

# **Testing the methodology for site descriptive modelling**

## **Application for the Laxemar area**

Johan Andersson, JA Streamflow AB

Johan Berglund, SwedPower AB

Sven Follin, SF Geologic AB

Eva Hakami, Itasca Geomekanik AB

Jan Halvarson, Svensk Kärnbränslehantering AB

Jan Hermanson, Golder Associates AB

Marcus Laaksoharju, Geopoint

Ingvar Rhén, Sweco VBB/VIK

Carl-Henric Wahlgren, Sveriges Geologiska Undersökning

August 2002

**Svensk Kärnbränslehantering AB**

Swedish Nuclear Fuel  
and Waste Management Co  
Box 5864

SE-102 40 Stockholm Sweden

Tel 08-459 84 00

+46 8 459 84 00

Fax 08-661 57 19

+46 8 661 57 19



# **Testing the methodology for site descriptive modelling**

## **Application for the Laxemar area**

Johan Andersson, JA Streamflow AB

Johan Berglund, SwedPower AB

Sven Follin, SF Geologic AB

Eva Hakami, Itasca Geomekanik AB

Jan Halvarson, Svensk Kärnbränslehantering AB

Jan Hermanson, Golder Associates AB

Marcus Laaksoharju, Geopoint

Ingvar Rhén, Sweco VBB/VIK

Carl-Henric Wahlgren, Sveriges Geologiska Undersökning

August 2002

# Preface

An important part of the Swedish Nuclear Fuel and Waste Management Company (SKB) preparation for the site investigations starting in 2002 concerns Site Descriptive Modelling. SKB has conducted two parallel subprojects in this area. The first entailed establishing the first version (version 0) of the Site Descriptive Model of the three sites North Tierp, Forsmark and Simpevarp. An essential part of this work is compiling existing data and interpretations of these sites in a regional scale. The other subproject, presented in this report, concerns testing the Methodology for Site Descriptive Modelling by applying it to the existing data obtained from investigation of the Laxemar area, which is a part of the Simpevarp site. This project is primarily a methodology test. The lessons learned will be implemented in the Site Descriptive Modelling during the coming site investigation.

The intent of the project has been to explore whether available methodology for Site Descriptive Modelling based on surface and borehole data is adequate and to identify potential needs for development and improvement in the methodology. SKB wants to demonstrate that a Site Descriptive Model can be established for a real site following structured and discipline integrated procedures in accordance with the intentions earlier presented. The project has also given the opportunity to test the different computer tools associated with building a site descriptive model.

The site specific data of Laxemar is comparable to the planned wealth of data after the Initial Site Investigation stage as envisaged by SKB. However, the data have been collected by different methods and the boreholes have partly been a test bed for new measurement techniques. The Site Descriptive Model should be reasonable, but should not be regarded as a 'real' model. There are limitations both in input data and in the scope of the analysis.

The work has been conducted by a project group with representatives from the main disciplines, geology, hydrogeology, hydrogeochemistry and rock mechanics. The different experts assessed and evaluated data and explored different modelling options. However, the full project group also met at regular intervals to discuss on a detailed level the current progress and ideas of the different modelling teams. In this way, the project also serves as a test bench for working interdisciplinary in order to reach a consistent understanding of a site.

Anders Ström  
Site Investigation – Analysis

## Summary

A special project has been conducted where the currently available data from the Laxemar area, which is part of the Simpevarp site, have been evaluated and interpreted into a Site Descriptive Model covering: geology, hydrogeology, hydrogeochemistry and rock mechanics. Description of the surface ecosystem has been omitted, since it was re-characterised in another, parallel, project. Furthermore, there has been no evaluation of transport properties. The project is primarily a methodology test. The lessons learnt will be implemented in the Site Descriptive Modelling during the coming site investigation.

The intent of the project has been to explore whether available methodology for Site Descriptive Modelling based on surface and borehole data is adequate and to identify potential needs for development and improvement in the methodology. The project has developed, with limitations in scope, a Site Descriptive Model in local scale, corresponding to the situation after completion of the Initial Site Investigations for the Laxemar area (i.e. 'version 1.2' using the vocabulary of the general execution program for the site investigations /SKB, 2001/). The Site Descriptive Model should be reasonable, but should not be regarded as a 'real' model. There are limitations both in input data and in the scope of the analysis.

### The modelling process

The measured (primary) data constitute a wide range of different measurement results including data from two deep core drilled boreholes. These data both need to be checked for consistency and to be interpreted into a format more amenable for three-dimensional modelling. Examples of such evaluations are estimation of surface geology, lineament interpretation, geological single hole interpretation, hydrogeological single hole interpretation and assessment of hydrogeochemical data. Furthermore, while cross-discipline interpretation is encouraged there is also a need for transparency. This means that the evaluations first are made within each discipline and after this compared to check for potential inconsistencies.

The processed data are used for three-dimensional modelling. The geological modelling provides the geometrical framework for the modelling in other disciplines and results in descriptions of geometry and properties of deformation zones of sizes down to 'local major zones' (1–10 km) and geometry and properties of rock domains. Two descriptions have been derived; the Base Geological Model and the Alternative Geological Model. Given the limited amount of data, regions of the model domain still have quite uncertain descriptions. The geometry is represented using a 3D CAD software (RVS), which is also used as an active interpretation tool for the geometric modelling.

The base for the hydrogeological modelling is the Geological Model with its identified volumetric objects. Essential hydrogeological evaluation tools include: assessment of single hole hydraulic tests, interpretation of interference tests and numerical modelling of groundwater flow tests and other observations. The resulting hydrogeological description comprises hydraulic properties for defined geometrical units and boundary conditions for the present day conditions for the rock volume defined by the Base Geological Model.

The major tasks for the hydrogeochemical evaluation include: (i) characterisation of undisturbed groundwater chemistry including the origin, depth/lateral distribution and the turnover time; (ii) focusing on data of importance for the safety evaluation such as pH, Eh, chloride, sulphide, colloids and microbes; (iii) identification of possible dissolved oxygen at repository depth. The hydrogeochemical description concerns distribution of the major water types, the water type mixing proportions and lists the major type of chemical reactions occurring at the site. Even if much of the modelling can be done in parallel with other disciplines, consistency checks with hydrogeology can and have been made. These comparisons enhance the confidence in the model.

The rock mechanics description comprises the initial (i.e. prior to excavation) stresses and the distribution of deformation and strength properties of the intact rock, of fractures and fracture zones, and of the rock mass. Only limited mechanics data exist from the Laxemar site, still predictions (with low confidence) are made using inferences from the nearby Äspö site combined with assessing the yet available site specific data.

## **Lessons learnt**

The resulting Laxemar Site Descriptive model can be regarded as a good illustration of the kind of description which will be produced at the end of the Initial Site Investigation stage ('version 1.2'). However, it should also be remembered that the description provided has been produced within the limitations in scope of the project. These limitations concerned the need to test new procedures, limitations in data as compared to the planned site investigations, and to some extent also limitations in resources. Should a version 1.2 model be needed for the area, the modelling work needs to be substantially revised, reflecting the data then being available.

The successful completion of the project also demonstrate that site descriptive modelling, as envisaged in the general execution program for the site investigations /SKB, 2001/, is indeed doable, even if it requires significant resources in time and staff. The project has tested a substantial part of the procedures to be applied in the 'real' modelling, and several potential improvements have been identified. When possible, these improvements have already been implemented during the course of the work. The remaining are listed, to be considered for the future site descriptive modelling.

# Contents

<b>1</b>	<b>Introduction</b>	11
1.1	Background	11
1.2	Scope and Objectives	12
1.2.1	Objectives	13
1.2.2	Limitations in scope	13
1.3	Methodology and organisation of work	14
1.3.1	What shall be estimated?	15
1.3.2	Evaluation of primary data	16
1.3.3	Estimating structures and properties in three-dimensions	17
1.3.4	Describing uncertainty	18
1.3.5	Organisation of work	19
1.4	This report	19
<b>2</b>	<b>Location and existing data</b>	21
2.1	Overview	21
2.2	Geoscientific investigation made	22
2.2.1	Surface based investigations	22
2.2.2	Core drilled boreholes	22
2.2.3	Percussion holes	24
2.3	Databases	24
2.3.1	SICADA and GIS data	24
2.3.2	Information not represented in GIS or SICADA	25
2.4	Initial modelling decisions	25
2.4.1	Co-ordinate system	25
2.4.2	Selecting the model domain	25
<b>3</b>	<b>Evaluation of primary data</b>	27
3.1	Geological evolution model	27
3.1.1	Introduction	27
3.1.2	Lithological development	30
3.1.3	Structural development	32
3.1.4	Development during the Quaternary period	37
3.2	Lineament identification	38
3.2.1	Detailed terrain model and resulting lineaments	38
3.2.2	Assessment of uncertainty in the digital terrain model	41
3.3	Surface geology	41
3.3.1	Quaternary deposits – distribution and description	41
3.3.2	Rock types – distribution, description and age	43
3.4	Geologic interpretation of borehole data	45
3.4.1	Aims of the single hole interpretation	45
3.4.2	Target parameters for single hole interpretation	47
3.4.3	Approach applied	48
3.4.4	Resulting single hole interpretation	50
3.4.5	Fracture mineralogical analysis	54
3.5	Seismic reflection and borehole radar measurements	54
3.5.1	Seismic reflection	54
3.5.2	Borehole radar measurements	58

3.6	Surface hydrogeology	59
3.6.1	Hydrological setting of the Simpevarp area	59
3.6.2	Quaternary deposits	65
3.6.3	Correlation with rock type?	65
3.6.4	Water table and piezometric levels	65
3.6.5	Baltic sea	66
3.7	Hydraulic interpretation of borehole data	67
3.7.1	Available data and test designs	67
3.7.2	Interpretation of single hole tests	75
3.7.3	Correlation between hydraulics and geology	78
3.8	Fracture Statistical Model	80
3.8.1	Input fracture and flow data	80
3.8.2	Fracture orientation distributions based on outcrop fracture data	81
3.8.3	Fracture orientation distribution based on fracture data from KLX01	84
3.8.4	Size distribution of fracture traces	86
3.8.5	Size distribution of the parent population	92
3.8.6	Spatial model	93
3.8.7	Fracture intensity	94
3.8.8	DFN model parameters	95
3.8.9	Analysis of flow data from KLX02	96
3.8.10	Fracture transmissivity distribution in the rock mass	98
3.9	Hydrogeochemical data evaluation	101
3.9.1	Introduction and aim	101
3.9.2	Data Set	101
3.9.3	Evaluation and simulation tools	102
3.9.4	Hydrogeochemical Evolution Model	104
3.9.5	Representativity of the data	106
3.9.6	Explorative analysis	108
3.10	Rock Mechanics Interpretation of Borehole Data	118
3.10.1	Collected SICADA data for rock mechanics	118
3.10.2	Stress measurement data from Laxemar	118
3.10.3	Stress measurement data from Äspö	120
3.10.4	Estimation of in situ stress along KLX02	121
3.10.5	Borehole seismic data from KLX02	124
3.10.6	Estimation of mechanical parameters for rock along KLX02	127
<b>4</b>	<b>Three-dimensional site descriptive modelling</b>	<b>129</b>
4.1	Geological and geometrical modelling	129
4.1.1	General modelling assumptions	129
4.1.2	Base geological model	130
4.1.3	Alternative geological model	136
4.1.4	Evaluation of uncertainties	147
4.2	Hydrogeological modelling	148
4.2.1	General modelling assumptions	148
4.2.2	Modelling strategy	150
4.2.3	Interference tests	151
4.2.4	Interpretation of hydraulic interferences	153
4.2.5	Estimating HCDs and HRDs directly from data	156
4.2.6	Interpretation of hydraulic interferences in the soil layers	158
4.2.7	Hydrogeological simulation approach	158

4.2.8	Numerical modelling approach for the Laxemar area	159
4.2.9	Identified uncertainties or unresolved issues in the model	170
4.3	Hydrogeochemical modelling	173
4.3.1	Geological information used in the hydrogeochemical modelling	173
4.3.2	Speciation, mass-balance and coupled modelling	173
4.3.3	M3 modelling	177
4.3.4	Visualisation of the groundwater properties	183
4.3.5	Comparison between hydrogeological and hydrogeochemical model	187
4.3.6	Site specific hydrogeochemical uncertainties	190
4.4	Rock mechanical modelling	192
4.4.1	State of stress	192
4.4.2	Mechanical property model	196
4.4.3	Uncertainty in rock mechanical property model	201
<b>5</b>	<b>The Laxemar Site Descriptive Model</b>	<b>205</b>
5.1	Geological description	205
5.1.1	General assumptions and uncertainties in the interpretations	205
5.1.2	Base geological model	207
5.1.3	Alternative geological model	230
5.1.4	Overall assessment of uncertainties in the geological description	235
5.2	Hydrogeological description	236
5.2.1	Hydraulic Conductor Domains (HCD)	236
5.2.2	Hydraulic Rock Domains (HRD)	237
5.2.3	Hydraulic Soil Domains (HSD)	239
5.2.4	Boundary Conditions	240
5.2.5	Groundwater flow pattern according to numerical simulations	241
5.2.6	Overall assessment of uncertainties in the hydrogeological description	242
5.3	Geochemical description	243
5.3.1	Model description	243
5.3.2	Conclusions and assessment of uncertainties	245
5.4	Rock mechanics description	247
5.4.1	In situ stress conditions	247
5.4.2	Mechanical properties of rock	248
5.4.3	Overall assessment of uncertainties in the rock mechanics description	248
<b>6</b>	<b>Lessons learned</b>	<b>251</b>
6.1	Methodology	251
6.1.1	Evaluation of primary data	251
6.1.2	Method for three-dimensional modelling	253
6.1.3	Traceability and Quality Assurance matter	255
6.1.4	Describing uncertainties	255
6.2	Working Procedures	256
6.3	The central SKB databases and software	257
6.3.1	GIS	257
6.3.2	Extracting data from SICADA	257
6.3.3	WellCad	257
6.3.4	RVS	258



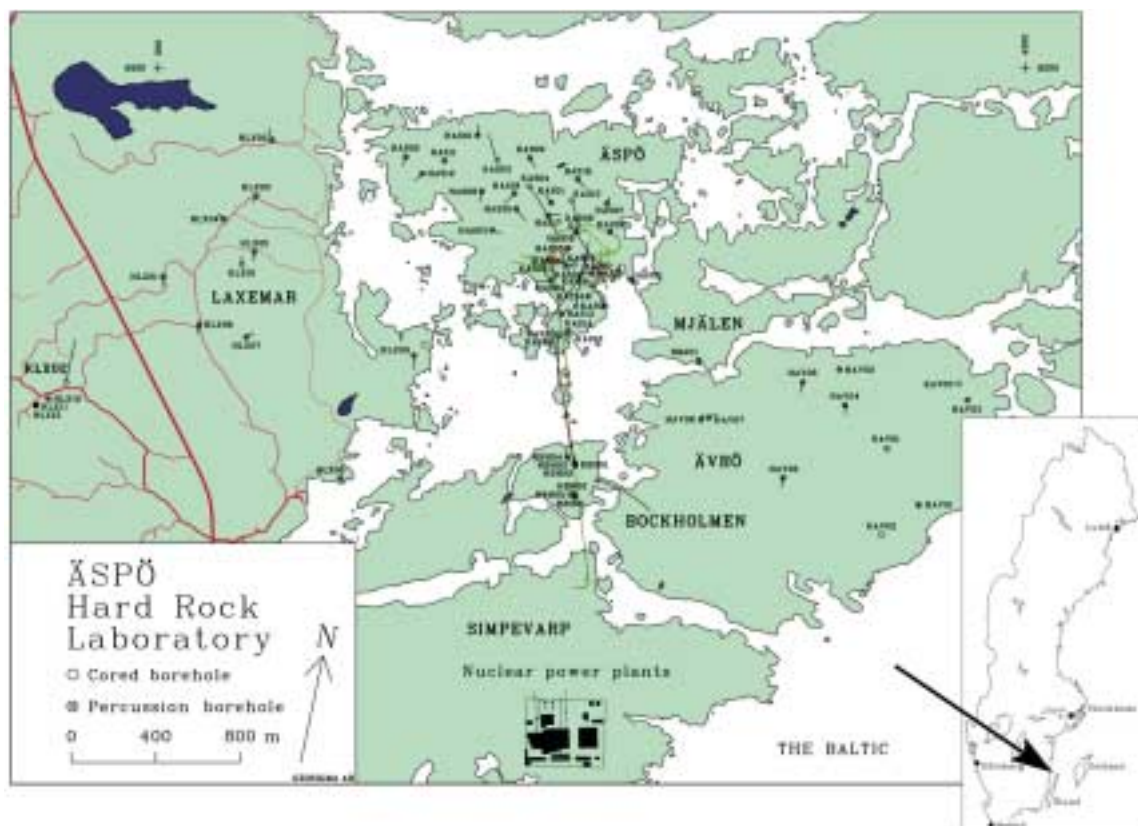
<b>References</b>	259
<b>Appendix A1</b>	269
<b>Appendix A2</b>	273
<b>Appendix A3</b>	275
<b>Appendix A4</b>	279
<b>Appendix A5</b>	281
<b>Appendix A6</b>	285
<b>Appendix A7</b>	293
<b>Appendix B1</b>	295
<b>Appendix B2</b>	309
<b>Appendix B3</b>	329
<b>Appendix B4</b>	337
<b>Appendix C1</b>	343

# 1 Introduction

The Swedish Nuclear Fuel and Waste Management Company (SKB) is preparing for the site investigations scheduled to start in 2002. An important part of these preparations is to test the methodology for Site Descriptive Modelling. A special project has been conducted where the currently available data from the Laxemar area, which is part of the Simpevarp site, have been evaluated and interpreted into a Site Descriptive Model covering geology, hydrogeology, hydrogeochemistry and rock mechanics. Description of surface ecosystems have been omitted in this tests, since they were being re-characterised in another, parallel, project. Furthermore, there has been no evaluation of transport properties. The project is primarily a methodology test. The lessons learned will be implemented in the Site Descriptive Modelling during the coming site investigation.

## 1.1 Background

An important part of the SKB preparation for the site investigations starting in 2002 concerns Site Descriptive Modelling. As a part of these preparations SKB has conducted a project, presented in this report, concerning testing the Methodology for Site Descriptive Modelling by applying the methodology to the existing data obtained from investigation of the Laxemar area, Figure 1-1, which is a part of the Simpevarp site.



*Figure 1-1. Overview of the Laxemar area. The selected model domain is displayed in Figure 2-1.*

The Laxemar area was included in the pre-investigations made for the Äspö Hard Rock Laboratory during 1986–1990. These investigations comprised different surface based methods, some percussion drilled bore holes and one deep core drilled borehole /Stanfors et al, 1997/. Later, a second borehole was core drilled in 1992, mainly to test investigation techniques at great depths. Several tests have since been performed /Ekman, 2001/. This means that the site specific data is comparable to the planned wealth of data after the Initial Site Investigation stage as envisaged in /SKB, 2001/. However, the data have been collected by different methods and the boreholes have partly been a test bed for new measurement techniques. The quality of the database may not meet the requirement envisaged for the initial stage of the site investigation. This will also impact on the quality of the models that can be produced from these data.

The basic ambitions, content and principles for Site Descriptive Modelling is described in the general execution program for the site investigations /SKB, 2001/. The Site Descriptive Model should be an integrated description of the site and its regional environments with respect to current state and naturally ongoing processes, covering geology, rock mechanics, thermal properties, hydrogeology, hydrogeochemistry, transport properties and surface ecosystems. The description is made in Regional and Local scale and should serve the needs for Safety Assessment and Design /SKB, 2000/.

Even if a ‘Site Descriptive Model’ mainly is a description, it is still a ‘model’. The selection of parameters and geometrical framework is based on an underlying conceptual model of the site. Estimation of geometry and parameter values into a full three-dimensional description rests on extrapolation of data measured at a few locations. Furthermore, the confidence in the description should be tested with simulations of e.g. groundwater flow or stress distribution to the extent useful. However, Site Descriptive Modelling does not concern simulation of e.g. the future site evolution (part of Safety Assessment) or estimation of tunnel stability (part of Design analyses). The Site Descriptive Model is, of course an essential input to such simulations. See also /SKB, 2000/.

/Munier and Hermanson, 2001/ provide the basic structure for geometrical geologic modelling, which is an essential element of the methodology for Site Descriptive Modelling. However, many other aspects of the methodology were in a developing phase during the conduct of the current project. In particular, documented “method descriptions” for modelling and intermediate products of modelling were only partly available when the project started. Instead, the project has partly been a test-bed for the finalisation of these method descriptions. Furthermore, although not documented as formal method descriptions, SKB and its consultants have developed considerable experience in site modelling over the years, and in particular during the characterisation of the Äspö HRL, see e.g. /Rhén et al, 1997/.

## **1.2 Scope and Objectives**

The intent of the project has been to explore whether available methodology for Site Descriptive Modelling based on surface and borehole data is adequate and to identify potential needs for development and improvement in the methodology. SKB wants to demonstrate that a Site Descriptive Model can be established for a real site following structured and discipline integrated procedures in accordance with the intentions presented in the general execution programme /SKB, 2001/.

### 1.2.1 Objectives

The project has developed, with limitations in scope, a Site Descriptive Model in local scale for the Laxemar Area, corresponding to the situation after completion of the Initial Site Investigations (i.e. ‘version 1.2’ using the vocabulary of /SKB, 2001/). The work has been conducted in order to reach the following specific objectives:

- test the evaluation of site specific information using the planned methodology with its requirements on integration and consistency between different disciplines and its requirement on documentation of data exchange,
- document experiences and suggest potential developments of current modelling methodology and
- (secondary) increase the understanding of the Laxemar area.

The Site Descriptive Model should be reasonable, but should not be regarded as a ‘real’ model. There are limitations both in input data and in the scope of the analysis, see next subsection.

### 1.2.2 Limitations in scope

The main tool for interpreting and visualising geometrical information in three dimensions is the Rock Visualisation System (RVS) – a Microstation-based 3D CAD software package developed by SKB. The version (2.3) of the RVS software available at the time of the start of the project did not have full compatibility with all intended functions in the geometric geological modelling report /Munier and Hermansson, 2001/. In particular, the used version of RVS primarily handles deformation zones, whereas space filling entities, i.e. ‘rock domains’ as well as the description of the three-dimensional distribution of properties in these domains had to be handled outside the RVS-environment. Later RVS versions (version 3 and onwards) handle these functions. The ‘alternative model’, which include several different ‘rock domains’ was in fact developed with an early release of RVS 3.0, see Chapter 4.

The amount and quality of data from Laxemar is not fully comparable to the ambitions of the Initial Site Investigations. The boreholes have been used as test beds for developing and assessing measurement techniques, which means that some tests have only been performed in one borehole, or in a part of a borehole. Many tests envisaged in the general programme /SKB, 2001/, including most rock mechanics tests, were not performed at Laxemar. The surface based investigations mainly date back to the pre-investigation of the Äspö HRL, and do not encompass all development and thought in the current plans.

The modelling is confined to develop a Site Descriptive Model in Local Scale. An updated regional model was developed in the parallel ‘version-0’ project, but was not practically available to the current project. Available regional knowledge was of course used also for the Laxemar modelling, but regional modelling was not performed, as this would have been an unnecessary duplication of efforts.

In addition, the following components of the Site Descriptive Modelling were omitted, or made with a low ambition level.

- There was limited consideration of previous model versions. Neither a version 0 (see above), nor a version 1.1 according to the format in the general execution programme were available.
- There was no description of the radionuclide transport properties of the rock. There are few, if any, transport specific measurements as envisaged in the general execution programme /SKB, 2001/. However, it should also be born in mind, that the (detailed) hydrogeological and hydrogeochemical descriptions provide the main input to the transport description. At least after the Initial Site Investigation.
- There was no description of thermal properties. This part, although very important, was not considered critical for the test and the amount of thermal data was also limited. Furthermore, the three-dimensional thermal model would to a large extent rely on the (rock type part of) the geological model.
- There was no description of surface ecosystems, as this was part of a parallel project ('the 0-version'), but near-surface hydrology was included.

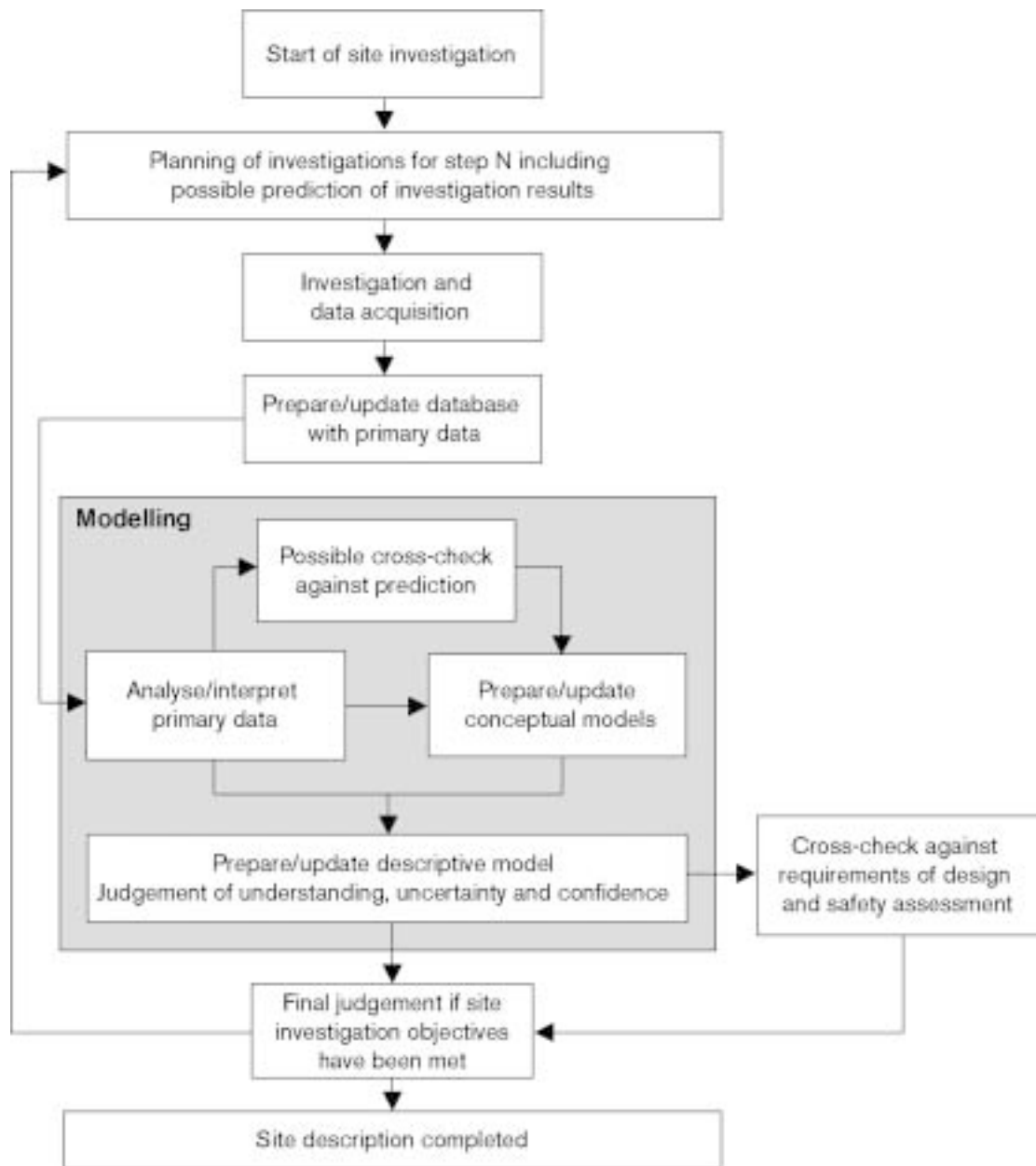
It should also be born in mind that the project primarily was a test and that the methodology for Site Descriptive Modelling was developed in parallel with the project. This also implied some time and resource limitations to the work, which would not be as active in the 'real' modelling.

### 1.3 Methodology and organisation of work

The general characterisation program /SKB, 2001/ describes objectives with the programme and its different stages, methods for characterisation, defines different characterisation stages and describes the interaction needed between different disciplines. To the extent possible and considering the limitations in scope outlined in Section 1.2.2 the current project has followed the methodology outlined in the general programme.

The site-descriptive model is devised and updated stepwise as the site investigation progresses, Figure 1-2. After a completed batch of measurements the primary data are first evaluated within each discipline; geology, rock mechanics, hydrogeology, hydrogeochemistry etc. This *evaluation of primary* data both concern quality control etc of data and 'intermediate interpretations' aiming at producing 'building blocks' for the three-dimensional description. The next main step, *three-dimensional modelling*, concerns estimation of geometry and properties in three-dimensions. This step also includes interdisciplinary assessments of the *confidence and uncertainty* in the produced description. One way of describing these uncertainties is to produce *alternative* models.

In principle, although not fully tested within the current project, the modelling also includes a step of comparison between previous models and discussion of how additional measurements may affect uncertainties in prediction. Also outside the scope of the current project are decisions whether additional loops of modelling or data acquisition are necessary. Such judgements are made by the end users (primarily Design and Safety Assessment).



*Figure 1-2. The site investigation phase consists of several steps with planning, investigations, interpretation and cross-checking (from /SKB, 2001/ Figure 2-5).*

### 1.3.1 What shall be estimated?

The selection of parameters to be estimated during the site characterisation programme rests on several assessments on what is required to be determined for the use of Safety Assessment and Design. Over the years SKB has developed a significant experience, from various field studies, safety assessments and from the work at the Äspö Hard Rock Laboratory (HRL) on what to measure. /Andersson et al, 2000/ formulate requirements and preferences on the rock, from a safety and engineering perspective, drawing upon the analyses and conclusions made in SR 97 /SKB, 1999/. Additional data are needed to obtain a geoscientific understanding of the site. The need for ecosystem information was explored by /Lindborg and Kautsky, 2000/. The intended content of the site descriptions is further specified in the general execution programme /SKB, 2001/.

The site investigation and the modelling will be developed in stages. A full description will only be available at the end of the complete site investigation stage. Specific to the version 1.2 description, which will be produced as a result of the Initial Site Investigation stage, the site descriptive modelling should be detailed enough to provide a basis for a decision to start the Complete Site Investigation step /SKB, 2001/. This means that the modelling should:

- allow identification of rock volumes potentially suitable for a repository as regards geological homogeneity and suitable rock types,
- allow an initial judgement of location, orientation and size of extensive deformation zones, i.e. regional and local major fracture zones and extensive ductile (plastic) shear zones,
- allow judgement of the absence of indications of unfavourable rock mechanical, hydrogeochemical and hydrogeological conditions.

/Andersson et al, 2000/ quantify what is considered to be unfavourable in respect to this situation and also stipulate criteria for conditions that can warrant discontinuation of a site investigation.

### **1.3.2 Evaluation of primary data**

The measured (primary) data constitute a wide range of different measurement results. These data both need to be checked for consistency and to be interpreted into a format more amenable for three-dimensional modelling. Furthermore, while cross-discipline interpretation is encouraged there is also a need for transparency. This means that the evaluations first are made within each discipline and after this compared to check for potential inconsistencies.

#### **Geology**

The generic geological knowledge as well as findings from some of the surface based investigations are combined into a description of the geological historical evolution, using 'standard methods' of the geological science, see Section 3.1. Arguments based on this geological evolution are often essential for justifying extrapolation of shape and size of units and of arguing size and direction of fracture zones. The surface information is also used for compiling surface geology (rock type) maps and lineament maps, see Sections 3.2–3.3.

Borehole geophysics and geological borehole logs are interpreted into a unified geological description along each borehole, see Section 3.4. This geological single-hole interpretation also identifies potential fracture zone intersections with the borehole.

The measured signals from reflection seismics and borehole radar can be interpreted into reflectors or reflection cones (see Section 3.5). These reflectors are then used in the three-dimensional modelling.

Lineaments and fracture data are evaluated statistically into a fracture statistical description, see Section 3.8.

## **Hydrogeology**

The surface hydrology data are compiled into a surface hydrogeological description, see Section 3.6. The different hydraulic tests carried out in the boreholes are interpreted into a hydrogeological single-hole interpretation of the permeability distribution along the boreholes and identification of potential hydraulic conductor intersections and some correlation studies of mapped core versus permeability distribution, see Section 3.7.

## **Hydrogeochemistry**

For hydrogeochemistry the primary data evaluation essentially concern quality checks of the collected water samples /Smellie et al, 2002/. The evaluation essentially aims at identifying representative data sets for further analysis, see Section 3.9.

## **Rock Mechanics**

The evaluation of stress measurements essentially concern assessing the origin of variation (if existent), is it likely to be measurement 'scatter' or is it potentially to be explained by geologic structures? Rock mechanics laboratory data obtained from bore cores (if existent) together with fracture statistics data are used for rock mechanics classification along boreholes /Andersson et al, 2002/. The current evaluation is given in Section 3.10.

### **1.3.3 Estimating structures and properties in three-dimensions**

The three-dimensional modelling, concern estimation of geometry and properties in three-dimensions. SKB has presented a methodology to construct, visualise and present the Site Descriptive Models /Munier and Hermanson, 2001/. The main tool for interpreting and visualising geometrical information in three dimensions is the Rock Visualisation System (RVS).

## **Geology**

The crystalline rock mass contain deformation zones on a large variety of scales ranging from micro-cracks in the 'intact rock', individual visible joints, to regional deformation zones. According to SKB nomenclature, see e.g. /SKB, 2000/, all *deformation zones* with essentially brittle deformation history are called 'fracture zones'. Furthermore, the Geological Site Descriptive Model only explicitly (deterministically) describes the fracture zones with a size larger than around 1 km. Such zones are called 'regional zones' (>10 km) and 'local major zones' (1–10 km). The remaining zones are described statistically within each rock domain. Identification of zones are mainly made from the lineament maps, the single-hole interpretation of the boreholes and from seismic and radar reflectors, see Section 4.1.

The geometrical distribution of rock properties and fracturing is described using the concepts of *rock units* and *rock domains*. A rock unit is a volume judged to have a reasonably statistically homogeneous distribution of lithology and fracture statistics. (Fracture zones are special cases of rock units). A rock unit may contain different rock types and also small scale inclusions of various rock types. Each rock unit is defined by its location and is described in terms of rock type distribution and fracture and fracture zone statistics. In addition, several rock units, e.g. those only separated by different fractures zones, may have similar properties. This information is also handled by logical connections in



the geological model, where several rock units are assembled into rock domains. A rock domain is a region of the rock mass for which the properties can be considered essentially the same in a statistical sense. The interpretation is mainly based on the surface geological description, combined with the single-hole interpretations of the boreholes, see Section 4.1.

### **Hydrogeology**

The hydrogeological description primarily contains information on the permeability distribution at various scales, see /SKB, 2001/ for the rock units. The distribution is based on the geological description of the rock domains and associated rock units, but the hydrogeological evaluation of data may lead to further divisions into different units, or that geologically distinct units are combined into hydraulic domains with the same (statistically) hydraulic properties. The hydraulic description may in turn be used for simulating different tests (e.g. interference tests) and measurements (i.e. salinity distribution) for further calibration or assessment of confidence of the model. See Section 4.2.

### **Hydrogeochemistry**

/SKB, 2001/ has defined the major task for hydrogeochemical evaluation to include: (i) characterise undisturbed groundwater chemistry including the origin, depth/lateral distribution and the turnover time; (ii) focus on data of importance for the safety evaluation such as pH, Eh, chloride, sulphide, colloids and microbes; (iii) identify possible dissolved oxygen at repository depth. Currently, SKB develops documented procedures for the hydrogeochemical modelling /Smellie et al, 2002/ to be used to attain these goals. The data evaluation becomes a complex and time-consuming process when the information has to be decoded. Manual evaluation, expert judgment and mathematical modelling is often combined dependent of the aspect of the modelling. The predicted water distribution can also be compared with simulations made on the hydrogeological description. See Section 4.3.

### **Rock mechanics**

SKB has developed a Rock Mechanics Descriptive Modelling Strategy /Andersson et al, 2002/. The model describes the initial stresses and the distribution of deformation and strength properties of the intact rock, of fractures and fracture zones, and of the rock mass. Rock mass mechanical properties are estimated by empirical relations and by numerical simulations but overall judgement is finally needed. The stress modelling approach integrates stress measurements, geological factors, numerical modelling and the uncertainties involved. The strategy should be reviewed and, if required, updated as appropriate. For the Laxemar project this methodology has been applied to some extent, see Section 4.4, but not fully. The main restriction was that there is comparatively little rock mechanics data from the Laxemar area making extensive rock mechanics evaluations difficult. More rock mechanics data are expected to be measured in the coming site investigations.

#### **1.3.4 Describing uncertainty**

The site description must also assess the uncertainty in the description. There are always uncertainties in interpreting measurements and in determining rock parameters, which vary in space.

The site descriptive modelling should deal with conceptual uncertainty, data uncertainty, spatial variability and confidence. Even if these concepts are related, it is useful to keep them separated. The three-dimensional description needs to describe the parameters with their spatial variability over a relevant scale and to describe the uncertainty in this description. One way of describing these uncertainties is to produce alternative models, but uncertainty may also be described as distributions or intervals. In addition, it is also necessary to describe the confidence in the model predictions. Confidence is more expressed in qualitative terms (e.g. high, fair, low) but such value statements must be supported by concrete observations from the modelling.

The uncertainty evaluation has been made within each discipline, but also includes interdisciplinary assessments of the confidence and uncertainty in the produced description.

### **1.3.5 Organisation of work**

The work has been conducted by a project group with representatives from the main disciplines, geology, hydrogeology, hydrogeochemistry and rock mechanics. The different experts assessed and evaluated data and explored different modelling options. However, the full project group also met at regular intervals to discuss on a detailed level the current progress and ideas of the different modelling teams. The progress of work essentially follows the outline of the report.

## **1.4 This report**

The report essentially follows the different modelling steps. Chapter 2 summaries the available data. Chapter 3 concerns the evaluation of the primary data. Chapter 4 concerns three-dimensional modelling including assessment of uncertainties. The final Site Descriptive model is presented in Chapter 5. Chapter 6 discusses lessons learned and concludes the project.

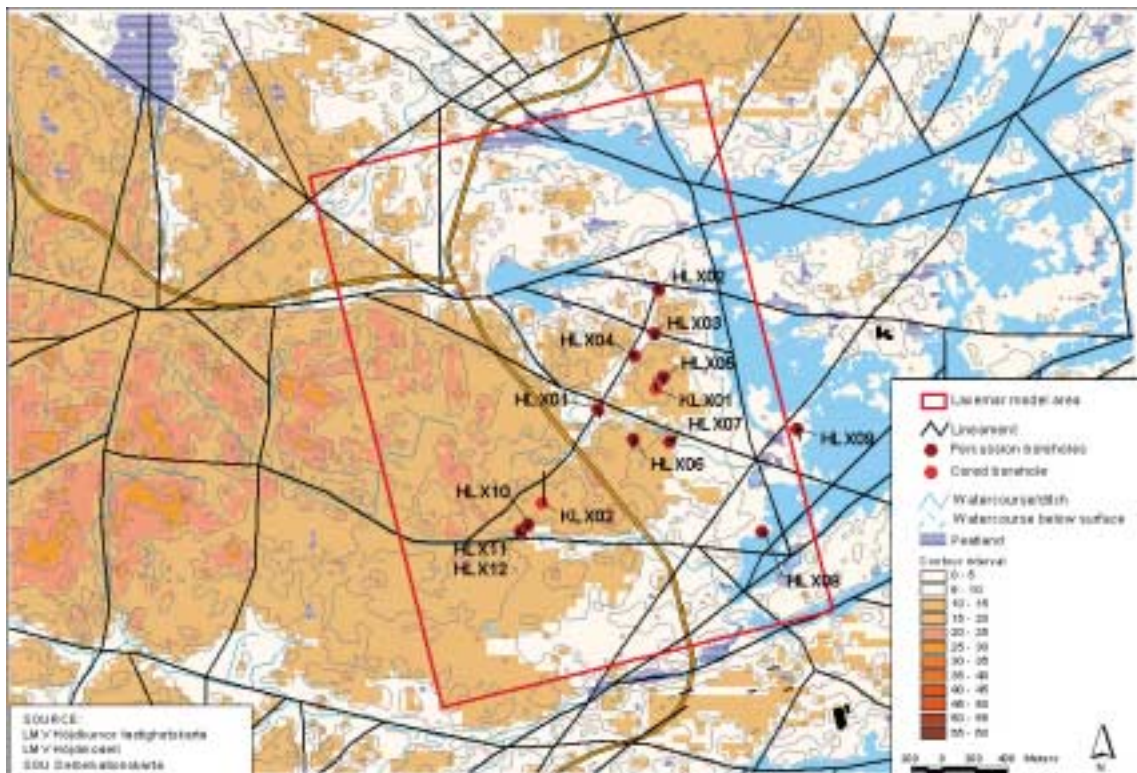
## 2 Location and existing data

This chapter provides an overview of the Laxemar area and of the available data from the site.

### 2.1 Overview

The Laxemar area constitutes the mainland immediately to the west alongside the island of Äspö, see Figure 2-1. The area is situated within the nature geographic region “Södermanlands and Götalands archipelagos”. The landscape is a mixture of open water areas, islands and skerries. The vegetation is characterised by relatively poor forest types, with pine as the dominating tree species, although spots of deciduous wood exist in the lower, sediment filled valleys. These sediments are partly cultivated or being used as pasture.

The predominant rock type is a reddish grey, c. 1800 Ma, medium- to coarse-grained, generally porphyritic granite to granodiorite belonging to the Transscandinavian Igneous Belt. Exposed bedrock or bedrock with a thin cover (<0.5 m) of Quaternary deposits, mostly till, dominates the area. In the topographic lows (valleys) glacial and post-glacial sediments dominate. The topography is slightly more accentuated compared to the conditions at Äspö with adjacent islands. The altitude slightly exceeds 22 m.a.s.l. in the southern part. (For more detail, see Sections 3.1 to 3.3).



*Figure 2-1. Laxemar area, location of boreholes and lineaments interpreted in Oskarshamn feasibility study. The figure also displays the selected model domain (see Section 2.4.2).*

## 2.2 Geoscientific investigation made

The Laxemar area was included in the pre-investigations made for the Äspö Hard Rock Laboratory during 1986–1990. These investigations comprised different surface based methods, some percussion drilled bore holes and one deep core drilled borehole /Stanfors et al, 1997/. Later the area has been used for testing equipment and methods. A second core drilled borehole was drilled in 1992 mainly to test investigation techniques at great depths. Several tests has since been performed /Ekman, 2001/. There were also additional percussion holes drilled. In total there are two deep core drilled boreholes in the area and 12 rather shallow percussion drilled holes, see Figure 2-1.

### 2.2.1 Surface based investigations

Most of the surface based investigations carried out until 2001 were part of the pre-investigations of the Äspö Hard Rock Laboratory between 1986 and 1990, but there has been additional measurement later. /Stanfors et al, 1997/ summarise these tests. The geological investigations comprise:

- airborne geophysical surveys (magnetic, slingram, VLF, radiometric),
- ground geophysics (gravity, magnetic, VLF and seismic refraction) measurements,
- petrophysics on 257 rock samples,
- bedrock mapping,
- tectonic analysis and fracture mapping.

Furthermore, as a test, ground geophysical measurements with half-regional resistivity measurements (HRR), electrical soundings (VES) and transient electromagnetic sounding (TE) were carried out in 1996–1997.

A reflection seismic study was conducted along two crossing lines in late 1999 /Bergman et al, 2001/. The crossing was located at the interception of borehole KLX02. The main goal of the investigation was to perform a full-scale test of newly developed methods. (For further discussion, see Section 3.5).

Investigations on hydrology and hydrogeology were mainly limited to compilation of available data in databases such as the SGU well database (see Section 3.6). Some surface water samples were collected for the hydrogeochemical exploration (see Section 3.9).

### 2.2.2 Core drilled boreholes

The first core drilled borehole, KLX01, reached 703 m at a first drilling effort in 1988 and was deepened to 1078 m in 1990. The second core drilled borehole, KLX02, reaches 1700 m. The drilling was performed during 1992, but logging and other investigations were carried out later, see /Ekman 2001/.

## Geology

In summary the geological investigations in the core drilled boreholes comprise

- Geological core logging (KLX01, KLX02).

- Petrophysical logging (KLX01, KLX02).
- Geophysical logging (KLX01, KLX02).
- Borehole radar (KLX01, KLX02).
- Fission track studies (KLX02).
- Borehole TV-logging with BIPS and also with a black and white CCD-camera (only KLX02).
- Vertical seismic profiling (VSP), (KLX02).

More detail as well as the evaluation of (some of these data) is given in Sections 3.4, 3.5 and 3.8.

### ***Hydrogeology***

In summary the hydrogeological investigations in the core drilled boreholes comprise:

- Airlift tests (KLX01, KLX02 and also some of the percussion drilled holes).
- Injection tests 3 m sections (between 106.00–691.00 m of KLX01).
- Injection tests 30 m sections (between 103.00–643.00 m of KLX01).
- Flowlogging with a probe of spinner type and with the UCM-flow probe (parts of KLX01).
- Difference flow measurement with or without pumping using the Posiva Flow Log (KLX02).
- Short term pumping test or capacity tests (KLX01, KLX02).
- Interference test with pumping in one section of KLX02, with monitoring in several sections of KLX01.

More detail as well as the evaluation of (some of these data) is given in Section 3.7.

### ***Hydrogeochemistry***

The hydrogeochemical investigations of the bore holes comprise various water samples and characterisation of fracture minerals. More detail, as well as the evaluation is given in Section 3.9.

### ***Rock mechanics***

In summary, the rock mechanics investigations in the core drilled boreholes comprise:

- Rock stress measurements (hydraulic fracturing) (KLX02).
- Measurement of the compressive and shear wave velocity by means of a 2SAA-1000 Sonic Probe equipment (KLX02).
- Temperature profiles in (KLX01, KLX02).

More detail is given in Section 3.10.

### **2.2.3 Percussion holes**

The first seven (HLX01–07) of the twelve percussion drilled boreholes were part of the Äspö HRL pre-investigation programme. The holes, about 100 m deep, were drilled to get a first indication of the hydrogeologic conditions of the upper parts of the investigation area and to explore preliminary indications of hydraulic structures. Information from these holes comprises drilling records, air-lift tests and pumping tests.

The holes HLX08 and HLX09 were drilled to get more information on the (extension of) fracture zone NE-1 (in the Äspö HRL terminology) found in the tunnel to the Äspö HRL. The holes HLX10–12 were drilled as water supply wells for the core drilled borehole KLX02.

## **2.3 Databases**

The investigation results are mainly stored in the SKB databases SICADA and the SKB GIS database. Data used in the current project has also mainly been obtained from these databases. However, some limited data, not stored in these official and Quality Assured databases have also been utilized.

### **2.3.1 SICADA and GIS data**

Most of the SICADA data are measurement results or results from evaluations of such data, stored in tables. Data for use in the current project have been obtained on-line using purpose designed software. The export format varies according to the importing software, e.g. RVS and WellCad have specific import routines connected to the SICADA structure.

For traceability a set of appendices are compiled, which should allow a complete trace to all information used in the project.

Appendix A1 provides a history record of which data have been extracted from SICADA. The table provides date, running identification number, who was ordering the information, name of project and a short description of the type of data ordered.

Geographically positioned data have been obtained from the SKB GIS databases. Such data have been used in the RVS geometrical modelling (see Section 4.1) and for describing the surface environment, hydrography etc, see Section 3.6. Appendix A2 lists the ordinary maps and ortophotos used. The maps and the ortophotos have mainly been used for a general description of land use within and close to the model area. Hydrographical data, such as streams, have been obtained from the topographic map.

The project has also utilised geological information compiled and evaluated in the Oskarshamn feasibility study in the form of geological maps and lineament maps etc, Appendix A3. The lineament map has then been updated within the project (see Section 3.2) using an updated topographic model. Appendix A3 summaries the type of information used.

Appendix A4 provides information on which Geological data have been imported to RVS from SICADA.

Appendix A5 provides information on which hydrogeological and metrological data have been ordered from the SKB databases. Appendix A6 contains a 'log-file' of ordered hydrogeochemical data from SICADA. The log-file provides information on which type of data has been ordered, the time, filename, parameter name, chemical variables and the criteria for selection. Appendix 6 provides information on which rock mechanics data have been ordered from the SKB databases.

### **2.3.2 Information not represented in GIS or SICADA**

In addition, to the data stored in official sources, the project has also used other information. Also these data sources are tabulated in the above appendices.

## **2.4 Initial modelling decisions**

### **2.4.1 Co-ordinate system**

Although it may be viewed as a trivial point past experience clearly show the need to be very precise about co-ordinate system. Throughout the modelling all co-ordinate data are handled and presented in the RT90 RH70 2,5gV system, which is the standard selection by SKB. Consequently, data not presented in this system were transferred into RT90, before further evaluation within the project.

### **2.4.2 Selecting the model domain**

After reviewing the available information the first step in the Laxemar modelling project was to determine the size and location of the model domain. According to plan /SKB, 2001/ a Local Site Descriptive Model should cover an area of about 5–10 km<sup>2</sup>. In addition, the following was considered for making the selection of the model domain:

- The deep core drilled boreholes KLX01 and KLX02 should be located in the centre of the domain.
- The domain should be deep enough for the hydrogeological flow simulations to be performed in Site scale and should also include the depth of the boreholes. In /SKB, 2001/ a depth down to 1000 m is anticipated, but the Laxemar boreholes extend to further depths. It was therefore decided to make the domain 2 km deep, and then evaluate potential disadvantages of such a deep model domain.
- The domain should include regional lineaments, which may serve as boundaries for subsequent hydrogeological simulations.
- The distribution of bodies of diorite to gabbro could be an essential element of the rock type description. The surface exposures, one in the south-western and two in the north-eastern part, should thus be included in the model domain.
- A small bay north-east of the boreholes has been characterised for chemical traces of deep groundwater discharge. This potential discharge area should be included in the model domain, in order to make it possible to evaluate this specific information.

- The reflection seismic profiles, which are considered to be an essential component of the site data during the initial site investigation stage should be included in the model domain.
- The model domain should not be too large as this would imply data needs outside the volume of interest. There are also practical limitations to the amount of information, which can be practically handled in the same RVS-model.

The resulting surface of the model domain is shown in Figure 2-1. The surface area is approximately 8.5 km<sup>2</sup>, i.e. typical of the envisaged Local models to be produced during the site investigation. Exact co-ordinates are provided in the RVS-representation.



## **3 Evaluation of primary data**

This chapter concerns the evaluation of the available primary data. These data both need to be checked for consistency and to be interpreted into a format more amenable for three-dimensional modelling. Furthermore, while cross-discipline interpretation is encouraged there is also a need for transparency. This means that the evaluations are first made within each discipline. The interpretations are then compared within the framework of the three-dimensional modelling, described in Chapter 4.

### **3.1 Geological evolution model**

The generic geologic knowledge as well as findings from some of the surface based investigations are combined into a description of the geological historical evolution, using 'standard methods' of the geological science. Arguments based on this geological evolution are often essential for justifying extrapolation of lithology and of arguing size and direction of fracture zones.

#### **3.1.1 Introduction**

The following brief outline of the geological evolution in the Oskarshamn region is mainly based on results published in reports in various SKB series as well as on research papers in scientific journals. The Oskarshamn region is put into a regional geological context (Figure 3-1), but the description is focussed on the geological evolution of rock types and structural elements that characterize the bedrock in the Oskarshamn local community and its immediate surroundings (Figure 3-2; /Bergman et al, 1998, 1999, 2000/).

The geological evolution of cratonic bedrock regions is generally the result of consecutive large-scale processes, e.g. orogenies, which have operated over a considerable period of time. In order to try to understand the geological development of the bedrock in southeastern Sweden, with focus on the Oskarshamn region, it is necessary to take into account also post-cratonization, i.e. after c. 1750–1700 Ma, large-scale processes to which the Oskarshamn region has had a more or less remote position, since these processes might have had a far-field effect in the already cratonized crust. The geological development in the Oskarshamn region, including the formation of existing rocks, as well as structural and tectonic overprinting, is complex and span over a time period of c. 1900 Ma. The following text gives a brief summary and for further information of the geological evolution and processes that might have affected the bedrock in the Oskarshamn region and the rest of the southern part of the Fennoscandian Shield, the reader is referred to e.g. /Larson and Tullborg, 1993; Milnes et al, 1998/.

The geological evolution in southeastern Sweden, with focus on the Oskarshamn region, is tentatively summarized in Table 3-1 (page 36).

# BEDROCK OF SWEDEN

## Fossil-bearing bedrock outside the Caledonides

Sandstone, shale and limestone, 545-55 m.y. in age

## Caledonides

Rocks 700-430 m.y. in age

- Granite and gabbro
- Sandstone, shale, limestone and volcanic rocks, mainly metamorphosed
- Mica schist, mica gneiss and amphibolite
- Sandstone with dolerite dykes
- Sandstone, fossil-bearing shale and limestone

Rocks older than 1500 m.y.

- Granite, syenite, gabbro, volcanic rocks and mica gneiss

## Precambrian shield

Rocks 1570-700 m.y. in age

- Granite and pegmatite
- Sandstone, shale and mafic volcanic rocks, partly metamorphosed
- Granite, monzonite, syenite, gabbro and dolerite, partly gneissose

Rocks 1850-1590 m.y. in age

- Mica gneiss and amphibolite
- Felsic volcanic rocks, gneissose
- Volcanic rocks, partly metamorphosed
- Gneiss, mainly granitic, granodioritic or tonalitic in composition
- Granite, pegmatite, monzonite, syenite and gabbro, partly gneissose

Rocks 1960-1850 m.y. in age

- Granite, monzonite, syenite and gabbro, partly metamorphosed
- Granite, granodiorite, tonalite and gabbro, partly gneissose
- Sandstone and shale, partly gneissose
- Volcanic rocks, metamorphosed

Rocks 2500-1960 m.y. in age

- Mafic volcanic rocks, sandstone, shale and limestone, metamorphosed

Rocks older than 2500 m.y.

- Gneiss, granitic, granodioritic or tonalitic in composition; granite

## Structures

- Impact structure
- Form line of tectonic foliation
- Fault, symbols in downthrown block
- Thrust in the Caledonides, symbols in elevated block
- Thrust or reverse deformation zone in the Precambrian shield, symbols in elevated block
- Deformation zone, symbols in downthrown block
- Deformation zone, arrows indicate horizontal component of movement
- Deformation zone, unspecified

LLDZ Loftahammar – Linköping Deformation Zone

SFDZ Sveconorwegian Frontal Deformation Zone

PZ Protogine Zone

SBDZ Småland – Blekinge Deformation Zone

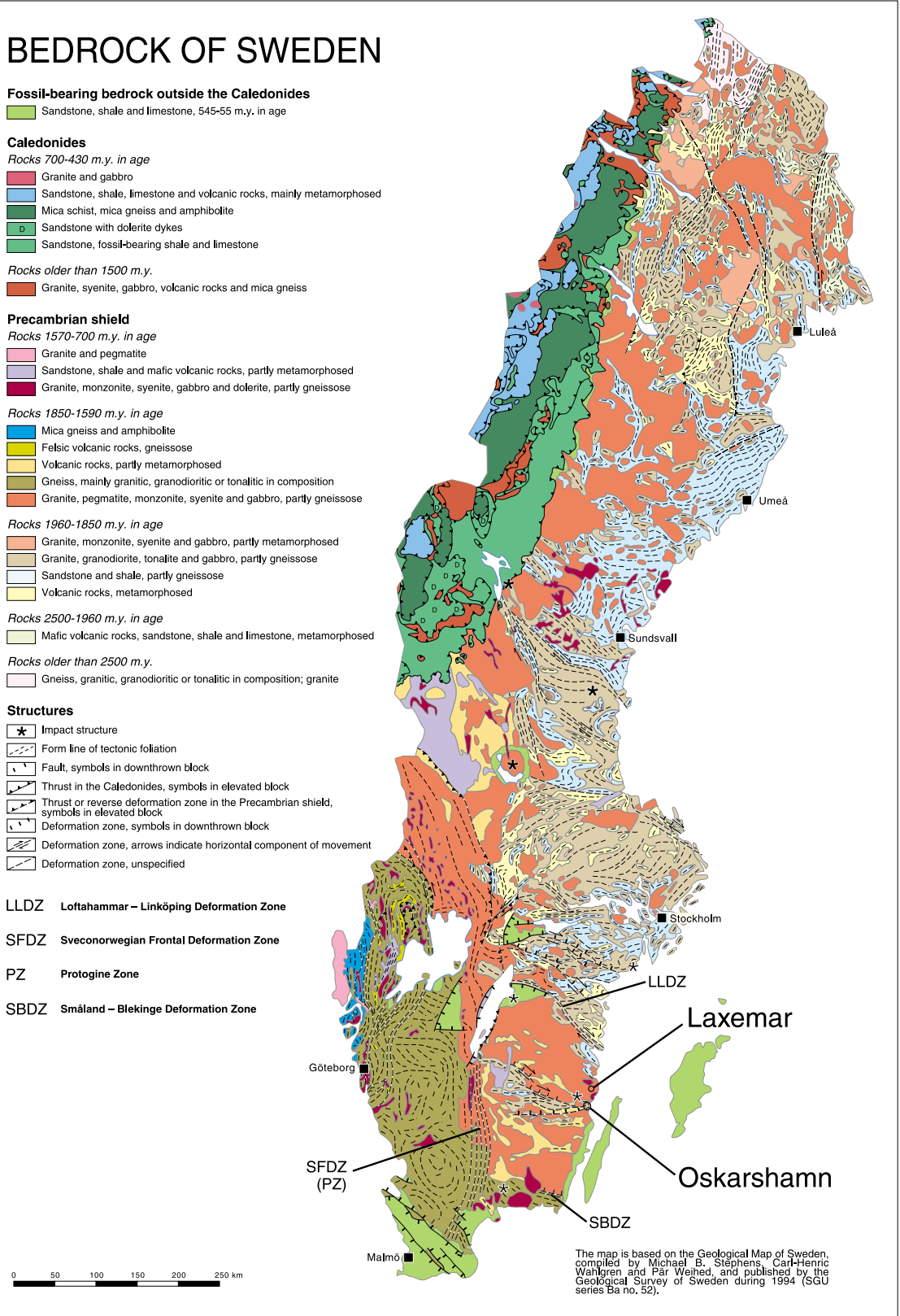


Figure 3-1. Bedrock map of Sweden.

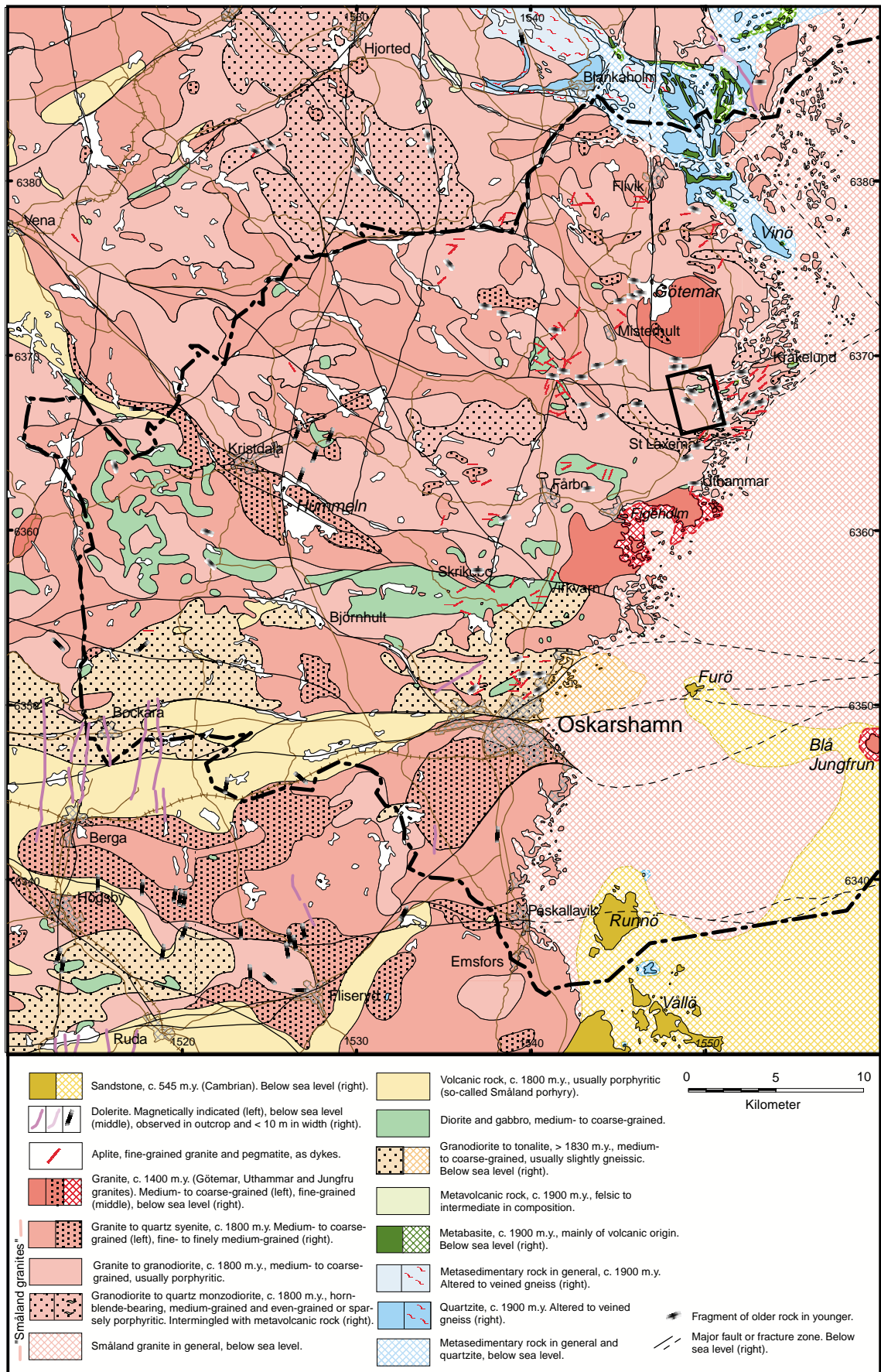


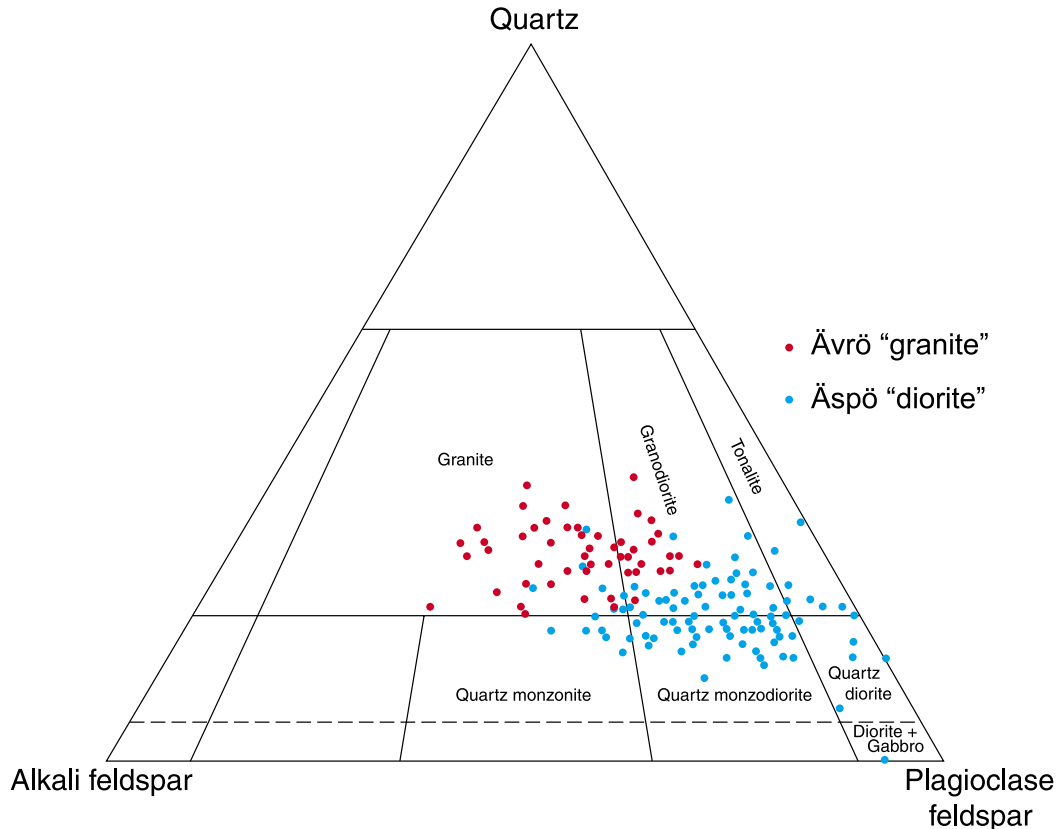
Figure 3-2. Bedrock map of the Oskarshamn local community and surrounding area. Slightly modified after Bergman et al, 1998/.

### 3.1.2 Lithological development

The oldest rocks in the Oskarshamn region, though subordinate, comprise more or less strongly deformed and metamorphosed supracrustal rocks of predominantly sedimentary but also of volcanic origin. The formation is constrained to the time interval c. 1890–1850 Ma, and the rocks have their main extension in the Blankaholm-Västervik area (Figure 3-2).

In the area immediately north of Oskarshamn and westwards, metagranitoids belonging to the E-W to WNW-ESE trending so-called Oskarshamn-Jönköping belt /Mansfeld, 1996/ constitute an important lithological component. These rocks were formed c. 1830–1820 Ma ago (/Mansfeld, 1996/, Åhäll, pers. comm.) and display a varying degree of tectonometamorphic overprinting of regional character, though locally they are relatively well-preserved.

The majority of the rocks at the present day erosional level of the Earth's crust in the major part of southeastern Sweden, were formed during a period of intense magmatism c. 1810–1760 Ma ago /e.g. Wikman and Kornfält, 1995; Kornfält et al, 1997/, during the waning stages of the Svecokarelian orogeny. The dominating rocks comprise granites, syenitoids, dioritoids and gabbroids, as well as spatially and compositionally related volcanic rocks. The granites and syenitoids, as well as some of the dioritoids are by tradition collectively referred to as Småland “granites” (Figure 3-2). Both equigranular, unequigranular and porphyritic varieties occur, and the compositional variation is displayed in Figure 3-3. Note the wide compositional range for both the Småland “granites” and what earlier has been classified as Äspö “diorite”. Hence, the Småland “granites” comprise a variety of rock types regarding texture, mineralogical and chemical composition.



*Figure 3-3. Modal compositional variation of Småland “granites”. Based on Figures 3-13 and 3-14 in /Wikman and Kornfält, 1995/.*

This generation of magmatic rocks belong to the so-called Transscandinavian Igneous Belt (TIB), which has a northnorthwest extension from southeastern Sweden through Värmland and Dalarna into Norway where it finally disappears beyond the Scandinavian Caledonides. It is characterized by repeated alkalicalcic-dominated magmatism during the time period c. 1850–1650 Ma ago. Magma-mingling and mixing processes, exemplified by the occurrence of enclaves, hybridization and diffuse transitions between different lithologies etc, are typical for TIB rocks and indicate a close relationship between the different rock types. In mesoscopic scale, these processes often result in a more or less inhomogeneous rock mass regarding texture, mineralogical and chemical composition. However, if larger rock volumes are considered these may be regarded as being more or less homogeneous, despite some internal variations.

Locally, fine- to medium-grained granitic to aplitic dykes and minor massifs are frequently occurring, e.g. in the Simpevarp area. Though volumetrically subordinate, these dykes constitute essential inhomogeneities in parts of the bedrock in the Oskarshamn region, especially in the Simpevarp area. These rocks are roughly coeval with the TIB host rock /Wikman and Kornfält, 1995; Kornfält et al, 1997/, but have been intruded at a late stage in the magmatic process. Furthermore, TIB-related dolerites and composite dykes are sparsely occurring.

After the formation of the TIB-related rocks, the next rock-forming period in the Oskarshamn region, including southeastern Sweden, did not take place until c. 1450 Ma ago, and is characterized by the local emplacement of granitic magmas in a more or less cratonized crust. However, this granitic magmatism is presumably a far-field effect of ongoing orogenic processes elsewhere, presumably farther to the southwest of present Scandinavia. In the Oskarshamn region, the c. 1450 Ma magmatism is exemplified by the occurrence of the Götömar, Uthammar and Jungfrun granites (Figure 3-2; /Kresten and Chyssler, 1976; Åhäll, 2001/). Except for the occurrence of TIB-related granitic dykes in the Oskarshamn region, fine- to medium-grained granitic dykes and pegmatites that are related to the c. 1450 Ma granites occur as well, e.g. in the Götömar granite. However, these dykes are inferred to only occur within the granite and in the immediate surrounding.

The youngest magmatic rocks in the region are scattered dolerite dykes that presumably are related to the regional system of N-S trending, c. 1000–900 Ma old dolerites that can be followed from Blekinge in the south to Dalarna in the north /Johansson and Johansson, 1990/. They are usually poorly outcropped, but due to their generally more or less high content of magnetite, they usually constitute linear, positive magnetic anomalies, and their occurrence and extension may, thus, be identified on the magnetic anomaly maps. Time-wise they are related to the c. 1100–900 Ma Sveconorwegian orogeny, which are responsible for the more or less strong reworking and present structural geometry in the bedrock of southwestern Sweden.

In late Precambrian and/or early Cambrian time, i.e. c. 600–550 Ma ago, arenitic sediments were deposited on a levelled bedrock surface, the so-called sub-Cambrian peneplain. The sediments were subsequently transformed to sandstones, which constitute the youngest rocks in the region (Figure 3-2). The remainder of these former extensively occurring sedimentary rocks cover the Precambrian crystalline rocks along the coast of the Baltic Sea from the area south of Oskarshamn in the north to northeastern Blekinge in the south. Furthermore, fractures filled with Cambrian sandstone are documented in e.g. the Götömar granite, east of the N-S trending fault that transects the latter /Kresten and Chyssler, 1976/ and at Enudden, c. 4 km northeast of Simpevarp /Talbot and Ramberg, 1990/.

### 3.1.3 Structural development

#### **Ductile deformation**

The bedrock of southeastern Sweden has gone through a long and complex structural development, including both ductile and brittle deformation, since the formation of the oldest c. 1890–1850 Ma supracrustal rocks. The oldest deformation is of regional, penetrative character, and is recorded in the supracrustal rocks in the Blankaholm-Västervik area. It pre-dates the intrusion of the c. 1850 Ma generation of TIB rocks which, however, are deformed themselves. At variance from the more or less penetrative pre-1850 Ma deformation in the supracrustal rocks, the deformation that has affected the 1850 Ma generation of TIB rocks, as well as the older supracrustal rocks, is heterogeneous in character. It is caused by dextral transpression in response to c. N-S to NNW-SSE regional compression, is constrained to the time-interval c. 1850–1800 Ma, and is exemplified by the dextral, strike-slip dominated Loftahammar-Linköping deformation zone (Figure 3-1; /Stephens and Wahlgren, 1996; Beunk and Page, 2001/). However, also the folding of the foliation in the pre-1850 Ma rocks is supposedly developed in response to the same stress field /Stephens and Wahlgren, 1996; Beunk and Page, 2001/.

The 1810–1760 Ma generation of TIB rocks, that dominates the bedrock in the Oskarshamn region, is post-tectonic in relation to the regional, penetrative deformation that is related to the peak of the Sveco Karelian orogeny. However, they are affected by a system of ductile deformation zones of the same character as the Loftahammar-Linköping deformation zone, though developed during more low-grade conditions, i.e. at shallower levels in the crust, than the initial phase of shearing in the Loftahammar-Linköping deformation zone. However, the latter zone displays ductile reactivation during low-grade conditions, which presumably is contemporaneous with the shearing in the 1810–1760 Ma TIB rocks. In the Oskarshamn region, these deformation zones are exemplified by the E-W trending Oskarshamn-Bockara and NE-SW trending Oskarshamn-Fliseryd deformation zones /Bergman et al, 1998/. Presumably, also the ductile, NE-SW trending so-called Äspö shear zone /Gustafsson et al, 1989; Bergman et al, 2000/, which is characterized by a sinistral strike-slip component, belongs to this system of ductile deformation zones.

Independent of the syn-deformational metamorphic grade, the dextral and sinistral strike-slip component in the WNW-ESE to NW-SE and NE-SW trending ductile deformation zones, respectively, indicate that a regional, c. N-S to NNW-SSE compression prevailed during their formation and subsequent ductile reactivation. Consequently, this regional stress field is inferred to have prevailed for a considerable period of time, at least from the time of the intrusion of the 1850 Ma TIB generation, or possibly earlier, until c. 1750 Ma ago. Most of the lithological contacts in the region, and also in the whole of southeastern Sweden, are more or less concordant to the orientation of the ductile deformation zones, which indicate that the emplacement of the TIB magmas was facilitated by ongoing shear zone activity. Together with the subsequent deformation of the TIB rocks, this testifies for an important influence of the deformation zones for the present structural and lithological framework in the bedrock of southeastern Sweden.

Apart from the mylonitic foliation in the ductile deformation zones, the 1810–1760 Ma TIB rocks locally display a more or less well-developed foliation /Kornfält and Wikman, 1987a/, e.g. preferred orientation of feldspar phenocrysts, mafic enclaves, biotite etc. However, it is often difficult to decide whether the foliation is syn-intrusive or caused by a subsequent tectonic overprinting. Independent of origin, the orientation of the foliation suggests that there is a genetic relationship between foliation development outside the ductile deformation zones and the shear zone activity.

### **Brittle deformation**

Since no ductile deformation has been observed in the c. 1450 Ma granites /e.g. Talbot and Ramberg, 1990; Munier, 1995/ or younger rocks, it is evident that only deformations during brittle conditions have affected the bedrock in the Oskarshamn region during at least the last c. 1450 Ma. However, the transition from ductile to brittle deformation presumably took place during the time interval c.1750–1700 Ma, i.e. during uplift and stabilization of the crust after the Sveconorwegian orogeny.

To unravel the brittle tectonic history in the bedrock in southeastern Sweden during the last c. 1450 Ma is difficult. It is plausible that tectonic activities that are related to more or less remote large-scale processes, such as e.g. the Gothian, Hallandian, Sveconorwegian and Caledonian orogenies, the opening of the Iapetus Ocean, the Late Palaeozoic Variscan and the Late Mesozoic to Early Cenozoic Alpine orogenies, as well as the opening of the present Atlantic Ocean, have had a far-field effect within the shield area. However, to which degree these large-scale processes have affected the bedrock in the Oskarshamn region and the rest of southeastern Sweden, and especially which brittle structure belongs to which process is difficult to decipher. The main reason for this uncertainty is the great lack of time markers for relative dating, except for the sub-Cambrian peneplain and the Cambro-Ordovician cover rocks, and the difficulties to date brittle structures radiometrically. In the absence of post-Cambrian markers it is difficult to determine which fracture zones or faults that were formed or reactivated during the last 495 million years.

The first brittle faults in the region probably developed in connection with the emplacement of younger granites. During the subsequent geological evolution, faults and older ductile deformation zones have been reactivated repeatedly, due to the increasingly brittle behaviour of the bedrock. Brittle reactivation of ductile deformation zones is a general phenomenon, and is also the case in the Oskarshamn region. Both the Oskarshamn-Bockara, Oskarshamn-Fliseryd and Äspö shear zones display clear evidence of being reactivated in the brittle régime (see also e.g. /Munier, 1995/). An inversion of the strike-slip component in the Äspö shear zone from sinistral during the older ductile deformation, to dextral during the younger brittle reactivation has been proposed by /Talbot and Munier, 1989/ and /Munier, 1989/.

K-Ar dating of biotites from the Småland “granites” /Åberg, 1978/ has yielded ages of c. 1500–1400 Ma. According to /Åberg,1978/, the obtained ages are caused by the c. 1500–1400 Ma magmatic activity in southern Sweden. However, /Tullborg et al, 1996/ considered the closure of the K-Ar system in this time interval to be the result of an uplift scenario. Independent of the explanation, there is no information about any explicit tectonic features that can be related to this time period.

The occurrence of c. 1000–900 Ma dolerites in southeastern Sweden testifies for a Sveconorwegian tectonic influence, since the intrusion of the parent magmas have been tectonically controlled. However, whether individual faults or fracture zones, which were not injected by mafic magma, were formed or reactivated during the Sveconorwegian orogeny, and if so which of them, is uncertain.

On the basis of titanite and zircon fission track studies in the Oskarshamn region, it has been suggested that sediments which were derived from the uplifted Sveconorwegian orogenic belt and deposited in a Sveconorwegian foreland basin, reached a thickness of c. 8 km in southeastern Sweden at around 850 Ma /Tullborg et al, 1996; Larson et al, 1999/. Subsequent exhumation of southeastern Sweden and erosion of the sedimentary pile were completed by the establishment of the sub-Cambrian peneplain at the end of the Neoproterozoic. Furthermore, apatite fission track ages in the Oskarshamn region indicate that Upper Silurian to Devonian sediments, which were derived from the uplift

of the Caledonian orogenic belt and deposited in a Caledonian foreland basin, covered most of Sweden and reached a thickness exceeding 2.5 km /Tullborg et al, 1995, 1996; Larson et al 1999/. Exhumation and subsequent erosion during the Early Mesozoic reduced the sedimentary cover almost completely /Tullborg et al, 1995, 1996; Larson et al, 1999/. During the Cretaceous, a new transgression initiated which resulted in a thin cover of marine sediments. In the Oskarshamn region the sedimentary cover was not completely removed until the Tertiary /Lidmar-Bergström, 1991/.

The above-mentioned repeated large-scale events of subsidence, deposition of sediments, and subsequent exhumation and erosion, reasonably must have been accompanied by tectonic activity, i.e. movements along faults. However, there is no information that help to decipher which fracture zones (faults) that possibly formed or were reactivated during these periods.

According to /Milnes and Gee, 1992/ and /Munier, 1995/, the Ordovician cover rocks along the northwestern coast of Öland are tectonically undisturbed, except for displacements in cm-scale. This suggests that the E-W trending fracture zones/faults in the Oskarshamn-Bockara deformation zone, which can be seen in the magnetic anomaly maps to continue eastwards under Öland, do not affect the Cambro-Ordovician cover sequences on Öland. Thus, this indicate that these brittle deformation zones of regional character were not active in post-Cambrian time, but are related to the Precambrian tectonic evolution. However, post-Cambrian fracture zones/faults do occur in the Oskarshamn region. On the northwestern part of Furö (see Figure 3-2), a small island c. 10 km east of Oskarshamn, a fault contact between a brecciated Cambrian sandstone and a brecciated red granite is recorded /Bergman et al, 1998/. Furthermore, the occurrence of joints filled with Cambrian sandstone east of, but not west of, the N-S trending fault in the western part of the Götemar granite, indicates that the eastern block has been down-faulted in relation to the western block in post-Cambrian time /Kresten and Chyssler, 1976; Bergman et al, 1998/.

As mentioned above the sub-Cambrian peneplain is a potential marker to demonstrate post-Cambrian brittle tectonics. In general, all pronounced depressions and distinct differences of topographic level in the Sub-Cambrian peneplain constitute potential fracture zones or faults. /Tirén et al, 1987/ studied the relative movements of regional blocks in southeastern Sweden, which were bounded by fracture zones and ranging in size between 25 km<sup>2</sup> and 100 km<sup>2</sup>. Differential movements were interpreted to have occurred along existing faults both during periods of uplift and subsidence.

A general problem is to decipher the relation between the formation and subsequent reactivation of faults and fracture zones. Especially the mutual age relationship between fracture zones with different orientation is difficult to determine, mainly due to the complex relationship between age of formation and age of (latest?) reactivation. Another, and perhaps the most important and complicating factor is that brittle deformation zones are very poorly exposed, since they mostly constitute topographical depressions filled with glacial cover, rivers, swamps etc.

The brittle deformation history of a region can be regarded as the combined effect of generation of new fractures or faults and reactivation of old fractures or faults. The ratio between generation of new structures and reactivation of older structures is presumed to decrease with time, since the orientation spectra of pre-existing structures increased with every new event of brittle deformation /Munier, 1995/. Relative age determinations of fractures, based on orientation and a succession of mineral filling with decreasing age, have been recorded on Äspö /e.g. Munier, 1995/, and it is reasonable to assume that these findings can be extrapolated to the surrounding parts of the Oskarshamn region. The oldest fractures are epidote- and quartz-bearing, and with decreasing age chlorite,



zeolite and calcite appear as fracture filling. Since the mineralogy in individual fractures within fracture zones is essentially similar to fractures in the intervening blocks /Munier, 1995/, the fracture filling is a tool for relative age determination of movements (reactivations) of the former. Consequently, the calcite-bearing fracture zones/faults represent the youngest reactivation, but the absolute age is uncertain.

Based on interpretation of data from Äspö, the orientation of the maximum compressive stress during the formation of the epidote- and quartz-bearing fracture zones was N-S/subhorizontal /Munier, 1989/, and had changed orientation to NE-SW when the chlorite-filled fracture zones/faults formed /Talbot and Munier, 1989/. The maximum horizontal compression was still NE-SW when the fractures formed which is filled with Cambrian sandstone /Talbot and Munier, 1989/. The orientation of the maximum horizontal compressive stress during the subsequent tectonic evolution is presumed to be NW-SE, i.e. the same as the present stress régime. Consequently, a roughly NW-SE maximum compressive stress is inferred to have prevailed for a considerable period of time, i.e. possibly for hundreds of million of years.

Attempts have been made to use palaeomagnetic, electron spin resonance (ESR) and isotopic dating (K-Ar, Rb-Sr) techniques of some brittle structures at the Äspö site /Maddock et al, 1993/, in order to constrain the minimum age of the most recent movements. Characterization of the sampled fault gouge material demonstrated that many fracture zones contain sequentially developed fault rocks and verifies that reactivation has occurred.

The ages given by the various dating methods reflect both inherent differences in the techniques and differences in the phase or phenomenon being dated. The interpretation of the ESR dating which was limited by the resolution of the method, yielded minimum ages of movements in the order of several hundred thousand to one million years. The results of the palaeomagnetic and K-Ar analyses strongly suggest that growth of the fracture infilling minerals took place at least 250 million years ago. The most recent fault movements are interpreted to have preceded this mineral growth. /Maddock et al, 1993/ conclude that any Quaternary and Holocene activity had little effect on the fracture zones they examined.

According to /Mörner, 1989/, a great number of supposed post-glacial faults occur on Äspö. However, none of the faults reported showed any positive evidence of kinematics /SKB, 1990/. Some of the reported faults did not display any disturbance of Precambrian markers, others had their bases exposed by excavation and ice plucking could be positively demonstrated. Talbot and /Munier, 1989/ discuss post-glacial faults in connection with studied fault scarps, i.e. abrupt steps in the glacially polished bedrock surface on Äspö. According to /Munier, 1995/, post-glacial reactivation of individual fractures has most likely occurred, but despite searches no evidence of such features has been found on outcrops.

Ongoing tectonic activity is manifested in seismic events and aseismic slip /Larson and Tullborg, 1993/. According to /Slunga et al, 1984/, the so-called Protogine Zone of southern Sweden (Figure 3-1) has been shown to be the border between a more seismic western Sweden and the more aseismic southeastern Sweden. Even though southeastern Sweden is a seismically very quiet area, an earthquake of magnitude 1.0 and focal depth of c. 16 kilometres was recorded c. 30 kilometres south of Oskarshamn in September 1988 /Slunga and Nordgren, 1990/. The orientation of the maximum horizontal principle stress relaxed by this earthquake, as well as other seismic events in Sweden, was c. NW-SE /Slunga et al, 1984; Slunga and Nordgren, 1990/. This is in agreement with the results from rock stress measurements at depths more than 300 metres /Stephansson et al, 1987/, and also with the stress field generated by the plate movements in the North

Atlantic Ocean /cf. Slunga, 1989; Gregersen et al, 1991; Gregersen, 1992/. According to /Slunga and Nordgren, 1990/, recent seismic activity in southeastern Sweden is related to plate-tectonic forces and not directly to land upheaval as a function of the last glaciation. /Gregersen et al, 1991/ and /Gregersen, 1992/ made the same conclusion based on focal mechanisms for present-day earthquakes in Fennoscandia. However, /Muir-Wood, 1993/ claimed that the recent seismicity appears to be a function of the post-glacial rebound.

**Table 3-1. Tentative synopsis of the geological evolution in south eastern Sweden with focus on the Oskarshamn region.**

Age (Ma)	Geological event
0.115–0	Glaciation; syn- to post-glacial fault movements?; NW-SE to WNW-ESE maximum horizontal principal stress.
95–0	Alpine orogeny (central Europe); opening and spreading of the Atlantic Ocean; <i>brittle deformation in the cratonic Oskarshamn region as a far-field effect?</i>
> 250	<i>Latest fault movements at Äspö? (K-Ar dating of gouge material)</i>
295–60	Tectonic activity in the Tornquist Zone (Fennoscandian border zone); <i>brittle deformation in the cratonic Oskarshamn region as a far-field effect?</i>
360–295	Hercynian-Variscan orogeny (central Europe). <i>Brittle deformation in the cratonic Oskarshamn region as a far-field effect?</i>
420–220	Subsidence related to the development of a Caledonian foreland basin, sedimentation followed by exhumation and erosion; <i>brittle deformation in the cratonic Oskarshamn region?</i>
510–400	Caledonian orogeny; closure of the Iapetus Ocean; formation of the Scandinavian Caledonides; WNW-ESE shortening (regional compression?) followed by extensional collapse; <i>brittle deformation in the cratonic Oskarshamn region as a far-field effect of orogenic deformation in western Baltica?</i>
550	Extensive sedimentation.
600	Opening of the Iapetus Ocean; <i>far-field effect in the cratonic Oskarshamn region?</i>
700–600	Peneplanation; Sub-Cambrian peneplain.
900–700	Subsidence related to the development of a Sveconorwegian foreland basin, sedimentation followed by exhumation and erosion; Rifting, graben formation, sedimentation in the Vättern area; Visingsö group; <i>brittle deformation in the cratonic Oskarshamn region?</i>
1100–900	Sveconorwegian orogeny; formation of the Sveconorwegian Frontal Deformation Zone ("Protogine Zone"); WNW-ESE to E-W regional compression; intrusion of dolerites – E-W extension; <i>Brittle deformation in the cratonic Oskarshamn region as a far-field effect of orogenic reworking of the crust in southwestern Sweden?</i>
1460–1420	Hallandian orogeny; <i>Brittle deformation in the cratonic Oskarshamn region as a far-field effect?</i>
1450	Intrusion of granite (e.g. Götemar and Uthammar granites).
1610–1560	Gothian orogeny; <i>Brittle deformation in the cratonic Oskarshamn region as a far-field effect?</i>
1750–1700	Transition from ductile to brittle tectonic régime.
1800–1750	Formation of transpressive, ductile deformation zones in response to c. N-S to NNW-SSE regional compression under low-grade conditions. Deformation zones with NW-SE to WNW-ESE and NE-SW direction display dextral and sinistral horizontal component, respectively.
1800	Intrusion of granite-syenitoid-dioritoid-gabbroid ("Småland granite"), composite dykes.
1830–1800	Regional, inhomogeneous deformation under (low)- to medium-grade conditions.
1830–1820	Intrusion of granitoids; volcanic activity?
1850(–1800)	Formation of transpressive, ductile deformation zones with a dextral horizontal component of movement, in response to c. N-S to NNW-SSE regional compression under medium-grade metamorphic conditions; folding of foliation in pre-1850 Ma rocks.
1850	Intrusion of granite-syenitoid-dioritoid-gabbroid.
1890–1850	Volcanic activity and sedimentation; regional deformation under medium- to high-grade conditions.
1960–1750	Svecokarelian orogeny.

### 3.1.4 Development during the Quaternary period

The Earth's youngest period, the Quaternary, that comprise the last 1635 Ma, is characterized by alternating glacial and interglacial stages. The landscape is largely influenced by the latest glaciation and its recession. Subsequently, the landscape has been reformed to a certain extent by isostatic uplift and wave-washing of the shores at that time.

The latest glaciation, the Weichselian, started c. 115 000 years ago. It is characterized by colder phases, stadials, interrupted by milder interstadials. The inland ice reached its maximum extension c. 20 000 years ago. According to mathematical and glaciological models, the maximum thickness of the ice cover in the Oskarshamn region was 2–2,5 km /Strömberg, 1989; Holmlund, 1993/. During the interstadials, the ice margin retreated to northernmost Sweden. Shorter periods of warmer climate have occurred in the Oskarshamn region.

Glacial striae on bedrock outcrops as well as the orientation of the eskers indicate main ice movement direction from NW–NNW in the region. Subordinate older striae indicate more westerly and northerly directions.

A marked improvement in climate took place about 18 000 years ago and the ice started to melt, a process that was completed after about 10 000 years. According to clay-varve chronology the Oskarshamn area was deglaciated c. 12 300 years ago. The retreat of the ice margin was c. 125–300 m/year /Kristiansson, 1986/.

The heavy inland ice pressed down the Earth's crust at least 800 m below its present position. As soon as the pressure started to decrease due to the deglaciation, the crust started to rise (land uplift). The highest situated traces of the shoreline, the highest shoreline, are at different altitudes throughout Sweden depending on i.a. how deep the crust had been depressed. The highest shoreline in the Oskarshamn region is c. 100 m above sea level, and, thus, the main part of the Oskarshamn local community is situated below the highest shoreline.

All the Quaternary deposits in the Oskarshamn region were formed during and after the latest glaciation. Deposits related to earlier glaciations or interglaciations are not known. The division of Quaternary deposits according to genesis and the environment in which they were formed consists of two main groups: glacial and post-glacial.

Glacial deposits were formed by the ice sheet or its melt-water. This group includes till, glaciofluvial gravel and sand. The glaciofluvial deposits are mainly deposited in eskers and deltas. The finest particles of glaciofluvial origin, i.e. clay, were dispersed in the sea and in large lakes. These particles formed glacial clays with varying properties.

Post-glacial deposits were formed independently of the melting of the ice sheet. Land uplift exposed older deposits to the influence of wave-washing and there was a more or less complete restratification. This group includes wave-washed sediments as shingle, gravel and sand. The restratification products with the finest particles, i.e. silt and clay particles, were deposited farthest away from the shore. Organic deposits are dominated by fen peat, but bog peat also occurs.

A major crustal phenomenon is the interplay between land uplift (isostasy) and sea level changes (eustasy) following the deglaciation. In the Oskarshamn region, shoreline regression prevails and the recent rate of land uplift is c. 1 mm/year /Ekman, 1996/.

Regarding syn- to post-glacial tectonic activity and recent seismicity, see Section 3.1.3 about "Brittle deformation".

## 3.2 Lineament identification

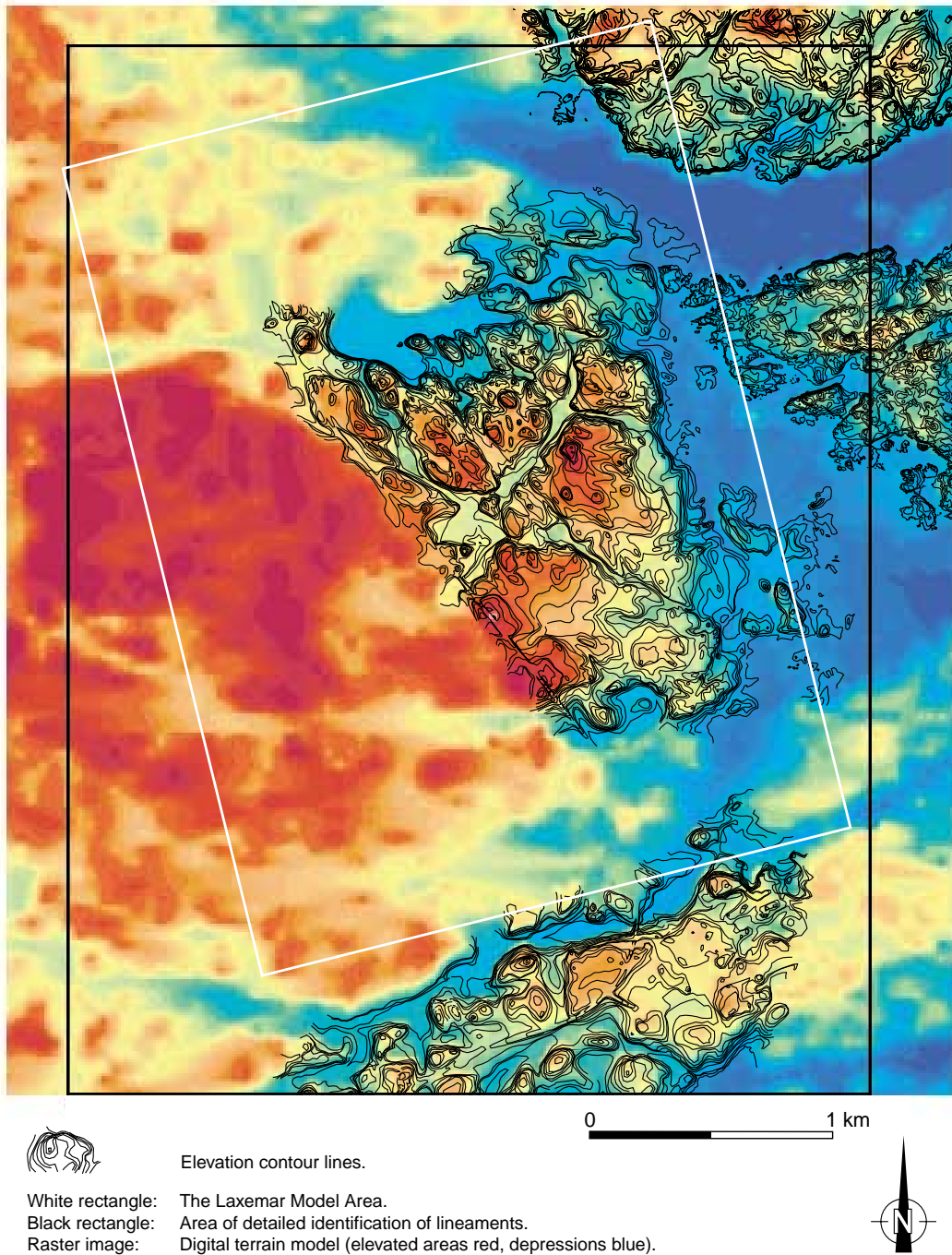
The compilation of identified lineaments in the Oskarshamn feasibility study /Bergman et al, 1998, 1999, 2000/ was used as a basis in this study. This identification was primarily based on topographic (50 metres grid) and airborne magnetic data, but as a complement, gravity and electromagnetic information was evaluated as well. In the sea area, the identified lineaments were mainly based on magnetic data, with the support of bathymetric information. Neither the lineaments from the feasibility study, nor those identified in this study, have been strictly characterized according to the methodology description for lineament identification /SKB, in prep./ concerning width, length, which data set each part of the lineament is based on etc. Still, as regards length the lineaments identified in this study have been characterized according to /Strähle, 2001/.

### 3.2.1 Detailed terrain model and resulting lineaments

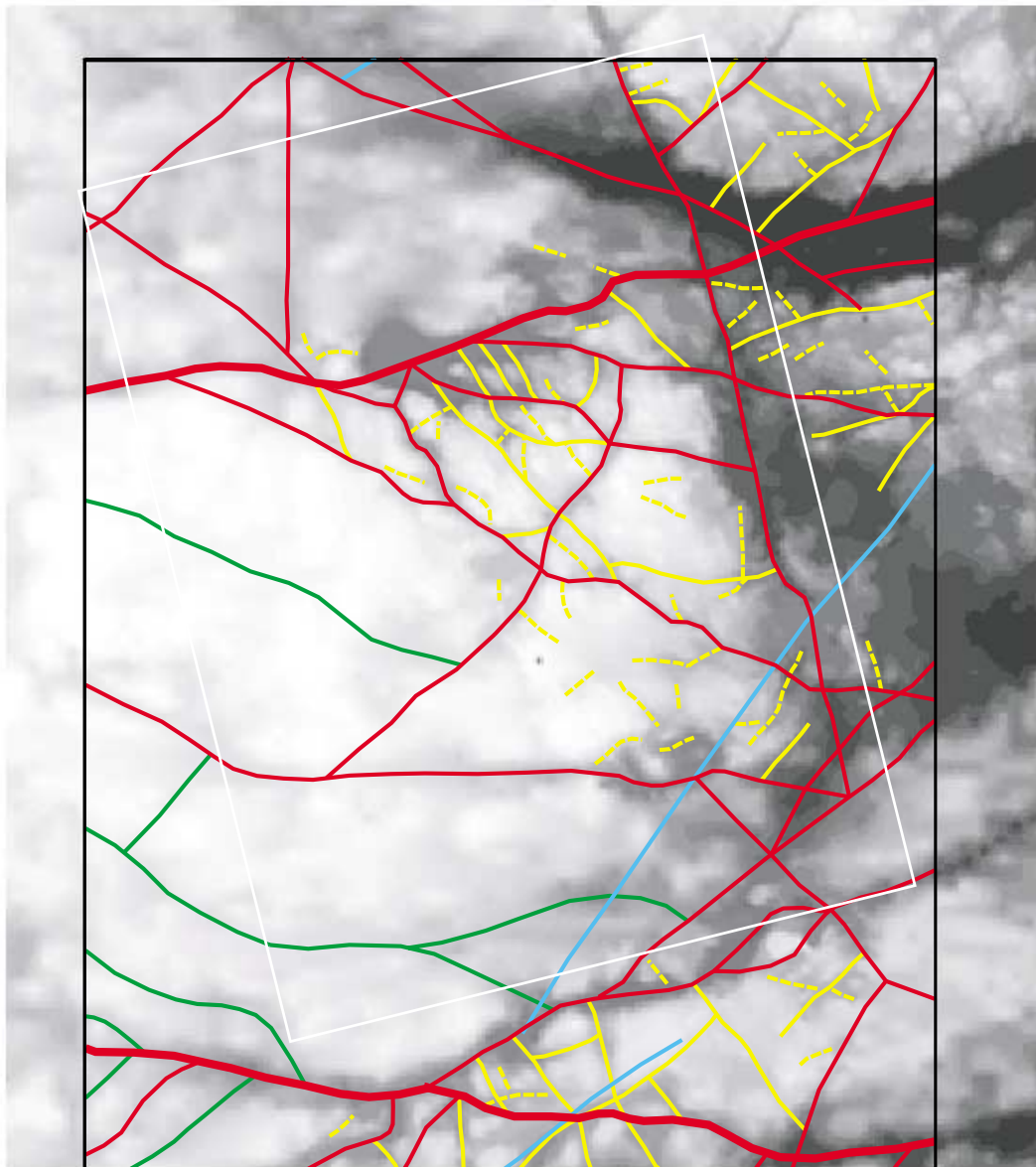
Because of the scale of presentation in the Oskarshamn feasibility study, only lineaments that could be traced for more than 2–5 kilometres were included in the compilation. Due to the need for more detailed information in the Laxemar Site Descriptive Model, the lineament compilation from the feasibility study has been complemented with new lineaments by use of a more detailed terrain model (Figure 3-4) and with the support of orthophotos. This terrain model was supplied by SKB and is based on contour lines with 1 metre equi-distance. However, it only covers parts of the Model Area and, accordingly, the complementary lineaments that have been identified are restricted to these parts. Nevertheless, also outside the area that is covered by the detailed terrain model, a more detailed evaluation of the topographical data in 50 metres grid revealed a few complementary lineaments with a length of c. 1–2 kilometres. Lineaments that were identified in the feasibility study have not been changed or omitted, but partly adjusted regarding the position according to the use of the more detailed terrain model.

The resulting lineament compilation of the Laxemar Model Area is displayed in Figure 3-5. In the compilation of the identified lineaments in the Laxemar Model Area, the following characterization of the lineaments has been applied:


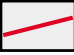
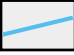



- Regional lineament, interpreted as a fault or fracture zone in the feasibility study. Length > 5 km. Position adjusted according to the detailed terrain model.
- Local major lineament, interpreted as a fault or fracture zone in the feasibility study. Length 1–5 km. Position adjusted according to the detailed terrain model.
- Local major lineament indicated in connection with the feasibility study. Based solely on magnetic data.
- Local major lineament of uncertain character, identified in this study. Length 1–2 km. Based on the Land Survey's topographic data in 50 m grid, with support of orthophotos.
- Local lineament, connected. Identified in this study. Length < 1 km. Based on the detailed terrain model with support of orthophotos.
- Local lineament, fragmented. Identified in this study. Length < 1 km. Based on the detailed terrain model with support of orthophotos.



**Figure 3-4.** Digital terrain model of the Laxemar Model Area and the immediate surroundings. In the area which is covered by the detailed contour lines (c. 1 m interval), the terrain model is based on 10 m grid; in the remaining part of the area on 50 m grid.



0 1 km

-  Regional lineament, interpreted as a fault or fracture zone in the feasibility study. Length > 5 km. Position adjusted according to the detailed terrain model.
-  Local major lineament, interpreted as a fault or fracture zone in the feasibility study. Length 1-5 km. Position adjusted according to the detailed terrain model.
-  Local major lineament identified in connection with the feasibility study. Based solely on magnetic data.
-  Local major lineament of uncertain character, identified in this study. Length 1-2 km. Based on the Land Survey's topographic data in 50 m grid with support of orthophotos.
-  Local lineament, connected. Identified in this study. Length < 1 km. Based on the detailed terrain model with support of orthophotos.
-  Local lineament, fragmented. Identified in this study. Length < 1 km. Based on the detailed terrain model with support of orthophotos.



- White rectangle: The Laxemar Model Area.
- Black rectangle: Area of detailed identification of lineaments.
- Raster image: Digital terrain model (elevated areas light grey, depressions dark grey).

*Figure 3-5. Lineament map of the Laxemar Model Area and the immediate surroundings.*

### 3.2.2 Assessment of uncertainty in the digital terrain model

The constructed 10 metres grid for the detailed terrain model used in the lineament identification in this study must be considered as preliminary, since no control of the quality of the input data has been performed. A quick look at the detailed terrain models of the Bussvik, Laxemar, Glostad and Äspö areas reveals many uncertainties, e.g.

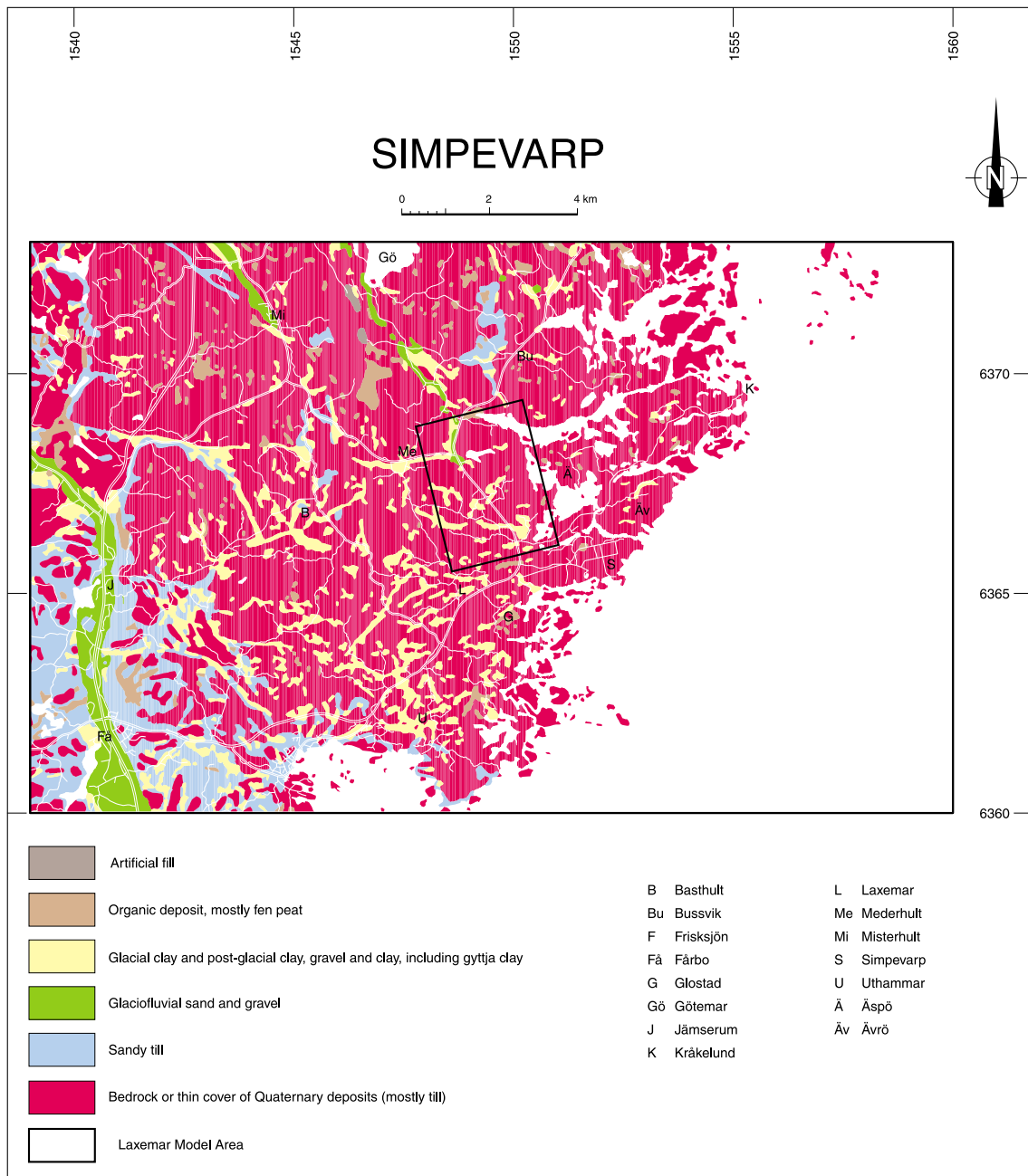
- The origin of the different terrain models is unclear and the many transformations between different coordinate systems might have added an error regarding the position. A comparison with the Land Survey's orthophoto, locally reveals a deviation in position of c. 5–20 metres.
- The contour lines have presumably been automatically drawn by the use of a computer program, and the lines are relatively crude in character (not on Äspö). More well-defined input data should have been available in the production of the contour lines.
- Apart from Äspö, the altitude along the iso-elevation contour lines displays a slight variation of c. 1 to 10 centimetres. However, deviations of one to several metres have been noted. Individual deviations of up to 0.5 metre have been noted in one and the same vector, from one node to the next. A consequence of this is that a large uncertainty exists, until the production of the detailed terrain models can be derived in detail.

### 3.3 Surface geology

The description of the surface geology, i.e. deposits and upper bedrock geology, is mainly based on the compilation of geological information that was performed during the Oskarshamn feasibility study /Bergman et al, 1998, 1999/. Certain results from the field control of the bedrock in connection with the latter have also been utilized /Bergman et al, 2000/. The distribution and characterization of the Quaternary deposits is only based on interpretation of aerial photographs, and they were not included in the field control work in connection with the feasibility study. Hence, the available surface geological information is of reconnaissance character, even though detailed bedrock geological mapping has been performed in parts of the Laxemar Model Area /Kornfält and Wikman, 1987b/. However, detailed information regarding existing rock types in the two cored boreholes KLX01 and 02 has been utilized /Stanfors, 1988, 1995; Wikman and Kornfält, 1995; Ekman, 2001/. A detailed field mapping and characterisation of the Quaternary deposits and the bedrock is needed in the initial stages of the site investigation programme.

#### 3.3.1 Quaternary deposits – distribution and description

Quaternary deposits, including glaciofluvial deposits, glacial clay, post-glacial sediments and organic deposits, are subordinate and occupy only c. 18% of the Laxemar Model Area, while exposed bedrock or bedrock with only a thin ( $\leq 0.5$  m) Quaternary cover make up the remaining c. 82% (Figure 3-6). In the percentage distribution of different Quaternary deposits, only deposits with an estimated thickness of more than c. 0.5 m are considered. Consequently, all numbers should be considered as minimum estimates. In particular, this is relevant for the percentage distribution of till that is not accounted for in the estimates, but which to a major extent constitutes the thin Quaternary cover. By consequence the true amount of exposed bedrock are presumed to be considerably less than 82%. However, the thickness of the Quaternary deposits in general is very limited, mostly only a few metres.



**Figure 3-6.** Quaternary deposit map of the Simpevarp regional model area. Laxemar Model Area is marked with a rectangle.

The only glaciofluvial deposit in the Model Area is the southern part of the esker that can be discontinuously followed from the area immediately west of the lake Frisksjön in a northerly to northwesterly direction to the southwestern shore of the lake Götemar (Figure 3-6). The esker occupies c. 2% of the area, which corresponds to 11% of the Quaternary deposits.

The predominating Quaternary deposits in the Model Area are glacial and post-glacial sediments, which occupy c. 15% of the Model Area, i.e. 83% of the Quaternary deposits. Due to the lack of detailed information, these are not distinguished in the Quaternary deposit map (Figure 3-6). The fine-grained glacial sediments are dominated by varved clay, while the post-glacial sediments are composed of coarse wave-washed sediments, dominated by gravel and sand, and fine-grained sediments dominated by clay



and gyttja clay. The wave-washed sediments can be found in connection with the esker, while the clay and gyttja clay mainly occur in topographical depressions and valleys. The thickness of the glacial and post-glacial sediments varies, but is commonly less than 3–4 m.

Post-glacial organic deposits are dominated by peat and occur in three places within the Model Area (Figure 3-6). Apart from two minor occurrences in the east-central part of the area, the peat is concentrated to an occurrence in the northernmost part of the area. Altogether, the peat occurrences occupy c. 1% of the Model Area, that correspond to c. 6% of the Quaternary deposits. Fen peat dominates, but bog peat also occurs. However, these two varieties have not been distinguished due to lack of information. The fen peat is usually 2–3 m thick, while the thickness of the bog peat varies between 0.5 and 2 m. The total thickness of peat where bog peat is underlain by fen peat is considered to be at the most 4–5 m /Bergman et al, 1998/.

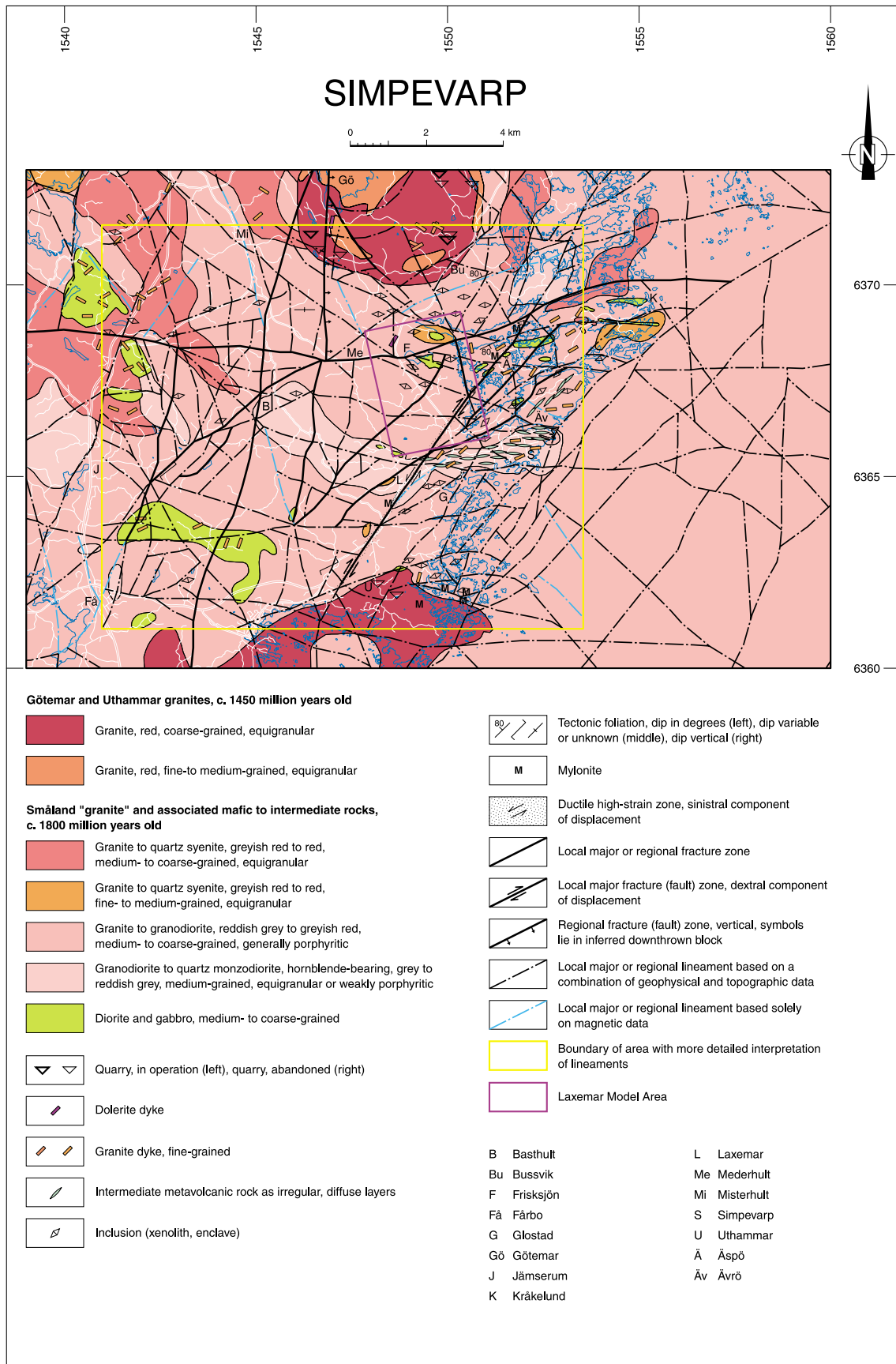
No indications of post-glacial, seismically related disturbances of the Quaternary deposits have been documented within the Model Area. However, fault scarps and boulder accumulations have been suggested to be of seismotectonic origin /Mörner, 1989/.

### **3.3.2 Rock types – distribution, description and age**

The bedrock in the Laxemar Model Area is predominated by a reddish grey to greyish red, medium- to coarse-grained, porphyritic granite to granodiorite which occupies c. 93% of the area. It belongs to the c. 1810–1760 Ma generation of granites, syenitoids, dioritoids and gabbroids (see Section 3.1.2). The feldspar phenocrysts are c. 1–3 cm large and usually relatively sparsely distributed, and locally, more or less even-grained varieties occur. Consequently, this granite to granodiorite is, from a textural point of view, relatively inhomogeneous. It is commonly more or less isotropic, but locally a foliation is developed. Occasionally it is difficult to decide whether the foliation is syn-intrusive or caused by a subsequent tectonic overprinting.

As can be seen in Figure 3-7, three bodies of diorite to gabbro occur, one in the southwesternmost and two in the northeastern part of the Model Area. Altogether they occupy c. 2.5% of the area. The diorite to gabbro together with unspecified mafic rocks, have traditionally been called “greenstone”. The northeasternmost diorite to gabbro is enveloped by a fine- to finely medium-grained, greyish red to red granite, while the diorite to gabbro in the southwesternmost corner of the area is surrounded by a reddish grey, medium-grained, granodiorite to quartz monzodiorite. The latter rock type only occupies 0.5% of the Model Area. However, it extends from the Simpevarp peninsula in the east to Basthult in the west (Figure 3-7), south of the Model Area, and only touches the southwesternmost corner of the latter.

During the field control in connection with the Oskarshamn feasibility study /Bergman et al, 2000/, the diorite to gabbro east of Lake Frisksjön was found to be intimately mixed with the surrounding granite to granodiorite. This is also evident from the detailed mapping carried out in this area by /Kornfält and Wikman, 1987b/. In general, the diorites to gabbros are relatively inhomogeneous in character, and commonly display a netveining of fine-grained granite to aplite, as well as a more or less strong mixing with the surrounding, synchronously formed, more felsic intrusive rocks. This indicate that the mafic plutonics belong to the same magmatic generation as the granite to granodiorite. Furthermore, xenoliths to enclaves and minor bodies of diorite to gabbro, as well as unspecified mafic rocks, are more or less commonly occurring in the predominating granite to granodiorite. The complex and intimate mixture of mafic rocks and the granite to granodiorite is also evident in the WellCAD plots from the boreholes KLX01 and KLX02 /Ekman, 2001/, see Section 3.4.



*Figure 3-7. Bedrock map of the Simpevarp regional model area. The Laxemar Model Area is marked with a rectangle.*

An important and frequently occurring rock type in the Laxemar Model Area, though volumetrically subordinate, is a greyish red to red, fine- to medium-grained granite, which primarily appears as more or less narrow dykes, but also as minor massifs (see e.g. Figure 10 in /Bergman et al, 2000/). This granite has yielded an age of c. 1800 Ma /Wikman and Kornfält, 1995; Kornfält et al, 1997/, which indicates that it belongs to the same magmatic suite as the granite to granodiorite and diorite to gabbro. The granite dykes usually display a width of a decimetre to a metre, and gradual transitions to pegmatitic and aplitic varieties occur. An example of a somewhat larger massif of a greyish red to red fine- to medium-grained granite envelopes the diorite to gabbro in the northeastern part of the Model Area. This granite occupies c. 4% of the area, and is presumably genetically related to the granite dykes. The latter constitute an important lithological inhomogeneity, and are commonly more strongly fractured than their country rock /e.g. Axelsson et al, 1990; Stanfors and Larsson, 1998; Bergman et al, 2000/. Hydraulic tests in boreholes have shown that sections dominated by fine-grained granite is generally more permeable compared to sections without fine-grained granite /Follin et al, 2000; Rhén and Forsmark, 2000/. Due to the lack of detailed bedrock information, the percentage of granite dykes in the area is difficult to estimate. They are considered to be more or less evenly distributed within the area, even though local variations in quantity may occur. Furthermore, one dolerite dyke exists in the area, ca 400 metres north-west of Lake Frisksjön.

For a more detailed description of the compositional variation and mineralogical and chemical characteristics of the different rock types in the Laxemar-Simpevarp area, the reader is referred to /Wikman and Kornfält, 1995/.

### **3.4 Geologic interpretation of borehole data**

The geological data observations cover many different aspects such as observations of lithology, fracturing, alteration, mineralisations, tectonic indications and hydraulic indications from flow etc. The tools for observing these characteristics are both by direct visual inspection, but also by indirect tools such as various types of geophysical logging tools, packer tests, down hole cameras, radar and seismics. The different observations show many different characteristics of the rock mass and can be used for different purposes. When constructing a geological model of the rock mass to be used for purposes such as design of tunnels, hydraulic modelling and safety performance studies it is useful to simplify the geological information into a few classes that describe certain characteristics of the rock. This simplification can be done in a single borehole interpretation methodology as described in this section.

#### **3.4.1 Aims of the single hole interpretation**

The aim of a geological single hole interpretation, within the framework of the Laxemar project, is to identify rock segments (*sections*) along the borehole having similar geological characteristics. These rock segments are then to be used in the 3D geometric modelling of rock domains<sup>1</sup> and deformation zones<sup>1</sup>. The geological sectioning of the borehole information can be viewed as a way to simplify and reduce the complex geological information to a few alternative interpretations that can be used in the 3D geometrical modelling.

---

<sup>1</sup> Rock and soil domains together with deformation zones are the main building blocks of the geological model as defined by /Munier and Hermanson, 2001/ and form a space filling geometry inside the model domain.

The simplification of the geology into rock segments with similar characteristics should be done avoiding subjectivity if possible. It is also vital that the steps leading to the interpretation of rock segments and deformation zones can be traced back to the original data. However, the complex nature of the different geological and geophysical (and other) indications, require consultation with expertise in the fields of interest. The aim is to present an analysis of geological and geophysical data mapped along the length of the borehole in an orderly way such that the results can be traced back to the original data, giving as little room as possible for “unknown” steps in the analysis.

To simplify geological and geophysical observations in a borehole into a manageable number it is useful to combine parameters in the core log for easier interpretation of the components inside the geological model. It is of course not possible to answer all questions by simplifying all the available information, but it is necessary to provide simple building blocks of each borehole to aid the development of a geological model. It is important to understand that in later uses of the geometrical model it will be necessary in many cases to go back to primary data to answer specific questions that may be obscured by the single hole interpretation. The methodology presented in this chapter is designed specifically for the information mapped in KLX 01 and KLX02 and may require to be tailored differently for future boreholes drilled during the site investigation phase.

The single hole interpretation done in the current project has an element of method development. Furthermore, all data have been analysed in a “desktop fashion”, i.e. without any chances of directly observing the actual drill core. However, the analysis has been developed and performed as if the core has been at hand. This approach has weaknesses such as:

- possible misinterpretation of geological and geophysical logs,
- possible misinterpretation of logged parameter values.

It is particularly difficult to assess how continuously changing parameters, such as alteration of the rock mass, have been classified and put into simplified categories in the database. Alteration of the core has been divided by the mapping geologist into either oxidized or not, chloritized or not etc. The strength of the alteration is given as medium or strong. The exact level of alteration required to fall into such a class is not defined a priori. In practice it is possible that the mapping geologist sets this level in light of the available material.

Another limiting factor is that the single hole interpretation covers only geological indications mapped in the two core drilled boreholes of the Laxemar site, KLX01 and KLX02. The single hole interpretation has not been performed on the percussion drilled HLX boreholes, as the data obtained from these holes essentially contain information about lithology and indicative data about fracturing from the drill sinking speed measurements. It is anticipated that a geological single hole interpretation is made on each of the core drilled boreholes in the coming site investigations as part of the standard mapping package.

The percussion holes at Laxemar HLX01–HLX12 were mainly drilled to supply the core drilling of KLX01 and KLX02 with water and to get shallow subsurface information from probable fracture zones. The boreholes were logged by different geophysical methods (see Section 3.5) and the resistivity values from the logging were used in geometrical modelling (Section 4.1). The measurements in the borehole do not include BIPS or any other logging tool to record the actual orientation of structures in the borehole.

### 3.4.2 Target parameters for single hole interpretation

The two KLX boreholes in Laxemar are mapped with a large number of geological parameters using both traditional geological observations of the core and by more indirect geophysical investigations, cf. Table 3-2. The data from the two boreholes have been collected for many different reasons and contain several incomplete data sets. The geological mapping has been performed using a modified Petrocore mapping technique. Petrocore has been the standard SKB mapping data tool, which has successively been replaced by the current mapping system Boremap. The Laxemar boreholes have been mapped with a hybrid between the two, called pc\_logging\_new in SICADA. It is not clear to what extent the collected data set departs from a standard petrocore mapping other than from the availability of BIPS images.

With the limited available time for this particular stage in the project the following data were considered most valuable for the construction of the geological model:

- Lithology (rock types).
- Alteration (oxidization, chloritization, epidotization, weathering, tectonization).
- Brittle deformation (i.e. observations of fracturing, core loss and crush).

These data also exist in complete sets for both boreholes.

The data presented in Table 3-2, apart from radar observations, are presented in WellCAD logs in Appendix B1 and B2.

**Table 3-2. Available geological and geophysical data from KLX01 and KLX02.**

Type of data	KLX01	KLX02	Used in the single hole interpretation
Lithology (rock types)	X	X	X
Fracture location	0–1072 m	229–1700 m	X
Fracture orientation (based on BIPS). Natural (mapped as open). Sealed (mapped as mineral filled)	0–1072 m	229–1700 m	
Fracture mineralisation	0–1072 m	229–1700 m	
Oxidization (alteration)	X	X	X
Chloritization (alteration)	X	X	X
Epidotization (alteration)	X	X	X
Weathering (alteration)	X	X	X
Tectonization (alteration)	X	X	X
Core loss	X	X	X
Crush	X	X	X
Salinity	X	X	
Fluid temp gradient	X		
Natural gamma	X	X	
Resistance	X	X	
Gamma gamma	X	X	
Radar observations	X	X	

By analysing these parameters the borehole geology can be simplified into what we call rock segments which have a similar geological characteristics over a borehole section length. The term *rock segment* is used here to describe each of the identified sections along the borehole in simplified terms and is the main output of the single hole interpretation. For 3D modelling reasons it is desirable that the number of different types of *rock segments* are as few as possible to be useful in the 3D interpretation between different boreholes.

One way to combine different geological parameters is to analyse them in a binary form so that, if possible, they can reduce the interpretations along the borehole to a few different types of rock segments. /Olsson (ed), 1992/ used a similar approach analysing borehole data in the Stripa project and developed a Fracture Zone Index (FZI) using a binary analysis of a number of key parameters.








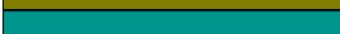
**3.4.3 Approach applied**

The proposed classification is based on the changes of character in lithology, alteration and fracturing along the boreholes. Table 3-3 shows eight different types of combinations that can occur when classifying lithology, alteration and fracturing in binary terms along the borehole. The classification is based on dividing the lithology into segments with either one dominating rock type (*single*) or with a mix of rock types (*mixed*). Alteration and brittle deformation is divided into sections of high or low proportion of alteration and fracture frequency. The color index shown in Table 3-3 refers to the WellCad log presented in Figure 3-8, illustrating the primary data visualisation.

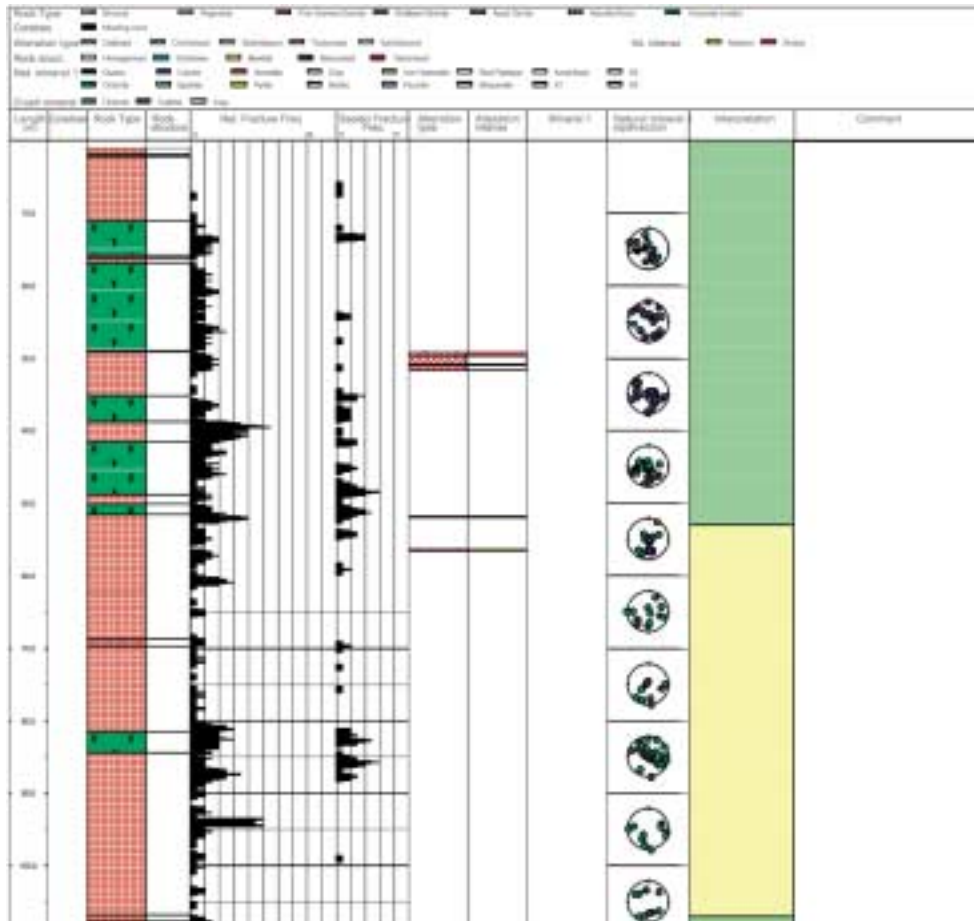
Each of the parameters is first studied independently of each other. The results are combined into rock segments after sections of lithology, alteration and fracturing of either *single*, *mixed*, *high* or *low* degree have been identified, cf. Figure 3-9. The process of combining these parameters into rock segments of types R1 to R8 is achieved by combining each parameter at each length section in the borehole. A section with *single* lithology, *low* alteration and *low* fracturing are thus classified as an R1 segment.

The interpretation is performed such that the three parameters are combined into as long rock segments as possible. The minimum length of rock segments using this approach will be dependent on the level of detail of the geological model. If the minimum length of rock segments is very short, then the single hole interpretation is of little value in the geometrical modelling as the data will remain to be very complex. On the other hand if the minimum length is too long, then important geological indications such

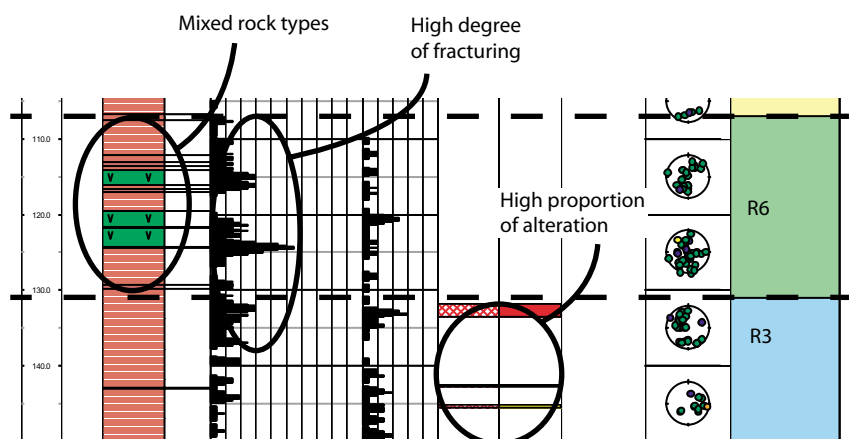
**Table 3-3. Classification of rock segments based on the geologic parameters lithology, alteration and brittle deformation.**

Lithology	Alteration	Fracturing	Rock Segments	Colour index used in WellCad
Single	Low	Low	R1	
Mixed	Low	Low	R2	
Single	High	Low	R3	
Single	Low	High	R4	
Mixed	High	Low	R5	
Mixed	Low	High	R6	
Single	High	High	R7	
Mixed	High	High	R8	

as narrow deformation zones may be obscured. To avoid making the single hole interpretation hide important data it is necessary that the geometrical modelling team always have the primary data at hand. For the Laxemar model 20 m segments have been considered as being the minimum length unless there are strong indications for smaller segments. The primary data for the Laxemar holes have also been used as a supportive data set in the geometrical modelling.



**Figure 3-8.** WellCad log of KLX01 showing lithology, fracturing and alteration along the borehole. The interpreted rock segments are shown as colored boxes in the interpretation column.



**Figure 3-9.** Illustration of how sections of lithology, alteration and fracturing are combined to rock segments.

### **3.4.4 Resulting single hole interpretation**

#### ***Lithology***

In KLX01 the dominating rock type is a medium- to coarse-grained, usually porphyritic granite to granodiorite (Småland “granite”). In the intervals 230–253 m and 525–547 m, a quartz monzodiorite (Äspö “diorite”) is present. A concentration of xenoliths to sheets (dm to tens of metre in scale) of unspecified, fine-grained mafic rocks (volcanic origin?) occur in the intervals 10–50 m, 82–84 m, 115–125 m, 325–385 m, 556–559 m, 611–617 m and 825–835 in the drillcore. Dykes or lenses of fine-grained granite usually accompany the mafic xenoliths to sheets.

The intensity in deformation/foliation of the granite to granodiorite varies along the borehole. The mapped alteration type refers to oxidation and tectonisation of varying intensities. The most frequent fracture minerals are chlorite and calcite. Hematite is common in the fracture zones, whereas pyrite seems to be more scattered. A few observations of Fe-oxyhydroxide have been made.

The rock type distribution in KLX02 is similar to that in KLX01, but the mafic xenoliths are more frequent and even larger, up to 50 metres in size is found between 800 to 920 metres depth. Mafic xenoliths of varying size are also found in the intervals 355–389 m, 540–553 m, 591–593 m, 605–609m, 680–725 m and 1380–1405m along the drillcore. Quartz monzodiorite (Äspö “diorite”) is found together with fine-grained granite in the upper 60 metres and from 1450 m and to the end of the core (c. 1700 m). Furthermore, there seems to be a spatial relationship between the fine-grained granite and the mafic rock components. It is also noticeable that the section with mixed rock types around 750 to 900 metres has an increased fracture frequency. There is also a section with high fracture frequency and alteration in the section dominated by quartz monzodiorite (Äspö “diorite”) at large depth (1550–1640 m).

Between c. 1450 and 1700 metres in borehole KLX02, i.e. the last c. 250 metres, the rock has been classified as Äspö “diorite” /e.g. Stanfors, 1995/. However, chemical and modal analyses of rock portions demonstrate a compositional variation between granodiorite and quartz diorite /Stanfors, 1995/. Consequently, it has a composition which is similar to the medium-grained granodiorite to quartz monzodiorite that occurs in the southwesternmost corner of the Model Area and occupies a relatively large area immediately south of the latter, from the Simpevarp peninsula in the east to Basthult in the west. Despite the lack of detailed information, it is from a compositional point of view reasonable to correlate these rocks and treat them as a coherent rock unit. Thus, a northward extension at depth is inferred.

#### ***Evaluation of data***

Lithology is a continuous parameter that can be studied in a binary fashion by analysing the frequency of rock contacts. Each rock contact represents a change in lithology from one rock type to another and can be treated as normal discontinuous data such as sealed fractures. However, a rock contact does not necessarily mean that the mechanical or hydraulic or other characteristics are different when crossing a rock contact. In the Laxemar area this can be exemplified by the quartz monzodiorite and granite, which have essentially the same hydraulic-, mechanical-, and fracture mineralisation properties and only differ in the mineral composition of the rock. The statistical analysis is based on the fact that the rock types are clearly distinguished along the borehole. As we have only performed a desktop analysis it is not known how precise the geological interpretation has been. It is known from previous core studies at Äspö that there is a gliding scale



between what is interpreted as a sealed fracture, a vein and a rock contact. The interpretation seems to vary between different mapping geologists. The statistics of rock contacts may therefore be influenced by the way sealed fractures, veins and contacts are entered in the SICADA data set.

The core (in this case the core log) is visually inspected to identify sections with homogeneous lithology (classified as *single*), with respect to its geological character. Other sections are classified as inhomogeneous (*mixed*). The lithology thus forms two classes, either a predominant single rock type in a section or a mix of several rock types. There may be many underlying reason for the occurrence of a mixed rock mass, such as magma mixing, ductile deformation, thermal solutions etc, but no such aspects are considered in the first step of the analysis.

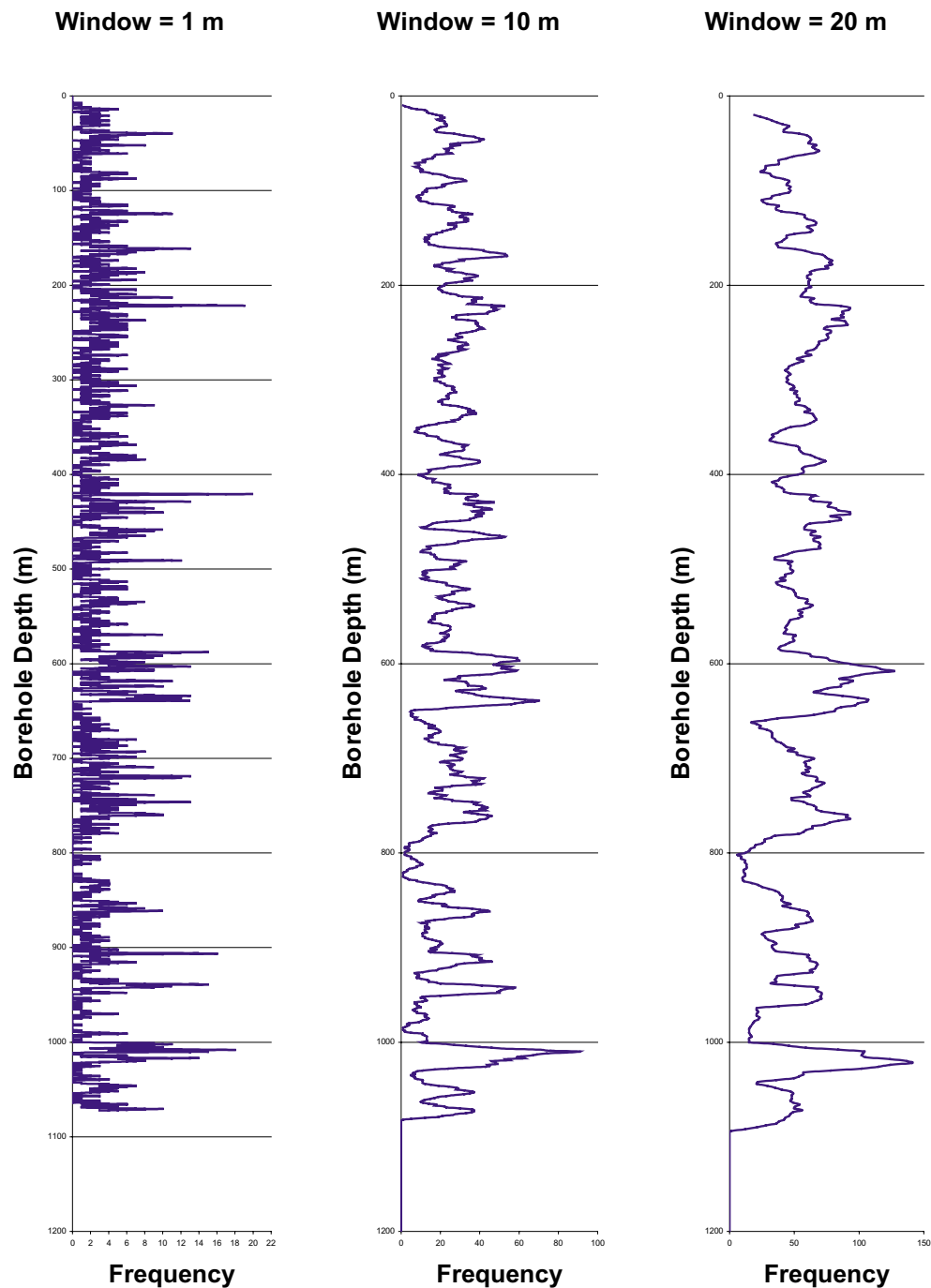
The same analysis is performed on the group of parameters labelled alteration in Table 3-2. This data set is more complex as the mapped parameter contains several types of alteration; chloritization, epidotization, seritization, oxidization, and mechanical alteration (tectonization). However, the analysis in the two holes was performed on the fact that they were recorded in SICADA as alteration regardless of the specific type. Further analysis is needed to understand how, for example, different types affect mechanical, hydraulic and transport characteristics in a complete analysis of the alteration parameters. It is anticipated that alteration is analysed somewhat differently in the site investigations when the single hole interpretation is performed in conjunction with the core mapping.

The analysis is performed by identifying highly altered sections along the borehole. The rest of the borehole is classified as *low* alteration. Thus alteration is divided into two classes, *high* and *low*. The core length proportion of low altered rock should be equal to or less than about 10–15% of the length of the segment. The distribution of altered pieces of rock within the identified section also provides information of what origin the alteration might have. Closely clustered altered pieces may indicate deformation zones with a distinct tectonic zone, whereas evenly spaced altered pieces may indicate a general background alteration of the host rock or the existence of a deformation zone much larger than the section of observation. Each type of spatial pattern is necessary to be investigated further so that larger trends can be captured.

Brittle deformation is analysed through the fracture frequency log. The fracture locations along the boreholes are analysed by utilising a moving average technique in order to identify different scales of fracturing. Several window sizes and step sizes are used to pinpoint which nature of fracturing that occurs in each borehole, see Figure 3-10.

Large deformation zones often have several narrow zones of highly fractured rock mixed with sections with average frequency of fracturing. These intensely fractured sections may be interpreted as individual zones if the standard frequency log is studied. The standard frequency log may also overlook narrow individual zones that are in the order of one meter as the normal frequency log plots fractures per meter. By using a moving average, narrow zones will show up if the window size is sufficiently small. Large window sizes may also reveal large-scale deformation zones that include several narrow zones of intensely fractured rock.

For simplicity, the WellCad log in Appendix B only presents fracture frequencies analysed with a moving average with a 1 m window and a 1 dm step size. However, Figure 3-10 shows an example of how the fracturing have been analysed with different window sizes using a moving average along the borehole. Varying the window size identifies larger deformation zones.



*Figure 3-10. Frequency analysis of fracturing in KLX01. This example shows the effect of analysing frequency using a moving average to find larger sections with increased fracturing. The frequency is based on natural fractures and crush sections.*

### **Rock segments**

The combination of all three parameters into rock segments of types R1 to R8 along KLX01 and KLX02 are presented in the WellCad log in Appendix B. The single hole analysis reveals that rock segments R1, R2, R3, R5, R6 and R8 are abundant in both boreholes but the rock segment types R4 and R6 are not encountered. Figure 3-11 illustrates the frequency of the different types of rock segments found in KLX01 and KLX02, respectively.

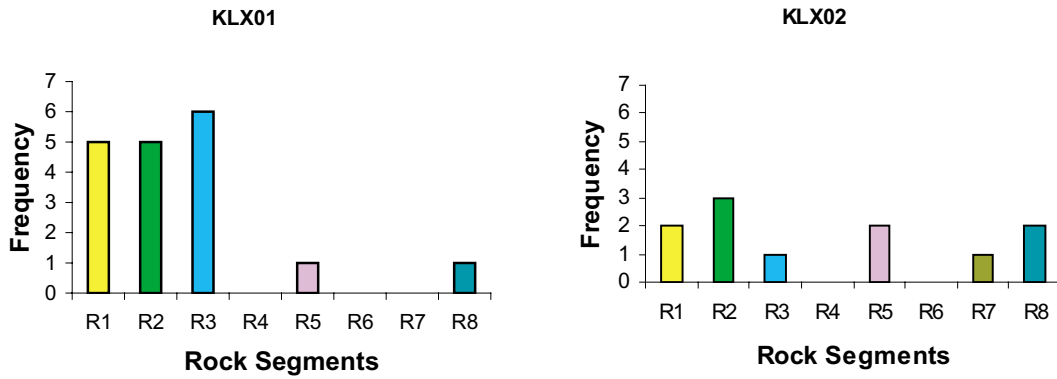


Figure 3-11. Frequency of rock segments found in KLX01 and KLX02.

It is likely that alteration is coupled to how lithology changes, such that a high proportion of alteration can exist in a section with mixed lithology. But this is not a given condition, the opposite may also occur in a weathered or chemically altered rock. The wide combination of different parameters under the concept of alteration makes interpretations difficult unless the specific type of alteration in each segment is investigated. Fracturing in the Laxemar rocks is weakly coupled to alteration and lithology such that sections with mixed lithology, high degree of alteration may also show an abundance of fracturing. When all three components are at a maximum it is interpreted as an R8, which is equivalent to a deformation zone, possibly with a ductile pre-cursor reactivated by brittle deformation. There also exists long sections which fall in to the category of R1:s, i.e. undeformed crystalline granites with no or very little influence from alteration and increased fracturing. The overall frequency of different rock segments is less in KLX02 (12) than in KLX01, which indicates that the rock mass in KLX01 is more heterogeneous than in KLX02. However, observing fracturing alone shows that KLX02 is more fractured and contains almost twice as many fractures, cf. Table 3-4 and also two R8 rock segments.

**Table 3-4. Fracture statistics in KLX01 and KLX02. Crush zones indicate sections that have not explicitly been mapped but are set to a default value of 40 fractures per meter.**

		KLX01	KLX02
Natural fractures and crush zones	Total amount	2893	6545
	# fractures/m	2.7	4.36
	spacing	0.37	0.23
Only natural fractures	Total amount	2573	3452
	# fractures/m	2.4	2.3
	spacing	0.41	0.44

### **Potential fracture zones along the boreholes**

Sections with more or equal to 10 fractures per meter over a section length larger than 1 m are considered to be *highly fractured* rock in the case of the Laxemar holes. The chosen threshold level is established after a careful review of both core logs in order to encompass the perspective of fracturing in this rock mass. New boreholes may change the truncation level depending on the observed fracturing.

There are 64 highly fractured sections identified in the Laxemar core drilled boreholes (16 in KLX01, 48 in KLX02) cf. Table 3-5. The fracturing is characterised by a relatively low background frequency of around 2-6 fractures per meter. Intense sections of fractures can have as many as 40 fractures per meter, characterised in the borehole log as crush sections. These sections are not explicitly mapped, but are identified and noted in a specific data table called “crush sections” as sec\_up and sec\_low values. For the frequency analysis all these sections have been converted to 40 fractures per meter.

### **3.4.5 Fracture mineralogical analysis**

Within different stages of the site investigation program fracture mineralogical investigations will be performed comprising mineralogical, textural and chemical composition of fracture minerals representing different depths, structures and groundwater chemistry environments.

Stable isotope analyses, mostly on fracture filling calcites and possibly sulphides, will together with corresponding analyses of the groundwater create a base for interpretations of past and present groundwater/mineral interactions at the site. Analyses of radioactive isotopes like U-series isotopes,  $^{14}\text{C}$  in calcite and K-Ar analyses of clay minerals can provide input to the description of the geological evolution of the area. In addition, textural studies (microscopy of fracture fillings and wall rock) may for example reveal crosscutting relations and sequence of events. Past and present depths of the redox front in the bedrock may be validated using fracture minerals and their chemical and isotopic composition. Also the deep stagnant groundwater environment may be validated using fracture minerals.

Interpretation of the data for fracture mineralogical studies will need input from and create output to several disciplines. However, from the Laxemar domain no systematic fracture mineral analysis has been performed. The only type of data present to interpret is the stable isotope data of calcites.

## **3.5 Seismic reflection and borehole radar measurements**

Seismic reflection measurements and borehole radar offer possibilities to local anomalies ‘inside’ the rock. Before three-dimensional modelling, the measurement signals need to be interpreted into potential reflecting surfaces etc.

### **3.5.1 Seismic reflection**

Using seismic reflection is an important tool in the 3D geological modelling work and it requires involvement of specific competence in this field. The identification of seismic profiles, as well as the statements concerning the seismicity in the area and the nature of the seismic reflectors, were made by the specialists that also made the measurements

**Table 3-5. Sections of fracturing equal to or more than 10 fractures per meter based on natural fractures and crush sections. These sections are potential fracture zones.**

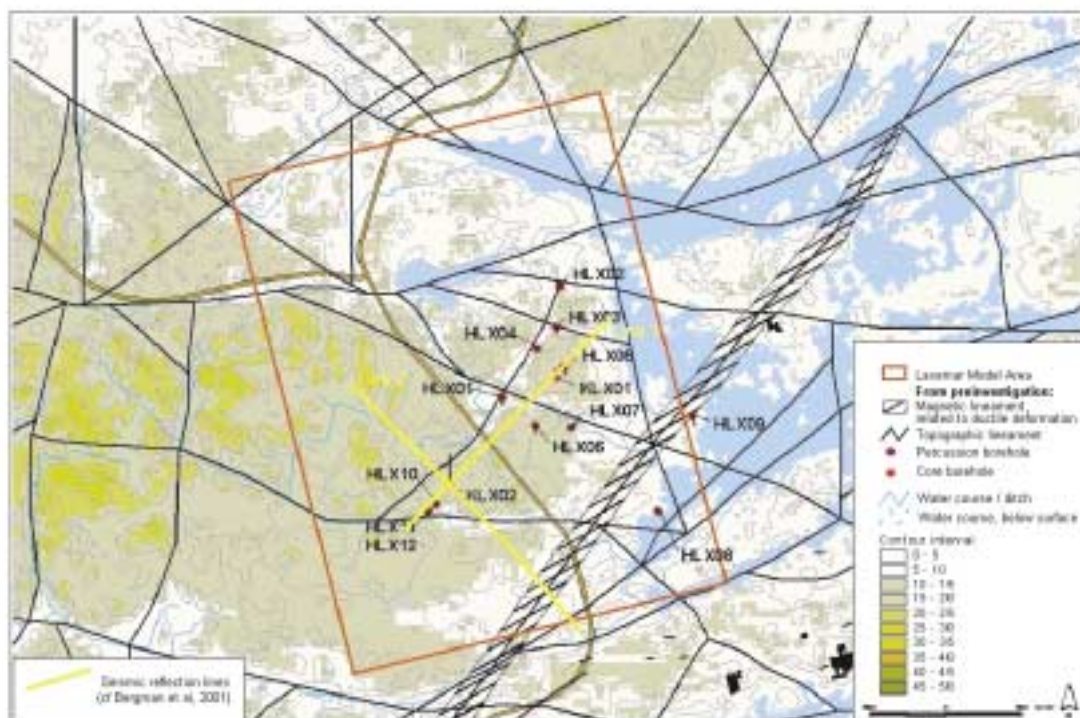
KLX02 Zones			KLX01 Zones		
sec up	sec low	length (m)	sec up	sec low	length (m)
252,6	253,8	1,2	160	163,7	3,7
339,3	340,7	1,4	220,7	222,4	1,7
385,1	386,5	1,4	420,3	421,5	1,2
435,4	437,8	2,4	587,6	588,7	1,1
466	468,5	2,5	633,6	634,9	1,3
530,6	531,7	1,1	697,5	698,7	1,2
623,4	625,9	2,5	759,4	760,5	1,1
662	663,5	1,5	805,1	806,2	1,1
732,5	733,6	1,1	858,6	859,9	1,3
750,9	752,5	1,6	905,6	907	1,4
779,4	781,7	2,3	912,6	913,9	1,3
786,8	788,8	2	938,4	939,5	1,1
799	801,7	2,7	945,5	947	1,5
811,9	813,8	1,9	1003,4	1004,4	1
816	820,4	4,4	1005,6	1010,5	4,9
828,8	829,8	1	1016,6	1018,4	1,8
846,1	847,4	1,3			
850	851,1	1,1			
853	858,3	5,3			
860,7	865,6	4,9			
881,8	883,9	2,1			
886,3	887,5	1,2			
892,3	896,7	4,4			
898,6	902,2	3,6			
919,3	921	1,7			
929,2	930,3	1,1			
943,3	950,1	6,8			
958,7	959,9	1,2			
995,1	996,2	1,1			
997,4	998,5	1,1			
1037,4	1046	8,6			
1050,2	1051,4	1,2			
1052,6	1055	2,4			
1056,1	1058,3	2,2			
1065,5	1082,2	16,7			
1085,6	1101,8	16,2			
1105,4	1112,8	7,4			
1309,2	1310,3	1,1			
1419,3	1420,4	1,1			
1564,8	1567,8	3			
1573,5	1575,1	1,6			
1586	1587,1	1,1			
1596,4	1597,6	1,2			
1601,4	1604	2,6			
1620,6	1622,3	1,7			
1628,9	1631,2	2,3			
1633,8	1635,2	1,4			
1697,8	1700	2,2			

(Juhlin pers. comm.). The interpretation of probable geological features related to seismic reflection in the three-dimensional geological modelling of the Laxemar Model Domain was performed by the geologists within the current project.

### **Measurements made and identification of seismic reflectors**

The Laxemar area was investigated by seismic reflection profiling in December 1999 along two perpendicular lines, each 2 km long (Figure 3-12). For a more complete description of the technique used and the acquired results see /Bergman et al, 2001/. Below follows a brief description of the data used in the geometrical modelling and what kind of ambiguities that are related to the data. The reflectors are digitally stored in RVS. An investigation using the VSP (Vertical Seismic Profiling) technique has also been conducted in KLX02, but was not available at the time of the current project and not considered in the geometrical modelling of the geology.

A large number of seismic reflexes show up in the Laxemar Model Domain and many of them are interpreted as lenses of diorite to gabbro (also referred to as “greenstones”, see Section 3.2). The high degree of reflectivity makes it hard to sort out relevant reflectors. The interpretation of reflectors by /Bergman et al, 2001/ differ somewhat from those made in the current project (Juhlin, pers. comm.), in that emphasis in the current project has been put on distinct reflectors showing a signature that could be related to fracture zones. In general the interpreted reflectors in the current project are shorter. Three dimensional seismic would increase the confidence level of the reflectors, especially with respect to their orientation in three dimensions. According to the interpretations by /Bergman et al, 2001/ six reflectors in line 1 and four in line 2 have been interpreted as fracture zones. There are nine more reflectors in each line, which probably are caused by lenses of diorite to gabbro (“greenstone”).



**Figure 3-12.** The seismic reflection lines at Laxemar (yellow) (from /Bergman et al, 2001/ Figure 2-2).

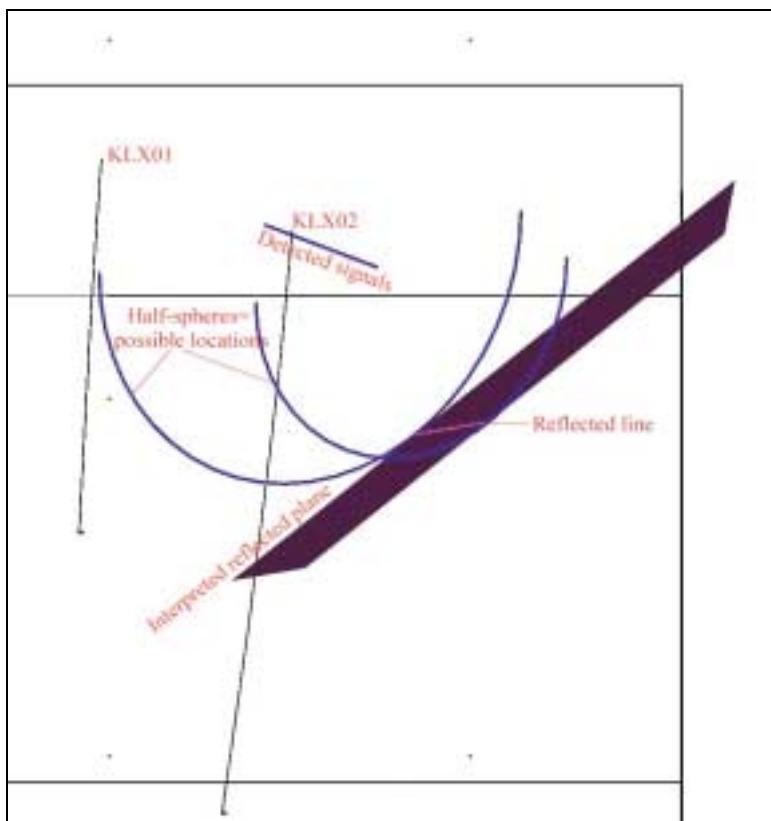
### **Visualisation of seismic reflectors in RVS**

Seismic reflectors are handled with a specific tool in the Rock Visualization System. The input data describe a line along the receiving geophones and shooting points at ground level ( $z = 0$  masl) and two half-spheres at the end of the reflecting plane at depth (see Figure 3-13). Actually the reflecting plane is a reflecting line that theoretically can be located at any position around the half-cone formed as a boundary to the half-spheres. The degree of sphericity of the cone is dependent on the velocity of the transmitted P waves in various directions in the bedrock. The velocity is different in different type of rocks and may well differ vertically and horizontally. In the Laxemar geometrical modelling (using RVS) a velocity of 6000 m/s vertically and 5500 m/s horizontally, has normally been used. The difference in velocity is used because of the higher fracture frequency near the surface and the probable existence of deeply eroded valleys.

### **Biases and use of information for further modelling**

There are a few properties related to the seismic reflection data, that makes the interpretation somewhat biased. This does not concern the interpreted reflectors, but with the current configuration of seismic lines it is difficult to identify reflectors in the model volume, having 'unfavourable' orientation and/or position. Most probably such surfaces exist in the model volume. The reported reflectors are only those that have favourable position in relation to the seismic lines.

The seismic lines at Laxemar (Line 1 and Line 2, see /Bergman et al, 2001/) are located in the central part of the modelled area (Figure 3-12). The lines cross each other at approximately right angle, with Line 1 in a SW – NE direction that passes KLX01 and



**Figure 3-13.** The interpretation tool for seismic reflection in RVS.

KLX02. Also the shooting points lie on these lines. Since the seismic signal has to pass from the shooting point to a reflecting plane and back to the geophone on the line, the reflecting plane has to dip in a direction towards these two points, or possibly be vertical. This means that reflecting planes dipping outwards from the central part of the model volume has small possibilities to gain support from the conducted seismic investigation. Other planes lie out of reach for the seismic profiles.

Obtaining the orientation of the reflecting planes in three dimensions by seismic information alone is possible when the reflectors are registered and correlated in both seismic lines. Close to the intersection between the two lines such correlation is more reliable. Reflecting planes (or actually lines) that only are registered in one of the lines have to be supported by other data in order to assign its orientation in three dimensions.

In summary, the seismic reflection information gives much valuable information in the central part of the model volume, but less information further away from the centre. The best information is gained from the crossing area between the two seismic lines. Section 4.1 shows how the seismic information was used in constructing a geological model of the site.

### **3.5.2 Borehole radar measurements**

Directional borehole radar is a method to localize structures in the bedrock, such as fractures, fracture zones, crush zones and lithological contacts being penetrated by the borehole or situated in its close surroundings. An electromagnetic pulse is sent from a transmitter and is generating reflections at surfaces with divergent electrical characteristics. There are two different types of sounding probes; dipole and directional antenna. Besides to measure the distance to the reflector and its angle to the borehole, the latter also gives the azimuth to the reflector. It is possible to apply frequencies between 25 and 250 MHz. Higher frequency gives lower penetration depth, but better resolution and vice versa. The directional antenna uses 60 MHz. A thorough description of the method is in preparation at SKB.

#### ***Identification of radar reflectors***

Borehole radar measurements have been done in both KLX01 (15–685 m) and KLX02 (210–~1405 m) /Niva and Gabriel, 1988/ and /Carlsten, 1993/. Both dipole antenna and directional antenna has been used, but at different levels in the boreholes. The equipment and technique used is described in these reports.

Radar reflexes can be registered a few tens of metres outside the borehole. The reflexes records differences in electrical properties and the larger this difference is, the thinner the reflecting structure can be in order to be detected. With a large contrast very thin objects can be detected. The dipole antenna was used in both boreholes and in KLX02 also a directional antenna was used (between 210 and 1035 m). The latter permits an absolute orientation of structures to be interpreted, but this equipment was only effective down to a depth of ca 1000 m. The radar pulse amplitude has been used as an aid in the interpretation of the reflexes. When the amplitude is damped the dielectric permittivity increases. This indicates a higher water or clay content.

A total of 63 reflectors (directional antenna) and 92 reflectors (dipole antenna) were identified from the directional antenna measurements in KLX02, between 57 and 1027 metres and 213–1392 metres depth, respectively. In KLX01 64 reflectors were identified between –57 (do not crosscut the borehole) and 762 metre. A cross-hole



correlation between KLX01 and KLX02 has also been conducted by /Carlsten, 1994/. An earlier cross-hole study has been done between boreholes at Äspö and KLX01 /Niva and Gabriel, 1988/.

### ***Biases and use of information for further modelling***

The result from conducted borehole radar measurements only describes structures with intermediate dip. No sub-vertical or sub-horizontal structures at all have been detected. This is in contrast to the situation at Äspö, where steep or sub-vertical and vertical fractures and fracture zones dominate. Different techniques have been used in KLX02 and KLX01 and different parts of the boreholes have been investigated in different ways, for various reasons. /Munier, 1994/ extrapolated potential fracture zones, as indicated by radar (directional antenna) data, to the surface. In summary the radar data may lend support to the RVS modelling for some interpretations in the model, but not for other. This is further discussed in Section 4.1.

## **3.6 Surface hydrogeology**

A description of the hydrology in Äspö region is found in /Larsson-McCann et al, 2002/, /Follin et al, 1998/ and /Rhén et al, 1997/. This section summarises the hydrology mainly based on /Larsson-McCann et al, 2002/ and gives some additional comments and figures that are related to the boreholes (HLX01–09 and KLX01–02) and the Laxemar Model Area.

### **3.6.1 Hydrological setting of the Simpevarp area**

Figure 3-14 and Figure 3-15 show the boundaries that are used for the Laxemar Model Area and include drainage basins, rivers and lakes. Figure 3-16 shows the model area as well as the position of the boreholes drilled up to 2001. /Follin et al, 1998/ show the drainage basins in Oskarshamns County.

As can be seen in the figures there are a large number of small drainage basins implying that there are small recharge and discharge areas. The annual recharge of ground water to deeper levels should be small in relation to the total recharge/discharge as long as the ground water is not utilized or drained to an underground facility.

According to /Larsson-McCann et al, 2002/ the mean air temperature varies between – 2°C in January-February to 16°C in July, see Figure 3-17. Figure 3-18 shows the yearly mean temperature.

The annual mean precipitation in Oskarshamn is 645 mm/year (corrected values, not the measured, for period 1961–2000), see Figure 3-19 and Figure 3-20, where about 20% falls as snow. The annual mean precipitation 1991 to 2000 was slightly higher; 681 mm. For the standard normal period 1961–1990 the annual mean precipitation is 633 mm. The annual potential evapotranspiration is about 560 mm /Nyberg et al, 2001/. In /Nyberg et al, 2001/. The annual and monthly mean values are shown for the period 1987 to 2000. The figures of annual specific discharge and precipitation indicate that the actual annual evapotranspiration is around 500 to 450 mm.

In /Larsson-McCann et al, 2002/ the relative humidity, global radiation, air pressure and wind (direction and speed coupled to frequencies) are also presented. Water level variation is also shown for lake Forshultesjön and the ice period for lake Gnötteln.

Close to the area for this study, there are two larger drainage basins; the Laxemarån and the Mistraån stream basins. No flow measurements have yet been performed in these watercourses. In /Larsson-McCann et al, 2002/ the measurement station 1619 Forshultesjön was chosen to represent the Oskarhamn area see Figure 3-21 and Figure 3-22. The annual mean specific runoff (here expressed as total runoff/total drainage area, Runoff some times also called discharge and specific runoff as specific discharge) is 5.7 L/s·km<sup>2</sup> (180 mm/year) for a drainage basin area of 103.2 km<sup>2</sup>.

Specific runoff was estimated for Virboån and Marströmmen Gerseboån and Laxemarån in /Svensson, 1987/ and was found to be between 150 and 200 mm/year.

The total groundwater-recharge contribution (baseflow) into the water courses and lakes is somewhat less than the specific runoff multiplied with the total area of the drainage basin. Some of the precipitation falls on lakes, water courses, discharge areas and on tight surfaces, where the water flows directly to a water course and some water is subsurface flow above the water table (interflow) that flows to the nearest water course. (The sum of flow on land surface, in water courses and lakes makes up overland flow). Also, some of the groundwater discharges directly to the sea (sub-sea outflow) as the area borders the Baltic Sea.

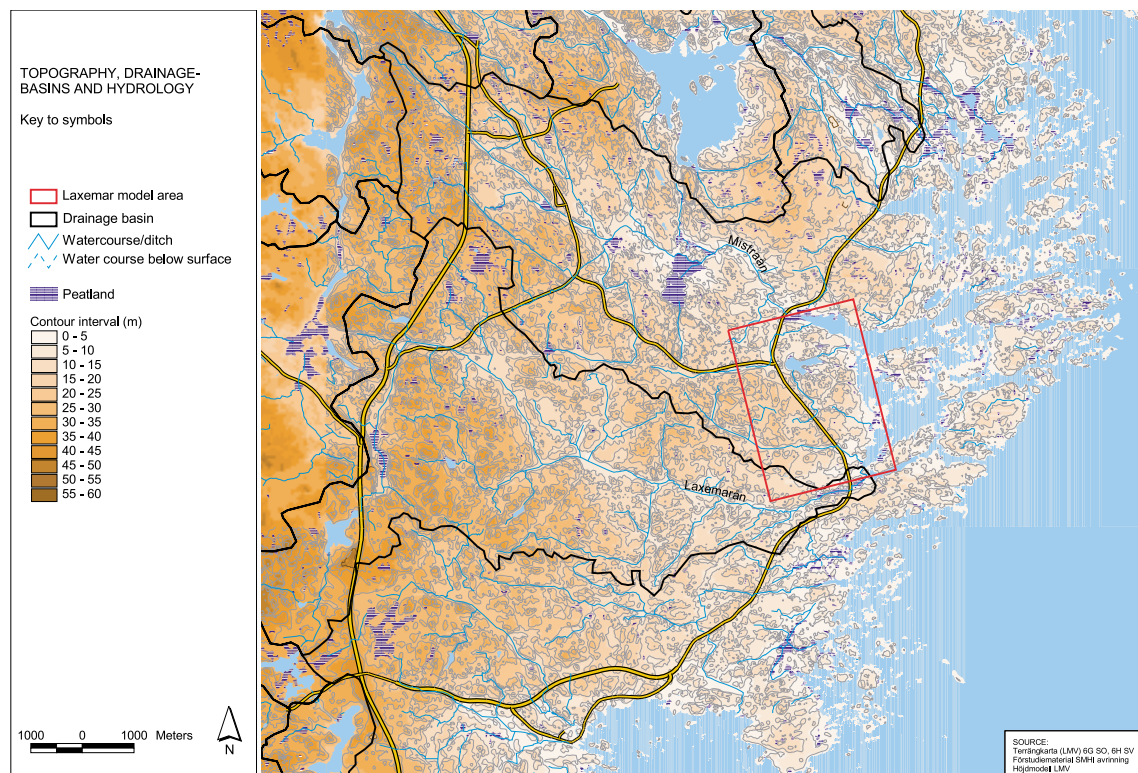
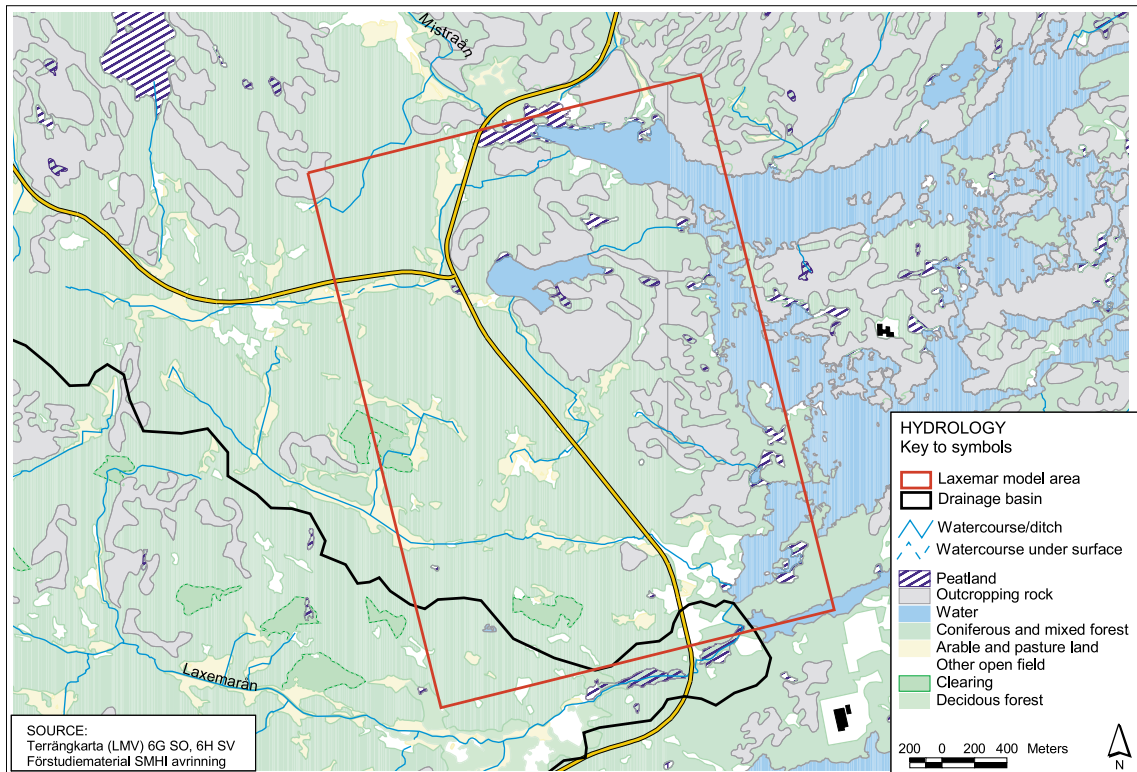
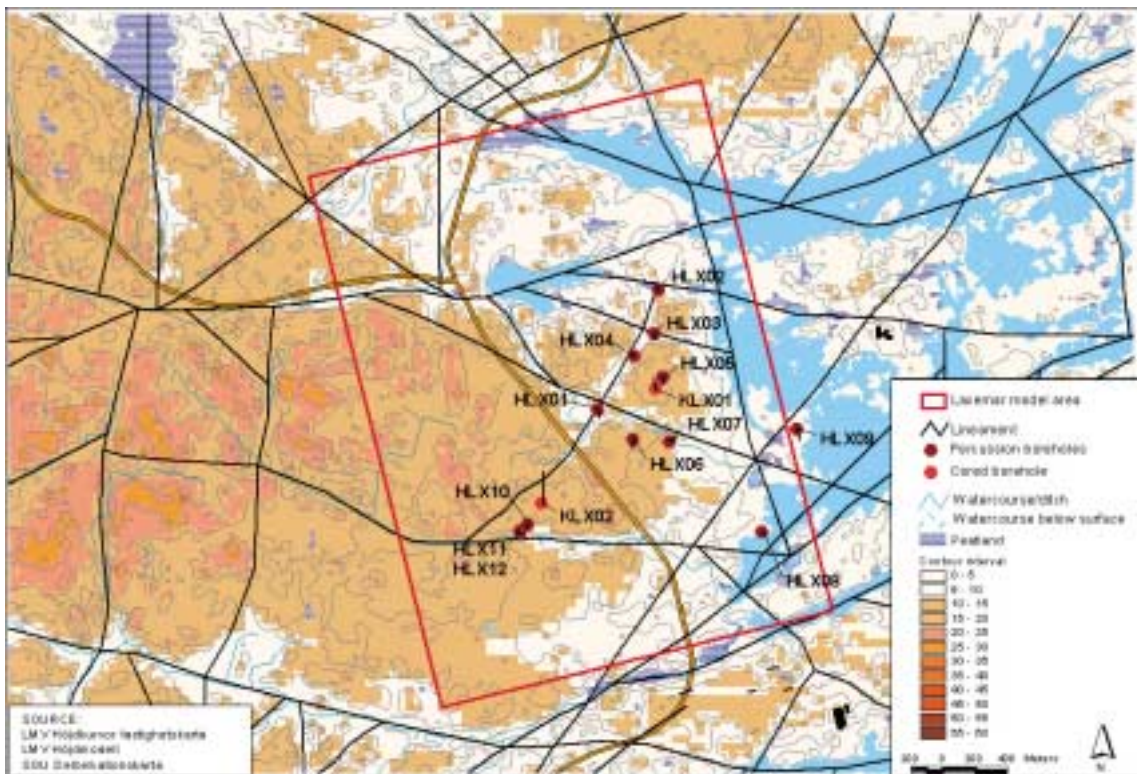


Figure 3-14. Drainage basins and rivers in the Simpevarp area.

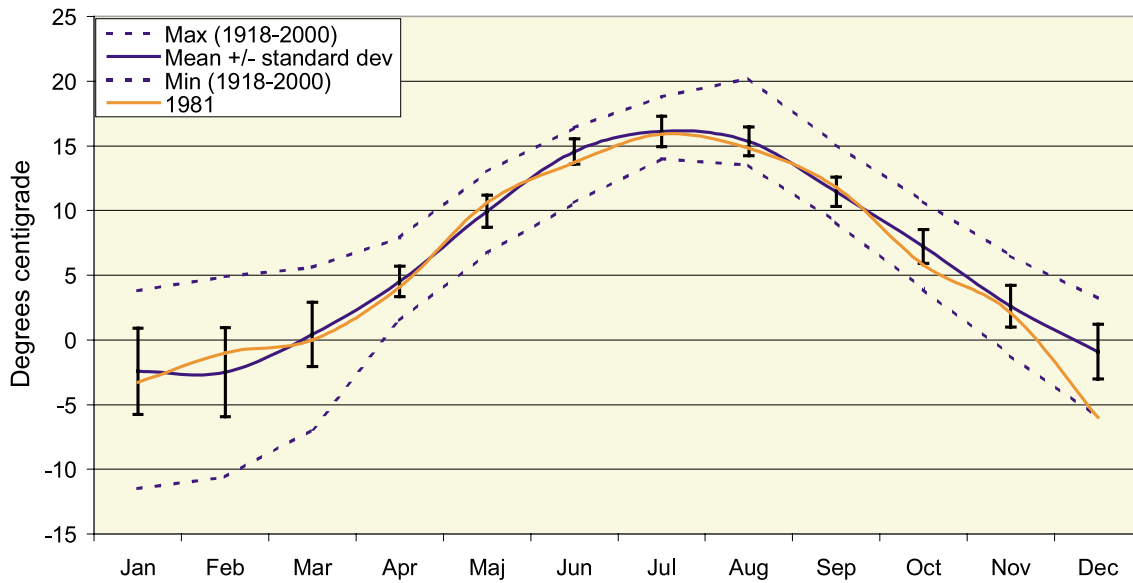


*Figure 3-15. Drainage basins and rivers in and near the Laxemar area.*



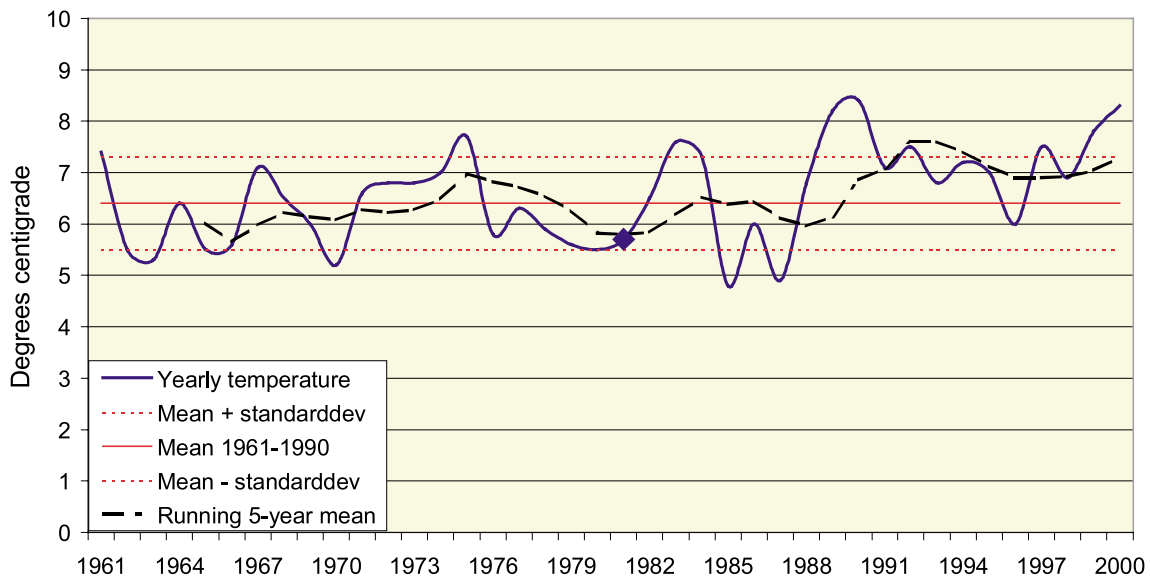
*Figure 3-16. Topography, rivers and boreholes in and near the Laxemar Model Area. (Lineaments as interpreted in the feasibility study.)*

### Monthly mean temperature, Oskarshamn, 1961 - 1990



**Figure 3-17.** Monthly mean temperature for the standard normal period 1961–1990, Oskarshamn. Vertical lines represent standard deviation and dashed lines maximum and minimum of the monthly mean temperature. Monthly means for the selected year 1981<sup>2</sup> are included (red line). /Larsson-McCann et al, 2002/.

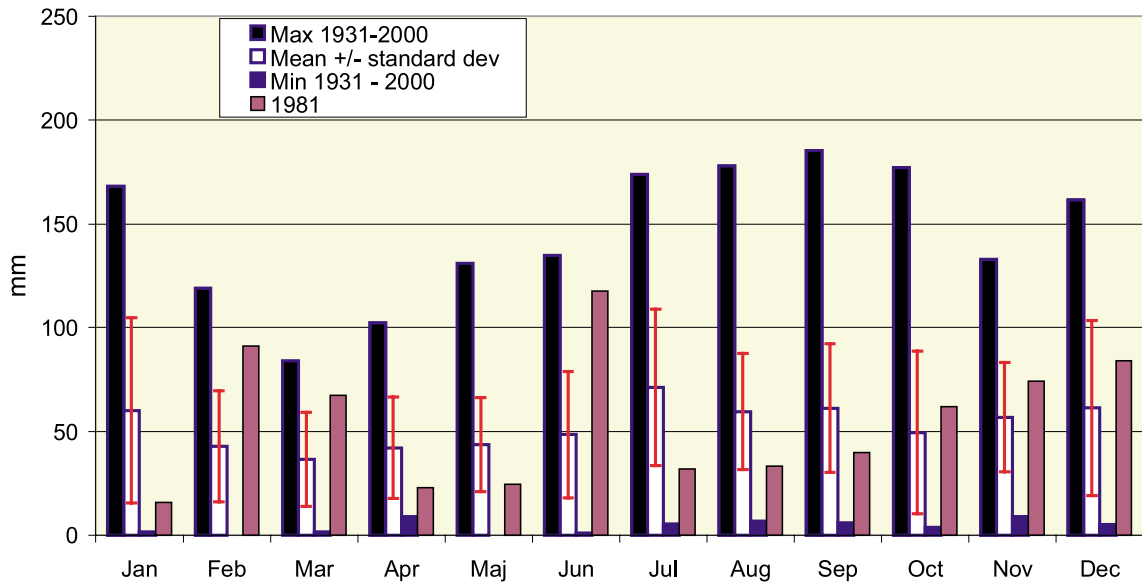
### Yearly mean temperature, Oskarshamn, 1961 - 2000



**Figure 3-18.** Yearly mean temperature for the period 1961–2000 and running 5-year mean temperature (dashed curve), Oskarshamn. Average yearly mean temperature for the standard normal period 1961–1990  $\pm$  one standard deviation is drawn (red continuous and dotted lines). /Larsson-McCann et al, 2002/.

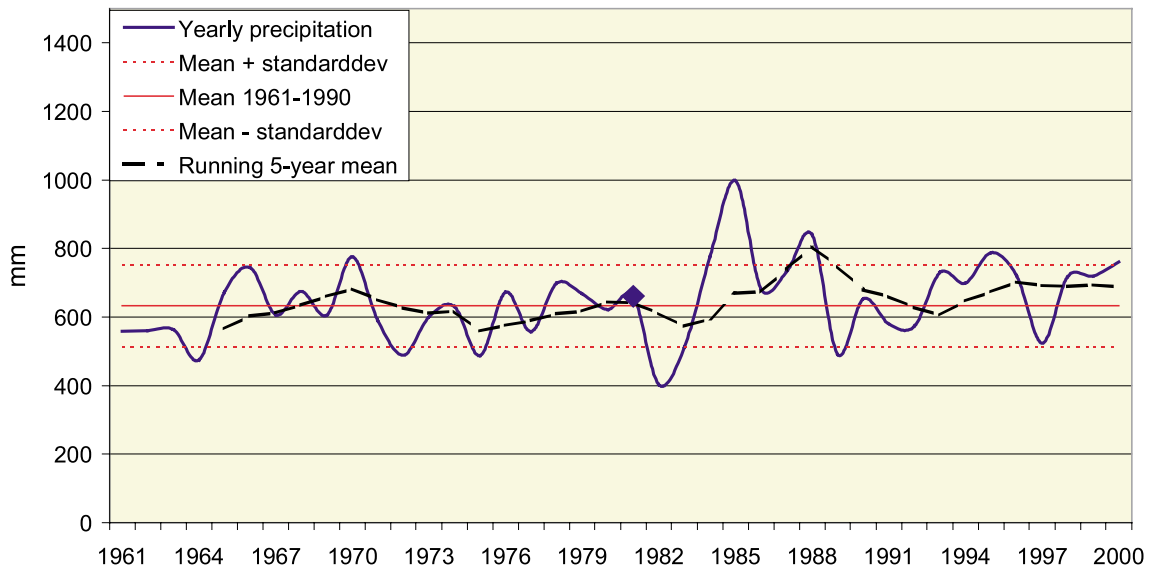
<sup>2</sup> One year (1981) has been selected to give high resolution in time for meteorological and hydrological variables for future use by SKB. It corresponds fairly well to the average year based on monthly mean air temperature.

### Monthly mean precipitation, Oskarshamn, 1961 - 1990



**Figure 3-19.** Average monthly sum of precipitation for the standard normal period 1961–1990, Oskarshamn (unfilled columns), max and min. Vertical lines represent standard deviation about mean. Monthly sums for selected year 1981 are also included (striped columns). /Larsson-McCann et al, 2002/.

### Yearly precipitation, Oskarshamn, 1961 - 2000



**Figure 3-20.** Yearly sums of precipitation (continuous curve) for the period 1961–2000, Oskarshamn and running 5-year mean sum of precipitation (dashed curve). Average yearly precipitation for the standard normal period 1961–1990 +/- one standard deviation is drawn (red continuous and dotted lines). The year 1981 is marked with a diamond. Corrected values. /Larsson-McCann et al, 2002/.

### Discharge 1619 Forshultesjön nedre 1955-2000

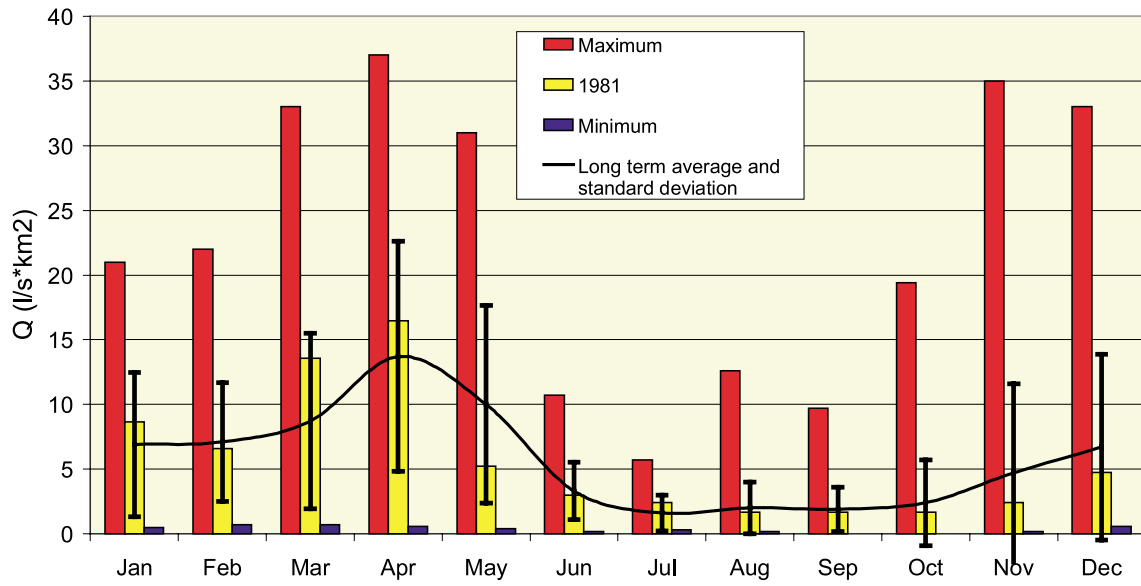


Figure 3-21. Monthly specific runoff 1619 Forshultesjön nedre 1955–2000. Maximum, minimum, long term average and standard deviation. 1981 specially selected year. /Larsson-McCann et al, 2002/

### Average discharge 1619 Forshultesjön nedre 1955-2000

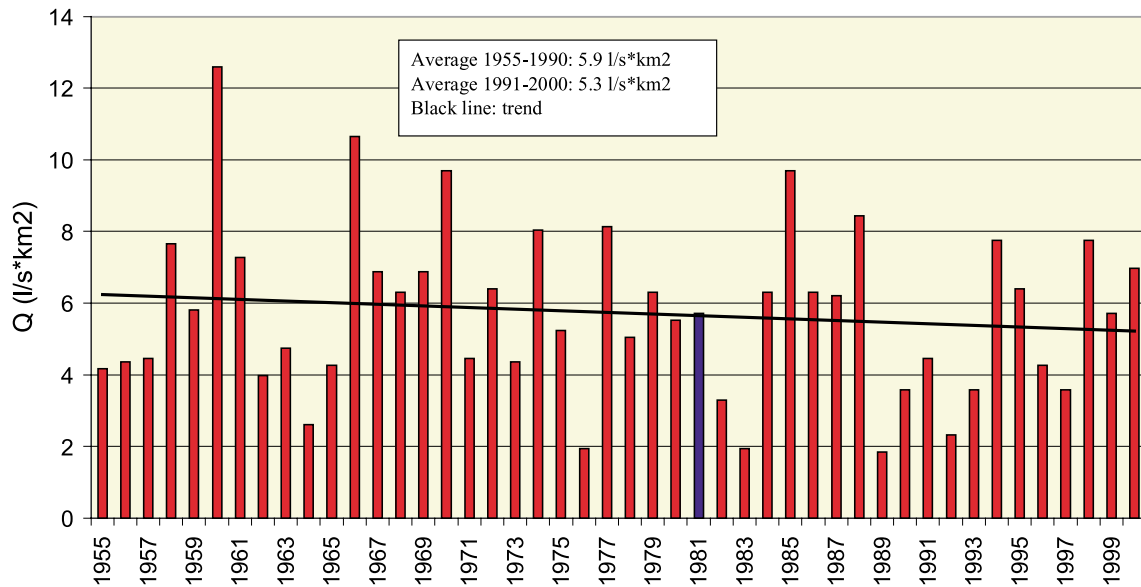


Figure 3-22. Average specific runoff 1619 Forshultesjön nedre 1955–2000 with trend (l/s\*km²). 1981 specially selected year. /Larsson-McCann et al, 2002/.

### 3.6.2 Quaternary deposits

The Laxemar Model Area is dominated by exposed bedrock or bedrock with only a thin layer of Quaternary deposits (< 0.5 m). Besides this thin layer, which mostly consists of till, the Quaternary deposits are dominated by glacial and post-glacial sediments, i.e. gravel, sand and clay. Furthermore, a glaciofluvial deposit (esker) and peat occur (see Section 3.3.1). No measurements of the hydraulic properties of the Quaternary deposits have been made. Table 3-6 shows typical ranges for Swedish conditions.

### 3.6.3 Correlation with rock type?

The main rock type within the area is a medium- to coarse-grained, porphyritic, more or less isotropic, granite to granodiorite. Texturally it is relatively inhomogenous, and locally a foliation is developed. There are also a few larger bodies of diorite to gabbro, traditionally called “greenstone” together with unspecified mafic rocks (see Section 3.3.2). Xenolites to enclaves and minor bodies of diorite to gabbro, as well as narrow dykes and minor massifs of fine-grained granite are rather common in the predominating granite to granodiorite.

Hydraulic tests (test scale approximately 3 m) in boreholes have shown that sections dominated by fine-grained granite are generally more permeable compared to sections without fine-grained granite /Rhen and Forsmark, 2000; Follin et al, 2000/. This may be valid also for the bedrock at surface.

In other sites in Sweden it has been observed that the bedrock surface may be more fractured on the stoss side compared to the leeside on a roche moutonnée. As the main direction of movement of the continental ice was from NW-NNW, the rock surface may have different fracturing on the NW-NNW side compared to the SE- SSE side of bedrock hills. The uppermost part of the bedrock may have a significantly higher hydraulic conductivity that affects the circulation of the groundwater.

### 3.6.4 Water table and piezometric levels

The maximum elevation of the water table (measured as the water level in the percussion holes in the upper part of the rock) is during the late autumn to spring and the minimum is found in late summer. The annual observed variation of the water table is around 1 m and less close to the coast and discharge areas. Measurements on Äspö, Ävrö and Bockholmen indicate that the water table ( $h_{WT}$ ) is correlated with topography with about  $h_{WT}=0.3z_{masl}$  /Rhen et al, 1997/. Possibly this relation can be approximately valid in the Laxemar area if the elevation above nearest discharge area is used. (This has not yet been tested on the available data in Laxemar Model Area).

**Table 3-6. Typical ranges for hydraulic properties of Quaternary deposits /Carlsson and Gustafson, 1997/.**

Soil type	Hydraulic conductivity (m/s)
Till	$10^{-5} - 10^{-11}$
Clay	$10^{-8} - 10^{-12}$
Silty soil	$10^{-5} - 10^{-9}$
Sandy soil	$10^{-3} - 10^{-6}$

The measured piezometric levels in the Laxemar area are shown in Appendix B3. The piezometric levels presented are the levels measured in standpipes from the packed off measurement section. The density of the water column down to the measurement section in the stand-pipes is approximately as in the packed-of borehole section. The shown levels are not entirely undisturbed, as hydraulic tests have been performed during several periods. The tests performed in KLX02 between 17 Dec. 1992 and 16 Jun. 1993 with three pump stops, and for Phase 2, pumping was performed between 19 Oct. 1995 and 25 Nov. 1995 with one pump stop /Follin, 1997/ is defined in the figure in Appendix B3. There are other activities that occasionally disturb the levels, but these activities are not compiled in this report. However, the figure gives an indication of the undisturbed levels and in Appendix B3 are also the interpreted undisturbed piezometric levels tabulated based on data from 1989 to 1992. In /Rhén et al, 1997/ a few time series of piezometric levels in borehole sections are presented in some detail, which show the variation in time of boreholes close to the coast line as well as boreholes situated inland.

The short time variation of the piezometric levels is influenced by a number of factors such as precipitation, earth tides, barometric pressure and sea level fluctuations. The influence of earth-tide on the piezometric levels is generally less than  $\pm 0.15$  m /Rhén et al, 1997/. The calculated level of ground surface relative to mean level is about  $-0.2$  to  $+0.4$  m due to the earth tide /Rhén et al, 1997/. The tidal wave is composed of two long-wave (half a month and half a year) and two short-wave (nearly half diurnal and half diurnal) oscillations and the piezometric level increases when the Earth crust is depressed and decreases when the crust rises.

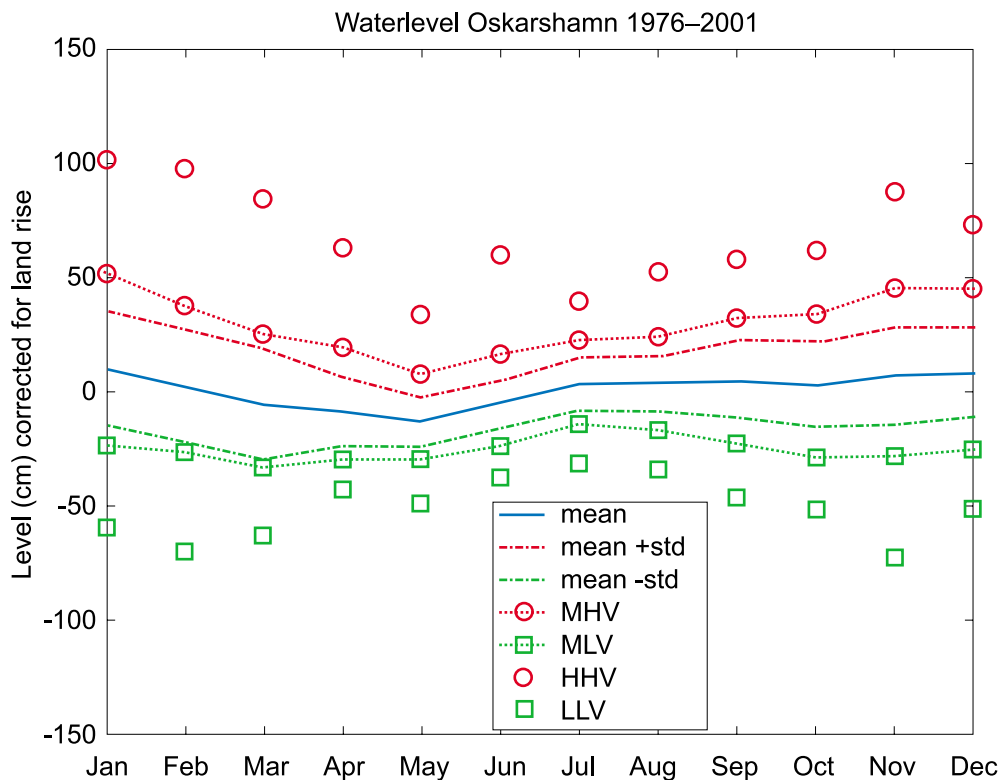
Some of the effects can be seen in borehole KLX01, where sections down to about 700 m show clear response from heavy rain or snow melting (Appendix B3, /Follin, 1996/). Tidal effects and barometric changes were mainly observed below 700 m in the Laxemar area and can be seen more superficial in other areas but are generally very small in the percussion drilled boreholes.

### **3.6.5 Baltic sea**

The sea water level is measured in Oskarshamn and Figure 3-23 shows the monthly mean sea level is shown. In /Larsson-McCann et al, 2002/ sea temperature (several measurement stations), salinity, nitrate+nitrite, total nitrogen, ammonium, phosphate phosphorus, total phosphorus, silicate-silicon, chlorophyll, oxygen, pH and alkalinity is shown for a few measurement stations. Temperature are shown for several measurement stations and the other parameters for a station east of Öland (BY38).

The salinity of the sea is about 7 g/L and is rather constant over the year and does not vary in the uppermost 20 m of the water column (Station BY38). Close to the coast where fresh water enters the sea from watercourses the salinity is less than 7 g/L. A few measurements around Äspö indicate a salinity of about 6 g/L but vary with location and time of sampling. One sample showed 4 g/L and a few others 5-6 g/L /Rhén et al, 1997/.





**Figure 3-23.** Monthly sea water level (cm) statistics at Oskarshamn 1976–2001. To obtain correct extreme value statistics, levels have been corrected for land rise. Monthly mean water level and one standard deviation are shown. MHV/MLV signifies mean high/low water level, i.e. mean of all years 1976–2001. HHV/LLV signifies highest/lowest water level ever during 1976–2001. Based on hourly measurements /Larsson-McCann et al, 2002/.

### 3.7 Hydraulic interpretation of borehole data

#### 3.7.1 Available data and test designs

Hydraulic tests of different kinds have been performed in the two deep core drilled holes (KLX01 and KLX02) and nine percussion boreholes (HLX01–09). Figure 3-24 to Figure 3-25 and Table 3-6 to Table 3-9 compile the types of tests that have been performed and what sections that have been tested in the different boreholes. The results are presented using type of test, borehole length and scale, where the “test scale” in the figures and tables represents the distance – approximate distance or distance class – between the upper and lower section of the tested borehole section.

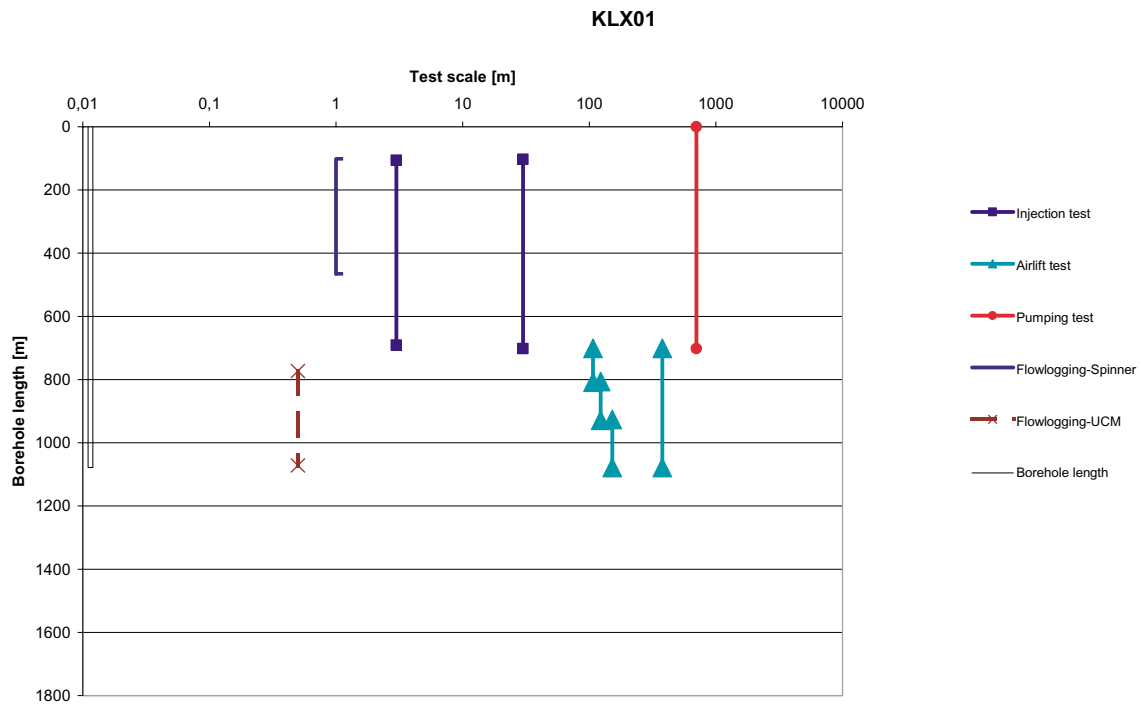


Figure 3-24. Hydraulic tests performed in KLX01.

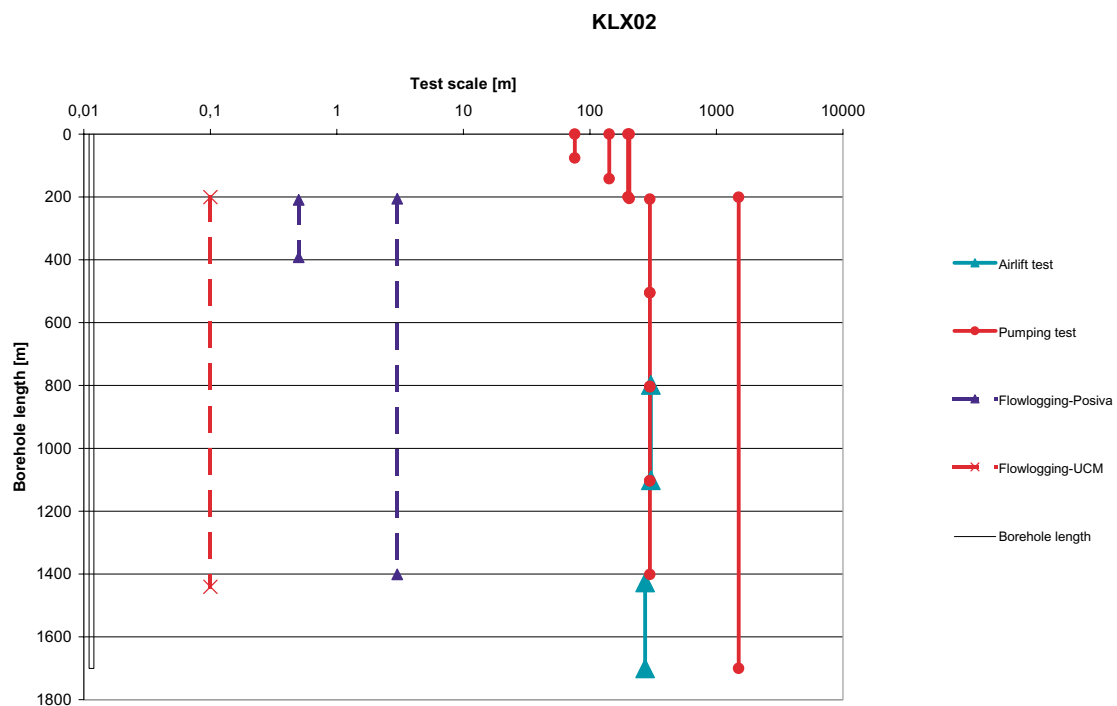


Figure 3-25. Hydraulic tests performed in KLX02.

**Table 3-7. Hydraulic tests performed in HLX boreholes.**

Borehole	Borehole length (m)	Tested part of bh, Secup (m)	Tested part of bh, Seclow (m)	Type of test performed	Test scale (L) (m)	Step length for moving measured section (dL) (m)
HLX01	100.00	0.00	100.00	Pumptest	~100	–
HLX02	132.00	0.00	132.00	Airlift test	~100	–
HLX03	100.00	0.00	100.00	Pumptest	~100	–
HLX04	125.00	0.00	125.00	Airlift test	~100	–
HLX05	100.00	0.00	100.00	Airlift test	~100	–
HLX06	100.00	0.00	100.00	Airlift test	~100	–
HLX07	100.00	0.00	100.00	Pumptest	~100	–
HLX08	40.00	0.00	40.00	Airlift test	~40	–
HLX09	151.00	0.00	151.00	Airlift test	~150	–

**Table 3-8. Hydraulic tests performed in KLX01. ((1): continuous logging, (2): secup last section).**

Borehole	Borehole length (m)	Tested part of bh, Secup (m)	Tested part of bh, Seclow (m)	Type of test performed	Test scale (L) (m)	Step length for moving measured section (dL) (m)
KLX01	1078.00	106.00	691.00 (688 (2))	Injection tests	3	3
		103.00	702.11 (673 (2))	Injection tests	30	30
		701.00	808.00	Airlift test	~100	–
		806.00	929.00		~100	
		926.00	1077.99		~150	
		701.00	1077.99		~300	
		0.00	702.11	Pumping test	700	–
		101.75	465.75	Flowlogging – Spinner	–	1.00
		700.05	1070.00	Flowlogging – UCM	–	0.05 (1)

**Table 3-9. Hydraulic tests performed in KLX02. ((1): secup last section).**

Borehole	Borehole length (m)	Tested part of bh, Secup (m)	Tested part of bh, Seclow (m)	Type of test performed	Test scale (L) (m)	Step length for moving measured section (dL) (m)
KLX02	1700.50	798.00	1101.50	Airlift test	~300	–
		1427.00	1700.50		~300	–
		0.0	76	Pumping test	~100	–
		0.0	142		~100	–
		0.0	200		~200	–
		0.00	205.00		~200	–
		207.00	505.00		~300	–
		505.00	803.00		~300	–
		805.00	1103.00		~300	–
		1103.50	1401.50	~300	–	
		201.00	1700.50		1500	–
		205.92	1399.92 (1396.92(1))	Flowlogging – Posiva Flow Log	3	3
		200.50	1440.50	Flowlogging – UCM	–	0.1

### **Observations during drilling**

During drilling, observations (judgements) of possible inflows and increased fracturing were made in some percussion boreholes.

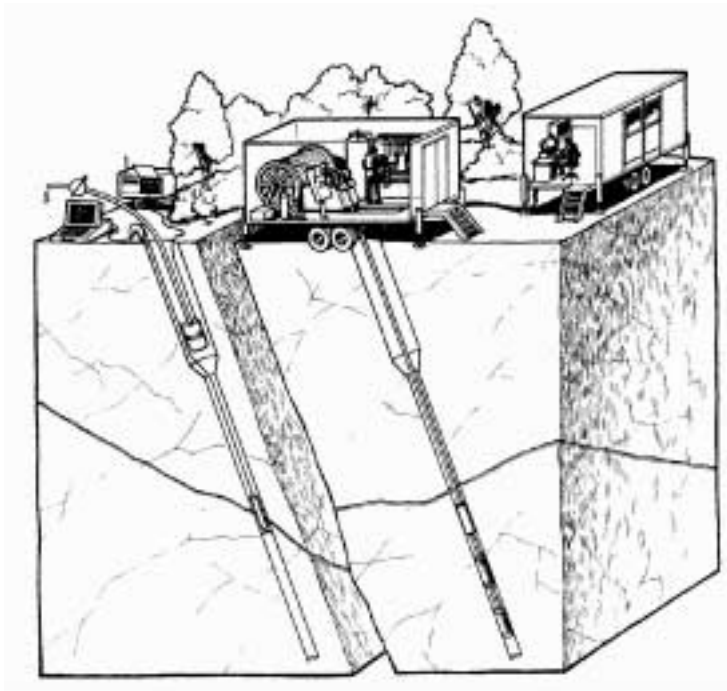
### **Flow logging, spinner**

Flow logging with spinner gives the cumulative water velocity along the borehole by measuring the rotation speed of a propeller. Flow logging can be made in a borehole during pumping or without pumping. Pumping gives possibilities to estimate the transmissivity distribution along the borehole if also a transmissivity value is available for a borehole section that has been flow logged. Generally is the procedure that the pumping for flow logging is also used as a pump test. If no pumping is made the flow logging shows the natural circulation in the borehole. Smaller anomalies cannot be measured with spinner due that the lower measurement limit is rather high. The advantage is that it is a fast method and that the upper measurement limit is rather high.

Flowlogging with a probe of spinner type was performed in KLX01, for 1 m intervals between 101.75–465.75 metres during the test pumping of the borehole. Data are recorded in counts per 10 seconds /Nilsson, 1989/.

### **Flow logging, UCM**

The measurement technique of the water flow rate in the UCM flow logging probe is estimated based on the velocity of sound in the flowing water. Otherwise the method is similar to spinner, see above.



*Figure 3-26. Flowmeter logging (left) is a method where the cumulative flow velocity change along the borehole is measured (spinner or UCM) or flow rate change within a defined test section is measured (Posiva Flow log).*

Continuous flow logging with the UCM flow probe was performed as a test in KLX01 in the interval 700.05–1070.00 m /Niva, 1991/ with or without pumping resulting in flow, temperature, resistivity and salinity. Logging was also made for KLX02 in the interval 200.50–1440.50 m, but for this test flow was not documented. A sketch of flow rate distribution for this test is presented in /Follin, 1996/.

### **Flow logging, Posiva Flow log (PFL)**

The Posiva Flow log /Rouhiainen, 2000/ is based on pulse transit time of a thermal pulse for small flows (0.1–10 ml/min) and thermal dilution rate for high flows (2–5000 ml/min). The method measures changes of flow along the borehole rather than the cumulative flow. The flow rate is measured in a test section (equal to test scale, L) limited by assemblies of soft rubber discs. The test section is moved in steps with step length dL. In this case the so-called “Sequential flow logging” mode (Test scale (L) = step length (dL)) was used to obtain hydraulic conductivity and fresh water head of the formation. When using a “Overlapping flow logging” mode (Test scale (L) > step length (dL), generally dL may be 0.1 m and L may be 1m) the aim is to determine the exact depth of fractures or fractures zones. The flow logging is performed with or without pumping.

Measurements with the Posiva Flow Log was included in the testing of KLX02 and the data set analysed contains hydraulic conductivities for 3 m section lengths (Test scale (L) = step length (dL)) in the interval 207.42–1398.42 m, see Table 3-9 /Rouhiainen, 2000/. Besides the flow, the electrical conductivity (EC) of groundwater was also measured.

Different drawdowns, test scales and step lengths were used in a second test campaign in borehole section 200–400m in KLX02 /Rouhiainen, 2000/ but these data has not been used in this report. Based on the data in borehole section 200–400m a correlation study between borehole TV- and radar images and difference flow logging results has also been made /Carlsten et al, 2001/. In this test the test scale 0.5 m with step length of 0.1 m was used for the evaluation. These results have not been used in this report. The details of the test of the Posiva Flow Logging in borehole section 200–400 m in KLX02 is presented in /Ludvigson et al, 2001/. Different drawdowns, test scales and step lengths were used and evaluated.

### ***Injection tests, test scale 3 m***

Hydraulic injection tests were made in borehole KLX01 in 3 m sections /Nilsson, 1989/ in the interval 106.00–691.00 m, see Table 3-8. For these tests a constant water pressure above the hydrostatic pressure was applied in the sections. Injection time and time for measurement of recovery are presented in Table 3-11. The total volume of water was measured by a flow meter. The location of sections along the borehole can possibly deviate about 1.2% /Follin et al, 2000/ in relation to true depth, due to tension in the measurement equipment (Umbilical Hose System) in long boreholes.

Tests were evaluated at transient conditions and the semilogarithmic approximation by /Cooper and Jacob, 1946/ was used to obtain section transmissivities. The elasticity of the hose (Umbilical Hose System) makes it questionable if the low flow rates are reliable. The possibilities to use the specific capacity when low flow rate have been measured to estimate the transmissivity in cases where the transient response does not indicate a clear radial flow is thus questionable. In this report the data in /Nilsson, 1989/ is used. Figure 3-28 presents an overview of the hydraulic conductivities for the 3 m sections along the borehole. (In Appendix 2 in /Rhén et al, 1997/ the specific capacity was used to estimate the hydraulic conductivity (K) for some sections and the low K-values should according to the above discussion be considered uncertain.)

### ***Injection tests, test scale 30 m***

In borehole KLX01, hydraulic injection tests were performed in 30 m sections /Nilsson, 1989/ in the interval 103.00–643.00 m, see Table 3-8. Pressure, injection time and measurements of pressure drop from injection stop are shown in Table 3-11. Evaluation was based on transient conditions and the semilogarithmic approach presented in /Cooper and Jacob, 1946/. The location of sections along the borehole can possibly deviate about 1% to the measurement equipment (Umbilical Hose System) in long boreholes. Figure 3-28 shows an overview of the resulting hydraulic conductivities related to the borehole length.

### ***Airlift tests***

Several boreholes at Laxemar were tested using airlift tests. These boreholes are the cored boreholes KLX01 (Table 3-8, /Rhén et al, 1991/) and KLX02 (Table 3-9, /Follin, 1993/). Further, airlift tests were performed in the percussion boreholes HLX02 and HLX04–06 /Nilsson, 1988/ and HLX08–09 /SKB, 1992/ see Table 3-6. The percussion boreholes HLX08–09 were mainly drilled with the intention to intersect the fracture zones ZLXNE06 and ZLXNE01 (NE1 and EW5 respectively in /Rhen et al, 1997/). When using airlift technique, the drawdown phase is commonly of lower quality than for a pumping test. There are no reported tests in HLX10–12.

According to /Nilsson, 1988/ a value of the specific capacity can be estimated using the total depth of the borehole and the measured flow. For HLX02 and HLX04–06 the specific capacity was calculated using the water filling up period from dry borehole.

In KLX01, airlift pumping was performed for a period of up to about 6 hours (Table 3-11) and the transmissivity was evaluated for sections 701.00–808.00 and 926.00–1077.99 m based on data from the recovery period and the semilogarithmic approximation /Cooper and Jacob, 1946/. Specific capacity only was obtained for section 806.00–929.00 m. In section 701.00–1077.99 in the same borehole, the hydraulic properties were estimated from the recovery phase. Estimated hydraulic conductivities related to borehole length for the airlift tests in KLX01 and KLX02 are presented in Figure 3-28 and Figure 3-29. Figure 3-27 shows the results for the percussion boreholes.

### **Pumping tests**

Pumping tests were performed in percussion boreholes HLX01, HLX03 and HLX07 /Nilsson, 1988/. “Pumping tests” also include test and rinse pumping and short pumping tests. For HLX01, transmissivity was evaluated from the recovery plot and for HLX03 and HLX07 both drawdown and recovery curves were used for analyses. Besides the tests in these percussion boreholes, a number of sections in KLX01 /Nilsson, 1989/ and KLX02 /Follin, 1993, 1996/ were also tested. For KLX02 two of the tests were performed as interference tests. The resulting hydraulic conductivities along the boreholes are compiled in Figure 3-29. The upper and lower sections of the tests are shown in Table 3-7 to Table 3-9.

**Table 3-10. Test data for hydraulic tests performed HLX boreholes.**

<b>Borehole</b>	<b>Tested part of bh, Secup (m)</b>	<b>Tested part of bh, Seclow (m)</b>	<b>Type of test performed</b>	<b>Pressure/ Draw down</b>	<b>Flow rate</b>	<b>Flow period (1)</b>	<b>Recovery period (1)</b>
HLX01	0.00	100.00	Pumptest	21.8 m	78 L/min 122.3 L/min (2)	29 hours 43 hours	~24 hours
HLX02	0.00	132.00	Airlift test	–	–	–	–
HLX03	0.00	100.00	Pumptest	42.5 m	4.3 L/min 5.9 L/min (3)	26 hours 22 hours	~5 hours
HLX04	0.00	125.00	Airlift test	–	–	–	–
HLX05	0.00	100.00	Airlift test	–	–	–	–
HLX06	0.00	100.00	Airlift test	–	–	–	–
HLX07	0.00	100.00	Pumptest	17.6 m	24.4 L/min	29 hours	~18 hours
HLX08	0.00	40.00	Airlift test	14.3 m	$3.28 \times 10^{-3} \text{ m}^3/\text{s}$	–	–
HLX09	0.00	151.00	Airlift test	56.4 m	$2.82 \times 10^{-3} \text{ m}^3/\text{s}$	–	–

(1) Some estimated from graphs.

(2) Increased after 29 hours.

(3) Increased after 26 hours.

**Table 3-11. Test data for hydraulic tests performed in KLX01.**

Borehole	Tested part of bh, Secup (m)	Tested part of bh, Seclow (m)	Type of test performed	Pressure / Drawdown	Flow rate	Flow period (3)	Recovery period (3)
KLX01	106.00	691.00 (688 (2))	Injection tests (3m scale)	200 kPa	–	10 min	10 min
	103.00	702.11 (643 (2))	Injection tests (30 m scale)	200 kPa	–	120 min	120 min
	701.00	808.00	Airlift test		1026 l/h	~4 hours	~1 hour
	806.00	929.00		53 l/h	1–3 hours	~1 hour	
	926.00	1077.99		700 l/h	~5.5 hours	~1 hour	
	701.00	1077.99		Max 46.9 m	1359 l/h	60 hours 12 min	~1200 min
	0.00	702.11	Pumping test	Max 30.9 m	148 L/min	41 hours	~3 hours
	101.75	465.75	Flow logging – Spinner	–	–	–	–
	700.05	1070.00	Flow logging – UCM (1)	≤ 72 m	17.3 L/min	–	–

(1) Continuous logging.

(2) Secup last section.

(3) Some estimated from graphs.

**Table 3-12. Test data for hydraulic tests performed in KLX02.**

Borehole	Tested part of bh, Secup (m)	Tested part of bh, Seclow (m)	Type of test performed	Pressure/ Drawdown	Flow rate	Flow period (5)	Recovery period (5)
KLX02	798.00	1101.50	Airlift test		$2.2 \times 10^{-4} \text{ m}^3/\text{s}$	600 min	120 min
	1427.00	1700.50		$2.1 \times 10^{-4} \text{ m}^3/\text{s}$	600 min	120 min	
	0.0	76	Pump test (2)	22 m	2400 L/h	100 min	60 min
	0.0	142	(2)	60 m	6900 L/h	465 min	105 min
	0.0	200	(2)	68 m	9045 L/h	475 min	120 min
	0.00	205.00	(3)	80 m	8000 L/min	2500 min	1400 min
	207.00	505.00	(4)		38 L/min	12 hours	12 hours
	505.00	803.00	(4)		4.9 L/min	15 hours	15 hours
	805.00	1103.00	(4)		9.0 L/min	864 hours	855 hours
	1103.50	1401.50	(4)		1.6 L/min	48 hours	47 hours
	201.00	1700.50	(4)		$3.0 \times 10^{-3} \text{ m}^3/\text{s}$	118100 min	21600 min
	205.92	1399.92 (1396.92 (1))	Flow logging – Posiva Flow Log	6.2 and 22m	–	–	–
	200.50	1440.50	Flow logging – UCM	–	$2.95 \times 10^{-3} \text{ m}^3/\text{s}$	–	–

(1) Secup last section.

(2) Test in percussion borehole with diameter 165 mm.

(3) Test in percussion borehole with diameter 215 mm.

(4) Test in core hole borehole with diameter 76 mm.

(5) Some estimated from graphs.



### 3.7.2 Interpretation of single hole tests

#### Percussion boreholes

Figure 3-27 shows the evaluated mean hydraulic conductivity for the percussion boreholes.

#### Cored boreholes – overview

Based on the flowlogging and the airlift test performed in the interval 700.50–1077.99 m of borehole KLX01, transmissivities related to the largest flow anomalies were estimated (referred to as a spinner survey in /Rhén et al, 1991/). This was made under the assumption that the bedrock is built up by parallel water conductors and that the transmissivity for each single conductor is proportional to the water inflow /Earlougher, 1977/. Based on the four anomalies, identified at 719–720 m, 737–738.5 m, 758–760 m, and 932–934 m, and the airlift test in section 701.00–1077.99 m ( $T = 1.2 \times 10^{-5} \text{ m}^2/\text{s}$ ), transmissivities of about  $1 \times 10^{-5}$ – $1 \times 10^{-6} \text{ m}^2/\text{s}$  were estimated.

Hydraulic conductivities along the boreholes for the tests presented above are compiled in Figure 3-28 and Figure 3-29. In Appendix B4 a more detailed view of the tests with a test scale less or equal to 30 m is shown. The fracture frequency presented in the figures includes estimated number of fractures for borehole section mapped as “crush” (based on number of mapped rock pieces in a section defined as “crush”. A section is defined as “crush” when the rock pieces are so small and crushed that they cannot be fitted together to orient the core) but in sections mapped as “core loss” no fractures are assumed. In Section 3.4 the fracture frequency of 40 fractures/m was used to estimate a possible (high) number of fractures in a borehole section mapped as “crush” and in sections mapped as “core loss” no fractures were assumed. Therefore above figures differ slightly from those in Section 3.4. The interpreted possible fracture zones in Section 3.4 are also plotted in Figure 28 and Figure 3-29.

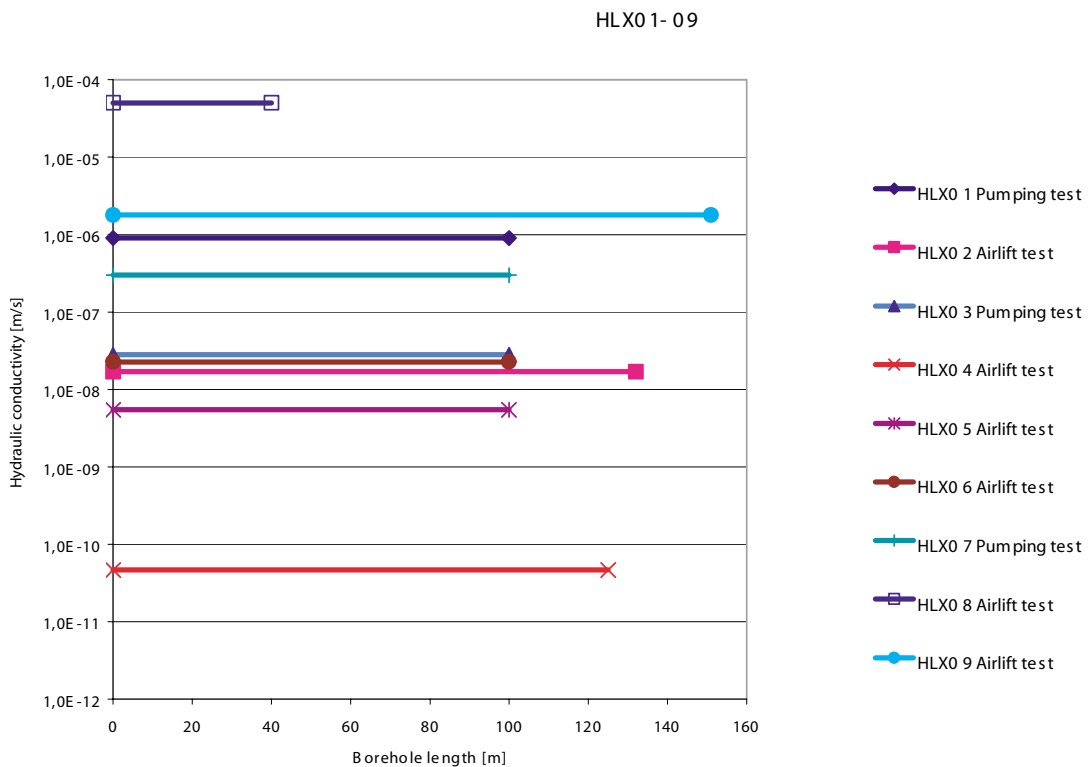
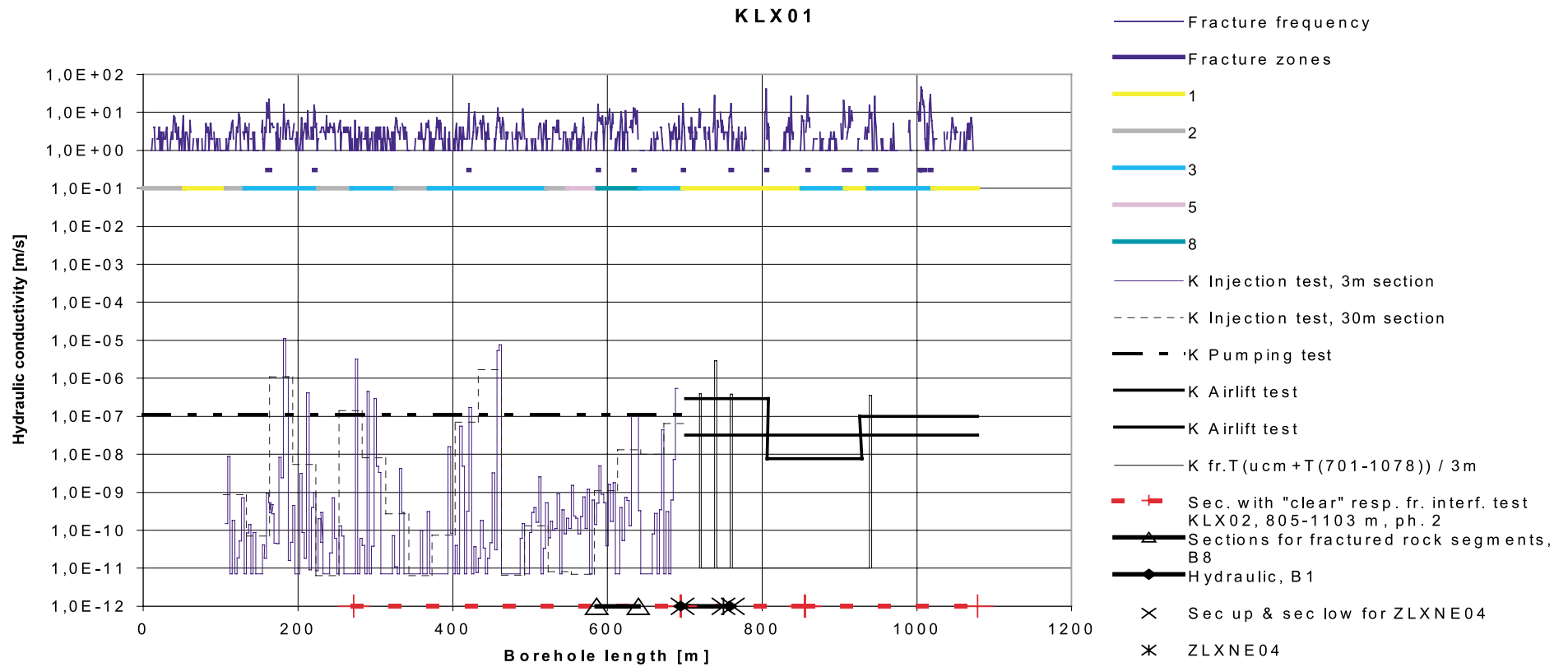
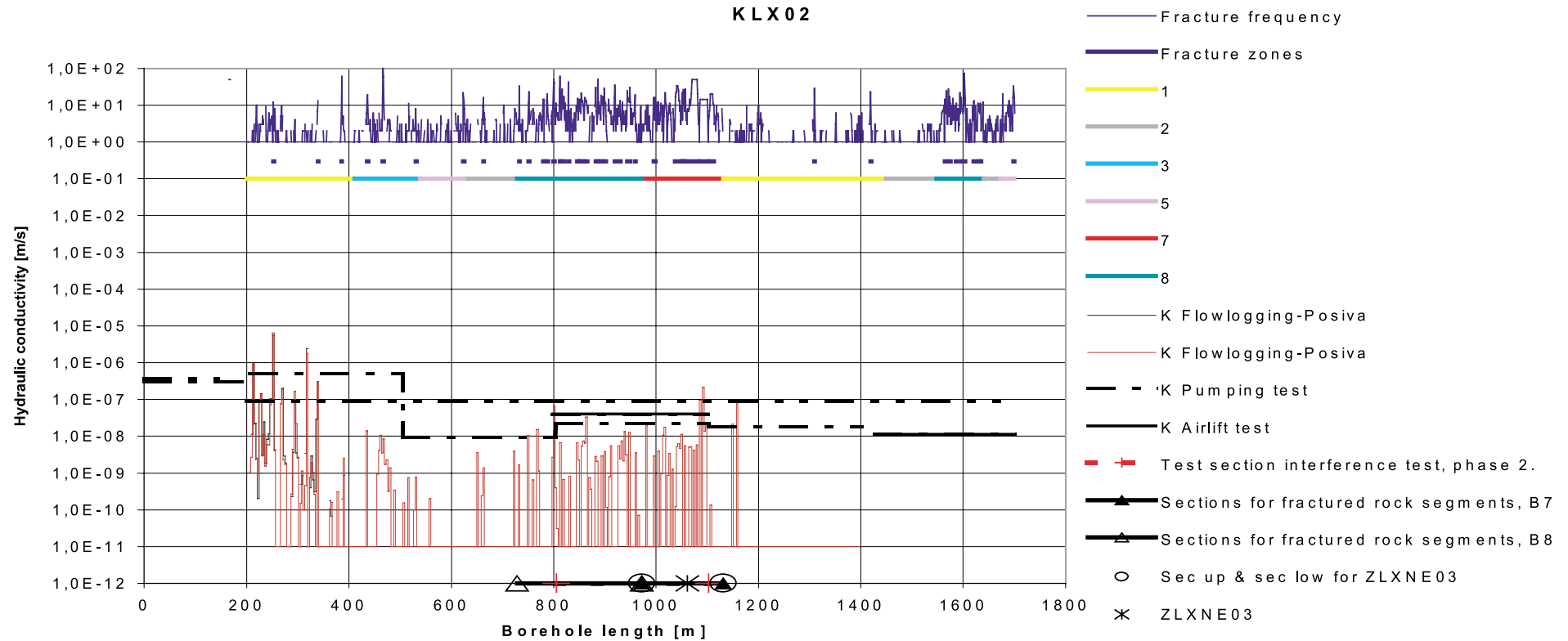


Figure 3-27. Hydraulic tests and estimated hydraulic conductivity for HLX boreholes.



**Figure 3-28.** Hydraulic tests and estimated hydraulic conductivity for KLX01. Fracture frequency in the figure includes borehole sections mapped as “Crush” and No of fractures in Crush sections are based on mapped pieces. “Fracture zone” is defined in Section 3.4 and is based on a fracture frequency > 10 fractures/m. The “rock segments” in the figure has number 1 to 8 according to Section 3.4. K(injection test) is based on transient condition.



**Figure 3-29.** Hydraulic tests and estimated hydraulic conductivity for KLX02. Fracture frequency in the figure includes borehole sections mapped as “Crush” and No of fractures in Crush sections are based on mapped pieces. “Fracture zone” is defined in Section 3.4 and is based on a fracture frequency > 10 fractures/m. The “rock segments” in the figure has number 1 to 8 according to Section 3.4. K(Flow logging-Posiva) is based on stationary condition.

Univariate statistics of all data from the testing of the cored and percussion boreholes are compiled in Table 3-13. The analysis of the distribution was made manually by fitting a line in a diagram for normal distribution of  $\text{Log}_{10}(K)$ . In KLX01 the measurement limit was set to  $7 \cdot 10^{-12}$  m/s in /Nilsson, 1988/. For the data from KLX02, where a large number of data are censored below the measurement limit, the resolution of flow measurements is better in the upper part of the borehole than in the lower part. Measurements below approximately 1100 m might be disturbed due to an increased salt concentration and/or clay particles in the water. A slight increase in noise level is observed already at 750 m and a distinct increase is seen at approximately 1100 m, see /Rouhiainen, 2000/. To improve the analysis, the measurement limit for the hydraulic conductivity is suggested to be approximately  $10^{-9}$  m/s, or possibly  $10^{-10}$  m/s down to approximately 800 m followed by  $10^{-9}$  m/s further down. In the analysis  $10^{-9}$  m/s is used as measurement limit.

### **3.7.3 Correlation between hydraulics and geology**

The hydraulic interpretation of the tests in the cored boreholes can be compared with the single hole geological interpretation described in Section 3.4. Of particular interest is any evidence of correlation between high permeability and potential fracture zones, or evidences of correlation between permeability and different rock segment types.

As mentioned previously, the correct depth of the measurements of the hydraulic conductivity in KLX01 may differ 1.2% from the core mapping due to tension in the equipment. Due to this fact correlation studies may be questionable in KLX01. This is of course valid for the below shown correlations.

#### ***Correlation with different geological logs***

The detailed measurements with test scale 3 m (injection tests and Posiva Flow Log) can be used to study if there exists any correlation between the hydraulic conductivity and any of the different geological logs along the boreholes. Such correlation studies may e.g. concern mapped rock type, rock contacts or rock veins or fracture frequency, but have not been conducted within this study.

In /Follin et al, 2000/ it is mentioned that boreholes with larger proportions of fine-grained granite show higher mean hydraulic conductivities. In /Rhén and Forsmark, 2000/ it was found that for core boreholes on Äspö, test sections including larger proportions of Fine-grained granite show a significant higher hydraulic conductivity.

The frequency of rock contacts or certain types of rock contacts can possibly be correlated to the hydraulic conductivity. Frequency of rock veins (Borehole section of one rock type with length less than 1 m and not considered to be fracture-filling mineral. In principal mapped "vein" is thus an indication smaller-scale rock contacts) can also possibly cause differences in hydraulic properties. However, for core boreholes on Äspö, /Rhén and Forsmark, 2000/ found no strong general correlation between existence of a rock contact or vein, but there was some correlation when fine-grained granite was one of the rock types in the rock contact or the vein was fine-grained granite. However it was also noted that it was difficult to be conclusive due to the test section scale and different methods for measurements.

In /Follin et al, 2000/ it was not found any clear evidences that increased fracturing (excluding what was defined as fracture zone) was correlated to changes in hydraulic conductivity.

### **Correlation with interpreted Rock Segments**

The potential correlation between hydraulic properties and the rock segments may be judged by visual inspection of Figure 3-28 and Figure 3-29. The fracture frequency in the figures includes borehole sections mapped as “Crush” and number of fractures in Crush sections are based on mapped pieces. “Fracture zone” is defined in Section 3.4 and is based on a fracture frequency > 10 fractures/m. The “rock segments” in the figure have number 1 to 8 according to Section 3.4. K(Flow logging-Posiva) is based on a stationary condition.

It is not obvious that there exist any correlation between the identified rock segments along the borehole in Section 3.4 and the measured hydraulic conductivity. In KLX02 there seem to be some correlation between high hydraulic conductivity and rock segment type 3 (single lithology, high alteration, low fracture frequency) above 700 m. But looking just on the fracture frequency in rock segment type 3 above 700 m indicate that there are short parts with high fracture frequency that partly correlate to high hydraulic conductivity. In this study no estimates of statistical distributions of the hydraulic conductivities (K) in the test scale 3 m have been made for the different rock segments.

### **Correlation with interpreted Possible Fracture Zones**

As indicated in Figure 3-28 and Figure 3-29 the possible fracture zones from Section 3.4 correlate rather well with high hydraulic conductivity. However, it is also evident that there exist permeable features outside these potential zones.

In this study no estimate of statistical distributions of the hydraulic conductivities (K) in test scale 3 m have been made for the possible fracture zones (i.e. fracture frequency  $\geq 10$  per m, including estimated fracture frequency, 40 fracture/m, for crush) and the rock outside these zones.

Sections of the core been mapped as “crush” may indicate larger and heavily fractured features that potentially have high permeability. A previous study /Follin et al, 2000/ estimated the statistical distributions of the hydraulic conductivities (K) in test scale 3 m for the borehole sections mapped as “crush”. The study indicated that the geometric mean K was 10–30 larger for “fracture zones” compared to the rest on the rock in KLX01 and KLX02, but the definition of fracture zone in /Follin et al, 2000/ was related to mapped crush and thus somewhat different compared to this study.

In /Rhén and Forsmark, 2000/ it was found that for core boreholes on Äspö, less than half of the High Permeability Features (HPF,  $T > 10^{-5}$  m<sup>2</sup>/s) could be found where crush was mapped and the rest in borehole sections with one or a few fractures. About 50% of the HPF:s were found where the core holes intersected the deterministically defined fracture zones. This indicated the presence of large features with fairly high transmissivities that should be modelled stochastically.

**Table 3-13. Univariate statistics KLX and HLX holes.**

Borehole	Secup	Seclow	Test scale	Meas. limit	Sample size	Hydraulic conductivity (K)		
	(m)	(m)	(m)	(m/s)		Mean (Log10(K) (m/s))	Median (Log10(K) (m/s))	Std (Log10(K) (m/s))
KLX01	106	688	3	$7 \cdot 10^{-12}$	197	-10.5	-	1.75
KLX02	207	1398	3	$10^{-9}$	398	-10.3	-	1.6
KLX02	207	800	3	$10^{-9}$	198	-10.5	-	1.7
KLX01	103	702	30	$7 \cdot 10^{-12}$	20	-8.94	-9.01	1.80
KLX02	0	1700	205-298	-	6	-7.37	-7.70	0.76
KLX02	500	1700	273-298	-	4	-7.85	-7.85	0.17
HLX 01-09	0	< 150	40-151	-	9	-7.13	-7.55	1.73
HLX 01-09 + KLX02 (depth 0-205m)	0	< 205	40-205	-	10	-7.07	-7.04	1.64
HLX 01-09 + KLX02 and KLX01	0	(1700)	40-300	-	18	-7.22	-7.60	1.29

### 3.8 Fracture Statistical Model

According to the programme /SKB, 2001/ fractures and local minor fracture zones could only be described in a statistical fashion. This section evaluates the available fracture and lineament data as well as connected flow data and performs statistical analyses.

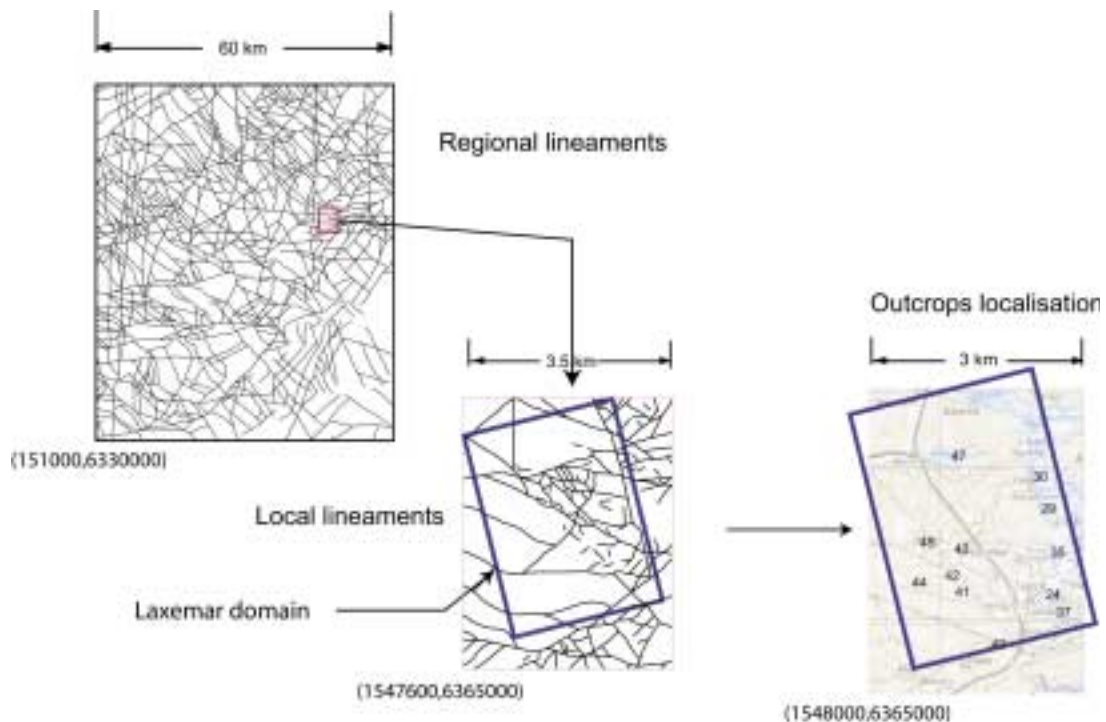
#### 3.8.1 Input fracture and flow data

Fracture data from the area exist in different scales and have different origins. The available and used fracture data in the Laxemar domain were:

- Fracture mapping in boreholes KLX01 and KLX02 as specified in Section 3.4. Data used for the fracture analysis are fracture orientation (KLX01), fracture locations (KLX01 and KLX02), and fracture flow (KLX01 and KLX02).
- Fracture traces mapped in 12 outcrops in the Laxemar /Ericsson, 1987/. Fracture orientation, trace lengths data and termination information have been used in the analysis.

Lineament maps at local and regional scale as specified in Section 3.2.

The maps provided support for analysis of lineament orientation and fracture size. The relation between regional, local and outcrop scales is shown in Figure 3-30.



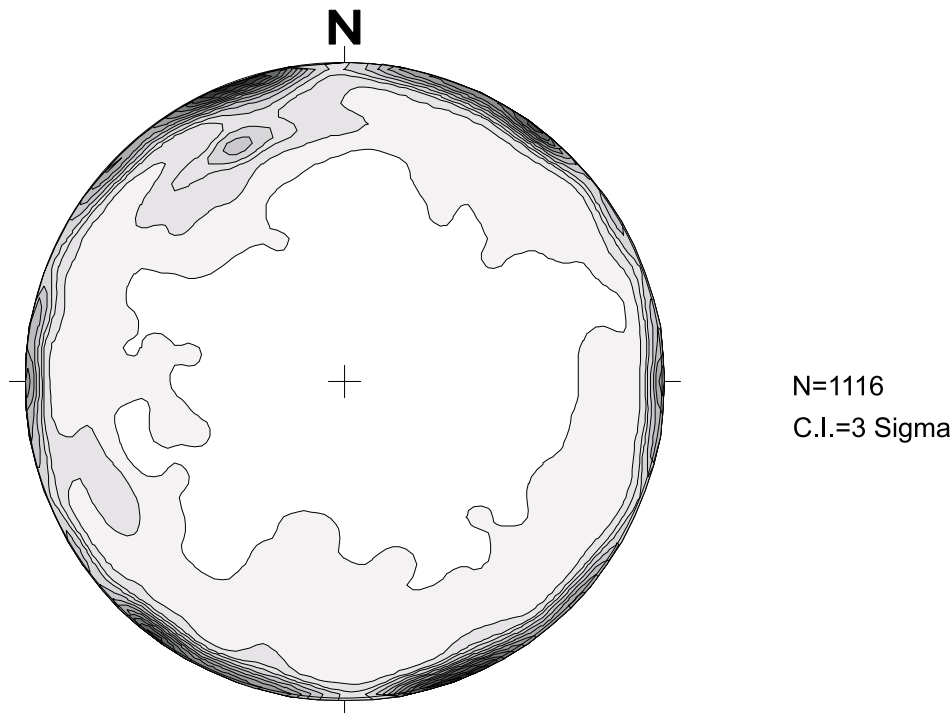
*Figure 3-30. Localisation and representation of the different mapping scales.*

### **3.8.2 Fracture orientation distributions based on outcrop fracture data**

Of the outcrops studied by /Ericsson, 1987/, twelve are located in the Laxemar domain. The denotations of those outcrops are PSM24, 29, 30, 35, 37, 40, 41, 42, 43, 44, 45 and 47, cf. Figure 3-30. Fracture data from these 12 outcrops were plotted on an equal area lower hemisphere projection, illustrated in Figure 3-31. At least three dominating fracture orientations are visible in the stereo plot, striking NS, WNW and ENE. All three are steeply dipping.

The fracture orientation distribution has been studied for each outcrop separately to illustrate the potential different fracture patterns, see Figure 3-32. The total numbers of analysed fractures are over eleven hundred, but the individual amount of fractures for each outcrop is highly variable. Some of the outcrops can be distinguished:

- Outcrop 37 is quite different from the other outcrops, with more gently dipping fractures.
- Outcrops 40, 43 and 44 exhibit mainly one dominating set of fractures, striking ENE.



**Figure 3-31.** Lower hemisphere projection of poles to fracture planes of all outcrops in the Laxemar domain (after /Ericsson 1987/).

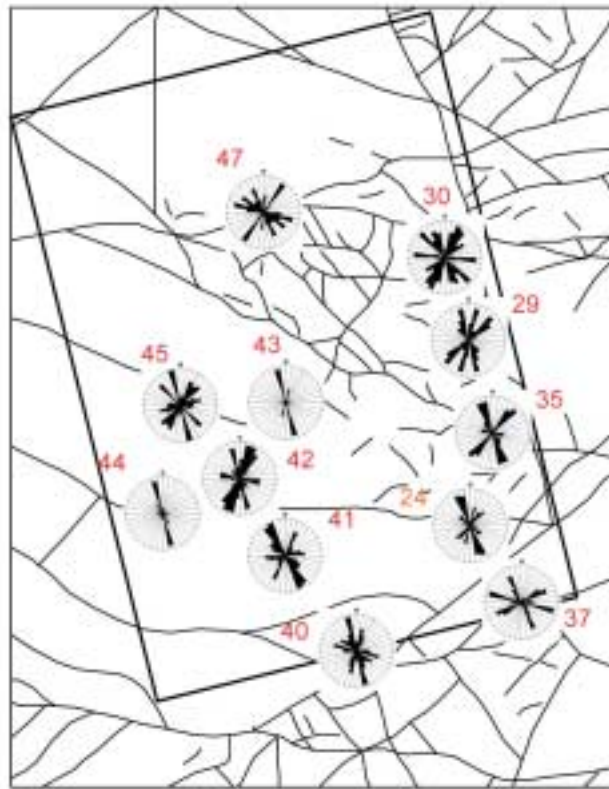
The ISIS (Interactive Set Identification System) module in FracMan was used for the fracture set identification /Dershowitz et al, 1995/. The fracture sets were defined as groups of fractures with similar properties including orientation, termination, infilling and mineralisation.

ISIS used an adaptive, probabilistic, pattern recognition algorithm. The user selects the characteristics and relative significance to be used for the allocation of fractures to fracture sets.

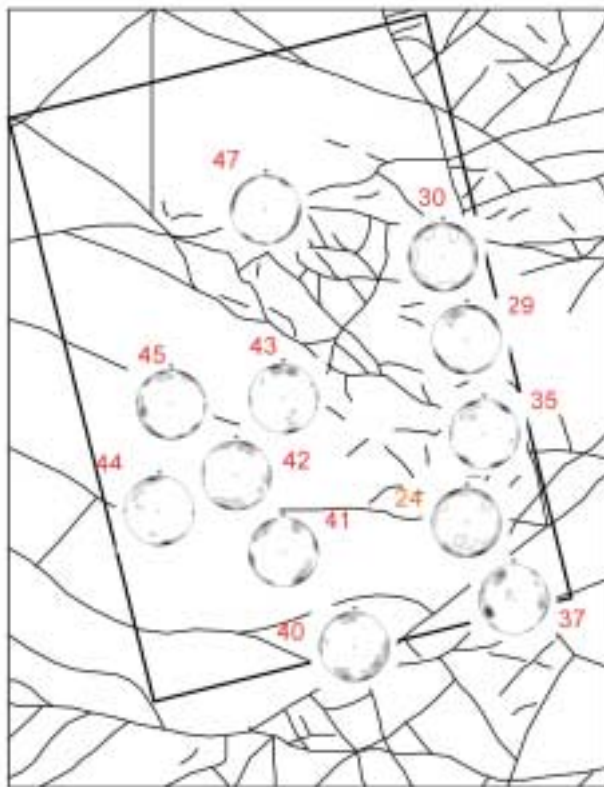
An initial estimation of the characteristics of each set is computed. The algorithm calculates the distribution of properties for the fractures assigned to each set, for each new realisation re-assigns fractures to sets according to a probability based upon the similarity of fractures to set characteristics. The properties of the sets are then recalculated and the process is repeated until the set assignment is optimised.

An initial estimation of three fracture sets in ISIS, based on the major clusters observed in Figure 3-31, gave the results shown in Table 3-14. The point projection of the poles to fracture planes of the different sets is illustrated in Figure 3-33. It should be noticed that the plot is not weighted, indicating that fractures having same strike and dip will appear as a single point.





a)

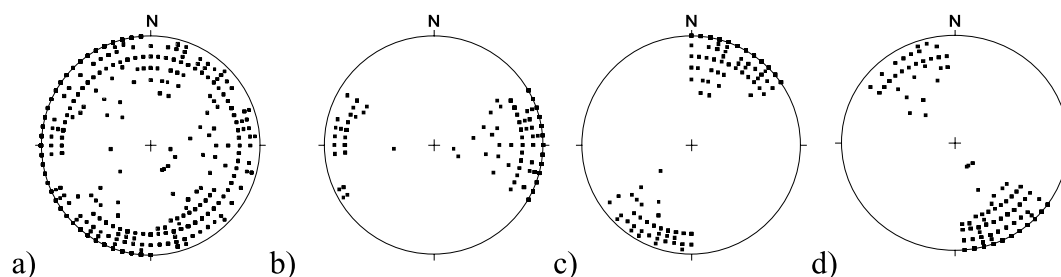


b)

**Figure 3-32.** a) Rosettes of poles to fracture planes; b) Contouring of poles to fracture planes,  $K=100$ ,  $C.I.=3\sigma$ . Outcrop data is set in geographical relation to the lineaments in the Laxemar domain.

**Table 3-14. Fracture sets derived from ISIS, from outcrops data.**

<b>Fracture set 1</b>		
Number and% of fractures	286	26.24
Orientation (pole trend, pole plunge)	89.2	3.6
Fisher K	12.47	
<b>Fracture set 2</b>		
Number and% of fractures	361	33.12
Orientation (pole trend, pole plunge)	206.9	0.3
Fisher K	16.89	
<b>Fracture set 3</b>		
Number and% of fractures	443	40.64
Orientation (pole trend, pole plunge)	151.6	4.1
Fisher K	15.27	

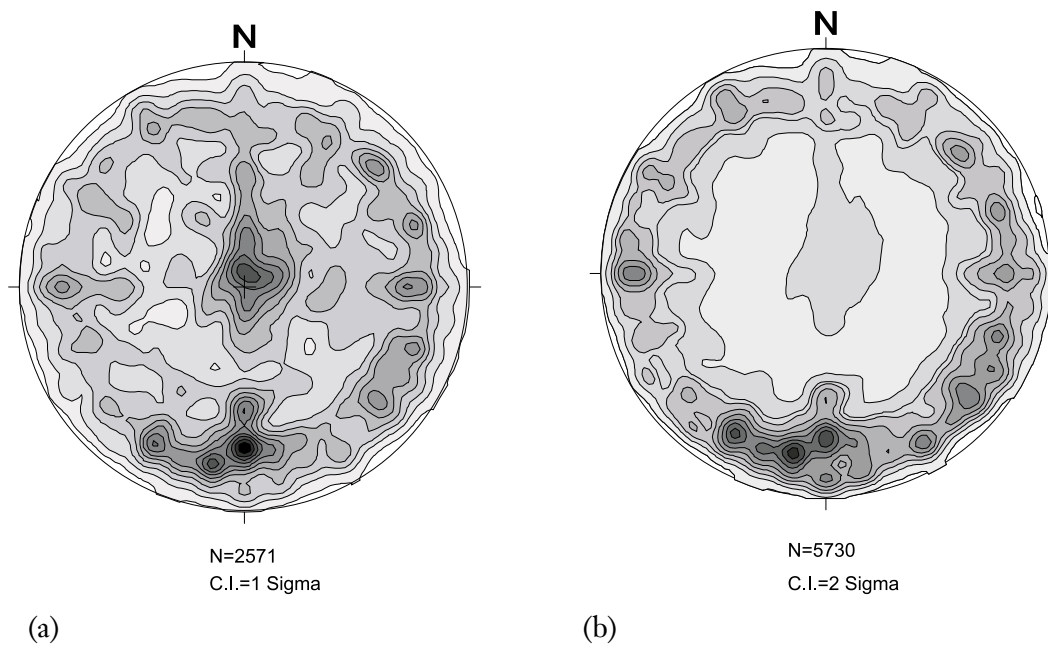


*Figure 3-33. Point plot of poles to fracture planes for sets derived from ISIS analysis; a) original data b) set 1, c) set 2, d) set 3.*

### 3.8.3 Fracture orientation distribution based on fracture data from KLX01

Fracture data from the boreholes KLX01 and KLX02 are not complete. Fracture orientations exist for KLX01 below the first 200 m down to the bottom of the borehole. KLX02 has partly, in several different sessions, been investigated by BIPS and parts of the material has been mapped but has not been entered into SICADA. Only fracture data from KLX01 were used in the orientation analysis.

The poles of the fractures measured in the borehole were plotted on an equal area lower hemisphere projection. The contour intervals, as calculated by the conventional angle on hemisphere method, are illustrated in Figure 3-34a. The plot shows at least 2 fracture sets, 1 subhorizontal, and one oriented EW steeply dipping. The importance of subhorizontal fractures might be overestimated because of the sampling bias induced by the orientation of the borehole, which is almost subvertical. To overcome this problem, a Terzaghi orientation correction was made on the values, using a maximum correction factor of 5. The selection of the correction factor is based on previous experience from /LaPointe et al, 1995/. The plot obtained, presented in Figure 3-34b, illustrates that there are at least 3 steeply dipping fracture sets, striking NS, WNW and NE and one subhorizontal set.

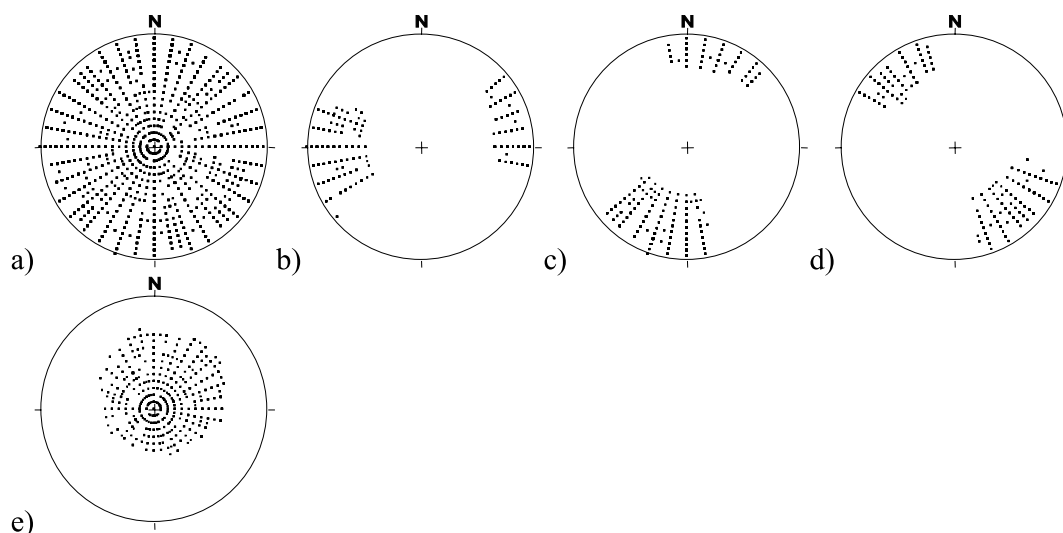


**Figure 3-34.** Lower hemisphere projection of poles to fracture planes in KLX01 a) without Terzaghi correction, b) with Terzaghi correction.

From the Terzaghi corrected stereonet plot of poles to fracture planes, an initial estimation for the orientation of the four fracture sets was made and analysed with ISIS. The results of the analysis are given in Table 3-15.

**Table 3-15. Fracture sets derived from ISIS, from borehole KLX01 Terzaghi corrected data.**

<b>Fracture set 1</b>		
Number and % of fractures	1427	24.9
Orientation (pole trend, pole plunge)	262	3.8
Fisher K	8.52	
<b>Fracture set 2</b>		
Number and % of fractures	1837	32.06
Orientation (pole trend, pole plunge)	195.9	13.7
Fisher K	9.26	
<b>Fracture set 3</b>		
Number and % of fractures	1485	25.92
Orientation (pole trend, pole plunge)	135.9	7.9
Fisher K	9.36	
<b>Fracture set 4</b>		
Number and % of fractures	981	17.12
Orientation (pole trend, pole plunge)	35.4	71.4
Fisher K	7.02	



**Figure 3-35.** Point plot of poles to fracture planes for sets derived from ISIS analysis of KLX01Terzaghi corrected data; a) original data b) set 1, c) set 2, d) set 3; e) set 4.

The stereonet point plot for each fracture set as defined after analysis with ISIS is shown in Figure 3-35. The interpretation of Figure 3-35a is supported by the contours plot presented in Figure 3-34b.

The results from the ISIS analysis shows that the orientation of fracture sets are consistent between outcrops and borehole KLX01.

### 3.8.4 Size distribution of fracture traces

In this study fracture size is expressed as the equivalent radius of a disc. Fracture trace length is the length of a fracture when it intersects a sampling plane, i.e. an outcrop.

The fracture size distribution of the parent population (i.e. the actual fractures in the rock mass) can be estimated by analysing trace length data of fractures mapped on outcrops and from lineaments.

Data for each mapping scale have been analysed separately. Three sets of data are available; the outcrops /Ericsson, 1987/, the lineaments in the Laxemar domain presented in Section 3.2, and the regional lineament maps presented in the Oskarshamn feasibility study /Bergman et al, 2000/.

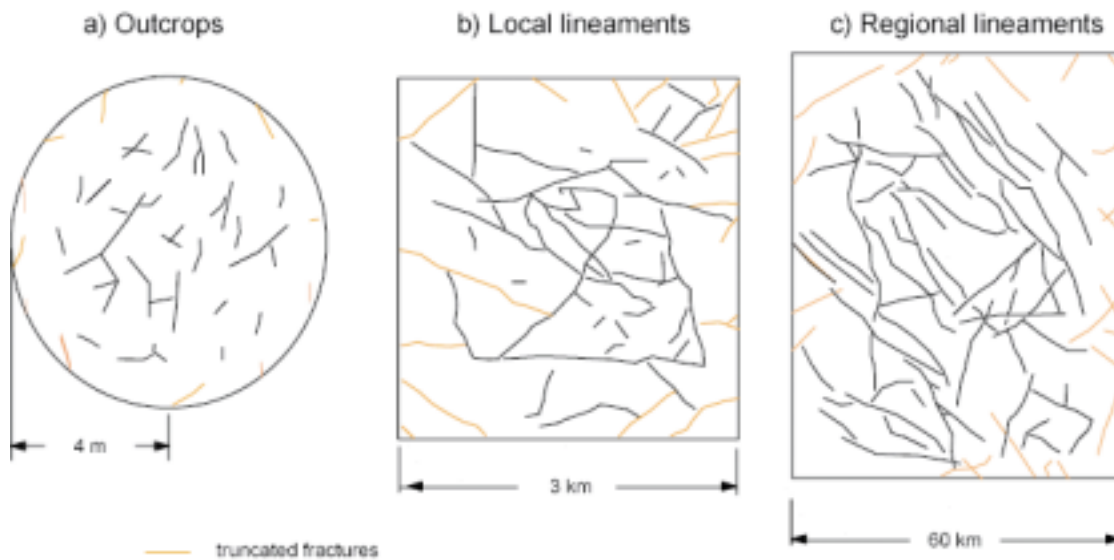
The distribution of the trace lengths is influenced by the truncation of the lineaments or fractures at the border of the mapping area. At the outcrop scale, two different length biases were identified. First, fractures have been mapped with an initial censoring level of 0.5 m. Secondly, fracture truncation occurs when fractures terminate against the border of the sampling window. Terminations of fractures on one or two sides to another fracture, and fractures overlaid and hidden by soil (on one or both sides) are identified and reported by /Ericsson, 1987/.

The size estimation method prescribed by /LaPointe et al, 2000b/ requires that fractures and lineaments that extend beyond the border of the mapping area, or into overlaying material, should be removed from the analysis. This is easily performed on lineament data at local and regional scales as there are trace maps showing the exact location of each lineament. The /Ericsson, 1987/ outcrop data sets are missing trace maps. However, raw data contains information of terminations' properties of fractures. Data for fractures with one or both end(s) overlaid/hidden by soils, or intersecting the outcrop's borders were removed from the data set in this study.

The size of truncated fractures is generally related to the size of the mapping area, see Figure 3-36. As a consequence, rejection of truncated fractures should not affect the distribution of trace lengths at a mapping scale. Retaining truncated fractures will mostly only affect the number of fractures identified in a delimited area. However, it cannot be excluded that the trace length distribution is biased in that the largest mapped fractures or lineaments are large in relation to the sampling window size. That might be the case if features cross the whole mapping area. In this case, if the truncated fractures are *not* removed, the mean trace length at this mapping scale would be overestimated.

The scaling properties of trace lengths have been approached by computation of the Complementary Cumulative Density Function (CCDF), for each fracture set at each mapping scale (Figure 3-37).

The fracture sets are those defined in Section 3.8.2, and their azimuthal ranges are presented in Table 3-16. The CCDF has been calculated for each set separately and then for the combined sets at a given scale, and the results are illustrated in Figure 3-37.



**Figure 3-36.** Visualisation of the effect of truncated fractures with regards to the mapping size. The outcrop map (a) is an illustration only as no such data exist for the /Ericsson, 1987/ data set. Lineament maps (b) and (c) illustrates the lineaments that have been removed from the data set.

**Table 3-16. Azimuthal ranges used for the fracture sets at different mapping scale.**

	Set number	Orientation	Azimuthal range
Outcrops	1	NW	90–160
	2	NS	160–210
	3	NE	30–90
Local	1	NE	0–60
	2	NW	110–180
	3	EW	60–110
Regional	1	NE	150–200
	2	NS	20–80
	3	EW	80–150

Analyses of CCDF at different scales showed that the best-fitted distribution to the trace lengths data is a Power law function. Hence, the probability that the trace length, X, is greater than x, P(X>x), is given by:

$$P(X > x) = G(x) = \left( \frac{x_0}{x} \right)^D$$

where G(x) is the Complementary Cumulative Density Function,  $x_0$  is the minimum fracture trace length, and D is the exponent of the function. D is the slope of the non-linear regression line (in a log-log diagram), and  $x_0$  is defined for each point of the non-linear regression by:

$$x_0 = x \cdot G(x)^{-D}$$

The mean value,  $\mu$ , of the distribution is expressed as:

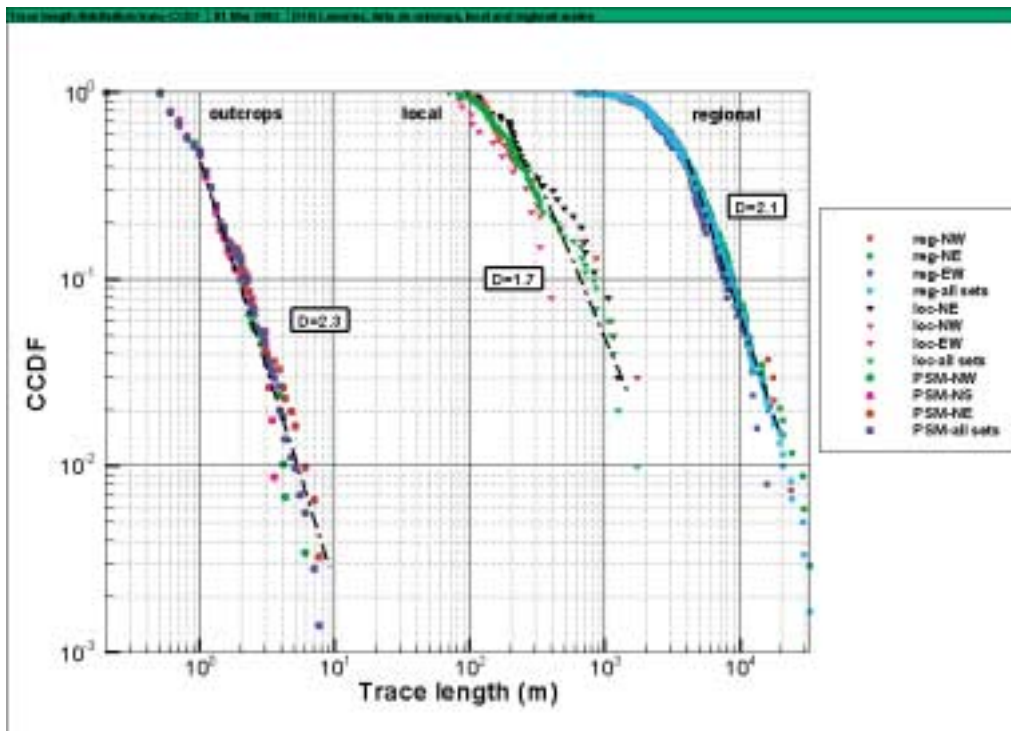
$$\mu = \frac{D \cdot x_0}{D - 1}$$

The CCDF has approximately linear portions for each data set over a wide size range. The analysis of the graph shows a relatively good consistency of the slope of the CCDF among the different fracture sets for each scale. This implies that all the sets scale in almost the same way at a given scale of observation. However, data are less consistent between the different sets at the local scale, see Figure 3-37.

The scaling of fractures is almost similar at outcrop and regional scales, but fractures at local scale seem to depart from this pattern.

Nevertheless, even if they present almost the same slope, different mean,  $\mu$ , and minimum trace length,  $x_0$ , can be assumed from the curves for the different sets, see Table 3-17. This is enhanced by the fact that the curves for different sets do not really overlap.

Figure 3-37 shows that there is a small gap in the data between the local and regional scales. Indeed, the curve at regional scale departs from linearity for trace lengths smaller than 2000 meters, and the trace length distribution at the local scale can be valid for trace lengths up to 1000 meters.



**Figure 3-37.** CCDF of trace lengths for lineaments at local (*loc*) and regional (*reg*) scales, and for outcrops (*PSM*).

There is also a greater gap in the data between the upper trace length of fracture traces on outcrops, around 10 meters, and the minimum trace length of fracture traces on local scale, around 70 meters. The representative trace length distribution at the local scale starts at trace lengths greater than 150 meters. The data provided in /LaPointe et al, 1999/ give support for the interpretation of trace lengths data in this gap. Indeed, on the basis of the range of values taken by trace lengths, the outcrops' mapping scale in Laxemar can be compared to the HRL mapping scale in Äspö, see Figure 3-39. According to the interpretation made by /LaPointe et al, 1999/ on Äspö data (scale 1:7000), the trace length distribution departs from linearity at trace lengths greater than 50 meters. The trace length distribution evaluated for data at HRL scale was then applied to generate the stochastic fracture pattern up to a size of 50 m.

Due to lack of sufficient data, the value of 50 m was also applied as the upper size for generation of stochastic fractures in Laxemar from outcrops' data. Hence, for fracture traces smaller than 50 meters, the trace length distribution is provided by measurements made on outcrops /Ericsson, 1987/. The CCDF is linear for fracture traces at a scale of 1 m up to 10 m, and the Power law function exponent,  $D$ , for all outcrops is 2.3 (Table 3-17). The trace length distribution obtained from outcrops data will be representative of the stochastic fractures in the model.

Fracture traces over 50 meters should be interpreted in another way.

The representative trace length distribution for fracture traces shorter than 50 meters is calculated for each fracture sets on outcrops data (Table 3-18). The definition of the fracture sets is presented in Table 3-16.

**Table 3-17. Power law parameters for fracture traces at different scales.**

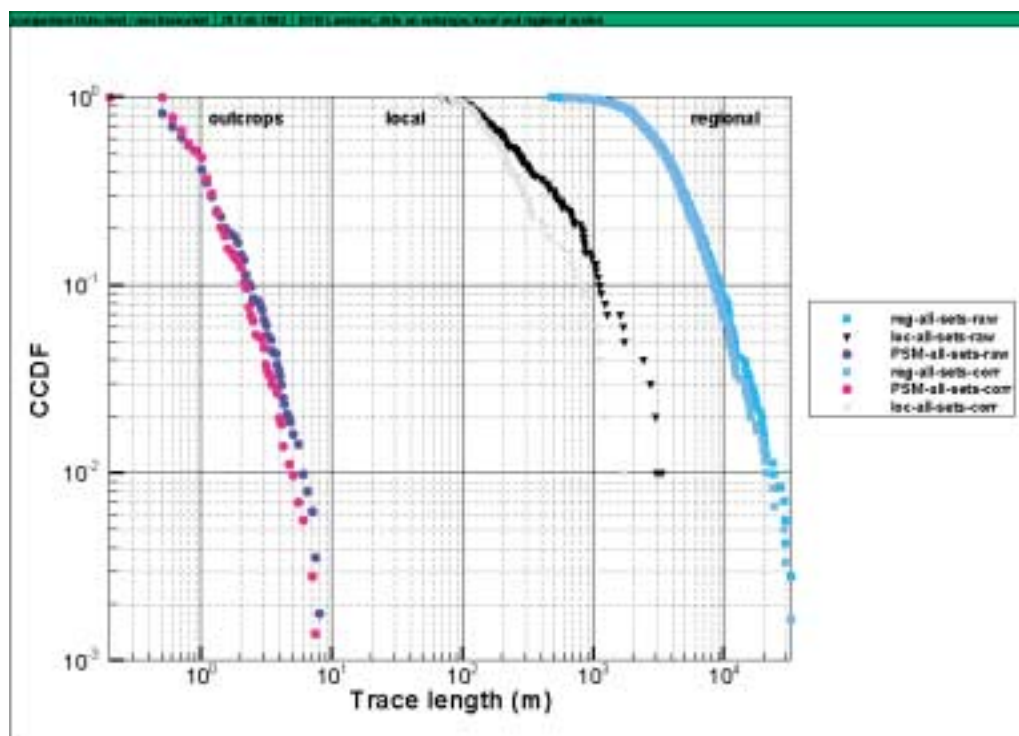
	Orientation of sets	D, trace length	$x_0$ (m), trace length	$\mu$ (m), trace length
Regional	NE, NW, EW	2.15	0.69	1.24
Local	NE, NW, EW	1.3	106.7	405.4
Outcrops	NW, NS, NE	2.3	2722.5	5113.6

**Table 3-18. Power law parameters for the fracture sets from outcrops.**

	Orientation of sets	D, trace length	$x_0$ (m), trace length
Set 1	NS	2.1	0.62
Set 2	NW	2.4	0.73
Set 3	NE	2	0.64
All sets	NS, NW, NE	2.3	0.69

The scaling of the fracture system is not so evident, since the difference in the Power law exponent is quite significant between the local scale and the outcrop and regional scales (Table 3-17). But the different fracture sets at outcrops and regional scale exhibit fractal length properties.

The CCDF for raw (including truncated fractures) and corrected trace lengths data are plotted in Figure 3-38. The curves are almost similar for outcrops and regional lineaments' data, but there is a significant discrepancy of data at the local scale. The relative amount of large fractures decreases when corrected data are analysed.



*Figure 3-38. CCDF for raw and corrected trace lengths' data, at the 3 observation scales.*



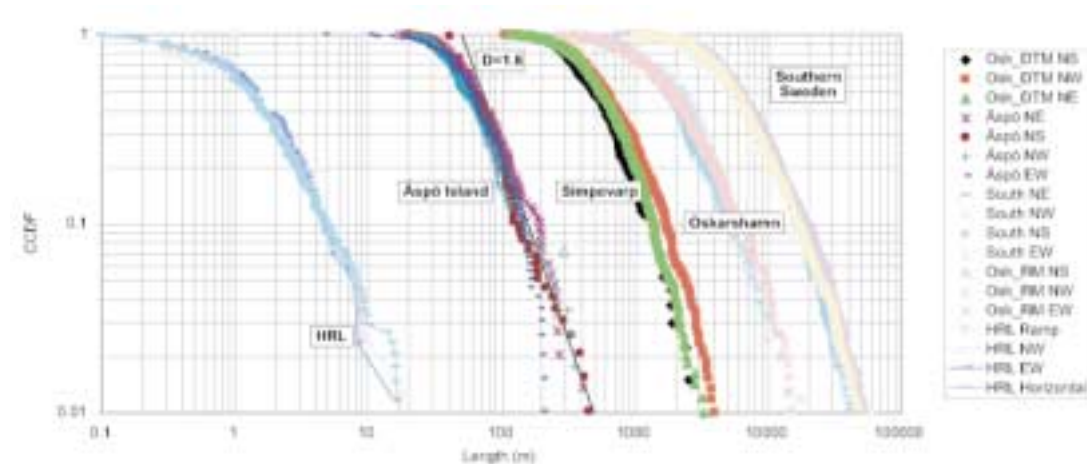
**Table 3-19. Influence of truncated fractures on Power law parameters, at different scales.**

	D, trace length		$x_0$ (m), trace length	
	Raw data	Corrected data	Raw data	Corrected data
Regional	2.06	2.15	2456	2722.5
Local	1.35	1.3	203.7	106.7
Outcrops	2.1	2.3	0.75	0.69

The Power law exponent, D, is similar or slightly lower when raw data are analysed, see Table 3-19. The influence of truncated fractures on the D exponent is fairly significant at all observation scales.

The fracture trace lengths at outcrops and regional scale suggests a fractal model, but this model does not fit at the local scale. An explanation of the discrepancy of data for different sets at this scale, and of data at this scale compared to other observation scales can be found in the unequal resolution of lineaments mapping at the local scale, see Figure 3-30. Fracture data are really sparse in the western part of the Laxemar domain, and are mostly large regional features. It is very likely that here would be many more short lineaments found if the topography data over the Laxemar domain would have the same resolution all over the map. The proportion of small traces would then increase and would be more similar to data from the regional scale as well as from the outcrops. Further, the overrepresentation of large fractures in relation to the sampling window size might be a cause of bias of trace length distribution at the local scale. When correcting data, most of the largest fractures are truncated and removed from the data set.

The results obtained in the Äspö area are shown in Figure 3-39. The fracture size follows a fractal model, and the Power law exponent is of the order of 1.6. This D value expresses that for a given observation scale, the range of trace lengths' values is more extended than at outcrop and regional scales in Laxemar.



**Figure 3-39. Trace length CCDF for Aberg and surrounding region /LaPointe et al, 1999/.**

### 3.8.5 Size distribution of the parent population

The Power law form of the observed CCDF for trace lengths suggest that the underlying fracture radius distribution may also follow a Power law distribution. Nevertheless, the parameters that characterise the Power law distribution for trace lengths can not be used directly to simulate the size distribution of the parent population, since the trace lengths are a biased form of the parent population.

Truncation and bias effects must be accounted for when transferring the parameters of the function from trace lengths, as determined in Section 3.8.4, to the parent population. Truncation of trace lengths' data is related to the orientation of the scanline or surface mapping towards the orientation of fracture sets, and to the edges of the mapping domain. Bias can be introduced in that larger fractures have a higher probability of intersecting the surface than do smaller ones.

The Power law function presents some specific characteristics useful to derive parameters on trace lengths to the parent population. With an assumption on the shape of the fractures, the size distribution of the fractures intersecting a trace plane can be related to the size distribution of the observed trace lengths, and the size distribution of the parent population is derived from the size distribution of the intersecting fractures. /LaPointe et al, 2000a/ presents the mathematical solutions for the calculation of the size distribution of the parent population from the distribution obtained on trace lengths, assuming circular fractures and a fractal fracture system. The following equations are applied to estimate the radius size distribution of the parent population.

From the trace length distribution to the size distribution of fractures intersecting a trace plane:

$$D_{intersecting} = D_{trace}$$

$$\mu_{intersecting} = \mu_{trace} \cdot 2/\pi$$

From the size distribution of fractures intersecting a trace plane to the size distribution of parent population:

$$D_{parent} = D_{intersecting} + 1$$

$$x_{0,parent} = x_{0,intersecting} = \mu_{intersecting} \cdot \left( \frac{D_{intersecting} - 1}{D_{intersecting}} \right)$$

with  $\mu$  mean value calculated from the Power law distribution,  $D$  Power law exponent,  $x_0$  minimum size of the Power law distribution. The Power law function and its parameters are defined in the equations in Section 3.8.4.

The size distribution of the fractures parent population is determined by applying the above equations on the parameters defined on the linear part of the CCDF curves.  $D_{parent}$  and  $x_{0,parent}$  define the input parameters for the size distribution for generating the DFN model. Table 3-20 gives the size distribution of the parent population of the fracture sets defined on outcrops.

**Table 3-20. Size distribution of the parent population, outcrop data.**

	<b>Azimet</b>	<b>Mean pole trend and plunge</b>	<b>D<sub>parent</sub></b>	<b>X<sub>0,parent</sub></b>
Set 1	NS	89.2 / 3.6	3.1	0.4
Set 2	NW	206.9 / 0.3	3.4	0.46
Set 3	NE	151.6 / 4.1	3	0.41
All sets	NW,NS,NE	–	3.3	0.44

### 3.8.6 Spatial model

The way fractures are located and scaled in space defines which geometrical conceptual model to use for generating the DFN model. This is assessed through a box fractal dimension calculation. The dispersion of fractures is evaluated by counting the amount of fractures or fracture centres in a stepwise increasing reference domain size. This computation is processed with the Fractal® software /LaPointe et al, 2000b/. There are mainly two methods to count the fractures: the fracture centres and random centres. When using the *fracture centres* option, a series of concentric circles is generated around a single point, and for each circle the number of fracture centres in each circle is counted. The number of fracture centres is plotted against the circle radius in a log-log graph. The slope of the regression line defines the box dimension. The *random points* option is very similar, except that one or several random points are selected along the trace. These methods are appropriate for determining the spatial model for generation of fractures in a DFN.

By definition, the values range from 1 to 2 for outcrops and lineaments data. A box dimension of 1 identifies a fracture pattern with fractures that are grouped and almost aligned in space. A box dimension of 2 represent a random fracture pattern that follows a Poisson distribution in space.

The box dimension was calculated for the local and regional corrected lineaments data by applying the *fracture centres* option. The box dimension for outcrops could not be calculated from the available set of raw data because no outcrop maps were available. The calculated box dimension is lower for local lineaments than for regional lineaments (Table 3-21). The calculated box dimension of 1.6 suggests that the fracture pattern is clustered, and the rock mass is divided into blocks of non-uniform size. The lower box dimension for local lineaments data suggest that the fracture pattern is more regularly structured in space. Moreover, the alignment of points in the graph at both scales suggests that the spatial fracture model is fractal (Figure 3-40). The fracture traces at local scale are long enough so that the data are not biased at small box dimensions and the slope represents the true box dimension. The true box dimension is assessed at regional scale by removing shorter fractures, which are far smaller than the smaller box dimensions.

**Table 3-21. Box dimension for lineaments at local and regional scale.**

	<b>Orientation of sets</b>	<b>D<sub>b</sub>, box dimension</b>
Regional	NE, NW, EW	1.64
Local	NE, NW, EW	1.47
Outcrops	NW, NS, NE	no map available

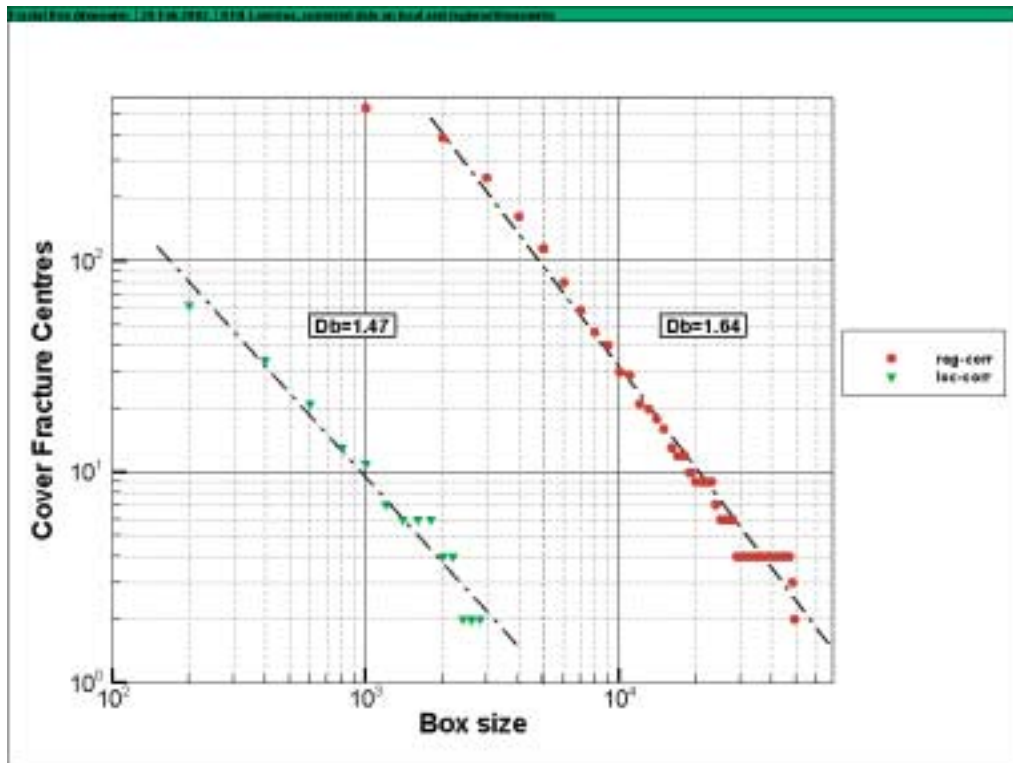


Figure 3-40. Fractal Box dimension on corrected data at local and regional scale.

A box fractal value of 1.6 is consistent with fracture statistics obtained in the Äspö area /LaPointe et al, 2000a/. However, detailed studies of fracturing in the HRL /LaPointe et al, 1995/ have shown box dimensions of 2.0 for traces mapped underground on the roof and walls, which is the expression of a Poissonian distribution. This implies that the spatial distribution of fracture centres in the rock mass outside the influence of large deformation zones is purely random. The discrepancy between the data could be related to the fact that smaller scale fractures are underrepresented on the lineament maps. If smaller were fractures included in the calculations, the resulting box dimension would increase. This observation cannot be checked in the Laxemar domain as the resolution of topography covers only parts of the area. Nevertheless, the fact that the amount of smaller fractures or lineaments might be underestimated at the local and regional scales must be considered. As a consequence, a Poissonian model was adopted for the spatial representation of stochastic fractures.

### 3.8.7 Fracture intensity

The fracture intensity is defined as the amount of fracture area per unit volume of rock,  $P_{32}$  ( $m^2/m^3$ ). This parameter cannot be assessed in the field but can be estimated on the basis of a linearly correlation with  $P_{10}$  ( $m^{-1}$ ), which is defined as the amount of fractures per meter (along a scanline or a borehole).

The asset of using  $P_{32}$  is that this parameter is independent of the orientation and size distribution of fractures. To determine  $P_{32}$ , a DFN model is generated on a “guessed” or simulated  $P_{32,sim}$ . Then, sampling boreholes are simulated in the model, with respect to the size and orientation of the borehole KLX01. The simulated  $P_{10,sim}$  is checked against

$P_{10,obs}$  calculated from the field data. The ratio of the true  $P_{10,obs}$  and of the simulated  $P_{10,sim}$  determines the constant of proportionality to multiplying  $P_{32,sim}$  and define the true  $P_{32}$ .

$$P_{32} = P_{32,sim} \cdot (P_{10,obs} / P_{10,sim})$$

The analysis of  $P_{32}$  was carried out by simulating a DFN model based on the 4 sets of fractures as defined in Section 3.8.3. The parameters used to simulate fracture size distribution are presented in Table 3-20. The values for  $P_{10,obs}$  are obtained from the core of KLX01, and in order to characterise the background fracturing, sections mapped as crush are not included in the calculation of  $P_{10,obs}$  (see also Chapter 3.1). The derived  $P_{32}$  data obtained from these simulations are presented in Table 3-22.

The equivalent  $P_{32}$  for the model is  $2.44 \text{ m}^2/\text{m}^3$ , which can be compared to other values determined in Äspö. /Stigsson et al, 2000/ report a global value of  $3.41 \text{ m}^2/\text{m}^3$  in the prototype repository domain of Äspö Hard Rock Laboratory. /Hermansson et al, 1998/ compute a global  $P_{32}$  for small and large fractures of  $2.75 \text{ m}^2/\text{m}^3$  in the Zedex tunnel domain.

The differences in the reported  $P_{32}$  values, besides the localisation, can be explained by the following factors:

- differences in the methodologies used to derive  $P_{10}$  or  $P_{21}$  from field data, and especially conductive fractures or fracture zones,
- different measurement equipments (core, outcrop, flow logs),
- different mapping methods and truncation value for the minimum size of mapped fractures.

### 3.8.8 DFN model parameters

Table 3-23 presents the calculated parameters for the DFN model defined for rock mechanics. In this case, the fracture frequency is related to all fractures (conductive and no conductive). The parameters of the model are used to simulate the rock mass, and do not represent values for the fracture zones.

**Table 3-22. Derived  $P_{32}$**

	$P_{10,obs}$	$P_{32,sim}$	$P_{10,sim}$	$P_{32}$
Set 1	0.60	2.99	0.70	<b>0.78</b>
Set 2	0.77	3.85	1.05	<b>0.66</b>
Set 3	0.62	3.11	0.74	<b>0.76</b>
Set 4	0.41	2.05	1.55	<b>0.24</b>
All	2.4	–	–	<b>2.44</b>

**Table 3-23. DFN parameters for a rock mechanic model.**

Parameter	Value	Comments
<b>Set 1</b>		
Orientation (Mean pole trend and plunge, dispersion)	262, 3.8, K=8.52 Fisher model	
Intensity ( $P_{32}$ , $m^2/m^3$ )	0.78	<i>all fractures</i>
Size	D=3.1, $x_0=0.4$	
<b>Set 2</b>		
Orientation (Mean pole trend and plunge, dispersion)	195.9, 13.7, K=9.26 Fisher model	
Intensity ( $P_{32}$ , $m^2/m^3$ )	0.66	<i>all fractures</i>
Size	D=3.4, $x_0=0.46$	
<b>Set 3</b>		
Orientation (Mean pole trend and plunge, dispersion)	135.9, 7.9, K=9.36 Fisher model	
Intensity ( $P_{32}$ , $m^2/m^3$ )	0.76	<i>all fractures</i>
Size	D=3, $x_0=0.41$	
<b>Set 4</b>		
Orientation (Mean pole trend and plunge, dispersion)	35.4, 71.4, K=7.02 Fisher model	
Intensity ( $P_{32}$ , $m^2/m^3$ )	0.24	<i>all fractures</i>
Size	D=3.3, $x_0=0.44$	
<b>All sets</b>		
Size	D=3.3, $x_0=0.44$	
Intensity ( $P_{32}$ , $m^2/m^3$ )	2.44	<i>all fractures</i>
Transmissivity ( $m^2/s$ ) (mean, standard deviation)	4.2E-08, 2E-07	
Spatial model	Baecher	

### 3.8.9 Analysis of flow data from KLX02

Flow data has been analysed to describe the properties of the conductive part of the fracture network. The available flow data comes from a series of difference flow measurements performed in KLX02 /Rouhiainen, 2000/. Three metre (3 m) packer tests have been conducted from 207 to 1398 m depth in KLX02. The measurement limit of the equipment is  $10^{-10}$  m/s down to 1150 m. Below this depth there is an increase of background noise /Rouhiainen, 2000/, the measurement limit increases below 1200 m /Rouhiainen, 2000/. In the transmissivity analysis values have been set to  $10^{-10}$  m/s when no conductivity data could be calculated.

The fracture transmissivity distribution is obtained by computation of the flow tests data with the Oxfilet module in FracMan. This method assumes that the net transmissivity of a test zone is equal to the sum of the transmissivities of the conductive fractures that intersect this test zone. A Poisson distribution defines the distribution of the conductive fractures. The algorithm will first generate conductive fractures in the test zones. Then, the user makes an estimation of fracture transmissivity distribution, and the algorithm calculates the packer test transmissivities of the zones from this set of data. The

transmissivity distribution is estimated by finding the best match between the observed distribution of packer interval transmissivities and the distribution of test zone transmissivities simulated for a given fracture frequency and fracture transmissivity distribution.

Transmissivity calculated from the test intervals follows a slightly skewed lognormal distribution, cf. Figure 3-41. In 122 intervals of 398, i.e. 30.65% of all sections, the transmissivity is below the threshold value and are set to the value of  $9.92 \cdot 10^{-12}$  m/s.

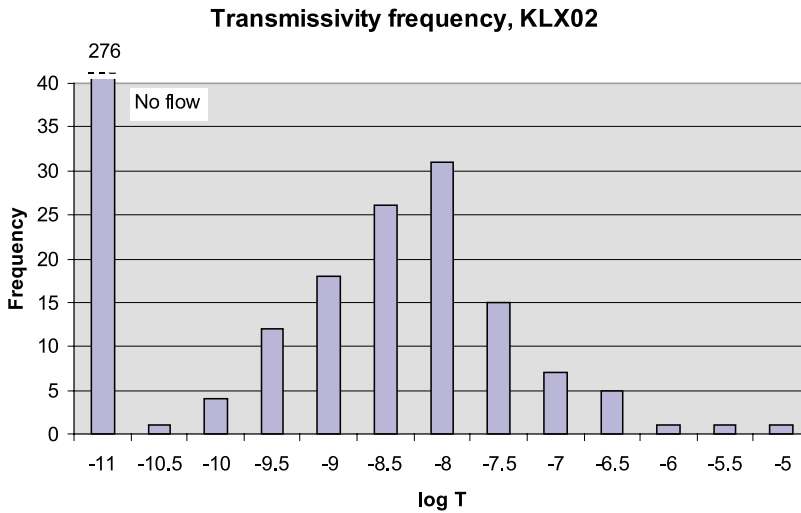


Figure 3-41. Distribution of the transmissivity in the 3-m intervals, KLX02.

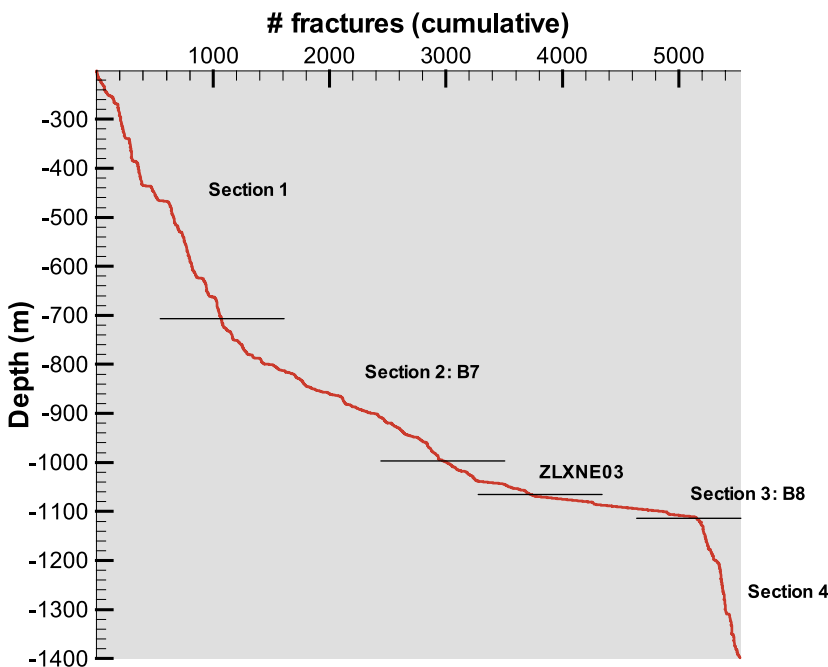


Figure 3-42. Fracture density ( $P_{10}$ ) in KLX02, natural joints and crush zones.

It is not possible to evaluate the transmissivity distribution in the sections below 1200 meters, because there are only two sections with a transmissivity over the threshold value.

The fracturing in KLX02 can be divided up into three distinctive groups, cf. Figure 3-42:

- background fracturing: defined by section 1 from 186.2 to 704.5 m, and section 4 from 1107 to 1398 m depth,
- highly fractured, and crushed, rock mass: defined by two sections, section 2 called R7 from 704.5 to 1011 m, and section 3 also called R8 from 1071 to 1107 m depth,
- fracture zone: ZLXNE03, from 1011 to 1071 m.

### 3.8.10 Fracture transmissivity distribution in the rock mass

The fracture frequency for conductive fractures,  $P_{10c}$ , influences the transmissivity distribution in the intervals, as well as the interpretation of the tests. The fracture frequency of conductive fractures ( $P_{10c}$ ) can be expressed as:

$$P_{10c} = \frac{-\ln(\# \text{ of no flow} / \# \text{ of tests})}{\text{Length of test zone}}$$

This expression assumes a totally random (i.e. Poisson distribution) of the conducting fractures.

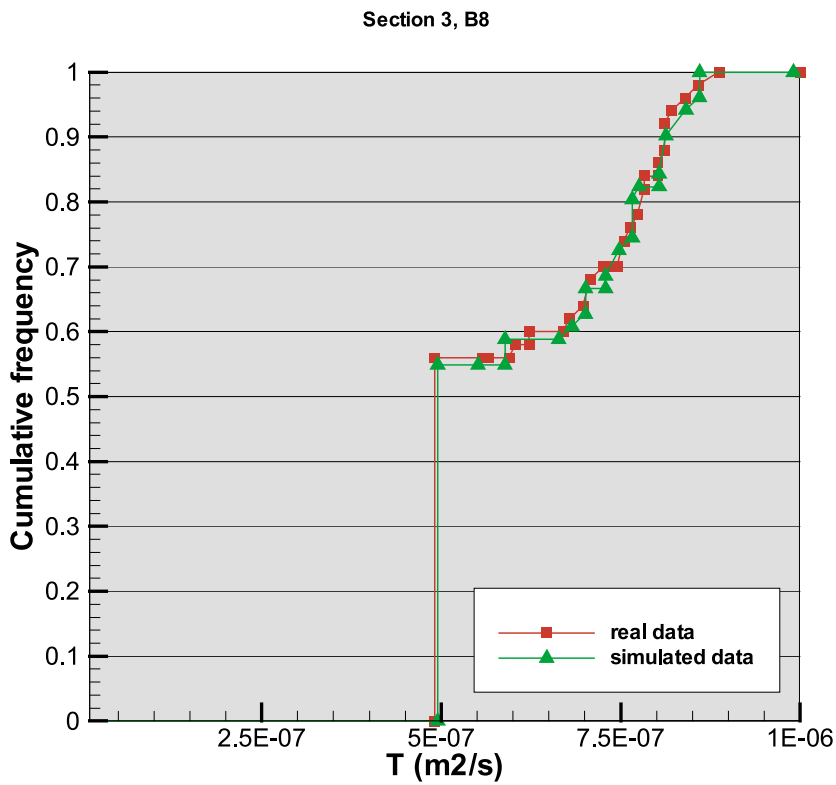
The intensity of conductive fractures,  $P_{32c}$ , was determined by following the same process as for all fractures (see Section 3.8.7), but the fracture data used for the simulation (fractures in KLX02) were bootstrapped. The observed fracture intensity,  $P_{10c,obs}$  used as an input represents frequency of all conductive fractures for the background fracturing. The derived  $P_{32c}$  for all conductive fractures is presented in Table 3-24. The fracture intensity for conductive fractures in each fracture set (Table 3-15) was then calculated from the percentage of occurrence of each set of fractures.

On the basis of the calculated  $P_{10c}$  (see Table 3-25) and assuming a log-normal distribution for the transmissivity (see Figure 3-41), the Oxfilet module in FracMan was used to simulate data that fit the real flow test data, see Figure 3-43. The results show quite small differences of transmissivity value in the different sections, see Table 3-25. The fracture zone is slightly more conductive than the other sections of the rock mass.



**Table 3-24. Derived  $P_{32c}$**

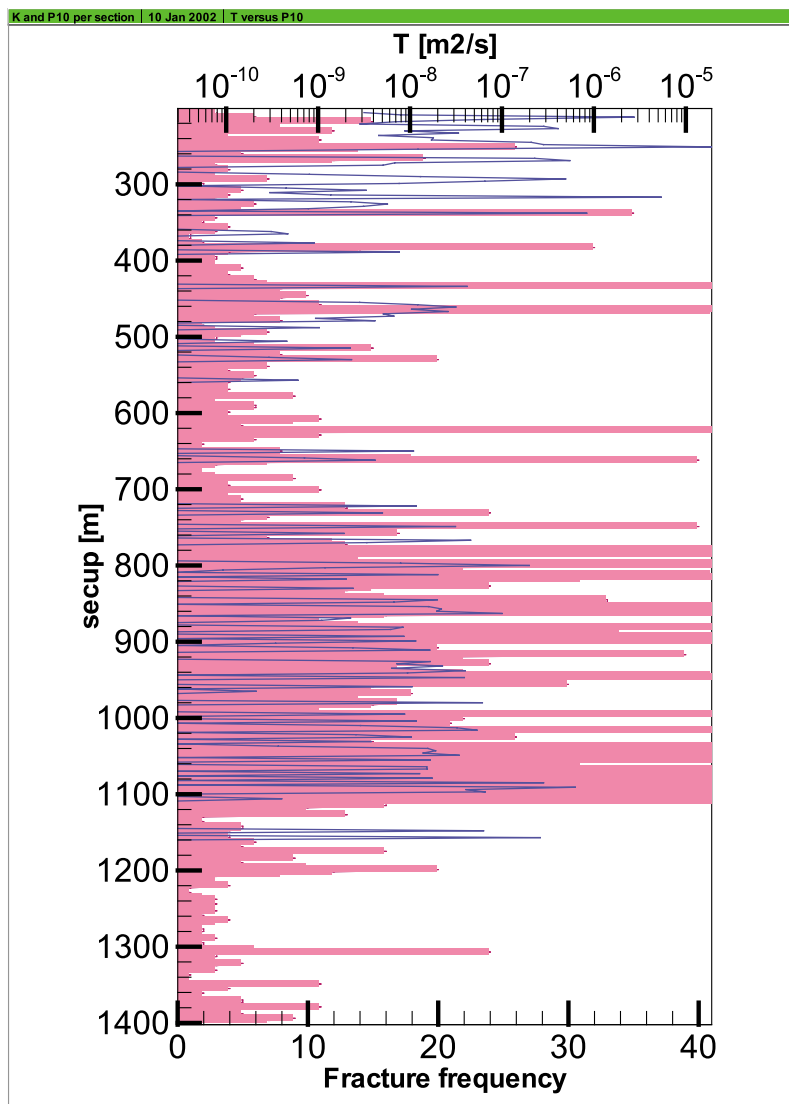
	$P_{10c,obs}$	$P_{32c,sim}$	$P_{10c,sim}$	$P_{32c}$
All conductive fractures	0.135	4	1.138	<b>0.48</b>
Set 1				<b>0.12</b>
Set 2				<b>0.15</b>
Set 3				<b>0.12</b>
Set 4				<b>0.08</b>



*Figure 3-43. Fit of simulated data with Oxfilet with real flow test data, section 3\_B8, KLX02.*

**Table 3-25. Transmissivity distribution in the different sections of the rock mass, from flow tests in KLX02.**

	Background fracturing	Highly fractured rock		Fracture zone
Segment type		R7	R8	
Transmissivity				
Mean value, m <sup>2</sup> /s	4.2E-08	7E-08	4.5E-08	1.5E-08
Standard deviation, m <sup>2</sup> /s	2E-07	5E-07	2E-07	5E-09
P <sub>10c</sub>	0.135	0.178	0.126	0.35



**Figure 3-44.** Comparison of the fracture frequency ( $P_{10}$ ) and the 3-m intervals transmissivity, in KLX02.

## 3.9 Hydrogeochemical data evaluation

This section describes the evaluation of the primary hydrogeochemical data. Most of these data are water sampled in the boreholes and at various surface locations. The evaluation essentially aims at identifying representative data sets for further analysis.

### 3.9.1 Introduction and aim

The aim of the hydrogeochemical data interpretation in association with the site investigation is to evaluate if the site is suitable from hydrogeochemical point of view for final disposal of spent nuclear fuel. A groundwater sample can be analysed for 20–30 water constituents, several isotopes, gas and microbe content, colloid content and properties such as pH, Eh and temperature. This information can e.g. indicate the origin of the water, the reactions affecting the water, palaeo hydrogeological regimes, present flow, the chemical aggressivity/stability of the water in contact with various materials such as bentonite and the copper capsules and finally the potential for the water to transport radionuclides from the repository to the biosphere.

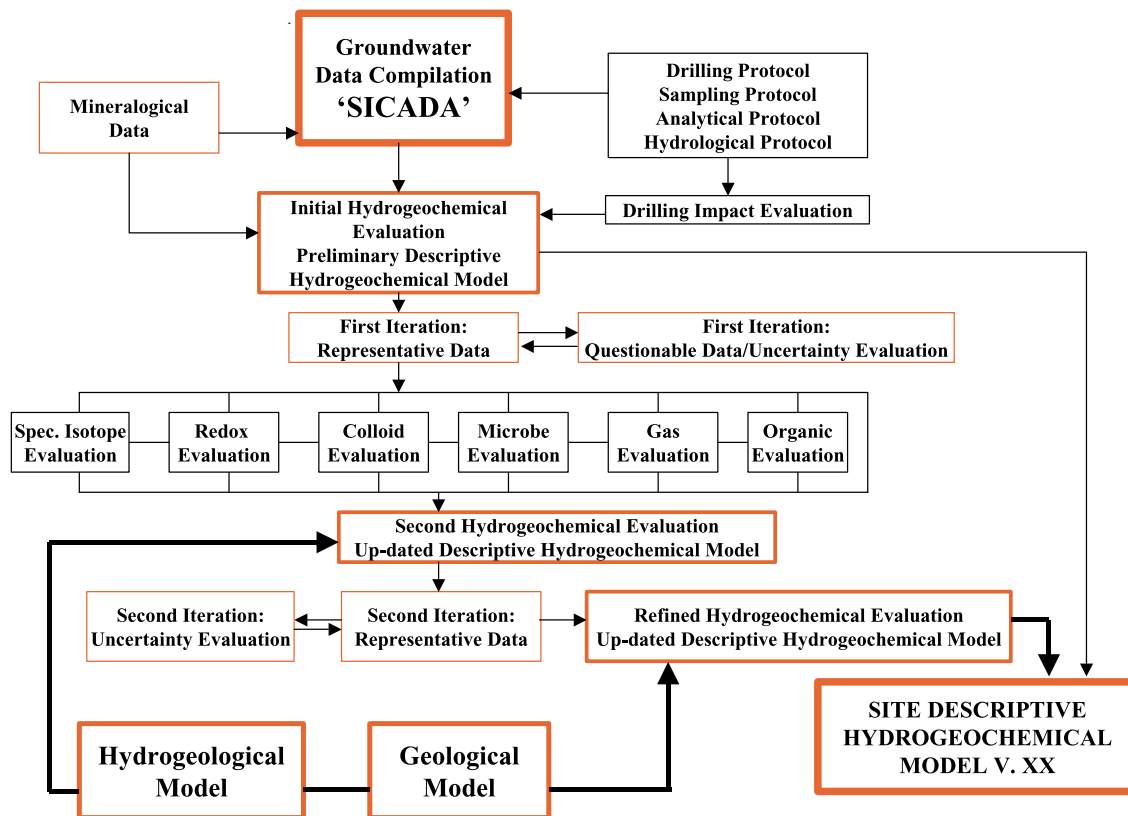
/SKB, 2001/ has defined the major task for hydrochemical evaluation to include: (i) characterization of undisturbed groundwater chemistry including the origin, depth/lateral distribution and the turnover time; (ii) focus on data of importance for the safety evaluation such as pH, Eh, chloride, sulphide, colloids and microbes; (iii) identification of possible dissolved oxygen at repository depth.

The data evaluation becomes a complex and time-consuming process when the information has to be decoded. Manual evaluation, expert judgment and mathematical modelling must normally be combined when evaluating groundwater information. A schematic presentation of how a site evaluation/modelling can be performed and its components are shown in Figure 3-45.

The geochemical evaluation and modelling presented in this work is a result of a method test and should not be regarded as an example of a final site modelling. A careful site modelling requires more resources for data evaluation, testing, modelling and uncertainty evaluation than was available within the framework of this project.

### 3.9.2 Data Set

The data used within this project was determined by the selected modelling area, the Laxemar domain (see Figure 3-46). A total of 253 samples were evaluated from the SKB database SICADA. The parameters and the observation gathered during the SICADA data collection are listed in A5. The groundwater data includes the deep boreholes (KLX01 and 02), percussion-drilled boreholes (HLX) soil tube samples /Laaksoharju and Gurban, 2002/, surface samples and samples from the Baltic Sea. The sampling was performed by using different techniques such as double packers for the deep boreholes /Laaksoharju et al, 1995a/ single packers for the percussion drilled boreholes and special samplers for the soil tubes /Laaksoharju and Gurban, 2002/.



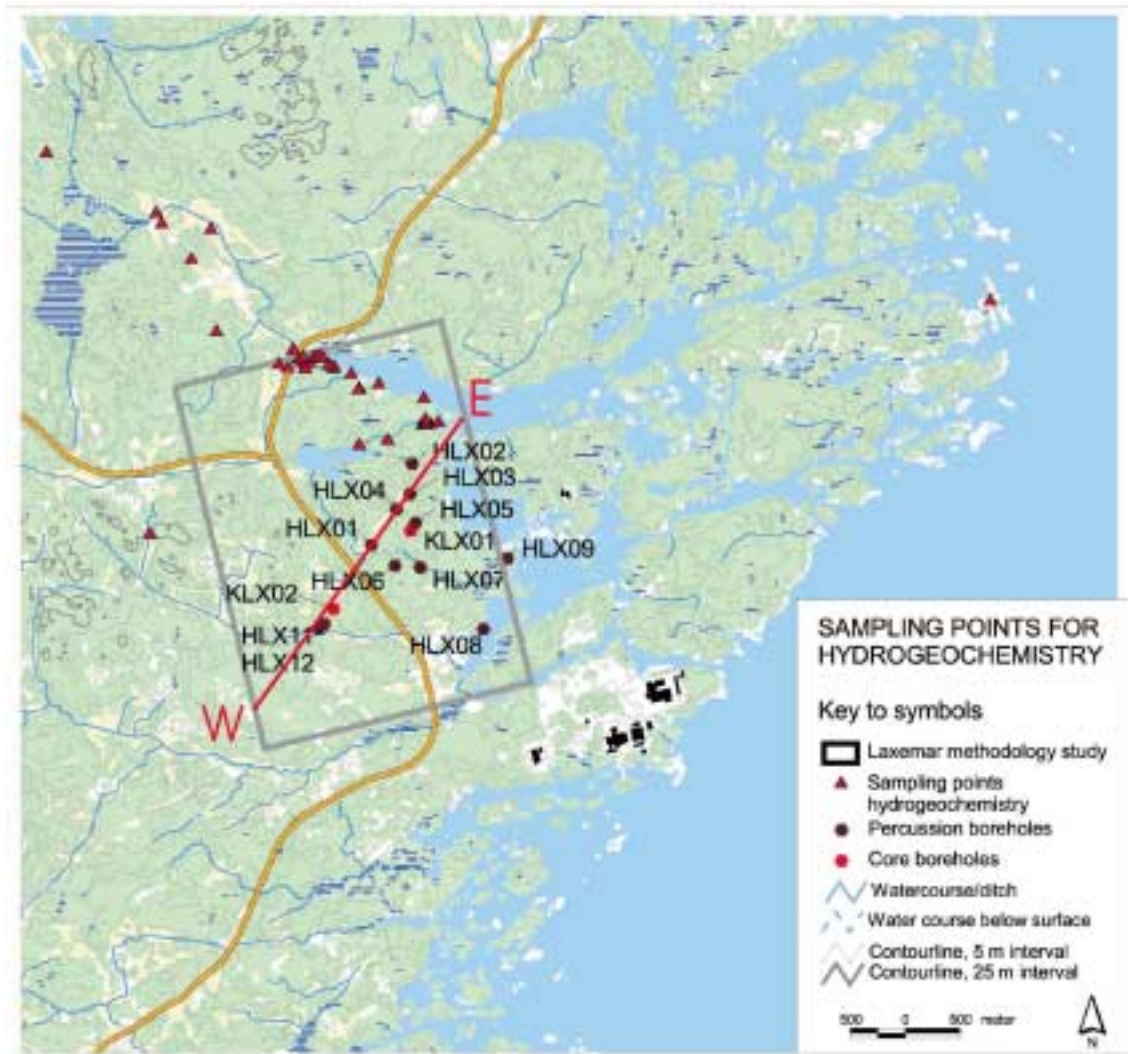
*Figure 3-45. A flow chart reflecting the methodology and the steps included in a site evaluation following the SKB method description /Smellie et al, 2002/. The steps used in this report are red labelled. The black marked evaluation steps were not tested due to lack of data.*

### 3.9.3 Evaluation and simulation tools

For the groundwater chemical calculations and simulations the following standard tools were selected:

For evaluation and explorative analyses of the groundwater:

- AquaChem: Aqueous geochemical data analysis, plotting and modelling tool (Waterloo Hydrogeologic).
- ChemStat: An advanced chemical statistical program (The scientific software group).
- Statgraphics: General statistical program (Manugistics Inc.).



**Figure 3-46.** The model domain (black square) and the locations of the boreholes and sampling points are shown. The red line represents the cutting plane W-E used for visualisation of the groundwater properties.

Mathematical simulation tools:

- PHREEQC: Chemical speciation and saturation index calculations, reaction path, advective-transport and inverse modelling /Parkhurst et al, 1980/.
- M3: Mixing and Massbalance modelling /Laaksoharju et al, 1999b/.

Visualisation/animation:

- TECPLOT: 2D/3D interpolation, visualisation and animation tool (Amtec Engineering Inc.).

### 3.9.4 Hydrogeochemical Evolution Model

The first step in the manual evaluation is to, based on known paleogeological events, construct a conceptual Hydrogeochemical Evolution Model for the site. This model can be helpful when evaluating data since it gives constraints to the possible groundwater types that may occur. No groundwater data are needed at this stage but discussion with hydrogeologists is recommended. The development of the description below are based on information on the glacial/post-glacial events that might have affected Laxemar compiled from /Björck, 1995/ and /Laaksoharju et al, 1999c,d/.

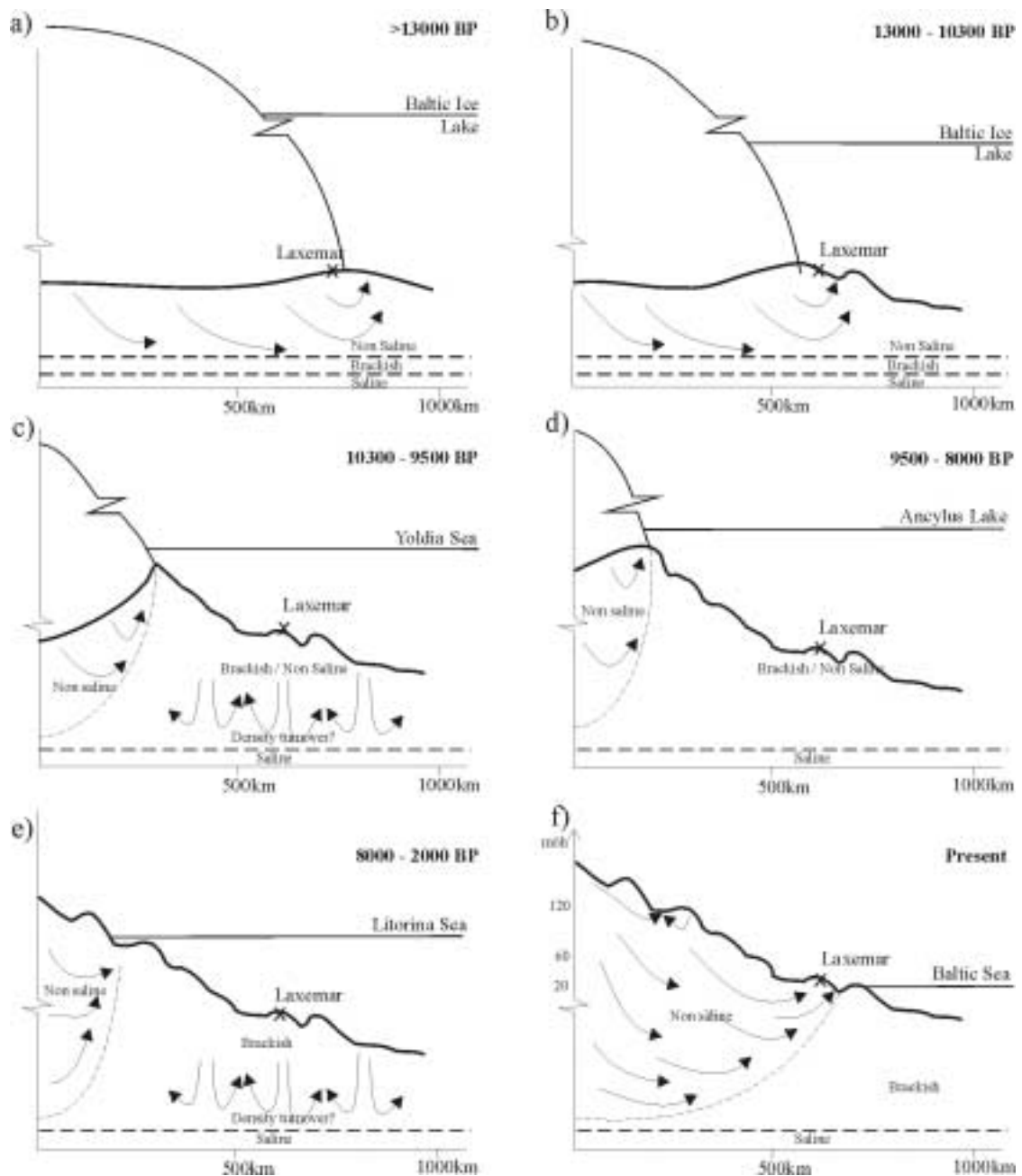
When the continental ice was formed >100,000BP permafrost formation could take place at a depth of several hundred meters which concentrated the existing groundwater by freezing /Bein and Arad, 1992/. The water formed had a higher density and could sink to the depth containing a water with the same salinity and density. (Highly saline waters may also be created from slow dissolution of fracture minerals etc.)

When the continental ice melted and retreated, glacial meltwater was hydraulically injected under considerable head pressure into the bedrock (>13,000BP). The exact penetration depth is still unknown, but a depth exceeding several hundred metres is possible according to hydrogeological modelling /Svensson, 1996/.

Different non-saline and brackish lake/sea stages then covered the Laxemar site (13,000BP–4,000BP). Of these only dense brackish sea water such as Yoldia (Yoldia represents a relative short time period and the effects may be difficult to trace) and Litorina Sea water could penetrate by density overturn and affect the groundwater in the more conductive parts of the bedrock. The density of the intruding sea water in relation to the density of the groundwater determined the final penetration depth of the sea water. The Litorina Sea stage (8,000 to 2,000BP) contained the most saline groundwater (twice the salinity of modern Baltic Sea water) and this water was supposed to have the deepest penetration depth. The result was that the glacial and brine groundwaters in the bedrock were affected by intruding brackish marine water.

When Laxemar subsequently rose above sea level a freshwater pillow of meteoric recharge water developed. The continuous land rise increased the hydraulic driving force so that the groundwaters in the upper part of the bedrock were flushed out gradually. This flushing started directly after deglaciation and, since this part of the bedrock had already risen above sea level, the postglacial marine water at these locations did not affect the groundwater composition.

Many of the natural events described above are repeated during a repository lifespan of hundred of thousands of years. The effects from the last glacial and de-glaciation event should therefore be easier to detect than from any previous glacial events which probably have been flushed out from the groundwater system. Some important origins of groundwater and events which may have affected the present groundwater at Laxemar is shown in Figure 3-47. As a result of the described sequence of events, brine, glacial, marine and meteoric groundwaters are expected to be mixed in a complex manner at various levels in the bedrock, depending on the hydraulic character of the fracture zones, groundwater density variations and borehole activities prior to groundwater sampling. For modelling purposes and based on the conceptual model of the site end-members compositions reflecting e.g. glacial meltwater was added to the data set (see Section 4.3.).



**Figure 3-47.** A conceptual Hydrogeochemical Evolution Model for the Laxemar site. Possible relation to different known post-glacial stages and land uplift which may have affected the hydrochemical evolution of the site is shown a) Glacial stage, b) Baltic Ice Lake stage, c) Yoldia Sea stage, d) Ancylus Lake stage, e) Litorina Sea stage and f) present day Baltic Sea stage, after /Laaksobarju et al, 1999c/.

### 3.9.5 Representativity of the data

By definition a representative sample is considered to be one which best reflects the undisturbed hydrological and geochemical in situ conditions for the sampled section. A sample which reflects in situ, on-line, at-line, on-site or off-site errors such as contamination from drilling, excessive pumping, contamination from tubes and downhole equipment of various compositions, contamination due to losses or uptake of atmospheric gases, analytical errors etc has a low representativeness. The errors mentioned above may be difficult or impossible to detect when examining analytical data. The representativeness may also be influenced by the location of the boreholes and selection of the sampling points. Some errors are easily avoided, others are difficult or impossible to avoid. Furthermore, chemical responses to these influences are sometimes, but not always, apparent.

Naturally there are no samples from undisturbed conditions prior to drilling and therefore much of the judgements lean on expert knowledge. For the future this judgement will be supported by a DIS (Drilling Impact Study) modelling where the aim is to model in detail the impact from drilling and other borehole activities on the individual fracture zones. A pilot test was performed on data from KOV01 /Gurban and Laaksoharju, 2002/ which indicated that the fracture zones in this case could be affected by 70% drilling water when a zone was penetrated during the drilling event. More than 1000L entered the individual fracture zones during the drilling event. All drilling water was removed prior to the start of the chemical sampling, leading to low drilling water content (<1%) in the samples. The general learning is that the risk of contamination is higher for the fracture zones with a higher permeability located in the upper part of the borehole due to the fact that the exposure time for drilling activities are longer.

The judgement of representativity for the Laxemar groundwater was in this case a straightforward task. From the deep boreholes there were generally time series of samples. The first sample was generally taken shortly after starting the sampling and the last sample generally after four weeks of low volume pumping. Generally the electrodes reflecting the Eh values stabilised at a negative value of around -200 mV during this pumping and therefore the last sample underwent a more rigorous analytical program than the first samples. The last sample was therefore more representative and thus also more useful for further modelling. For the Laxemar borehole KLX02 several sampling campaigns have been performed. The first sampling campaign was regarded to be more representative than the last sampling campaign since the borehole had been open (short circuited) for several years and the water is known to flow down vertically along the borehole to a depth of 1000 m. The samples from this borehole may therefore reflect more local conditions than regional conditions. From the shallow boreholes (HLX), soil tubes and surface locations there were generally only one or a few samples available. The sample selected was generally the last sample since most of the first samples were collected shortly after drilling or establishing the sampling device.

The learning is that the sampling strategy and the representative sample are selected already during the sampling campaign and few options are left for the modeller. From a total of 253 samples, 29 samples (11 deep boreholes samples, 11 shallow boreholes samples and 10 surface samples) were regarded to be representative. The average change in Cl concentration during sampling was 25% between the first and last sample.

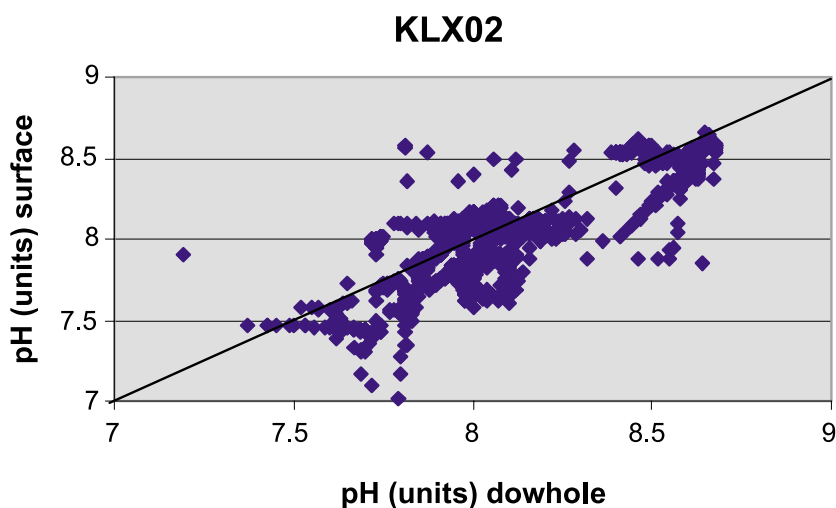
For the future the sampling campaigns should focus on getting representative Eh values as a measure of representative sampling but also to focus on the volume injected/ extracted from the fracture zones. Guided by the DIS modelling, which can indicate the amount of foreign water residing in different fracture zones, the sampling should be



aiming at removing foreign water volumes until “native” groundwater (a so called 0 sample) is reached but avoiding excessive extraction which can cause new groundwater mixtures. These samples should be analysed with a high enough (SKB class 4–5) accuracy so they can be selected as representative samples. The accuracy of the DIS modelling can be checked with the samples taken during drilling and during chemical sampling by analysing the drilling water content. The pumping should continue until representative Eh values (generally negative values) are recorded but also using the volume as an important criterion for sampling. All samples should have a representativity calculation reflecting if the sample reflects added borehole water (e.g. +1m<sup>3</sup>), native groundwater (0 m<sup>3</sup>) or excessively extracted groundwater (e.g. –1m<sup>3</sup>). By doing so the choice can be more objective and the representativity evaluation procedures suggested by /Smellie et al, 2002/ can be better employed. The planning and sampling work should be conducted in close cooperation between the modellers and persons in charge for sampling.

For identification the representative samples from Laxemar were marked in the data table used for modelling (see Appendix A5). From the representative data set two *target samples* (KLX01:456–461m and KLX02:335–340.8m) were identified in the data set since they were sampled closest to a potential repository depth. The uncertainty in the groundwater data was addressed in the modelling by using the average variability in all samples. The changes in e.g. salinity (25%) during sampling can be such an indicator. In addition the known analytical uncertainties generally ±5% was used in the modelling together with model uncertainties (10%). The Ion Charge Balance (ICB) was not satisfying (>5%) in some surface and shallow samples that may indicate analytical problems for some of these samples.

The changes caused due to uplifting of water is generally handled in a specific detailed modelling where the downhole/versus surface measurements are examined (see Figure 3-48). The variability of, in this example 1 unit (average), can be used in specific uncertainty modelling in e.g. mass-balance calculations where the effects on the calculations are measured. Generally the downhole measurements are regarded to be more representative and are used when available.



*Figure 3-48. pH measurements downhole (in situ) versus surface measurements are compared for the data sampled at KLX02. All measurements are presented here and some represent measurements taken early during the pumping cycle and are therefore less representative.*

The fundamental question in the modelling is generally if the uncertainties lead to a risk of misunderstanding the information in the data (for further discussions see Section 6.3). Generally the uncertainties from the analytical measurements are lower than the uncertainties caused by the modelling but the variability during sampling is generally higher than the model uncertainties.

### 3.9.6 Explorative analysis

A commonly used approach in groundwater modelling is to start the evaluation by explorative analysis of different groundwater variables and properties. The next phase often includes a groundwater classification based on the salinity or major constituents of the groundwater. The effects from the major water rock interactions are modelled using some of the standard mass-balance codes.

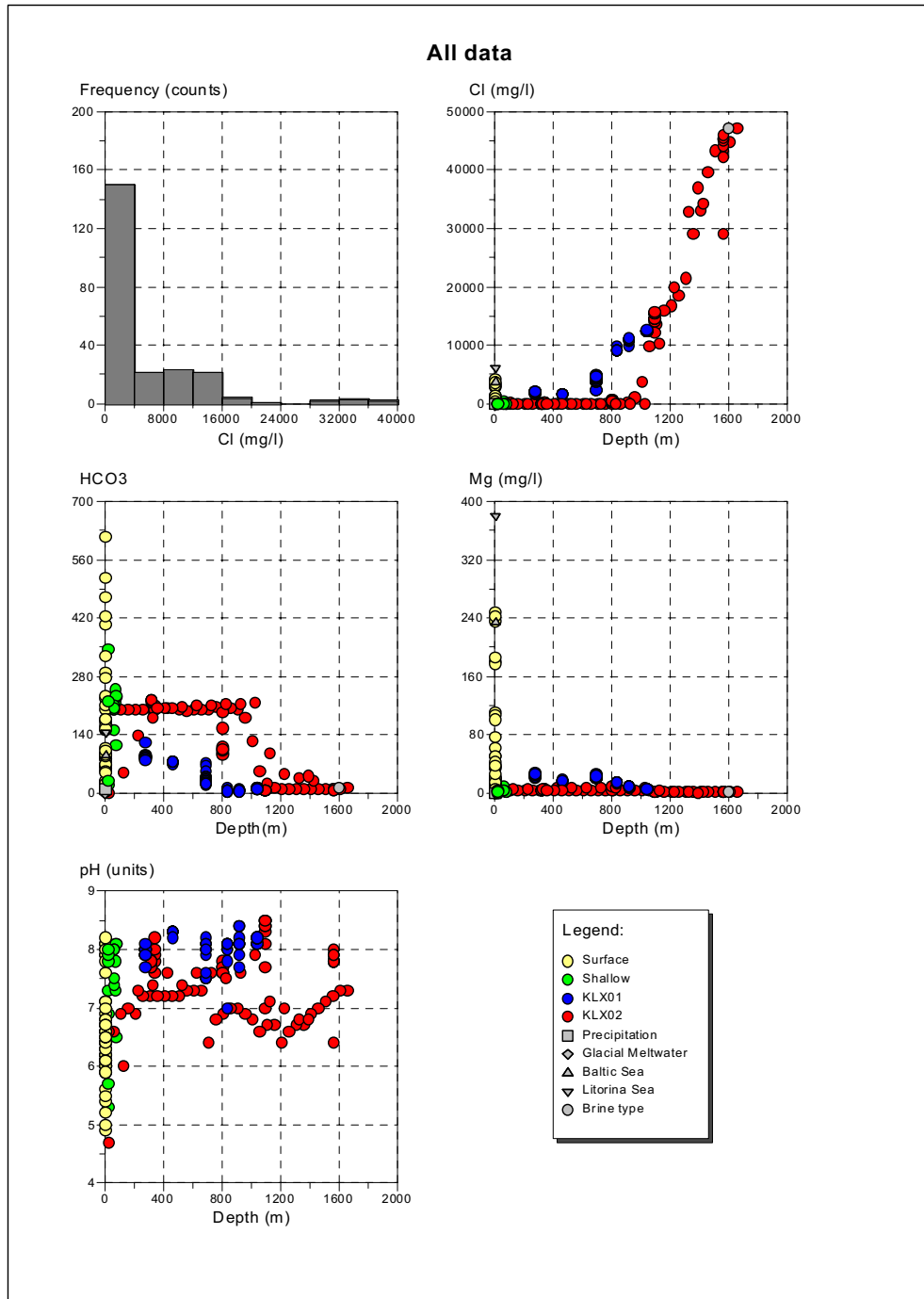
This section gives examples of how classical geochemical evaluation and modelling can be applied on site data by using the computer code AquaChem. The starting point is scatter plots where the data set is examined see Figure 3-49 and Figure 3-50, followed by classification in Figure 3-51. The plots such as Cl/depth shows that the freshwater saline interface is located at a greater depth in KLX02 compared with KLX01. The HCO<sub>3</sub>/depth plot indicates that the surface component indicated by high bicarbonate values are traceable to a greater depth in KLX02 than in KLX01. The Mg/depth plot shows that seawater is generally affecting the shallow samples. The Oxygen-18/Cl plot shows that most of the samples plot between precipitation, marine (Baltic Sea, Litorina Sea) and brine end-members indicating a possible mixing pattern.

The Piper plot clearly demonstrates the large spread of groundwater composition with two distinct groupings. One represents non-saline and brackish groundwaters characterised by a sodium, alternatively a calcium, bicarbonate-type water. The other is characterised as a sodium/calcium-chloride type of deep water. An evolutionary trend from non-saline water through brackish water to the saline water was observed in the Piper plot.

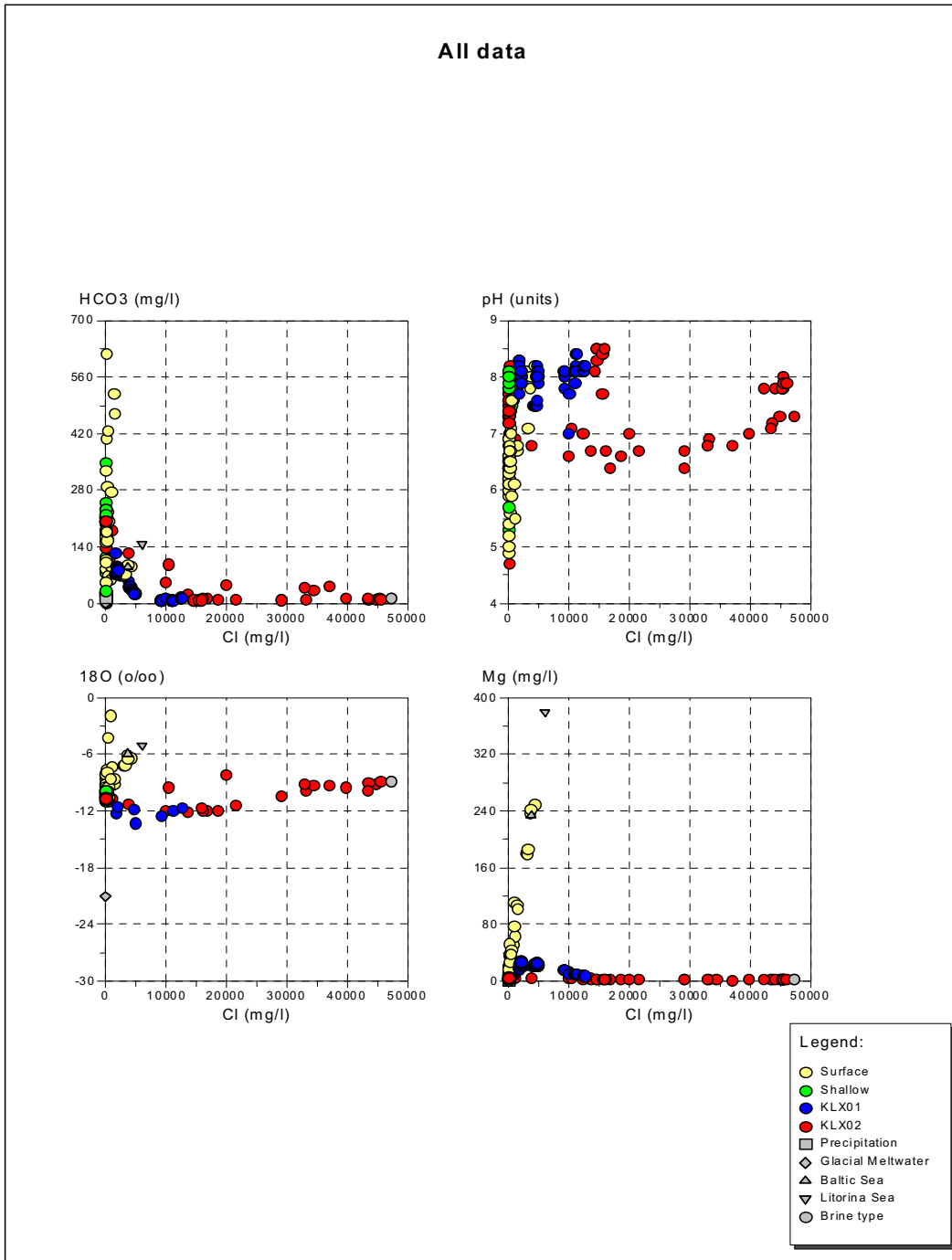
The disadvantage of Piper plots and other standard classification system in areas such as Laxeamar is the higher resolution for the non-saline waters than for the intermediate and saline groundwaters, with the latter usually forming tight clusters. For example, important changes in some variables such as SO<sub>4</sub> may be masked by larger changes in other variables such as Cl. The often crucial isotopic information is not included in the Piper plot.

The above procedure was repeated on the 29 representative samples (Figure 3-52 to Figure 3-54) in order to check that the general groundwater information is maintained in the reduced data set and to make detailed water type classification (Table 3-26). Table 3-27 lists general statistics for the representative samples. Table 3-28 shows an example of simple mixing calculations where deep water is mixed with rain water. This calculation can be used for a first test of possible mixing patterns although a too simplistic approach in a complex groundwater system can lead to over simplifications of the water origin, residence times and reactions taking place. The test should therefore always be repeated by using alternative end-members. In Table 3-29 Baltic Sea water composition is compared with the composition of representative samples. This test can be used to trace possible end-member influences on the observed groundwater composition. The aim is to trace possible influence of Baltic Sea water on the sampled groundwater. This test has to be repeated by including alternative elements and isotopes such as d<sup>18</sup>O before any judgements can be made. Table 3-30 lists general measured or calculated properties such as TDS (Total Dissolved Solids), Hardness, Alkalinity, different element ratios and possible dissolved minerals for the target sample KLX01:456–461m.

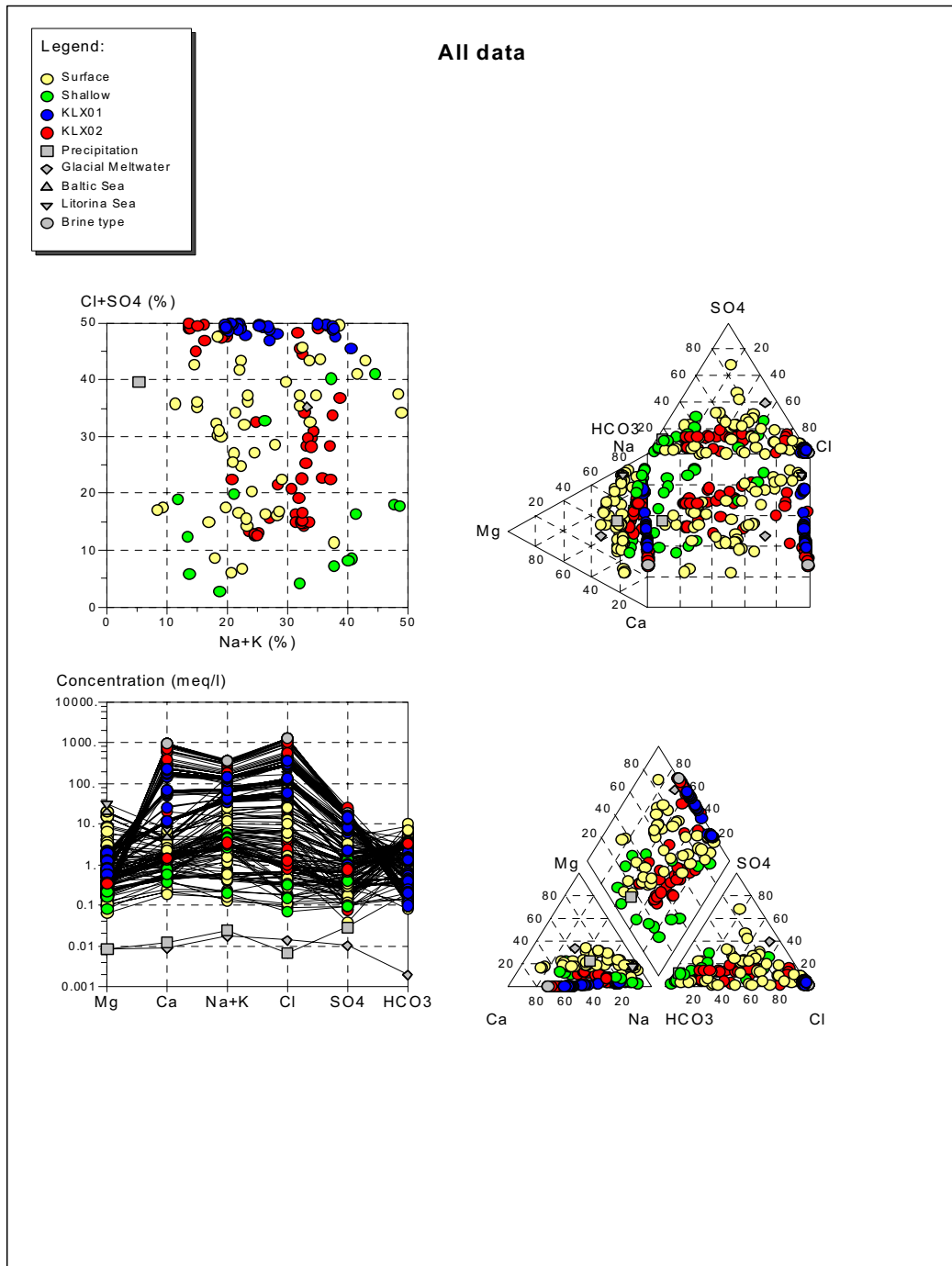
The above steps are used for identifying reaction and flow patterns in the data and to summarise and simplify the information. The information is included in the geochemical description of the site, see Section 5.3 and for other examples see e.g. /Smellie and Laaksoharju, 1992; Laaksoharju et al, 1995a, 1999d/.



*Figure 3-49. The frequency of the Cl samples, Cl/depth, HCO<sub>3</sub>/Depth, Mg/depth and pH/depth are plotted for all Laxemar data using AquaChem.*



*Figure 3-50. The HCO<sub>3</sub>/Cl, pH/Cl, Oxygen-18/Cl and Mg/Cl are plotted for all Laxemar data using AquaChem.*



**Figure 3-51.** Multicomponent plots used for classification of the data. From top left to top right to bottom left and bottom right: Ludwig-Langelier plot, Durov plot, Shoeller plot and Piper plot applied on all Laxemar data using AquaChem.

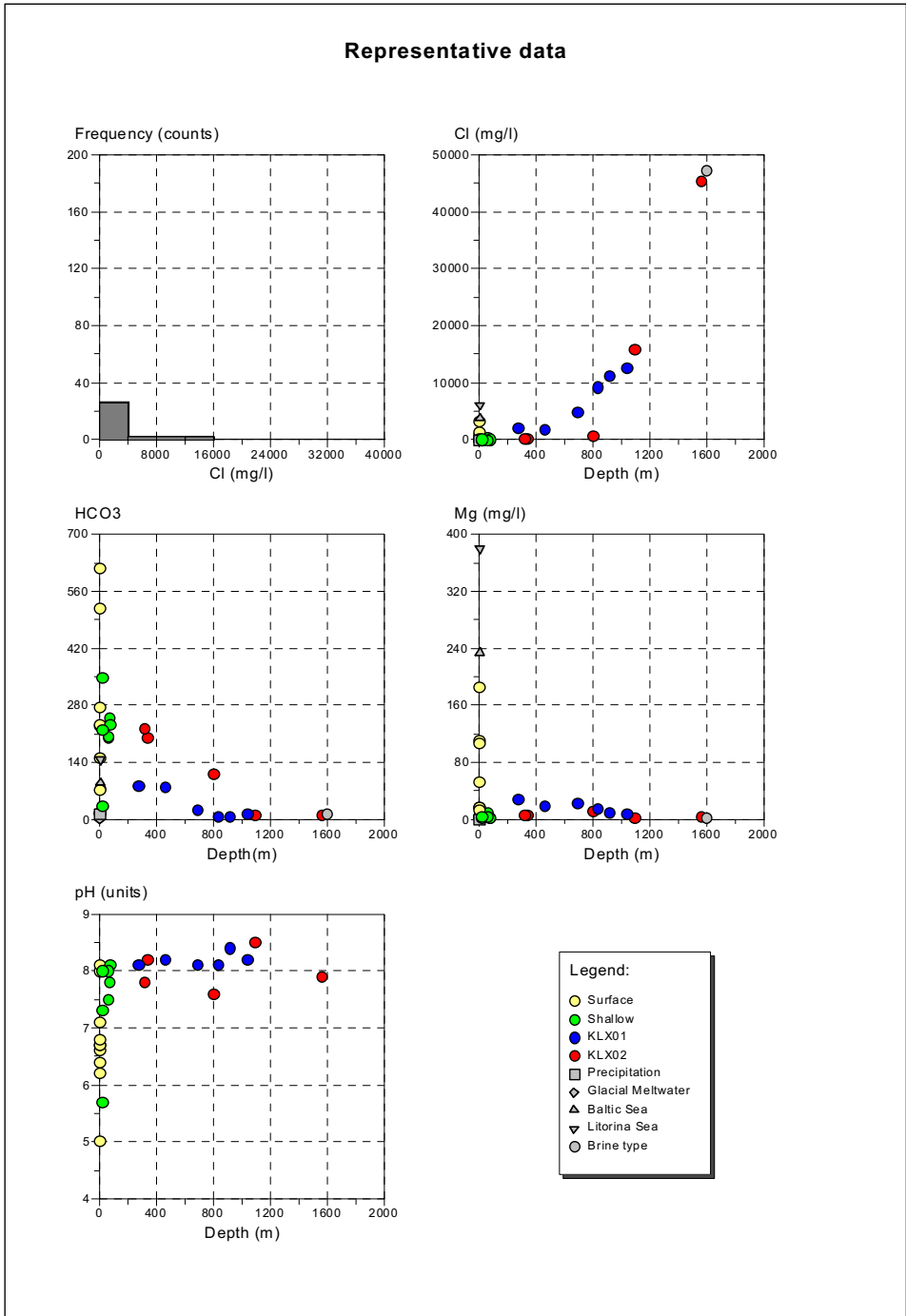
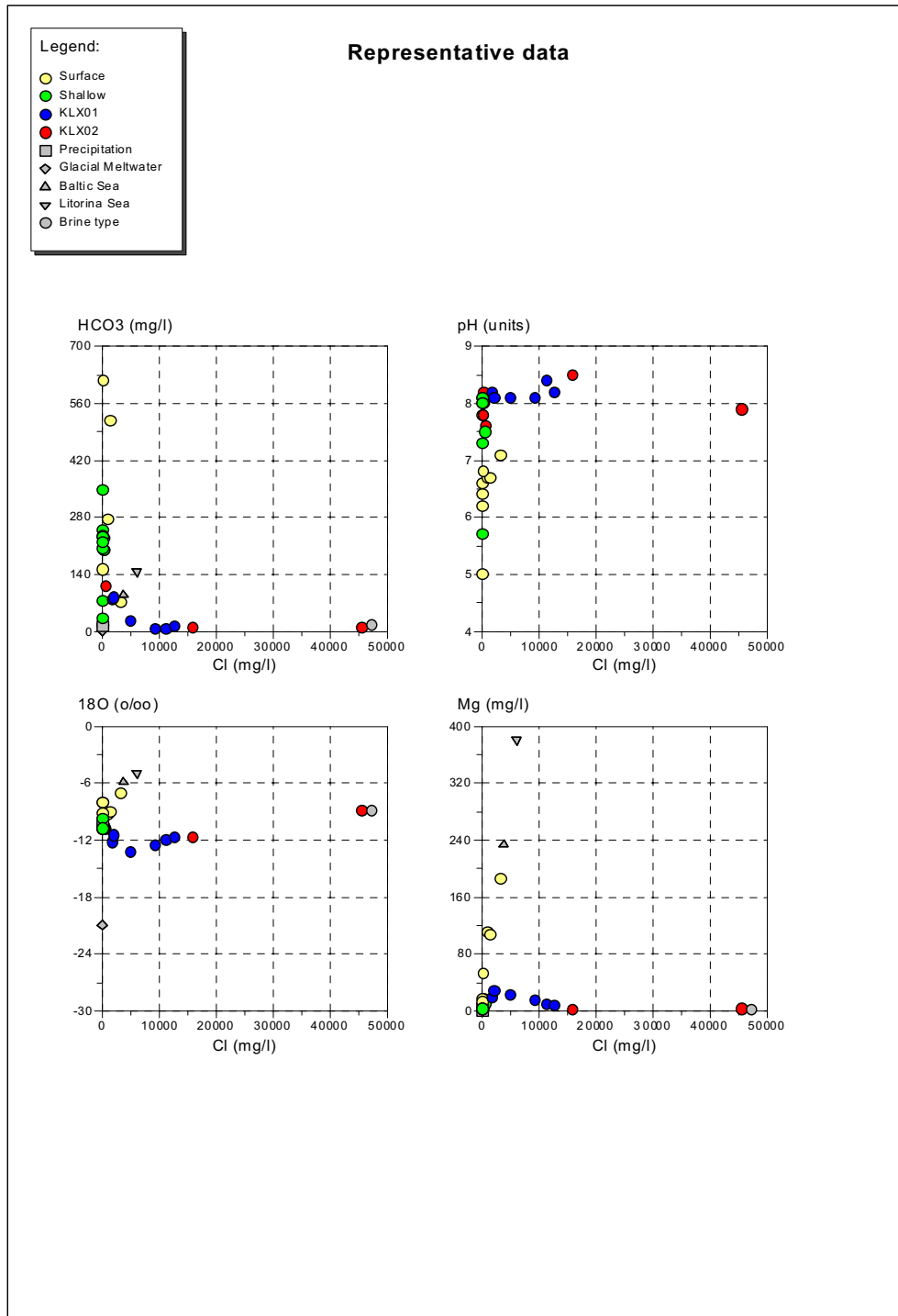
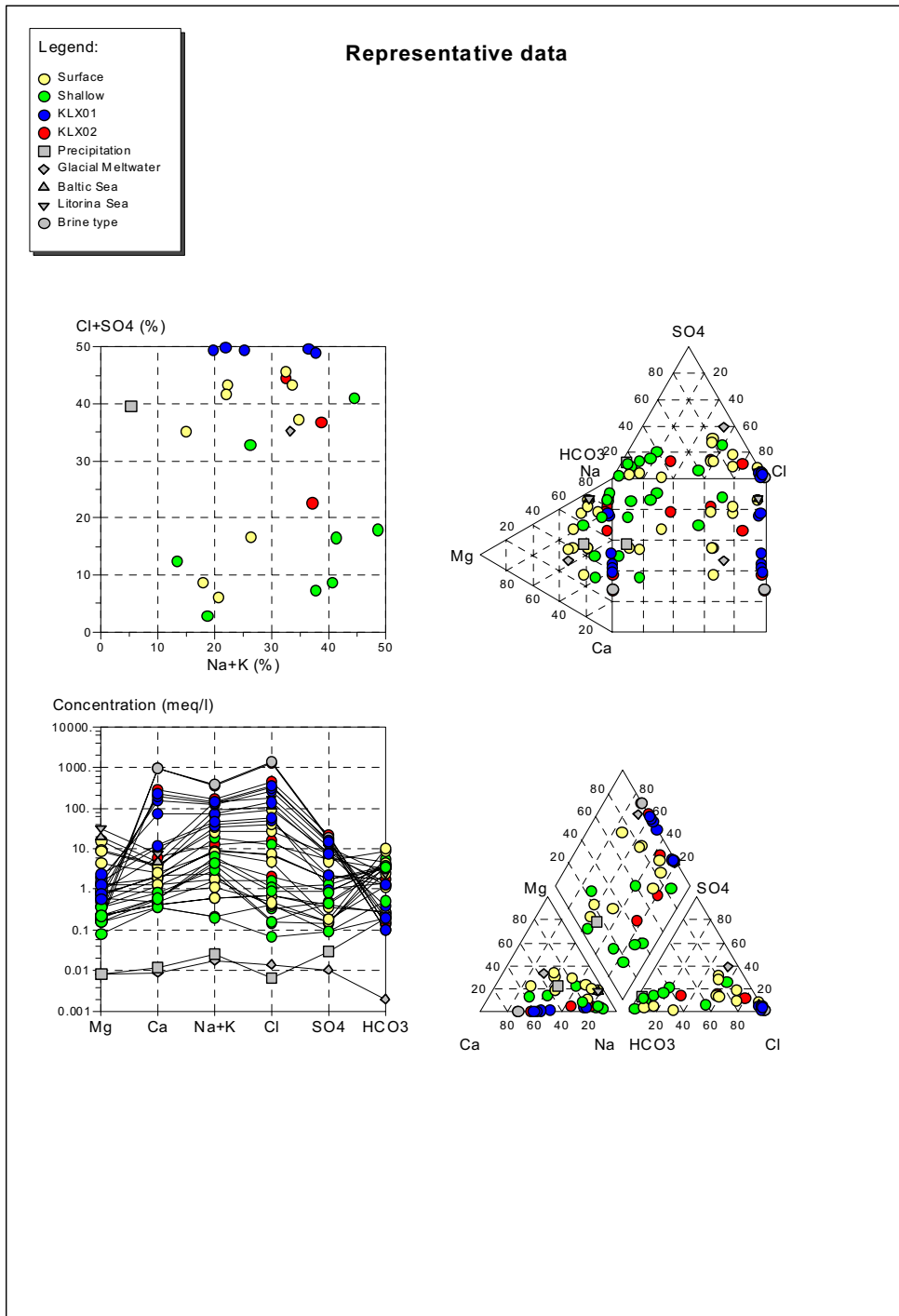


Figure 3-52. The frequency of Cl measurements, Cl/depth, HCO<sub>3</sub>/Depth, Mg/depth and pH/depth are plotted for representative Laxemar data using AquaChem.



*Figure 3-53. The HCO<sub>3</sub>/Cl, pH/Cl, Oxygen-18/Cl and Mg/Cl are plotted for representative Laxemar data using AquaChem.*



**Figure 3-54.** Multicomponent plots used for classification of the data. From top left to bottom left and bottom right: Ludwig-Langelier plot, Durov plot, Shoeller plot and Piper plot applied on representative Laxemar data using AquaChem.



**Table 3-26. Water type classification of the 29 representative samples and end-members by using AquaChem. Index.no = row number in the original SICADA table, Location = sampling location, Depth = sampling depth in the borehole, Watertype = classification based on major components, Dbase no. = sample number in the AquaChem data base.**

Index.no	Location	Depth m	Watertype	Dbase no.
10	Laxemar	19.5	Ca-Na-HCO3	2359 (01) •
12	Laxemar	72.5	Na-HCO3	2361 (01) •
135	Laxemar	337.9	Na-Cl-HCO3	2484 (03) •
142	Laxemar	800.9	Na-Ca-Cl	2491 (03) •
15	Laxemar	60	Na-Cl-SO4	2364 (01) •
152	Laxemar	1093.1	Ca-Na-Cl	2501 (03) •
161	Laxemar	1562.5	Ca-Na-Cl	2510 (03) •
167	Laxemar	318.3	Na-HCO3-Cl	2516 (03) •
17	Laxemar	6.5	Na-Mg-Cl-HCO3	2366 (01) •
207	Laxemar	1	Na-Cl-HCO3	2556 •
219	Laxemar	1	Na-Mg-Ca-HCO3	2568 •
220	Laxemar	1	Ca-Na-Mg-Cl-HCO	2569 •
221	Laxemar	1	Na-Ca-Cl-SO4	2570 •
222	Laxemar	1	Na-Ca-Cl-SO4-HC	2571 •
226	Laxemar	1	Na-Cl	2575 •
235	Laxemar	1	Na-Mg-Cl	2584 •
236	Laxemar	1	Na-Cl	2585 •
238	Laxemar	1	Na-Mg-Ca-HCO3	2587 •
241	Laxemar	1	Na-Mg-HCO3-Cl	2590 •
254	Deep_EndM	1600	Ca-Na-Cl	2603 (08)
255	Sea_EndM	5	Na-Cl	2604 (06)
256	Galcial_EndM	0	K-Ca-Mg-Na-Cl-S	2605 (05)
257	Rain_EndM	0	HCO3-SO4	2606 (04)
258	Litorina_End	5	Na-Cl	2607 (07)
3	Laxemar	75	Na-HCO3	2352 (01) •
32	Laxemar	691.1	Na-Ca-Cl	2381 (02) •
44	Laxemar	458.5	Na-Ca-Cl	2393 (02) •
5	Laxemar	19.5	Ca-Na-HCO3	2354 (01) •
53	Laxemar	274.5	Na-Ca-Cl	2402 (02) •
7	Laxemar	62.5	Na-Ca-HCO3	2356 (01) •
73	Laxemar	835.5	Ca-Na-Cl	2422 (02) •
84	Laxemar	915.5	Ca-Na-Cl	2433 (02) •
9	Laxemar	19.5	Na-HCO3	2358 (01) •
96	Laxemar	1038.5	Ca-Na-Cl	2445 (02) •

**Table 3-27. Example of general statistics for the representative samples and end members.**

34 samples, concentrations in mg/l

---

Sample No	Min	Max	Average	St. Dev.	Dev. CoeffVar%	
Na	0.17	8500.0	1266.258	2111.573	166.757	100.0 34
Ca	0.18	19300.0	1695.745	4599.408	271.232	100.0 34
Mg	0.1	380.0	37.889	80.632	212.811	100.0 34
Cl	0.23	47200.0	4924.725	11264.6	228.736	100.0 34
SO4	0.5	1010.0	236.435	307.268	129.958	100.0 34

**Table 3-28. A test where the rain water is mixed with the deep water. This test can reveal mixing patterns although the test has to be repeated by using alternative end-members before judging the results.**

Mixing two samples					
Solution 1:	257	Rain_EndM	0	HCO3-SO4	2606
(04)					
Solution 2:	254	Deep_EndM	1600	Ca-Na-Cl	2603
(08)					
Percentage of solution 1 in target solution:					
Sol 1	1.0	0.25	0.25	0.25	0.0
Sol 2	0.0	0.75	0.75	0.75	1.0
NA	0.4	6375.1	6375.1	6375.1	8500.0
CA	0.24	14475.06	14475.06	14475.06	19300.0
MG	0.1	1.615	1.615	1.615	2.12
CL	0.23	35400.059	35400.059	35400.059	47200.0
SO4	1.4	679.85	679.85	679.85	906.0

**Table 3-29. Example of an option in Aquachem where Baltic Sea water composition is compared by using the correlation and Euclidean distance with the composition of the representative samples.**

Location	Index	Corr Coeff	Euclidean distance	Points used for correlation
SEA01	2604	1.0	0.0	5
Litorina	2607	1.0	1185.708	5
PLX00048	2585	0.998	1202.615	5
PLX00039	2575	0.996	338.051	5
HLX08	2366	0.994	1874.989	5
KLX01	2393	0.99	1054.982	5
KLX01	2402	0.989	884.529	5
KLX02	2491	0.974	1625.527	5
PLX00047	2584	0.968	1400.197	5
PLX00022	2556	0.956	1758.206	5
KLX01	2381	0.924	782.575	5
KLX02	2484	0.922	1767.234	5
KLX01	2422	0.894	2778.989	5
KLX01	2433	0.88	3758.676	5
KLX01	2445	0.867	4465.012	5
PLX00053	2590	0.86	1801.9	5
KLX02	2501	0.858	5990.162	5
HLX07	2364	0.832	1638.337	5
SGKX02	2603	0.806	21443.314	5
KLX02	2510	0.804	20600.321	5
PLX00033	2569	0.786	1898.075	5
PLX00035	2571	0.739	1892.277	5
KLX02	2516	0.691	1852.014	5
PLX00034	2570	0.663	1892.11	5
PLX00050	2587	0.466	1892.731	5
Glacial	2605	0.462	1904.916	5
HLX04	2358	0.379	1870.344	5
HLX01	2352	0.347	1858.457	5
HLX06	2361	0.234	1880.819	5
HLX03	2356	0.095	1888.292	5
PLX00032	2568	0.063	1890.776	5
HLX05	2359	-0.149	1891.955	5
Rain '60	2606	-0.26	1904.944	5
HLX02	2354	-0.32	1903.052	5

**Table 3-30. General chemical information such as TDS (Total Dissolved Solids), Hardness, Alkalinity, different element ratios and possible dissolved minerals for the target sample KLX01:456-461m.**

SampleID	: 44			
Location	: KLX01			
Site	: Iaxemar			
Sampling Date	: 1988-11-23			
Geology	: granite			
Watertype	: Na-Ca-Cl			
Sum of Anions (meq/l)	: 51.5189			
Sum of Cations (meq/l)	: 50.4227			
Balance:	: -1.08%			
Calculated TDS (mg/l)	: 3013.4			
Hardness	: meq/l	°f	°g	mg/l CaCO3
Total hardness	: 12.61	63.04	35.30	630.4
Permanent hardness	: 11.33	56.65	31.72	566.5
Temporary hardness	: 1.28	6.39	3.58	63.9
Alkalinity	: 1.28	6.39	3.58	63.9
(1 °f = 10 mg/l CaCO3/1 1 °g = 10 mg/l CaO)				
Major ion composition				
	mg/l	mmol/l	meq/l	meq%
-----	-----	-----	-----	-----
Na+	860.0	37.408	37.408	36.696
K +	6.1	0.156	0.156	0.153
Ca++	223.0	5.564	11.128	10.916
Mg++	18.0	0.74	1.481	1.453
Cl-	1700.0	47.951	47.951	47.038
SO4--	106.0	1.104	2.207	2.165
HCO3-	78.0	1.279	1.279	1.255
Ratios				
	mg/l	mmol/l	Comparison to Seawater	
			mg/l	mmol/l
-----	-----	-----	-----	-----
Ca/Mg	12.389	7.514	0.319	0.194
Ca/SO4	2.104	5.042	0.152	0.364
Na/Cl	0.506	0.78	0.556	0.858
Cl/Br	261.538	589.456	287.5	648.1
Dissolved Minerals:				
	mg/l	mmol/l		
-----	-----	-----	-----	
Halite (NaCl)	: 2188.343	37.4076		
Sylvite (KCl)	: 11.631	0.157		
Carbonate (CaCo3)	: 372.363	3.7236		
Dolomite (CaMg(CO3)2)	: 136.314	0.74		
Anhydrite (CaSO4)	: 150.3	1.104		
SiO2 as Quartz	: 8.683	0.145		
or Feldspar (NaAlSi3O8)	: 37.915	0.145		

### 3.10 Rock Mechanics Interpretation of Borehole Data

This section presents and evaluates the input data available to support a rock mechanics modelling at Laxemar. First the stress measurements are discussed, then seismic logging results from KLX02 and finally the core logging information used to estimate deformation and strength parameters.

#### 3.10.1 Collected SICADA data for rock mechanics

For the rock mechanics descriptive model of Laxemar the type of data collected from SICADA are listed in Table 3-31. Apart from this some data were also collected from SKB reports and from the geological description within the Laxemar project. References to sources are given in the text in each case.

#### 3.10.2 Stress measurement data from Laxemar

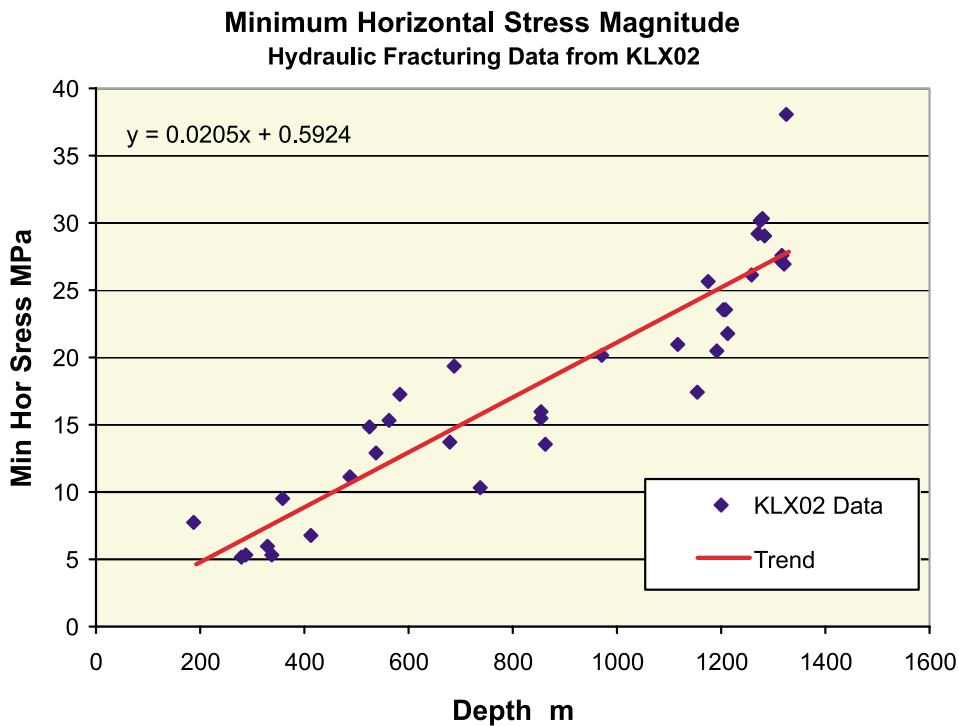
Within the Laxemar area stress measurements have been performed in one borehole, KLX02. The measurement technique used was the hydraulic fracturing method using the second breakdown method, i.e. using the reopening pressure. The interpretation technique applied and measurement results are reported in /Ljunggren and Klasson, 1997/. The data were collected from SICADA (Table 3-31).

**Table 3-31. Input data collected for the rock mechanics descriptive model. Shaded data have been explicitly used in the analysis. KLX01 and KLX02 are situated inside the Laxemar domain.**

<b>Measurements and parameters</b>	<b>Borehole</b>	<b>Comment</b>
Hydraulic fracturing stress measurements	KLX02	
Fracture frequency	KLX01 and KLX02	Only KLX02 used
Crush	KLX01 and KLX02	Only KLX02 used
Natural joints	KLX01 and KLX02	
Rock type	KLX01 and KLX02	
RQD	KLX01 and KLX02	Only KLX02 used
Overcoring stress measurements	KZ0059B, KXZSD8HR, KXZSD8HL, KXZSD81HR, KK0045G01, KAS05, KA3579G, KA3068A, KA2870A, KA2510A, KA2198A, KA1899A, KA1625A, KA1623A, KA1192A, KA1054A, KA1045A, KA1626A	All boreholes located at ÅHRL. Not all of the data are used in the analysis
Uniaxial compressive strength	KA0667B, KA0745B, KA0747A, KA1054A, KA1061A, KA1131B, PA1653, PA1654, PA1655, PAS00103, PAS00104, PAS00105, PAS00106, PAS00107, KXZA4, KXZA5, KXZA6, KXZC3, KXZC4, KXZC5, KXZC6, KXZC6, KA3545G, KA3557G	All boreholes located at ÅHRL
Sonic logging	KLX02	Not yet in SICADA#

The deepest test point is located 1337 m below ground surface and a total of 35 successful measurements were conducted. Test points between 200–850 m depth were completed using a hydrofracturing field truck unit, whereas the deeper tests were conducted using a pipe string and loose hydraulic hoses. The results obtained are shown in Figure 3-55 and they indicate an interval between ca 750–1100 m depth where less increase in magnitude occurs than a linear trend would indicate. This interval coincides with two rock segments interpreted as R8 (728–972) and R7 (972–1131) corresponding to high alteration and high fracturing, see Section 3.4 and Appendix B1. There are also several potential fracture zones in these segments.

The azimuth of the maximum horizontal stress is fairly constant between 200–1100 m depth, 151° (or N29°W), Figure 3-56, but shows significant azimuth rotation after that. The orientation of *principal* stresses is not directly measured with this method, rather it is assumed that the maximum and minimum principal stresses are perpendicular to the borehole, i.e. in this case horizontal. The maximum principal stress is commonly close to horizontal in Sweden and it is therefore reasonable to assume that the azimuth of the maximum principal stress is the same as for the maximum horizontal stress. The azimuth of the horizontal stress is determined by measuring the orientation of the induced fracture plane, which is assumed to develop perpendicular to the minimum stress, i.e. parallel to the maximum stress.



*Figure 3-55. Stress measurement results from KLX02. The minimum horizontal stress was determined using the hydraulic fracturing method.*

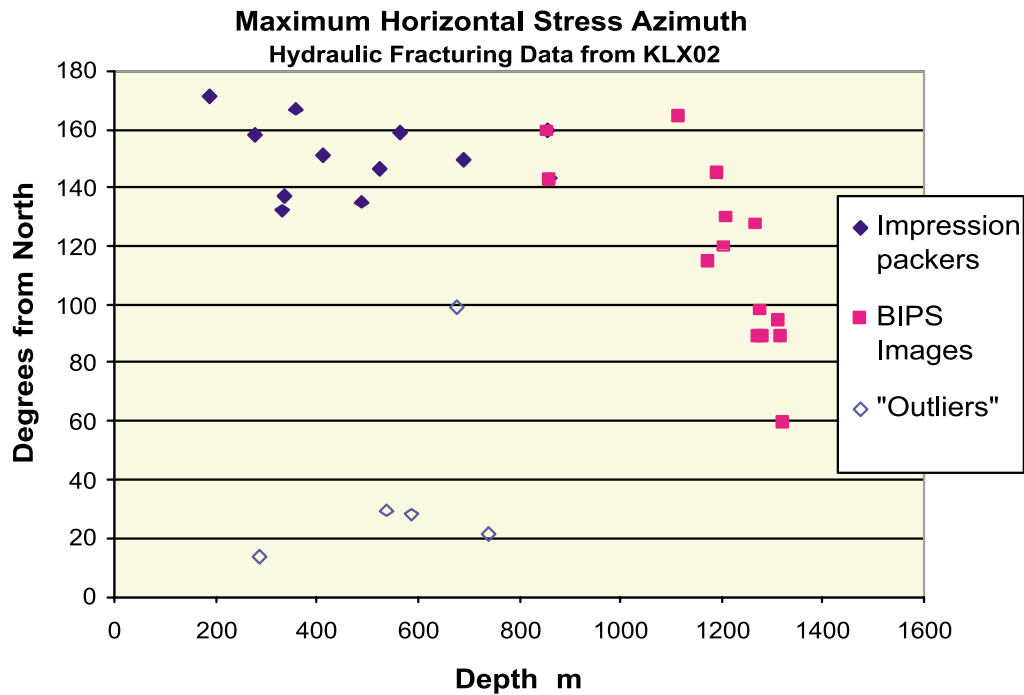
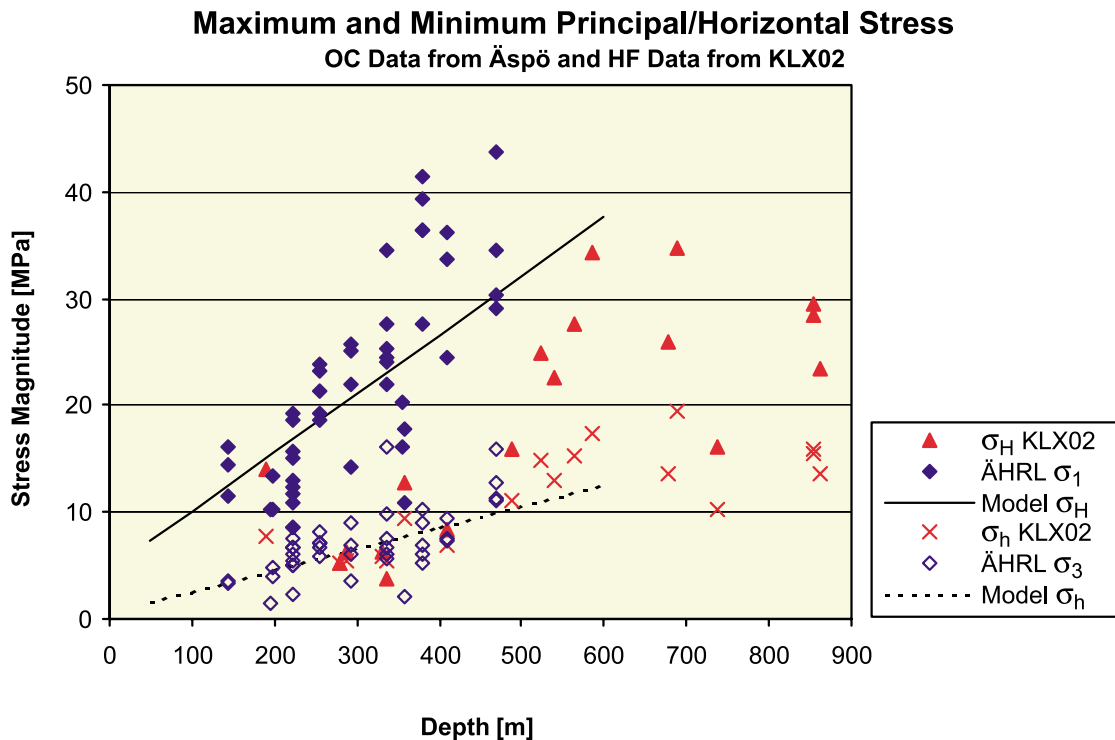


Figure 3-56. Azimuth of the maximum horizontal stress, measured with hydraulic fracturing method in borehole KLX02. At points below 850 m depth the orientation of the induced fracture is determined using BIPS images and above 800 m by traditional impression packers.

### 3.10.3 Stress measurement data from Äspö

Since the amount of data from the Laxemar area was limited it was decided to use also some of the data from the Äspö area, situated close to Laxemar, as a base for the stress estimation. The data were collected from SICADA (Table 3-31 and Appendix A7) and included only results from measurements using overcoring techniques. This technique provides all three principal stress magnitudes and orientations and therefore these data were considered useful as a complement to the hydraulic fracturing data from Laxemar. In a future site investigation, it is expected that some overcoring data will be available from the sites. (Hydraulic fracturing data also exist from Äspö but they were not used here since they would not provide any help for the maximum stress estimation).

Figure 3-57 shows a compilation of overcoring stress measurement results from 11 boreholes, totally 48 measurement points. The measurements are taken in the depth interval 145–470, mostly in short boreholes from the ÄHRL tunnel system. Only measurement points at a distance (>10 m) from the tunnel are included in this compilation (to avoid any data with stress influence from the tunnel excavation itself). The selected model depicted in the figure will be further described in Section 4.4.



*Figure 3-57. Compilation of stress measurement results from Äspö HRL. Maximum and minimum principal stress vs. depth. Data from hydraulic fracturing measurements in KLX02 are shown for comparison. (The linear trends used as stress model will be explained in Section 4.4).*

### 3.10.4 Estimation of in situ stress along KLX02

#### **Stress orientation**

The data from borehole KLX02 show fairly consistent orientation down to about 1100 m depth (Figure 3-56). Below 1100 depth the orientation is different. In the measurement report /Ljunggren and Klasson, 1997/ it is stated that the uncertainty of the orientation is higher at depth >850 m because BIPS images were used to locate the induced fractures (instead of the ordinary impression packers). This was very difficult because the fractures close very tightly after the test and only in one case could the fracture be found without doubt. For the majority of fractures identified with this technique there still exist, according to the report, uncertainty regarding the orientation. At a few test points no fractures could be found on the BIPS images. Therefore it was decided that, for the Laxemar exercise, the measurements using the BIPS technique should not be used in the estimation of the stress orientation (in particular for the upper part of the domain).

The mean orientation presented by /Ljunggren and Klasson, 1997/ for 200 to 1000 m depth (with 5 outliers excluded) is 151°. The explanation for the different values in “outlying” points is suggested to be either that weakness planes have been opened during fracturing or that misinterpretation have occurred when the imprints were transferred onto plastic films. No reinterpretation of the raw data from measurements has been performed within the framework of the Laxemar project.

## **Stress magnitude**

Stress measurement data for the minimum horizontal stress is determined from the shut-in pressures in hydraulic fracturing tests as presented by /Ljunggren and Klasson, 1997/. Numerical modelling of reopening test also shows that in most practical situations the apparent (the measured) reopening pressure is similar to the minimum horizontal stress, and also similar to the shut-in pressure /Rutqvist et al, 2000; Ratigan, 1992/. For the Laxemar case a linear trend of the data from hydraulic fracturing results in KLX02 was calculated, and this linear relationship with depth was used as an estimation of the minimum horizontal stress.

To estimate the *maximum* principal stress it was decided not to use the data based on the 'second breakdown method' (using the reopening pressure, see /Ljunggren and Klasson, 1997/). Numerical modelling has shown that for normal field conditions concerning well-bore storage the reopening pressure measured has no correlation with the maximum principal stress. It is only possible to obtain a reopening pressure that is dependent on the maximum horizontal stress, if the fracture opening is limited to a distance smaller than one borehole radius and if the well-bore storage is extremely small. In practise the fracture will propagate about 1 meter, and even if the fracture growth would have been limited the reopening would probably not be noticed because the compliance of such fracture would be very small compared to the well-bore storage of the field test equipment /Rutqvist et al, 2000/.

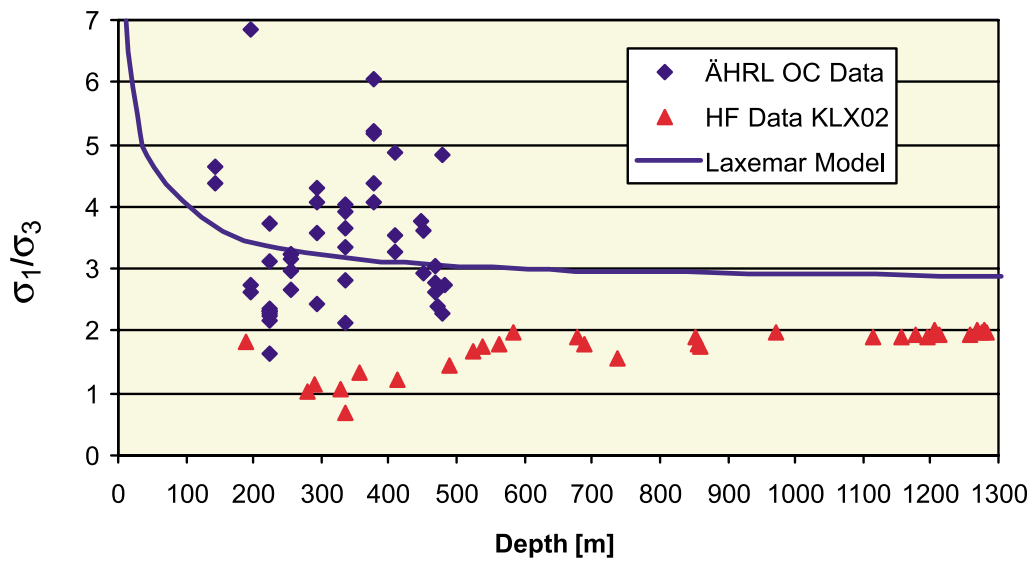
Instead, to estimate the magnitude of the *maximum* principal stress, the approach chosen was to multiply estimated minimum stress with the ratio between maximum and minimum stress, as measured with overcoring at Äspö. In this way potential local differences in stress level between the sites (or more precisely between borehole KLX02 and the boreholes at ÄHRL) could be preserved in the approach while still reaching a reasonable estimate of the maximum stress along KLX02. This assumption is, however, only correct if actually the ratio between the stresses can be considered fairly constant over a regional area. Still, an advantage of this approach, rather than using the measured stress magnitudes from Äspö directly as an estimation, is that the uncertainty introduced with the Young's modulus determination in overcoring method is avoided. The *ratio* between principal stresses is not expected to be very sensitive to changes in the determined Young's modulus, while the absolute *magnitude* changes in proportion to the Young's modulus.

Looking again at the data from Äspö, the ratio between the maximum and the minimum principal stress ( $\sigma_1/\sigma_3$ ) is plotted against depth (Figure 3-58) and against the minimum stress (Figure 3-59). In the plots also the ratios for the reported hydrofracturing data are given for comparison. The overcoring data have a considerable scatter in the ratio, but only one value lower than 2. The mean value is 3.5. It should be noted that the hydraulic fracturing results for maximum stress gives much lower values and never higher than 2. Actually, the often used way of estimating maximum horizontal stress from hydraulic fracturing *always* gives a ratio around 2, and therefore will not give reasonable estimates of the maximum stress in areas where the ratio is not 2. The overcoring results in Figure 3-58 indicates, although data are scattered, that the ratio is not equal to 2 at Äspö and this supports the decision to use hydrofracturing results for minimum stress determination only.

The minimum stress level measured at Äspö is of the same order of magnitude as the minimum horizontal stress in KLX02 (Figure 3-57). This further supports the idea that the general stress field is similar in the whole region.

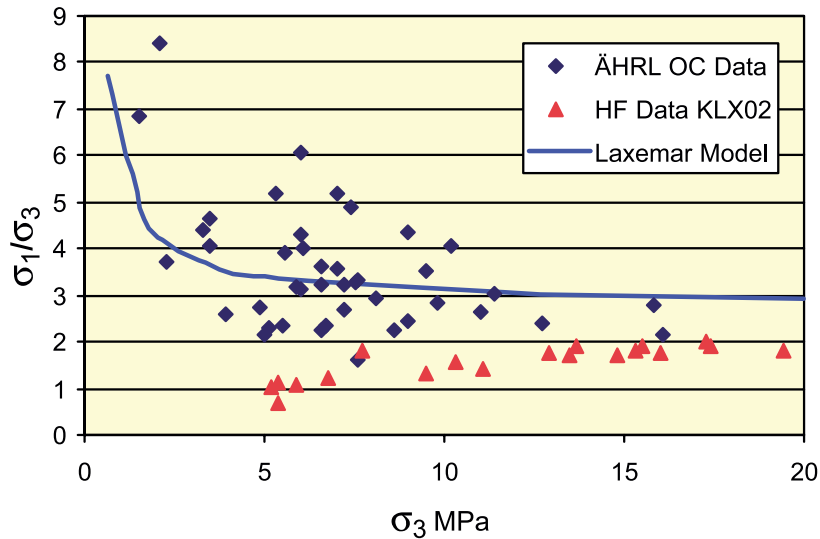


### Ratio between Maximum and Minimum Principal Stress



**Figure 3-58.** Ratio between maximum and minimum principal stress measured with overcoring techniques in several boreholes in the Äspö HRL (The function chosen as stress model for Laxemar will be explained in Section 4.4).

### Ratio between Maximum and Minimum Principal Stress



**Figure 3-59.** Ratio between maximum and minimum principal stress vs. the minimum principal stress from overcoring data. ( $\sigma_{H1}/\sigma_b$  vs.  $\sigma_b$  for hydraulic fracturing data is given for comparison).

The borehole KLX02 intersects a more fractured area between 700–1100 m depth (see previous discussion) and in this part of the borehole few measurements could be made. It can be expected that the fractured zone may influence the results in some way, either by influencing the measurements as such or that the actual stress levels are influenced at the zone /Hakami et al, 2002/. The variation observed in the data along the hole is also not negligible. The general trend is however clearly a stress increase with depth.

Another observation to be made is that there are no overcoring measurements from Äspö at 500 m depth or deeper and only two points with minimum stress levels higher than 15 MPa. This makes it uncertain to predict the maximum stress in the deeper parts of the borehole. Figure 3-55 indicates that the minimum horizontal stress in KLX02 is expected to be about 15 MPa or higher from 500 m depth and deeper. Although there is a lack of data, the Figure 3-59, showing less scatter with higher minimum stress, suggests that a  $\sigma_1/\sigma_3$  ratio in the span between 2 to 4 should cover the actual conditions also at depth.

Observed  $\sigma_1/\sigma_3$  ratios from other overcoring stress measurements in the Fennoscandian shield (Swedish and Finnish data from /Martin et al, 2001/) show similar span but on the average lower values, around 2. The fact that Äspö is located south of the other points in the database could be a potential explanation, but there may be other explanations to the differences. A detailed study of the stress database was outside the scope of this project.

### 3.10.5 Borehole seismic data from KLX02

Currently there are no rock mechanics property measurements from Laxemar. However, the project has explored the possibilities to use the borehole seismic data in the characterization of rock mechanics properties along a borehole. The compressive and shear wave velocity has been measured along KLX02 by means of a 2SAA-1000 Sonic Probe equipment. A measurement point is expected to have a rock volume of influence in the order of 1 m<sup>3</sup> (The distance between transmitter and receiver is 0.9 m). The wave velocities along the whole borehole are shown in Figure 3-60.

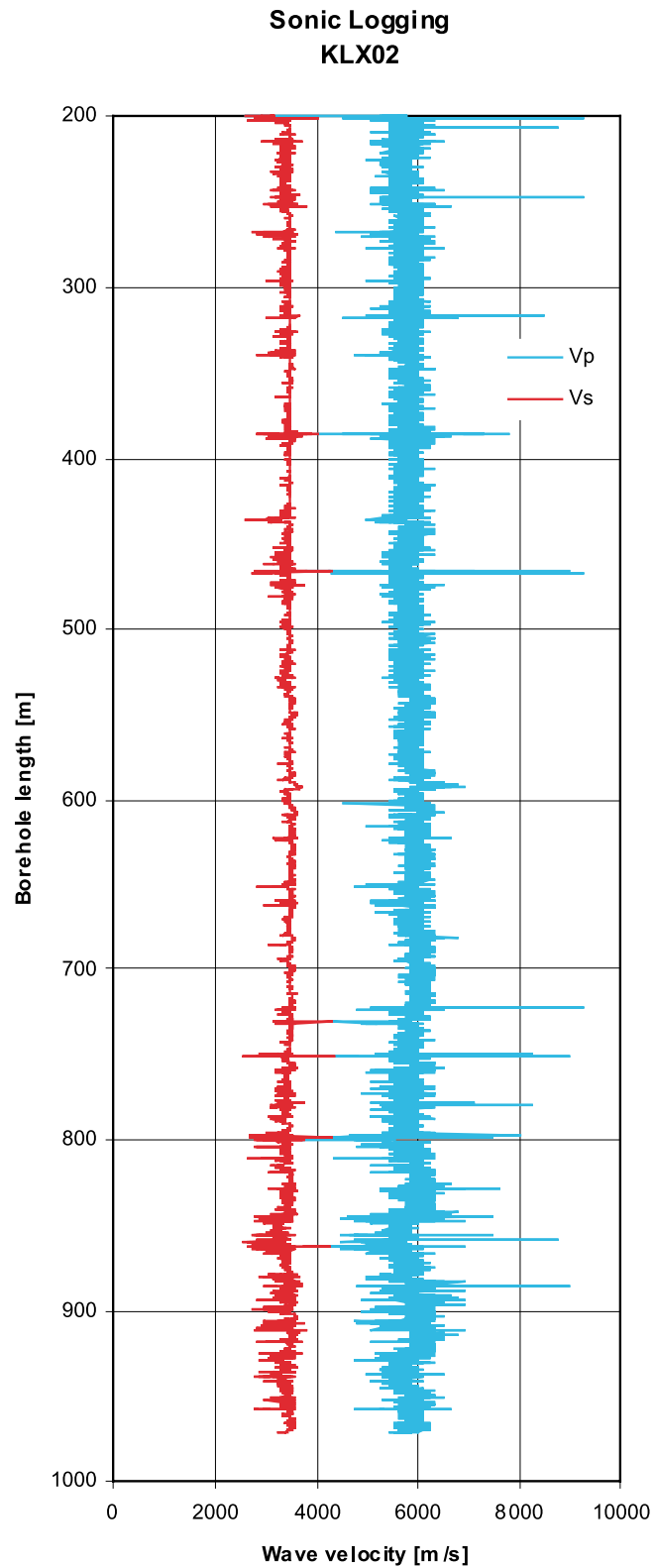
Two 50 m long sections of the borehole at different depths were chosen for this limited study. The analysed sections are located between 450–500 m depth and 900–950 m depth, respectively. The reason behind the choice of depths was, for the upper section, a depth corresponding to the Prototype Repository Test area at Äspö and inside a rock volume of good quality. The upper section is located inside rock segment R3 (high alteration and low fracturing). The lower section was selected as a section with higher fracturing and expected lower rock mass quality. This section is located inside a rock segment R8 (high alteration and high fracturing, see Section 3.4).

Empirical relations correlating the wave velocity with RQD (Rock Quality Designation) has been proposed by /Glen and Nelson, 1979/ and /Vuillermin, 1991/. RQD is a parameter that is determined for every meter during the core loggings and was available in SICADA for KLX02. The RQD tells how large percentage of the meter core that consists of pieces  $\geq 10$  cm. The two suggested relationships are:

$$RQD = 36.7 V_p^{0.52} \quad \text{/Glen and Nelson, 1979/}$$

$$RQD = 0.61 QI^{1.05}, \quad QI = 100 \frac{V_p}{V_t} \quad \text{/Vuillermin, 1991/}$$

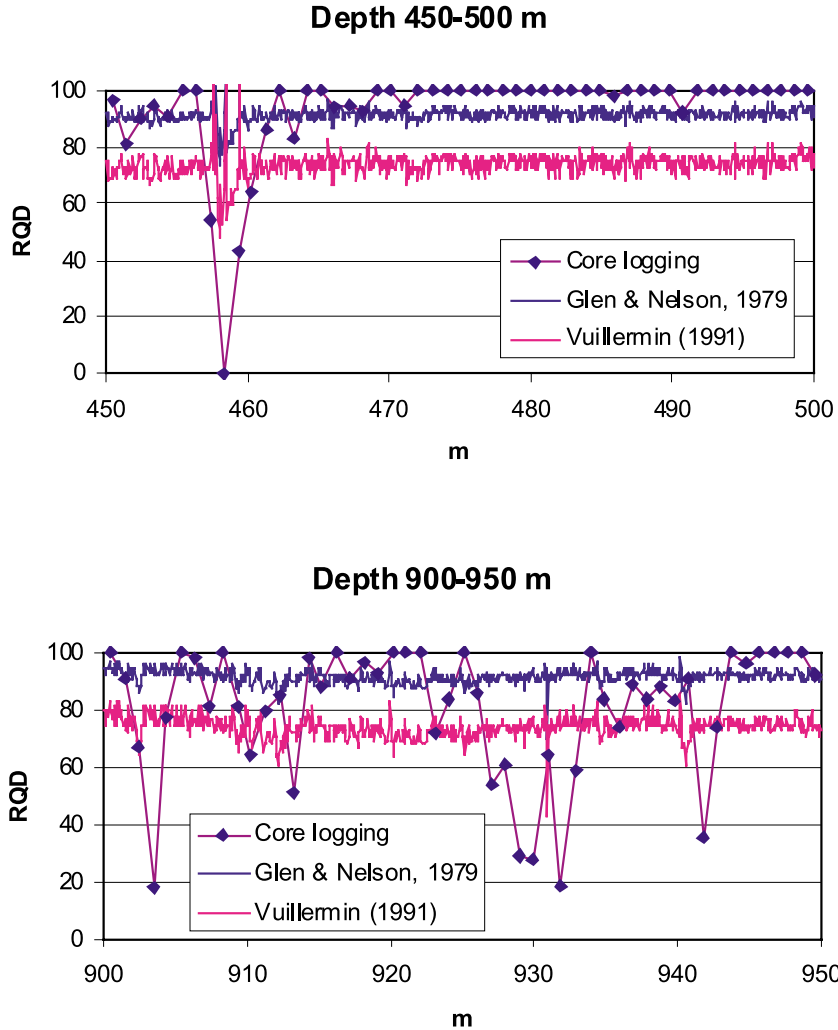
where  $V_p$  and  $V_t$  are compressional and shear wave velocities, respectively.



*Figure 3-60. Wave velocities from sonic logging in KLX02. A measurement is made every 5 cm and all data points are shown in the plot. ( $V_p$  = Compression wave velocity,  $V_s$  = Shear wave velocity).*

In Figure 3-61 the RQD determined with the two equations above are shown together with the actual RQD from the core log for the selected sections of KLX02. The wave velocities of the two sections do not differ much and thus the estimated RQD based on the sonic logging does not show a clear difference between the two sections. The fracture zone at 420 m depth is detected in the sonic log data but a similar correlation at the low RQD points of the lower section is not found. The value for the RQD determined with the Vuillemin relation is underestimating the real RQD.

Similarly, there are empirical equations relating the wave velocities with other rock mechanics parameters (Q, RMR). Given that the wave velocity does not vary significantly between the two sections, the use of any of these relationships would not reveal any major differences between the two sections.



**Figure 3-61.** Comparison of the RQD obtained from the analysis of the seismic data and from the actual logging of the drill core, for two different sections of KLX02. The upper section is within a R3 rock segment and the lower section is within a R8 segment (See geologic interpretation of borehole data, Section 3.4.3).

The sonic logging result is in contrast to the fact that the two compared sections are classified differently in Section 4.3, as R3 and R8 (low and high fracturing). The possible explanation for these apparently contradictory results may be one, or a combination of, the following:

- The empirical equations based on wave velocity might not be developed for the conditions of KLX02, but for comparison of rock sections with lower velocities. Also, the empirical equations do not consider the variation in in situ stress.
- The sonic log does not reflect differences in fracturing but reflects mainly the *intact* (small scale) rock compression modulus, which might not differ much between the sections.
- The rock mass deformation modulus at the two sections are actually fairly similar, even if the fracturing is different, considering the fairly high in situ stresses prevailing during the logging for both sections. If so, the wave velocity, which is related to the stiffness of the material in which the wave is propagating, will not be a good indicator of the degree of fracturing.

The sonic logging results indicate that the deformation modulus, for the different prevailing in situ stresses, should be expected to be similar along the whole depth of KLX02. However, it should be noted that the deformation modulus is not the only rock mechanical parameter of interest. For design purposes the rock mass strength properties during excavation conditions are desired, and the fracturing is expected to be important with respect to this.

In this project only two 50 m sections, at different depths in the same borehole, has been compared. These limited results points in the direction that sonic logging is not a useful method to reveal differences in the rock mass corresponding to differences in degree of fracturing.

### **3.10.6 Estimation of mechanical parameters for rock along KLX02**

Based on empirical and analytical relationships between rock mechanics data from borehole mapping and laboratory testing mechanical property parameters for the rock mass may be estimated. These methods are described in /Röshoff et al, 2002/ and /Staub et al, 2002/. For the Laxemar exercise there were no laboratory data available and no specific rock mechanics analysis has been performed within the scope of the Laxemar project. Nevertheless, an estimation of parameters suggested for the site investigation /Andersson et al, 2002/ has still been performed based on 1) limited Laxemar data and 2) the experiences from the Test Case project at Äspö and 3) the common understanding of the subject (see further Section 4.4).

As a first step in the characterization, the “input” parameters to be used for further empirical or theoretical analysis must be estimated. The most dominating factor for the rock mechanics description is the fracturing, which can be characterized using several different parameters (fractures frequency, fracture spacing, block size, number of fracture sets etc), and we here selected to use RQD which is one of the core logging parameters used for existing cores. Further, the discrete fracture network analysis that was described in Section 3.8 returns the intensity parameters  $P_{10}$  and  $P_{32}$ , also reflecting the degree of fracturing along a borehole and within a volume. Using RQD in combination with other rock conditions factors, empirical indexes such as RMR and Q may be estimated, but such classification was not performed for KLX01 or KLX02 in this project.  $P_{10}$  and  $P_{32}$  may be used in discrete element modelling studies of fractured rock behaviour (no existing empirical relation uses  $P_{10}$  or  $P_{32}$  today).

In Table 3-32 values or ranges for RQD,  $P_{10}$  and  $P_{32}$  are predicted for KLX02 in four different “categories” depending on whether a volume inside or outside a deformation zone is considered and depending on the depth. (The term “Deformation zone” here refer to a unit in the RVS model that has a defined width and this unit takes up a geometrically specified volume of the domain. The determination of deformation zones are described in Section 4.1). Inside the deformation zone volumes the fracturing is expected to vary strongly. In the upper part the fracture zones are expected to be generally wider and the width and location better known compared to at depth. To reflect this the judged possible span is estimated from 0 to 60 in upper part of domain and from 20 to 100 at lower parts. The scale for the estimated value is the mean RQD for 5 m borehole segment. KLX02 does not cross any fracture zone close to ground surface and through most of other fracture zones there are no boreholes available. Therefore the values of estimated RQD for deformation zones is selected also based on the knowledge from Äspö where the largest zones showed fairly thick soft clay cores. Such large zones may also exist in the Laxemar domain (The geological model for Laxemar will be presented in Section 4.1).

The division into two different depths are performed to indicate the expected depth dependence of variables. No sharp changes in properties should of course be inferred from this division. The fracture frequency logging has not shown any clear tendency for less fracturing with depth (in the rock outside fracture zones), Section 3.8. The upper 200 m log from KLX02 is also missing. The mechanical argument why it could be expected to have generally less fractures at depth is that at depth the rock is confined by higher stresses and fractures should therefore be created and propagate to a lesser extent. However, any evidence or investigation showing that this is true is not available. The difficulty in making such investigation is that it has to be determined what parts of a borehole that belongs to a “fracture zone” and what parts that belong to “background” rock (cf. Section 3.8).

**Table 3-32. Estimation of rock mechanics parameters along boreholes in Laxemar domain. Estimations based on data from borehole KLX02.**

Parameter	Rock Units 0–500 m depth	Rock Units 500–2000 m depth	Confidence	Comment
RQD	90–100	90–100	Medium	
$P_{10}$	2.4	<2.4	Medium Low at depth	Fractures in “Crush” not included. See Section 3.8.
$P_{32}$	2.4	<2.4	Medium Low at depth	–”–

Parameter	Deformation Zones 0–500 m depth	Deformation Zones 500–2000 m depth	Confidence	Comment
RQD	0–60	20–100	Low	Depends on definition of Deformation zone width. No boreholes through most zones.
$P_{10}$ and $P_{32}$	n.a.	n.a.		Not applicable for deformation zones.

## 4 Three-dimensional site descriptive modelling

This chapter concerns the three-dimensional descriptive modelling process. The modelling builds on the primary data evaluation described in Chapter 3.

### 4.1 Geological and geometrical modelling

The geological modelling provides the geometrical framework for the modelling in other disciplines. The modelling should provide /SKB, 2001/ geometry and properties of deformation zones of sizes down to ‘local major zones’ (1–10 km) and geometry and properties of rock domains. Fracture zones and fractures not explicitly defined should be described statistically and be given as properties of the rock domains. The model should also include uncertainty estimates. Some aspects of uncertainty may be illustrated by presenting alternative models.

#### 4.1.1 General modelling assumptions

##### ***Model properties***

The identified geological units within the model boundary define the geometry of site descriptive model. The modelling is performed such that geometries of identified geological units are defined in space within the model boundary. All geometries are constrained by the model boundary. The extent and termination of geometries within the model are defined by the modeller. When the geometries are defined then each object is described in terms of its geological character. There are two main object types in the Laxemar model that are assigned geological properties;

- Rock units
- Deformation zones

A *rock unit* is defined as a volume of the rock mass that is interpreted to have similar geological character /Munier and Hermanson, 2001/. This is the smallest entity that can be defined in the rock mass. Soil units are the equivalent for the soil cover at the site. Rock units can be combined to *rock domains* to illustrate parts of the rock mass that are geometrically separated but has similar geological characteristics. *Deformation zones* are a special case of a rock domain from a geometrical point of view. The criteria for a deformation zone are such that the geological indications show increased deformation of the rock (see e.g. /Bergman et al, 1999/). Furthermore, according to SKB nomenclature (see e.g. /Andersson et al, 2000/), a *fracture zone* is a deformation zone which has mainly undergone brittle deformation. Soil units have not been defined in the Laxemar geometrical model and are thus not part of the base geological modelling. The properties of the Quaternary deposits in Laxemar are described in Chapter 3, Section 3.3.1.

Normally, the location, extent and width of deformation zones are entered into the model, together with identified rock and soil units at the site. The geometrical model is completely space filling, i.e. there are geometries filling up all available space within the boundaries of the model. The main input to the geometrical modelling is surface observations such as lineaments and geological maps and subsurface data such as seismics, radar and the geological single hole interpretation as described in Chapter 3.

## **Modelling process and alternatives**

Chains of more or less strong indices build up the pieces of a geological model. There has to be, however, at least one very strong indication of existence and size, for every geometrical element in the model volume, to justify its presence there. A part of the modelling and uncertainty evaluation is thus to document the support for each deformation zone or rock unit introduced.

The geometrical modelling of the Laxemar site is an iterative process that have passed several stages of model versions and alternatives as more data from the site was considered. Two different geometric models have been produced for the site. The primary geometrical model is a *base geological model* that has been focussed on the deformation zones, interpreting the rock mass between the zones as being one single homogeneous rock domain. Secondly, an *alternative geological model* has been produced that describe an updated, more complex, interpretation of the deformation zones and several rock domains. Thus, it could be argued the alternative model is only a more updated *version* of the base model. However, uncertainties in interpretation are such that also the (original) base model should be retained as a potential possibility, thereby illustrating the uncertainty in geometry when there is only limited information.

## **RVS modelling tool and model versions**

Geometrical modelling in three dimensions requires a tool that can handle not only the creation of complex geometries, but also the visualisation of geographical data in space. SKB has developed RVS (Rock Visualisation System) for this purpose.

RVS version 2.3 has been used in the present project. RVS Version 3.0 was considered, but was not yet ready for productive use within the time frame of the project. Part of the project group have been testing version 3.0 concurrently during the present project, but it has not been possible to convert quality controlled models to version 3.0. Several comments and issues regarding the RVS functionality have been left out as the new version indicates that these things will be solved. Notes have been made only when there are clear indications that this functionality is needed, but is not known to be included in the new RVS version.

### **4.1.2 Base geological model**

The derivation of the base geological model has been focussed on the deformation zones, interpreting the rock mass between the zones as being one single homogeneous rock domain. As a part of the current analysis the existing data were evaluated regarding reliability and confidence. It was decided that a general hierarchy for three-dimensional modelling should prevail among the primary input data on the basis of its source:

- Geological mapping of the surface (Section 3.3) and of the two cores from KLX01 and KLX02 (see Section 3.4), but also some field data from the Oskarshamn feasibility study /Bergman et al, 1998, 2000/.
- Lineament map of this project (see Section 3.2).
- Seismic reflection data (see Section 3.5).
- Radar reflection data (see Section 3.5).



- Regional, external and older lineament studies as well as geological structures in the region extending into the present investigation area (see Section 3.2).
- Information from percussion drillings made in the area (HLX01–HLX12). The information from the percussion holes has only briefly been used to confirm the existence of a few deformation zones.

Other data that has been considered but not used is VLF-data, aeromagnetic data and resistivity data. Seismic refraction data are important to indicate deformation zones at the surface but where not available within the model boundaries.

### **Deformation zones**

The lineament study of the Laxemar area is the starting point in the interpretation of the geometrical units of the Laxemar model. Without the possibility to check the geological characteristics of each lineament in the field or through more investigations it is, as a primary working hypothesis, assumed that the following lineament classes (cf. Figure 4-1) are indeed deformation zones of some kind;

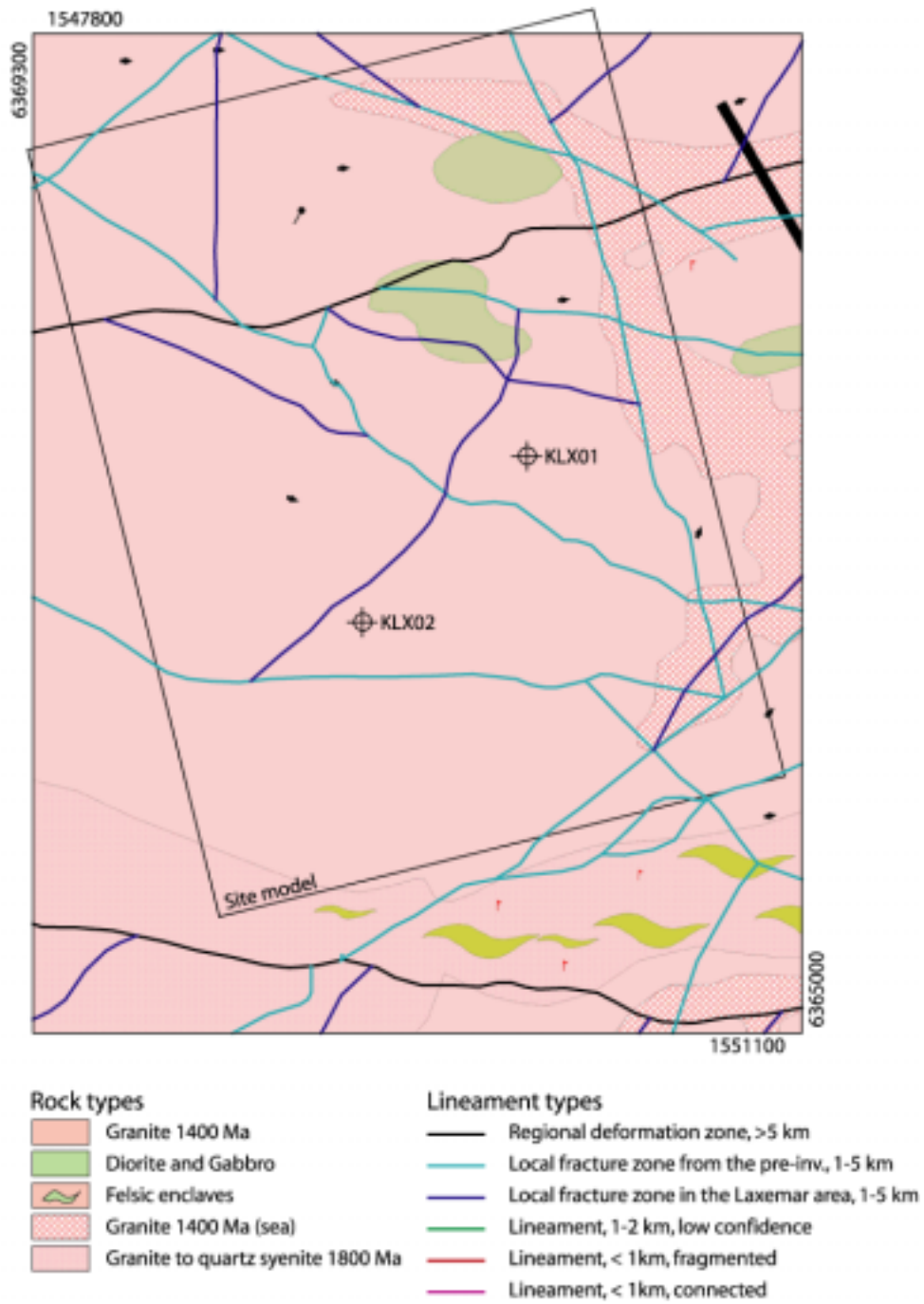
- Regional lineaments including regional magnetic lineaments, (verified as ductile deformation zone in the field) identified in the feasibility study, > 5km
- Local lineaments from the feasibility study, 1–5 km
- Local lineaments in the Laxemar area, 1–5 km as listed in Section 3.2.

This assumption is thus pre-defined in the primary data analysis and is not subject to any exclusion in the *base geometrical* model. Smaller lineaments have not been modelled deterministically, but form part of the fracture statistical analysis of the region, cf. Chapter 3.8.

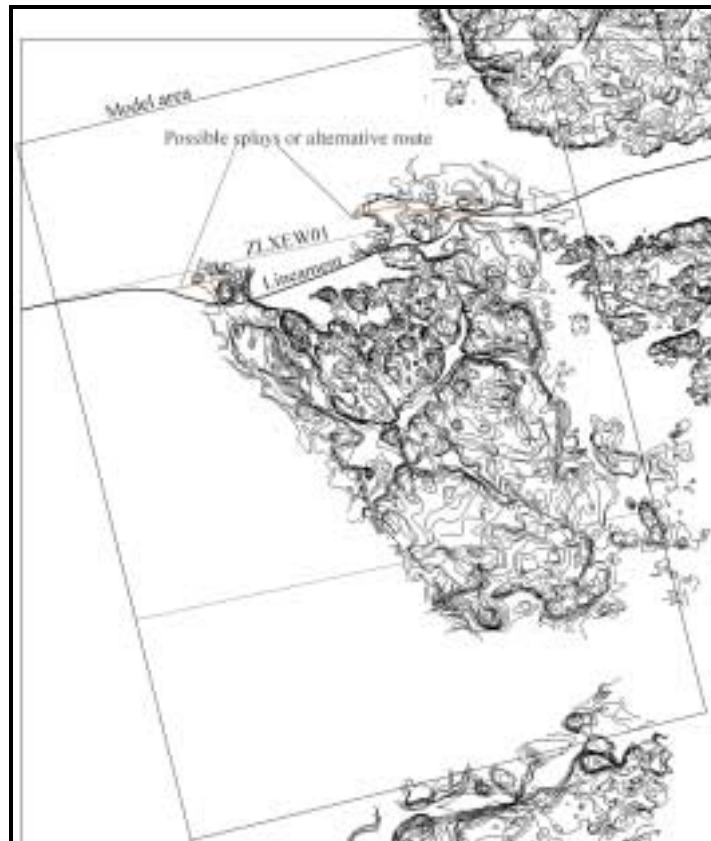
The lineaments provide input to the location of the zones on the surface. As a first assignment a best-fit line was drawn along the lineaments. This was done by hand through visual observation. As an example the zone ZLXEW01, in Figure 4-2, was drawn along the northern part of the lineament. This position takes into consideration the extension of the zone outside the model area, but also the possible existence of splays or alternative routes.

It was attempted to allocate a probable zone width based on the topographic map expression, but it was abandoned, as the topography alone is highly uncertain as a width indicator. Another attempt was made to interpret geometrical zones as rectangular blocks with a width that would encompass the undulation of the lineament. As an example, the width of ZLXEW01 was set to 350 metres. However, this interpretation shows not only the location of the zone, but also the geometrical uncertainty of where the zone may be located. This type of interpretation may be useful for estimating the uncertainty of the geometries but does not give useful input to subsequent use of the model in other geoscientific disciplines.

Finally, it was decided that interpretations based only on lineaments should be used to produce geometries of zones with no width and vertical dips that are planar to as great extent as possible. The reason for choosing vertical rather than some other dip, was primarily done on empirical grounds. A majority of observed zones as they appear on Äspö and on the Simpevarp peninsula (and elsewhere in Sweden) are steeply dipping. Also earlier studies of zones in the Laxemar area have indicated steep dips of existing zones /Rhén et al, 1997/.



*Figure 4-1. The subset of lineaments that have been used in the geometric modelling.*



*Figure 4-2. Illustration of a modelled zone (ZLXEW01) in relation to the associated lineament.*

Due to time constraints, the base geological model development has been limited to considering lineament and single hole interpretations (see Chapter 3.4). The resulting model is illustrated in Figure 4-3. Table 4-1 summarises the geometry and basis for the modelled zones. The model has the following characteristics:

- With subsurface data from only two boreholes the base geological model is dominated by a majority of vertically dipping zones.
- Two zones, ZLXNE03 and ZLXNE04 cf. Figure 4-3, are based both on lineaments and intersections in boreholes KLX01 and KLX02. To interpret the dip of these zones as well as estimating the geological width the highly fractured sections, cf. Table 4-1, and the identified rock segments (R8) have been used together with hydraulic inflow measurements, (see Chapter 4.2).
- ZLXNE01 was modelled based on a regional and a magnetic lineament (lineament on magnetic maps), as primary input. Two field observations exist from this zone (see Chapter 5.1) and indicate a southerly dip of the zone.
- ZLXEW01 is the most significant zone interpreted to cross the model domain. The lineament has regional extent and other lineaments seem to be truncated, end or be faulted along this lineament. It has also been verified by “semi-regional resistivity measurements” /Eriksson et al, 1998/. ZLXEW01 has been modelled as a vertical plane in the base case model and all other zones are truncated against this structure.

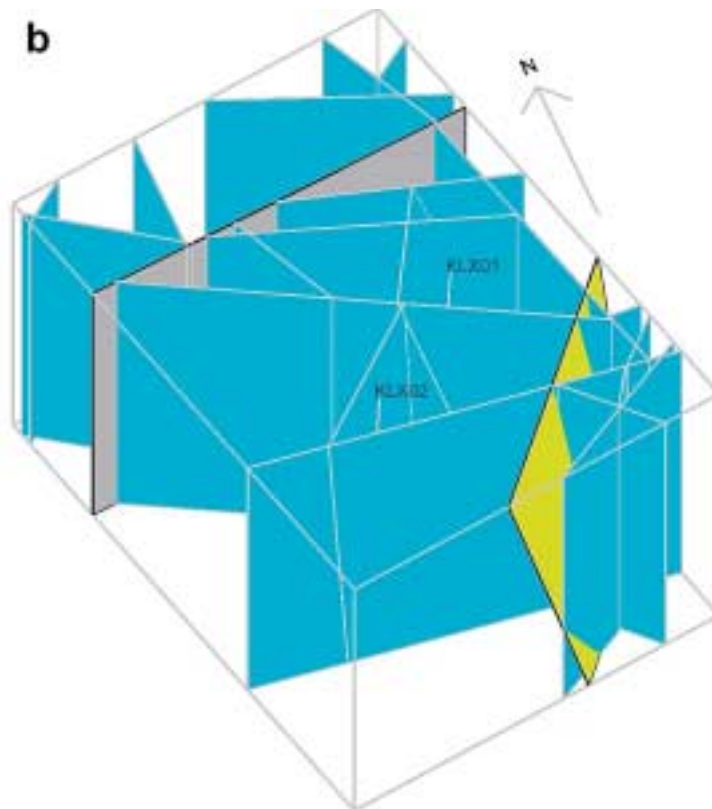
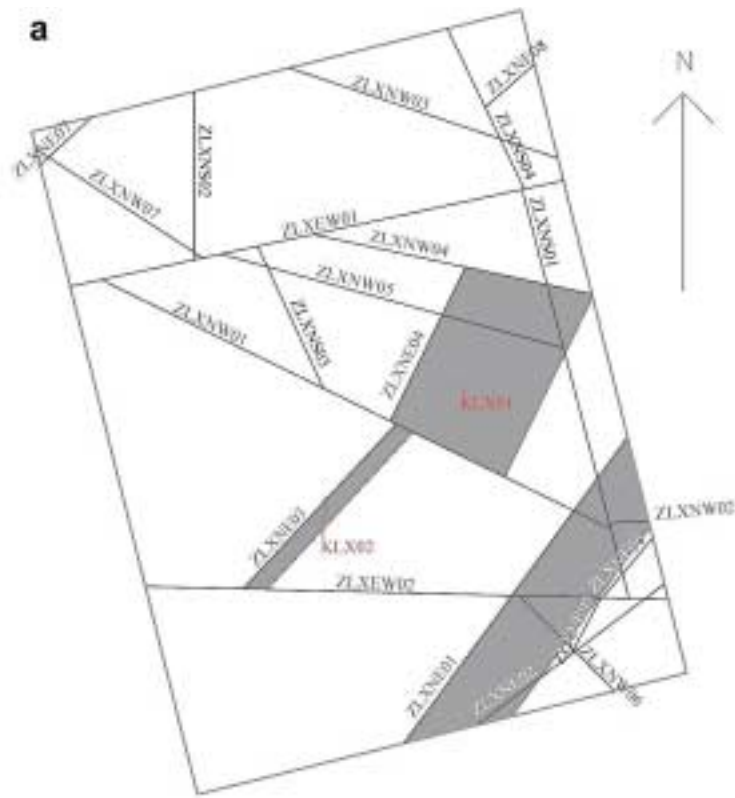


Figure 4-3. Base geological model. Figure a) show a top view with zone names indicated and b) an isometric view.

The geometrical RVS-representation of the base geological model for Laxemar comprises all together 21 zones and hence 18 of these are modelled as vertical planes. The final co-ordinates for the corners of modelled zones (rectangles and polygons) are presented in Appendix C1.

**Table 4-1. Brief zone description, base geological model.**

<b>Zone name</b>	<b>Surface observation</b>	<b>Subsurface observation</b>	<b>Geophysical indication</b>	<b>Orientation</b>	<b>Truncation – termination</b>	<b>Comment</b>
ZLXEW01	Topography: Regional lineament		HRR Magnetic	78/90	Model boundary	Probable/ Certain
ZLXEW02	Topography: Local major lineament			91/90	Model boundary	Probable
ZLXNE01	Field data		Magnetic lineament	36/80	Model boundary	Certain
ZLXNE02	Topography: Local lineament			53/90	Model boundary	Probable
ZLXNE03	Topography: Local major lineament	Rock segment in KLX02, HLX01, Regional support		43/87.5	ZLXEW02 ZLXNW01	Probable/ Certain
ZLXNE04	Topography: Local major lineament	Rock segment in KLX01, HLX04, HLX02		27.5/72	LXNW01 ZZLXNW04 Model boundary	Probable/ Certain
ZLXNE05	Topography: Local lineament			28/90	ZLXNE02 ZLXEW02	Possible
ZLXNE06	Topography: Local lineament	HLX08 Regional support		40/90	ZLXEW02 Model boundary	Probable
ZLXNE07	Topography: Local lineament			47/90	Model boundary	Possible
ZLXNE08	Topography: Local major lineament			49/90	ZLXNS04 Model boundary	Possible
ZLXNS01	Topography: Local major lineament	Regional support		165/90	ZLXEW02 ZLXEW01	Possible
ZLXNS02	Local major lineament			0/90	ZLXEW01 Model boundary	Possible
ZLXNS03	Topography: Local lineament			155/90	ZLXNW01 ZLXEW01	Possible
ZLXNS04	Topography: Local major lineament			154/90	ZLXEW01 Model boundary	Possible
ZLXNW01	Topography: Local major lineament	HLX01		116/90	ZLXNS01 ZLXEW01	Probable
ZLXNW02	Topography: Local lineament			86/90	ZLXNS01 Model boundary	Possible
ZLXNW03	Topography: Local major lineament			109/90	Model boundary	Possible
ZLXNW04	Topography: Local lineament			102/90	Model boundary ZLXEW01	Probable
ZLXNW05	Topography: Local major lineament			105/90	ZLXNS01 ZLXEW01	Possible
ZLXNW06	Topography: Local major lineament			135/90	Model boundary ZLXEW02	Possible
ZLXNW07	Topography: Local lineament			123/90	ZLXEW01 Model boundary	Possible

### **Rock domains in the base geological model**

The bedrock geology in the Laxemar model is based on the bedrock map in the scale 1:250 000 over the area as described in Section 3.3. The bedrock map over the model domain is very schematic and has few details, as is illustrated in Figure 4-1. In the base geological model the bedrock geology is simplified to one single rock domain that is described as granite with a minor contribution of diorite to gabbro together with unspecified mafic rocks ('greenstones'), cf. Table 4-2. Thus the base geological model contains geometries for twenty-one deformation zones and one rock domain. The soil cover on the surface has not been included in the model due to its small relative thickness compared to the depth of the model domain.

#### **4.1.3 Alternative geological model**

The alternative geological model in this study represents a more thorough analysis of the available data set including seismics, radar and selected hydraulic data from the boreholes. It also presents a more detailed sub-division of the rock mass. As already mentioned, it could be argued that the alternative model is only a more updated version of the base model. However, uncertainties in interpretation are such that also the base model should be retained as a potential possibility, thereby illustrating the uncertainty in geometry when there is only limited information.

#### **Deformation zones**

Every zone was individually re-examined for more detailed indications that could verify the existence of the zone, its orientation and character. Again, the hierarchic list of used criteria and indications at the beginning of Section 4.1 has been used to evaluate the character of each zone. In addition, the position of the dipping zones in relation to the location in the boreholes was reinterpreted using the following criteria:

- The borehole intersection point should be at or close to fractured and altered sections.
- Radar reflections that are close to the intersection point is considered in the interpretation of the orientation of the zone.
- Information from geophysical logging of percussion boreholes was used if available.
- Correlation was done with zones in the Äspö area and with interpretation during the feasibility study.

**Table 4-2. Basis for Rock domain description in Base Geological Model. The actual description is given in Section 5.1.**

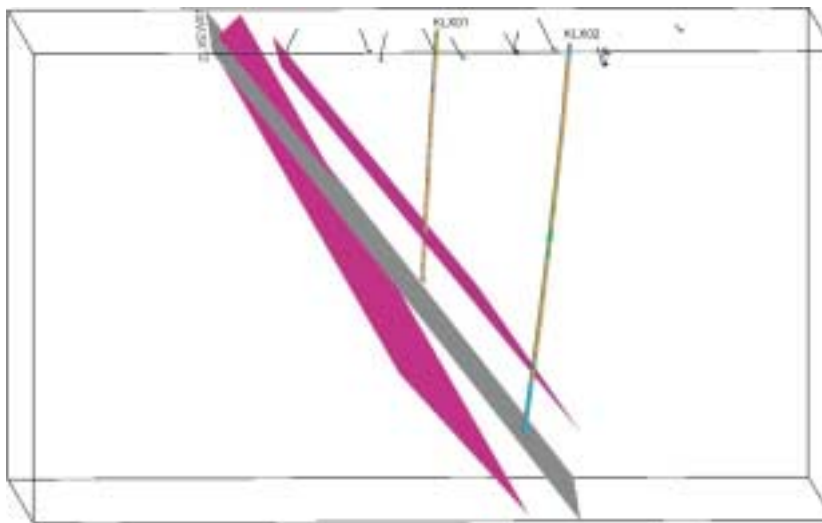
<b>Domain name</b>	<b>Surface observation</b>	<b>Subsurface observation</b>	<b>Geophysical indication</b>	<b>Truncation</b>	<b>Comment</b>
RLXA	Geological map	not accounted for	not accounted for	Model boundary	

The interpreted seismic reflectors were modelled in RVS in accordance with the interpretations and considerations made from the seismics and radar observations (see Chapter 3.6). Several of the zones do have reflectors parallel and close to their position in the model domain. In the case the interpreted orientation of a zone was sub parallel to a seismic reflector the zone was matched with the reflector. This procedure was conducted for all zones in the alternative geological model in relation to all interpreted reflectors. The result was that three more zones, ZLXEW01, ZLXEW02 and ZLXNE06, were modelled with a non-vertical dip. Seismic observations also instigated a reinterpretation of the dip angle of ZLXNE04.

The resulting zone geometry is displayed in Figure 4-12 and Table 4-3. The development of the model, and the support for the different zones is discussed in the following.

### Seismic reflectors etc

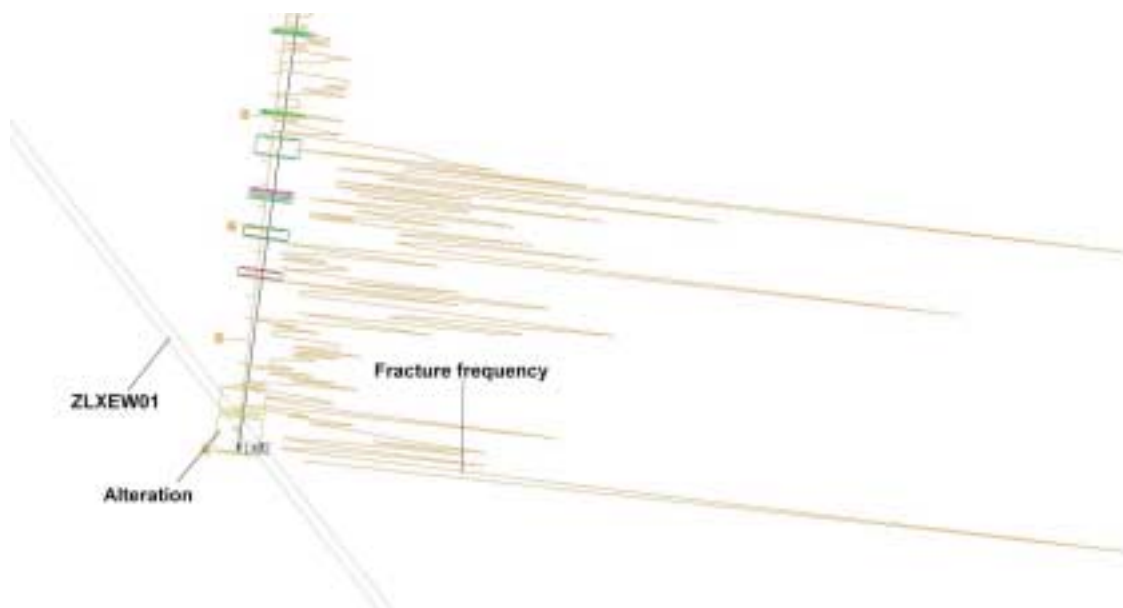
Seismic reflectors support the interpreted orientation of ZLXEW01. Particularly from reflector 4 in Line 1 (Reflector C in /Bergman et al, 2001/), cf. Figure 4-4, which indicate that the zone might dip towards the south. This reflector approximately parallels the modelled zone when the dip of the zone and reflector is set to 52 degrees. The reflected signal comes mainly from the northwest part of the model volume and is situated approximately 200 metres south of the modelled zone.



**Figure 4-4.** Seismic support for ZLXEW01. Purple planes represent the interpreted seismic reflectors that may be correlated with ZLXEW01.

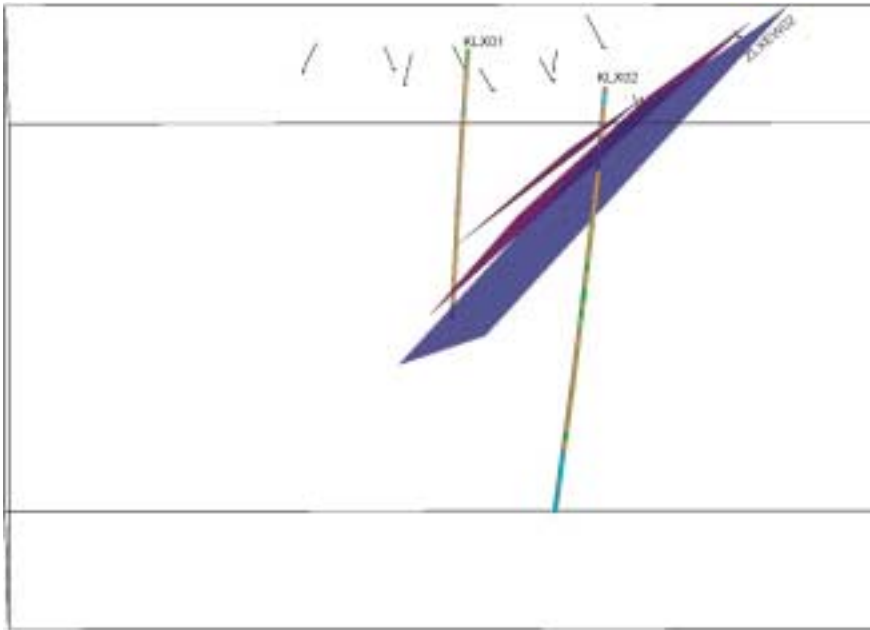
If this reflector actually reflects the location of ZLXEW01 this may imply several things. Either the velocity of the reflected wave is different from what has been assigned or the zone undulates, has offsets or parallel zones. A strong undulation of ZLXEW01 is indicated by the trend of the lineament itself. Also reflector 4 in Line 2 /Bergman et al, 2001/ may indicate that ZLXEW01 dips towards the south. The reflectors are not perfectly parallel with the modelled zone, but since it probably undulates or has developed splays (or both), it is considered a valid interpretation. The chosen position of ZLXEW01 coincides with a fractured and altered section in the lowermost part of KLX02, cf. Figure 4-5.

ZLXEW02 is also indicated in both seismic lines. Especially reflector 1 (“A” in /Bergman et al, 2001/), cf. Figure 4-6, has the character of a deformation zone. It is semi-parallel with the modelled zone when a dip of 38 degrees is applied and utilising a vertical velocity of 6000 m/s and a horizontal velocity of 5500 m/s. The two indicative reflexes from the two lines are approximately parallel with the zone at an assigned dip of 40–45 degrees. Also in this case the reflectors lie closer to the seismic line than the modelled zone (~ 175 m). However, if the reflexes come from the zone, this may suggest an undulation of the zone or that parallel zones and/or splays occur, which again are indicated by the strike of the lineament. The chosen position of ZLXEW02 coincides with a fractured and altered section at a depth of 340 metres in KLX02, cf. Figure 4-7. There are also two radar reflectors that seem to correlate with ZLXEW02 at this location.

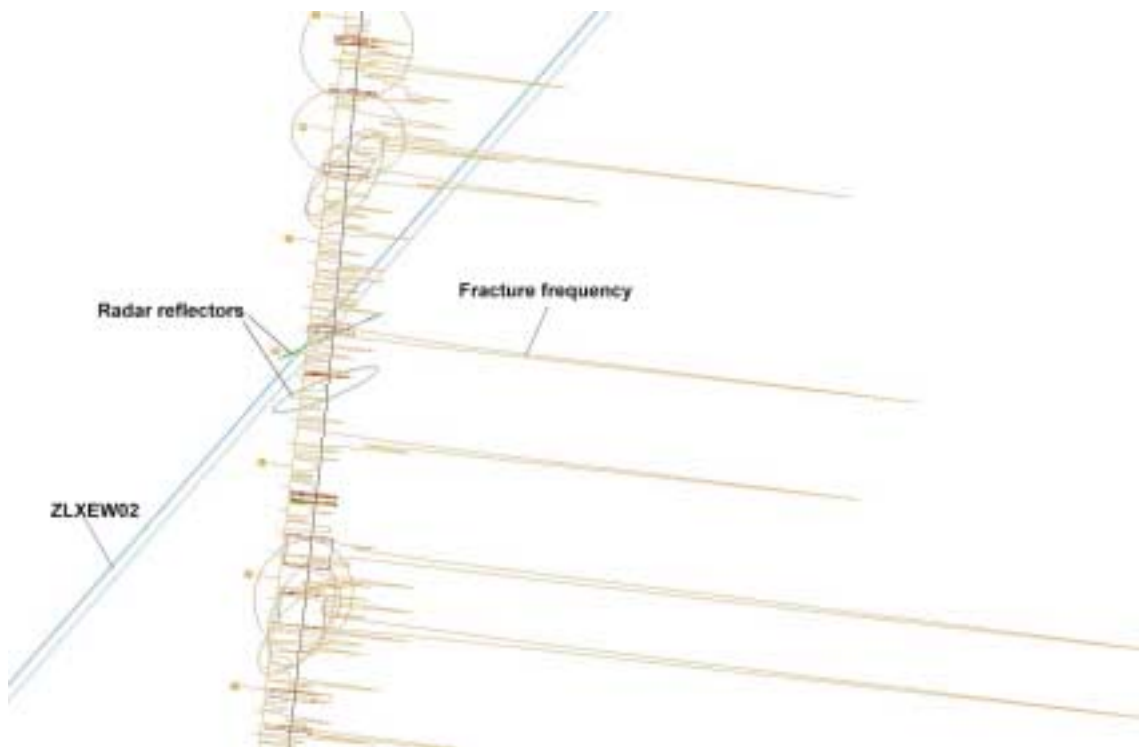


*Figure 4-5. Close-up of the intersection with zone ZLXEW01 in the lower part of KLX02.*





*Figure 4-6. Seismic support for ZLXEW02. Purple planes represent the interpreted seismic reflectors that may be correlated with ZLXEW02.*

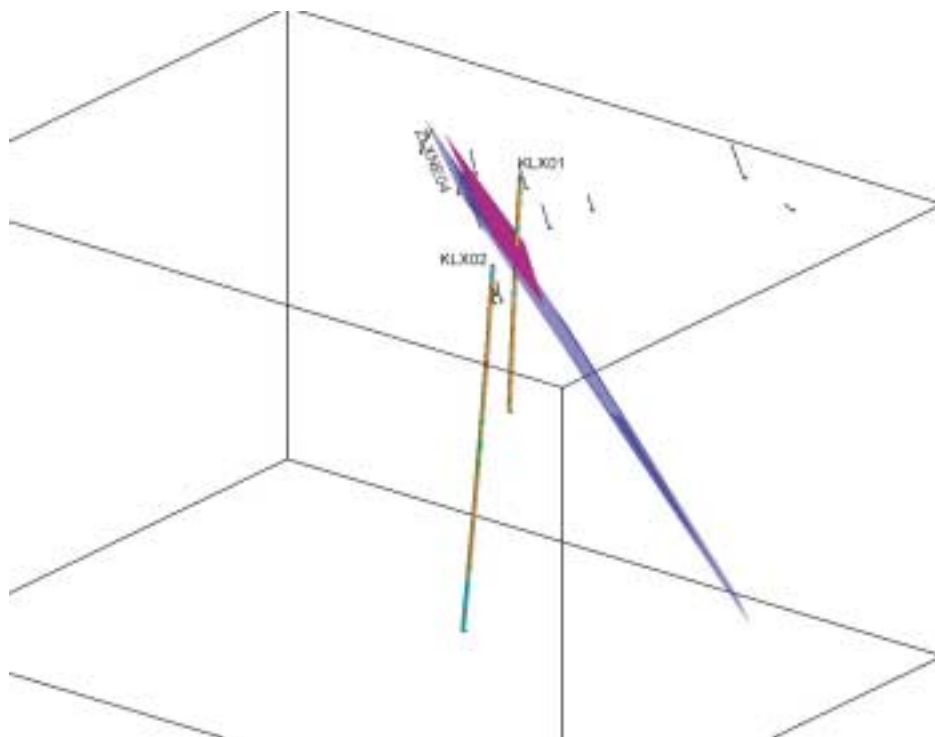


*Figure 4-7. Close-up of the intersection with zone ZLXEW02 in KLX02.*

In line 1, reflector 5 /Bergman et al, 2001/ is a strong indicator that zone ZLXNE04 may be dipping towards the SE and crosscut KLX01, cf. Figure 4-8. This was assumed in the base geological model, but with a steeper dip than what is suggested by this seismic reflector. Again the position of the reflector is sensitive to assigned velocity. In this case 6000 m/s is used as vertical velocity and 5500 m/s as horizontal velocity. This results in a plane that dips 56 degrees and reaches the ground surface very close to the topographic valley where the lineament is drawn. The modelled zone is 40 metres further away from the reflector, a position that correlates with the lineament on a larger scale. Hydraulic significant sections in HLX04 were considered, but correlation between zone dip and position in such boreholes has to be done with the actual zone on a local scale, rather than with a planar interpretation based on a lineament, cf. Figure 4-9.

Reflector 6 in Line 1 /Bergman et al, 2001/ may suggest that there exist a zone dipping 37 degrees towards KLX01 at the position where zone ZLXNW01 is modelled, cf. Figure 4-10. The fairly long and straight lineament along which ZLXNW01 was modelled indicates a steep zone. Because of the geometric uncertainty of the lineament interpretation ZLXNW01 is left vertical.

There are four seismic reflectors, two in each line, that represent potential fracture zones dipping from the southern border of the model area and just south of the area, cf. Figure 4-11. They may be correlated to represent two planes that crosscut KLX02 (/Bergman et al, 2001/; reflectors D and G).



**Figure 4-8.** Seismic support for ZLXNE04. Purple plane represents the interpreted seismic reflector that may be correlated with ZLXNE04.

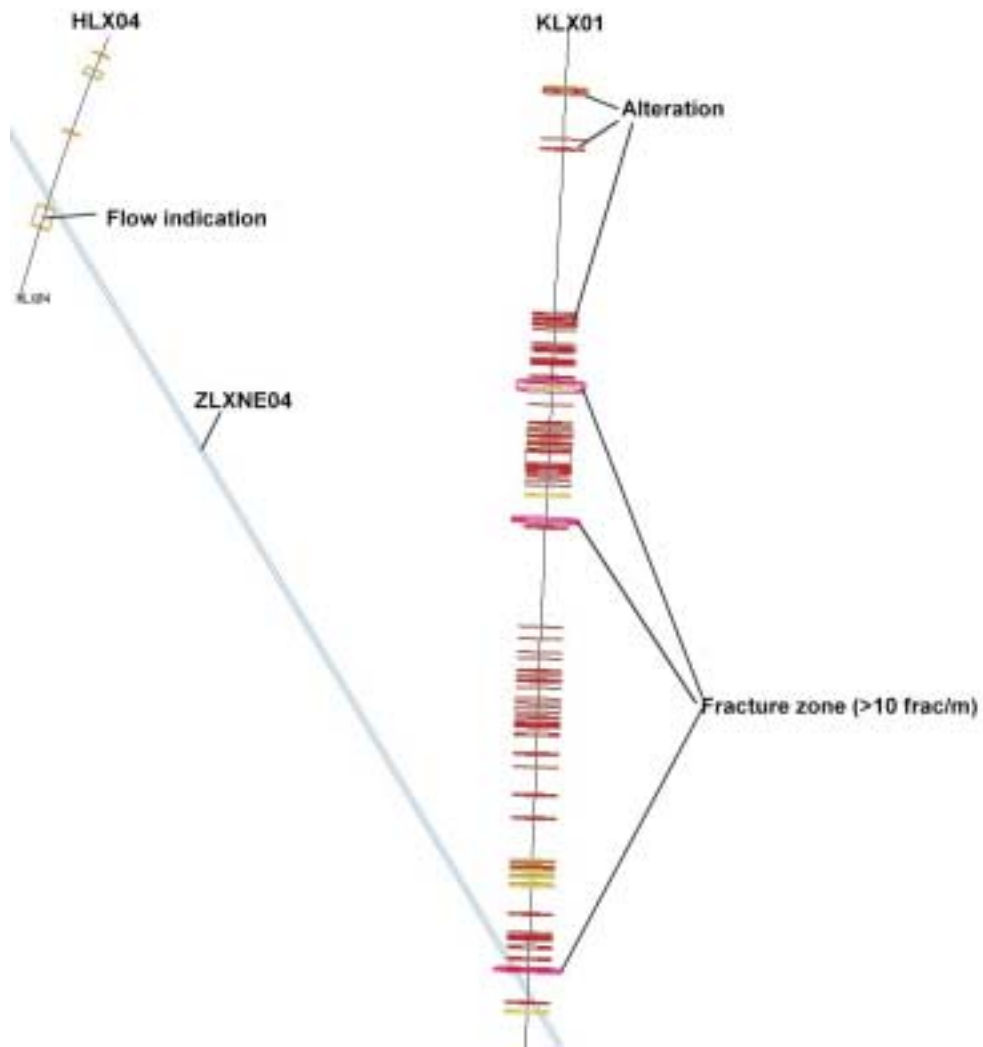


Figure 4-9. Illustration of the support for ZLXNE04 in HLX04 and the fractured sections in KLX01.

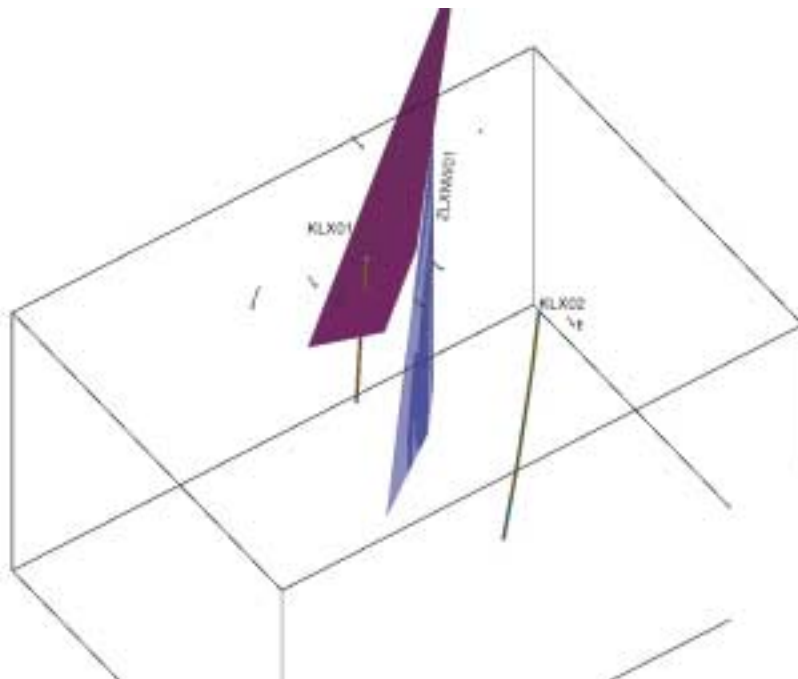
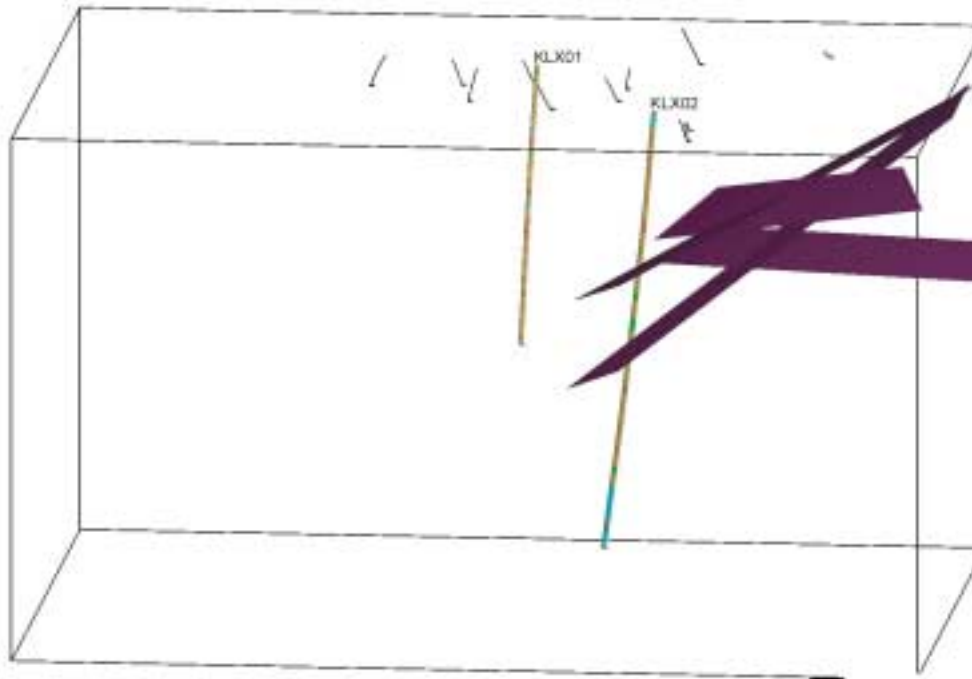


Figure 4-10. Purple plane represents the interpreted seismic reflector that may be correlated with ZLXNW01.

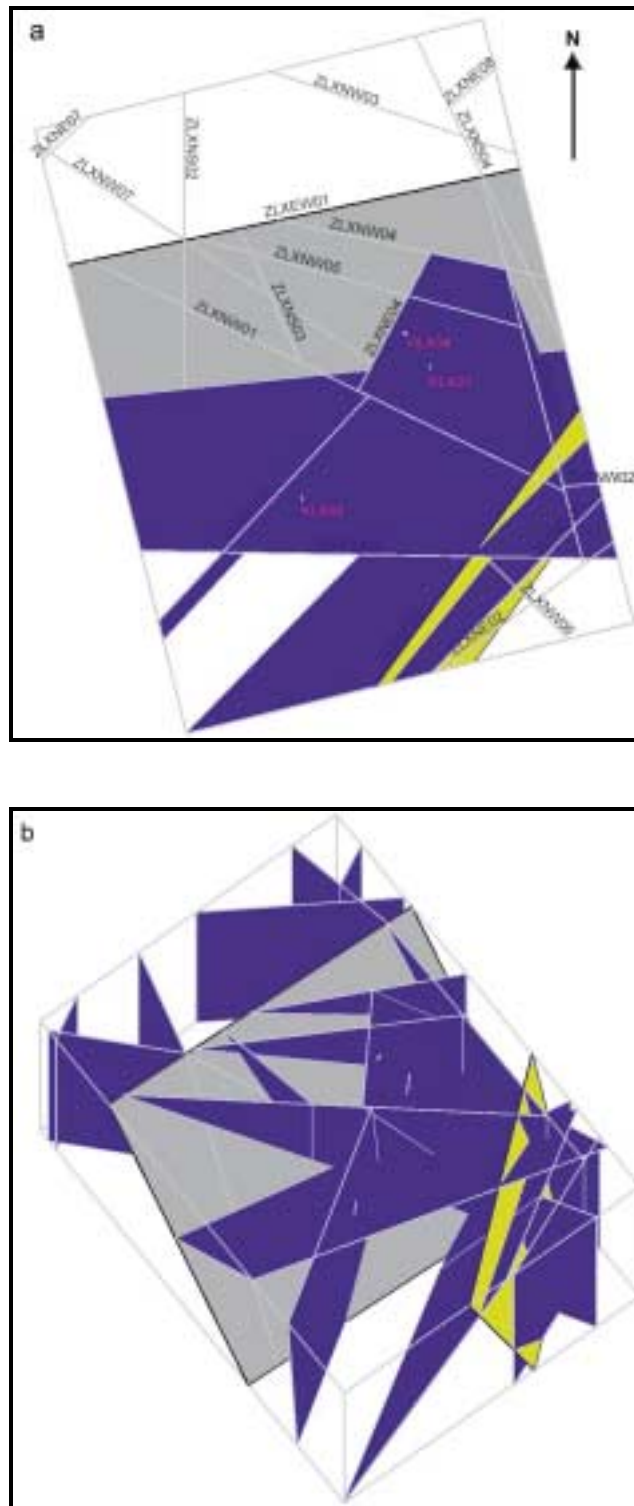


*Figure 4-11. Seismic support for potential fracture zones from south of the model area.*

### **Radar reflectors**

In KLX01 only one radar reflector has been visualized and used in the RVS modelling, due to the lack of oriented data. The visualised radar reflector has earlier been interpreted as a candidate for possible cross-hole correlation between KLX01 and the boreholes KAS02 and KAS03 at Äspö /Niva and Gabriel, 1988/. In KLX02 19 radar reflectors from /Carlsten, 1994/ (Table 3.3) have been used to correlate with suggested zone indications. However, the interpreted radar reflections normally have a large variation in orientation due to physical limitations in the methodology. Therefore radar data has been used with a lower level of confidence than direct observations. A modelled zone is primarily located in 3D with data obtained from the lineament study, field data and borehole geology, with or without support from the reflection seismic interpretation. In practise, the position in KLX02 has only been slightly adjusted if a nearby radar reflector suggested so. No zone was modelled with radar data as the primary support.

The supportive data behind the alternative geological model, illustrated in Figure 4-12, is not only very sparse, but also favour certain interpretations in a biased way. For example, the usage of the seismic data set is highly speculative as reflectors only indicate dipping directions towards the seismic lines and therefore disfavour potential dips outwards from the model centre. The subsequent usage of the model needs to keep all sources of uncertainty in mind, in order not to over-interpret the modelled structures.



**Figure 4-12.** *Alternative geological model. a) Top view and b) isometric view. The different colour denotes the size of the lineament, related to the zone; grey = regional; blue = local major and local; yellow = regional magnetic.*

**Table 4-3. Brief zone description, alternative geological model.**

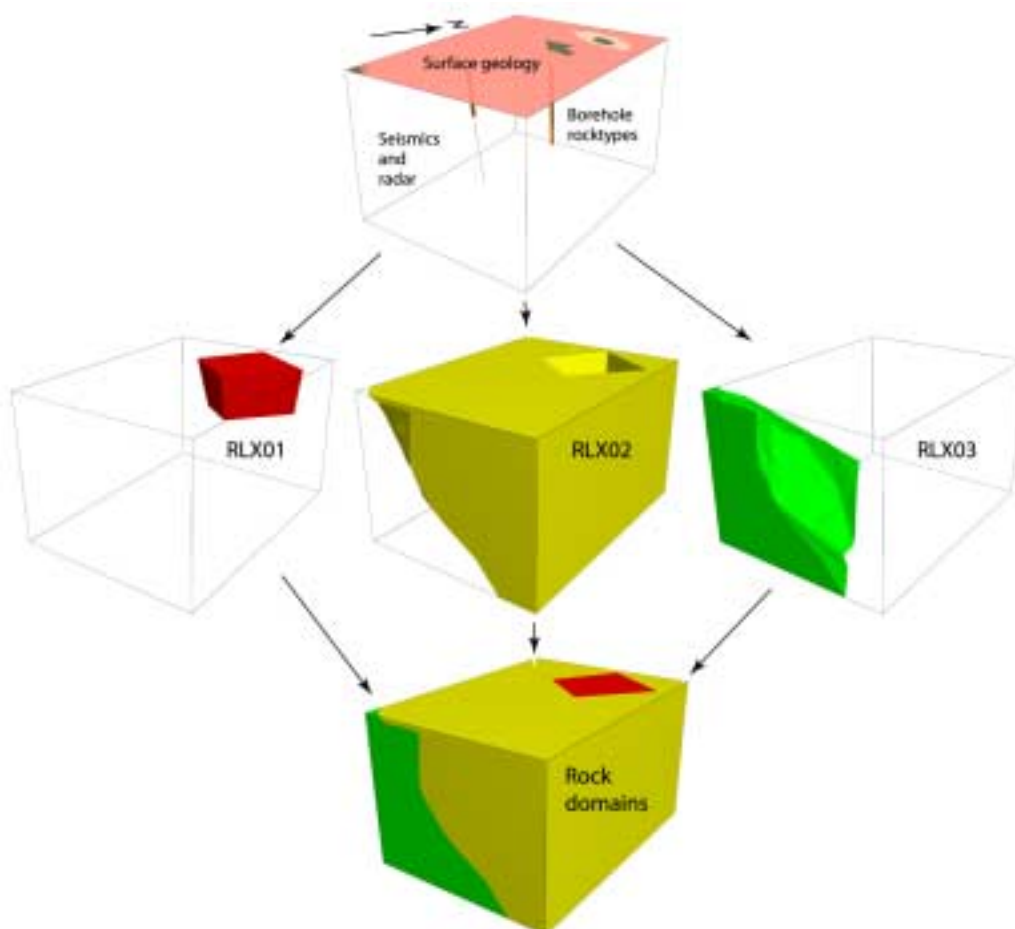
<b>Zone name</b>	<b>Surface observation</b>	<b>Subsurface observation</b>	<b>Geophysical indication</b>	<b>Orientation</b>	<b>Truncation – termination</b>	<b>Comment</b>
ZLXEW01	Topography: Regional lineament	Fractured and altered section in KLX02	HRR, Seismic refl., Magnetic data	78/53	Model boundary	Probable/ Certain
ZLXEW02	Topography: Local major lineament	Fractured and altered section in KLX02	Seismic refl. Radar refl.	271/49	Model boundary ZLXEW01	Probable/ Certain
ZLXNE01	Field data Regional support		Magnetic lineament	36/80	Model boundary	Certain
ZLXNE02	Topography: Local lineament Regional support			53/90	Model boundary	Probable
ZLXNE03	Topography: Local major lineament	Rock segment in KLX02, HLX01 Regional support	Seismic refl.	43/87.5	ZLXEW02 ZLXNW01 ZLXEW01 Model boundary	Probable/ Certain
ZLXNE04	Topography: Local major lineament	Rock segment in KLX01, HLX04, HLX02	Seismic refl.	27.5/59	ZLXNW01 ZLXNW04 ZLXEW01 Model boundary	Probable/ Certain
ZLXNE05	NOT APPLICABLE					
ZLXNE06	Topography: Local lineament	HLX08 Regional support		224/70	ZLXEW01 Model boundary	Probable
ZLXNE07	Topography: Local lineament			47/90	Model boundary	Possible
ZLXNE08	Topography: Local major lineament			49/90	ZLXNS04 Model boundary	Possible
ZLXNS01	Topography: Local major lineament	Regional support		165/90	ZLXEW02 ZLXEW01 Model boundary	Probable
ZLXNS02	Topography: Local major lineament			0/90	ZLXEW01 Model boundary	Possible
ZLXNS03	Topography: Local lineament			155/90	ZLXNW01 ZLXEW01 Model boundary	Possible
ZLXNS04	Topography: Local major lineament			154/90	ZLXEW01 Model boundary	Possible
ZLXNW01	Topography: Local major lineament	HLX01		116/90	ZLXNS01 ZLXEW01 Model boundary	Probable
ZLXNW02	Topography: Local lineament			86/90	ZLXNS01 Model boundary	Possible
ZLXNW03	Topography: Local major lineament			109/90	Model boundary	Possible
ZLXNW04	Topography: Local lineament Regional support	HLX02		102/90	Model boundary ZLXEW01	Probable
ZLXNW05	Topography: Local major lineament			105/90	ZLXNS01 ZLXEW01 Model boundary	Possible
ZLXNW06	Topography: Local major lineament			135/90	Model boundary ZLXEW02	Possible
ZLXNW07	Topography: Local lineament			123/90	ZLXEW01 Model boundary	Possible

### **Rock domains**

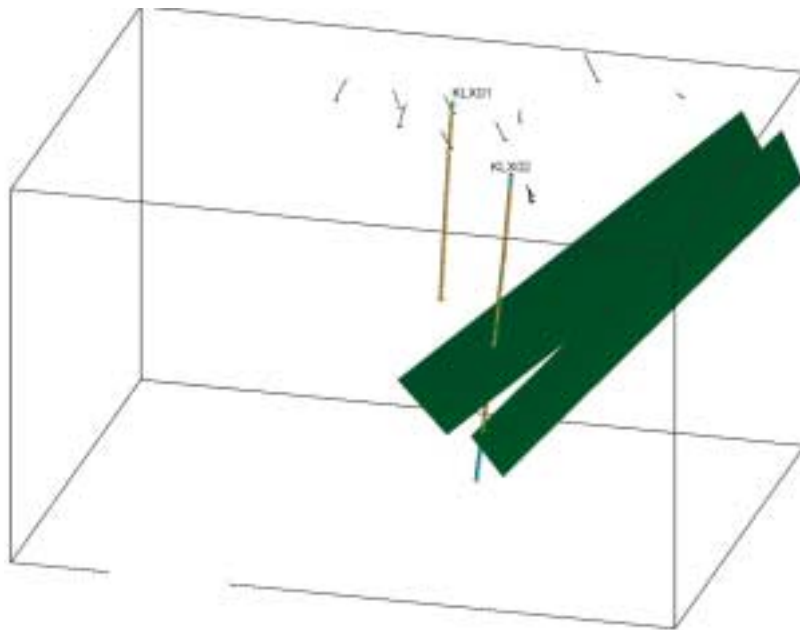
Three rock domains have tentatively been identified, based mainly on the surface distribution of rock types, and on seismic and radar indications. The geometry of the three rock domains is illustrated in Figure 4-13 and summarised in Table 4-4.

In addition to the seismic reflectors from potential fracture zones reported above there are several reflectors probably caused by diorite to gabbro ('greenstones') or similar rock types. Such reflectors are particularly common between ca 600 and ca 900 metres depth in the central part of the model volume. These reflectors generally dip at a low angle, most of them towards south, southeast and southwest. In KLX02 several occurrences of diorite to gabbro have been recorded at depth.

Many radar reflectors in KLX02, at a depth of 680–960 meters, have been interpreted as fractured diorite to gabbro. Most of them strike NW-SE and dip towards NE. This may lend support to an interpretation where a rock domain exposed in the south-western most part of the model area (composed of granodiorite to quartz monzodiorite, with intercalated mafic rock) is dipping towards the north-east. In the model the granodiorite to quartzmonzodiorite on the geological map has been correlated with the Åspödiorite mapped in KLX02 below 1450 metres. However, the interpreted diorite to gabbro has not been modelled outside the core of KLX02. This is justified by the fact that the existing reflectors are short in relation to the model volume.



*Figure 4-13. Flowchart showing the basis and interpretation of rock domains in the alternative geological model.*



*Figure 4-14. Potential seismic support for rock boundaries.*

Based on existing rock types, three rock domains have tentatively been defined, i.e. RLX001, RLX002 and RLX003. In the northeastern part of the model area, the more or less intimate mixture of diorite to gabbro and different varieties of granite to granodiorite constitute the rock domain RLX001. The deformation zone ZLXNW03 delimits this rock domain in the northeastern part, since no diorite to gabbro or red, fine- to finely medium-grained granite is documented northeast of the zone. Due to the lack of information at depth, the rock domain has been modelled with a simple box shape downwards, that does not reach the bottom of the model volume. This is an unrealistic, but simplistic interpretation of the extension at depth. The rock domain RLX002 includes the porphyritic granite to granodiorite, which is the dominating rock type at the surface in the Laxemar Model Area. The third rock domain, RLX003, is based on the inferred correlation between the granodiorite to quartz monzodiorite in the southwesternmost corner and immediately south of the Model Area, and the granodiorite to quartz diorite (“Åspö diorite”) that has been mapped in the borehole KLX02, from a depth of 1450 m and downwards ( $Z=-1421$ ). Hence, this rock domain has a presumed northward extension at depth, and dominates the southern lower part of the model volume (Figure 4-13). Due to the lack of detailed information, the frequently occurring red, fine-grained granitic dykes, as well as the occurrence of dioritic to gabbroic xenoliths to enclaves and minor bodies, are treated as being more or less evenly distributed in the rock domains.

**Table 4-4. Basis for rock domain description, alternative geological model. The actual description is given in Section 5.1.**

Domain name	Surface observation	Subsurface observation	Geophysical indication	Truncation	Comment
RLX01	Geological map			Model boundary, RLX02	Certain
RLX02	Geological map	Core logs		Model boundary, RLX01, RLX03	Certain
RLX03	Geological map	Core log of KLX02	Seismic reflection	Model boundary, RLX02	Probable



### **Confidence in alternative model**

The alternative geological model represents the sum of alternative geometries, having reasonably high probabilities. However, it is possible to present an alternative model for every possible combination of zone geometries in the modelled volume. Available geological and geophysical data alone cannot produce a reliable model to be used for other geoscientific purposes. Table 4-3 and Table 4-4 show the existing elements in the model and the basis for their interpretation.

#### **4.1.4 Evaluation of uncertainties**

The uncertainties in geological modelling can be divided into four general types;

- *Data uncertainty* which involves measurements errors of point observations, errors in the interpretation of the parameter, assumptions of conceptual models or extrapolation between point observations with a spatial distribution.
- *Conceptual uncertainties* such as the extent or variability of the geometry of a deformation zone or rock/soil unit.
- *Resolution of interpretation* (or scale dependence) of the representation of geometries and parameters in the model. For example fractures and fracture zones are represented differently a different scale of resolution, i.e. at scales with less resolution than the target site, small fracture zones may be represented as stochastic features and at more detailed scales the same zone size may be represented as a deterministic structure.
- *Confidence* level of the interpretation. This uncertainty is qualitative but can be measured in various ways by a consequent interpretation of the input data and by presenting variations of parameter estimates as statistical distributions. A further measure of the confidence level is to compare early estimates with interpretations made at a later stage with more detailed data available.

#### **Assessing uncertainty in deformation zone geometry**

The deformation zones in the Laxemar base geological model are based on lineament data having uncertainties in the location and extent of each of the identified lineaments. The length and in many cases the width of the lineaments have then been used in the interpretation of deformation zones. In zones with no other primary data information than lineaments, the dip has been set to vertical. The width has been estimated based on generic assumptions about length/width relationships or from the topographic expression on the surface of Laxemar. All these small assumptions and simplifications add to the total uncertainty of location, extent, width and geological character of the interpreted zones.

To better define the zones and decrease the uncertainty of their nature, other data such as seismic measurements, flow data, detailed borehole characterizations etc, have been used in the alternative geological model. The detailed data mostly stem from a local area of the model with a considerably more detailed resolution. All interpretations outside this area is uncertain.

Each of the detailed data sources have their specific uncertainties, which are related to the way they are sampled, equipment limitations, limited level of effort etc. For example, the seismic survey was done such that only reflectors dipping towards the intersection

between the two survey lines were possible to detect. Other possible orientations were not covered. Such uncertainties tint the underlying primary database for the interpretation in such a way that it is not possible to have the same level of certainty in the interpretations at all places in the model.

In summary, the level of geological information is of such different detail at different scales of resolution and at different locations within the modelling domain that the interpreted structures in both the base and alternative geological models are subject to extensive uncertainties. However, the interpretations have been made in the simplest possible way at all stages, such that zones have been kept planar with an identical width throughout their extent, not to infer any unnecessary uncertainties. By this modelling approach it is possible to increase the detail in the interpretation when new data becomes available.

### ***Assessing uncertainty in rock domains***

The bedrock map, which is utilised in the Laxemar model area, is of a reconnaissance character. Due to its lack of detailed information, the bedrock is simplified to one rock domain in the base geological model. However, the alternative geological model also takes into account the background fracturing, the rock types in the boreholes and seismic interpretations that extend beyond the Laxemar model domain.

### ***Assessing uncertainty in properties***

The geological model also concerns properties of the deformation zones and of the rock domains. The property predictions are provided in Section 5.1. In the latter each structure is presented in table form indicating a quantitative estimate for each parameter, a span in which the parameter is likely to occur and an estimate of the confidence level of the quantitative estimate. The span is estimated by indications in the primary data, references to similar type of structures in similar environment (Åspö) or by expert judgement. The confidence level reflects how much support in the data there is for the quantitative estimate.

## **4.2 Hydrogeological modelling**

Three-dimensional site descriptive modelling of the hydrogeology requires integrated evaluation with several other disciplines. Essential hydrogeological tools are interference tests and numerical groundwater flow modelling. This section concerns the three-dimensional site descriptive modelling, which will lead to a site descriptive model summarised in Chapter 5. The single-hole evaluation presented in Section 3.7 is the hydrogeological starting point for the evaluation, and generally the single-hole evaluations made during different investigations can be used directly for assigning hydraulic parameters. However, if some criteria used in the analysis of the single-hole results has been changed, for example definition of possible fracture zones, parts of the old single-hole evaluation has to be updated.

### **4.2.1 General modelling assumptions**

The base for the hydrogeological modelling is the Geological model with its identified volumetric objects; *Deformation Zones*, *Rock Units*, *Rock Domains* and *Soil Units*, see Section 4.1. Deformation zones may be Brittle Deformation Zones (Fracture zones)

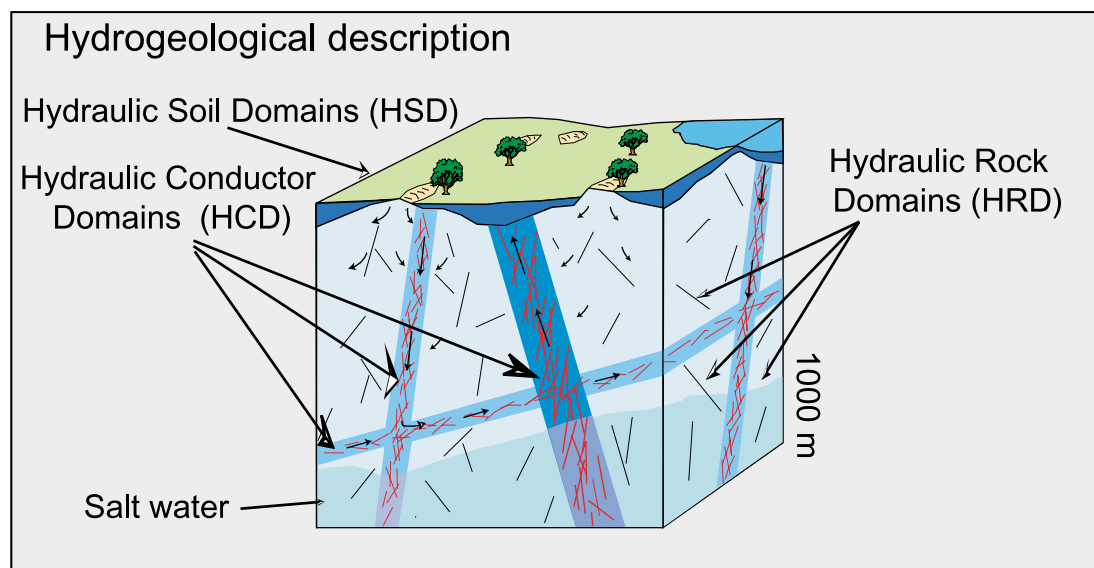
or Ductile Deformation Zones. Rock units with similar geological character but e.g. separated by deformation zones can be combined into a *Rock Domain*. *Soil units* are based on the interpretation of the spatial distribution of different types of Quaternary deposits. As for rock units, soil units with similar geological character can be combined into a *Soil Domain*.

Due to limitations in scope, only the base geological model (see Section 4.1) has been considered as input to the hydrogeological description. Potential implications of considering the alternative geological model are discussed though.

The results from the hydraulic single-hole tests, together with the single hole geological evaluation indicate where deformation zones intersect the boreholes but give no or uncertain information about their possible extent and orientation. (Even if orientation of individual fractures can be made with good accuracy with Borehole-TV and core mapping, such local information is of little value for determining the large scale orientation of zones.) High transmissivity zones are likely the result of brittle deformation (i.e. the zones should be regarded as fracture zones), but possibly there also exists reactivated Ductile Deformations zones with significant transmissivity. Lacking further information all zones are called Deformation zones in this analysis.

Based on results from interference tests the existence of some of the deformation zones can be strengthened or confirmed. Within a relatively large rock volume the orientation, size and properties of the features can be analysed and discussed. The result from the interference tests may also give reasons to revise the positions (in bore holes), orientations, extent (and termination) and connectivity (to other zones) of some deformation zones. Such potential revisions should then be fed back to the geological modelling in order to explore whether revisions of the geological model would be feasible.

The analysis of the hydraulic single-hole tests and interference tests together with the geometrical description of the deformation zones and the rock domains gives as result assigned properties to *Hydraulic Conductor Domains (HCD)* and *Hydraulic Rock Domains (HRD)* that generally coincide with the defined deformation zones and rock domains respectively, see Figure 4-15. However, a deformation zone or a rock domain may be subdivided into two or more HCD or HRD respectively, if the hydraulic properties vary significantly within the geologically defined domain.



*Figure 4-15. Principal illustration of features in a hydrogeological model.*

The initial base for the hydrogeological modelling is the single-hole tests results as presented in Section 3.6 and 3.7 together with the first version of the geological model with its deformation zones and rock domains. The geometrical description provided by the geologist is the base for more accurate analysis of the single-hole tests and the subsequent interference tests. (The evaluation of an interference test can start, as soon as the data are available but cannot be finished without having accurate geometrical information.) The analysis provides the foundation for the internal discussion, mainly with the geologists but also with the other disciplines, about the relevance in the geometrical description of the suggested deformation zones (as deterministic objects) and rock domains and other alternatives to the geometrical description. When one or several geometrical alternatives are agreed upon within the project as *Model Version X.Y* (as *base model* and *alternatives*) the data has generally to be re-analysed to some extent to define the properties of the domains for the base model and the alternatives. Parameters for a domain may be constants or stochastic variables with or without spatial correlation.

The geometrical description of the Quaternary deposits, their geological character (mainly grain size distribution) and hydraulic test results are used to make hydro-geological model of the soil layers. *Soil Domains*, which are considered to have significant different hydraulic properties, form *Hydraulic Soils Domains (HSD)* with specified hydraulic properties. If interference tests have been performed (in geological formations with relatively high permeability) they may give information for a better definition of the extent of the HSD and may also give information of differences in vertical and horizontal permeability and leakage conditions between aquifers or aquifers and lakes/water courses. However, the geometrical description will mainly be based on the geological judgement of how the quaternary deposits are spatially distributed and thus geometrically defined as soil units.

By implementing the geometries and parameters of the HCDs, HRDs and HSDs in a numerical groundwater flow model, the Model Version X.Y can now be tested. Parameters are implemented and as a first step tested if they reproduce the single-hole test results. To some extent the properties estimated along the boreholes will be used to local conditioning of the parameters in the numerical model. As a second step measured piezometric levels, considered to represent undisturbed conditions, measured salinity distributions in boreholes and measured salinity of the sea (if bounded by the sea) as well as run-off data are used to test and further condition the model. As a third step interference tests are used for tests and further conditioning. The simulation results may show differences that indicate that the geometries and/or properties of the HCDs , HRDs and HSDs should be revised. The follow-up discussions may lead to modification of the geometrical description and thus a re-analysis of the properties that should be assigned to each HCD, HRD and HSD. The revised model is then considered to be the official *Descriptive Version X.Y Model* that should be used for further analysis with regards to design and safety assessment. However, the limited scope within the Laxemar project did not allow for completion of this iterative loop.

#### **4.2.2 Modelling strategy**

##### **Rock**

The first step in the development of the site descriptive hydrogeological model is to use single-hole tests and the geometrical geological model to analyse the different parts of the boreholes based on where deformations zones and rock units are expected to intersect the boreholes, see Section 3.7. Hydraulic tests straddling a specified deformation zone with longer test time (and subsequent evaluation period) is generally considered to give a more representative estimate of the average properties of the zone.

Measured interferences (pressure responses in surrounding boreholes) during drilling, relatively short-time hydraulic tests (for example 100 m test-scale test during drilling of core holes, hydraulic tests in percussion boreholes etc) may give useful information for interpretation of the general pattern of hydraulic anisotropy or specific fracture zones. However, well-controlled interference tests give most reliable information to examine (some of) the fracture zones in the geological model just by studying the pressure responses. This second step gives indications of how the geometrical model should be modified and is reported in Section 4.2.4.

A third step is to use a preliminary geometrical model with hydraulic properties and implement it in a numerical groundwater flow model and perform explorative simulations with natural (undisturbed) conditions and interference tests, see Section 4.2.7. These simulations will first of all indicate if the assigned properties to HCDs and HRDs are reasonable. These explorative simulations may indicate that geometry and/or properties of HCD should be changed. Some observation sections will be positioned outside the HCD and the responses in these indicate something about the conductivity, storativity and connectivity of the features in within the HRD. In a late stage, when there are a large number of observation sections available, these observations will be useful for testing the assigned properties to the HRD.

A limitation of the interference tests is that if the contrast in hydraulic properties is low, between for example a HCD and the rest of the rock mass, or the permeability of the HCD is low, the responses in the observation sections may be insignificant or non-conclusive. In such a case the geological interpretation and the single-holes tests is the base for assigning properties for the fracture zone.

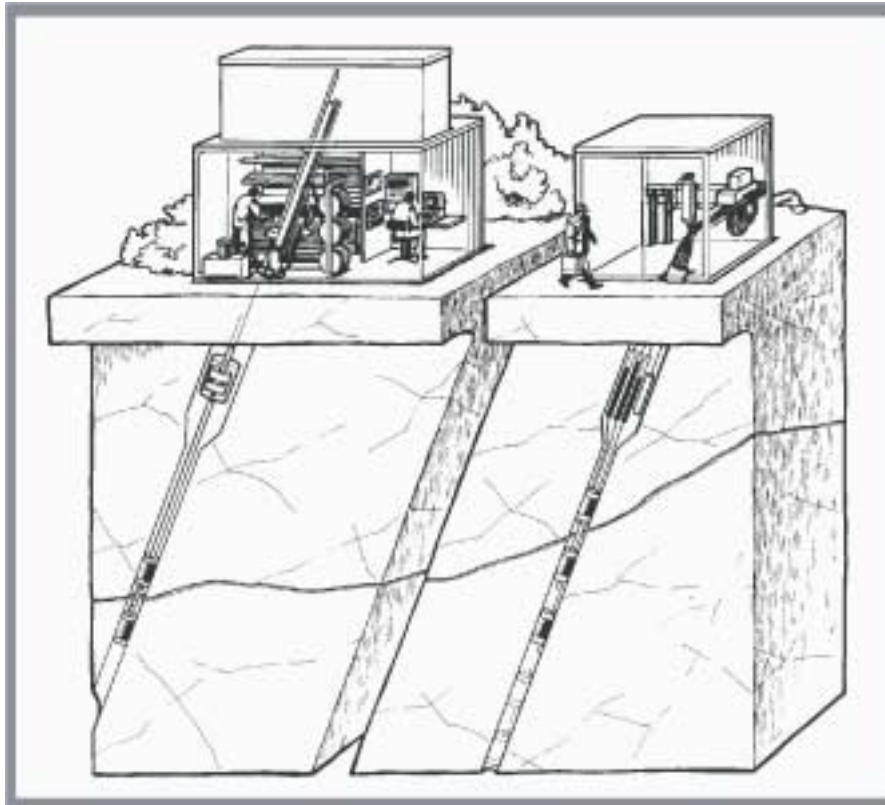
If no hydraulic tests have been performed in a specific zone, *possible* hydraulic properties estimated are assigned to the fracture zone based on the geological description of the fracture zone and the general knowledge of the hydraulic properties of the deformation zones in the area.

### **Quaternary deposits**

Grain size distribution curves (sieve analysis graphs) and single-hole tests in soil layers is the base for assigning properties to the geological soil units. If interference tests have been performed, these tests can be useful for defining the extension of some soil units and leakage conditions between different soil units or soil unit and watercourse or lake.

### **4.2.3 Interference tests**

During an interference test water is pumped from a borehole, or a section of it, and the drawdown is measured in the pumped borehole as well as in a number of other boreholes, called observation boreholes (Figure 4-16). These boreholes are generally equipped with several packers making it possible to monitor the drawdown at different sections along a borehole. Generally pumping has to be carried out for a few days in order to observe the pressure responses in observation boreholes several hundred metres away from the pumped borehole. In the text below ‘test section’ denotes the borehole section that is pumped.



*Figure 4-16. Interference test with observation boreholes.*

**Interference test – test section part of borehole – short-term pumping**

If the test section in a borehole is sealed off by packers it is possible to test an individual fracture zone. This procedure offers good opportunities for evaluating the flow regime for early, middle and late times and thus provides a generally good estimate of the flow properties of the fracture zone close to the borehole. The drawdown and recovery periods generally last around 3 days each.

Depending on the length of the test section and the structure of the flow paths, the flow regime may vary from 1D for early times, 2D for the middle period and sometimes 3D for the longer times. A transmissivity can be evaluated from the pressure-time curve assuming radial flow /Cooper and Jacob, 1946/. An Agarwal time correction may be used for the evaluation of the recovery phase /Earlougher, 1977/.

If one of the observation sections in the nearby observation boreholes intersect the same HCD as the pumped one, it is possible to estimate the storage coefficient of the HCD provided that flow is radial and that no other hydraulic features significantly affect the draw-down for the evaluation period considered. Generally the observation section has to be within a few 100 of meters from the pumped borehole section.

The responses in the observation sections can sometimes provide information about position and size of the HCDs. Occasionally, large hydraulic features, with hardly any firm geological evidences can be observed in the interference test data, but generally geological and geophysical data have to be used to support the discussion of the location and extent of the HCDs.

### ***Interference test – open borehole – short-term pumping***

In some cases the entire borehole is pumped (open-borehole test). In this case the transmissivity of the entire borehole is evaluated. Depending on whether one or several HCDs intersects the pumped borehole and the way in which the observation sections in nearby boreholes are situated it may be possible to evaluate the storage coefficient of a HCD. However, compared with interference tests, where a HCD has been sealed off, it is generally more difficult to draw conclusions from the location and extent of water-bearing zones. The drawdown and recovery period lasts generally about 3 days each.

### ***Interference test – open borehole/test section part of borehole – long-term pumping***

Long-term Pumping Tests (LPT) are considered to have drawdown and recovery periods of a month or more. The purpose is the same as for other interference tests with one exception; LPT provide a means to obtain better information about hydraulic boundary conditions, groundwater recharge and large-scale anisotropy and connectivity within a larger rock volume.

All interference tests are valuable as calibration cases for the numerical groundwater flow model, but the long-term pumping tests are generally considered most valuable.

## **4.2.4 Interpretation of hydraulic interferences**

### ***Indications of anisotropy or deformation zone orientation***

Drilling of a borehole and hydraulic tests during drilling causes hydraulic pressure responses that sometimes can be observed in nearby boreholes, usually closer than 500 m from the drilled borehole. These responses can be useful for the first assessment of larger-scale anisotropy and connectivity between HCDs. No such data has been available for the Laxemar model area.

### ***Interpretation of interference tests***

Two interference tests were performed using KLX02 as discharge well and KLX01 as observation well. The horizontal distance between the wells are approximately 1000 m. For the first test, Phase 1 /Follin, 1993/, pumping lasted between 1992-12-17 and 1993-06-16 with three pump stops, and for Phase 2, pumping was performed between 1995-10-19 and 1995-11-25 with one pump stop /Follin, 1996/. During Phase 1, KLX02 was tested in the interval 201–1700 m and all monitored sections of KLX01 reacted on the pumping. In Phase 2 /Follin, 1996/, the interval 805–1103 m of KLX02 was tested and responses referred to as “clear” were found in the KLX01 intervals 272–694, 695–855 and 856–1078 m, see Section 3.7.2. Based on these tests, it is of interest to determine the location of (a) possible zone(s) connecting the two boreholes.

For borehole KLX02, the lower part of the tested interval 805–1103 m has a high frequency of fractures (highest fracture frequency: 1035–1100 m). The largest transmissivities estimated using Posiva Difference Flow Meter are found in the sections between approximately 1086 and 1092 m along the borehole. Summarizing the transmissivities between 1035–1086 m gives a transmissivity of approximately  $1 \times 10^{-7} \text{ m}^2/\text{s}$ , whereas the interval 1086–1100 m would have a transmissivity of about  $1 \times 10^{-6} \text{ m}^2/\text{s}$ .

During the interference tests, responses referred to as “clear” /Follin, 1996/ were found in the intervals 272–694 m, 695–855 m and 856–1078 m of borehole KLX01. Analyses of data indicate that the interval 695–855 m is a possible location for a connecting zone between these two boreholes. This is supported by the following arguments:

Based on /Follin, 1996/, the computed flow rates divided by the actual discharge rate would be 48% and 11% for intervals 695–855 and 856–1078 m respectively. The remaining 41% was assumed to originate from the interval between 272–694 m in KLX02.

Good agreement was found between summarized transmissivities ( $8-9 \times 10^{-5} \text{ m}^2/\text{s}$ ) for 3 m and 30 m injection tests as well as for an airlift test for the interval 0–700 m for KLX01. The interval 600–700 m, which early was suggested a possible zone location, has a summarized transmissivity of  $3 \times 10^{-6} \text{ m}^2/\text{s}$ . However, this is approximately one order of magnitude lower than what was found for a test in the lower interval between 701–808 m.

For the interference tests, the distance between the interval tested in KLX02 and intervals for observations are similar. However, the observed changes in water level were larger and more “distinct” in the interval 695–855 m compared to the other intervals, see Figure 4-17. This indicates that the best hydraulic connectivity between the two boreholes is found between intervals 805–1103 m (KLX02) and 695–855 m (KLX01).

Further, flow anomalies from the UCM-flowlogging, which should originate from larger inflows, agree with some of the higher fracture frequencies found in lower part of the borehole (approximately 720, 740 and 760 m), see Section 3.7. If relating flow to transmissivity, the anomaly at 740 m would be slightly lower than  $1 \times 10^{-5} \text{ m}^2/\text{s}$ . This was made under the assumption that the bedrock is built up by parallel water conductors and that the transmissivity of each single conductor is proportional to the water inflow /Earlougher, 1977/. The lower part of borehole KLX01 (700–1050 m) is more fractured than the rest of the borehole, which may explain the response observed for the lowest section.

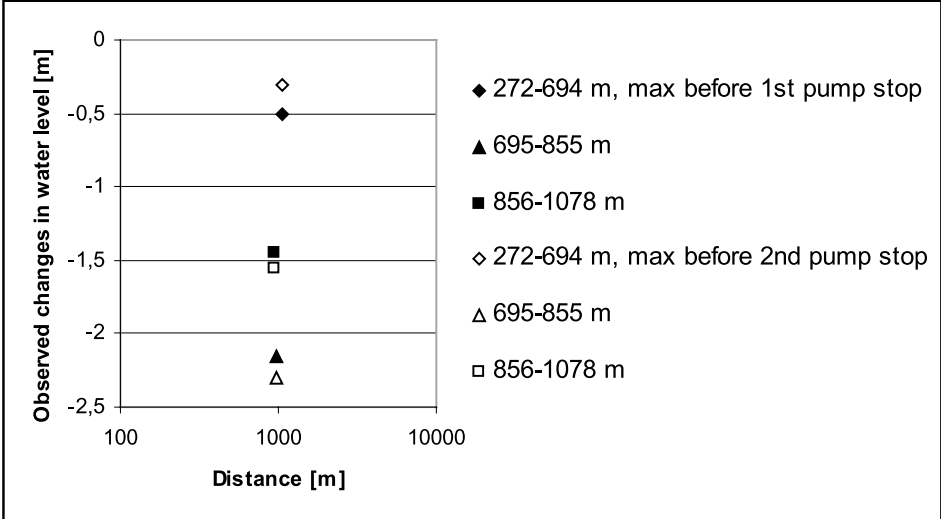


Figure 4-17. Distance between sections of boreholes KLX01 and KLX02, and observed changes in water level in borehole KLX01.



Initially, pumping during the full-length test of KLX02 (Phase 1) was performed with a flow of either  $2.95 \times 10^{-3}$  or  $1.95 \times 10^{-3}$  m<sup>3</sup>/s and to estimate what proportion of these flows that may originate from the interval 805–1103 m, the transmissivities from pumping tests in KLX02 (test scale approximately 300 m, see Section 3.7.2, Figure 3-29) were used ( $0.03 \times 2.95 \times 10^{-3} \approx 8.4 \times 10^{-5}$  m<sup>3</sup>/s and  $0.03 \times 1.95 \times 10^{-3} \approx 5.6 \times 10^{-5}$  m<sup>3</sup>/s). Subsequently, the change in water level after 25 days of pumping was divided by this flow, resulting in “specific drawdowns” for the sections 272–694, 695–855 and 856–1078 m of KLX01. Figure 4-17 and Table 4-5 presents these drawdowns as well as the results for the section test of KLX02 during phase 2.

Based on these calculations, the transmissivity of KLX02 below 500 m was estimated to be about 10% of the total borehole transmissivity. Further, the differences between specific drawdowns for the sections 272–694 m, 695–855 m and 856–1078 m in KLX01 are not very large when comparing the results for the full length and section tests (Table 4-5). This can be explained by a situation where the upper sections of KLX02 have little connection to KLX01. This was indicated by the small response in KLX01 during the full-length test of KLX02 (Phase 1) even though the transmissivity is considerably higher in the upper part of the borehole. This was also confirmed by /Carlsten et al, 2001/, which show that the interpreted flow anomalies for the upper 200–400 m of KLX02 are oriented towards WNW-NW. The differences there are between the specific drawdowns can be explained by the higher fracture frequency found in the lower part of KLX01, which can make the flow deviate from radial to more spherical flow.

During the later part of the pumping period of KLX02, Phase 1 (see Appendix B4), boreholes HLX01, HLX02, HLX05, HLX06 and HLX07 show a general decrease in piezometric level. This indicates that the pumping of KLX02 influences the boreholes. For boreholes HLX03, HLX04 and HLX09 data are lacking for this period. Further, if looking at the pump stop preceding this last pumping period, a clear increase in piezometric level is observed for the lower sections of KLX01 and simultaneously a smaller response is seen for HLX06 and possibly also for HLX05, HLX01 and HLX07. The percussion borehole HLX05 is found in the vicinity of KLX01 and seems to follow the response of this same borehole. HLX01, HLX06 and HLX07 might be influenced by a zone with an approximately NW direction, but the response can also be a result of a generally fractured upper aquifer.

**Table 4-5. Estimated specific drawdowns for borehole KLX01 during interference tests Phase 1 (full length test) and Phase 2 (section test).**

Borehole	Sec up – sec low	Change in water level Phase 1 (m)	Specific drawdown ( $Q \approx 8.4 \times 10^{-5}$ m <sup>3</sup> /s) (s/m <sup>2</sup> )	Specific drawdown ( $Q \approx 5.6 \times 10^{-5}$ m <sup>3</sup> /s) (s/m <sup>2</sup> )	Change in water level Phase 2 (m)	Specific drawdown ( $Q \approx 1.5 \times 10^{-4}$ m <sup>3</sup> /s) (s/m <sup>2</sup> )
KLX01	0.00–140.00	small	–	–	–	–
	141.00–271.00	small	–	–	–	–
	272.00–694.00	–0.6	$7.1 \times 10^3$	$10.8 \times 10^3$	0.5	$3.3 \times 10^3$
	695.00–855.00	–1	$11.9 \times 10^3$	$18.0 \times 10^3$	–2.15	$14.3 \times 10^3$
	856.00–1078.00	–1.8	$21.4 \times 10^3$	$32.4 \times 10^3$	–1.45	$9.7 \times 10^3$

## 4.2.5 Estimating HCDs and HRDs directly from data

In Section 4.1 several observations have been used to test different geometrical alternatives of possible deformation zones. KLX01 and KLX02 intersects a few of the possible deformation zones and the HLX-boreholes probable intersects or are very close to several deformation zones, see Figure 3-16 in Section 3.6. Most of these percussion boreholes were originally intended to intersect possible zones. In Table 4-6 the observations are compiled and the hydrogeological observations are added.

### Hydraulic Conductor Domains

A few HLX are associated with two zones in Table 4-6. The reason is that the boreholes are close to an intersection between two zones and it is presently uncertain if the data from these bore holes represent one or both (possible in terms of transmissivity estimate) of the zones Whether the observations in the HLX-holes should in all cases actually represent the zones in Table 4-6 is presently uncertain. Possibly the available material can be used for further analysis but to some extent new borehole investigations should be performed.

The early-middle time responses for the test November 1995 in KLX02 has not been evaluated. The results here are based on the late-time responses. Based on the suggested location of zones (Table 4-6) along the boreholes, Table 4-7 presents univariate statistics for different sections of the boreholes. This is needed to describe the hydraulic properties of both zones and the rock mass.

Based on geological and hydrogeological data the project team decided that zone ZLXNE03 could probably intersect borehole KLX02 in the interval 972–1131 m and mean, average and standard deviation of the hydraulic conductivity are thus presented for the zone and for the rock while excluding this zone. For KLX02 the mean conductivity of the upper section is higher than the value found for the suggested deterministically defined zone.

**Table 4-6. Transmissivity, type of test and secup/seclow used as guidance when suggesting location and transmissivity of HCDs.**

HCD	Bh	Indication in bh-section (m)	BH inter- section in RVS	Type of tests performed	Hydr. section Secup (m)	Hydr. section Seclow (m)	Transmissivity (m <sup>2</sup> /s)
ZLXNE03	KLX02	1040 (w:10–30m)	n/a	Pumping test (interf. test)	1035 (1086)	1100 (1092)	6.6×10 <sup>-6</sup>
ZLXNE03	HLX01		n/a	Pumping test			9×10 <sup>-5</sup>
ZLXNE04	KLX01	750 (w:10–20m)	n/a	Airlift test UCM	720	760	~1×10 <sup>-5</sup>
ZLXNE04	HLX02		n/a	Airlift test			2.2×10 <sup>-6</sup>
ZLXNE04	HLX04		n/a	Airlift test			2.8×10 <sup>-6</sup>
ZLXNE06	HLX08		n/a	Airlift test			2×10 <sup>-3</sup>
ZLXNW01	HLX01		n/a	Pumping test			9×10 <sup>-5</sup>
ZLXNW01	HLX07		n/a	Pumping test			6.6×10 <sup>-6</sup>
ZLXNW04	HLX02		n/a	Airlift test			2.8×10 <sup>-6</sup>

In KLX01 the injection tests in 30 m scale in the upper part of the borehole indicate a higher hydraulic conductivity but the tests in 3m scale a lower. The reason is the spatial distribution of permeable features; rather few with large transmissivities.

### Hydraulic Rock Domains

The statistical distributions summarised in Table 4-7 can be used to estimate hydraulic properties of the rock mass between fractures zones. Table 4-8 presents suggested parameters describing the hydraulic conductivity of the rock mass between fracture zones. Only one Hydraulic Rock Domain is suggested based on this information.

It is difficult to estimate the average storage capacity as “specific storativity ( $S_s$ )” in a fractured media. However, considering the porosity and compressibility of rock mass it should not become much less than  $S_s = 1 \cdot 10^{-7} \text{ m}^{-1}$ , see /Rhen et al, 1997/ for further details.

**Table 4-7. Univariate statistics for KLX01 and KLX02. The estimates of the distribution characteristics (mean and standard deviation  $\text{Log}_{10}K$ ) are based on the fitting a straight line to values above the measurement limit in a normal probability plot of  $\text{Log}_{10}K$ .**

Borehole/ Rock/Zone	Secup	Seclow (m)	Test scale (m)	Meas. limit (m)	Sample size (m/s)	Hydraulic conductivity (K)	
						Mean ( $\text{Log}_{10}(K)$ ) (m/s)	Std ( $\text{Log}_{10}(K)$ ) (m/s)
<b>KLX01</b>	106	691	3	$7 \cdot 10^{-12}$	197	-10.5	1.75
Rock	106	463	3	$7 \cdot 10^{-12}$	121	-10.5	2.0
Rock	463	691	3	$7 \cdot 10^{-12}$	76	-9.8	1.2
<b>KLX01</b>	103	702	30	$7 \cdot 10^{-12}$	20	-9.01	1.80
Rock	103	463	30	$7 \cdot 10^{-12}$	12	-8.66	1.90
Rock	463	702	30	$7 \cdot 10^{-12}$	8	-9.42	1.63
<b>KLX02</b>	207	1398	3	$10^{-9}$	398	-10.3	1.6
Zone	972	1131	3	$10^{-9}$	54	-9.3	1.07
Rock <sup>1</sup>	207	1398	3	$10^{-9}$	344	-10.5	1.9
Rock	207	340	3	$10^{-9}$	45	-8.6	1.4

<sup>1</sup> Values in section 972–1131 not included.

**Table 4-8. Lognormal distributions based on univariate statistics for KLX01 and KLX02, with zones in Table 5-30 excluded in the data set for analysis. Data represent measurements along sub-vertical boreholes.**

HRD	Test scale (m)	Hydraulic conductivity (K)	
		Median( $\text{Log}_{10}(K)$ ) (m/s)	Std( $\text{Log}_{10}(K)$ ) (m/s)
HRD1	3	-10.5	1.8
	30	-9.0	1.8

## 4.2.6 Interpretation of hydraulic interferences in the soil layers

No hydraulic tests have so far been made.

## 4.2.7 Hydrogeological simulation approach

### **General**

SKB's systems approach to hydrogeological modelling described in Chapter 7 of the general program for site investigations /SKB, 2001/. In short, a site's hydrogeological properties and states are described by means of parameters, which detail the hydraulic properties of the Quaternary deposits (soil) and the crystalline bedrock, and the hydrological processes that govern the hydraulic interplay between surface water, precipitation and groundwater flow. Section 4.2.1 describes the general modelling assumptions concerning how the model volume is divided into separate volumes; Hydraulic Soils Domains (HSD), Hydraulic Conductor Domains (HCD) and Hydraulic Rock Domains (HRD). The geometries of these volumes, HSD etc, define hydrogeological-property regions that should be implemented in a numerical groundwater flow model. The size and the position of the boundaries in a numerical model depends on the purpose of the modelling, hydrological conditions on the upper boundary and strive to find simple and trustworthy boundary conditions on the vertical and bottom boundaries.

In this section a numerical groundwater flow model is used to test how well the hydrogeological descriptive model compares to different large-scale hydrogeological condition, as run-off rates, level of the water table and water-salinity towards depth. Among other things these data may also be used to calibrate near-surface parameters. Interference tests are also essential for the testing and calibration of a numerical model. A basic test, that has to be checked throughout the modelling, is that the single-hole test results can be reproduced. This can be made on different levels and it has to be decided what level that is considered sufficient, and comparable, to how the descriptive model has been implemented in the numerical groundwater flow model. To some extent these single-hole results can be used to local conditioning of the model. However, the single-hole results, together with the defined domains, are used to control how the stochastic distributions of the hydraulic properties in the descriptive model compare to the values in the numerical model.

The use of a numerical groundwater flow model to integrate detailed information within generally a large volume can increase the confidence that the descriptive model is reasonable in a sense that it can reproduce several measured entities and some processes considered essential for PA. A result from a tested and calibrated model is a judgement of major uncertainties; what type and where they are. This information is useful for the planning of future investigations. The tested and calibrated model can also be used to simulate future hydraulic tests to see if one can expect responses in available or planned boreholes. The results can give some guidance of for future investigation boreholes, although there are several other considerations than just hydrogeological responses that has to be considered for the position and direction of new boreholes. The final tested and calibrated model, based on the descriptive model is of course a tool useful for parts of the Design and Safety Assessments.

In this section the test and calibration of the numerical groundwater flow model is shown. Some of the results from the calibrated model are also part of the site descriptive model in Section 5.2.

## **Numerical code**

The code used is DarcyTools, which is a volume-integrated finite-difference code for variable-density groundwater flow /Svensson, 2002a,b/. DarcyTools uses a mixed DFN/Continuum approach for the simulation of groundwater flow through fractured rocks. That is, the geometries and the transmissivities of all discrete features (HCDs as well as the random hydraulic features) are transformed to equivalent inter-node conductivities prior to the solution of the flow equations. Hence, DarcyTools models flow through an anisotropic and heterogeneous continuum. The modelling technique is described in detail by /Svensson et al, 2002a,b/ and more briefly in /Follin and Svensson, 2002/.

Besides the major deterministic zones (HCDs) the model also contains random hydraulic features (conductive fractures and minor conductive fracture zones not modelled deterministically) in the HRDs. Hydraulic features with smaller size than the cell size in the numerical model cannot directly be considered in the same way as features larger than the cell size. The latter type of random fractures is modelled as discrete features whereas the former type is taken into account as a background (bulk) hydraulic conductivity.

### **4.2.8 Numerical modelling approach for the Laxemar area**

The parameter values presented in this Chapter and of the final descriptive hydrogeological model of the Laxemar model area (Chapter 5) have been used as input data to a quantitative (numerical) model /Follin and Svensson, 2002/. The model size is 2400 x 3400 x 2000 m<sup>3</sup> (Appr E-W X Appr N-S X Depth). The Cell size in the model is 30 m, except for close to the surface where the cells become thinner.

The numerical model is based the Base Geological Model containing about 21 major fracture zones in the modelled volume, some of which are also confirmed hydraulically by means of single-hole tests in the deep core holes KLX01 and KLX02. Figure 4-18 shows a perspective view of the deterministic zones modelled, the Hydraulic Conductor Domains (HCD). The transmissivity of the red, yellow and blue coloured zones (planes) in Figure 4-18 is shown in Table4-9.

The near surface deposits are not modelled explicitly but uppermost cells in the model are more conductive than the rock mass to facilitate surface run-off in case the water table reaches the topography, see /Follin and Svensson, 2002/ for details. No watercourse is modelled as no significant watercourse within the model area was identified.

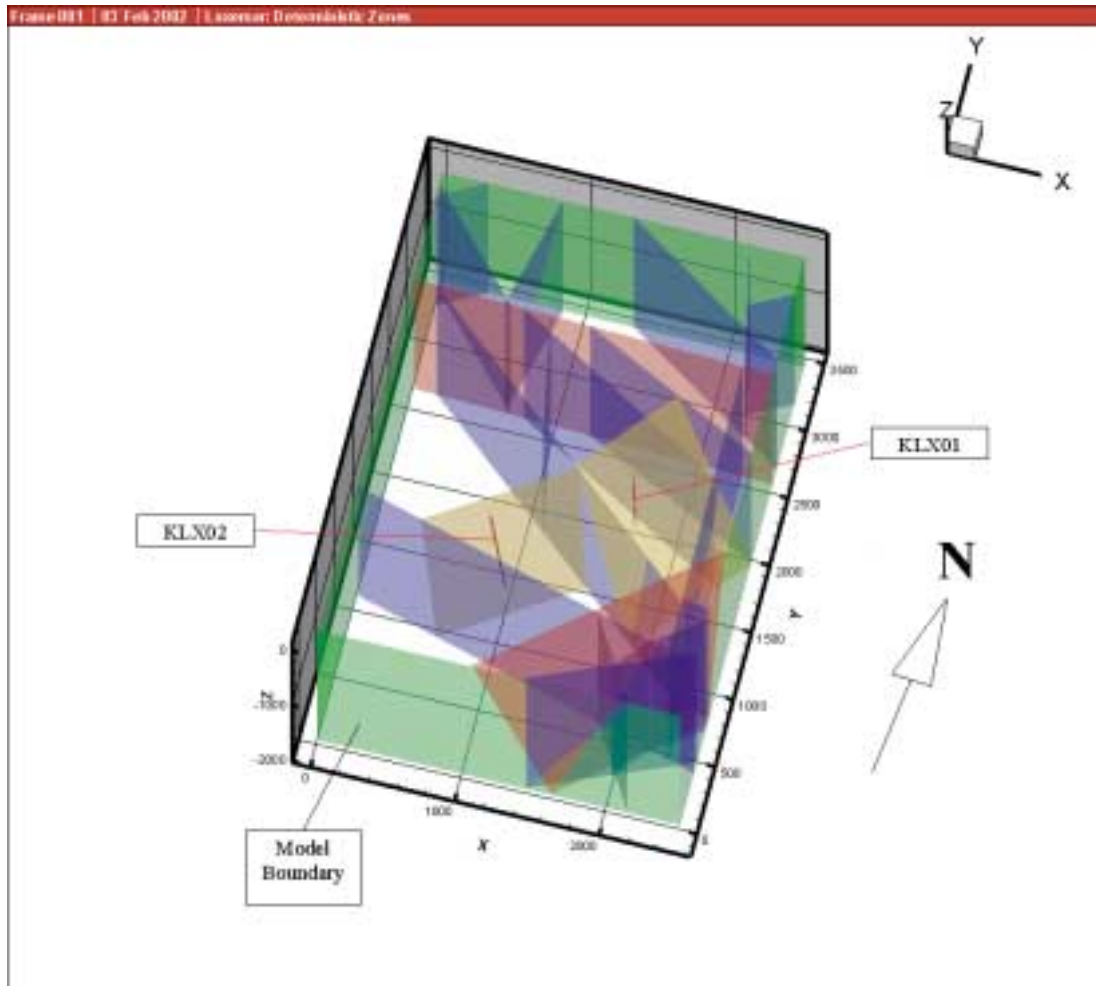
Only the Base Geological Model in Section 4.1 (and 5.1) has been considered and not the presented alternative. The reason is the limited scope for the present work. A few realisations of stochastic properties of the HRDs were made to test the model. All general assumptions are presented in the section for the Base Geological Model.

## **HCD**

The Properties of the HCDs are taken from the initial estimate (see above) and are also given in Table 4-9.

## **HRD**

For assigning properties to the Hydraulic Rock Domains the injection tests in the 30 m test scale was considered to be most useful for calibration the material properties since the grid cell size was chosen to 30m.



**Figure 4-18.** 3D visualisation of the Laxemar model domain. The vertical boundaries of the model domain are coloured in green. The strike direction of the model's y-axis is N14°W. Slightly different hydraulic properties have been assigned to the 21 HCDs based on deterministic fracture zones and lineaments for the Base Geological Model. Coordinate system used:RT90/RHB70. The properties are compiled in Table 4-9. (Figure 3-8 in /Follin and Svensson, 2002/).

**Table 4-9. Hydraulic properties of the 21 deterministic HCDs based on identified fracture zones and lineaments /Follin and Svensson, 2002/.**

No. of fracture zones	Transmissivity (m <sup>2</sup> /s)	Thickness (m)	Colour in Figure 4-18
2	1·10 <sup>-4</sup>	10	Red
2	7·10 <sup>-6</sup>	10	Yellow
17	3·10 <sup>-6</sup>	10	Blue

To assign the properties to the HRDs, models for the spatial distribution of the hydraulic features, the size and form and orientation of these features, and finally, the hydraulic properties of the features are needed. Base for the spatial model of the geometrical properties are the interpreted lineaments, mapped fractures on outcrops and mapped fractures in the core holes, see Section 3.8.

It is noted that it was not possible to assess the Power Law exponent for fracture size with certainty from the available trace map data in this project due to a varying quality in the data and censoring. In contrast to the inferred value of  $-3.2$ , /La Pointe et al, 1999/, has previously advocated that a value of  $-2.6$  should be diagnostic for probabilistic 3D structural-hydrogeological simulations in the region where the Laxemar area is located. The latter value has been tested in several models with good results, see for example /Svensson, 2001/. For the purpose of the present project it was decided to use  $-2.6$  since the DFN-analysis in Section 3.8 was not completed at the time of the numerical flow simulations. As indicated by /Follin and Svensson, 2002/, the difference has very little practical implications as the chosen grid cell size (30 m) is sufficiently large in order to filter out most of the minor fractures that are associated with the  $-3.2$  value.

Two basic concepts are presently used for assigning hydraulic properties the random hydraulic features. The first assumes no correlation between the size of the feature and the transmissivity value, see Section 3.8.9. The second assumes that there is a positive correlation between the size of the feature and the transmissivity value, which have been tested in several models, for example /Svensson, 2001/. /Follin and Svensson, 2002/ discusses in detail the available data and the possible interpretations. In the present model the positive correlation model between the size of the feature and the transmissivity value is used, with the formulation below:

Four fracture sets are assumed for the non-deterministic fracturing within the Laxemar model domain. The deduced parameter values for orientation, spatial distribution and intensity are compiled in Table 4-10, all values except D are taken from Section 3.8.

Given the value of the Power Law exponent,  $D$ , and the volume,  $V$ , of the Laxemar model domain the number of fractures (squares in DarcyTools),  $N[L_1, L_2]$ , within a specified size range,  $L_1$  to  $L_2$ , can be estimated using the following equation /Svensson, 2001/:

$$N[L_1, L_2] = \frac{V I}{D} \left[ \left( \frac{L_2}{L_{ref}} \right)^D - \left( \frac{L_1}{L_{ref}} \right)^D \right] \quad (1)$$

where  $L_1 < L_2$ ,  $I$  and  $L_{ref}$  are two coefficients that determine the position of the power law distribution in a log-log plot of  $N$  versus  $L$ . For the structural-hydraulic model of the prototype repository at Äspö, /Svensson, 2001/ used  $I = 10^{-8}$  and  $L_{ref} = 500$  m with good results.

**Table 4-10. Geometric and hydraulic properties for the non-deterministic fractures.**

Set No.	Orientation statistics of the mean normal vector (pole)				Fracture size D	Spatial distribution Type	Fracture intensity	
	Type	Trend	Plunge	Dispersion			P <sub>32</sub>	P <sub>32c</sub>
1	Fisher	262.0	3.8	8.52	-2.6	Baecher	0.78	0.12
2	Fisher	195.9	13.7	9.26	-2.6	Baecher	0.66	0.15
3	Fisher	135.9	7.9	9.36	-2.6	Baecher	0.76	0.12
4	Fisher	35.4	71.4	7.02	-2.6	Baecher	0.24	0.08
All	$T \in \log N(4.2 \cdot 10^{-8}, 2 \cdot 10^{-7})$ m <sup>2</sup> /s [ $\approx \log_{10} T \in N(-8.06, 0.773)$ log <sub>10</sub> (m <sup>2</sup> /s)]						2.44	0.48

A positive correlation between the size of the hydraulic features and the transmissivity ( $T_f$ ) is assumed:

$$T_f = \begin{cases} \alpha \left( \frac{L_f}{100} \right)^2 \text{ m}^2/\text{s} & \text{for } L_f \leq 100 \text{ m} \\ \alpha & \text{m}^2/\text{s} \text{ for } L_f > 100 \text{ m} \end{cases} \quad (2a)$$

$$b = 0.01 L_f \quad (2b)$$

The value of the coefficient  $\alpha$  in Equation (2a) was set to  $10^{-5} \text{ m}^2/\text{s}$  in the study by /Svensson, 2001/. By means of trial and error, this value was altered to  $10^{-8} \text{ m}^2/\text{s}$  in the /Follin and Svensson, 2002/ in order to obtain a good fit with measured conductivities on a 30 m scale in the core-drilled boreholes KLX01 and KLX02. The plot in Figure 4-19 visualises the different proposals for the definition of fracture transmissivity discussed so far.

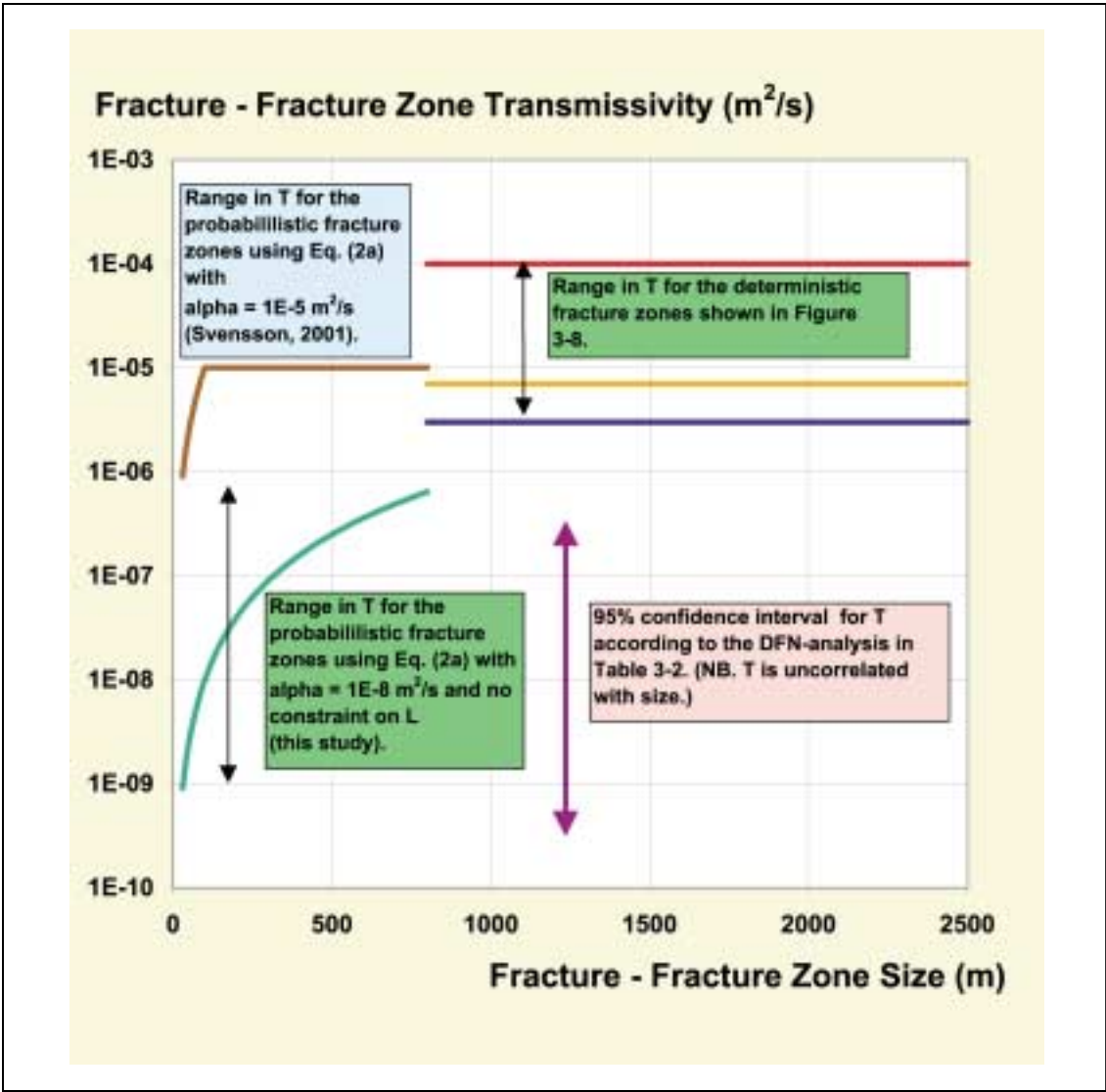


Figure 4-19. Visualisation of the different proposals for the definition of fracture transmissivity discussed in this study (Figure 3-11 in /Follin and Svensson, 2002/).



/Follin and Svensson, 2002/ also points out that fracture area per volume,  $P_{32}$ , shown in Section 3.8 is not comparable to the  $P_{32}$  in the numerical model, because smaller features than 30 m are not included in the numerical model but are included in the analysis in Section 3.8. For the chosen discretisation of the Laxemar structural-hydraulic flow model (30 m), the  $P_{32}$  value is  $0.023 \text{ m}^2/\text{m}^3$ .

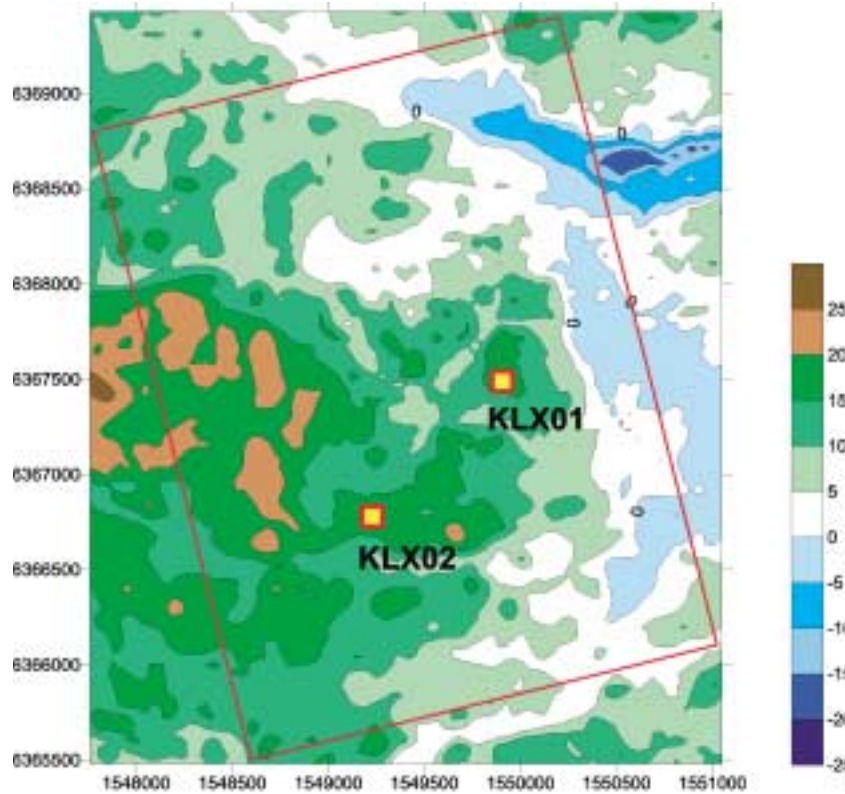
### **Boundary conditions**

Figure 4-20 shows a map of the Laxemar model area. The western boundary coincides with a local topographic ridge, see Figure 4.21. The north and south boundaries almost coincide with the outlets of two small rivers, the Mistraån stream to the north and the Laxemarån stream to the south. The eastern boundary coincides with the shoreline to the Baltic Sea. The topography of the Laxemar model area is shown in Figure 4-21. The maximum altitude within the Laxemar model area (red border line) slightly exceeds 22 m.a.s.l. in the western part. The maximum topographic gradient within the area is c. 30‰. The top boundary coincides with ground surface and is modelled as a specified flux boundary with a specified net precipitation of 200 mm/year.

All vertical boundaries are assumed to be no-flow boundaries, except for the eastern boundary that is modelled with a prescribed pressure profile. The nature of the pressure profile versus depth follows the prescribed TDS concentration versus depth that has been used in the regional modelling of the hydrogeological conditions around the Äspö HRL /Svensson, 1997/. The boundary conditions are shown in Figure 4-22. A major difference is the thickness of the two model domains. The bottom boundary of the locaa model used in this study was set to c. -2 000 m, whereas the bottom of the regional model was c. -3 000 m.



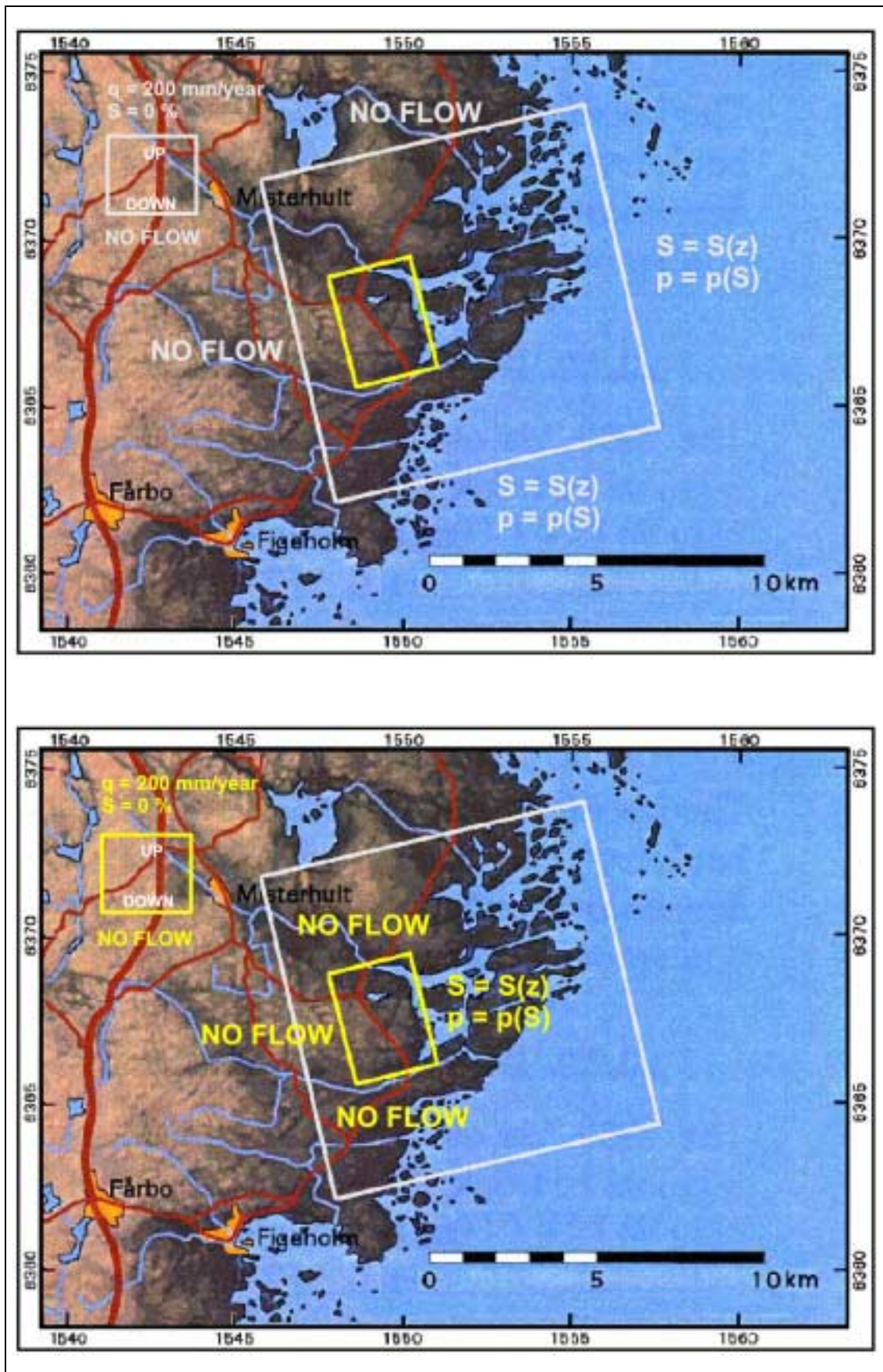
**Figure 4-20.** The location of the Laxemar area model domain in RT90/RHB70 coordinates.



**Figure 4-21.** Topography within the Laxemar model area. Coordinates in RT90/RHB70. /Follin and Svensson, 2002/.

The realism of the used boundary conditions has not been possible to assess in detail within the given time frame. However, /Follin and Svensson, 2002/ show that the aforementioned boundary conditions render an almost identical initial pressure and salinity distributions as that of the regional flow model carried out by /Svensson, 1997/. The rationale behind this result can best be explained by the fact the models have similar boundary conditions although the sizes of the model domains are different. Moreover, the equations of flow and salt have been solved for steady state conditions. Hence, the porosity has no impact on the solution and that there are no considerations made to transients such as seasonal changes in groundwater recharge or shore level displacement. From a hydraulic point of view, the adopted boundary conditions will create a balance between fresh and saline groundwater that is not dependent on the geology within the domain. The soundness of this fact is scrutinised by /Follin and Svensson, 2002/, but it may be noted that the Ghyben-Herzberg relation indeed is a balance of forces solely.

It should be noted that the results from the regional model by /Svensson, 1997/ were discussed by the project team, but the transfer of the boundary conditions from this model to the Laxemar Local model was considered too time consuming and not necessary considering the objectives to test the methodology of how to implement a descriptive model within a numerical groundwater flow model.



*Figure 4-22. The top figure shows the boundary conditions that were used by /Svensson, 1997/ in the regional model for Aspö HRL. The bottom figure shows the boundary conditions of the present study.  $S$  = salinity,  $p$  = pressure and  $q$  = volumetric flux.*

### **Model calibration – general**

As mentioned above, only three realisations form the possible variation of the random field that is analysed in this section. The calibration has been directed to treat two different hydrogeological performance measures, namely:

- The coefficient  $\alpha$  in the equation that relates fracture transmissivity to fracture size, see Eq. 2a in this Section. The value of  $\alpha$  was altered until a reasonable agreement was obtained between the *CDF* of the inter-node hydraulic conductivity field in the flow model and the *CDFs* of the  $K_{30}$  measurements carried out in the two deep core-drilled boreholes KLX01 and KLX02.
- The hydraulic conductivity  $K$  of the uppermost four cell layers of the flow model. The value of  $K$  was tuned for each layer until a reasonable agreement was obtained between simulated and known surface water conditions within the entire Laxemar model domain.

The first performance measure was chosen because of the presumed importance of probabilistic fractures and fracture zones for the hydraulic conductivity of the bedrock and the groundwater flow distribution at depth. The second performance measure was chosen because of the extreme importance of the top boundary condition.

No attempts were made to condition the local hydraulic properties along the boreholes.

### **Model calibration – hydraulic conductivity versus depth**

Figure 4-23 shows five graphs that represent different cumulative density functions (*CDFs*) for the hydraulic conductivity of the bedrock on a 30 m support scale ( $K_{30}$ ). Three of the five *CDFs* represent field data (light green, cerise and red) measured between c. 100 m–1660 m in the specified core-drilled boreholes, KLX01, KLX02 and KAS02–03. The remaining two *CDFs* (blue and dark green) are numerical simulations of  $K_{30}$ , denoted by DT\_C-1 and DT\_C-2. Each realisation consists of three sources of data; the deterministic fracture zones of the Base geological model, a Monte Carlo simulation of probabilistic fractures and fracture zones and a Monte Carlo simulation of a heterogeneous subgrid hydraulic conductivity field. Figure 4-26 shows an example of such a realisation.

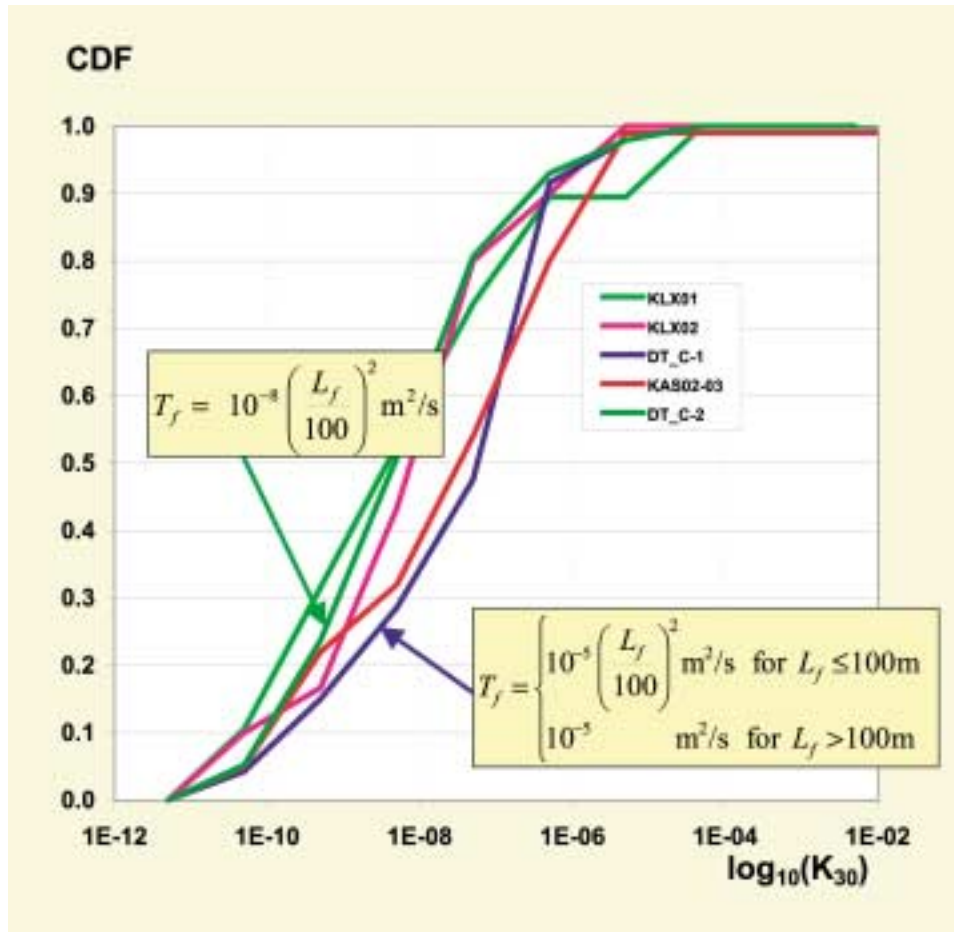
Figure 4-24 and Figure 4-25 show the measured and simulated  $K_{30}$  values along the stretch of the two boreholes KLX02 and KLX01.  $K_g$  denotes the geometric mean of the simulated directional cell wall conductivities  $K_{x+}$ ,  $K_{y+}$ ,  $K_{z+}$ ,  $K_{x-}$ ,  $K_{y-}$  and  $K_{z-}$ . The blue graphs represent “measured”  $K_{30}$  values. For KLX02, the measured values were deduced by and divide the sum by 30. For KLX01, the measured values were obtained by means of 30 m double-packer injection tests..

The two *CDFs* representing Laxemar data are not entirely alike, but their median values are c. one order of magnitude less than the median of the *CDF* representing Äspö data. Hence, the *CDFs* indicate that hydraulic differences may exist between the two areas.

The  $K_{30}$  realisations DT\_C-1 and DT\_C-2 are geometrically identical but differ in the value of the coefficient that relates transmissivity to fracture size. That is, the simulation DT\_C-1 has an  $\alpha$ -value of  $10^{-5}$  m<sup>2</sup>/s whereas DT\_C-2 has an  $\alpha$ -value of  $10^{-8}$  m<sup>2</sup>/s. Given the used equations, Figure 4-23 indicates that probabilistic fractures have a significant impact on the bedrock hydraulic conductivity and the groundwater flow distribution at depth. It should be noted, however, that this study merely points at the importance of

the issue without making any real attempt to address it as such. Indeed, the DFN-analyses in Section 3.8 do not provide any information for assessing potential correlation between fracture transmissivity and fracture size of the kind used in this study.

The other two unconditional realisations of this study, DT\_C-3 and DT\_C-4, are geometrically different from each other and from DT\_C-2. Despite their geometric differences, however, the CDFs of the three unconditional realisations are quite alike, which implies that the size of the Laxemar model domain is sufficiently large in order to appeal to this type of ergodicity test.



**Figure 4-23.** Cumulative density functions (CDFs) for the hydraulic conductivity on a 30 m support scale. The CDFs denoted DT\_C-1 and DT\_C-2 are based on simulations with DarcyTools and the CDFs denoted KLX01, KLX02, and KAS02-03 are based on measurements. /Follin and Svensson, 2002/.

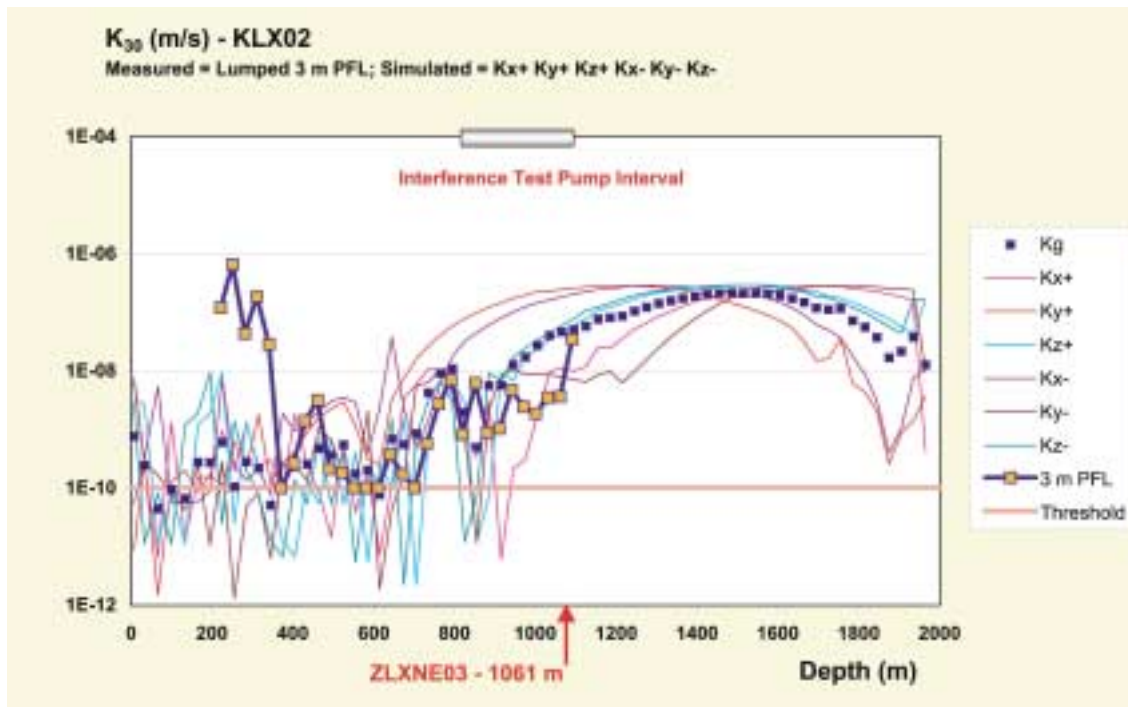


Figure 4-24. Measured and simulated  $K_{30}$  values in the pumped borehole KLX02. Midpoint for HCD indicated in the figure. /Follin and Svensson, 2002/.

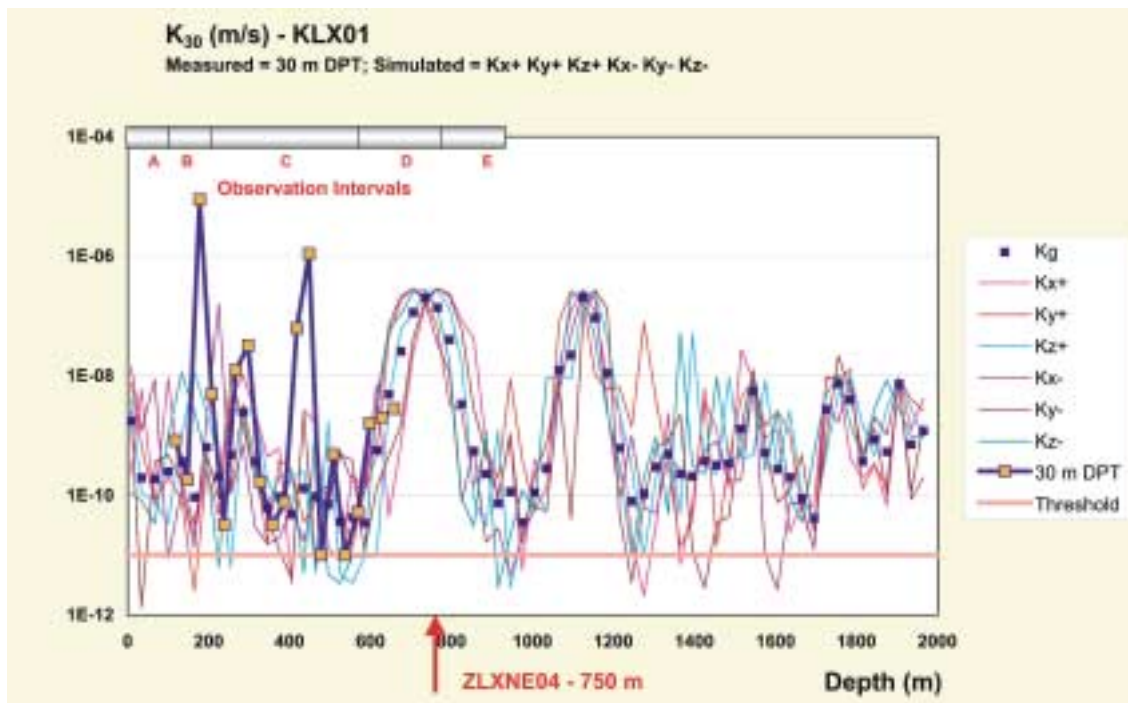
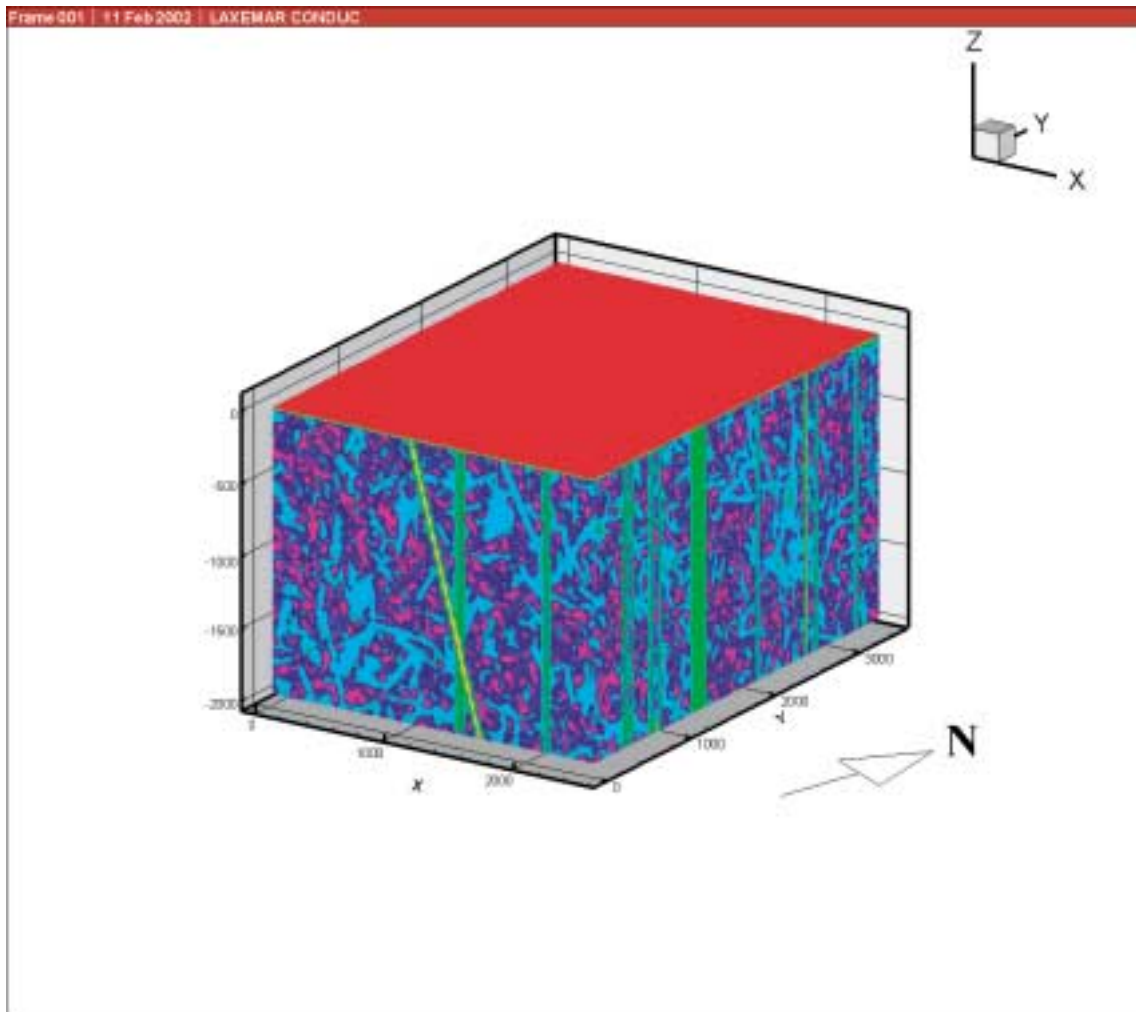


Figure 4-25. Measured and simulated  $K_{30}$  values in the observation borehole KLX01. Midpoint for deterministic zone indicated in the figure. /Follin and Svensson, 2002/.



**Figure 4-26.** 3D visualisation of a conductivity realisation of the Laxemar model domain. The realisation is obtained by mean of superposition of deterministic and probabilistic sources. The colouring in the figure represents the contribution from four different sources. Three of these (purple-blue, turquoise and green-yellow) represent different types of bedrock structures, see Figure 4-18. The fourth (red), represents high conductivities close to the surface, e.g., Quaternary deposits. (Figure 3-13 in /Follin and Svensson, 2002/).

### **Hydraulic conductivity close to ground surface**

The hydraulic conductivity of the uppermost part of the subsurface is generally much greater than that of the bedrock at repository depth. If the contrast in hydraulic conductivity between the upper and lower parts of the modelled flow system is sufficiently large, e.g., two orders of magnitude or more /Freeze and Cherry, 1979/, it can be concluded that it is the topography and the near-surface hydrogeological conditions that govern the surface runoff, the groundwater recharge and the location of the water table. The hydraulic properties of the bedrock structures at depth have little influence, unless they reach ground surface. Moreover, the location of the water table is known to play an important role in coastal aquifer systems for location of the freshwater/saltwater interface. According to the approximate Ghyben-Herzberg relation the location of the interface is independent of the geology provided that the flow system is at steady state. The uppermost four layers of the numerical flow model of the Laxemar area have been conceptualised as Quaternary deposits and outcropping bedrock. The values of the

hydraulic conductivity of the uppermost four layers of the numerical flow model were chosen so that the size of Lake Frisksjön was approximately correct, cf. Figure 4-20. It should be noted, however, that this study merely points at the importance of the issue without making any real attempt to address it as such. Unfortunately there are no other lakes or streams of similar importance within the Laxemar model area to calibrate against. Moreover, the current knowledge about the Quaternary Deposits is also limited. Hence, it has not been possible to elaborate the calibration of the hydraulic conductivity of the uppermost layers in this project.

## **Results**

/Follin and Svensson, 2002/ provide a detailed description of the modelling and all results. In what follows, the results are commented briefly.

The results from the 35 days long interference test conducted between drillhole KLX02 (pumping hole) and KLX01 (observation hole) in 1996 /Follin, 1997/ was chosen by the methodology test project team as a reference test for the numerical exploration of the “calibrated” flow model. Due to the constrained timetable it was decided to work with one of the three realisations only for the numerical simulation of the interference test.

In Figure 4-27 all the HCDs, the pumped borehole KLX02, the observation borehole KLX01, with 5 sealed-off sections is shown. In Figure 4-26 the steady-state drawdown in a vertical sections is shown. The modelled drawdowns in the borehole sections in KLX01 rather close to the measured, with one major difference; the maximum drawdown is switched between the two deepest borehole sections, see Table 4-11.

The salinity distribution in the groundwater was also compared to the measured values in KLX01 and KLX02 and the hydrogeochemical model, based on interpolation between observations, see Section 4.3.5.

### **4.2.9 Identified uncertainties or unresolved issues in the model**

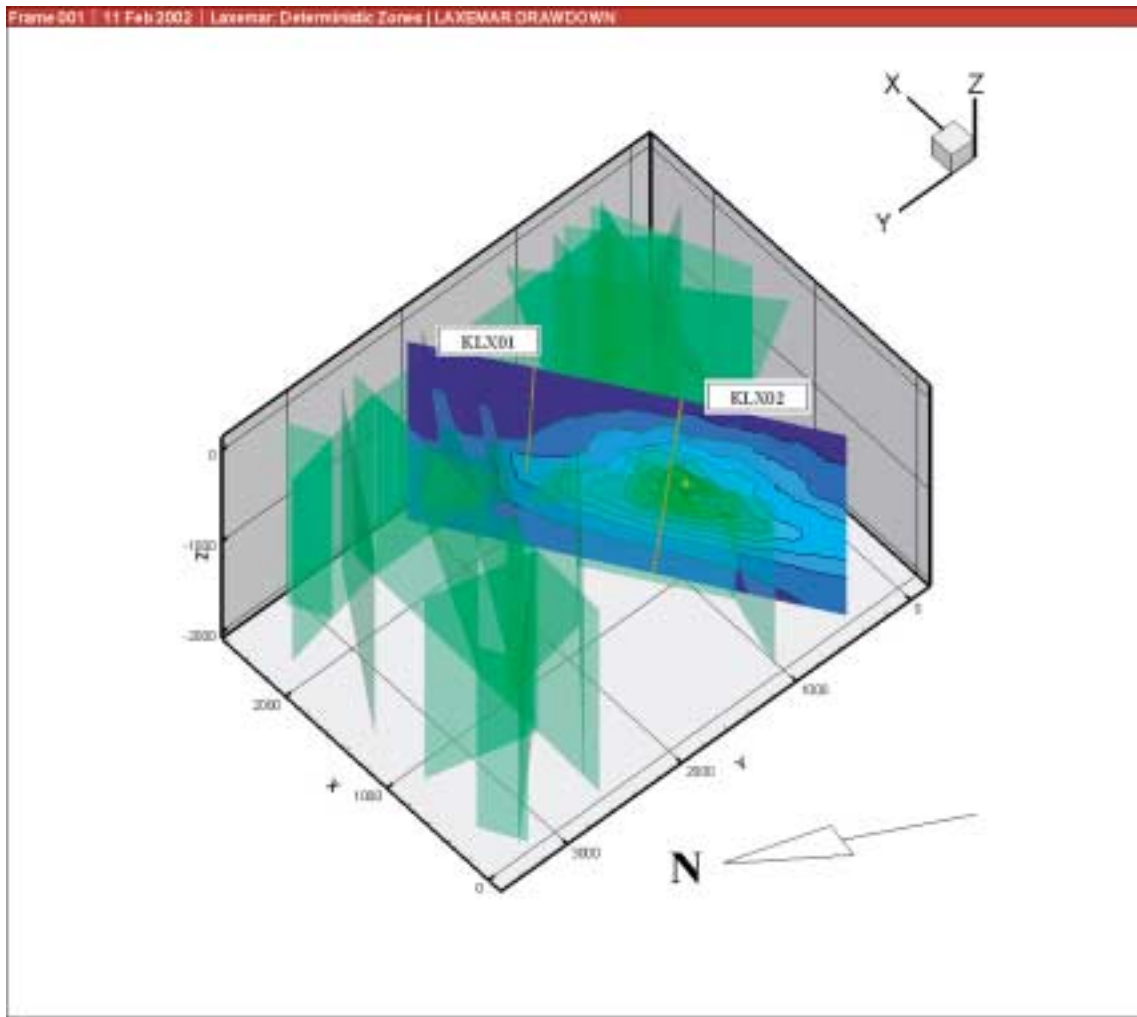
There are several potential uncertainties of the hydrogeological model as presented. These uncertainties may be divided between the uncertainty in transmissivity distribution of deformation zone and fracture transmissivity and the uncertainties regarding the hydrogeology of the near surface.

#### ***Deformation zone and fracture transmissivities – Conditioning***

The uncertainty in transmissivity distribution both regards the distributions as such and the associated geometry as given by the geological model.

A problem with the single-hole data that have been used in this project is that the field methods differ between the holes, do not cover the entire borehole lengths and the positions of the injection test-sections are uncertain in KLX01. Another problem is that only limited testing has been performed in the percussion boreholes, compared to what is planned for the site investigations. All these factors combined limit the analysis and the conclusions that can be drawn. Despite these site-specific shortcomings, however, there is one major limitations of general interest that need to be highlighted and resolved as soon as possible.





*Figure 4-27. Visualisation of the drawdown in a vertical cross-section running through the two boreholes (KLX02 to the right). The green surfaces represent the deterministic zones of the Base geological model. (Figure 4-7 in /Follin and Svensson, 2002/).*

**Table 4-11. Measured and simulated drawdown in KLX01 for the interference test made in November 1995, see /Follin, 1997/ and Section 4.2.4. /Follin and Svensson, 2002/. Pumped borehole section in KLX02 805–1103 m.**

Test Section	Measured drawdown in freshwater head	Simulated drawdown in freshwater head
KLX01: 0–140 m	~ 0 m	0.15 m
KLX01: 141–271 m	~ 0 m	0.23 m
KLX01: 272–694 m	0.6 m	0.83 m
KLX01: 695–855 m	2.3 m	1.07 m
KLX01: 856–1078 m	1.5 m	2.12 m

The limitation in mind can be seen in Figure 4-25, where the measured hydraulic conductivity in the upper part of KLX02 between 200–300 m is not captured by the studied realisation. Obviously, there is something missing in this portion of the model, e.g. a geometric structure with a fairly high transmissivity. The problem with the missing hydraulic structure could be claimed to be due to the used Base geological model, which does not contain any fracture zone at this position. In contrast, it can be concluded that the Alternative geological model does contain sub-horizontal fracture zones at this depth. The Alternative model is not constructed on the basis of hydraulic anomalies but on reflection seismic anomalies, which makes it even more interesting. From a Monte Carlo simulation point of view, it may be advocated that the Base geological model could be all right and that the problem is solely probabilistic, i.e., the realisation with the random features is not sufficiently conditioned to match the local observations.

The situation in KLX01 is somewhat similar, see Figure 4-24. Besides the missing hydraulic structure required in order to explain the elevated conductivity values in the upper part of this borehole, it may also be noted that there is a highly conductive probabilistic feature in the studied realisation at the bottom of KLX01. The anomaly cannot be assessed critically since there are no hydraulic data at this depth to support the argumentation.

Although the issue of conditioning shows up to be a very important issue, it must be recognised that the solution to the problem is not as straightforward as for the stochastic continuum approach, which does not bother at all about geometry. /Follin and Svensson, 2002/ discusses a few alternatives that may be feasible from a practical point of view but these need to be evaluated, and perhaps also elaborated, before they are subjected to a peer review.

### ***Near surface deposits and groundwater recharge***

The hydraulic conductivity of the uppermost layers of a numerical flow model in DarcyTools have been used to tune the position of the water table and hence the spatial distribution of recharge and discharge areas. If the hydraulic conductivity of the uppermost layer is high, saturated grid cells in the topographic lows will form a flow pattern that resembles the surface hydrological conditions, i.e., wetlands, lakes and streams. Unfortunately, the present knowledge about the hydrology of the Laxemar area is quite limited. Except for the elevation of Lake Frisksjön, there are no other hydrological data to calibrate against. According to the geological description in Section 3.3, however, the uppermost part of the subsurface consists of a thin layer of flushed till or outcropping bedrock, which suggests that the surface runoff should be quite high.

The performed tuning of the hydraulic conductivity of the uppermost layers carried out in support of this project is by no means exhaustive. The point made by /Follin and Svensson, 2002/ is that the hydrogeological conditions on the top boundary are important for the credibility of the environmental impact assessment. The near-surface conditions determine the relation between the net precipitation and the maximum groundwater recharge. Questions like “How large will the radius of influence be once the construction of the deep repository has started?” require a good understanding of the near-surface processes. Conclusively, it is important to have a good control of surface runoff parameters such as lake elevation, stream flow rates, but also the thickness and conductivity of the Quaternary deposits. If these parameters are unknown, the performance assessment modelling of the subsurface can still be performed as planned although the gradients would need to be assumed.

## 4.3 Hydrogeochemical modelling

Hydrogeochemical modeling involves several sciences such as geology and hydrogeology. This information is used as background information, supportive information or as independent information when models are constructed or compared. The following chapters describes how geological information can be used in the modeling and how speciation, mass-balance, coupled modeling and mixing modeling can be used. The results from the modeling are generally presented by using 2D/3D visualization tools. Examples of this is given in the final subsection of this section.

### 4.3.1 Geological information used in the hydrogeochemical modelling

#### ***Borehole specific information***

Geological information is used in hydrogeochemical modelling as a direct input in to mass-balance modelling but also to judge the feasibility of the results from e.g. saturation index modelling (see Table 4-12). For this particular modelling exercise geological data from KLX01 and 02 was summarized by using WellCad information (see Section 3.4.4) and the information was reviewed and the relevant rock types, fracture minerals and mineral alteration were identified.

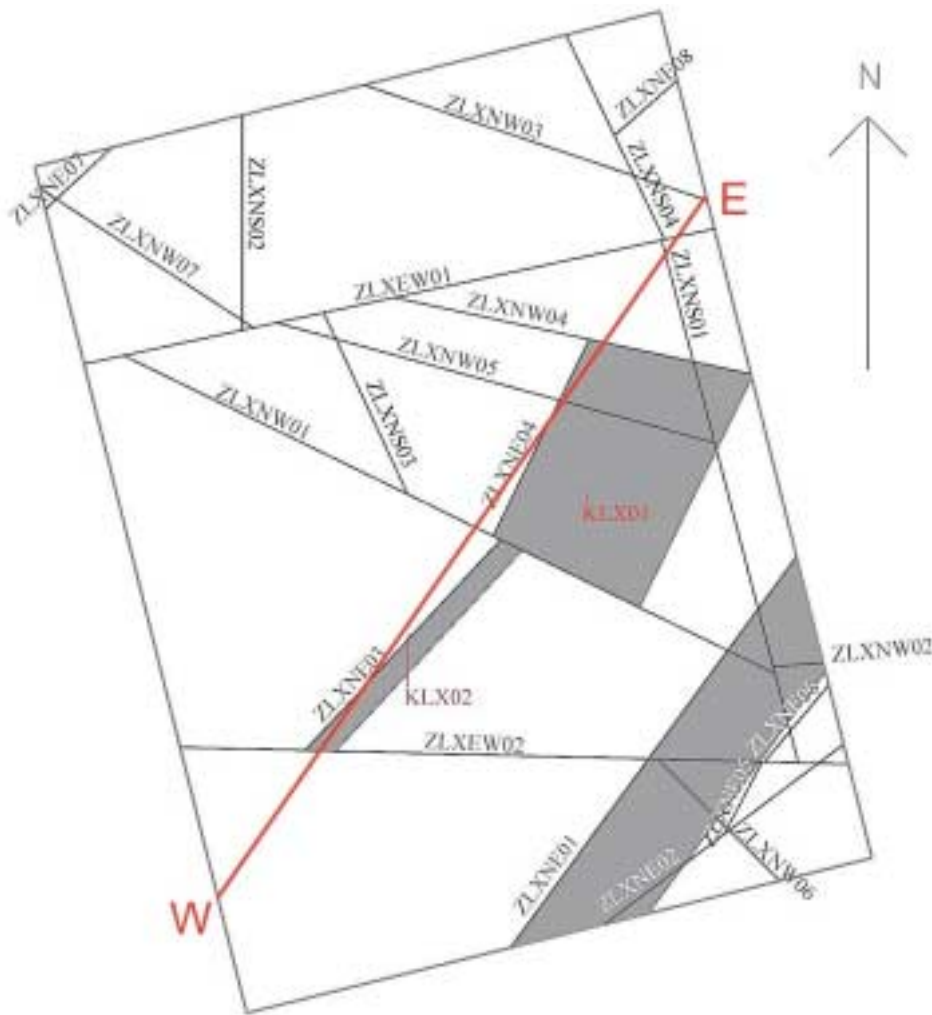
#### ***Geological model used for visualisation***

The base geological structural model (see Section 4.1) provides important information of fractures conducting groundwater. This is used for the understanding and modelling of the hydrodynamics. The cutting plane used for visualisation of groundwater properties was selected with respect to the geological model (see Figure 4-28). The cutting plane was located along the major fracture zones ZLXNE03 and ZLXNE04 since most of the groundwater samples are located in association or in the near vicinity of these fracture zones. The alternative geological model presented in Section 4.1 would not change the selection of the cutting plane. It was also tested to visualise the groundwater samples in relation to the base geological model. But this was not possible with the present version of RVS.

### 4.3.2 Speciation, mass-balance and coupled modelling

#### ***Speciation modelling***

Speciation modelling with PHREEQC has been carried out. The main purpose of such *speciation modelling* is to calculate, based on thermodynamic properties, the mineral saturation indices. The indices are indicators of the saturation state of a mineral with respect to a given water composition. A positive value indicates that thermodynamically a mineral can precipitate, a negative value that it can dissolve. A value close to zero indicates that the mineral is not reacting. The saturation index indicates the potential for the process, not the rate, at which the process will proceed. From this information conclusions concerning possible major reactions taking place and indirect indications of the dynamics of the system can be drawn.



**Figure 4-28.** The base geological model and the cutting plane W-E (in red) used for visualization of the groundwater properties. (The coordinates for the cutting plane are: Point West: 1548500, 6365850, 501548500, 6365850, -1950 and point East: 1550325, 6368825, 501550325, 6368825, -1950.)

An advantage with the speciation modelling that it is relatively easy to modify the model to include new species and elements and there is extensive literature on test cases and on complexation reactions and estimates of the stability constants. The following types of major reactions can generally be modelled:

1. Introduction of CO<sub>2</sub> gas in the unsaturated zone.
2. Dissolution of calcite and dolomite, and precipitation of calcite.
3. Cation exchange.
4. Oxidation of iron containing minerals, pyrite and organic matter.
5. Reduction of oxygen, nitrate, and sulphate, with production of sulphide.

6. Reductive production of methane.
7. Dissolution of gypsum, anhydrite and halite.
8. Incongruent dissolution of primary silicates with formation of clays.

The following difficulties can occur (after Parkhurst and Plummer in /Alley, 1993/):

- The theory used (Debye-Hückel) or its modification can be applied only on dilute water or on sodium chloride groundwater of maximum seawater concentration.
- Insufficient laboratory work has been performed to reproduce mineral solubilities.
- The thermodynamic data is based on high temperatures because of slow equilibrium in low temperatures (~25°C).
- Minerals can have a range of stability due to their composition and structure.
- Lack of mechanisms to account for repulsive forces in mixed electrolytes.
- Sensitive to accuracy of chemical analyses especially for pH and Eh. One unit change in the pH (see Figure 3-48) changes the SI calculations with one unit. This means that pH measurements recorded at surface rather than down-hole can lead to misunderstanding concerning the precipitation/dissolution of a mineral phase.
- Many of the reactions such as redox reactions are biologically mediated or kinetically slow and therefore not in equilibrium.

For low-temperature calculations, the number of minerals for which meaningful saturation indices can be calculated is relatively small. Reliable indications can be obtained for fast reactions such as: carbonate, sulphate and chloride minerals. For kaolinite, clays, feldspars and other aluminium silicates qualitative results can be obtained due to uncertainties in the thermodynamic data and the aluminium measurements.

The results of saturation index modelling performed on the target sample (KLX02: 235–341 m) is shown below as an example (see Table 4-12). A positive saturation index SI indicates that the water is supersaturated in respect to that mineral or gas phase. If the value is negative the water is undersaturated and the mineral or gas can dissolve. A value close to 0 ( $SI \pm 0.5$ ) indicates saturation. SI = saturation index, IAP = ionic activity product and  $K_T$  = equilibrium constant.

The results indicate that the water is in equilibrium ( $SI \pm 0.5$ ) with Aragonite, Calcite, Chalcedony, Dolomite, Quartz, Rhodochrosite and Talc. This may indicate that the water is in equilibrium with many of the rock minerals. The validity of the calculations have always to be checked by means of geological information (see Chapter 4.4.1) where the mineralogical data has to support the existence of the various mineral phases. In this particular case the geological information indicated that Chlorite (not calculated due lack of aluminium data) and Calcite are the major fracture minerals at this depth. Additional site modelling indicated that the shallow water (<100 m) is generally under saturated with respect to Calcite but deeper water (>100 m) is saturated or supersaturated, which can indicate dissolution of this mineral at shallow depths and precipitation at larger depths. A more detailed and extensive modelling was regarded to be outside the scope of the project.

**Table 4-12. Saturation index calculations for the target sample KLX02:235-341 m.**

-----Saturation indices-----

Phase	SI	log IAP	log KT	
Anhydrite	-2.23	-6.57	-4.33	CaSO <sub>4</sub>
Aragonite	0.18	-8.09	-8.26	CaCO <sub>3</sub>
Calcite	0.33	-8.09	-8.42	CaCO <sub>3</sub>
Celestite	-2.33	-8.95	-6.63	SrSO <sub>4</sub>
Chalcedony	-0.05	-3.76	-3.71	SiO <sub>2</sub>
Chrysotile	-3.76	30.17	33.92	Mg <sub>3</sub> Si <sub>2</sub> O <sub>5</sub> (OH) <sub>4</sub>
CO <sub>2</sub> (g)	-3.00	-21.21	-18.21	CO <sub>2</sub>
Dolomite	0.03	-16.74	-16.77	CaMg (CO <sub>3</sub> ) <sub>2</sub>
Fe(OH) <sub>3</sub> (a)	3.35	21.59	18.24	Fe(OH) <sub>3</sub>
FeS (ppt)	-68.28	-107.90	-39.62	FeS
Goethite	9.24	21.59	12.35	FeOOH
Gypsum	-1.98	-6.57	-4.59	CaSO <sub>4</sub> : 2H <sub>2</sub> O
H <sub>2</sub> (g)	-24.45	-24.40	0.05	H <sub>2</sub>
H <sub>2</sub> S (g)	-73.57	-117.29	-43.72	H <sub>2</sub> S
Hausmannite	-9.15	55.33	64.47	Mn <sub>3</sub> O <sub>4</sub>
Hematite	19.44	43.19	23.75	Fe <sub>2</sub> O <sub>3</sub>
Jarosite-K	-2.47	29.44	31.91	KFe <sub>3</sub> (SO <sub>4</sub> ) <sub>2</sub> (OH) <sub>6</sub>
Mackinawite	-67.54	-107.90	-40.36	FeS
Manganite	-2.83	22.51	25.34	MnOOH
Melanterite	-7.92	-10.30	-2.39	FeSO <sub>4</sub> : 7H <sub>2</sub> O
O <sub>2</sub> (g)	-39.00	48.80	87.80	O <sub>2</sub>
Pyrite	-110.51	-200.79	-90.28	FeS <sub>2</sub>
Pyrochroite	-4.89	10.31	15.20	Mn (OH) <sub>2</sub>
Pyrolusite	-8.90	34.71	43.61	MnO <sub>2</sub>
Quartz	0.42	-3.76	-4.19	SiO <sub>2</sub>
Rhodochrosite	0.18	-10.90	-11.08	MnCO <sub>3</sub>
Sepiolite	-2.28	13.84	16.13	Mg <sub>2</sub> Si <sub>3</sub> O <sub>7</sub> .5OH:3H <sub>2</sub> O
Sepiolite(d)	-4.82	13.84	18.66	Mg <sub>2</sub> Si <sub>3</sub> O <sub>7</sub> .5OH:3H <sub>2</sub> O
Siderite	-1.01	-11.82	-10.81	FeCO <sub>3</sub>
SiO <sub>2</sub> (a)	-0.93	-3.76	-2.83	SiO <sub>2</sub>
Strontianite	-1.19	-10.47	-9.28	SrCO <sub>3</sub>
Sulfur	-55.22	-92.89	-37.68	S
Talc	-0.34	22.64	22.99	Mg <sub>3</sub> Si <sub>4</sub> O <sub>10</sub> (OH) <sub>2</sub>

### **Mass balance and coupled modelling**

The aim of *mass-balance modelling* is to determine the type and amount of geochemical reactions that are occurring in a groundwater system. This is done by identifying the minerals that are reacting and determining the amounts of the minerals that dissolve or precipitate. The modelling of an important group of minerals such as aluminium silicates (e.g. feldspars and clay minerals) are hindered or made uncertain at Laxemar due to difficulties associated with aluminium determinations. Reactions such as Ion exchange, sulphate reduction and Calcite dissolution can be modelled but was regarded to be outside the framework of the method test.

*Coupled reaction-transport modelling* (1D modelling in PHREEQC) can be used to solve geochemical reactions and processes of advection, dispersion and diffusion. The aqueous model used is based on thermodynamic speciation modelling and the uncertainties are therefore the same as those discussed above. The model has to calculate the flow field for a steady state or possibly transient aquifer that is under study and hence the hydraulic properties of the aquifer must be known. Inverse modelling starts from a known target

solution and tries to quantify the processes that led to the observed chemistry. The mass-balance, reaction transport (coupled code) and the inverse modelling possibilities in PHREEQC were outside the framework of this project but will be used in future site modelling /see Smellie et al, 2002/.

### **4.3.3 M3 modelling**

A challenge in groundwater modelling is to reveal the origin, mixing and reactions altering the groundwater samples. The groundwater modelling concept M3 (Multivariate Mixing and Mass-balance calculations) /Laaksoharju and Skårman, 1995; Laaksoharju et al, 1999b/ can be used for making judgement on this.

#### ***Introduction and model description***

In M3 modelling the assumption is that the groundwater is always a result of mixing and reactions. M3 modelling uses a statistical method to analyse variations in groundwater compositions so that the mixing components, their proportions, and chemical reactions are revealed. The method quantifies the contribution to hydrochemical variations by mixing of groundwater masses in a flow system by comparing groundwater compositions to identified reference waters. Subsequently, contributions to variations in non-conservative solutes from reactions are calculated.

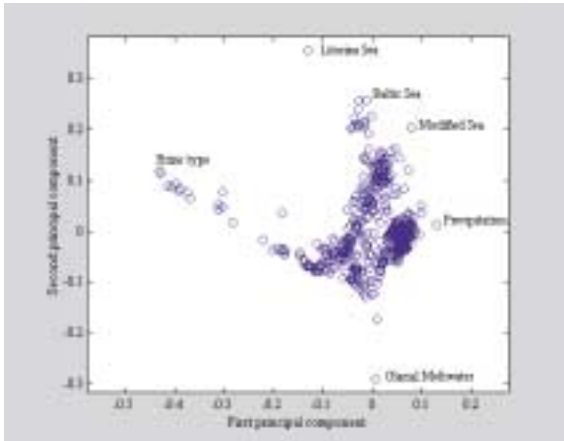
The M3 method has been tested, evaluated, compared with standard methods and modified over several years within domestic and international research programmes supported by the SKB. The main test and application site for the model has been the Äspö HRL /Laaksoharju and Wallin, 1997; Laaksoharju et al, 1999c/. Mixing seems to play an important role at many crystalline and sedimentary rock sites where M3 calculations have been applied such as in different Swedish sites /Laaksoharju et al, 1998/, Canada /Smellie and Karlsson, 1996/, Oklo in Gabon /Gurban et al, 1998/ and Palmottu in Finland /Laaksoharju et al, 1999a/.

The features of the M3 method are:

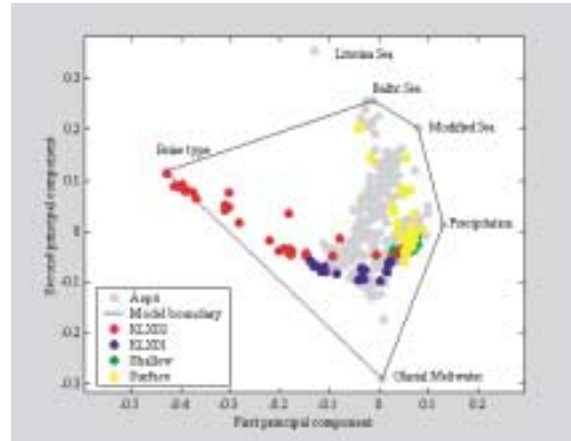
- It is a mathematical tool which can be used to evaluate groundwater field data, to help construct a conceptual model for the site and to support expert judgement for site characterisation.
- It uses the entire hydrochemical data set to construct a model of geochemical evolution, in contrast to a thermodynamic model that simulates reactions or predicts the reaction potential for a single water composition.
- The results of mixing calculations can be integrated with hydrodynamic models, either as a calibration tool or to define boundary conditions.
- Experience has shown that to construct a mixing model based on physical understanding can be complicated especially at site scale. M3 results can provide additional information of the major flow paths, flow directions and residence times of the different groundwater types which can be valuable in transport modelling.
- The numerical results of the modelling can be visualised and presented for non-expert use.

The M3 method consists of 4 steps where the first step is a standard principal component analysis (PCA), selection of reference waters, followed by calculations of mixing proportions, and finally mass balance calculations (for more details see /Laaksoharju et al, 1999b; Laaksoharju, 1999d/). The four modelling steps employed on Laxemar data are illustrated in Figure 4-29.

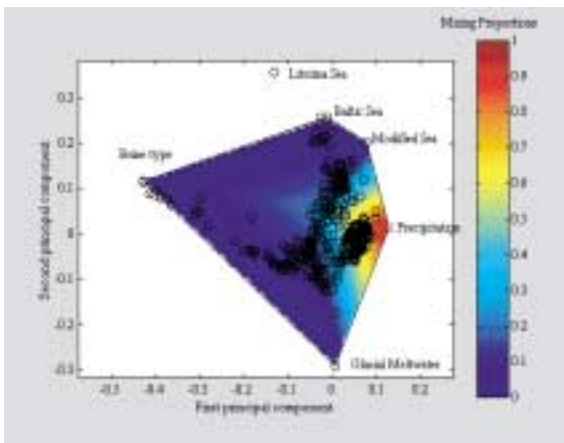
a) Principal component analysis



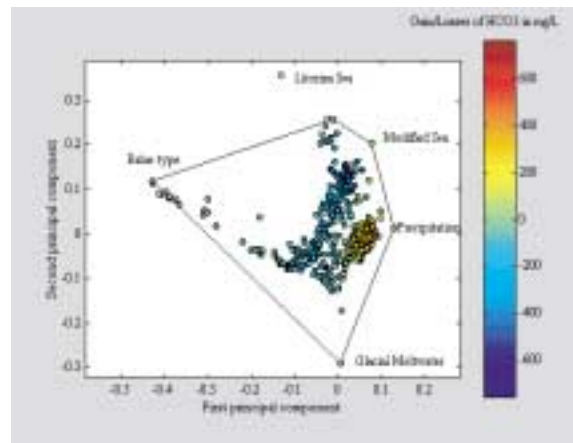
b) Identification of Reference waters



c) Mixing calculations



d) Mass-balance calculations



**Figure4-29.** Different steps in the M3 modelling: a) Identification of principal components with the maximum resolution, b) selection of reference waters, c) mixing calculations where the linear distance of a sample to the reference waters e.g. the portions of meteoric water (%) are shown, d) Mass-balance calculations, the sources and sinks (mg/l) of carbonate ( $\text{HCO}_3$ ) are shown which cannot be accounted for by using the ideal mixing model.



Five reference waters were chosen at the Laxemar site using the M3 method: Brine type, Glacial, Sea Water, Modified Sea and Precipitation. The existence of these reference waters is also supported by the conceptual post-glacial scenario model (Figure 3-47) of the site. This type of modelling should be repeated by using different types and numbers of reference waters and testing different data sets containing both local and regional data. The selected reference waters for the current modelling are:

- **Brine type of reference water:** Represents the sampled deep brine type (Cl = 47,000 mg/L) of water found in KLX02:1631–1681m /Laaksoharju et al, 1995a/. An old age for the Brine is suggested by the measured <sup>36</sup>Cl values indicating a minimum residence time of 1.5 Ma for the Cl component /Laaksoharju and Wallin, 1997/.
- **Glacial reference water:** Represents a possible melt-water composition from the last glaciation >13,000BP. Modern sampled glacial melt water from Norway was used for the major elements and the δ<sup>18</sup>O isotope value (–21 ‰ SMOW) was based on measured values of d<sup>18</sup>O in calcite surface deposits /Tullborg and Larson, 1984/. The δ<sup>2</sup>H value (–158 ‰ SMOW) is a modelled value based on the equation (δH = 8 × δ<sup>18</sup>O + 10) for the meteoric water line.
- **Sea Water:** Represents sampled modern Baltic Sea water.
- **Modified Sea water:** Represents Baltic Sea affected by microbial sulphate reduction.
- **Precipitation water:** Corresponds to infiltration of meteoric water (the origin can be rain or snow) from 1960. Sampled modern meteoric water with a modelled high tritium (100 TU) content was used to represent precipitation from that period.

For groundwater analytical data see Table 4-13.

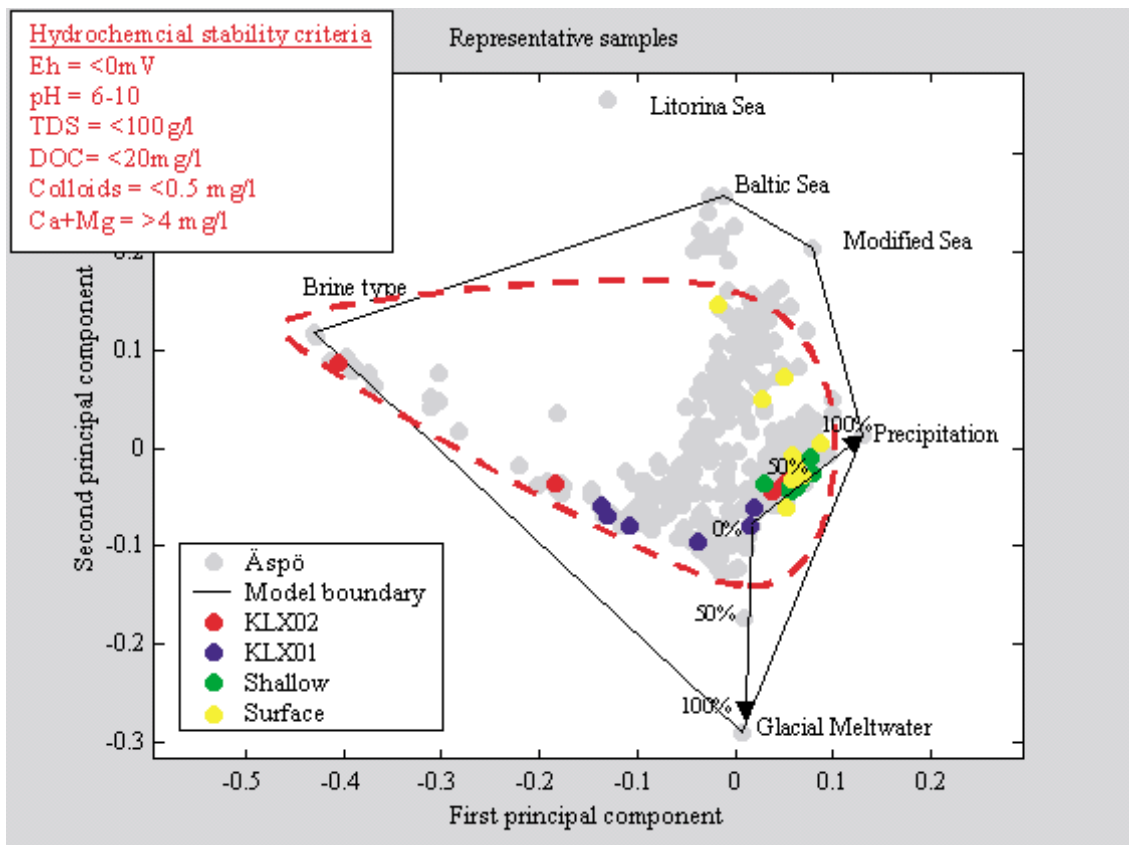
**Table 4-13. Groundwater analytical or modelled data\* used as reference waters in the M3 modelling for Laxemar.**

	Cl (mg/L)	Na (mg/L)	K (mg/L)	Ca (mg/L)	Mg (mg/L)	HCO <sub>3</sub> (mg/L)	SO <sub>4</sub> (mg/L)	<sup>3</sup> H (TU)	δ <sup>2</sup> H ‰	δ <sup>18</sup> O ‰
Brine	47200	8500	45.5	19300	2.12	14.1	906	4.2	–44.9	–8.9
Glacial	0.5	0.17	0.4	0.18	0.1	0.12	0.5	0	–158*	–21*
Baltic Sea	3760	1960	95	94	234	90	325	42	–53.3	–5.9
Modified Sea	4920	2300	29	730	233	1200	36	14	–50.4	–7.3
Precipitation	0.23	0.4	0.29	0.24	0.1	12.2	1.4	100*	–80	–10.5

The following six reactions have been considered, with comments on the qualitative outcomes of mixing and mass balance modelling with M3:

1. *Organic decomposition*: This reaction is detected in the unsaturated zone associated with Meteoric water. This process consumes oxygen and adds reducing capacity to the groundwater according to the reaction:  $O_2 + CH_2O \rightarrow CO_2 + H_2O$ . M3 reports a gain of  $HCO_3$  as a result of this reaction.
2. *Organic redox reactions*: An important redox reaction is reduction of iron III minerals through oxidation of organic matter:  $4Fe(III) + CH_2O + H_2O \rightarrow 4Fe^{2+} + 4H^+ + CO_2$ . M3 reports a gain of Fe and  $HCO_3$  as a result of this reaction. This reaction takes place in the shallow part of the bedrock associated with influx of Meteoric water.
3. *Inorganic redox reaction*: An example of an important inorganic redox reaction is sulphide oxidation in the soil and the fracture minerals containing pyrite according to the reaction:  $HS^- + 2O_2 \rightarrow SO_4^{2-} + H^+$ . M3 reports a gain of  $SO_4$  as a result of this reaction. This reaction takes place in the shallow part of the bedrock associated with influx of Meteoric water.
4. *Dissolution and precipitation of calcite*: There is generally a dissolution of calcite in the upper part and precipitation in the lower part of the bedrock according to the reaction:  $CO_2 + CaCO_3 \rightarrow Ca^{2+} + 2HCO_3^-$ . M3 reports a gain or a loss of Ca and  $HCO_3$  as a result of this reaction. This reaction can take place in any groundwater type.
5. *Ion exchange*: Cation exchange with Na/Ca is a common reaction in groundwater according to the reaction:  $Na_2X_{(s)} + Ca^{2+} \rightarrow CaX_{(s)} + 2Na^+$ , where X is a solid substrate such as a clay mineral. M3 reports a change in the Na/Ca ratios as a result of this reaction. This reaction can take place in any groundwater type.
6. *Sulphate reduction*: Microbes can reduce sulphate to sulphide using organic substances in natural groundwater as reducing agents according to the reaction:  $SO_4^{2-} + 2(CH_2O) + OH^- \rightarrow HS^- + 2HCO_3^- + H_2O$ . This reaction is of importance since it may cause corrosion of the copper capsules. Vigorous sulphate reduction is generally detected in association with marine sediments that provide the organic material and the favourable salinity interval for the microbes. M3 reports a loss of  $SO_4$  and a gain of  $HCO_3$  as a result of this reaction. This reaction modifies the seawater composition by increasing the  $HCO_3$  content and decreasing the  $SO_4$  content.

The above information is included in the geochemical description of the site, see Section 5.3. The PCA in M3 modelling can be used for several purposes, one example /Puigdomenech, 2001/ is to test which samples meet the requirements and preferences of /Andersson et al, 2000/. All representative samples at Laxemar meet these criteria. The individual samples can be tested for how much disturbances (e.g from changing climate) can be allowed before the hydrochemical stability criteria are no longer met (Figure 4-30). In this modelling example the target sample can have an addition of 75% precipitation water and 30% glacial meltwater and still meet the SKB criteria.



**Figure 4-30.** PCA plot illustrate whether the samples meeting the requirements and preferences of /Andersson et al, 2000/. All the representative samples at Laxemar meet these criteria. The black arrows indicate how much changes the target depth sample can undergo before some of the criteria is no longer met.

### **Model uncertainties**

The following factors can cause uncertainties in M3 calculations:

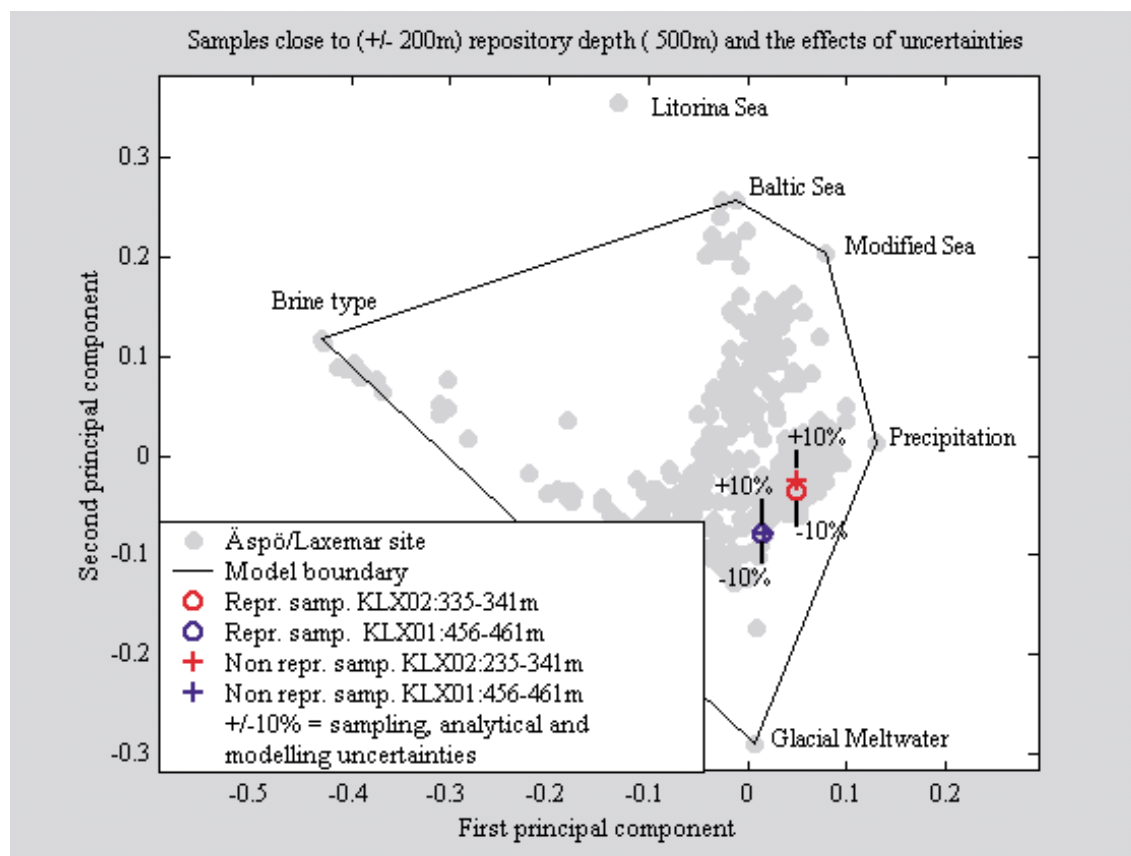
- Input hydrochemical data errors originating from sampling errors caused by the effects from drilling, borehole activities, extensive pumping, hydraulic short-circuiting of the borehole and uplifting of water which changes the in situ pH and Eh conditions of the sample, or as analytical errors.
- Conceptual errors such as wrong general assumptions, selecting wrong type/number of end-members and mixing samples that are not mixed.
- Methodological errors such as oversimplification, bias or non-linearity in the model, and the systematic uncertainty which is attributable to use of the centre point to create a solution for the mixing model.

An example of a conceptual error is assuming that the groundwater composition is a good tracer for the flow system. The water composition is not necessarily a tracer of mixing directly related to flow since there is not a point source as there is when labelled water is used in a tracer test.

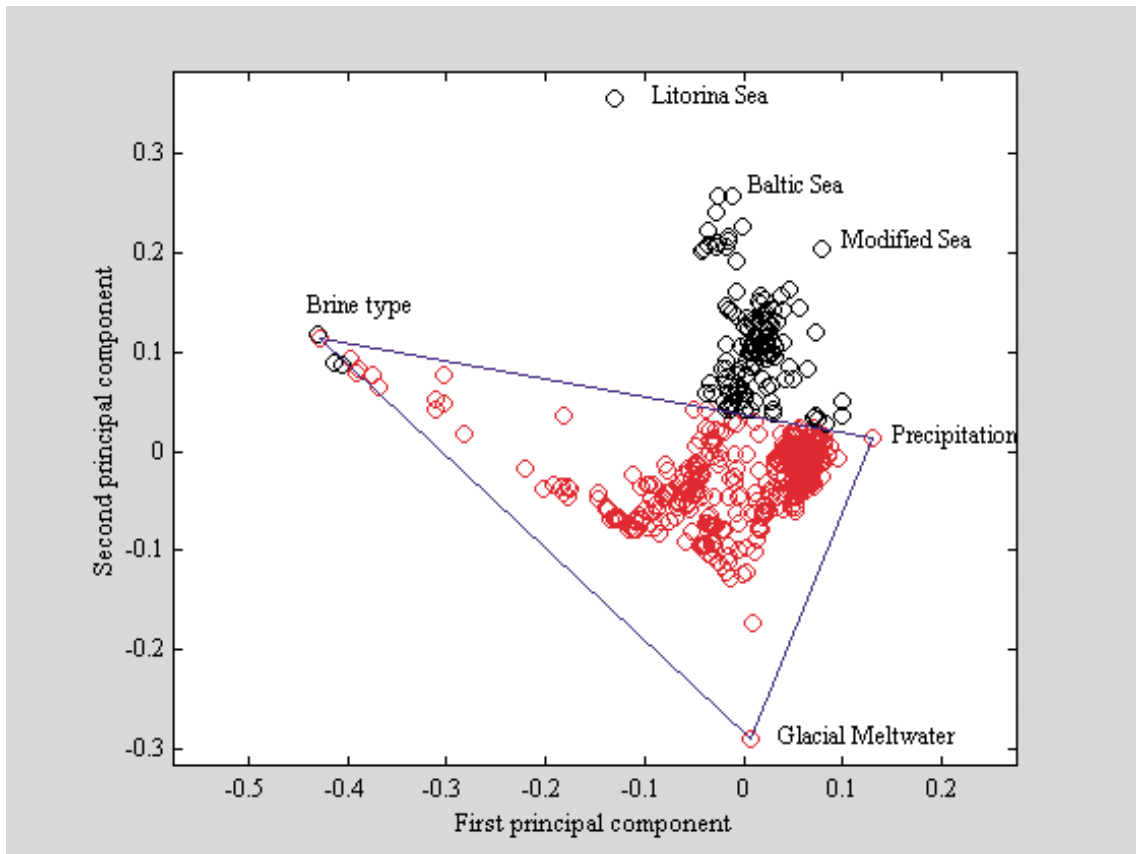
Another source of uncertainty in the mixing model is the loss of information in using only the first two principal components. The third principal component gathers generally around 10% of the groundwater information compared with the first and second principal components which contain around 70% of the information. A sample could appear to be closer to a reference water in the 2D surface than in a 3D volume involving the third principal component. In the latest version of M3 the calculations can also be performed in 3D.

Uncertainty in mixing calculations is smaller near the boundary of the PCA polygon and larger near the centre. The uncertainties have been handled in M3 by calculating an uncertainty of 0.1 mixing units (with a confidence interval of 90%) and stating that a mixing portion <10% is under the detection limit of the method. The effects from data uncertainties and model uncertainties are shown in Figure 4-31. The changes in KLX02:335-340.8 m expressed as Cl concentrations are 126–235 mg/L between the first and the last sample. The changes in KLX01:456–461 m expressed as Cl concentrations is 1650–1700 mg/L between the first and the last sample.

An example of an alternative model employing different reference waters (precipitation, glacial meltwater and brine) is shown in Figure 4-32. The alternative model cannot explain the observations close to the Sea but can explain the observations from the deep



**Figure 4-31.** The effect from the data uncertainties and model uncertainties are plotted on a PCA for the two target . The Model uncertainty  $\pm 10\%$  is shown here as error bars the analytical uncertainty is  $\pm 5\%$  and represents therefore half of the error bars.



**Figure 4-32.** Example of alternative model for the Laxemar site by selecting alternative reference waters. The aim of this modelling is to test the uncertainties but also to test how various models will change the scientific understanding of the site. This alternative model can explain the deep borehole observations at Laxemar but not the shallow observations sampled close to the Baltic Sea.

boreholes KLX01 and KLX02 and may therefore indicate that the influence from modern Baltic Sea water is minor. This contradicts the two-component model tested in Table 3-29, which is indicating Sea water contributions at large depths in KLX01.

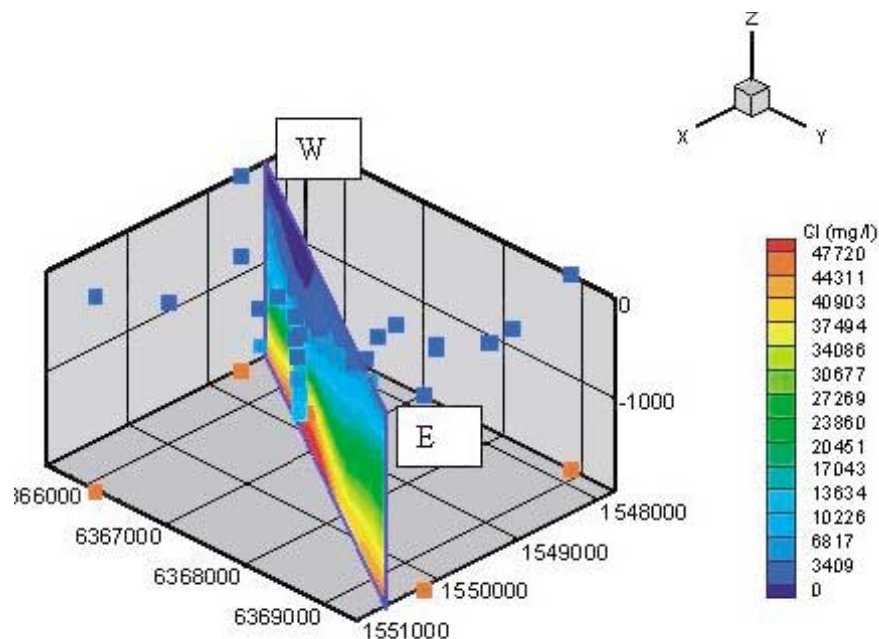
#### 4.3.4 Visualisation of the groundwater properties

To visualise the measured and modelled groundwater properties at Laxemar, and to summarise the information from all the samples a 3D interpolation by using TecPlot was performed. The interpolation method used was 3D Kriging. To show the results a 2D cutting plane was chosen based on the geological model (see Figure 4-28). The cutting plane goes through the Laxemar mainland in a SW-NE direction. For simplification the cutting plane is named W-E. To reduce uncertainties the cutting plane was chosen where most of the sampling from depth was located.

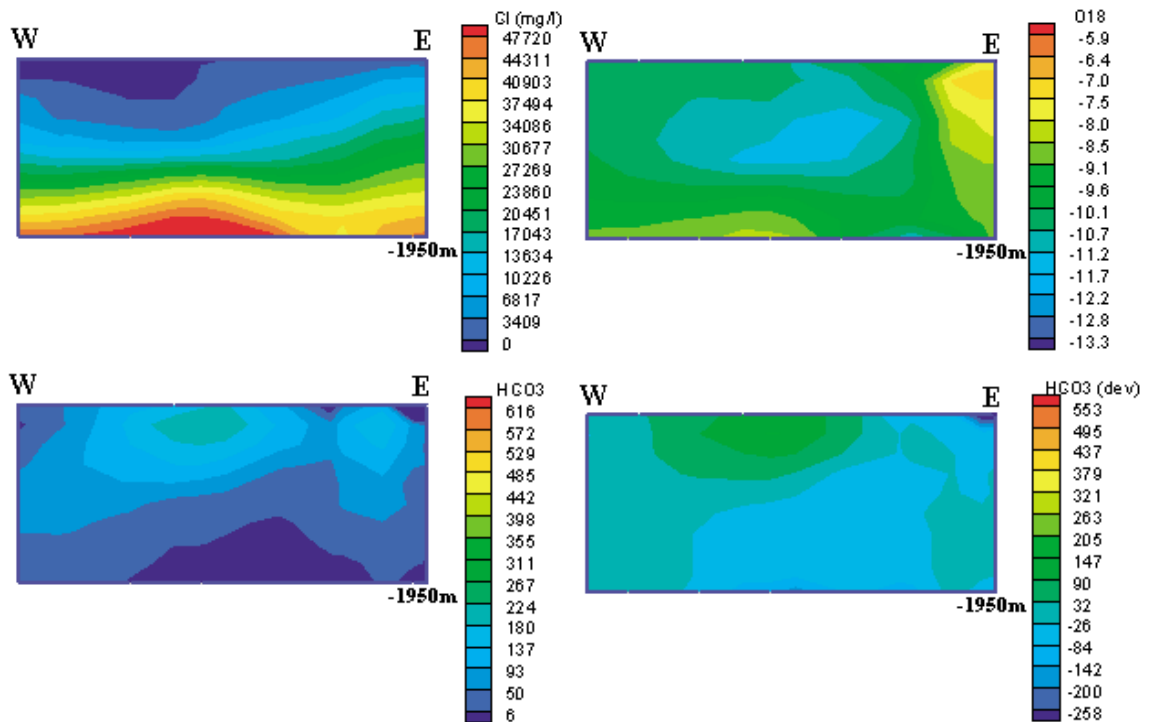
The interpolation is uncertain at large depths (>500 m) and in the corners of the cutting plane, where there are few or no observations. It is important to note that it is assumed that the sampled waters represent conductive and connected fractures and not the rock matrix. The results of the interpolation should be regarded as a potential map for a certain groundwater property to occur at a given bedrock location. The map has a high

degree of accuracy only close to the sampling points. The 3D interpolation was based on a total of 29 representative samples from the site. At the surface rain water alternatively Sea water was used dependent of the geographical location of the corners. In the lower corners of the model at -1950 m depth the information from the nearest deep borehole was used. At the W corner of the cutting plane a point was added at 700 m depth from the nearest borehole (KLX02). The Cl values is similar to what can be calculated by using Gben-Hertzberg's relation (the relation describes the depth of the interface between saline and non-saline water at coastal sites) and offers therefore an alternative for future simulations of boundary conditions. The results of the Cl interpolation is shown in Figure 4-33. Figure 4-34 shows Cl,  $\delta^{18}\text{O}$ ,  $\text{HCO}_3$  and the M3 deviation of  $\text{HCO}_3$  along the W-E cutting plane. The deviation calculations in M3 can be used as an indication of mass-balance reactions.

Figure 4-35 shows the M3 calculated mixing proportions of Baltic Sea water, precipitation, modified Sea water, glacial meltwater, brine water and the operational age. The calculated operational age can be used to illustrate a possible age distribution of the groundwaters. The mixing proportions and the assumed ages of the reference waters are used to suggest ages for the water masses. Clearly, water age is not a well defined quantity since different species migrate at different velocities. The evaluation still provides some insight. In this particular example the assumed ages for the reference waters were: Baltic Sea = 3,000 year, Precipitation = 0 year, Modified Sea = 3,000 year, Glacial meltwater = 10,000 year and Brine= >100,000 years. A sensitivity calculation should be performed where alternative ages are tested for the reference waters and where the results are compared with e.g.  $^{14}\text{C}$  determinations of the water, deviations from the



**Figure 4-33.** The 3D view of the interpolated Cl distribution, and the representative groundwater samples used in the interpolations. The boundary conditions used in the model are points added in the corners of the model.

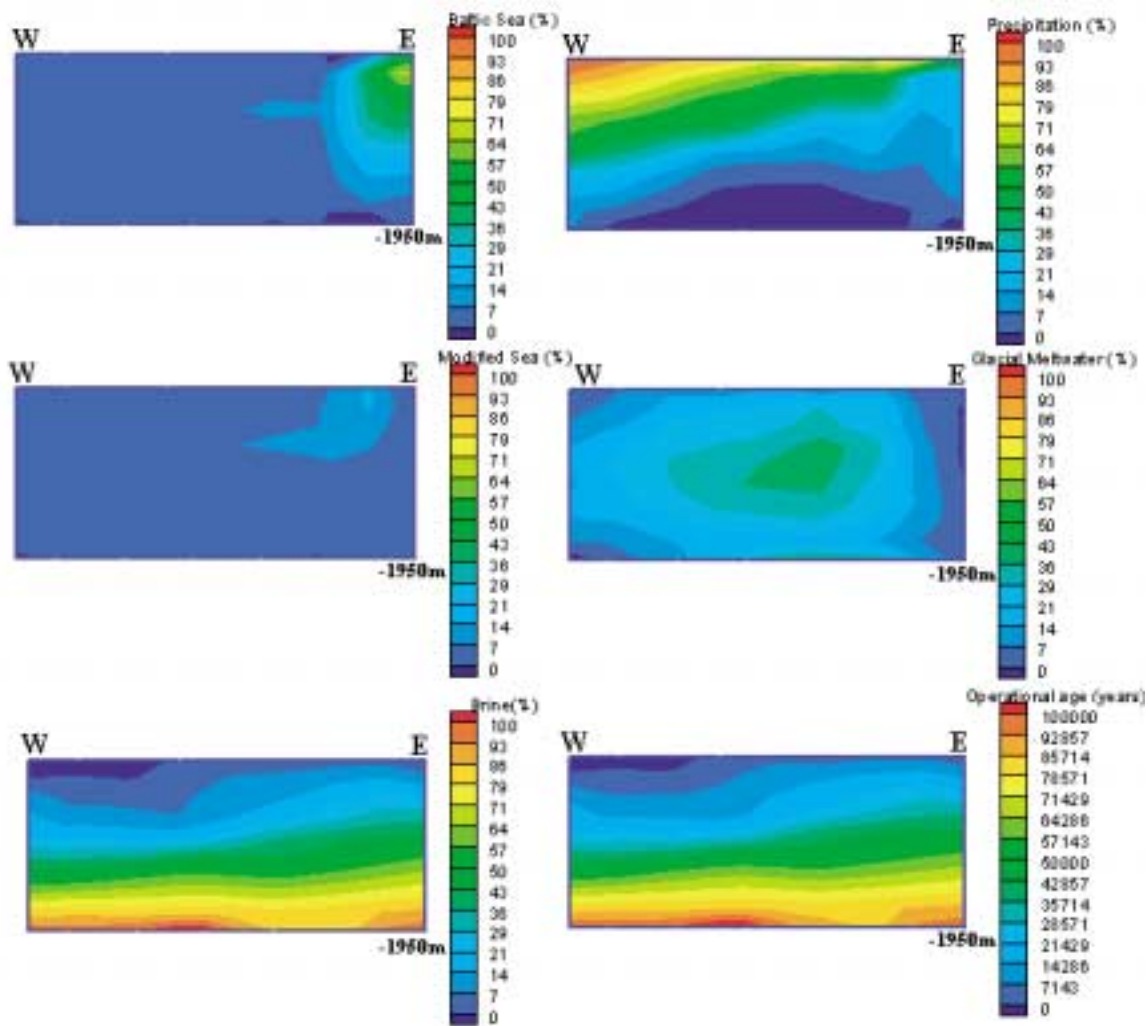


**Figure 4-34.** The cutting planes showing the results of the 3D interpolation of the measured values of Cl,  $\delta^{18}\text{O}(\text{O}-18)$  and  $\text{HCO}_3$  along the W-E cutting plane. These plots can be used for showing the distribution of measured values and to indicate effects from reactions. The deviation of  $\text{HCO}_3$  (dev) is shown as an example of deviation calculations in M3 which is used as an indication of mass-balance reactions. A gain (positive value) can be due to calcite dissolution, decomposition of organic matter or sulphate reduction. A loss (negative value) can indicate calcite dissolution.

meteoric water line based on the  $\delta^{18}\text{O}/\delta^2\text{H}$  plot,  $\text{Cl}^{36}$  age determinations, Tritium concentrations, fracture mineralogy, Uranium isotopes and Helium determinations. Also independent hydrogeological modelling can be used to calculate residence times and for independent comparison of the modelling results. The information from the above modelling is included in the geochemical description of the site, see Chapter 5.3.

### **Test of interpolation uncertainties**

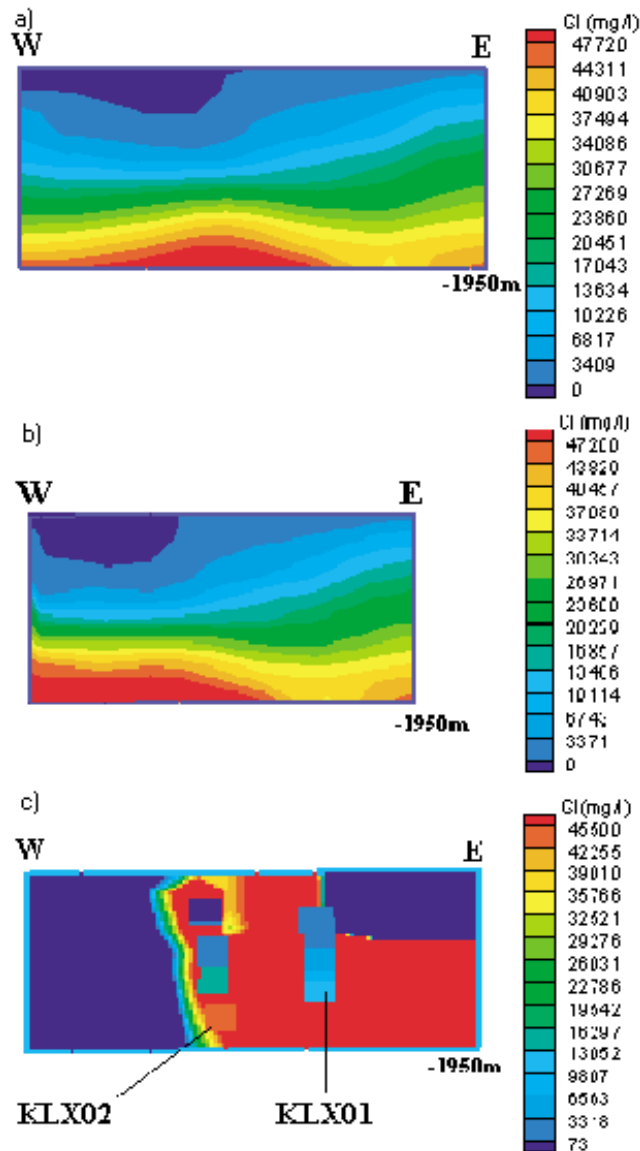
An advantage with 3D interpolation is that the model boundaries can be easily selected and uncertainties can be investigated in various parts of the model. Different cutting planes can be visualised for different fracture zones using the same model and boundary conditions. Finally the comparison between independent modelling such as hydro-modelling is easier since various cutting planes along the fracture zones or in the modelled area can be compared. The drawback is that larger uncertainties can occur and therefore local models will as well be constructed at a site investigation phase.



*Figure 4-35. The cutting planes W-E showing the results of the 3D interpolation of the M3 calculated mixing proportions of Baltic Sea, Precipitation, Modified Sea, Glacial meltwater and Brine. This information is used for indicating the possible origin of the water and possible flow patterns. The calculated operational age can be used to illustrate a possible age distribution of the groundwaters.*

The uncertainties can be tested in various ways. Figure 4-36 shows the effects from changing the boundary conditions. Figure 4-37 shows the differences when interpolating in 3D versus 2D. Figure 4-38 shows the effect from modelling the M3 uncertainty range of  $\pm 10\%$  by adding 10% precipitation water. The increase leads to a 10% higher content of precipitation water at larger depths. The uncertainty does not lead to misinterpretations and should not affect the final judgement of the site. The results show that it is necessary to test the effects of uncertainties to build confidence in the codes and models used. Unrealistic effects on site modelling are generally easily detected when using mathematical modelling.



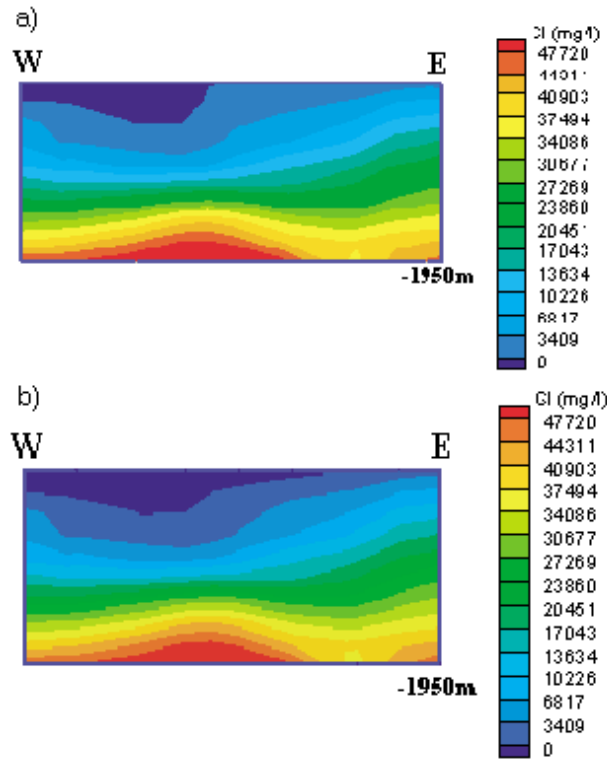


*Figure 4-36. Test of effects from changing the boundary conditions in the interpolation of the cutting plane W-E: a) the original Cl model b) using the samples from KLX02 as a boundary for the W corner; c) using only measured values and no boundaries, this brings the deep saline brine water up to the surface and the location close to measured values cannot be correctly modelled.*

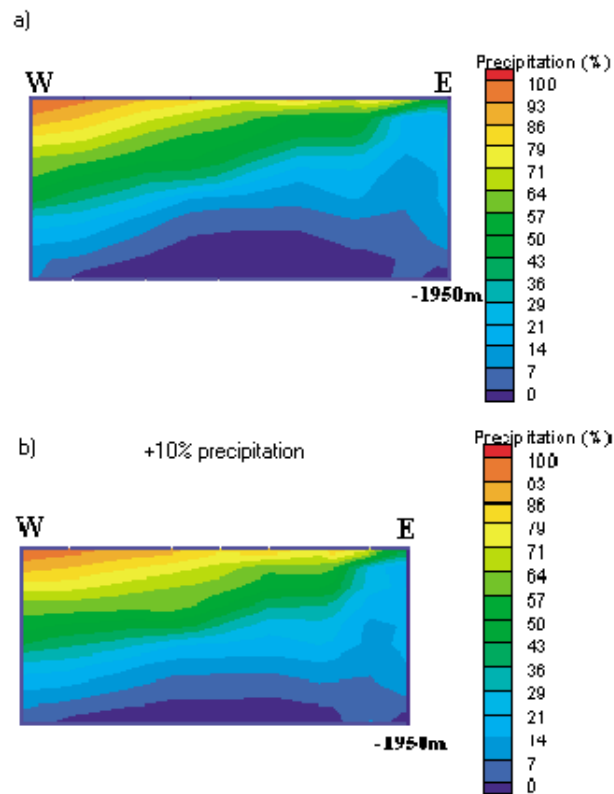
### 4.3.5 Comparison between hydrogeological and hydrogeochemical model

#### General

The hydrogeology and geochemistry deals with the same media of describing the groundwater properties. Therefore these two sciences should be able to describe the groundwater system in a similar way. In the on going SKB project /Wikberg 1998; Svensson et al, 2002c; Rhen and Smellie, 2002/ the method of integration was tested. Here the Cl and the M3 mixing proportions based on chemical sampling and modelling were compared with the results from independent hydrogeological modelling. The measured values and the modelled values were compared and despite discrepancies all



**Figure 4-37.** Test of the effects on the interpolation from using 3D versus 2D interpolations. a) the original Cl model based on 3D interpolation b) 2D interpolation, here the points outside the cutting plane have been deleted. The result show minor differences between the 3D and 2D interpolation since Kriging interpolation in 3D gives lower weight to points outside the cutting plane.



**Figure 4-38.** The M3 result uncertainty is in the range of  $\pm 10\%$  and therefore a test was conducted where the proportion of precipitation was increased with 10% in all the samples. a) the original model b) the proportion of precipitation is increased with 10%.

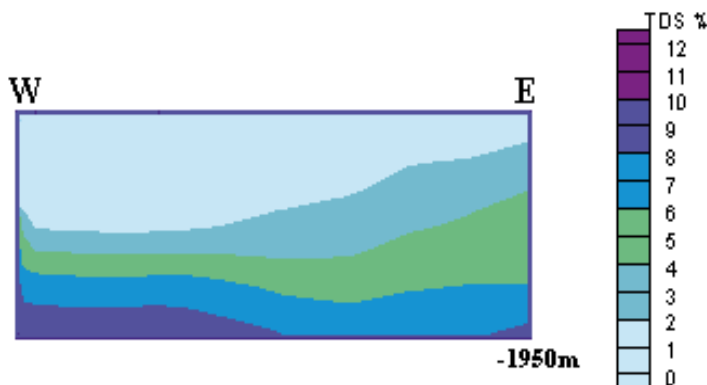
the codes could basically describe the Äspö site in terms of similar mixing proportions. The advantages with integration are:

- Hydrogeological models will be constrained by a new data set. If, as an example, the model cannot produce any Meteoric water at a certain depth and the hydrogeochemical data indicates that there is a certain fraction of this water type at this depth, then the model has to be revised.
- Hydrogeochemical models generally focus on the effects from reactions on the obtained groundwater rather than on the effects from transport. An integrated modelling approach can describe flow directions and hence help to understand the origin of the groundwater, the turn over time of the groundwater system can indicate the age of the groundwater, and knowing the flow rate can be used to indicate the reaction rate. The obtained groundwater chemistry is a result of reactions and transport, therefore only an integrated description can be used to correctly describe the measurements.
- By comparing two independent modelling approaches a consistency check can be made. As a result a better confidence in processes active, geometrical description and material properties can be gained.

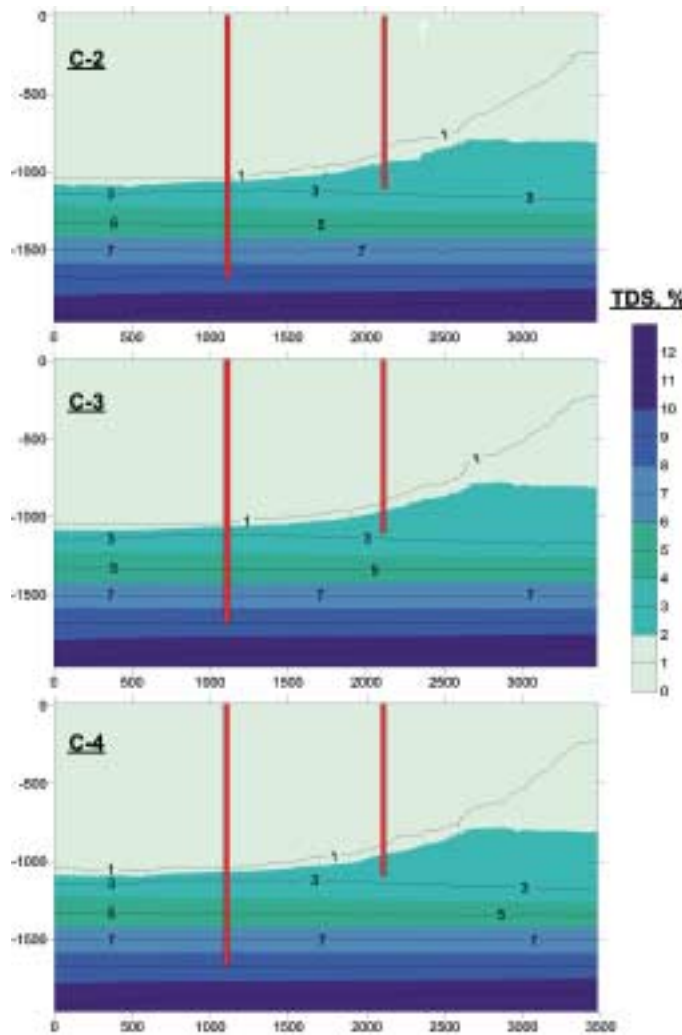
#### **Comparison of the hydrogeological and the hydrogeochemical models of the Laxemar area**

In this study only the Cl concentrations modelled along the same cutting plane W-E (see Figure 4-28 for orientation) are compared by using two independent models. In the future site investigations also M3 mixing proportions will be used for comparison and integration. TecPlot was used for 3D interpolation of TDS as described in the previous section. The result from the chemical model is shown in Figure 4-39. In Figure 4-40 the results from the hydrogeological modelling (see Section 4.2) is shown.

There are many similarities between the geochemical and hydrogeological modelling shown above. The major differences are in the amount of TDS in the east corner of the cutting plane. The chemical interpolations indicate that a more saline water could exist closer to the surface than indicated by the hydrogeological model but also at larger



**Figure 4-39.** TDS (Salinity) distribution based on interpolation of measured TDS in KLX01, KLX02, HLX holes, Baltic Sea and Meteoric water (at ground surface) within a box of the same size as in Figure 4-36b. Assumed TDS values at the lower corners of the box based on KLX02 values. Vertical cutting plane striking NW through boreholes KLX01 and KLX02.



*Figure 4-40. The TDS cutting plane based on the hydrogeological model using the same cutting plane as in Figure 4-39.*

depth. No deep borehole (only 100 m deep) exists in this part of the rock, which could be used for confirmation. The discrepancies can be due to the differences in the boundary conditions used in the models or in the assumptions made. The discrepancies should be a subject for further site investigations and model testing which is outside the framework for the current project.

#### **4.3.6 Site specific hydrogeochemical uncertainties**

At every phase of the hydrogeochemical investigation programme – drilling, sampling, analysis, evaluation, modelling – uncertainties are introduced which have to be accounted for, addressed fully and clearly documented to provide confidence in the end result, whether it will be the site descriptive model or repository safety analysis and design /Smellie et al, 2002/. The uncertainties can be conceptual uncertainties, data uncertainty, spatial variability of data, chosen scale, degree of confidence in the selected model, and error, precision, accuracy and bias in the predictions. Some of the identified uncertainties recognized during the Laxemar modeling exercise are discussed below.

The following data uncertainties have been estimated, calculated or modelled for the data and models used for the Laxemar Model Domain:

- drilling; may be  $\pm 10$ –70% at Laxemar,
- effects from drilling during sampling; is <5%,
- sampling; may be  $\pm 10$ % at Laxemar,
- influence associated with the uplifting of water; may be  $\pm 10$ %,
- sample handling and preparation; may be  $\pm 5$ %,
- analytical error associated with laboratory measurements; is  $\pm 5$ %,
- mean groundwater variability at Laxemar during groundwater sampling (first/last sample); is about 25%,
- the M3 model uncertainty; is  $\pm 0.1$  units within 90% confidence interval.

Conceptual errors can occur from e.g. the paleohydrogeological conceptual model. The influences and occurrences of old water end-members in the bedrock can only be indicated by using certain element or isotopical signatures. The uncertainty is therefore generally increasing with the age of the end-member. The relevance of an end-member participating in the groundwater formation can be tested by introducing alternative end-member compositions or by using hydrodynamic modelling to test if old water types can resign in the bedrock during prevailing hydrogeological conditions.

Uncertainties in the PHREEQC depend on which model is used in PHREEQC. Generally the analytical uncertainties and uncertainties concerning the thermodynamic data bases are of importance. Care also is required to select mineral phases which are realistic (even better if they have been positively identified) for the systems being modelled. The errors can be addressed by using sensitivity analyses, alternative models and descriptions. Such analysis was regarded to be outside the scope of this exercise.

The uncertainty due to 3D interpolation and visualization depends on various issues i.e. data quality, distribution, model uncertainties, assumptions and limitations introduced. The uncertainties are therefore often site specific and some of them can be tested such as the effect of 2D/3D interpolations. The site specific uncertainties can be tested by using quantified uncertainties, alternative models, and comparison with independent models such as hydrogeological simulations. Test performed on Laxemar data showed minor differences.

The integration part between the different modelling approaches was limited due to the nature of the project but should always play a central part in the site evaluation. There are many similarities between the geochemical and hydrogeological modelling. The major differences are in the amount of salinity predicted in the east corner of the cutting plane. The chemical interpolations indicate that a more saline water could exist closer to the surface than indicated by the hydrogeological model but also at larger depth. No deep borehole exists in this part of the rock, which could be used for confirmation. The discrepancies can be due to the differences in the boundary conditions used in the models or in the assumptions made. The discrepancies between models should be used as an important validation and confidence building opportunity to guide further modelling efforts.

## 4.4 Rock mechanical modelling

A strategy to be used when building a rock mechanics descriptive model is presented in /Andersson et al, 2002/. This approach has been followed to the extent possible with the data and time available for this project. The rock mechanics model consists of two main parts, the stress model describing the load conditions and the rock mass property model, describing the rock quality, including deformability and strength parameters. The *combination* of stress and mechanical properties at a certain location (place and depth) will determine the stability conditions for a future repository at this location. It is therefore necessary to get an acceptable characterization of both factors during the site investigation.

### 4.4.1 State of stress

Following the approach suggested in /Hakami et al, 2002/ Figure 4-41, the first question to try to answer in the process of making a stress model is whether the stresses as observed from measurements vary within the domain. For the Laxemar case this question is not easy to answer simply because only one borehole with measurements exists. For this borehole some variation is observed (Section 3.10.1), but how to interpret this variation (in minimum horizontal stress) is uncertain.

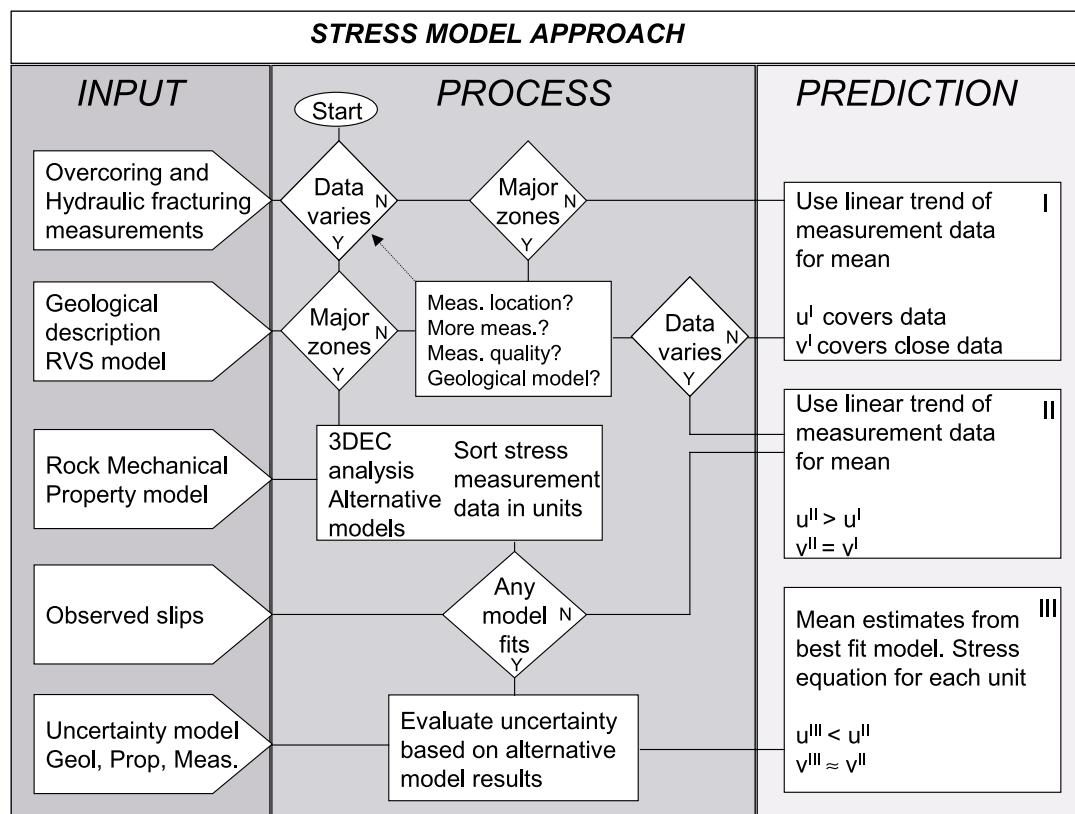


Figure 4-41. Flowchart of the stress model approach /Hakami et al, 2002/.

The next question is whether there are structures in the domain of such significance that they could cause major stress influence. The geological modelling (Section 4.1) clearly shows that fracture zones do exist and their location at ground surface is fairly well known. However, the orientation, and thus locality towards depth is uncertain.

The geological history of the Laxemar area was described in Section 3.1. Of particular importance for the stress model are the observations concerning the structural development and brittle deformation. It was concluded that the Laxemar area today is constituted of a structure controlled region, i.e. there are many already existing fault (fracture zone) structures that have been reactivated several times.

Further it is interpreted that, the current stress field has prevailed for a long period of time, and that magnitude and orientation of the stresses are controlled by the tectonic movements (shear traction and ridge push forces). The orientation of the maximum principal stress is often found to be roughly NW-SE in the whole region, also on a scale including the northern part of Europe /Müller et al, 1992/. This general direction has been noted through measurements but is also consistent with concepts of plate movements. There is no particular reason to believe that the stress field of Laxemar should deviate significantly from this general pattern since the geology of the area is similar to the surrounding areas.

According to the base geological model (Figure, 4-3) the zone ZLXNE03, intersected by borehole KLX02, has a strike which is about perpendicular to the maximum principal stress. This stress orientation is seen not only from the regional pattern but also from the actual measurement data at Laxemar as was shown in Figure 3-56, in Section 3.10. Therefore zone ZLXNE03 is not among those who are expected to show clear stress influence. This is also in accordance with the stress results from KLX02, which show stress variability but a fairly gradual increase occurring *after* the end of the zone intersection. Furthermore, the zone is interpreted to be steeply oriented and thus a slip on this zone would not likely have caused a clear stress change in terms of magnitude.

The zone in the domain that is most likely to show stress influence is the regional large zone ZLXEW01 having an east-west strike. A dextral strike-slip movement has been observed which is also what would fit to a NW-SE oriented maximum stress. Thus, inside and close to ZLXEW01 the orientation of stress should be expected to vary more and turn to be more perpendicular to the zone, on the average.

Following the flowchart in Figure 4-41 this possible case should lead to a three-dimensional analysis of the potential mechanisms at the site. However, for this project there were several reasons not to make a numerical model of the site.

- The geometry of the fracture zones was fairly uncertain and it would therefore be quite arbitrary how to select a geometrical model to analyse.
- Input data on the mechanical properties of the fracture zones in the domain was also scarce.
- The time limitations for rock mechanical effort in the project did not allow for such exercise.
- A meaningful interpretation of a numerical model needs more measurement data than what was available. It would otherwise not be possible to prefer one model from another.

The prediction for Laxemar has thus been built in line with prediction Case II of the flowchart. The uncertainty (u) is a parameter that describes the spans in the actual mean stress value is expected to lie within. This span increases if there is lack of data, poor geological understanding, contradictory measurement results etc. The variability (v) is a measure of the actual spatial variation around the mean stress. In Case II the uncertainty in the model are fairly large, but the spatial variability does not change with certainty.

Stress is here regarded as an entity on a scale of about 0.1–1 m, i.e. much larger than grain size and similar fine joints but on a scale smaller than the large faults and fracture zones. The scale used for stress determines what variation one should expect around the mean stress. This scale is used of practical reasons because it corresponds to the influence volume of a single measurement. The scale of overcoring measurements is smaller and shows a larger scatter compared to hydraulic fracturing measurements, which must be considered when interpreting the data.

In Section 3.10 the available site-specific data concerning stresses was presented and the linear trend for the minor stress was shown in Figure 3-55 in Section 3-10. Following the suggested procedure in the flow chart the prediction for the stress should use the linear trend of the data as the prediction for the mean stress at a site. The equation of the linear trend for the hydraulic fracturing data in KLX02 is:

$$\sigma_3 (= \sigma_h) = 0.02z + 0.6 \text{ MPa} \quad (\text{rounded figures})$$

The selected model has horizontal and vertical mean principal stresses and the model relationship for  $\sigma_3$  becomes the same as for  $\sigma_h$ . It should also be pointed out that the denotation 2 and 3 for intermediate and minimum principal stress might become switched with this model, depending on the principal stresses relative size at each point. However, the major stress is clearly larger than the other two and its orientation is therefore more certain.

The model for the magnitude of the maximum principal stress was selected to be a linear function with depth, such that the ratio between  $s_1$  and  $s_3$  towards depth approaches is about 3. The stress values at the ground surface should not be zero, because we know from shallow measurements from other places that the maximum horizontal stress is considerable and that the minimum horizontal stress also often is higher than zero. The equation selected for the (mean of) maximum principal stress was

$$\sigma_1 = 0.055z + 4.6 \text{ MPa}$$

The way to choose these figure was simple trial and comparison with data from Äspö (see Figures 3-57 to 3-59 in Section 3.10). The ratio will with these models increase towards ground surface. The measurements give some support for such conditions, but data are scattered. Using this relationship the stress close to ground surface is 4.6 MPa which is a reasonable figure. From Laxemar we have no data at all from the first 200 m depth so the uncertainty of the model is larger (in %) in the upper part. But, for the purpose of design and safety assessment of a repository it is mainly important to have a good estimation at depth, where stresses are higher and where the deposition tunnels and deposition holes will be excavated.

It may be interesting to compare the Laxemar stress model equation with the prediction made within the Test Case project /Hudson, 2002/. There the mean maximum principal stress were determined by

$$\sigma_1 = 0.065z + 1.0 \text{ MPa}$$



This equation gives fairly similar maximum stress values as the Laxemar model (for ca 100–500 m depth a maximum difference of 2.5 MPa). Note that these two models have been arrived at using almost fully different borehole data (KAS05 and KA3545G was the only overcoring data available for the Test Case and the hydraulic fracturing data are not the same for the Test Case and for Laxemar). The amount of overcoring data at a future site will not be as high as the number used to choose a  $\sigma_1/\sigma_3$  ratio from Äspö, but will on the other hand be of more value since they give site specific and locally measured stress values. More importantly, overcoring stress measurement result from different points at the actual site will give the possibility to detect a variation in the  $\sigma_1/\sigma_3$  ratio.

For the intermediate principal stress  $\sigma_2$ , a model corresponding to the overburden weight, oriented vertically, was chosen. This model has been suggested in the literature and has been shown to fit measurement at many locations in the world including Scandinavia, although a local variation may occur (Amadei and Stephansson, 1997; Martin et al, 2001). The density and stiffness of the rock types at Laxemar is not expected to vary significantly (Section 3.10 and Section 4.1). The fairly fractured character of the rock mass in the Laxemar also argues against large arching effects. Movements along fractures and the friction forces developed at the fracture planes may however cause the principal stress to rotate locally from the overall vertical direction.

A stress prediction should be given for the whole Laxemar volume, down to 2000 m depth. There is a general poor knowledge of the magnitudes of stress magnitudes at these depths due to the lack of measurements. A few very deep measurements have been performed and the deep hydraulic fracturing measurements at the KTB site (Te Kamp et al, 1995) is one of them. These measurements show a continuously increasing magnitude for the minimum horizontal stress down to the deepest point at 9 km depth, reaching. Therefore we have chosen to use the same linear increasing model for the whole block but to divide the model into depth intervals, 0–500 and 500–2000 m depths. This division makes it possible to describe the depth-dependent differences in the model, in this case differences in the uncertainty levels.

Furthermore the stress model separates between points located inside units characterised as deformation zones and the more intact rock mass blocks between the zones. This division makes it possible to describe the clear difference in expected stress variation that is correlated to the complex geometry and heterogeneity of a deformation zone. The mechanical properties of the rock lying inside or close to a zone can be substantial and change rapidly. Some parts may be strongly altered and other parts being fairly intact. Several smaller zones rather than a single continuous fracture plane may build up the zone, and this can well give rise to stress concentrations at fracture ends or “bridges”. The complex geometry is not known, but it is clear that the stress variation should be expected to be higher inside, and in the vicinity of, a deformation zone of these reasons. The extent of the variation is also difficult to investigate because the measurement methods require a fairly homogeneous rock to have a high accuracy. This leads to fewer measurements from fracture zones and to a larger scatter in the data located at zones.

Lacking more data, the estimation of the spatial variation must be based on judgement. The coincidence in stress orientation between KLX02 and the two other Hydraulic fracturing boreholes at Äspö (Ljunggren and Klasson, 1997) indicates that the differences within the region may be limited and this also gives some further confidence to the use of Äspö data (i.e. the Test Case results) for the Laxemar model. The values for spatial variation is here selected to be similar to the stress model of the Test Case, 15 and 50% for rock mass and fracture zones respectively (see further (Hakami et al, 2002)).

The model for the Laxemar domain is summarized in Table 4-14 and Table 4-15 and is also illustrated in Figure 4-42. The chosen model, i.e. the total span for possible stress values to be found in the block, covers all site-specific data from Laxemar. The span also covers the overcoring data from Äspö. The plot shows the predicted *mean* stress values. The actual, point-to-point stress magnitude is expected to vary around this mean value,  $\pm$  a “spatial variation” percentage.

#### 4.4.2 Mechanical property model

The mechanical properties of the bedrock at a site must be characterized with respect to certain selected parameters as discussed by /Andersson et al, 2002/. Since the geological conditions varies greatly from place to place in the world and the characterization needed for different underground constructions varies strongly (deep mines, shallow tunnels, large caverns etc), there is no accepted single standard way of selecting parameters. /Andersson et al, 2002/ consider the needs and conditions for repository construction in expected conditions of the Swedish basement crystalline rock. We have here tried to follow the parameters and procedures suggested in /Andersson et al, 2002/, as much as possible. In principal two different approaches is available, the “theoretical” approach, (see further /Staub et al, 2002/) and the “empirical” approach /Röshoff et al, 2002/. The results from both approaches should be compared and the uncertainty span for the parameters be selected based on an evaluation of both approaches.

The parameters selected for this project are:

- Uniaxial compressive strength of intact rock.
- Elastic deformation modulus (Young’s modulus) for rock mass.
- Poisson’s ratio for rock mass.
- Uniaxial compressive strength of rock mass.
- Cohesion of rock mass.
- Internal friction of rock mass.

Each of these parameters is explained in the following.

The potential variation of mechanical properties within the Laxemar domain is directly corresponding to the expected variation in lithology and structures in the domain (Section 4.1). It may be concluded from the geological model that the rock mass blocks of the domain would show some minor differences in mechanical properties but that the major differences should be related to the increased fracturing and fracture alteration in deformation zones. The accuracy in property prediction at a certain point will thus be a direct function of the certainty in the geometry of geological model at this point.

The Laxemar project does not allow for a differentiation (classification) in character between different deformation zones in the domain. However, at a site where boreholes have been drilled through the major different structures this should be possible. It is expected that the structures at Laxemar identified as “deformation zones” (see Table 4.1) will show quite different mechanical properties, because of differences in extent, width, complexity, mineralogy etc. Especially, the occurrence of thick soft, infilling materials would be of decisive importance for the strength of the zones.

**Table 4-14. Predicted in situ stress magnitudes at Laxemar (see text).**

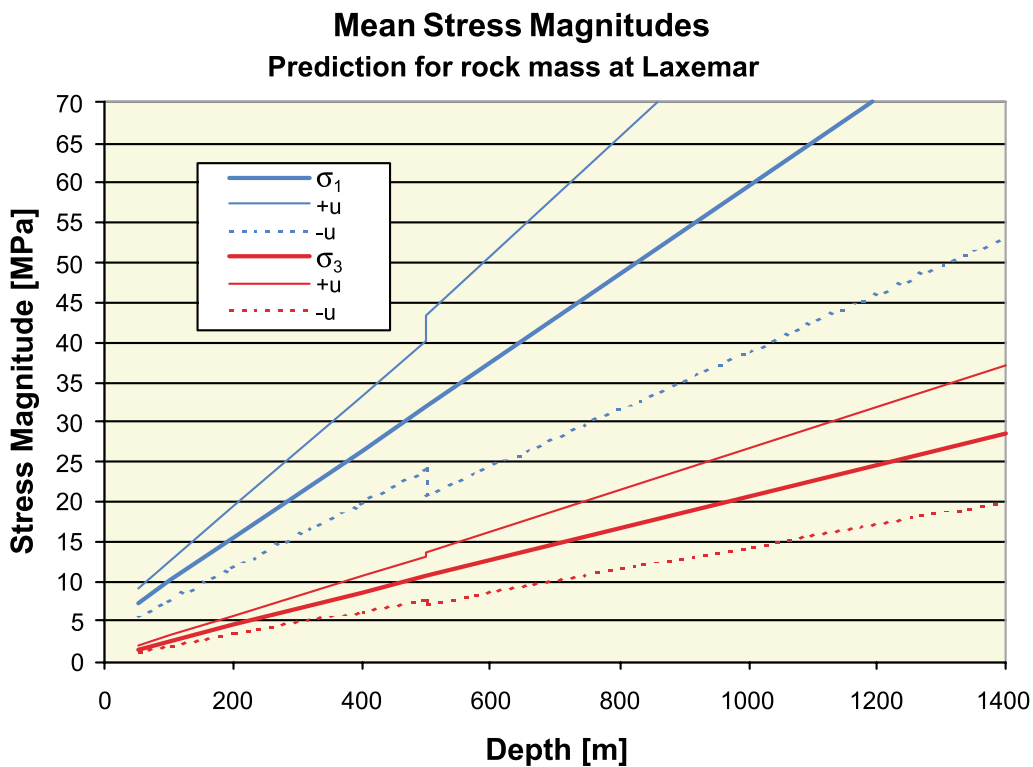
Parameter	$\sigma_1$	$\sigma_2$	$\sigma_3$
Mean stress magnitude, MPa	$0.055 \cdot z + 4.6$	$0.027 \cdot z$	$0.020 \cdot z + 0.6$
Uncertainty (u), 0–500 m	$\pm 25\%$	$\pm 25\%$	$\pm 25\%$
Uncertainty (u), 500–2000 m	$\pm 35\%$	$\pm 30\%$	$\pm 30\%$
Spatial variation (v), rock mass	$\pm 15\%$	$\pm 15\%$	$\pm 15\%$
Spatial variation (v), fracture zones	$\pm 50\%$	$\pm 50\%$	$\pm 50\%$

**Table 4-15. Predicted in situ stress orientation at Laxemar (see text).**

Parameter	$\sigma_1$ , azimuth	$\sigma_1$ , dip	$\sigma_3$ , dip
Mean stress orientation	$150^\circ$	$0^\circ$	$0^\circ$
Uncertainty, 0–500 m d	$\pm 15^\circ$	$\pm 10^\circ$	$\pm 15-45^\circ$ **
Uncertainty, 500–2000 m	$\pm 20^\circ$	$\pm 10^\circ$	$\pm 10^\circ$
Spatial variation, rock mass	$\pm 15^\circ$	$\pm 15^\circ$	$\pm 15^\circ$
Spatial variation, fracture zones	$\pm 25^\circ$	$\pm 30^\circ$	$\pm 30^\circ$

\* The azimuth and dip of all three principal stress componine can be derived from the three parameters given, because they are perpendicular in each point.

\*\* At some level  $\sigma_2$  and  $\sigma_3$  may have similar magnitude and the dip can then be any.



**Figure 4-42.** In situ stress model for the Laxemar domain. Predicted maximum and minimum principal stress magnitudes, with the uncertainty spans  $\pm u$ . (The spatial (local) variation around the mean,  $\pm v$ , is not shown in the diagram).

### **Uniaxial compressive strength of intact rock**

Laboratory strength tests on intact cores performed by SKB in the Laxemar and Äspö area are presented in Figure 4-43. A large spread in the obtained uniaxial compressive strength can be observed. The lowest values are clearly lower than what is normally expected for this type of rock material /e.g. Hoek & Brown, 1980/, possibly due to some measurement errors. However, given the expected variation in rock type, even if some further scrutinizing of data (not performed within this project) might narrow the span for reliable results, it would probably still remain that the uniaxial strength for intact rock must be expected to vary in a fairly wide range over the domain. The mean value of the strength data from SICADA is 184 MPa with a standard deviation of 74 MPa. The span 100–280 MPa is here considered to cover possible values for the intact rocks in the Laxemar domain.

### **Deformation modulus of rock mass**

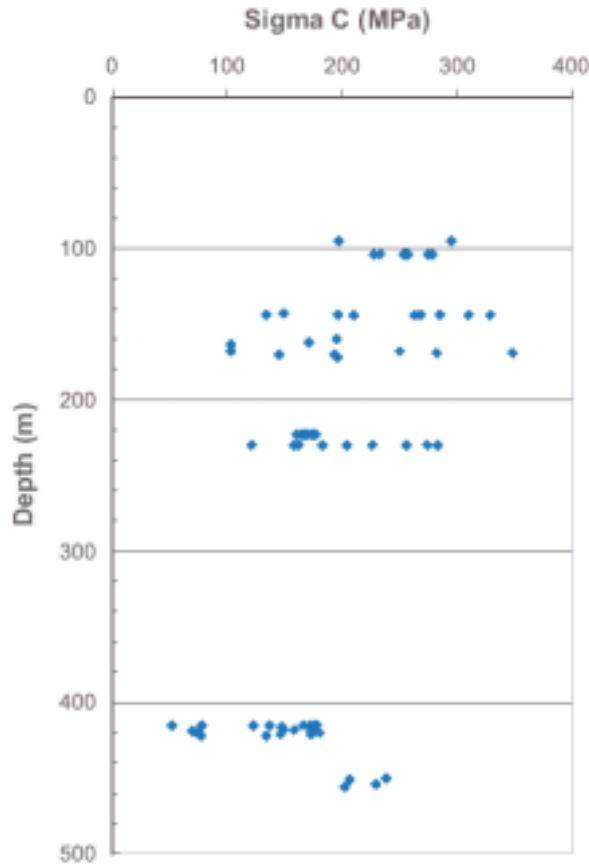
The elastic parameters for the rock mass is governed by the elastic properties of the intact rock material and the elastic properties of the assembly of fractures in the considered volume. The rock mass is here considered as a homogeneous material with equivalent properties. The estimation of this parameter relies on results from the empirical analysis in the Test Case project /Röshoff et al, 2002/ and the numerical analysis performed in the same project /Staub et al, 2002/. Neither empirical nor numerical analysis based on Laxemar data has been performed. The span for Young's modulus has been estimated based on judgement and interpretation of expected influence of trends in indata parameters.

The mean for Young's modulus in the Target area of Test Case (400–500 m depth), estimated with numerical modelling, was 40.3–42.5 GPa with a standard deviation of 4.6–5.1 GPa /Staub et al, 2002/. The corresponding values estimated with empirical approach was a mean of 37–47 GPa with a standard deviation of 13 GPa using Rock Mass Rating (RMR) and mean 25–29 GPa (6–9 GPa st.dev.) using Tunnelling Quality Index (Q) and 39 GPa determined using geophysical data /Röshoff et al, 2002/.

The span selected here is 40–55 GPa for the upper 500 m and 50–65 GPa for the 500–2000 m depth interval. The values for Laxemar were selected slightly higher than the result from the Test Case because the fracturing was reported to be slightly higher at Äspö compared to Laxemar (the  $P_{32}$  was 2.44 m<sup>2</sup>/m<sup>3</sup> for Laxemar and 3.41 m<sup>2</sup>/m<sup>3</sup> for the Test Case, See Section 3.8). The relation between  $P_{32}$ -values and the deformation modulus (and the other strength parameters described in following sections) in the theoretical approach have not been investigated, and the estimated influence from fracture intensity is therefore uncertain. The direction of the influence is however clear, more fractures give lower stiffness and strength. The deformation modulus can not be higher than the intact rock so this sets the absolute upper level for the rock mass. The deformation modulus of the intact rock for Äspö and Laxemar rocks are expected to lie in the span 60–90 GPa /Martin et al, 2001; Staub et al, 2002/.

Note that the differences between the two depth interval are *not* supposed to reflect the influence from stress dependence, but the strength parameters are here all estimated to correspond to the same (high) confining stress (10 MPa). The differences between the depth intervals in the property model stems from expected differences in fracturing and fracture properties.

Both the empirical and the theoretical approaches have a number of sources for uncertainty. For the theoretical approach these factors are: uncertainty in estimation of necessary indata to numerical models, uncertainty in the influence of problem simplifi-



**Figure 4-43.** Results from uniaxial testing of 83 samples from 24 boreholes at Äspö and Laxemar; uniaxial compressive strength vs. depth. The data below 400 m depth are from Zedex and Prototype experimental areas at ÄHRL. From /Martin et al, 2001/ (72 of the values available in SICADA).

cation for the numerical modelling etc. For the empirical approach the uncertainty lies in the applicability of the empirical relationships, the sensitivity of selected input parameters etc. These issues are brought up further in the strategy report /Andersson et al, 2002/ and the underlying reports /Staub et al, 2002/ and /Röshoff et al, 2002/.

The figures of the selected spans for the property model are not calculated but selected by judgement, as described above, and rounded figures (dividable with 5) were chosen to reflect the uncertainty (and not give any false impression of accuracy).

### **Poisson's ratio**

Lacking any empirical classification from Laxemar, or theoretical analysis based on Laxemar data it was judged that the sonic log data from KLX02 should be used. The measurement of wave velocity both for compression and shear wave gives the possibility to have a measure of Poisson's ratio. The borehole seismic data (sonic logging) was used to estimate the span for the Poisson's ratio. The empirical relation proposed by /McDowell, 1990/ was used:

$$\nu = \frac{1}{2} \left( \frac{r^2 - 2}{r^2 - 1} \right), \quad r = \frac{V_p}{V_s} \quad \text{/McDowell, 1990/}$$

where  $V_p$  and  $V_s$  are the compression and shear wave velocities, respectively.

The mean  $\pm$  the standard deviation for single measurements in the section 450–500 m in KLX02 was used as the uncertainty span (cp. Section 3.10). The selected span for Poisson's ration is 0.23–0.28. This was also supported by comparing with the result from the numerical analysis in Test Case project /Staub et al, 2002/. The result presented there was 0.25–0.27 for the mean and 0.02 in standard deviation.

### **Rock mass compressive strength**

The uniaxial compressive strength for a rock mass is a term most often understood as the compressive strength for a case with zero confining stress. However, the strength is much dependent on the confinement and, since only one confinement level should be used to get a single parameter value to compare, a high confinement stress was chosen. In this project the following definition has been used: The “Rock mass compressive strength” should correspond to the maximum (axial) load that can be applied on a rock mass (ca 30x30x30 size) with a confining (surrounding) stress of 10 MPa. This definition is important to remember and to consider when the values are compared with other similar parameters in the literature. Using other definitions of axial compressive strength might well give significantly different values.

It is not easy to calculate or determine the rock mass strength because mechanical behaviour of a fractured rock is a complex subject. The size of the problem makes testing and validation almost impossible. For this model estimates are partly based on estimated parameters describing the fracturing (RQD and P) estimated for KLX02 (see Section 3.10) and again assuming that the other conditions would be similar to what was found in the Test Case at Äspö.

The numerical simulations from the Test Case gave a strength of about 120 MPa with 10 MPa confining stress for Granodiorite and a comparison with empirically estimation using GSI and Hoek and Browns strength relationships giving a strength of 110–175 MPa /Staub et al, 2002/. The strength values determined using different empirical methods gives a large span of values for the Test Case, depending on the relation used.

The selected span for the property model of Laxemar was 100–125 MPa for 0–500 m depth and 100–160 MPa 500–2000 m depth in the domain, for rock mass in the rock unit. In the deformation zone units the strength is estimated to 55–75 MPa and 60–85 MPa, respectively.

### **Rock mass cohesion**

Rock mechanical characterization parameters for rock *mass* is a subject with less common standards and methods compared to *intact* rock. If a constitutive model for the rock mass as a continuous material is to be used, the Mohr-Coulomb model is one of the most common. This model includes a parameter determining the strength for zero confining stress, the rock mass cohesion. The Mohr-Coulomb strength criterion is linear while the actual strength is expected to be non-linearly stress-dependent. Often used is also the Hoek&Brown relationship which gives a non-linear relationship. It is therefore important to clearly state how the characterization parameters used are defined. Here we use a definition where the strength values for 10 and 20 MPa confinement were used to construct the strength parameters (i.e. an apparent cohesion from this *linear* relationship based on high level confinement levels, not for a true zero confinement).

The difference in  $P_{10}$  and  $P_{32}$  (Section 3.8) between Äspö and Laxemar indicates that a higher strength should prevail at Laxemar. The importance of DFN parameters for the mechanical parameters determined with the theoretical approach (UDEC calculations) has not been investigated. The cohesion for the rock mass is however expected to generally decrease with increasing fractures. The maximum cohesion for the rock mass is definitely the cohesion of the intact rock, which would be the situation in cases where the fractures play no role for the failure.

Inside the fracture zone the cohesion is expected to be lower than inside the less fractured rock mass units.

The selected span for mean cohesion in the rock units is 10–25 MPa and 15–30 MPa, for 0–500 m and 500–2000 m depth, respectively. Corresponding values selected for rock mass inside deformation zone units was 5–15 MPa and 5–20 MPa. The reasoning behind figures is similar as for deformation modulus and compressive strength (see above).

### ***Rock mass internal friction angle***

As for cohesion, the rock mass internal friction angle is a parameter related to the Mohr-Coulomb strength criterion, which is commonly used. The same two confining stress values were considered for the definition of the friction angle, 10 and 20 MPa. Friction angle estimated in Test Case are about 40° (st. dev. about 5) using theoretical approach and 47° using RMR and Hoek and Brown relations.

The absolute maximum value possible for the rock mass is equal to the internal friction angle for intact rock. The laboratory testing from ÄHRL show that the friction angle of intact samples can reach up to about 50°.

The selected span for the Laxemar property model was 40°–45° (0–500 m) and 40°–50° (500–2000 m) in rock units. The higher uncertainty with depth is because of the possibility to have less fracturing with depth. (Remember that the stress dependence should not be reflected in the parameter. The stress level for comparison is held constant.)

### **4.4.3 Uncertainty in rock mechanical property model**

The uncertainty in the property model can be ascribed many different sources. Generally the property model for the intact rock will be less uncertain because these parameters are defined for small scale and standard testing methods exist. For the “rock mass” (30 m scale) properties there is a general difficulty with validating the concepts used (whether “theoretical” or “empirical”) because field scale testing is almost impossible and the material that is to be characterized is very complex.

The existing empirical relations may not be fully applicable for the conditions and requirements of the repository of different reasons, mainly that the number of (non-mining) excavations made at these depths is limited. The theoretical approach has not yet been established as standard methodology for rock characterization purposes but is normally used as a tool in solving specific rock engineering design or stability problems.

A specific confidence question related to the aim of this project is how to make the estimations for large volumes of rock with sparse data. For ordinary underground excavation projects the characterization to be done involves a more limited volume of rock.

The large scale makes it necessary to simplify the geological and geometrical model largely and to include only the largest deformation zones. The local minor fracture zones that exist must be considered as part of the “rock units” and treated non-deterministically.

This circumstance gives the effect that, if for example during the stages of site investigation, the degree of detail in geometrical geological modelling increases (smaller zones are identified and included), the rock mechanics properties of the rock units must be re-evaluated. The rock mass becomes stiffer as the rock units become smaller.

The contribution to the compliance (opposite of stiffness) from the local minor fracture zones can well be in the same order as the contribution from fractures of smaller scale as is illustrated by the following example. Consider the case where a local minor fracture zone (say 2.5 m wide) occurs every hundred meter (less than in KLX02) and is a hundred times more compliant than the smaller fractures (2.5 m x 40 fractures/m). Then this zone will be as compliant as the smaller fracture set in the same orientation if the frequency is about 1 fracture/m. The stiffness would be half if the local minor zone was considered (the possible additional influence from alteration not included).

In the Laxemar project an important parameter used to quantify fracturing has been the DFN model parameters based on fracture statistics (Section 3.8). Using these parameters the crush zones may not be properly represented considered. In the theoretical approach applied in the Test Case project /Staub et al, 2002/ all fractures of the network for numerical modelling were given the same mechanical properties independent of the size (selected to correspond to small fractures). The influence of less compliance in the local minor fracture zones (treated as single features in the DFN model) was thus possibly not well represented. Therefore the stiffness and strength may have been overestimated for rock units of the model.

The interaction between the geological and rock mechanical models could be further developed, as discussed by /Andersson et al, 2002/. For example, further consideration may be put on how to estimate the stiffness and strength of the rock mass at any scale in a more systematic way. A possible way could be to make statistical analysis on the fracture data again after the RVS units are identified, such that the statistics on fractures (including minor fracture zones) located in rock domains can be separated from fractures located in the identified deformation zones of the RVS model. The mechanical modelling, based on fracture statistics (and other core logging) parameters, may then change if the geometrical model changes. There is also a need to develop the theoretical approach such that the difference in mechanical properties of both large-scale features (minor zones) and small-scale features (joints) are considered.

The selected spans for the rock mechanics parameters are summarized in Table 4-16. An attempt is also made to summarize the discussion on uncertainty and confidence by giving a high, medium or low rate to the confidence.



**Table 4-16. Predicted rock mechanical properties in Laxemar domain.**

Parameter	Rock Units 0–500 m	Rock Units 500–2000 m	Confidence	Comments
Uniaxial compressive strength, <i>intact rock</i> *	100–280 GPa	100–280 GPa	High	The span may be decreased with more data.
Elastic Modulus, rock mass*, (30x30x30 m)	40–55 GPa	50–65 GPa	Low	Depends on how minor fracture zones are treated.
Poisson's ratio, rock mass*	0.23–0.28	0.23–0.28	Medium	
Uniaxial strength, rock mass*	100–125 MPa	100–160 MPa	Low	Is related to the strength for intact rock. See text about definition. Depends on how minor fracture zones are treated.
Friction angle, rock mass**	40°–45°	40°–50°	Medium	Difficult to validate material models for large scale.
Cohesion, rock mass**	10–25 MPa	15–30 MPa	Low	See text about definition.
Parameter	Def. Zones 0–500 m	Def. Zones 500–2000 m	Confidence	Comments.
Uniaxial compressive strength*, <i>intact rock</i> inside deformation zones	100–280 GPa	100–280 GPa	Low	No laboratory tests available from zones. Weak rocks may be difficult to sample. Large spatial variation expected.
Elastic Modulus*, rock mass (fractures, intact rock and fracture filling, 30x30x30 m)	10–40	10–40	Low	Geological characterization uncertain. Variation between zones and within zones expected.
Poisson's ratio*, rock mass	0.20–0.26	0.20–0.26	Low	D:o
Uniaxial strength*, rock mass	55–75 MPa	60–85 MPa	Low	D:o
Friction angle**, rock mass	25°–35°	25°–40°	Low	D:o
Cohesion**, rock mass	5–15 MPa	5–20 MPa	Low	D:o See text about definition.

\* Confining stress 10 MPa.

\*\* Linear model between 10 and 20 MPa confining stress.

## 5 The Laxemar Site Descriptive Model

This chapter summarises the resulting Laxemar Site Descriptive model. It builds on the results of the evaluation in Chapters 3 and 4. It should also be remembered that the description provided has been produced within the limitations in scope of the project, as defined in Chapter 1. Still it is likely that the description is a good illustration of the kind of description which will be produced at the end of the Initial Site Investigation stage ('version 1.2' using the vocabulary of /SKB, 2001/).

### 5.1 Geological description

The geological description concerns geometry and properties of deformation zone of sizes down to 'local major zones' (1–10 km) and geometry and properties of rock domains, with uncertainties.

#### 5.1.1 General assumptions and uncertainties in the interpretations

Figure 5-1 illustrates the base and alternative geological models respectively. The descriptions are first presented for the base geological model, Section 5.1.2, and then for the alternative geological model, Section 5.1.3. Properties of deformation zones and rock domains are provided in tables in these sections.

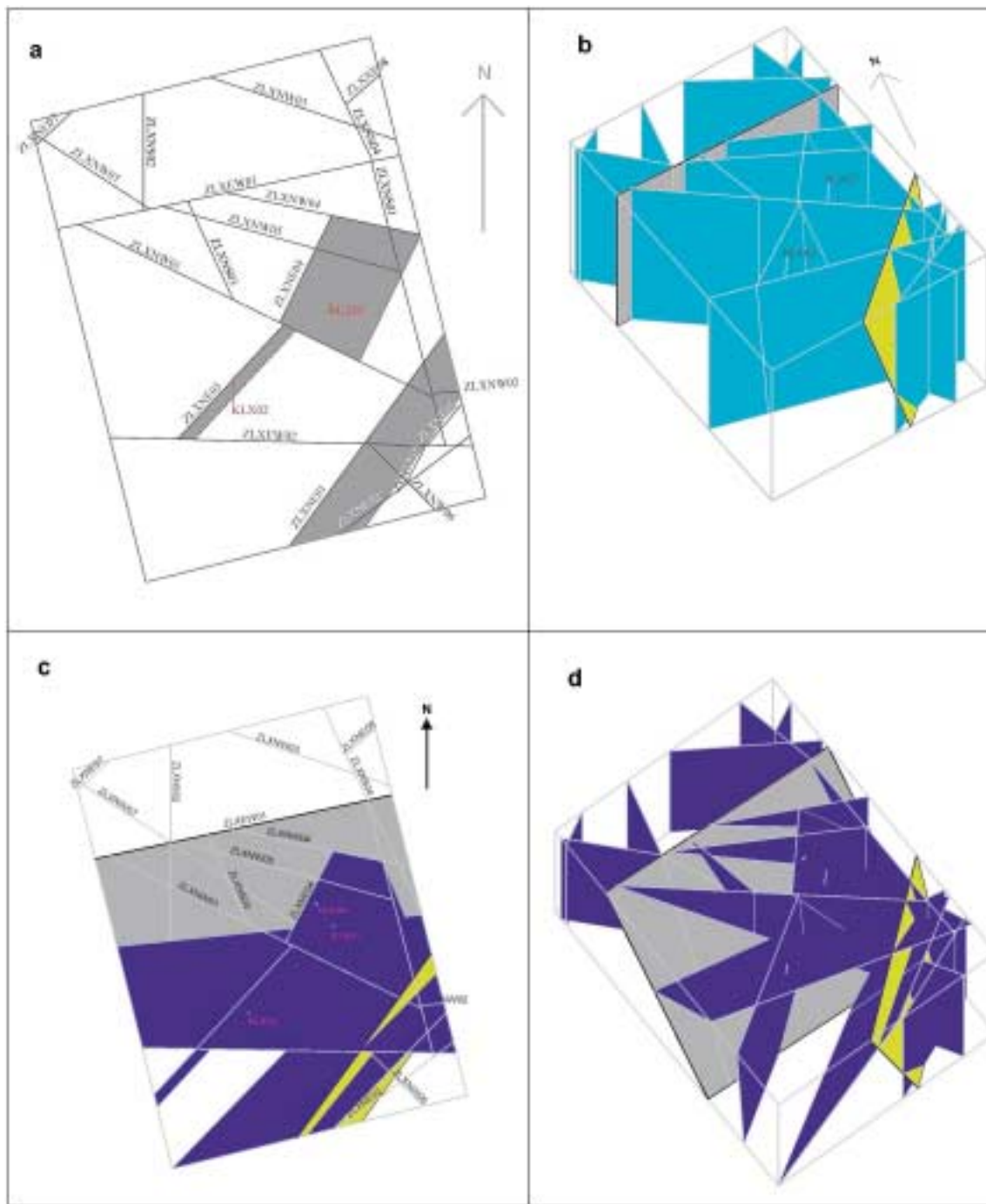
##### ***Basis for description***

The geology of the Laxemar model domain is crudely known outside of the immediate vicinity of the two boreholes, KLX01 and KLX02. Several other data sources exist but do not cover the whole domain, or have a low level of detail made for a much larger area than the Laxemar site:

- The bedrock map only exists on a regional scale.
- Detailed mapping of the bedrock has not been performed in the major part of the model area.
- No field control has been carried out of the lineaments assigned as deformation zones.

If not else stated, in the following description all fracture zones are based on lineaments, which are indicated by topographic and magnetic data. The lack of field control or core samples from boreholes that intersect lineaments and suspected deformation zones make most statements regarding their character uncertain.

There is limited information regarding deformation in the core logs. The only deformation zones interpreted in the boreholes are mapped as brittle crush-zones. In the core logs fracture zones have been defined as  $\geq 10$  fractures/metre for a section of at least 1.0 metre. Highly fractured sections ( $\geq 10$  fractures/metre) that are shorter than 1 metre have been neglected. This definition of fracture zones has been chosen based on an overall judgement of the fracturing in boreholes KLX01 and KLX02 and is specific to this particular project. It is advised that a more a well-founded level of truncation is defined in the methodology program for single hole interpretation that SKB are currently conducting.



*Figure 5-1. Illustration of the (a) base geological model and c) alternative geological model. Illustrations b) and c) shows the base and alternative geological models in isometric view respectively.*

## ***Uncertainties***

In the following subsections each structure is presented in table form indicating a quantitative estimate for each parameter, a span in which the parameter is likely to occur and an estimate of the confidence level of the quantitative estimate. The span is estimated by indications in the primary data, references to similar type of structures in similar environment (Äspö) or by expert judgement. The confidence level reflects how much support in the data there is for the quantitative estimate. A low confidence level means that there is little information available and that the estimate is based on more qualitative information. Medium confidence level means that the data gives some form of support but that the span may be very large. A high confidence level usually indicates that there are detailed information available and that the span may be possible to narrow down. There is also a column which indicates what data are behind this interpretation and a column for additional comments to each parameter value.

The quantification of parameter values are usually subject to very large uncertainties due to the sparse primary data and especially the very sparse spatial coverage of the data. In many cases the tables are presented with practically no hard data other than the lineaments. But these tables also serve the purpose of pointing out what is needed to investigate in order to have a model with the same level of uncertainties in all part of the model domain.

### **5.1.2 Base geological model**

A short description follows below of the interpreted rock domains and deformation zones in the base geological model. The description contains information on the underlying data and the geological characteristics of the deformation zones. Generally, the spatial variability of the characteristics over the extent of the zone is uncertain due to the small number of observation points. The geological character has therefore been presented in descriptive terms unless there are good reasons (i.e. more data) for more quantitative estimates. Each structure is presented in table form indicating a quantitative estimate for each parameter, a span in which the parameter is likely to occur and an estimate of the confidence level of the quantitative estimate.

#### ***RLXA***

The rock mass in the base geological model has been interpreted in the most simplistic way to one single rock domain covering the whole model domain. The characteristic of this rock domain, RLXA, is dominated by commonly porphyritic granite to granodiorite. A smaller proportion of the rock mass also contains gabbro and granodiorite to quartz diorite (“Äspö diorite”). Table 5-1 describes the detailed geological information about this rock domain.

**Table 5-1. Description of the interpreted geological characteristics for RLXA.**

<b>RLXA</b>					
<b>Property</b>	<b>Quantitative estimate</b>	<b>Span</b>	<b>Confidence</b>	<b>Basis for interpretation</b>	<b>Comments</b>
Volume	1.4·10 <sup>10</sup> m <sup>3</sup>	0	Medium	Geological map	Entire volume of the model domain
Ductile deformation	Analysed (N/A)			No observations	
Rock type	Granite 77% Aplite 3% Granodiorite 10% Diorite to gabbro and mafic rocks, 10%	Granite ± 5% Aplite ± 2% Granodiorite ± 2% Diorite to gabbro and mafic rocks ± 2%	Medium	Geological map and KLX01 and KLX02	
Grain size	N/A			No observations	
Alteration	15% of the complete length of the boreholes are altered	± 7%		KLX01 and KLX02	
Mineralogical description	Not Analysed (N/A)			–	
Density	N/A			No observations	
Fracture orientation	Set 1: 352/86 Set 2: 286/76 Set 3: 226/92 Set 4: 125/18	Set 1: K=8.52 Set 2: K=9.26 Set 3: K=9.36 Set 4: K=7.02	High	Section 3.8	Fracture data from the whole region Fisher distribution
Fracture size	Set 1: D=3.1, x0=0.4 Set 2: D=3.4, x0=0.46 Set 3: D=3, x0=0.41 Set 4: D=3.3, x0=0.44	Set 1: D±0.3 Set 2: D±0.3 Set 3: D±0.3 Set 4: D±0.3		Section 3.8	Power Law
Fracture intensity	Set 1: 0.78 Set 2: 0.66 Set 3: 0.76 Set 4: 0.24	Set 1: ± 0.2 Set 2: ± 0.2 Set 3: ± 0.2 Set 4: ± 0.2	High	Section 3.8	P <sub>32</sub> .(m <sup>2</sup> /m <sup>3</sup> )
Fracture mineralogy	Chl, Ep, Ca			KLX01 and KLX02	

### **ZLXEW01**

ZLXEW01 strikes approximately east-west and the lineament that it is based on is of regional character and continues well outside the model volume. It ends in a bay to the Baltic sea in the north-eastern part of the model area. Traditionally the lineament has been called the Mederhult line in earlier work and SFZ03 is an earlier name of the presumed fracture zone /e.g. Rhen et al, 1997/. The zone has been verified within the Laxemar Model Domain, its existence has been verified by ground magnetic and VLF measurements /Stenberg and Sehlstedt, 1989/, as well as by a refraction survey /Rydström and Gereben, 1989/ outside the model domain and half-regional resistivity measurements /Ericsson et al, 1998/. No boreholes penetrate the zone.

Other regional lineaments (fracture zones) are normally truncated and possibly faulted by ZLXEW01. Both dextral and sinistral movements are possible to infer from the symmetry of lineaments on either side.

The reflection seismic data may lend support to the zone geometry. This is considered in the alternative modelling.

From a geological perspective, the size of this deformation zone, indicates that the zone may function as a hydraulic barrier between the northern and southern part of the model domain. The deformation zone EW-1 on the Äspö island is similar in size and is reported to be partly acting as a hydraulic barrier, Rhén et al 1997, although its flanks are highly conductive. Table 5-2 presents the interpreted geological description.

**Table 5-2. Description of the interpreted geological characteristics for ZLXEW01.**

<b>ZLXEW01</b>					
<b>Property</b>	<b>Quantitative estimate</b>	<b>Span</b>	<b>Confidence level</b>	<b>Basis for interpretation</b>	<b>Comments</b>
Orientation (strike/dip)	078/90	±10/±35	Medium	Regional lineament airborne geophysics	See also Section 4.1
Width	100 m	20–200 m	Low	Ground magnetic, VLF, regional lineament	See also Section 4.1
Length <sup>1</sup>	>10 km	10–100 km	High	Regional lineament	
Ductile deformation	Yes		Medium		
Brittle deformation	Cataclastic		High	Ground magnetic, VLF, topography	See also Section 4.1 Based on one observation
Rock type	Granite	Variable	Medium	Geological map	
Grain size	N/A			No observations	
Alteration	N/A			No observations	
Mineralogical description	N/A			No observations	
Density	N/A			No observations	
Fracture orientation	N/A			No observations	
Fracture frequency	Increased fracturing		High	No observations	
Fracture mineralogy	N/A			No observations	

<sup>1</sup> Concerns total length (i.e. not truncated by model domain).

## ZLXEW02

This zone is based on a local major lineament but has not been verified in the field and is not penetrated by any borehole. A seismic reflection has been identified, which is interpreted to correlate with a zone along the lineament. This has been taken into consideration in the alternative model. Table 5-3 presents the interpreted geological description.

**Table 5-3. Description of the interpreted geological characteristics for ZLXEW02.**

<b>ZLXEW02</b>					
<b>Property</b>	<b>Quantitative estimate</b>	<b>Span</b>	<b>Confidence level</b>	<b>Basis for interpretation</b>	<b>Comments</b>
Orientation (strike/dip)	271/90	±20/±?	Medium	Local major lineament	See also Section 4.1
Width	20 m	5–200 m	Low	Local major lineament	
Length	2.5 km	2.3–>10 km	High	See above	
Ductile	N/A				
Brittle deformation	Cataclastic		Medium	No observation	
Rock type	Granite and quartz monzonite	Variable	Medium	Geological map, core log KLX02	
Grain size	N/A			No observations	
Alteration	N/A			No observations	
Mineralogical description	N/A			No observations	
Density	N/A			No observations	
Fracture orientation	N/A			No observations	
Fracture frequency	Increased fracturing		High	No observations	
Fracture mineralogy	N/A			No observations	

## ZLXNE01

ZLXNE01 is indicated in the airborne magnetic data and by ground magnetic measurements /Stenberg and Sehlstedt, 1989/. It has been verified in two field localities /Bergman et al, 2000/ in or close to the model domain. It is described as a steeply dipping, ductile or semi-ductile shear zone of local major character, which constitutes a narrow belt characterized by an increased concentration of separate, discontinuous high-strain zones. These have been developed during low-grade metamorphic conditions and are composed of strongly deformed to mylonitic varieties of the surrounding Småland “granites”. There are no boreholes that have penetrated the zone within the model domain. Ground VLF /Stenberg and Sehlstedt, 1989/ and seismic refraction measurements /Rydström and Gereben, 1989/ have verified brittle reactivation along the zone south of the model domain. It can be correlated with the so-called Äspö shear zone on the Äspö Island in the east, which is both described from surface information and from core mapping in several boreholes. On the Äspö Island it is also mylonitic in the central part with intensely fractured and faulted border zones (see e.g. /Rhen et al, 1997/ and /Mazurek et al, 1996/). The width of the mylonitic core can be approximated to ca 50 meters and approximately 200 hundred meters including the brittle and intensely deformed outer parts of the zone /Rhen et al, 1997/. Table 5-4 presents the interpreted geological description.

**Table 5-4. Description of the interpreted geological characteristics for ZLXNE01.**

ZLXNE01					
Property	Quantitative estimate	Span	Confidence level	Basis for interpretation	Comments
Orientation (strike/dip)	036/80	±10/±10	Medium	Field data, airborne magnetic	See also Section 4.1
Width	200 m	100–250 m	High	Airborne magnetic, field data, Äspö data	
Length	>10 km	10–100 km	High	Magnetic lineament	
Ductile deformation	Mylonitic		High	Field data, Äspö data	
Brittle deformation	Cataclastic		High	Field data, ground geophysics, Äspö data	
Rock type	Granite	Variable	Medium	Geological map	
Grain size	N/A			No observations	
Alteration	N/A			No observations	
Mineralogical description	N/A			No observations	
Density	N/A			No observations	
Fracture orientation	N/A			No observations	
Fracture frequency	Increased fracturing		High	No observations	
Fracture mineralogy	N/A			No observations	



## ZLXNE02

The zone ZLXNE02 is indicated by a local, major lineament. The zone has not been verified by field observations and is not penetrated by any borehole. However, this lineament extends into the area south of Äspö, where it may be correlated with three different zones, NE-1, EW-3 and EW-2, /Rhén et al, 1997/, that is penetrated by the tunnel of the Äspö laboratory. These have somewhat different strike, dip and characteristics, and hence it is hard to use information from that area in the current model. Table 5-5 presents the interpreted geological description.

**Table 5-5. Description of the interpreted geological characteristics for ZLXNE02.**

<b>ZLXNE02</b>					
<b>Property</b>	<b>Quantitative estimate</b>	<b>Span</b>	<b>Confidence level</b>	<b>Basis for interpretation</b>	<b>Comments</b>
Orientation (strike/dip)	053/90	±10/±?	Medium	Local, major lineament	See also Section 4.1
Width	50 m	10–100 m	Low	No observations	
Length	2 km	1–5 km	Medium	Local, major lineament	
Ductile deformation	N/A				
Brittle deformation	Cataclastic		Medium	No observations	
Rock type	Granite	Variable	Medium	Geological map	
Grain size	N/A			No observations	
Alteration	N/A			No observations	
Mineralogical description	N/A			No observations	
Density	N/A			No observations	
Fracture orientation	N/A			No observations	
Fracture frequency	Increased fracturing		High	No observations	
Fracture	N/A			No observations	

### ZLXNE03

The deformation zone ZLXNE03 is indicated by a local lineament. The subsurface below this valley has been investigated by means of a percussion borehole (HLX01) and geophysical logging in this hole. The suggested zone has been correlated with a fractured rock segment at an approximate depth of 1040 metres depth in KLX02. This rock segment (named R7 in the single hole interpretation, (Section 3.4), is characterised by several crushed zones and fracture zones, but also by a high proportion of alteration (22%, see Appendix B2). Chlorite, calcite and hematite are the dominating mineral in fractures and fracture zone (including crush zones). The segment is dominated by Småland granite, with a few thin greenstone sheets and fine-grained granite. The angle between the borehole and the proposed zone is low and if the zone geometry is interpreted correct it is approximately 20 metres wide at this depth. The lower section of the rock segment (between 1037 and 1113 m borehole length) is particularly fractured and altered. No clay or core loss has been registered in the core.

No other observations from the zone exist. The borehole radar investigation ends above this section in the borehole. The seismicity in this rock segment is generally sub-horizontal or dip at low angle including the VSP data. Table 5-6 presents the interpreted geological description.

**Table 5-6. Description of the interpreted geological characteristics for ZLXNE03.**

<b>ZLXNE03</b>					
<b>Property</b>	<b>Quantitative estimate</b>	<b>Span</b>	<b>Confidence level</b>	<b>Basis for interpretation</b>	<b>Comments</b>
Orientation (strike/dip)	043/87	±10/±5	Medium	Local, major lineament, HLX01, KLX02 (1040 m)	See also Section 4.1
Width	20 m	10–30 m	Medium	KLX02	Based on one estimate
Length	2 km	1–5 km	Medium	Local major lineament	
Ductile deformation					
Brittle deformation	Increased fracturing Cataclastic		Medium	HLX01, KLX02 (1040 m)	Appendix B1 and Section 3.4
Rock type	Granite	Variable	Medium	Geological map	
Grain size	N/A			No observations	
Alteration	21.2% of segment R7		Medium	KLX02 (1040 m)	
Mineralogical description	N/A			No observations	
Density	N/A			No observations	
Fracture orientation	N/A			KLX02 (1040 m)	
Fracture frequency	14.7 fractures per metre in R7		Medium	KLX02 (1040 m)	Based on one observation
Fracture mineralogy	Chlorite, epidote, FeOH		Medium	KLX02 (1040 m)	Based on one observation

## ZLXNE04

This deformation zone is indicated by a local, major lineament. The lineament follows an undulating valley, and the subsurface below this valley has been investigated by means of two percussion boreholes (HLX01 and HLX04) and geophysical logging of these holes. The angle between the boreholes and the assumed zone is probably very small, particularly for HLX01, which is drilled almost parallel with the supposed dip direction. The information from the HLX holes has not been used when the dip of the zone was modelled, but resistivity data indicate that the zone is conductive.

The modelled zone is a plane that represents an average strike of the lineament and with a dip according to its location in KLX01, at approximately 750 metres depth. The assigned depth correspond to a rock segment with generally low fracture frequency, but with a few, narrow fracture zones. Three of these zones correlate with sections with distinct hydraulic flow, at 720–740 metre (see Chapter 3.7). The segment is dominated by Småland granite and the lower part of the section (746–760 m) has a high proportion of alteration. No crush zones, clay or core losses have been identified. The mineralogy in fractures in this rock segment is dominated by chlorite and calcite. The zone is estimated to have a thickness of 15 metre based on the observed intersection with KLX01.

The reflection seismic data lends some support to the modelled zone, which was considered in the alternative model. Table 5-7 presents the detailed geological description for this zone.

**Table 5-7. Description of the interpreted geological characteristics for ZLXNE04.**

<b>ZLXNE04</b>					
<b>Property</b>	<b>Quantitative estimate</b>	<b>Span</b>	<b>Confidence level</b>	<b>Basis for interpretation</b>	<b>Comments</b>
Orientation (strike/dip)	027/72	±10/±35	Medium	Local, major lineament, HLX01, HLX04, KLX01 (750 m)	See also Section 4.1
Width	15 m	10–20m	Low	KLX01 (750 m)	Based on one observation
Length	1 km	0.8–1.2 km	High	Local major lineament	
Ductile deformation				No observations	
Brittle deformation	Cataclastic		High	HLX01, HLX04, KLX01 (750m)	Appendix B1 and Section 3.4
Rock type	Granite	Variable	Medium	Geological map	
Grain size	N/A			No observations	
Alteration	8.4% oxidization in segment R1		Medium	KLX01 (750 m)	Appendix B1. Based on one observation
Mineralogical description	N/A			No observations	
Density	N/A			No observations	
Fracture orientation	N/A			Segment R1 in KLX01 (697–762 m)	Appendix B1
Fracture frequency	3.6 fractures per metre		Medium	Segment R1 in KLX01 (697–762 m)	Appendix B1. Based on one observation
Fracture mineralogy	N/A			KLX01 (750m)	Appendix B1

## ZLXNE05

This short zone is modelled as a continuation of the zone ZLXNE06, but with an angle to the latter according to a local lineament. Ground geology, ground geophysics or any borehole has not verified the zone. The lineament is physically located in a bay of the Baltic sea. Table 5-8 presents the detailed geological description for this zone.

**Table 5-8. Description of the interpreted geological characteristics for ZLXNE05.**

ZLXNE05					
Property	Quantitative estimate	Span	Confidence level	Basis for interpretation	Comments
Orientation (strike/dip)	028/90	±10/±?	Medium	Local, major lineament	See also Section 4.1
Width	N/A			Local, major lineament	Lineament located in a bay of the Baltic Sea
Length	200 m	100–300 m	High	Local, major lineament	Lineament located in a bay of the Baltic Sea
Ductile deformation	N/A			No observations	
Brittle deformation	Cataclastic		Low	Topography	
Rock type	Granite	Variable	Medium	Geological map	
Grain size	N/A			No observations	
Alteration	N/A			No observations	
Mineralogical description	N/A			No observations	
Density	N/A			No observations	
Fracture orientation	N/A			No observations	
Fracture frequency	N/A			No observations	
Fracture mineralogy	N/A			No observations	

## ZLXNE06

The zone ZLXNE06 is modelled with support from a local lineament. It is verified in a percussion borehole (HLX08) as fractured sections with low resistivity.

The modelled zone is probably related to a zone at the southern part of Äspö, which was penetrated by the access ramp down to the Äspö laboratory (NE-1). Documentation from the Äspö tunnel was only considered during modelling of the alternative model.

No other field data exist for this zone. Table 5-9 presents the detailed geological description for this zone.

**Table 5-9. Description of the interpreted geological characteristics for ZLXNE06.**

ZLXNE06					
Property	Quantitative estimate	Span	Confidence level	Basis for interpretation	Comments
Orientation (strike/dip)	040/90	±10/±?	Medium	Local, major lineament	See also Section 4.1
Width	N/A			Local, major lineament	Lineament located in a bay of the Baltic Sea
Length	300 m	200->1000 m	High	Local, major lineament	Lineament located in a bay of the Baltic Sea
Ductile deformation	N/A			No observations	
Brittle deformation	Cataclastic		Low	Topography	
Rock type	Granite	Variable	Medium	Geological map	
Grain size	N/A			No observations	
Alteration	N/A			No observations	
Mineralogical description	N/A			No observations	
Density	N/A			No observations	
Fracture orientation	N/A			No observations	
Fracture frequency	N/A			No observations	
Fracture mineralogy	N/A			No observations	

**ZLXNE07**

This zone is based on a local major lineament but it has not been verified in the field and is not penetrated by any borehole. Table 5-10 presents the detailed geological description for this zone.

**Table 5-10. Description of the interpreted geological characteristics for ZLXNE07.**

<b>ZLXNE07</b>					
<b>Property</b>	<b>Quantitative estimate</b>	<b>Span</b>	<b>Confidence level</b>	<b>Basis for interpretation</b>	<b>Comments</b>
Orientation (strike/dip)	047/90	±10/±?	Medium	Local major lineament	See also Section 4.1
Width	N/A			Local major lineament	
Length	>300 m	300→1000 m	High	Local major lineament	
Ductile deformation	N/A			No observations	
Brittle deformation	Cataclastic		Low	Topography	
Rock type	Granite	Variable	Medium	Geological map	
Grain size	N/A			No observations	
Alteration	N/A			No observations	
Mineralogical description	N/A			No observations	
Density	N/A			No observations	
Fracture orientation	N/A			No observations	
Fracture frequency	N/A			No observations	
Fracture mineralogy	N/A			No observations	

## ZLXNE08

This zone is based on a local, major lineament but it has not been verified in the field and is not penetrated by any borehole. Table 5-11 presents the detailed geological description for this zone.

**Table 5-11. Description of the interpreted geological characteristics for ZLXNE08.**

<b>ZLXNE08</b>					
<b>Property</b>	<b>Quantitative estimate</b>	<b>Span</b>	<b>Confidence level</b>	<b>Basis for interpretation</b>	<b>Comments</b>
Orientation (strike/dip)	049/90	±10/±?	Medium	Local major lineament	See also Section 4.1
Width	N/A			Local major lineament	
Length	300 m	200->1000 m	High	Local major lineament	
Ductile deformation	N/A			No observations	
Brittle deformation	Cataclastic		Low	Topography	
Rock type	Granite	Variable	Medium	Geological map	
Grain size	N/A			No observations	
Alteration	N/A			No observations	
Mineralogical description	N/A			No observations	
Density	N/A			No observations	
Fracture orientation	N/A			No observations	
Fracture frequency	N/A			No observations	
Fracture mineralogy	N/A			No observations	

**ZLXNS01**

This zone is based on a local, major lineament but has not been verified in the field and is not penetrated by any borehole. Table 5-12 presents the detailed geological description for this zone.

**Table 5-12. Description of the interpreted geological characteristics for ZLXNS01.**

<b>ZLXNS01</b>					
<b>Property</b>	<b>Quantitative estimate</b>	<b>Span</b>	<b>Confidence level</b>	<b>Basis for interpretation</b>	<b>Comments</b>
Orientation (strike/dip)	165/90	±10/±?	Medium	Local major lineament	See also Section 4.1
Width	N/A			Local major lineament	
Length	2.5 km	2–2.8 km	High	Local major lineament	
Ductile deformation	N/A			No observations	
Brittle deformation	Cataclastic		Low	Topography	
Rock type	Granite	Variable	Medium	Geological map	
Grain size	N/A			No observations	
Alteration	N/A			No observations	
Mineralogical description	N/A			No observations	
Density	N/A			No observations	
Fracture orientation	N/A			No observations	
Fracture frequency	N/A			No observations	
Fracture mineralogy	N/A			No observations	



## ZLXNS02

This zone is based on a local major lineament but has not been verified in the field and is not penetrated by any borehole. Table 5-13 presents a detailed geological description of the zone.

**Table 5-13. Description of the interpreted geological characteristics for ZLXNS02.**

<b>ZLXNS02</b>					
<b>Property</b>	<b>Quantitative estimate</b>	<b>Span</b>	<b>Confidence level</b>	<b>Basis for interpretation</b>	<b>Comments</b>
Orientation (strike/dip)	000/90	±10/±?	Medium	Local major lineament	See also Section 4.1
Width	N/A			Local major lineament	
Length	700 m	500->1000 m	High	Local major lineament	
Ductile deformation	N/A			No observations	
Brittle deformation	Cataclastic		Low	Topography	
Rock type	Granite	Variable	Medium	Geological map	
Grain size	N/A			No observations	
Alteration	N/A			No observations	
Mineralogical description	N/A			No observations	
Density	N/A			No observations	
Fracture orientation	N/A			No observations	
Fracture frequency	N/A			No observations	
Fracture mineralogy	N/A			No observations	

### **ZLXNS03**

This zone is based on a local major lineament but has not been verified in the field and is not penetrated by any borehole. Table 5-14 presents a detailed geological description of the zone.

**Table 5-14. Description of the interpreted geological characteristics for ZLXNS03.**

<b>ZLXNS03</b>					
<b>Property</b>	<b>Quantitative estimate</b>	<b>Span</b>	<b>Confidence level</b>	<b>Basis for interpretation</b>	<b>Comments</b>
Orientation (strike/dip)	155/90	±10/±?	Medium	Local major lineament	See also Section 4.1
Width	N/A			Local major lineament	
Length	700 m	500–1000 m	High	Local major lineament	
Ductile deformation	N/A			No observations	
Brittle deformation	Cataclastic		Low	Topography	
Rock type	Granite	Variable	Medium	Geological map	
Grain size	N/A			No observations	
Alteration	N/A			No observations	
Mineralogical description	N/A			No observations	
Density	N/A			No observations	
Fracture orientation	N/A			No observations	
Fracture frequency	N/A			No observations	
Fracture mineralogy	N/A			No observations	

## ZLXNS04

This zone is based on a local major lineament but has not been verified in the field and is not penetrated by any borehole. Table 5-15 presents a detailed geological description of the zone.

**Table 5-15. Description of the interpreted geological characteristics for ZLXNS04.**

<b>ZLXNS04</b>					
<b>Property</b>	<b>Quantitative estimate</b>	<b>Span</b>	<b>Confidence level</b>	<b>Basis for interpretation</b>	<b>Comments</b>
Orientation (strike/dip)	154/90	±10/±?	Medium	Local major lineament	See also Section 4.1
Width	N/A			Local major lineament	
Length	900 m	700->1000 m	High	Local major lineament	
Ductile deformation	N/A			No observations	
Brittle deformation	Cataclastic		Low	Topography	
Rock type	Granite	Variable	Medium	Geological map	
Grain size	N/A			No observations	
Alteration	N/A			No observations	
Mineralogical description	N/A			No observations	
Density	N/A			No observations	
Fracture orientation	N/A			No observations	
Fracture frequency	N/A			No observations	
Fracture mineralogy	N/A			No observations	

## **ZLXNW01**

The deformation zone ZLXNW01 is based on a local major lineament. There are two percussion boreholes, HLX01 and HLX07, which are possibly related to the lineament. It has not been possible to use the information from the boreholes to assign a dip of the modelled zone. However, the resistivity data from these boreholes is not in conflict with the interpretation of a vertical zone.

Seismic reflection data support a fracture zone dipping towards and crosscutting the KLX01. This is considered in the alternative model. Table 5-16 presents a detailed geological description of the zone.

**Table 5-16. Description of the interpreted geological characteristics for ZLXNW01.**

<b>ZLXNW01</b>					
<b>Property</b>	<b>Quantitative estimate</b>	<b>Span</b>	<b>Confidence level</b>	<b>Basis for interpretation</b>	<b>Comments</b>
Orientation (strike/dip)	116/90	±10/±?	Medium	Local major lineament, HLX01 and HLX07	See also Section 4.1
Width	N/A			Local major lineament	
Length	2.5 km	2.2–3 km	High	Local major lineament	
Ductile deformation	N/A			No observations	
Brittle deformation	Cataclastic		Low	Topography, resistivity	
Rock type	Granite	Variable	Medium	Geological map	
Grain size	N/A			No observations	
Alteration	N/A			No observations	
Mineralogical description	N/A			No observations	
Density	N/A			No observations	
Fracture orientation	N/A			No observations	
Fracture frequency	N/A			No observations	
Fracture mineralogy	N/A			No observations	

## ZLXNW02

This zone is based on a local major lineament but has not been verified in the field and is not penetrated by any borehole. Table 5-17 presents a detailed geological description of the zone.

**Table 5-17. Description of the interpreted geological characteristics for ZLXNW02.**

<b>ZLXNW02</b>					
<b>Property</b>	<b>Quantitative estimate</b>	<b>Span</b>	<b>Confidence level</b>	<b>Basis for interpretation</b>	<b>Comments</b>
Orientation (strike/dip)	086/90	±10/±?	Medium	Local major lineament	See also Section 4.1
Width	N/A			Local major lineament	
Length	200 m	100->500 m	High	Local major lineament	
Ductile deformation	N/A			No observations	
Brittle deformation	Cataclastic		Low	Topography	
Rock type	Granite	Variable	Medium	Geological map	
Grain size	N/A			No observations	
Alteration	N/A			No observations	
Mineralogical description	N/A			No observations	
Density	N/A			No observations	
Fracture orientation	N/A			No observations	
Fracture frequency	N/A			No observations	
Fracture mineralogy	N/A			No observations	

### **ZLXNW03**

This zone is based on a local, major lineament but has not been verified in the field and is not penetrated by any borehole. Table 5-18 presents a detailed geological description of the zone.

**Table 5-18. Description of the interpreted geological characteristics for ZLXNW03.**

<b>ZLXNW03</b>					
<b>Property</b>	<b>Quantitative estimate</b>	<b>Span</b>	<b>Confidence level</b>	<b>Basis for interpretation</b>	<b>Comments</b>
Orientation (strike/dip)	109/90	±10/±?	Medium	Local major lineament	See also Section 4.1
Width	N/A			Local major lineament	
Length	1.5 km	1.3-→2 km	High	Local major lineament	
Ductile deformation	N/A			No observations	
Brittle deformation	Cataclastic		Low	Topography	
Rock type	Granite	Variable	Medium	Geological map	
Grain size	N/A			No observations	
Alteration	N/A			No observations	
Mineralogical description	N/A			No observations	
Density	N/A			No observations	
Fracture orientation	N/A			No observations	
Fracture frequency	N/A			No observations	
Fracture mineralogy	N/A			No observations	

## ZLXNW04

The ZLXNW04 is based on a local major lineament. There is one percussion drilled borehole, HLX02, that penetrates a zone that probably is related to the lineament. A steep dip is indicated, but no precise dip was possible to interpret from the data.

No other observation regarding the modelled zone are available. Table 5-19 presents a detailed geological description of the zone.

**Table 5-19. Description of the interpreted geological characteristics for ZLXNW04.**

ZLXNW04					
Property	Quantitative estimate	Span	Confidence level	Basis for interpretation	Comments
Orientation (strike/dip)	102/90	±10/±?	Medium	Local major lineament, HLX02	See also Section 4.1
Width	N/A			Local major lineament	
Length	1.5 km	1.3->2 km	High	Local major lineament	
Ductile deformation	N/A			No observations	
Brittle deformation	Cataclastic		Low	Topography	
Rock type	Granite	Variable	Medium	Geological map	
Grain size	N/A			No observations	
Alteration	N/A			No observations	
Mineralogical description	N/A			No observations	
Density	N/A			No observations	
Fracture orientation	N/A			No observations	
Fracture frequency	N/A			No observations	
Fracture mineralogy	N/A			No observations	

## ZLXNW05

This zone is based on a local, major lineament but has not been verified in the field and is not penetrated by any borehole. Table 5-20 presents a detailed geological description for the zone.

**Table 5-20. Description of the interpreted geological characteristics for ZLXNW05.**

<b>ZLXNW05</b>					
<b>Property</b>	<b>Quantitative estimate</b>	<b>Span</b>	<b>Confidence level</b>	<b>Basis for interpretation</b>	<b>Comments</b>
Orientation (strike/dip)	105/90	±10/±?	Medium	Local major lineament	See also Section 4.1
Width	N/A			Local major lineament	
Length	1.6 km	1.4–1.9 km	High	Local major lineament	
Ductile deformation	N/A			No observations	
Brittle deformation	Cataclastic		Low	Topography	
Rock type	Granite	Variable	Medium	Geological map	
Grain size	N/A			No observations	
Alteration	N/A			No observations	
Mineralogical description	N/A			No observations	
Density	N/A			No observations	
Fracture orientation	N/A			No observations	
Fracture frequency	N/A			No observations	
Fracture mineralogy	N/A			No observations	



## ZLXNW06

This zone is based on a local major lineament but has not been verified in the field and is not penetrated by any borehole. Table 5-21 presents a detailed geological description of the zone.

**Table 5-21. Description of the interpreted geological characteristics for ZLXNW06.**

<b>ZLXNW06</b>					
<b>Property</b>	<b>Quantitative estimate</b>	<b>Span</b>	<b>Confidence level</b>	<b>Basis for interpretation</b>	<b>Comments</b>
Orientation (strike/dip)	135/90	±10/±?	Medium	Local major lineament	See also Section 4.1
Width	N/A			Local major lineament	
Length	800 m	600-->1000 m	High	Local major lineament	
Ductile deformation	N/A			No observations	
Brittle deformation	Cataclastic		Low	Topography	
Rock type	Granite	Variable	Medium	Geological map	
Grain size	N/A			No observations	
Alteration	N/A			No observations	
Mineralogical description	N/A			No observations	
Density	N/A			No observations	
Fracture orientation	N/A			No observations	
Fracture frequency	N/A			No observations	
Fracture mineralogy	N/A			No observations	

**ZLXNW07**

This zone is based on a local major lineament but has not been verified in the field and is not penetrated by any borehole. Table 5-22 presents a detailed geological description of the zone.

**Table 5-22. Description of the interpreted geological characteristics for ZLXNW07.**

<b>ZLXNW07</b>					
<b>Property</b>	<b>Quantitative estimate</b>	<b>Span</b>	<b>Confidence level</b>	<b>Basis for interpretation</b>	<b>Comments</b>
Orientation (strike/dip)	123/90	±10/±?	Medium	Local major lineament	See also Section 4.1
Width	N/A			Local major lineament	
Length	1 km	0.8->1.5 km	High	Local major lineament	
Ductile deformation	N/A			No observations	
Brittle deformation	Cataclastic		Low	Topography	
Rock type	Granite	Variable	Medium	Geological map	
Grain size	N/A			No observations	
Alteration	N/A			No observations	
Mineralogical description	N/A			No observations	
Density	N/A			No observations	
Fracture orientation	N/A			No observations	
Fracture frequency	N/A			No observations	
Fracture mineralogy	N/A			No observations	

### 5.1.3 Alternative geological model

The alternative geological model considers the available site data at a deeper level. A few of the structures in the base geological model have new interpretations and the rock mass at the site has been divided into rock domains to better reflect the variability of the rock mass characteristics.

Below follows a detailed description of interpretations that have changed from the base geological model. Please note that interpretations that are identical to the base geological model are not repeated in this section. To get the complete geological description of the alternative geological model structures not mentioned in this section can be found in Section 5.1.2.

#### **Rock Domains**

Based on existing rock types, the bedrock in the model area has been divided in three rock domains RLX01, RLX02 and RLX03 (see Figure 4-9). The main rock domain (RLX02), cf. Table 5-24, includes the dominating, commonly porphyritic granite to granodiorite and makes up c. 70% of the volume in the geological model. In the north-eastern part of the model area, the more or less intimate mixture of diorite to gabbro and different varieties of granite to granodiorite constitute a separate rock domain (RLX01), cf. Table 5-23, which is estimated to occupy less than 5% of the volume. A fracture zone (fault) along Kärsviken delimits this rock domain in the northeastern part, since no diorite to gabbro or red, fine- to finely medium-grained granite is documented northeast of the fault. Due to the lack of information at depth, the rock domain has been given the geometrical shape of a box that does not reach the bottom of the model volume. The

**Table 5-23. Description of the interpreted geological characteristics for rock domain RLX01.**

<b>Rock domain RLX01</b>					
<b>Property</b>	<b>Quantitative estimate</b>	<b>Span</b>	<b>Confidence</b>	<b>Basis for interpretation</b>	<b>Comments</b>
Volume	5.4·10 <sup>8</sup> m <sup>3</sup>	± 2·10 <sup>8</sup> m <sup>3</sup>	Medium	Geological map	Estimated from the RVS model
Ductile deformation	N/A			No observations	
Rock type	Granite 10% Gabbro 70% Granite to granodiorite 20%	Granite ± 10% Gabbro ± 20% Granite to granodiorite ± 10%	Medium	Geological map	
Grain size	N/A			No observations	
Alteration	N/A			No observations	
Mineralogical description	N/A			Not performed	
Density	N/A			No observations	
Fracture orientation	N/A			No observations	
Fracture size	N/A			No observations	
Fracture intensity	N/A			No observations	
Fracture mineralogy	N/A			No observations	

third rock domain (RLX03), cf. Table 5-25, is based on the inferred correlation between the granodiorite to quartz monzodiorite immediately south of the model area and the granodiorite to quartz diorite (“Äspö diorite”) in the bottom of the borehole KLX02 (from 1450 m depth and downwards; see Section 3.3 above). Hence, this rock domain has a presumed northward extension at depth, and dominates the southern lower part of the model volume, which corresponds to c. 20–25% of the latter.

Due to the lack of detailed information, the frequently occurring red, fine-grained granitic dykes, as well as the occurrence of dioritic to gabbroic xenoliths to enclaves and minor bodies, are treated as being more or less evenly distributed in the rock domains. This is also indicated in the WellCAD plot of the drillcores from boreholes KLX01 and KLX02 /Ekman, 2001/, which also show the relatively inhomogeneous character of the bedrock in the Laxemar project area, regarding the occurrence of fine-grained granite and minor mafic bodies. The distribution of rock types in boreholes KLX01 and KLX02 has been calculated from the information in the SICADA database.

**Table 5-24. Description of the interpreted geological characteristics for RLX02.**

<b>RLX02</b>					
<b>Property</b>	<b>Quantitative estimate</b>	<b>Span</b>	<b>Confidence</b>	<b>Basis for interpretation</b>	<b>Comments</b>
Volume	10 <sup>10</sup> m <sup>3</sup>	± 2·10 <sup>9</sup> m <sup>3</sup>	Medium	Geological map	Estimated from the RVS model
Ductile deformation	N/A			No observations	
Rock type	Granite 77% Aplite 3% Granodiorite 10% Diorite to gabbro and mafic rocks 10%	Granite ± 5% Aplite ± 2% Granodiorite ± 2% Diorite to gabbro and mafic rocks ± 2%	Medium	Geological map and KLX01 and KLX02	
Grain size	N/A			No observations	
Alteration	15% of the complete length of the boreholes are altered	± 7%		KLX01 and KLX02	
Mineralogical description	N/A			Not performed	
Density	N/A			No observations	
Fracture orientation	Set 1: 352/86 Set 2: 286/76 Set 3: 226/92 Set 4: 125/18	Set 1: K=8.52 Set 2: K=9.26 Set 3: K=9.36 Set 4: K=7.02	High	Section 3.8	Fracture data from the whole region Fisher distribution
Fracture size	Set 1: D=3.1, x0=0.4 Set 2: D=3.4, x0=0.46 Set 3: D=3, x0=0.41 Set 4: D=3.3, x0=0.44	Set 1: D±0.3 Set 2: D±0.3 Set 3: D±0.3 Set 4: D±0.3		Section 3.8	Power Law
Fracture intensity	Set 1: 0.78 Set 2: 0.66 Set 3: 0.76 Set 4: 0.24	Set 1: ± 0.2 Set 2: ± 0.2 Set 3: ± 0.2 Set 4: ± 0.2	High	Section 3.8	P <sub>32</sub> ·(m <sup>2</sup> /m <sup>3</sup> )
Fracture mineralogy	Chl, Ep, Ca			KLX01 and KLX02	

**Table 5-25. Description of the interpreted geological characteristics for RLX03.**

<b>Rock Domain RLX03</b>					
<b>Property</b>	<b>Quantitative estimate</b>	<b>Span</b>	<b>Confidence</b>	<b>Basis for interpretation</b>	<b>Comments</b>
Volume	2.2·10 <sup>9</sup> m <sup>3</sup>	± 2·10 <sup>9</sup> m <sup>3</sup>	Medium	Geological map	Estimated from the RVS model
Ductile deformation	N/A			No observations	
Rock type	Granite 10% Aplite 5% Granodiorite 80% Diorite to gabbro and mafic rocks 5%	Granite ± 2% Aplite ± 2% Granodiorite ± 10% Diorite to gabbro and mafic rocks ± 2%	Medium	Geological map and KLX02	KLX02 are the only indication within the site
Grain size	N/A			No observations	
Alteration	N/A			KLX01 and KLX02	
Mineralogical description	N/A			Not performed	
Density	N/A			No observations	
Fracture orientation	N/A			No observations	
Fracture size	N/A			No observations	
Fracture intensity	N/A			No observations	
Fracture mineralogy	N/A			No observations	

## **Deformation zones**

### **ZLXEW01**

The alternative interpretation reflects changes based on the tectonized section in KLX02 at 1685 m. Details of the reinterpretation are presented in Section 4.1. Table 5-26 presents the alternative geological interpretation.

### **ZLXEW02**

ZLXEW02 has a more gentle dip in the alternative geological model based mainly on an interpreted intersection with a fracture zone in KLZ02 at 340 m depth. The new intercept constrains the width and gives quantitative estimates for alteration and fracture frequency. Details of the reinterpretation are presented in Section 4.1. Table 5-27 presents the alternative geological interpretation.

**Table 5-26. Alternative geological interpretation for ZLXEW01. See also Section 5.1.2 for complementary information. This table only reflects changes in the alternative model.**

<b>ZLXEW01 Alternative model</b>					
<b>Property</b>	<b>Quantitative estimate</b>	<b>Span</b>	<b>Confidence level</b>	<b>Basis for interpretation</b>	<b>Comments</b>
Orientation (strike/dip)	078/52	±5/±0.5	Medium	Regional lineament, tectonized section in KLX02 (1685 m), airborne geophysics	See also Section 4.1 Based on one observation
Width	30 m	30–200 m	Low	Tectonized section in KLX02 (1685 m), ground magnetic, VLF, regional lineament	See also Section 4.1 Based on one observation
Alteration tectonized	92%			Segment R7 in KLX02 (1685 m)	Appendix B1. Based on one observation
Fracture frequency	7.2 fractures per metre		Medium	Segment R7 in KLX02 (1685 m)	Based on one observation
Fracture mineralogy	Chlorite		Medium	No observations	Based on one observation

**Table 5-27. Alternative geological interpretation for ZLXEW02. See also Section 5.1.2 for complementary information. This table only reflects changes in the alternative model.**

<b>ZLXEW02 Alternative model</b>					
<b>Property</b>	<b>Quantitative estimate</b>	<b>Span</b>	<b>Confidence level</b>	<b>Basis for interpretation</b>	<b>Comments</b>
Orientation (strike/dip)	271/49	±5/0.5	Medium	Local major lineament	See also Section 4.1 Dip based on one observation
Width	2 m	1.5–3 m	Medium	Local major lineament	Based on one observation
Length	5 km	5–>10 km	Medium	Local major lineament	
Brittle deformation	Cataclastic		Medium	Crush zone and Fracture zone in KLX02 (340 m)	Appendix B1. Based on one observation
Rock type	Granite and quartz monzonite	Variable	Medium	Geological map, core log KLX02 (340 m)	Appendix B1
Alteration	Ca 50% medium strong oxidization			Altered section in KLX02 (340 m)	Appendix B1. Based on one observation
Fracture frequency	24.3 fractures per metre		High	Crush zone and fracture zone in KLX02 (340 m)	Based on one observation

## ZLXNE04

Details of the reinterpretation are presented in Section 4.1. Table 5-28 presents the detailed geological interpretation.

## ZLXNE05 and ZLXNE06

Zone ZLXNE05 and ZLXNE06 have been combined into one zone, named ZLXNE06 in the alternative geological model. This change was implemented to converge with regional lineament interpretation. The ZLXNE06 was also correlated with zone “NE01 in the access tunnel to the Äspö Laboratory. From tunnel mapping a dip of 70° and a thickness of 28 m was assigned /Rehn et al, 1997/.

**Table 5-28. Alternative geological interpretation for ZLXNE04. See also Section 5.1.2 for complementary information. This table only reflects changes in the alternative model.**

ZLXNE04 Alternative model					
Property	Quantitative estimate	Span	Confidence level	Basis for interpretation	Comments
Orientation (strike/dip)	027.5/59	±5/±0.5	Medium	Local major lineament, HLX04, altered fracture zone in KLX01 (421 m)	See also Section 4.1
Width	1 m	0.5–1.5m	Low	HLX04, altered fracture zone in KLX01 (421 m)	Based on one observation
Brittle deformation	Cataclastic		Medium	HLX04, altered fracture zone in KLX01 (421 m)	Appendix B1 and Section 3.4. Based on one observation
Alteration	100% medium strong oxidization		Medium	Altered fracture zone in KLX01 (421 m)	Appendix B1. Based on one observation
Fracture orientation	NNE		Medium	Fracture zone in KLX01 (421 m)	Appendix B1. Based on one observation
Fracture	14.2 fractures		Medium	Fracture zone in KLX01 (421 m)	Appendix B1. Based on one observation
Fracture mineralogy	Calcite, Chlorite		Medium	Fracture zone in KLX01 (421 m)	Appendix B1. Based on one observation

**Table 5-29. Alternative geological interpretation for ZLXNE06. See also Section 5.1.2 for complementary information. This table only reflects changes in the alternative model.**

<b>ZLXNE06 Alternative model</b>					
<b>Property</b>	<b>Quantitative estimate</b>	<b>Span</b>	<b>Confidence level</b>	<b>Basis for interpretation</b>	<b>Comments</b>
Orientation (strike/dip)	224/70	±10/±5	Medium	Local major lineament, HLX04, altered fracture zone in KLX01 (421 m) Correlation with Äspö tunnel; zone "NE-01"	See also Section 4.1
Width	28 m	15–40m	Medium	HLX04, altered fracture zone in KLX01 (421 m) Correlation with Äspö tunnel; zone "NE-01"	Based on one observation
Brittle deformation	Cataclastic		Medium	HLX04, altered fracture zone in KLX01 (421 m)	Appendix B1 and Section 3.4.
Length	800 m	600→1000 m	High	Local, major lineament	Lineament located in a bay of the Baltic Sea

#### **5.1.4 Overall assessment of uncertainties in the geological description**

The basis for the uncertainty assessment of the geological model is provided in Section 4.1.4. This assessment has resulted in the uncertainty spans, confidence levels etc in the above descriptions.

In summary, the level of geological information is of such different detail at different scales of resolution and at different locations within the modelling domain that the interpreted structures in both the base and alternative geological models are subject to extensive uncertainties. However, the interpretations have been made in the simplest possible way at all stages, such that zones have been kept planar with an identical width throughout their extent, not to infer any unnecessary uncertainties. By this modelling approach it is possible to increase the detail in the interpretation when new data becomes available.

The overall uncertainty in the geological model is also illustrated by the presentations of the base model and the alternative model. Even if it could be argued that the alternative model only is a more updated version of the base model, uncertainties in interpretation are such that also the base model should be retained as a potential possibility, yet with lower confidence than the alternative model. Additional alternatives are clearly possible, there are potential zones in the boreholes not connected to deterministic zones in the presented models and more importantly as already discussed, the current data only covers a limited region of the model domain.



## 5.2 Hydrogeological description

The description below comprises hydraulic properties for defined geometrical units and boundary conditions for the present day conditions for a rock volume defined by the Base Geological model. The geometrical units in the hydrogeological description are: Hydraulic Conductor Domains (HCD), Hydraulic Rock Domains (HRD) and Hydraulic Soil Domains (HSD), see Section 4.2.

### 5.2.1 Hydraulic Conductor Domains (HCD)

#### General

The hydraulic properties within the Hydraulic Conductor Domains (HCDs) are represented by constant values. No spatial models for stochastic distribution of properties are suggested. However, the values are certainly subject to high uncertainty since the majority of the HCDs have not been tested.

#### Defined HCD

All deformation zones deterministically defined in the Base Geological Model, Section 5.1, are considered as HCDs. Two of the HCDs, ZLXNE03 and ZLXNE04, are penetrated by core holes and local estimates of the transmissivities (T) are available from these holes. Data are also available from a few percussion holes that possibly intersect the same HCDs as KLX01 and KLX02. Transmissivities in these HLX holes indicate the same magnitude for T. However, there remains uncertainties of how well these HLX holes represent the HCDs. Some of the other HLX holes possibly also intersect other HCDs but as for the previously mentioned HLX holes there remains uncertainties in the evaluation, and therefore the results are not included explicit as representative values for the HCDs.

The rest of the HCDs are assigned the mean transmissivity of HCDs reported for Äspö /Rhén et al, 1997/, see Table 5-30. However, ZLXNE01 is probably the same deformation zone as NE-1, just South of Äspö /Rhén et al, 1997/. The interpreted transmissivity for NE-1 is  $2.2 \times 10^{-4} \text{ m}^2/\text{s}$  ( $\text{std}(\text{Log}_{10}(T))=0.5$ ), which compares with also a high transmissivity in HLX08 ( $T= 2. \times 10^{-3} \text{ m}^2/\text{s}$ ), interpreted to intersect ZLXNE01.

The base for the suggested range of the effective transmissivity (as a constant value for the entire HCD) shown in Table 5-30 should be interpreted as that the “true” constant value is expected to be within the suggested range. It compares approximately to the upper and lower quartiles found for all the HCDs at Äspö /Rhén et al, 1997/.

**Table 5-30. Base Hydrogeological Model. Suggested transmissivity for Hydraulic Conductor Domains (HCD).**

Zone name	Transmissivity (T) (m <sup>2</sup> /s)	Estimated possible range for T (m <sup>2</sup> /s)	Comment
ZLXNE03	$7 \times 10^{-6}$	$0.1T < T < 10T$	
ZLXNE04	$7 \times 10^{-6}$	$0.1T < T < 10T$	
ZLXE01	$1 \times 10^{-4}$	$0.1T < T < 10T$	Regional zone
ZLXNE01	$1 \times 10^{-4}$	$0.1T < T < 10T$	Regional zone
Other zones	$3 \times 10^{-6}$	$0.1T < T < 10T$	Local zones

**Table 5--31. The power law relationship between transmissivity (T) and Storativity (S). Test scale approximately 100 m.  $S = aT^b$ . R = Correlation coefficient. n = sample size /Rhén et al, 1997/.**

Scale (m)	a	b	R	n
100	0.009	0.79	0.71	5

There are very few interference tests at Äspö HRL that are judged to be useful for direct evaluation of the storage coefficient (S) of a hydraulic conductor, where the radial flow assumption can be interpreted to be valid. The reason is that the distance between the observation sections is relatively long in comparison with the distances between hydraulic conductors with higher transmissivities (T). The relationship between T and S was in /Rhén et al, 1997/ approximated to a power law relationship, which is also presented in /Rhén et al, 1997/.

However, the relation in Table 5-31 seems to give unrealistic low S values for very low T values. There are few points for the regression analysis which makes the relation uncertain. Probably the slope should be less than shown. The variability of S is however probably relatively large, which the figure in /Rhén et al, 1997/ indicates.

## **5.2.2 Hydraulic Rock Domains (HRD)**

### **General**

Only one Hydraulic Rock Domain (HRD) is considered for the entire descriptive model. No depth dependency of the distribution of the properties is suggested. However in the numerical groundwater flow model the near surface conditions, representing rock as well as Quaternary deposits, are set to a higher hydraulic conductivity compared to HRD1 in Table 4-8. See /Follin and Svensson, 2002/ for details.

The description of the properties is made in two (alternative) ways:

- Statistical distributions (stochastic continuum) of hydraulic conductivity based on measurements in different test scales.
- Statistical distributions of transmissivity for the fractures in a discrete fracture network (DFN) description.

### **Stochastic continuum description of HRD**

Table 4-8 presents suggested parameters describing the hydraulic conductivity of the rock mass between fracture zones. Only one Hydraulic Rock Domain is suggested. These parameters were estimated based on the previous analyses and the statistics presented in Section 4.2.

**Table 5-32. Lognormal distributions based on univariate statistics for KLX01 and KLX02, with zones in Table 5-30 excluded in the data set for analysis. Data represent measurements along sub-vertical boreholes.**

HRD	Test scale (m)	Hydraulic conductivity (K)	
		Median(Log10(K)) (m/s)	Std(Log10(K)) (m/s)
HRD1	3	-10.5	1.8
	30	-9.0	1.8

It is difficult to estimate the average storage capacity as “specific storativity ( $S_s$ )” in a fractured media. However, considering the porosity and compressibility of rock mass it should not become much less than  $S_s = 1 \cdot 10^{-7} \text{ m}^{-1}$ , see /Rhen et al, 1997/ for further details.

### **DFN approach for HRD description**

To assign the properties to the HRDs, models for the spatial distribution of the hydraulic features, the size and form and orientation of these features, and finally, the hydraulic properties of the features are needed. Four fracture sets are assumed for the non-deterministic fracturing within the Laxemar model domain. The deduced parameter values for orientation, spatial distribution and intensity are compiled in Table 5-33.

**Table 5-33. Geometric and hydraulic properties for the non-deterministic fractures.**

Set No.	Orientation statistics of the mean normal vector (pole)				Fracture size D	Spatial distribution Type	Fracture intensity	
	Type	Trend	Plunge	Dispersion			$P_{32}$	$P_{32c}$
1	Fisher	262.0	3.8	8.52	-2.6	Baecher	0.78	0.12
2	Fisher	195.9	13.7	9.26	-2.6	Baecher	0.66	0.15
3	Fisher	135.9	7.9	9.36	-2.6	Baecher	0.76	0.12
4	Fisher	35.4	71.4	7.02	-2.6	Baecher	0.24	0.08
All	$T \in \log N(4.2 \cdot 10^{-8}, 2 \cdot 10^{-7}) \text{ m}^2/\text{s} [\approx \log_{10} T \in N(-8.06, 0.773) \log_{10}(\text{m}^2/\text{s})]$						2.44	0.48

Given the value of the Power Law Exponent,  $D$ , and the volume,  $V$ , of the Laxemar model domain the number of fractures (squares in DarcyTools),  $N[L_1, L_2]$ , within a specified size range,  $L_1$  to  $L_2$ , can be estimated using the following equation (taken from /Svensson, 2001/):

$$N[L_1, L_2] = \frac{V I}{D} \left[ \left( \frac{L_2}{L_{ref}} \right)^D - \left( \frac{L_1}{L_{ref}} \right)^D \right] \quad (1)$$

where  $L_1 < L_2$ .  $I$  and  $L_{ref}$  are two coefficients that determine the position of the power law distribution in a log-log plot of  $N$  versus  $L$ . For the structural-hydraulic model of the Laxemar model domain the following coefficients are used:  $D = -2.6$ ,  $L_{ref} = 500$  m and  $I = 10^{-8}$ .

A positive correlation between the size of the hydraulic features and the transmissivity ( $T_f$ ) is assumed:

$$T_f = \begin{cases} \alpha \left( \frac{L_f}{100} \right)^2 \text{ m}^2/\text{s} & \text{for } L_f \leq 100 \text{ m} \\ \alpha \text{ m}^2/\text{s} & \text{for } L_f > 100 \text{ m} \end{cases} \quad (2a)$$

$$b = 0.01 L_f \quad (2b)$$

The value of the coefficient  $\alpha$  in Equation (2a) was set to  $10^{-8}$  m<sup>2</sup>/s in the /Follin and Svensson, 2002/.

### 5.2.3 Hydraulic Soil Domains (HSD)

The mapped Quaternary deposits are shown in Section 3.3. Very little is known about the soil depth apart from that it is generally thin. About 82% of the area is exposed bedrock or with thin cover of Quaternary deposits, generally till. In Table 5-34 possible values for hydraulic properties of different HRDs is given.

Typical ranges for specific storage ( $S_s$ ) and kinematic porosities ( $n_e$ ) can be found in several text books on hydrogeology.

**Table 5-34. Typical ranges for hydraulic properties of the soil units /Carlsson and Gustafson, 1997/.**

Soil type	Hydraulic conductivity (m/s)
Till	$10^{-5}$ – $10^{-11}$
Clay	$10^{-8}$ – $10^{-12}$
Silty soil	$10^{-5}$ – $10^{-9}$
Sandy soil	$10^{-3}$ – $10^{-6}$

## **5.2.4 Boundary Conditions**

### ***Precipitation and air temperature***

According to /Larsson-McCann et al, 2002/ the mean air temperature varies between about  $-2^{\circ}\text{C}$  in January-February to about  $16^{\circ}\text{C}$  in July. The annual mean precipitation in Oskarshamn is 645 mm/year (corrected values, not the measured, for period 1961–2000), where about 20% falls as snow.

### ***Drainage basins and run-off***

The larger drainage basins was shown in Section 3.6, Figure 3-14, and the smaller drainage basins within the modeled area has not been defined but the sizes are indicated by the topography in Figure 3-16.

No measurement stations of the flow rates in water courses in or close to the modeled area are available. Based on nearby watercourses the run-off is estimated to 150–200 mm/year /Larsson-McCann et al, 2002; Svensson, 1987/.

The actual total groundwater-recharge contribution (baseflow) to the water courses and lakes is somewhat less than the specific runoff multiplied with the total area of the drainage basin. Some of the precipitation falls on lakes, water courses, discharge areas and on tight surfaces, where the water flow directly to a water course, (flow on land surface and in water courses and lakes summarized as: overland flow) and some water is subsurface flow above the water table (interflow) that flows to nearest water course. Some of the groundwater recharge will also flow directly to sea (subsea outflow) as the area borders the Baltic sea.

The above figures of annual specific discharge and precipitation indicate that the actual annual evapotranspiration is around 500 to 450 mm.

### ***Recharge and discharge areas***

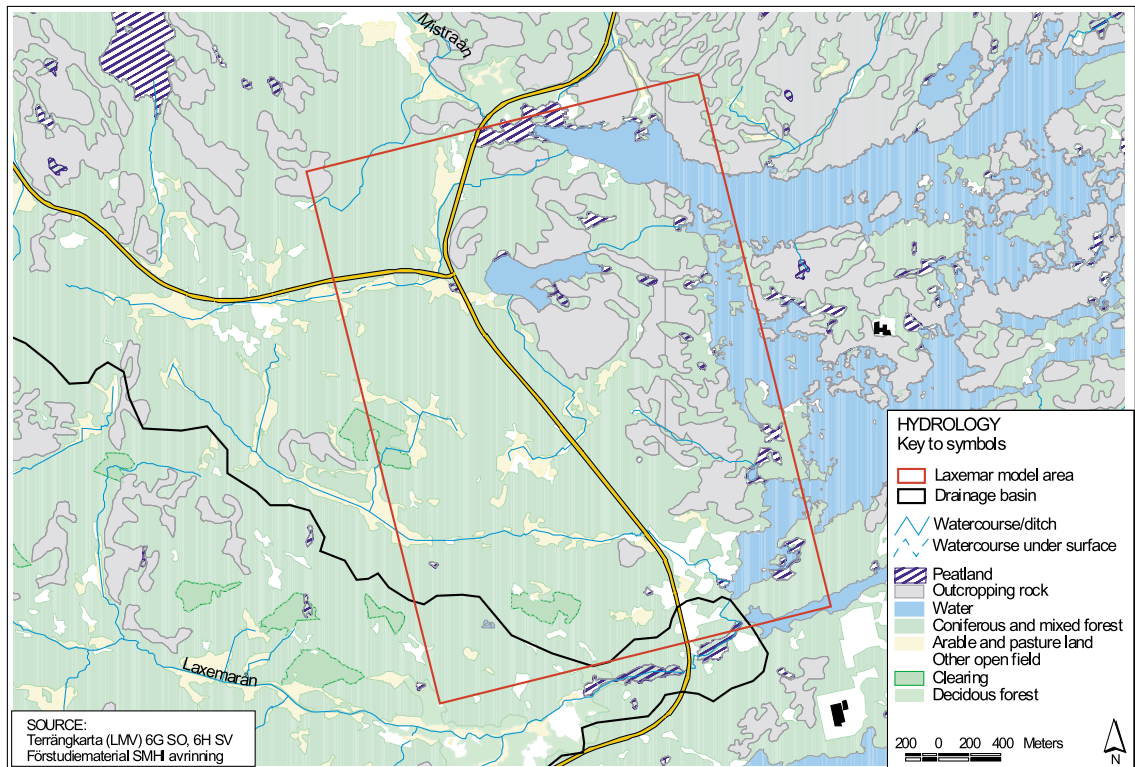
Discharge areas are indicated by watercourses and peat land in Figure 5-2. The rest of the land-surface can be considered as recharge areas. However, outcropping rock, which has no or a thin soil layers, covers a rather large area of the model. The recharge is probably less on outcropping rock areas compared to the rest of Laxemar Model Area. Discharge areas are also located along the coastline, below the sea. The discharge area below the sea may be rather wide.

### ***Water table***

Only a few observations within the modeled area are available. These indicate, as generally found, that water table follows the topography with the largest distances between the topography and the water table near top of the hills.

### ***Baltic Sea level variation and salinity***

The daily changes of the sea level are generally less than  $\pm 1.0$  m /Larsson-McCann et al, 2002/. The salinity of the sea is about 7g/L and is rather constant over the year and does not vary in the top 20 m of the water column /Larsson-McCann et al, 2002/. Close to the coast where fresh water enters the sea from watercourses the salinity is less than



*Figure 5-2. Drainage basins and rivers in and near the Laxemar area.*

7 g/L. A few measurements around Äspö indicate a salinity of about 6 g/L but vary by location and time for sampling. One sample showed 4 g/L and a few others 5–6 g/L (Rhén et al, 1997).

### **Vertical boundaries**

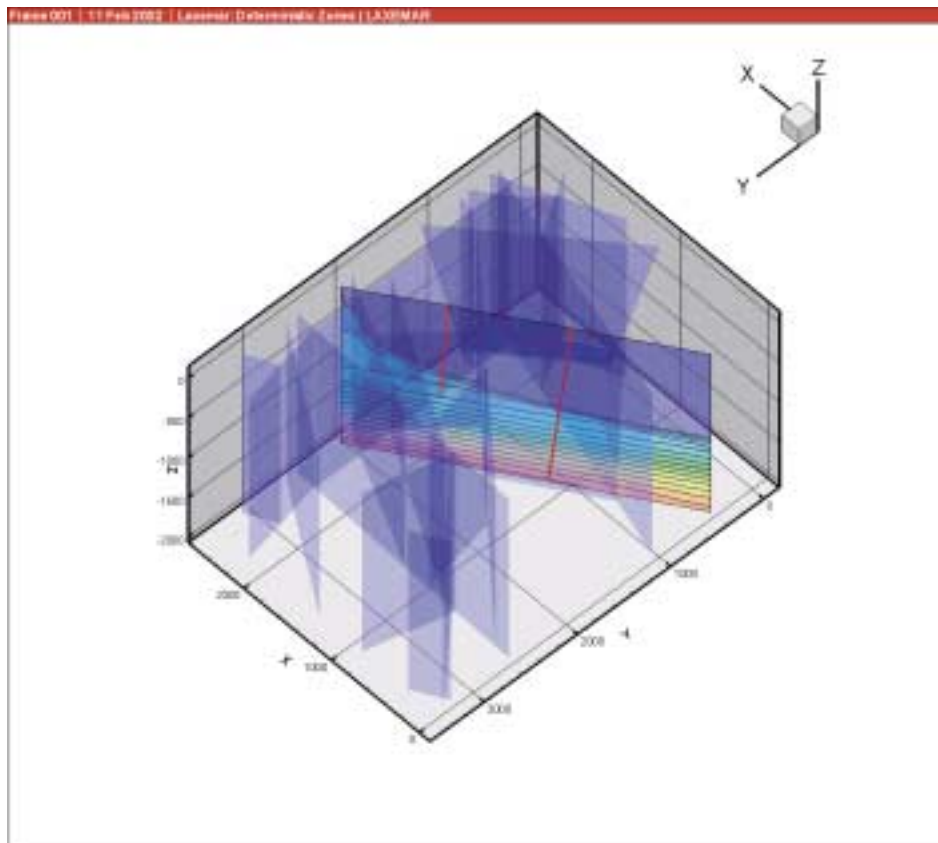
The salinity distributions in KLX01 and KLX02 indicates possible conditions on the western, northern and southern model boundary.

### **Tidal effects**

Earth tidal affects the pressure responses but generally the amplitude is less than 0.1 mvp and even less in the upper most 100–200 m of the rock.

### **5.2.5 Groundwater flow pattern according to numerical simulations**

The numerical groundwater flow model, see Section 4.2, based on the Base Hydrogeological Model, gives indications of the flow pattern and salinity distribution within the Laxemar Model Domain under natural (undisturbed) conditions (see Figure 5-3). For more information see (Follin and Svensson, 2002).



*Figure 5-3. Simulated salinity distribution on a vertical plane through the model. Natural conditions. Base Hydrogeological Model. (For more information see /Follin and Svensson, 2002/).*

## 5.2.6 Overall assessment of uncertainties in the hydrogeological description

The basis for the uncertainty assessment of the hydrogeological model is provided in Section 4.2.10. This assessment has resulted in the uncertainty spans, confidence levels etc in the above descriptions. The evaluation has resulted in a description with a fair representation of the measured data. Still it is evident that significant uncertainties are connected to this description.

The uncertainty in transmissivity distribution both regards the distributions as such and the associated geometry as given by the geological model.

- Clearly, there are hydraulic observations not properly explained by the current description. This may indicate a need to revise the base geological model or to spend further efforts in conditioning the current model. Some initial assessments /see Follin and Svensson, 2002/ suggest that the Alternative Geologic Model offers a better structure for the hydrogeological model, but a full test of this possibility has not been carried out. Evaluation of the geological model jointly with the geologists would probably be much fruitful. However, the limitations in geological input data (see Section 5.1) need also be considered.
- Many of the presented HCDs have not been hydraulically tested. The provided hydraulic properties of these thus have low confidence.

- The fracture transmissivity distribution in the DFN-description match fairly well with measured results, but there are substantial uncertainties as regards size distributions, size-T correlations and spatial variability which cannot be tested without additional numerical and hydraulic tests from more bore holes and in more testing sections. /Follin and Svensson, 2002/ discuss a few alternatives that may be feasible from a practical point of view but these need to be evaluated, and perhaps also elaborated, before they are subjected to a peer review.

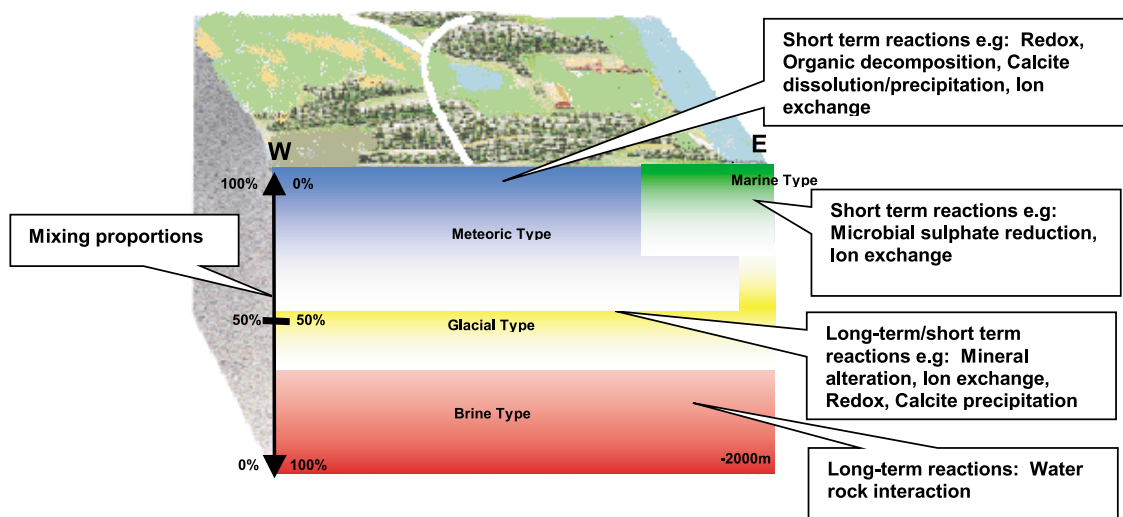
The hydraulic conductivity of the uppermost layers of a numerical flow model in DarcyTools have been used to tune the position of the water table and hence the spatial distribution of recharge and discharge areas. Unfortunately, the present knowledge about the hydrology of the Laxemar area is quite limited. Except for the elevation of Lake Frisksjön, there are no other hydrological data to calibrate against. The performed tuning of the hydraulic conductivity of the uppermost layers carried out in support of this project is by no means exhaustive.

### 5.3 Geochemical description

To summarise the results from the modelling of the Laxemar site a *Site descriptive model* can be constructed. This model can consist of one or several illustrations where various observed or modelled geochemical properties are summarised.

#### 5.3.1 Model description

An example of a site descriptive model is shown in Figure 5-4. The illustration shows distribution of the major water types, indicates the mixing proportions and lists the major type of reactions occurring at the site. The figure can also be completed with flow lines from the hydrodynamic modelling.



**Figure 5-4.** General components in the site descriptive model for Laxemar shown along the W-E cutting plane (for orientation see Section 4.3). The dominating water types Brine Type (Ca-Na-Cl rich water type), Glacial Type (K-Ca-SO<sub>4</sub> rich water type), Marine Type (Na-Cl rich water type) and Meteoric Type (HCO<sub>3</sub>-SO<sub>4</sub> rich water type) water are illustrated as mixing proportions (%) and major massbalance reactions occurring within the domains. The mixing proportions add up to 100% in all points.



The major characteristics of the dominating waters types (Meteoric, Marine, Glacial and Brine) at the Laxemar site are:

**Meteoric Type ( $\text{HCO}_3\text{-SO}_4$  to  $\text{Na-HCO}_3$  rich water type):** As seen in Figure 5-4, the upper area of the W-E cutting plane is dominated by meteoric water (named Precipitation in M3 calculations) to a depth of approximately 500–1000 m. This water type is altered by fast short-term reactions such as redox reactions that prevent deep oxygen penetration into the bedrock. Oxygen consumption and carbonate production linked to organic decomposition, iron reduction and methane production is generally the dominating redox reaction /Pedersen and Karlsson, 1995; Banwart et al, 1996/. Saturation index calculations and M3 modelling indicated dissolution of calcite in the upper recharge part of the bedrock and the resulting precipitation of calcite in the lower part of the bedrock which can alter the direction of the groundwater flow paths in fractured bedrock. Sinks and sources of anions and cations due to sorption/desorption (i.e. surface complexation and ion exchange) can alter the water composition of the meteoric groundwater /Laaksoharju and Wallin, 1997/.

**Marine Type (Na-Cl rich water type):** The east corner of the cutting plane is dominated by marine water (Figure 5-4). The exact penetration depth is not known because of lack of observations and is therefore based on M3 modelling. (The water type is named Baltic Sea and Modified Sea in M3 calculations). The source of Mg is shown to be associated with an influx of marine water, present Baltic Sea or possibly Litorina Sea water. Identified fast short-term reactions that have modified the Sea water are a sink of Na and a gain of Ca, due to ion exchange with clays. Marine water is characterised by fast, short-term reactions that modify the waters when they enter the bedrock and have been identified as a sink of K and Na, and a gain of Ca, due to ion-exchange with clays /Laaksoharju and Wallin, 1997/. The Marine water can undergo decomposition of organic material due to microbiological sulphate reduction (Modified Sea water) which has been detected by M3 modelling as a sink for  $\text{SO}_4$  and a source for  $\text{HCO}_3$ . The calculations correlate well with the measured content of sulphate-reducing bacteria at locations at Äspö-HRL /Laaksoharju et al, 1995b/.

**Glacial Type (K-Ca- $\text{SO}_4$  rich water type):** An important water type found at Laxemar has been affected by a component of cold climate recharge /Tullborg, 1997/. The low  $\delta^{18}\text{O}$  value indicates a climate which corresponds to a mean annual temperature of  $-3^\circ\text{C}$  using Dansgaard's formula /Dansgaard, 1964/. Such a low temperature has not prevailed during post-glacial times in the area. Cold climate signatures are found in many samples from 800–1200 m depths on the mainland of Laxemar /Laaksoharju et al, 1995b/. The interpretation from the conceptual model (see Figure 3-47) and the M3 calculations are that this water type has been formed by the continental ice sheet melting and the water has been injected into the saline water. The amount, oxidation state, penetration depth of glacial meltwater are not completely known. Despite the many indications of glacial meltwater at great depth, there is no clear evidence from the fracture mineral distribution that this water was oxygenated to more than 50–100 m in the upper part of the bedrock /Tullborg, 1997/. The calculated sink for Ca may be due to calcite precipitation during injection of glacial groundwater and consequent mixing with calcite-saturated saline groundwater which caused super saturation of calcite /Laaksoharju and Wallin, 1997/.

**Brine Type (Ca-Na-Cl rich watertype):** At depths below 1000–1200 m the Brine groundwater mixing portion starts to play an important role. The origin of the brine component at the Laxemar site is unknown. Alternatives such as ancient metamorphic fluids, water/rock interaction, fluid inclusions, leaching of paleozoic sediments, and

localised freezing have been discussed /Laaksoharju and Wallin, 1997/ as a source for the brine water component. The stable isotope data ( $\delta^{18}\text{O} = -10.4$  to  $-8.9$  ‰;  $\delta^2\text{H} -60.2$  to  $-44.9$  ‰) from the deep saline groundwaters show significant deviation from MWL (Meteoric Water Line). Characteristics similar to these low temperature Precambrian granitic shield areas are shown for the deep Canadian brines /Frape et al, 1984; Frape and Fritz, 1987/. The deviation from MWL is ascribed to water/rock interaction during long periods of time. Saturation index calculations indicate equilibrium between the water and the rock forming minerals. An old age for the Brine is also suggested by the measured  $^{36}\text{Cl}$  values indicating a minimum residence time of 1.5 Ma for the Cl component /Laaksoharju and Wallin, 1997/. The origin may be unclear but the mean residence time for the groundwater is considerable.

### 5.3.2 Conclusions and assessment of uncertainties

The conclusion is that the complex groundwater evolution and patterns at Laxemar are a result of many factors such as: a) the closeness to Baltic Sea resulting in relative small hydrogeological driving forces which can preserve old water types from being flushed out, b) the changes in hydrogeology related to glaciation/deglaciation and land uplift, c) repeated Sea/lake water regressions/transgressions and d) organic or inorganic alteration of the groundwater caused by microbial processes or in situ water/rock interactions. The sampled groundwater reflects in various degrees modern or ancient water/rock interactions and mixing processes. This means that in order to understand the origin and evolution of the groundwater, the geology as well as past and present hydrogeology, has to be understood.

The modelled present-day groundwater conditions of the Laxemar site consist of a mixture in varying degrees of the following water types: Brine, Glacial, Marine and Meteoric waters. The location, depth and hydraulic properties of the rock determine the degree of groundwater mixing e.g. at KLX02 the saline interface can exist at larger depth than at the more coastal borehole KLX01. To a depth of 500–1000 m the dominating mixing portion is meteoric water. Close or under the Baltic Sea marine water of different origins dominates. Some of this water especially in association with the Sea bed sediments can have ongoing sulphate reduction. At depths of 800–1200 m a brackish-saline water consisting of proportions of glacial melt water occurs. Below this level and down to the 1800 m and below saline water contains more proportions of brine water of which the major portion has been stagnant for periods of time extending from 10000 to perhaps millions of years.

The performed evaluation indicated that the water composition is such that the representative samples can meet the SKB chemical stability criteria for Eh, pH, TDS, DOC, Colloids and Ca+Mg (see /Anderson et al, 2000/ and Table 5-35). The modelling of the target sample (KLX01:456–461m) reflecting the repository depth indicates that the sample can undergo considerable changes (from land uplift and changing climate) before some of the criteria is no longer met. In this modelling example the sample can have an addition of 75% precipitation water and 30% glacial meltwater.

**Table 5-35. The hydrochemical stability criteria defined by SKB which are valid for the representative samples from the Laxemar site. The chemical criteria are also met for the analysed properties and elements sampled at the target depths at KLX01 and KLX02. \* = Colloids where determined only from some deep samples at KLX02, \*\* = calculated value, N/A = not analysed.**

	Eh mV	pH (units)	TDS (g/l)	DOC (mg/l)	Colloids* (mg/l)	Ca+Mg (mg/l)
Criterion	<0	6–10	<100	<20	<0.5	>4
KLX01:456–461m	–308	8.2	3	1.4	N/A	241
KLX02:335–341m	–200 **	8.2	0.6	N/A	N/A	42

Many of the uncertainties associated with hydrochemistry are difficult to describe since there are no ‘undisturbed’ samples to provide a reference point. This difficulty can be partly compensated for by controlling (and modelling) those major disturbing influences on groundwater quality and hence to reduce uncertainties. For example:

- Collect data that reflect the spatial and temporal groundwater variations.
- Measure/model the input and output water volumes along different fractures/fracture zones in association with drilling and other borehole activities (i.e. DIS Drilling Impact Study).
- Measure the chemical variation during sampling which can indicate the ‘natural’ variability.
- Measure the direct influence of the spiked flushing water resulting from drilling.
- Measure/model the effect of transporting water from depth to the surface (e.g. to quantify the influence of in- and out-gassing processes on redox measurements).
- Use alternative models, sensitive analyses and independent models for during groundwater modelling.
- Comparison and integration between models.
- Use discrepancies between models to guide further modelling efforts.

The deep information in this exercise was limited to two boreholes KLX01 and KLX02. This makes interpolation between the observations uncertain. Minimum three deep boreholes should be available at a site. KLX02 can reflect local hydrogeological conditions rather than regional conditions, which may increase the uncertainty in the interpolations and evaluation. In addition important information from the evaluations such as: special isotopes, redox, colloid, microbe, gas and organic matter is missing in this test and therefore increase the uncertainties. The integration part between the different modelling approaches was limited due to the nature of the project but should always play a central part in the site evaluation. The tests performed in this report suggest that expert knowledge is needed in all parts of the modelling and evaluation processes.

## 5.4 Rock mechanics description

The rock mechanics model consists of two main parts, the stress model describing the load conditions and the rock mass property model, describing the rock quality, including deformability and strength parameters at a site. The combination of stress and mechanical properties at a certain location (place and depth) will determine the stability conditions for a future repository at this location.

### 5.4.1 In situ stress conditions

The model for the state of stress in the Laxemar domain is presented in Table 5-36 and Table 5-37. For the uncertainty span the domain is divided into two different depth levels because of the differences in general knowledge as well as site specific data at depth (see Sections 3.10.3 and 4.4.3). For the estimation of spatial variation the domain is divided into units regarded as deformation zone and the more intact rock mass units between them (Section 5.1).

**Table 5-36. Predicted in situ stress magnitudes in Laxemar domain.**

Parameter	$\sigma_1$	$\sigma_2$	$\sigma_3$
Mean stress magnitude, MPa	$0.055 \cdot z + 4.6$	$0.027 \cdot z$	$0.020 \cdot z + 0.6$
Uncertainty, 0–500 m	$\pm 25\%$	$\pm 25\%$	$\pm 25\%$
Uncertainty, 500–2000 m	$\pm 30\%$	$\pm 30\%$	$\pm 30\%$
Spatial variation, rock mass	$\pm 15\%$	$\pm 15\%$	$\pm 15\%$
Spatial variation, deformation zones	$\pm 50\%$	$\pm 50\%$	$\pm 50\%$

**Table 5-37. Predicted in situ stress orientations in Laxemar domain.**

Parameter	$\sigma_1$ , trend	$\sigma_1$ , dip	$\sigma_3$ , dip
Mean stress orientation	$150^\circ$	$0^\circ$	$0^\circ$
Uncertainty, 0–500 m d	$\pm 15^\circ$	$\pm 10^\circ$	$\pm 15\text{--}45^\circ$ *
Uncertainty, 500–2000 m	$\pm 20^\circ$	$\pm 10^\circ$	$\pm 10^\circ$
Spatial variation, rock mass	$\pm 15^\circ$	$\pm 15^\circ$	$\pm 15^\circ$
Spatial variation, deformation zones	$\pm 25^\circ$	$\pm 30^\circ$	$\pm 30^\circ$

\* At some level  $\sigma_2$  and  $\sigma_3$  may have similar magnitude and the dip can then be any.

#### **5.4.2 Mechanical properties of rock**

Table 5-38 presents the rock mechanical parameters predicted for the rock mass and the rock in the deformation zones, respectively. The given span represents the expected range for the mean of the parameters with a scale for the rock mass (including intact parts and fractures) in the order of 30x30x30 m. A local variation of the parameters around the mean should also be anticipated. The division of the Laxemar domain into two categories, depending on depth, should not be interpreted as an abrupt change. The division is simply done to describe the expected trends (depth-dependency) and the uncertainty differences with depth.

The different parameters used for rock mass characterization do not have any standard definition and it is important to consider this properly when comparing the values with others. How the parameters were defined here, and how they were selected, is described in Section 4.4.2.

#### **5.4.3 Overall assessment of uncertainties in the rock mechanics description**

The basis for the uncertainty assessment of the rock mechanics description is provided in Section 4.4.1 (state of stress) and in Section 4.4.4 (properties). This assessment has resulted in the uncertainty spans, confidence levels etc in the above descriptions. For the Laxemar project, the available mechanics data were much less than is expected to exist already after the Initial Site Investigation. This means that uncertainty spans had to be set larger and with less confidence than can be expected when producing the rock mechanics model at that stage.

**Table 5-38. Predicted rock mechanical properties in Laxemar domain. (For parameter definitions see Section 4.4.2. The uncertainty and confidence are discussed in Section 4.4.3.)**

Parameter	Rock Units 0–500 m	Rock Units 500–2000 m	Confidence	Comments
Uniaxial compressive strength, <i>intact rock</i> *	100–280 GPa	100–280 GPa	High	The span may be decreased with more data.
Elastic Modulus, rock mass*, (30x30x30 m)	40–55 GPa	50–65 GPa	Low	Depends on how minor fracture zones are treated.
Poisson's ratio, rock mass*	0.23–0.28	0.23–0.28	Medium	
Uniaxial strength, rock mass*	100–125 MPa	100–160 MPa	Low	Is related to the strength for intact rock. See text about definition. Depends on how minor fracture zones are treated.
Friction angle, rock mass**	40°–45°	40°–50°	Medium	Difficult to validate material models for large scale.
Cohesion, rock mass**	10–25 MPa	15–30 MPa	Low	See text about definition.
Parameter	Def. Zones 0–500 m	Def. Zones 500–2000 m	Confidence	Comments.
Uniaxial compressive strength*, <i>intact rock</i> inside deformation zones	100–280 GPa	100–280 GPa	Low	No laboratory tests available from zones. Weak rocks may be difficult to sample. Large spatial variation expected.
Elastic Modulus*, rock mass (fractures, intact rock and fracture filling, 30x30x30 m)	10–40	10–40	Low	Geological characterization uncertain. Variation between zones and within zones expected.
Poisson's ratio*, rock mass	0.20–0.26	0.20–0.26	Low	D:o
Uniaxial strength*, rock mass	55–75 MPa	60–85 MPa	Low	D:o
Friction angle**, rock mass	25°–35°	25°–40°	Low	D:o
Cohesion**, rock mass	5–15 MPa	5–20 MPa	Low	D:o See text about definition.

\* Confining stress 10 MPa.

\*\* Linear model between 10 and 20 MPa confining stress.



## **6 Lessons learned**

As stated in the introduction the intent of the project has been to explore whether available methodology for Site Descriptive Modelling is adequate and to identify potential needs for development and improvement in the methodology. The current chapter summarises lessons learnt in this respect.

### **6.1 Methodology**

This very report demonstrates that a Site Descriptive Model can be established for a real site following structured and discipline integrated procedures in accordance with the intentions presented in the general execution programme /SKB, 2001/. The projects primary objective is thus fulfilled. There are, however, several instances where methods and practices could be improved, primarily to enhance the speed and optimise the workload, but also at instances enhancing the quality of the work.

#### **6.1.1 Evaluation of primary data**

##### ***Geology***

When the project started, SKB routines for lineament evaluation, single hole interpretation and fracture statistics were still being developed. In fact, these routines have then been established, partly based on the experiences and suggestions made by participants in the Laxemar project.

The Laxemar Model Area as a whole has not been mapped in detail and, consequently, the surface geological information is of reconnaissance character. In particular, this is relevant for the Quaternary deposits, the distribution of which is only based on interpretation of aerial photographs. The lack of detailed surface information renders problem in the definition of well-characterised rock units and domains, as well as the correlation between the surface information and the information from the cored boreholes. The latter is also complicated by a somewhat loose bedrock nomenclature. However, these shortcomings will be avoided in the forthcoming site investigation phase, since a detailed mapping will be carried out, and the rock types and Quaternary deposits will be strictly characterised according to a modern nomenclature.

##### ***Hydrogeology***

There are also some observations made as regards the hydrogeological evaluation of primary data.

- There were some difficulties to compile all data available. As several hydraulic tests had been made as tests of methods or equipment, all data had not been properly reported and to relevant extent included in SICADA. It was time consuming to try to find relevant reports and data files as well as interpret the results. Some data are possibly still missing and some data can possibly be better evaluated. Furthermore, it may be quite relevant to run new tests in the boreholes with the new methods to get all measurements, in old and future boreholes on the 'same level'. These problems are likely to be much less severe during the site investigation phase where data collection and storage is subject to consistent Quality Assurance.



- Techniques for evaluating hydraulic tests against the geological single hole interpretation could be further developed. The criteria of a potential fracture zone along a borehole turned out to be different when old data was compared to what was suggested by the geological single hole interpretation. This caused some confusion. It is not obvious what criteria should be used in the single-hole analysis, but it should be a very clear definition in the beginning of the investigations. If the criterion changes, one has to update all databases with the stored potential fracture zones, as most likely it is a part of a parameter that is visualised in RVS for example.
- It is essential to visualise the single-hole measurement in a comprehensive way. This can be made in WellCad. However, the hydrogeological group had not the software, and there were some problems to get a proper overview of the data. This can however be improved quite easily by preparing standard designs for single-hole presentations in WellCad.
- The statistical treatment of data can be improved and made more efficient in such a way that a standard evaluation is 'streamlined' with standard plots and standard tables for presenting the analysis.

### **Hydrogeochemistry**

Observations made by the hydrogeochemistry evaluation of the primary data mainly concern the interaction between modelling and site investigation practices. The following is suggested:

- The modellers should play a more active role in the planning/executing of the field campaign. This could increase awareness of field/modelling difficulties.
- The risk of contamination is higher for a shallow fracture zone (longer exposure time for borehole activities) of high permeability than for a fracture zone at larger depths with low permeability /Gurban and Laaksoharju, 2002/.
- The groundwater disturbances can be modelled and the modelling can be verified if the water is analysed for drilling water when starting the water extraction and not when starting the sampling.
- The measure of representativity is often low Eh values rather than the volume injected/extracted from the fracture zone.
- The representative samples are not selected by the modeller but by the field personnel by applying an extensive analytical program for one or some samples. A larger data set of carefully analysed samples could give a larger choice but could also provide valuable information of the chemical variability and these samples could be used in alternative site models.
- There is a need for improved WellCad presentation of geological data to be used for hydrochemical modelling.

Generally it should also be noted that the hydrochemical depth information from only two deep boreholes add uncertainties in the modelling and interpretation work. At least three deep boreholes per site should be investigated with care.

## **Rock Mechanics**

The procedures outlined in the Rock Mechanics Site Descriptive Modelling Strategy /Andersson et al, 2002/ was found workable, but were not fully tested. The main reason for this limited effort was that most of the rock mechanics data anticipated during the site investigation, even its early phases, were not available at Laxemar. As regards data and data interpretations the following observations have been made by the rock mechanics team:

- Depending on the depths that are considered for the future repository (currently 400–700 m depth), measurement interpretation may need further development. The overcoring method has a limitation for high stress conditions. If stresses are high, microfracturing or core discing during overcoring may make measurements with this technique impossible. In the available database there are no data from overcoring showing a maximum stress level higher than 44 MPa. This means that there is little experience in stress measurements in very high stress conditions. In this project the stress estimations at depth was partly based on extrapolations from data at lower stress levels.
- The existing data from laboratory strength testing of intact rock show a large spread between samples, and also differences between laboratories. The possibility for test procedure explanations to the spread cannot be neglected. It is recommended that the testing methods used are scrutinised and that standard procedures are established such that the reliability of the data is assured.

### **6.1.2 Method for three-dimensional modelling**

#### ***Geological modelling***

Even if substantial earlier experience in geologic modelling existed prior to the start of the project, specific routines for the RVS supported geological modelling were not available. These were developed during the course of the project and the experiences gained are now considered when formulating routines to be used during the site investigation modelling.

#### ***Hydrogeological modelling***

The following observations have been gained from the hydrogeological modelling perspective.

- The interface with the RVS representation of the geological (and geometrical) model could be improved. A big problem from the beginning was to get the relevant intersections (secup-seclow) of the deterministic deformation zones as interpreted in RVS and as actual geological core mapped indications. This is essential for the comparison with the hydraulic data. One big reason was that the initial RVS version used could not handle deterministic deformation zones as 3D objects in a proper way. Another reason was that the hydrogeological team did not have a good way of transferring information between the geological and hydrogeological group. The hydrogeological group had little experience of RVS at that time, which is part of the reason, but a stricter tabulated format for the exchange of information would have been useful.
- There is a need to further ‘streamline’ statistical treatment of data also needed for the modelling.

- The analysis of properties for the DFN distributions can probably be improved. In particular, there was expressed concern on the reliability of estimated “power law exponents” resulting from trace map statistical analysis.
- The groundwater flow modelling was shown to be a crucial element in evaluating the data. Still the modelling had to have a limited scope as the software (DarcyTools, /Svensson et al, 2002a,b/) was under development and lacks several features in terms of post- and pre-processing as well as hydrogeological processes needed. For example is a routine missing that transfers the RVS geometry to a format suitable for DarcyTools. DarcyTools will be improved during 2002. The testing and calibration of the numerical model is time consuming and it is therefore important that the transfer of data to the numerical model are effective to get a ‘flying start’. There are several tools that could be used to make the testing and calibration of the model much more effective. Several realisations have to be tested and in a later stage of the site investigations there will be a large number of boreholes and a fairly large number of interference tests. This is not easily and effectively handled unless one has prepared good tools for it. There is also a question of how local conditioning should be made in an effective and correct way.
- It is also essential that the hydrogeologist and the hydrogeochemist can view, understand and comment the numerical model results. This can possibly be improved in the future by exporting the simulation results in a format that can be visualised in a separate postprocessor. The used visualisation software for hydrogeology and hydrogeochemistry (TecPlot) was not fully tested for that purpose.

### ***Hydrogeochemical modelling***

The hydrogeochemical modelling capability should include various approaches. For example, this includes modelling and interpretation based on expert knowledge, standard geochemical modelling, coupled hydrochemical and hydrogeological modelling and chemical descriptions by using only hydrogeological models. In developing the models various tests should be undertaken. Examples of such tests include:

- More tests of comparing, integrating and visualising results from different codes describing different groundwater properties.
- Tests of differences when applying different codes on identical data and how this will affect the understanding.
- Tests of how much uncertainties can be allowed before there is a risk of misunderstanding the site data.

### ***Rock Mechanical Modelling***

The procedures outlined in the Rock Mechanics Site Descriptive Modelling Strategy /Andersson et al, 2002/ was found workable, but were not fully tested (see above). Nevertheless, it was possible to produce motivated rock mechanics properties of the site even if uncertainty ranges are wide and confidence low. As regards potential development needs, the reader is referred to the concluding sections of the Rock Mechanics Site Descriptive Modelling Strategy report.

### **6.1.3 Traceability and Quality Assurance matter**

The project has strived for high traceability between measurement, data, primary evaluation and three-dimensional modelling. The strict routines for importing data from the acknowledged data sources (SICADA and GIS) has been followed, and data obtained outside these sources are documented. In addition, visualisation and data quality checks have been applied at many levels. Clearly, and despite the routines employed, occasional mistakes in data transfer (i.e. use old version data or use of 'corrupted' data) have been found in these quality checks. All found mistakes have been corrected.

It has also been possible to maintain the intention of clearly keeping track of the justification for geometric structures and associated properties. Specifically, the intention has been to first assess the information within each discipline, document the findings, and then compare the results with findings made in other disciplines. While these procedures produce significant documentation, it is still judged essential to maintain this strict principle of traceability.

For the future it is evident that proper procedures for data quality assessment and quality control in data transfer can always be improved. Still, the actual experiences also point to the fact that every user of information need to take some provision in checking adequacy in information obtained. The extensive use of visualisation tools enhances such possibilities. For example, three dimensional visualisation of the HCD in the hydrogeologic model allows quick visual inspection for controlling if the HCD geometry as intended coincides with the Deformation Zone geometry of the Geological Model.

### **6.1.4 Describing uncertainties**

Considerable efforts have been made in assessing and describing uncertainties in the descriptions. There is, however, room for further improvement. In particular:

- Structures for reporting and describing uncertainties were developed during the course of the project. Had these structures been well established from the beginning, more consideration of uncertainties might have developed from the onset of the analysis.
- The project did not fully use the information in the feedback loop from e.g. hydrogeology to geology. It seems likely that important observations could be made on e.g. the plausibility of the Base Model and the Alternative Model using such information. A more streamlined assessment of the primary data, see below, would allow more time for this potentially essential cross-evaluation of information.
- The level of information at the early stages of the site investigation clearly warrants the need to produce alternative descriptions. Still, in practice, maintaining several alternatives leads to a substantially increased workload. Furthermore, the distinction between alternative and updated version is not always easy to uphold. Insights gained in producing the first 'alternative' are hard to put aside when developing additional ones. Careful planning and a project commitment to produce alternatives is required. Furthermore, it should be understood that it not necessary for different alternatives to be equally plausible.

## 6.2 Working Procedures

The work has been conducted by a project group with representatives from the main disciplines, geology, hydrogeology, hydrogeochemistry and rock mechanics. The different experts assessed and evaluated data and explored different modelling options. The full project group also met at regular intervals to discuss on a detailed level the current progress and ideas of the different modelling teams. A reference group also followed the progress of work.

Overall the organisational set up of the work is judged to be successful. The regular project team meetings enabled continuous cross discipline information flow and feedback. The achieved integration was stimulating and enhanced multidisciplinary insights hard to achieve by any other means.

Having said this, interdisciplinary Site Descriptive Modelling is a huge undertaking with lots of necessary subanalyses and issues. Care is needed to make the integrating project team meetings fruitful information and thought exchange occasions. Attention on the following seems motivated:

- The size of the project group was eight persons. This was still manageable, although discussions on important ‘details’ may be cumbersome for participants of very different competence. However, increasing the group membership above the current number may have a detrimental impact on the usefulness of the group interaction and information flow.
- The evaluation is a learning process – and takes time. There is a need to get acquainted with site and data. For the Laxemar project much effort and time was also spent on tracking data and on the evaluation of primary information. In comparison more of the available time could have been spent on the three-dimensional modelling. This meant that concrete multidisciplinary feedback only came late in the project. Several routines for data interpretation also had to be developed during the course of the project. Clearly, streamlining the routines for primary data interpretation would make it easier to focus on integration and site modelling.
- The three dimensional interpretation and visualisation techniques were essential both for the geometric modelling and for communication of results within the group. While the currently used software may have some shortcomings (see below), the technique as such has proven its value and efforts should be spent in spreading its use to a wide range of users.

Finally, a substantial amount of documentation is produced when aiming for traceability. Careful documentation also takes time. While full documentation is essential for the end products produced during the Site Investigation (e.g. after completion of the Initial Site Investigation and after completion of the Complete Site Investigation), less ambitious documentation may be contemplated for the intermediate versions of the models. On the other hand, the current report provides a structure, which should make future documentation efforts less cumbersome. Also the project Web-site for storing documents and other information greatly enhanced information exchange within the project. Use of a flexible, project controlled, Web-site is recommended also for future project.

## **6.3 The central SKB databases and software**

It has been possible to use the central SKB databases and software (i.e. GIS, SICADA and RVS) in accordance with the intended uses. However, many difficulties have been revealed. Some are already adjusted, whereas others may be worth additional consideration.

### **6.3.1 GIS**

The GIS database was generally found useful. Identified points for further improvement include:

- The structure of the data and the correct labels for the information was not always easy to find.
- Some data was not in GIS format. This caused some problems in the beginning when maps were to be made.
- There are many potential users of the GIS data base. Efforts should be spent on making it more accessible to many users.
- Some problems were encountered in retrieving the correct versions of the GIS-information. This is evidently not acceptable and efforts to improve the version handling system are needed.

### **6.3.2 Extracting data from SICADA**

In essence the means of importing data from the SICADA-database has worked according to plans. Still, some problems are noted, which could be considered when deciding for updates of the database and the procedures:

- Initially there was some problem with the deliveries of the requested data. Data were delivered fast but some data was missing. This has been discussed and new routines for extracting data from SICADA are now being implemented. The structure of the hydrogeological data in SICADA will also be improved.
- The extraction of hydrochemical data revealed that some of the data lacked coordinates and unique sample numbers. Important values such as Ion Charge Balance (ICB) and TDS (total dissolved solids) are calculated in SICADA but the values cannot be extracted with the current SICADA interface. These values have therefore to be recalculated when using the data. Values under the detection limit are currently reported negative e.g. -1 in SICADA, but the values should be reported as <1 in order to avoid confusion in the numerical models or with negative values such as  $\delta^{18}\text{O}$  isotopes and Eh values. In this modelling half of the detection limit was used so if the detection limit was 1 the value 0.5 was used in the modelling.

### **6.3.3 WellCad**

The borehole visualisation system (WellCad) appears to be a working and useful tool. However, for optimal use it requires trained users. In this context it is a need to assess the range of different people who may be potential users of the WellCad information. Relying on very few trained operators and few licenses, may not be sufficient.

WellCad pictures based on core logging gives good possibilities to study the geological information. The large information can create problems to visualise everything in an optimal way. The choice of colours can cause confusion, e.g. to distinguish different alteration types such as oxidized (red), tectonised (darker red) and weathered (orange), as well as fine-grained granite (red) from “Småland granite” (dark orange). The column showing rock structures has one colour for homogenous and one for schistose, and no possibility of showing gradual changes (weak to strong foliation etc) is indicated.

#### **6.3.4 RVS**

As already stated, three-dimensional CAD-based visualisation tools are essential for the site descriptive modelling. There are several potential users, and again, knowledge in using information from the 3D systems needs to be comparatively widely spread.

The currently used RVS software was capable of handling the information from Laxemar, and with the significantly improved functionality in version 3.0, RVS, can be used for purpose. This is particularly true for handling and visualisation of borehole information. Still, there are several shortcomings with RVS, which should be considered. For example:

- RVS is weak in handling surface information. Topography and GIS data cannot be imported in an acceptable manner.
- There is a need for efficient exporting possibilities from RVS to e.g. numerical codes etc.

Nevertheless, the principle methodology of working with 3D CAD based software is now well established.

## References

- Alley W M (ed), 1993.** Regional groundwater quality. ISBN 0-442-00937-2. Van Nostrand Reinhold, New York, USA, pp 634.
- Amadei A, Stephansson O, 1997.** Rock stress and its measurement, Chapman and Hall, London, ISBN 0412447002.
- Andersson J, Ström A, Svemar C, Almén K-E, Ericsson L O, 2000.** What requirements does the KBS-3 repository make on the host rock? Geoscientific suitability indicators and criteria for siting and site evaluation. SKB TR 00-12, Svensk Kärnbränslehantering AB.
- Andersson J, Christiansson R, Hudson J A, 2002.** Site Investigations Strategy for Development of a Rock Mechanics Site Descriptive Model, SKB TR 02-01, Svensk Kärnbränslehantering AB, Stockholm.
- Axelsson C, Jonsson E-K, Geier J, Dershowitz W, 1990.** Discrete fracture modelling. SKB PR 25-89-21, Svensk Kärnbränslehantering AB, Stockholm, Sweden.
- Banwart S, Tullborg E-L, Pedersen K, Gustafsson E, Laaksoharju M, Nilsson A-C, Wallin B, Wikberg P, 1996.** Organic carbon oxidation induced by large-scale shallow water intrusion into a vertical fracture zone at the Äspö Hard Rock Laboratory (Sweden). *Journal of Contaminant Hydrology* 21 (1996), Elsevier Science B. V., pp115–125.
- Bein A, Arad A, 1992.** Formation of saline groundwaters in the Baltic region through freezing of seawater during glacial periods. *Journal of Hydrology*, 140, Elsevier Science B.V., pp75–87.
- Bergman T, Isaksson H, Johansson R, Lindén A H, Lindgren J, Lindroos H, Rudmark L, Wahlgren C-H, 1998.** Förstudie Oskarshamn. Jordarter, bergarter och deformationszoner. SKB R-98-56, Svensk Kärnbränslehantering AB.
- Bergman T, Follin S, Isaksson H, Johansson R, Lindén A H, Lindroos H, Rudmark L, Stanfors R, Wahlgren C-H, 1999.** Förstudie Oskarshamn. Erfarenheter från geovetenskapliga undersökningar i nordöstra delen av kommunen. SKB R-99-04, Svensk Kärnbränslehantering AB.
- Bergman T, Isaksson H, Rudmark L, Stanfors R, Wahlgren C-H, Johansson R, 2000.** Förstudie Oskarshamn. Kompletterande geologiska studier. SKB R-00-45, Svensk Kärnbränslehantering AB.
- Bergman B, Juhlin C, Palm H, 2001.** Reflektionsseismiska studier inom Laxemarområdet. SKB R-01-07, Svensk Kärnbränslehantering AB.
- Beunk F F, Page L M, 2001.** Structural evolution of the accretional continental margin of the Paleoproterozoic Svecofennian orogen in southern Sweden. *Tectonophysics* 339, 67–92.
- Björck S, 1995.** A review of the history of the Baltic Sea, 13.0–8.0 Ka BP. In: *Quaternary International*, Vol. 27, Elsevier Science Ltd., 1040-6182/95, pp19–40



- Carsson L, Gustafson G, 1997.** Provpumpning som geohydrologisk undersökningsmetodik. Chalmers Tekniska Högskola, Geologiska Inst., Publ C62.
- Carlsten S, 1993.** Drilling KLX02 – Phase 2. Lilla Laxemar, Oskarshamn. Borehole radar measurements in KLX02. SKB AR 93-43, Svensk Kärnbränslehantering AB.
- Carlsten S, 1994.** Drilling KLX02 – Phase 2. Lilla Laxemar, Oskarshamn. Correlation of radar reflectors between boreholes KLX01 and KLX02. SKB AR 94-28, Svensk Kärnbränslehantering AB.
- Carlsten S, Strähle A, Ludvigson J-E, 2001.** Conductive fracture mapping. A study on the correlation between borehole TV- and radar images and difference flow logging results in borehole KLX02. SKB R-01-48, Svensk Kärnbränslehantering AB.
- Cooper H H Jr, Jacob C E, 1946.** A generalized graphical method for evaluating formation constants and summarizing well field history. Trans. Am. Geophys. Un., 27, 526–534.
- Dansgaard W, 1964.** Stable isotopes in precipitation. In: Tellus 16, pp436–468.
- Dershowitz W, Lee G, Geier J, Foxford T, LaPointe P, Thomas A, 1995.** FracMan, interactive discrete feature data analysis, geometric modeling and exploration simulation. User documentation, version 2.5. Golder Associates Inc. Seattle, Washington.
- Earlougher, R C, 1977.** Advances in well test analysis. SPE monograph Volume 5, Henry L, Doherty Series.
- Ekman M, 1996.** A consistent map of the postglacial uplift of Fennoscandia. Terra nova 8, 158–165.
- Ekman L, 2001.** Project Deep Drilling KLX02, Phase 2. Methods, scope summary and results, Summary report, SKB TR-01-11, Svensk Kärnbränslehantering AB.
- Ericsson L O, 1987.** Fracture mapping on outcrops. Äspölaboratoriet. SKB PR 25-87-05, Svensk Kärnbränslehantering AB.
- Ericsson L, Johansson R, Thunehed H, Triumf C-A, 1998.** Metodtester ytgeofysik, 1996. Bestämning av berggrundens bulkresistivitet och djupet till salint grundvatten med halvregional resistivitetsmätning, elektrisk sondering samt transient elektromagnetisk sondering. SKB PR D-98-01, Svensk Kärnbränslehantering AB.
- Follin S, 1993.** Djupborrning KLX02 -Etapp 1, Lilla Laxemar, Oskarshamns kommun, Evaluation of the hydraulic testing of KLX02. SKB AR 94-21, Svensk Kärnbränslehantering AB.
- Follin S, 1996.** Djupborrning KLX02 -Etapp 2, Lilla Laxemar, Oskarshamns kommun, Interpretation of the hydraulic testing of KLX02. SKB Project Report U-96-32, Svensk Kärnbränslehantering AB.
- Follin S, Årebäck M, Axelsson C-A, Stigsson M, Jacks G, 1998.** Förstudie Oskarshamn, Grundvattnets rörelse, kemi och långsiktiga förändringar, R-98-55, Svensk Kärnbränslehantering AB.
- Follin S, Askling P, Carlsten S, Strähle A, 2000.** Smålandgranitens vatten-genomsläpplighet, Jämförelse av borrhålsdata från Äspö, Laxemar och Klipperås, SKB R-00-46, Svensk Kärnbränslehantering AB.

- Follin S, Svensson U, 2002.** Groundwater flow simulations in support of the Local Scale Hydrogeologic Description developed within the Laxemar Methodology Test Project, SKB R-02-29, Svensk Kärnbränslehantering AB.
- Frape S K, Fritz P, McNutt R H, 1984.** The role of water/rock interaction in the chemical evolution of groundwaters from the Canadian shield. In: *Geochim. et Cosmochim. Acta* 48, pp1617–1627.
- Frape S K, Fritz P, 1987.** Geochemical trends for groundwaters from the Canadian shield. In: Fritz P and Frappe S K, *Saline water and gases in crystalline rocks*. Geol. Assoc. of Canada Spec. Pap., 33:19–38.
- Freeze R A, Cherry J A, 1979.** *Groundwater*, (Prentice-Hall, Inc.), London.
- Glen W E, P H Nelson, 1979.** Borehole logging techniques applied to base metal ore deposits, in *Geophysics and Geochemistry in the Search for Metallic Ores* (Hood ed.), Geological Survey of Canada, Economic Geology Report 31, pp. 273–294
- Gregersen S, Korhonen H, Husebye E S, 1991.** Fennoscandian dynamics: Present-day earthquake activity. *Tectonophysics* 189, 333–344.
- Gregersen S, 1992.** Crustal stress regime in Fennoscandia from focal mechanisms. *Journal of Geophysical Research* 97, B8, 1, 1821–1827.
- Gurban I, Laaksoharju M, Ledoux E, Made B, Salignac A L, 1998.** Indications of uranium transport around the reactor zone at Bagombé (Oklo). SKB TR-98-06, Svensk Kärnbränslehantering AB.
- Gurban I, Laaksoharju M, 2002.** Drilling Impact Study (DIS); Evaluation of the influences of drilling, in special on the changes on groundwater parameters. SKB report in progress.
- Gustafsson G, Stanfors R, Wikberg P, 1989.** Swedish Hard Rock Laboratory. First evaluation of 1988 year pre-investigations and description of the target area, the island of Äspö. SKB TR 89-16, Svensk Kärnbränslehantering AB.
- Hakami E, Hakami H, Cosgrove J, 2002.** Strategy for a Rock Mechanics Site Descriptive Model - Development and testing of an Approach to modelling the State of Stress. SKB R 02-03, Svensk Kärnbränslehantering AB.
- Hermansson J, Stigsson M, Wei L, 1998.** A discrete fracture network model of the Äspö Zedex tunnel section. SKB HRL-98-29, Svensk Kärnbränslehantering AB.
- Hoek E, Brown E T, 1980.** *Underground Excavation in Rock*. The Institute of Mining and Metallurgy, London, 527 p.
- Holmlund P, 1993.** Den senaste istiden i Skandinavien. En modellering av Weichselisen. SKI Teknisk Rapport 93:44, Swedish Nuclear Power Inspectorate, Stockholm, Sweden.
- Hudson (ed), 2002.** Strategy for a Rock Mechanics Site Descriptive Model. A Test Case based on data from the Äspö HRL, SKB R-02-04, Svensk Kärnbränslehantering AB.
- Johansson L, Johansson Å, 1990.** Isotope geochemistry and age relationships of mafic intrusions along the Protogine Zone, southern Sweden. *Precambrian Research* 48, 395–414.

- Kornfält K-A, Wikman H, 1987a.** Description of the map of solid rocks around Simpevarp. SKB PR 25-87-02, Svensk Kärnbränslehantering AB.
- Kornfält K-A, Wikman H, 1987b.** Description to the map (No 4) of solid rocks of 3 small areas around Simpevarp. SKB PR 25-87-02a, Svensk Kärnbränslehantering AB.
- Kornfält K-A, Persson P-O, Wikman H, 1997.** Granitoids from the Äspö area, south-eastern Sweden – geochemical and geochronological data. GFF 119, 109–114.
- Kresten P, Chyssler J, 1976.** The Götömar massif in south-eastern Sweden: A reconnaissance survey. Geologiska Föreningens i Stockholm Förhandlingar 98, 155–161.
- Kristiansson J, 1986.** The ice recession in the south-eastern part of Sweden. Kvärtärgeologiska institutionen, Stockholms universitet. Report 7.
- Laaksoharju M, Skärman C, 1995.** Groundwater sampling and chemical characterisation of the HRL tunnel at Äspö, Sweden. SKB PR 25-95-29, Svensk Kärnbränslehantering AB.
- Laaksoharju M, Smellie J, Nilsson A-C, Skärman C, 1995a.** Groundwater sampling and chemical characterisation of the Laxemar deep borehole KLX02. SKB TR 95-05, Svensk Kärnbränslehantering AB.
- Laaksoharju M (ed), Gustafson G, Pedersen K, Rhén I, Skärman C, Tullborg E-L, Wallin B, Wikberg P, 1995b.** Sulphate reduction in the Äspö HRL tunnel. SKB TR 95-25, Svensk Kärnbränslehantering AB.
- Laaksoharju M, Wallin B (eds), 1997.** Evolution of the groundwater chemistry at the Äspö Hard Rock Laboratory. Proceedings of the second Äspö International Geochemistry Workshop, June 6–7, 1995. SKB International Co-operation Report ISRN SKB-ICR-91/04-SE. ISSN 1104-3210, Stockholm, Sweden.
- Laaksoharju M, Gurban I, Skärman C, 1998.** Summary of the hydrochemical conditions at Aberg, Beberg and Ceberg. SKB TR 98-03, Svensk Kärnbränslehantering AB.
- Laaksoharju M, Gurban I, Andersson C, 1999a.** Indications of the origin and evolution of the groundwater at Palmottu. The Palmottu Natural Analogue Project. SKB TR 99-03, Svensk Kärnbränslehantering AB.
- Laaksoharju M, Skärman C, Skärman E, 1999b.** Multivariate Mixing and Mass-balance (M3) calculations, a new tool for decoding hydrogeochemical information. Applied Geochemistry Vol. 14, #7, 1999, Elsevier Science Ltd., pp861–871.
- Laaksoharju M, Tullborg E-L, Wikberg P, Wallin B, Smellie J, 1999c.** Hydrogeochemical conditions and evolution at Äspö HRL, Sweden. Applied Geochemistry Vol. 14, #7, 1999, Elsevier Science Ltd., pp835–859.
- Laaksoharju M, 1999d.** Groundwater Characterisation and Modelling: Problems, Facts and Possibilities. Dissertation TRITA-AMI-PHD 1031; ISSN 1400-1284; ISRN KTH/AMI/PHD 1031-SE; ISBN 91-7170-. Royal Institute of Technology, Stockholm, Sweden. Also as SKB TR-99-42, Svensk Kärnbränslehantering AB.
- Laaksoharju M, Gurban I, 2002.** Sampling of surface water and shallow groundwater at Laxemar: Possible indicators for interaction between deep groundwater in contact with the Biosphere. SKB report in progress.

- Larson S Å, Tullborg E-L, 1993.** Tectonic regimes in the Baltic Shield during the last 1200 Ma – A review. SKB TR 94-05, Svensk Kärnbränslehantering AB.
- Larson S Å, Tullborg E-L, Cederbom C, Ståberg J-A, 1999.** Sveconorwegian and Caledonian foreland basins in the Baltic Shield revealed by fission-track thermochronology. *Terra Nova* 11, 210–215.
- Larsson-McCann S, Karsson A, Nord M, Sjögren J, Johansson L, Ivarsson M, Kindell S, 2002.** # Compilation of existing meteorological, hydrological and oceanographic data. Oskarshamn (tentative title), SKB TR xxxxx. Svensk Kärnbränslehantering AB.
- LaPointe P, Wallmann P, Follin S, 1995.** Estimation of effective block conductivities based on discrete network analyses using data from the Äspö site, SKB TR-95-15, Svensk Kärnbränslehantering AB.
- LaPointe P, Cladouhos T, Follin S, 1999.** Calculation of displacements on fractures intersecting canisters induced by earthquakes: Aberg, Beberg and Ceberg examples. SKB TR-99-03, Svensk Kärnbränslehantering AB.
- LaPointe P, Cladouhos T, Outters N, Follin S, 2000a.** Evaluation of the conservativeness of the methodology for estimating earthquake-induced movements of fractures intersecting canisters. SKB TR-00-08, Svensk Kärnbränslehantering AB.
- LaPointe P, Burago A, Lee K, Dershowitz B, 2000b.** GeoFractal: Geostatistical and Fractal Analysis for Spatial Data. User manual, version 1.0. FracMan Technology Group, Golder Associates.
- LaPointe P, Cladouhos T, Follin S, 2002.** A methodology to estimate possible damage to high-level nuclear waste repositories due to future earthquakes. Accepted for publication by *Bulletin of the Seismological Society of America*.
- Lidmar-Bergström K, 1991.** Phanerozoic tectonics in southern Sweden. *Zeitschrift für Geomorphologie N.F.* 82, 1–16.
- Lindborg T, Kautsky U, 2000.** Variabler och parametrar för att beskriva ytnära ekosystem vid platsundersökningar. SKB R-00-19. Svensk Kärnbränslehantering AB.
- Ljunggren C, Klasson H, 1997.** Drilling KLX02 – Phase 2 Lilla Laxemar Oskarshamn – Deep hydraulic fracturing Rock stress measurements in Borehole KLX02, Laxemar. SKB Project Report U-97-27, Svensk Kärnbränslehantering AB.
- Ludvigson J-E, Hansson K, Rouhiainen P, 2001.** Methodology study of Posiva Difference Flow Meter in borehole KLX02 at Laxemar, SKB R-01-52, Svensk Kärnbränslehantering AB.
- Maddock R H, Hailwood E A, Rhodes E J, Muir Wood R, 1993.** Direct fault dating trials at the Äspö Hard Rock Laboratory. SKB TR 93-24, Svensk Kärnbränslehantering AB.
- Mansfeld J, 1996.** Geological, geochemical and geochronological evidence for a new Paleoproterozoic terrane in southeastern Sweden. *Precambrian Research* 77, 91–103.
- Martin C D, Christiansson R, Söderhäll J, 2001.** Rock stability considerations for siting and constructing a KBS-3 repository. Based on experiences from Äspö HRL, AECL's URL, tunnelling and mining. SKB TR-01-38, Svensk Kärnbränslehantering AB.

- Mazurek M, Bossart P, Eliasson T, 1996.** Classification and characterization of water-conducting features at Äspö: Results of investigations on the outcrop scale. SKB ICR 97-01, Svensk Kärnbränslehantering AB.
- McDowell P W, 1990.** The determination of the dynamic elastic modulus of rock masses by geophysical methods, in *Field Testing in Engineering Geology*, (Bell, Culshaw, Cripps & Coeffy eds.), Engineering Special Publication No. 6, Geological Society, London, U.K, pp. 267–274.
- Milnes A G, Gee D G, 1992.** Bedrock stability in southeastern Sweden. Evidence from fracturing in the ordovician limestones of northern Öland. SKB TR 92-23, Svensk Kärnbränslehantering AB.
- Milnes A G, Gee D G, Lund C-E, 1998.** Crustal structure and regional tectonics of SE Sweden and the Baltic Sea. SKB TR 98-21, Svensk Kärnbränslehantering AB.
- Muir-Wood R, 1993.** A review of the seismotectonics of Sweden. SKB TR 93-13, Svensk Kärnbränslehantering AB.
- Müller B, Zoback M L, Fuchs K, Mastin L, Gregersen S, Pavoni N, Stephansson O, Ljunggren C, 1992.** Regional Patterns of Tectonic Stress in Europe. *Journal of Geophysical Research*, 97, No. B8, 11, 783–803.
- Munier R, 1989.** Brittle tectonics on Äspö, SE Sweden. SKB PR 25-89-15, Svensk Kärnbränslehantering AB.
- Munier R, 1993.** Drilling KLX02 – Phase 2. Lilla Laxemar, Oskarshamn. Description of geological structures in and near boreholes KLX02 and KLX01, Laxemar. SKB AR 94-23, Svensk Kärnbränslehantering AB.
- Munier R, 1995.** Studies of geological structures at Äspö. Comprehensive summary of results. SKB PR 25-95-21, Svensk Kärnbränslehantering AB.
- Munier R, Hermanson J, 2001.** Metodik för geometrisk modellering. Presentation och administration av platsbeskrivande modeller (In Swedish: Methodology for geometrical modelling. Presentation and administration of site descriptive models). SKB R-01-15, Svensk Kärnbränslehantering AB.
- Mörner N-A, 1989.** Postglacial faults and fractures on Äspö. SKB PR 25-89-24, Svensk Kärnbränslehantering AB.
- Nilsson L, 1988.** Hydraulic tests, pumping tests at Laxemar. SKB PR 25-87-11b, Svensk Kärnbränslehantering AB.
- Nilsson L, 1989.** Hydraulic tests at Äspö and Laxemar. SKB PR 25-88-14, Svensk Kärnbränslehantering AB.
- Niva B, Gabriel G, 1988.** Borehole radar measurements at Äspö and Laxemar – Boreholes KAS02, KAS03, KAS04, KLX01, HAS02, HAS03 and HAV07. SKB PR 25-88-03, Svensk Kärnbränslehantering AB.
- Niva B, 1991.** Testmätning med UCM-flödessond. SKB AR 92-02, Svensk Kärnbränslehantering AB.
- Nyberg G, Jönsson S, Wass E, 2001.** Äspö Hard Rock Laboratory, Hydro monitoring program, Report for 2000. SKB IPR-01-29, Svensk Kärnbränslehantering AB.

- Olsson, O (ed), 1992.** Site Characterization and Validation – Final Report. Stripa 92-22, Svensk Kärnbränslehantering AB.
- Parkhurst D L, Thorstenson D C, Plummer L N, 1980.** PREEQE – A computer program for geochemical calculations: U.S. Geological Survey Water Resources Investigation Report 80-96, pp210.
- Pedersen K, Karlsson F, 1995.** Investigation of subterranean bacteria – Their importance for performance assessment of radioactive waste disposal. In: SKB TR 95-10, Svensk Kärnbränslehantering AB.
- Puigdomenech I (ed), 2001.** Hydrochemical Stability of Groundwater Surrounding a Spent Nuclear Fuel Repository in a 100,000 year perspective. SKB TR-01-28, Svensk Kärnbränslehantering AB.
- Ratigan J L, 1992.** The use of fracture reopening pressure in hydraulic fracturing stress measurements. *Rock Mech Rock Engng*, 25, 225–36.
- Rhén I, Forsmark T, Nilsson L, 1991,** Hydraulic tests on Äspö, Bockholmen and Laxemar 1990 in KAS 09, KAS 11-14, HAS 18-20, KBH 01-02 ang KLX01 Evaluation. SKB PR 25-91-01, Svensk Kärnbränslehantering AB.
- Rhén I, Bäckblom G, Gustafson G, Stanfors R, Wikberg P, 1997.** Äspö HRL – Geoscientific evaluation 1997/2. Results from pre-investigations and detailed site characterization. Summary report. SKB TR 97-03, Svensk Kärnbränslehantering AB.
- Rhén I, Forsmark T, 2000.** Äspö Hard Rock Laboratory, High-permeability features (HPF). SKB IPR-00-02, Svensk Kärnbränslehantering AB.
- Rhen I, Smellie J, (eds), 2002.** Comparison and summary of TASK#5. SKB-IC report in preparation.
- Rouhiainen P, 2000.** Äspö Hard Rock Laboratory Difference flow measurements in borehole KLX02 at Laxemar, SKB IPR-01-06. Svensk Kärnbränslehantering AB.
- Rutqvist J, Tsang C-F, Stephansson O, 2000.** Uncertainty in the maximum principal stress estimated from hydraulic fracturing measurements due to the presence of the induced fracture. *Int. J. of Rock Mechanics and Mining Sciences*, 37, 107–120.
- Rydström H, Gereben L, 1989.** Seismic refraction survey on Äspö and Hålö. SKB PR 25-89-18, Svensk Kärnbränslehantering AB.
- Röshoff K, Lanaro F, Jing L, 2002.** Strategy for a Rock Mechanics Site Descriptive Model – Development and testing of the Empirical Approach, SKB R 02-01, Svensk Kärnbränslehantering AB.
- SKB, 1990.** Granskning av Nils-Axels Mörnars arbete avseende postglaciala strukturer på Äspö. SKB AR 90-18, Svensk Kärnbränslehantering AB.
- SKB, 1992.** Passage through water-bearing fracture zones, compilation of technical notes, passage through fracture zone NE-1. Hydrogeology and groundwater chemistry, SKB PR 25-92-18c, Svensk Kärnbränslehantering AB.
- SKB, 1999.** SR 97 – Post-closure safety. Deep repository for spent nuclear fuel. Main Report (Volumes I and II). Svensk Kärnbränslehantering AB.

- SKB, 2000.** Geoscientific programme for investigation and evaluation of sites for the deep repository. SKB TR 00-20, Svensk Kärnbränslehantering AB.
- SKB, 2001.** Site investigations: Characterisation methods and general execution programme, SKB TR 01-29, Svensk Kärnbränslehantering AB.
- Slunga R, Norrman P, Glans A-C, 1984.** Baltic shield seismicity, the results of a regional network. Geophysical research letters 11, 1247–1250.
- Slunga R, 1989.** Analysis of the earthquake mechanisms in the Norrbotten area. In Bäckblom & Stanfors (eds), Interdisciplinary study of post-glacial faulting in the Lansjärv area northern Sweden. 1986–1988. SKB TR 89-31, Svensk Kärnbränslehantering AB.
- Slunga R, Nordgren L, 1990.** Earthquake measurements in southern Sweden APR 1 1987 – NOV 30 1988. SKB AR 90-19, Svensk Kärnbränslehantering AB.
- Smellie J, Laaksoharju M, 1992.** The Äspö hard rock laboratory: final evaluation of the hydrogeochemical pre-investigations in relation to existing geologic and hydraulic conditions. SKB TR 92-31, Svensk Kärnbränslehantering AB.
- Smellie J, Karlsson F, 1996.** A reappraisal of some Cigar-Lake issues of importance to performance assessment. SKB TR-96-08, Svensk Kärnbränslehantering AB.
- Smellie et al, 2002.** Hydrochemistry, Guidelines for evaluation and modelling. Draft SKB report, Svensk Kärnbränslehantering AB.
- Stanfors R, 1988.** SKB Hard Rock Laboratory. Geological borehole description KAS02, KAS03, KAS04, KLX01. SKB PR 25-88-18, Svensk Kärnbränslehantering AB.
- Stanfors R, 1995.** Drilling KLX02 – phase 2 Lilla Laxemar, Oskarshamn. Brief geological description of the cored borehole KLX02. SKB AR 95-37, Svensk Kärnbränslehantering AB.
- Stanfors R, Erlström M, Markström I, 1997.** Äspö HRL – Geoscientific evaluation 1997/1. Overview of site characterisation 1986–1995. SKB TR 97-02, Svensk Kärnbränslehantering AB.
- Stanfors R, Larsson H, 1998.** Förstudie Oskarshamn. Simpevarpshalvön – Sammanställning av befintlig geoinformation. SKB AR L-98-24, Svensk Kärnbränslehantering AB.
- Staub I, Fredriksson A, Outters N, 2002.** Strategy for a Rock Mechanics Site Descriptive Model – Development and testing of the Theoretical Approach SKB R-02-02, Svensk Kärnbränslehantering AB.
- Stenberg L, Sehlstedt S, 1989.** Geophysical profile measurements on interpreted regional aeromagnetic lineaments in the Simpevarp area. SKB PR 25-89-13, Svensk Kärnbränslehantering AB.
- Stephansson O, Dahlström L-O, Bergström K, Sarkka P, Vitinen A, Myrvang A, Fjeld O, Hansen T H, 1987.** Fennoscandian Rock Stress Database – FRSDDB. Research report TULEA 1987:06, Luleå University of Technology, Luleå.
- Stephens M B, Wahlgren C-H, 1996.** Post-1.85 Ga tectonic evolution of the Svecokarelian orogen with special reference to central and SE Sweden. GFF 118, Jubilee Issue, A26–27.

**Stigsson M, Outters N, Hermanson, J, 2000.** Prototype repository – Hydraulic DFN model n2. Final draft. SKB report, Svensk Kärnbränslehantering AB.

**Strähle A, 2001.** Definition och beskrivning av parametrar för geologisk, geofysisk och bergmekanisk kartering av berg. SKB R-01-19, Svensk Kärnbränslehantering AB.

**Strömberg B, 1989.** Late Weichselian deglaciation and clay varve chronology in east-central Sweden. Sveriges geologiska undersökning Ca 73.

**Svensson U, 1987.** Hydrological conditions in the Simpevarp area. SKB PR-25-87-09, Svensk Kärnbränslehantering AB.

**Svensson U, 1996.** SKB Palaeohydrogeological programme. Regional groundwater flow due to advancing and retreating glacier-scoping calculations. In: SKB Project Report U 96-35, Svensk Kärnbränslehantering AB.

**Svensson U, 1997.** A regional analysis of groundwater flow and salinity distribution in the Äspö area. SKB TR 97-09. Svensk Kärnbränslehantering AB.

**Svensson U, 2001.** Äspö Hard Rock Laboratory, Prototype Repository, Groundwater flow, pressure and salinity distributions around the Prototype Repository. Continuum model No 1, SKB IPR-01-40, Svensk Kärnbränslehantering AB.

**Svensson U, Kuylenstierna H-O, Ferry M, 2002a** (in prep). DarcyTools, Software description and documentation, Version 1.0 (Tentative title), SKB XXX-YY-YY.

**Svensson U, Kuylenstierna H-O, Ferry M, 2002b** (in prep). DarcyTools, Concepts, methods, equations and tests, Version 1.0 (Tentative title), SKB XXX-YY-YY.

**Svensson U, Laaksoharju M, Gurban I, 2002c.** Impact of the tunnel construction on the groundwater chemistry at Äspö. SKB report in progress.

**Talbot C, Munier R, 1989.** Faults and fracture zones in Äspö. SKB PR 25-89-11, Svensk Kärnbränslehantering AB.

**Talbot C, Ramberg H, 1990.** Some clarification of the tectonics of Äspö and its surroundings. SKB PR 25-90-15, Svensk Kärnbränslehantering AB.

**Te Kamp L, Rummel F, Zoback M D, 1995.** Hydrofrac stress profile to 9 km at the German KTB site, in Proc. Workshop on Rock Stresses in the North Sea, Trondheim, Norway, NTH and SINTEF Publ., Trondheim, pp. 147–53.

**Tirén S A, Beckholmen M, Isaksson H, 1987.** Structural analysis of digital terrain models, Simpevarp area, southeastern Sweden. Method study EBBA II. SKB PR 25-87-21, Svensk Kärnbränslehantering AB.

**Tullborg E-L, Larson S Å, 1984.**  $\delta^{18}\text{O}$  and  $\delta^{13}\text{C}$  for limestones, calcite fissure infillings and calcite precipitates from Sweden. Geologiska föreningens i Stockholm förhandlingar 106(2).

**Tullborg E-L, Larson S Å, Björklund L, Samuelsson L, Stigh J, 1995.** Thermal evidence of Caledonide foreland, molasse sedimentation in Fennoscandia. SKB Technical Report TR-95-18, Svensk Kärnbränslehantering AB.

**Tullborg E-L, Larson S Å, Stiberg J-A, 1996.** Subsidence and uplift of the present land surface in the southeastern part of the Fennoscandian Shield. GFF 118, 126–128.



**Tullborg E-L, 1997.** Recognition of low-temperature processes in the Fennoscandian shield. Ph.D. thesis at Geological Department at the Institution for Geosciences. Geovetarcentrum, Göteborgs Universitet, 41381 Göteborg, Sweden.

**Vuillermin F, 1991.** Possibilità e limitazione della prospezione geoelettrica e sismica a rifrazione nella caratterizzazione geomeccanica degli ammassi rocciosi (in Italian) (Possibility and limitations of the geoelectric and seismic logging for the geomechanical characterisation of rock masses), in “La meccanica delle rocce a piccola profondità” (Rock mechanics at shallow depth), October 1991, Italy.

**Wikberg P, 1998.** Äspö Task Force on modelling of groundwater flow and transport of solutes. SKB progress report HRL-98-07, Svensk Kärnbränslehantering AB,

**Wikman H, Kornfält K-A, 1995.** Updating of a lithological model of the bedrock of the Äspö area. SKB PR 25-95-04, Svensk Kärnbränslehantering AB.

**Åberg G, 1978.** Precambrian geochronology of south-eastern Sweden. Geologiska Föreningens i Stockholm Förhandlingar 100, 125–154.

**Åhäll K-I, 2001.** Åldersbestämning av svårdaterade bergarter i sydöstra Sverige. SKB R-01-60, Svensk Kärnbränslehantering AB.

## Appendix A1

### Summary log of data ordered from the SICADA – data base (in Swedish)

Date	Nr	Orderer/project	Ordered data	Status	Comments
010912	54	Jan Hermansson Golder Metodik för platsbeskrivning Laxemar	Data från sprickceller PSM; Läkta och naturliga sprickor KLX02, borsjunkning HLX01–07	Klart	
	53	Marcus Laaksuharju Geopoint Modelleringstest av Laxemar inför PLU, KEA	Samtliga kemidata från Laxemar	Klart	Ann-Chatrin
	06	Ingvar Rhén Sweco SKI Platskaraktisering – analys av data Metod för presentation/jämförelse av försvarsområden.	Koordinater från object_location	Klart	Leverat enligt beställning. Tillkommit flera efterbeställningar.
010924	59	Ingvar Rhén VBB VIAK – Sweco AB Metodik för platsbeskrivning Laxemar	Parameterar: • Nederbörd • Lufttemperatur • Potentiell evopotranspiration • Havsnivå på Östersjön (Baltic sea) • Avrinning (runoff ), flöde för vatten drag, finns det inlagt (mätt eller beräknat) för tex Laxemar ån eller annan? Tidsupplösning: ett värde per dygn. Period: Alla kvalitetskontrollerade data. Format: På ett format så att det går att ta in i ett EXCEL ark och kunna få det i kolumner samt att få tidpunkt som år och löptid i EXCEL.	Klart 010926	
010924	58	Ingvar Rhén VBB VIAK – Sweco AB Metodik för platsbeskrivning Laxemar	Grundvattennivådata för Laxemar området. Tidsupplösning: ett värde per dygn. Period: Alla kvalitetskontrollerade data. Bh: KLX01, KLX02, HLX01–12, alla tillgängliga bh-sektioner. Uppgifter. Bhnamn, sektions nr, secup, seclow, tidpunkt, nivå. Format: På ett format så att det går att ta in i ett EXCEL ark och kunna få det i kolumner samt att få tidpunkt som år och löptid i EXCEL.	Klart 010926	

	56	Ingvar Rhén VBB VIAK –Sweco AB Metodik för platsbeskrivning Laxemar	Estimated hydraulic conductivity, transmissivity Flowlogging data (Posiva, UCM)	Klart 010921	
011002	69	Anders Ström SKB Platsbeskrivande modell Laxemar	WellCadbilder för KLX01 och KLX02	Klart	WellCad-bilder Henry Pilstål Även skickade till Johan Berglund Swedpower
011009	67	Åsa Fransson SWECO Metodik för platsbeskrivning Laxemar	KLX01, packer test, 106–691 m i 3-m intervall KLX01, packer test, 103–702 m i 30-m intervall KLX01, airlift test, 701–808 m, 806-929m, 926–1078 m, 701–1078 m HLX02, HLX04, HLX05, (airlift tror jag)	Klart 011010	
011009	65	Johan Berglund Swedpower KLX02	BIPS-data från KLX02	Klart	Allan Strähle
	62	Åsa Fransson SWECO Metodik för platsbeskrivning Laxemar	Komplettering enligt fil databeställning.xls som bifogas mail Flowlogging data (spinner, Posiva)	Klart	Skickat 011002 lista över Pekkas filer
011024	70	Åsa Fransson Sweco AB Metodik för platsbeskrivning Laxemar	Fracture frequency och läge för naturliga öppna sprickor för KLX01 och KLX02	Klart	
011115	78	Marcus Laaksoharju GeoPoint AB Metodik för platsbeskrivning Laxemar	KLX01 och KLX02: 1) Geologisk data (bergarter/sprickmineral) i tabellformat. 2) WellCad översiktsbilder för borrhålen som visar bergarterna, sprickmineralen och sprickornas läge. Om det dessutom går att visa CI halten längs med borrhålen skulle det vara ypperligt.	Klart	WellCad ss/hp Två leveransfiler 01_78_1.zip, 01_78_2.zip Även skickat till Eva-Lena Tullborg Terralogica
011116	79	Eva Hakami ITASCA Geomekanik AB Metodik för platsbeskrivning Laxemar	1) Spänningsmättningsdata (Hydraulisk spräckning) från KLX02. 2) Sprickkarteringsdata från KLX02 och KLX01 (RQD, Q, RMR, sprickfrekvens, kartering naturliga sprickor och krosszoner). 3) Spänningsmättningsdata med överborrning från Åspö (inte hydraulisk spräckning) oavsett borrhål.	Klart 011121	
011120	80	Eva-Lena Tullborg Terralogica Metodik för platsbeskrivning Laxemar	Från KLX01–02. Filtrera ut HM, FE och PY för naturliga sprickor ur mineral1-4. Slå samman detta till en mineralcolumn per borrhål och sortera på djup.	Klart 011122	Skickad till Allan Strähle 011121

011120	81	Åsa Fransson Sweco AB Metodik för platsbeskrivning Laxemar	Jag är intresserad av data ifrån interferenstester i KLX02 med observation i KLX01 (referens: AR 94-21 och U-96-32). Pumpningen genomfördes i sektion 805–1103 m. Observationer skedde i sektionerna 0–140 m, 141–271 m, 272–694 m, 695–855 m och 856–1078 m. Jag önskar mig: Data ifrån pumpningen av KLX02 (tryck, flöde, tid...) Data ifrån observationsbrunnen KLX01 (tryck, tid...) Helst excelformat (alternativt .mio) XYZ-koordinater för packerlägen (sec up och sec low, tror att det som står ovan stämmer, men jämför gärna med data ifrån testerna). XYZ-koordinater för topp, botten i hammarborrhålen HLX01–09.		Delleverans 1 skickad 011121
011123	82	Martin Stigson Golder Metodik för platsbeskrivning Laxemar	Naturliga och läkta sprickor från KLX02 i excelfil.	Klart	Muntlig beställning via SS

---

### Used Geographic Information System data from SKB:s data base

#### General maps and orthophotos

Maps/orthophotos	Contents	Field of application
Topographic Maps (LMV T5 version) 6G SO, 6H SV	Geographic Sweden Data (GSD). General landscapes information	Basis for map presentation
Cadastral Maps 6G 1h-j, 2h-j, 3i-j, 4i-j, 6H 1a-4a, 3b,4b	Geographic Sverigedata (GSD). General landscapes information, with elevation	Basis for map presentation
Ortophotos 6G 1h-j, 2h-j, 3i-j, 4i-j, 6H 1a-4a, 3b,4b	Ortophotos in a raster format (TIFF) Produced by scanning and manipulation high quality diapositive	Foundation for analysis of landscapes

## Data input from SKB GIS 5.0

### Data from the Oskarshamn Feasibility Study

Type of data	Filename	Contents	Field of application	Used in layout
<b>SGU - - deformations-karta;</b>	formlinje	Foliation trend, field measurements of structures	Geological Map from Feasibility Study and Airborne geophysics Map in RVS/hydrology	RVS model
	magform	Magnetic form lines, anomalies	Geological Map from Feasibility Study and Airborne geophysics Map in RVS/hydrology	RVS model
	Monly	Fracture zone; magnetically indicated (low magnetic)	Geological Map from Feasibility Study and Airborne geophysics Map in RVS/hydrology	RVS model Fig. 3-2, 3-7
	Namn	Names	Geological Map from Feasibility Study and Airborne geophysics Map in RVS/hydrology	RVS model Fig. 3-2
	Plastisk_skjuvzon_r00_45fig6	Ductile deformation zone	Geological Map from Feasibility Study and Airborne geophysics Map in RVS/hydrology	RVS model Fig. 3-7
	Regh1	Regional fracture zone below sea level, northern part	Geological Map from Feasibility Study and Airborne geophysics Map in RVS/hydrology	RVS model Fig. 3-2, 3-7
	Regh2	Regional fracture zone below sea level, southern part	Geological Map from Feasibility Study and Airborne geophysics Map in RVS/hydrology	RVS model Fig. 3-2
	Regl1	Regional fracture zone on land, southern part	Geological Map from Feasibility Study and Airborne geophysics Map in RVS/hydrology	RVS model Fig. 3-2
	Regl2	Regional fracture zone on land, northern part	Geological Map from Feasibility Study and Airborne geophysics Map in RVS/hydrology	RVS model Fig. 3-2, 3-7
	Symbol	Symbols; tectonic breccia, mylonite, vertical displacement etc.	Geological Map from Feasibility Study and Airborne geophysics Map in RVS/hydrology	RVS model Fig. 3-7
	Zonhav	Local fracture zone, below sea level	Geological Map from Feasibility Study and Airborne geophysics Map in RVS/hydrology	RVS model Fig. 3-7
	Zonland	Local fracture zone, on land	Geological Map from Feasibility Study and Airborne geophysics Map in RVS/hydrology	RVS model Fig. 3-7
	Sprickzon_r00_45fig6	Regional-local fault or fracture zone	Geological Map from Feasibility Study	Fig. 3-7
	Berggrund	Rock types; on islands and on land	Map in RVS Geological Map from Feasibility Study	RVS model Fig. 3-2
	Bghav	Rock types; below sea level	Map in RVS ?? Geological Map from Feasibility Study	RVS model Fig. 3-2
	Bgoar	Rock types on islands	Not used Geological Map from Feasibility Study	Fig. 3-2
Bgytland	Rock types on mainland	Map in RVS/hydrology Geological Map from Feasibility Study	RVS model Fig. 3-2	

Type of data	Filename	Contents	Field of application	Used in layout
<b>SGU - - deformations-karta;</b>	Diabas	Dolerite dykes	Not used Geological Map from Feasibility Study	Fig. 3-2, 3-7
	Gang	Greenstone- and granite dykes	Map in RVS Geological Map from Feasibility Study	RVS model Fig. 3-2, 3-7
	Inneslut	Fragments of older rocks	Map in RVS Geological Map from Feasibility Study	RVS model Fig. 3-2
	Namn	Names	Not used Geological Map from Feasibility Study	Fig. 3-2
	Spirill	Veined gneiss	Map in RVS Geological Map from Feasibility Study	RVS model Fig. 3-2
	Streck	Structural measurements	Not used Geological Map from Feasibility Study	Fig. 3-7
	Stenbrott_idrift_r98_56	Quarry, in operation	Not used Geological Map from Feasibility Study	Fig. 3-7
	Stenbrott_nedlagda_r98_56	Quarry, abandoned	Not used Geological Map from Feasibility Study	Fig. 3-7
	Punkt-symboler_r00_45fig6	Inclusions, quarries, foliation	Not used Map in RVS	RVS model Fig. 3-7
	Sgab_kns	Quaternary deposits	Hydrology Geological Map from Feasibility Study	Fig. 3-6
Berggrunstytor_r00_45 fig6	Rock types	Map in RVS Geological Map from Feasibility Study	RVS model Fig. 3-7	

### Complementary data not stored in SKB GIS 5.0

Content	Application	Used in layout
Bedrock surfaces in Simpevarp regional model area, Vers. 0	Map in RVS	Fig. 3-7, RVS model
New lineaments identified in the Simpevarp regional model area, Vers. 0		Fig. 3-7

### Digital terrain model

Type of data	Filename	Contents	Field of application	Used in layout
Terrain model	Lax_Area	Area of interpretation: 1547800–1551100, 6365000–6369300	RVS model	Fig. 3-4

**Lineament - identification within the area defined by the coordinates 1547800-1551100, 6365000-6369300**

Type of data	Filename	Contents	Field of application	Used in layout
<b>Lineament</b>	RegZon2	Regional fault or fracture zone (according to the feasibility study). Extension >5 km. Now more accurately positioned.	RVS	Laxemar/detail/hydrology lineament Fig. 3-5
	LokZon	Local fault or fracture zone (according to the feasibility study). Extension >5 km. Now more accurately positioned.	RVS	Laxemar/detail/hydrology lineament Fig. 3-5
	LokZonLax	Local fracture zone in the Laxemar area, (according to the feasibility study). Extension 1-5 km. Now more accurately positioned.	RVS	Laxemar/detail/hydrology lineament Fig. 3-5
	MagOnly	Deformation zone (fracture zone?) only magnetically indicated. Not modified in this version (more detailed magnetic data was not available).	RVS	Laxemar/detail/hydrology lineament Fig. 3-5
	LineH50m	Lineament, extension 1-2 km, uncertain character. Not interpreted as fracture zones in the feasibility study. Based on the DTM 50m grid from LMV (Land Survey) supported by ortho photo.	RVS	Laxemar/detail/hydrology lineament Fig. 3-5
	LineH10m Conn	Lineament, < 1 km, (connected). Interpretation based on detailed DTM data (Lax_AreaHxyz) supported by ortho photo.	RVS	Laxemar/detail/hydrology lineament Fig. 3-5
	LineH10m Frag	Lineament, < 1km, (not connected). Interpretation based on detailed DTM data (Lax_AreaHxyz) supported by ortho photo.	RVS	Laxemar/detail/hydrology lineament Fig. 3-5
<b>Altitude data</b>	Laxareah. xyz LaxAreaH. doc	Topographic data, XYZ (grid format)	DTM-modell of topography. Not used in RVS. Send to SF to be Used in DarcyTools.	

**Yellow map, Metria**

Type of data	Filename	Contents	Field of application	Used in layout
<b>Terrain map</b>		Sample of terrain map		Laxemar/hydrology/regional Laxemar/detail/hydrology lineament Hydrology/catchment area etc.
		Sample of terrain map		Laxemar/hydrology/regional Laxemar/detail/hydrology lineament Hydrology/catchment area etc.



<b>Type of data</b>	<b>Filename</b>	<b>Contents</b>	<b>Field of application</b>	<b>Used in layout</b>
<b>Terrain map</b>		Elevation data		Laxemar/hydrology/regional Laxemar/detail/hydrology lineament
		Catchment area		Laxemar/hydrology/regional Hydrology/catchment area etc.

<b>Type of data</b>	<b>Filename</b>	<b>Contents</b>	<b>Field of application</b>	<b>Used in layout</b>
<b>Map of landed property</b>	oh.shp	Contour map		Laxemar/hydrology/regional

## Geological data imported to RVS from SICADA and other sources

### Data from SICADA

Science	Subject	Method	Parameter name	Description	Available data (0= do not exist 1= imported to RVS)			Data used (0= not used 1= used)
					KLX01 0--700m	700- ~1100m	KLX02 HLX	
Geology (From SICADA)	core_logging	pc_logging_new	colour		1	1	1	0
			natural_joint_min1	Mineral 1 from Petrocore	1	1	1	1
			natural_joint_min2	Mineral 2 from Petrocore	1	1	1	1
			natural_joint_min3	Mineral 3 from Petrocore	1	1	1	0
			natural_joint_min4	Mineral 4 from Petrocore	1	1	1	0
			natural_joint_roghn	Roughness from Petrocore	1	1	1	0
			natural_joint_skin	Skinfactor from Petrocore	1	1	1	0
			natural_joint_surface	Surface from Petrocore	1	1	1	0
			natural_joint_width	Fracture width from Petrocore	1	1	1	0
			rock		1	1	1	1
	rqd		1	0	0	0		
	structure		1	1	1	1		
	core logging	petrocore	alteration_intensity	Intensity type code	1	1	1	1
			alteration_type	Alteration type	1	1	1	1
			pe_core_loss_missingcore	Core loss length	1	1	1	1
			pe_core_loss_type	Type of coreloss code	1	1	1	1
			pe_crush_min1	Fracture mineral 1	1	1	1	1
pe_crush_variable			Variable	1	1	1	1	
pe_rock_colour			Rock colour	1	1	1	1	

Local (Created from SICADA data and reports)	Core logging	Resistivity log (ref: pers. comm. Ingvar Rehn)	HLX_zone	Fracture zone indication				1
		Interpretation (ref: this project)	Rock_seg	Interpreted rock segments in KLX	1	1	1	1
		Fracture data (ref: SICADA)	Frac/metre	Fracture frequency per metre, crushzone included	1	1	1	1
			Fracfreq_ma	Moving average of the fracture frequency	1	1	1	1
			Fracture zones	>10 fr/metre	1	1		1
		Radar (ref: Carlsten, 1993 and 1994)	Radar	Radar reflector from crosshole study	1	0	0	1
			Reflexion	Radarreflexion			1	1
Vsp (ref: pers. comm.. Christopher Juhlin)	vsp	Reflectors from vertical seismic profiling			1	0		

### Other input to RVS

Typ of data	Source	Reference
Lineaments map	SKB GIS-database	
Geological map	SKB GIS-database	
Contour map	SKB GIS-database	
Magnetic map	SKB GIS-database	
Reflection seismic data	Christopher Juhlin, Uppsala university	Personal communication

## Appendix A5

### Hydrogeological data used

#### Hydrology (see appendix A1, data number 59)

Observation	Meas. station	Time period for data set	Source for data	Time for delivery of data
Precipitation, Air temperature	PSM7616	1987-01-01 to 1994-04-30, 1995-07-01 to 1999-12-31	SICADA	Sept 2001
Precipitation, Air temperature	PSM7647	1994-05-01 to 1995-06-30	SICADA	Sept 2001
Potential evapotranspiration	PSM7524	1995-08-01 to 1995-09-30	SICADA	Sept 2001
Potential evapotranspiration	PSM7647	1987-01-01 to 1999-12-31	SICADA	Sept 2001
Potential evapotranspiration	PSM7722	1987-01-01 to 1995-07-31	SICADA	Sept 2001
Potential evapotranspiration			/Rhen et al, 1997/ (TR 97-06) /Nyberg et al, 2001/ (IPR-01-29)	
Snow				
Run-off			/Svensson, 1987/ (PR 25-87-09)	

#### Piezometric levels (see appendix A1, data number 58)

Observation	Boreholes	Time period for data set	Time resolution	Source for data	Time for delivery of data
Piezometric levels in core holes	KLX01 all available borehole sections	1989-05-19 to 1999-12-31	1 value/day	SICADA	Sept 2001
Piezometric levels in core holes	KLX02	No data		SICADA	Sept 2001
Piezometric levels in percussion holes	HLX 01–09, all available borehole sections	1987-10-26 to 1999-12-31	1 value/day	SICADA	Sept 2001
Piezometric levels in percussion holes	HLX 10–12	No data		SICADA	Sept 2001

**Borhole data Hydraulic tests performed in HLX- and KLX holes. Data type: Transmissivity=T, Hydraulic conductivity=K, Counts=C, Flow rate=F, Temperature=Te, Electrical conductivity=EC, Resistivity=R, Salinity=S. (1) continuous logging, (2) secup last section, (3) preliminary data delivered from SKB), see appendix 1 order number 56, 62, 67, 70, 81.**

Bore-hole	Bore-hole length	Tested part of bh, Secup	Tested part of bh, Seclow	Type of test	Date for test	Test scale (L)	Step length for moving measured section (dL) (m)	Data type	Source for data	Time for delivery of data
	(m)	(m)	(m)			(m)				
HLX01	100.00	0.00	100.00	Pumptest	198x-xx-xx	~100	-	T	SICADA	Sept-Dec 2001
HLX02	132.00	0.00	132.00	Airlift test		~100	-	T	SICADA	Sept-Dec 2001
HLX03	100.00	0.00	100.00	Pumptest		~100	-	T	SICADA	Sept-Dec 2001
HLX04	125.00	0.00	125.00	Airlift test		~100	-	T	SICADA	Sept-Dec 2001
HLX05	100.00	0.00	100.00	Airlift test		~100	-	T	SICADA	Sept-Dec 2001
HLX06	100.00	0.00	100.00	Airlift test		~100	-	T	SICADA	Sept-Dec 2001
HLX07	100.00	0.00	100.00	Pumptest		~100	-	T	SICADA	Sept-Dec 2001
HLX08	40.00	0.00	40.00	Airlift test		~40	-	T	SICADA	Sept-Dec 2001
HLX09	151.00	0.00	151.00	Airlift test		~150	-	T	SICADA	Sept-Dec 2001
KLX01	1078.00	106.00	691.00 (688 (2))	Injection tests		3	3	K <sub>JACOB</sub>	SICADA	Sept-Dec 2001
		103.00	702.11 (643 (2))	Injection tests		30	30	K <sub>JACOB</sub>	SICADA	Sept-Dec 2001
		701.00 806.00 926.00 701.00	808.00 929.00 1077.99 1077.99	Airlift test		~100 ~100 ~150 ~300	-	T	SICADA	Sept-Dec 2001
		0.00	702.11	Pumping test		700	-	T	SICADA	Sept-Dec 2001
		101.75	465.75	Flowlog – Spinner		-	1.00	C, F	SICADA	Sept-Dec 2001
		700.05	1070.00	Flowlog – UCM		-	0.05 (1)	F, R, S, Te	SICADA	Sept-Dec 2001

KLX02	1700.50	798.00	1101.50	Airlift test	~300	-	T	SICADA	Sept-Dec
		1427.00	1700.50		~300				2002
		0.00	205.00	Pumping	~200	-	T	SICADA	Sept-Dec
		207.00	505.00	test	~300				2001
		505.00	803.00		~300				
		805.00	1103.00		~300				
		1103.50	1401.50		~300				
		201.00	1700.50		1500				
		205.92	1399.92	Flow-					
			(1396.92	logging -					
		(1))	PDFM	3	3	K, EC	SICADA	Sept-Dec	
						(3)		2001	
	200.50	1440.50	Flowlog -	-	0.1	R, S,	SICADA	Sept-Dec	
			UCM			Te		2001	

---

## Hydrogeochemical data

**Table 1. The variables from SICADA used as an input for the hydrogeochemical modelling.**

Column n	Domain	Description
ba	ug/l	Barium
br	mg/l	Bromide
ca	mg/l	Calcium
ce	ug/l	Cerium
cl	mg/l	Chloride
cond	mS/m	El. conductivity
cs	ug/l	Cesium
doc	mg/l	Dissolved Organic Carbon
drill_water	per_cent	Drilling water residue
dy	ug/l	Dysprosium
Er	ug/	Erbium
Eu	ug/l	Europium
f	mg/l	Fluoride
Fe	mg/l	Total Iron by ICP-AES
feii	mg/l	Ferrous Iron , spectrophotometric method
fetot	mg/l	Total Iron , spectrophotometric method
gd	ug/l	Gadolinium
hco3	mg/l	Hydrogen carbonate (alkalinity)
Hf	ug/l	Hafnium
ho	ug/l	Holmium
i	mg/l	Iodide
ldcode		Object or borehole id. code
indium	ug/l	Indium
k	mg/l	Potassium
La	ug/l	Lanthanum
li	mg/l	Lithium
Lu	ug/l	Lutetium
Mg	mg/l	Magnesium
mn	mg/l	Manganese
Na	mg/l	Sodium
Nd	ug/l	Neodymium
Nh4_n	mg/l	Ammonium as Nitrogen
No2_n	mg/l	Nitrite as Nitrogen
No2no3_n	mg/l	Nitrite + Nitrate as Nitrogen
No3_n	mg/l	Nitrate as Nitrogen
Ph	pH_unit	pH
Po4_p	mg/l	Phosphate as Phosphorus
Pr	ug/l	Praseodymium
Rb	ug/l	Rubidium
s2	mg/l	Hydrogen sulphide analysed as total sulphide
sample_no	sample_num.	Sample number
Sb	ug/l	Antimony

Column n	Domain	Description
Column n	Domain	Description
Sc	ug/l	Scandium
seclow	m	Lower section limit
secup	m	Upper section limit
si	mg/l	Silicon
Sm	ug/l	Samarium
smpl_flow	l/min	Water flow rate at the sampling occasion
So4	mg/l	Sulphate
So4_s	mg/l	Sulphate as Sulphur (total Sulphur by ICP-AES)
Sr	mg/l	Strontium
start_date	date	Start date
stop_date	date	Stop date
Tb	ug/l	Terbium
tl	ug/l	Thallium
Tm	ug/	Thulium
y	ug/l	Yttrium
Yb	ug/l	Ytterbium
Zr	ug/l	Zirconium
age_bp	year	C-14 age BP
c13	per_mill	Delta C-13 per mille PDB (the standard PeeDee Belemnite)
d	dev_SMOW	Deuterium, deviation from SMOW (Standard Mean Oceanic Water)
idcode	Object or boreh.	id. code
o18	dev_SMOW	Oxygen-18, deviation from SMOW (Standard Mean Oceanic Water)
pmc	pmc	PMC (Percent Modern Carbon)
Ra226	Bq/l	Ra-226
Ra228	Bq/l	Ra-228
Rn222	Bq/l	Rn-222
sample_no	sample_number	Sample number
seclow	m	Lower section limit
secup	m	Upper section limit
start_date	date	Start date
stop_date	date	Stop date
Th	ug/l	Thorium
Th228	mBq/kg	Th-228
Th230	mBq/kg	Th-230
Th232	mBq/kg	Th-232
tr	TU	Tritium
u	ug/l	Uranium
u234	mBq/kg	U-234
u235	mBq/kg	U-235
u238	mBq/kg	U-238
Ba	ug/l	Barium
Br	mg/l	Bromide
Ca	mg/l	Calcium
Ce	ug/l	Cerium
cl	mg/l	Chloride



Column n	Domain	Description
cond	mS/m	El. conductivity
Cs	ug/l	Cesium
doc	mg/l	Dissolved Organic Carbon
Column n	Domain	Description
drill_water	per_cent	Drilling water residue
Dy	ug/l	Dysprosium
Er	ug/	Erbium
Eu	ug/l	Europium
f	mg/l	Fluoride
Fe	mg/l	Total Iron by ICP-AES
feii	mg/l	Ferrous Iron , spectrophotometric method
fetot	mg/l	Total Iron , spectrophotometric method
gd	ug/l	Gadolinium
hco3	mg/l	Hydrogen carbonate (alkalinity)
Hf	ug/l	Hafnium
ho	ug/l	Holmium

**Table 2. The database index, boreholes, coordinates and the depth for the groundwater samples are listed in the table. Representative samples are grey shaded and the selected target depths (depths reflecting repository depth) are framed.**

DBINDEX	SampleID	Location	Date	Y	X	z	Depth
1	-1	HLX01	23.10.87	6367317.3	1549572.7	-56.177	75.0
2	-1	HLX01	24.10.87	6367317.3	1549572.7	-56.177	75.0
3	-1	HLX01	25.10.87	6367317.3	1549572.7	-56.177	75.0
4	2555	HLX01	16.06.98	6367344.8	1549570.4	-8.01	19.5
5	2562	HLX02	17.06.98	6368102.8	1549936	-7.681	19.5
6	-1	HLX03	05.11.87	6367795.6	1549918.7	-46.674	62.5
7	-1	HLX03	06.11.87	6367795.6	1549918.7	-46.674	62.5
8	2556	HLX03	16.06.98	6367812.1	1549920.3	-7.016	19.5
9	2557	HLX04	17.06.98	6367683.8	1549788.6	-7.522	19.5
10	2558	HLX05	17.06.98	6367546.8	1549967.8	-1.742	19.5
11	-1	HLX06	01.11.87	6367128.5	1549780.9	-46.41	72.5
12	-1	HLX06	03.11.87	6367128.5	1549780.9	-46.41	72.5
13	2559	HLX06	17.06.98	6367155.9	1549784	-1.126	19.5
14	-1	HLX07	04.11.87	6367171.1	1550035.1	-43.947	60.0
15	-1	HLX07	05.11.87	6367171.1	1550035.1	-43.947	60.0
16	2560	HLX07	17.06.98	6367160.3	1550020.7	-7.67	19.5
17	2561	HLX08	17.06.98	6366585.8	1550591.3	-2.408	6.5
18	1501	KLX01	04.10.88	6367527	1549914.4	-672.947	691.1
19	1502	KLX01	05.10.88	6367527	1549914.4	-672.947	691.1
20	1503	KLX01	11.10.88	6367527	1549914.4	-672.947	691.1
21	1504	KLX01	17.10.88	6367527	1549914.4	-672.947	691.1
22	1505	KLX01	18.10.88	6367527	1549914.4	-672.947	691.1
23	1506	KLX01	19.10.88	6367527	1549914.4	-672.947	691.1

DBINDEX	SampleID	Location	Date	Y	X	z	Depth
24	1507	KLX01	20.10.88	6367527	1549914.4	-672.947	691.1
25	1508	KLX01	21.10.88	6367527	1549914.4	-672.947	691.1
26	1509	KLX01	24.10.88	6367527	1549914.4	-672.947	691.1
27	1510	KLX01	25.10.88	6367527	1549914.4	-672.947	691.1
28	1511	KLX01	26.10.88	6367527	1549914.4	-672.947	691.1
29	1512	KLX01	27.10.88	6367527	1549914.4	-672.947	691.1
30	1513	KLX01	28.10.88	6367527	1549914.4	-672.947	691.1
31	1514	KLX01	31.10.88	6367527	1549914.4	-672.947	691.1
32	1516	KLX01	03.11.88	6367527	1549914.4	-672.947	691.1
33	1517	KLX01	08.11.88	6367514.6	1549916.2	-440.733	458.5
34	1518	KLX01	09.11.88	6367514.6	1549916.2	-440.733	458.5
35	1519	KLX01	10.11.88	6367514.6	1549916.2	-440.733	458.5
36	1520	KLX01	11.11.88	6367514.6	1549916.2	-440.733	458.5
37	1521	KLX01	14.11.88	6367514.6	1549916.2	-440.733	458.5
38	1522	KLX01	15.11.88	6367514.6	1549916.2	-440.733	458.5
39	1523	KLX01	16.11.88	6367514.6	1549916.2	-440.733	458.5
40	1524	KLX01	17.11.88	6367514.6	1549916.2	-440.733	458.5
41	1525	KLX01	18.11.88	6367514.6	1549916.2	-440.733	458.5
42	1526	KLX01	22.11.88	6367514.6	1549916.2	-440.733	458.5
43	1527	KLX01	22.11.88	6367514.6	1549916.2	-440.733	458.5
44	1528	KLX01	23.11.88	6367514.6	1549916.2	-440.733	458.5
45	1529	KLX01	25.11.88	6367504	1549918.3	-257.055	274.5
46	1531	KLX01	29.11.88	6367504	1549918.3	-257.055	274.5
47	1530	KLX01	29.11.88	6367504	1549918.3	-257.055	274.5
48	1532	KLX01	30.11.88	6367504	1549918.3	-257.055	274.5
49	1533	KLX01	01.12.88	6367504	1549918.3	-257.055	274.5
50	1534	KLX01	05.12.88	6367504	1549918.3	-257.055	274.5
51	1535	KLX01	06.12.88	6367504	1549918.3	-257.055	274.5
52	1536	KLX01	07.12.88	6367504	1549918.3	-257.055	274.5
53	1537	KLX01	08.12.88	6367504	1549918.3	-257.055	274.5
54	1538	KLX01	09.12.88	6367504	1549918.3	-257.055	274.5
55	1626	KLX01	23.10.89	6367527	1549914.4	-672.947	691.1
56	1627	KLX01	24.10.89	6367527	1549914.4	-672.947	691.1
57	1628	KLX01	25.10.89	6367527	1549914.4	-672.947	691.1
58	1629	KLX01	26.10.89	6367527	1549914.4	-672.947	691.1
59	1630	KLX01	27.10.89	6367527	1549914.4	-672.947	691.1
60	1631	KLX01	30.10.89	6367527	1549914.4	-672.947	691.1
61	1632	KLX01	31.10.89	6367527	1549914.4	-672.947	691.1
62	1633	KLX01	01.11.89	6367527	1549914.4	-672.947	691.1
63	1751	KLX01	21.09.90	6367534.4	1549913.1	-817.194	835.5
64	1752	KLX01	24.09.90	6367534.4	1549913.1	-817.194	835.5
65	1753	KLX01	25.09.90	6367534.4	1549913.1	-817.194	835.5
66	1754	KLX01	26.09.90	6367534.4	1549913.1	-817.194	835.5
67	1755	KLX01	27.09.90	6367534.4	1549913.1	-817.194	835.5
68	1756	KLX01	01.10.90	6367534.4	1549913.1	-817.194	835.5
69	1757	KLX01	02.10.90	6367534.4	1549913.1	-817.194	835.5
70	1758	KLX01	03.10.90	6367534.4	1549913.1	-817.194	835.5

DBINDEX	SampleID	Location	Date	Y	X	z	Depth
71	1759	KLX01	04.10.90	6367534.4	1549913.1	-817.194	835.5
72	1760	KLX01	05.10.90	6367534.4	1549913.1	-817.194	835.5
73	1761	KLX01	09.10.90	6367534.4	1549913.1	-817.194	835.5
74	1763	KLX01	12.10.90	6367538.6	1549912.3	-897.084	915.5
75	1764	KLX01	15.10.90	6367538.6	1549912.3	-897.084	915.5
76	1765	KLX01	16.10.90	6367538.6	1549912.3	-897.084	915.5
77	1766	KLX01	17.10.90	6367538.6	1549912.3	-897.084	915.5
78	1767	KLX01	18.10.90	6367538.6	1549912.3	-897.084	915.5
79	1768	KLX01	19.10.90	6367538.6	1549912.3	-897.084	915.5
80	1769	KLX01	24.10.90	6367538.6	1549912.3	-897.084	915.5
81	1770	KLX01	25.10.90	6367538.6	1549912.3	-897.084	915.5
82	1771	KLX01	26.10.90	6367538.6	1549912.3	-897.084	915.5
83	1772	KLX01	29.10.90	6367538.6	1549912.3	-897.084	915.5
84	1773	KLX01	30.10.90	6367538.6	1549912.3	-897.084	915.5
85	1774	KLX01	31.10.90	6367538.6	1549912.3	-897.084	915.5
86	1775	KLX01	05.11.90	6367544.9	1549911.2	-1019.916	1038.5
87	1776	KLX01	06.11.90	6367544.9	1549911.2	-1019.916	1038.5
88	1777	KLX01	07.11.90	6367544.9	1549911.2	-1019.916	1038.5
89	1778	KLX01	08.11.90	6367544.9	1549911.2	-1019.916	1038.5
90	1779	KLX01	09.11.90	6367544.9	1549911.2	-1019.916	1038.5
91	1780	KLX01	12.11.90	6367544.9	1549911.2	-1019.916	1038.5
92	1781	KLX01	13.11.90	6367544.9	1549911.2	-1019.916	1038.5
93	1782	KLX01	14.11.90	6367544.9	1549911.2	-1019.916	1038.5
94	1783	KLX01	15.11.90	6367544.9	1549911.2	-1019.916	1038.5
95	1784	KLX01	16.11.90	6367544.9	1549911.2	-1019.916	1038.5
96	1785	KLX01	19.11.90	6367544.9	1549911.2	-1019.916	1038.5
97	-1	KLX02	03.08.93	6366810.6	1549223.6	-435.691	456.0
98	-1	KLX02	03.08.93	6366805.3	1549223.6	-385.976	406.0
99	-1	KLX02	03.08.93	6366800.2	1549223.7	-336.24	356.0
100	-1	KLX02	03.08.93	6366795.5	1549223.9	-286.455	306.0
101	-1	KLX02	03.08.93	6366791.1	1549224	-236.653	256.0
102	-1	KLX02	03.08.93	6366786.7	1549224.2	-186.85	206.0
103	-1	KLX02	03.08.93	6366782.2	1549224.4	-137.048	156.0
104	-1	KLX02	03.08.93	6366777.7	1549224.5	-87.251	106.0
105	-1	KLX02	03.08.93	6366963.3	1549227.1	-1625.86	1656.0
106	-1	KLX02	03.08.93	6366956.2	1549226.7	-1576.359	1606.0
107	-1	KLX02	03.08.93	6366773	1549224.7	-37.471	56.0
108	-1	KLX02	03.08.93	6366949.2	1549226.4	-1526.858	1556.0
109	-1	KLX02	03.08.93	6366769.8	1549224.8	-1.614	20.0
110	-1	KLX02	03.08.93	6366942.2	1549226	-1477.356	1506.0
111	-1	KLX02	03.08.93	6366935.1	1549225.6	-1427.855	1456.0
112	-1	KLX02	03.08.93	6366928.1	1549225.3	-1378.35	1406.0
113	-1	KLX02	03.08.93	6366921.1	1549225	-1328.842	1356.0
114	-1	KLX02	03.08.93	6366914.1	1549224.8	-1279.331	1306.0
115	-1	KLX02	03.08.93	6366907.3	1549224.4	-1229.809	1256.0
116	-1	KLX02	03.08.93	6366900.5	1549224.2	-1180.274	1206.0
117	-1	KLX02	03.08.93	6366893.8	1549224.1	-1130.721	1156.0

DBINDEX	SampleID	Location	Date	Y	X	z	Depth
118	-1	KLX02	03.08.93	6366887.4	1549223.9	-1081.131	1106.0
119	-1	KLX02	03.08.93	6366881.2	1549223.6	-1031.513	1056.0
120	-1	KLX02	03.08.93	6366875.2	1549223.5	-981.885	1006.0
121	-1	KLX02	03.08.93	6366869.1	1549223.6	-932.252	956.0
122	-1	KLX02	03.08.93	6366863.2	1549223.9	-882.609	906.0
123	-1	KLX02	03.08.93	6366857.2	1549224.1	-832.971	856.0
124	-1	KLX02	03.08.93	6366851.1	1549224	-783.334	806.0
125	-1	KLX02	03.08.93	6366845.3	1549223.9	-733.678	756.0
126	-1	KLX02	03.08.93	6366839.3	1549223.8	-684.035	706.0
127	-1	KLX02	03.08.93	6366833.3	1549223.7	-634.393	656.0
128	-1	KLX02	03.08.93	6366827.6	1549223.6	-584.725	606.0
129	-1	KLX02	03.08.93	6366821.8	1549223.5	-535.057	556.0
130	-1	KLX02	03.08.93	6366816.1	1549223.6	-485.384	506.0
131	2701	KLX02	01.11.93	6366798.4	1549223.8	-318.222	337.9
132	2702	KLX02	03.11.93	6366798.4	1549223.8	-318.222	337.9
133	2703	KLX02	04.11.93	6366798.4	1549223.8	-318.222	337.9
134	2704	KLX02	05.11.93	6366798.4	1549223.8	-318.222	337.9
135	2705	KLX02	08.11.93	6366798.4	1549223.8	-318.222	337.9
136	2706	KLX02	09.11.93	6366798.4	1549223.8	-318.222	337.9
137	2707	KLX02	11.11.93	6366850.5	1549224	-778.27	800.9
138	2708	KLX02	12.11.93	6366850.5	1549224	-778.27	800.9
139	2709	KLX02	15.11.93	6366850.5	1549224	-778.27	800.9
140	2710	KLX02	18.11.93	6366850.5	1549224	-778.27	800.9
141	2711	KLX02	19.11.93	6366850.5	1549224	-778.27	800.9
142	2712	KLX02	23.11.93	6366850.5	1549224	-778.27	800.9
143	2713	KLX02	24.11.93	6366850.5	1549224	-778.27	800.9
144	2714	KLX02	02.12.93	6366885.8	1549223.8	-1068.331	1093.1
145	2715	KLX02	03.12.93	6366885.8	1549223.8	-1068.331	1093.1
146	2716	KLX02	07.12.93	6366885.8	1549223.8	-1068.331	1093.1
147	2717	KLX02	08.12.93	6366885.8	1549223.8	-1068.331	1093.1
148	2718	KLX02	09.12.93	6366885.8	1549223.8	-1068.331	1093.1
149	2719	KLX02	13.12.93	6366885.8	1549223.8	-1068.331	1093.1
150	2720	KLX02	14.12.93	6366885.8	1549223.8	-1068.331	1093.1
151	2721	KLX02	15.12.93	6366885.8	1549223.8	-1068.331	1093.1
152	2722	KLX02	16.12.93	6366885.8	1549223.8	-1068.331	1093.1
153	2723	KLX02	22.12.93	6366950.1	1549226.4	-1533.293	1562.5
154	2724	KLX02	28.12.93	6366950.1	1549226.4	-1533.293	1562.5
155	2725	KLX02	04.01.94	6366950.1	1549226.4	-1533.293	1562.5
156	2726	KLX02	05.01.94	6366950.1	1549226.4	-1533.293	1562.5
157	2727	KLX02	11.01.94	6366950.1	1549226.4	-1533.293	1562.5
158	2728	KLX02	12.01.94	6366950.1	1549226.4	-1533.293	1562.5
159	2729	KLX02	13.01.94	6366950.1	1549226.4	-1533.293	1562.5
160	2730	KLX02	14.01.94	6366950.1	1549226.4	-1533.293	1562.5
161	2731	KLX02	17.01.94	6366950.1	1549226.4	-1533.293	1562.5
162	2732	KLX02	18.01.94	6366950.1	1549226.4	-1533.293	1562.5
163	2734	KLX02	31.01.94	6366796.6	1549223.9	-298.656	318.3
164	2735	KLX02	01.02.94	6366796.6	1549223.9	-298.656	318.3

DBINDEX	SampleID	Location	Date	Y	X	z	Depth
165	2736	KLX02	08.02.94	6366796.6	1549223.9	-298.656	318.3
166	2737	KLX02	09.02.94	6366796.6	1549223.9	-298.656	318.3
167	2738	KLX02	10.02.94	6366796.6	1549223.9	-298.656	318.3
168	2421	KLX02	25.09.97	6366807.3	1549223.6	-404.87	425.0
169	2417	KLX02	25.09.97	6366802.1	1549223.7	-355.144	375.0
170	2416	KLX02	25.09.97	6366797.2	1549223.8	-305.377	325.0
171	2415	KLX02	25.09.97	6366792.8	1549224	-255.577	275.0
172	2422	KLX02	25.09.97	6366788.3	1549224.2	-205.777	225.0
173	2414	KLX02	25.09.97	6366783.9	1549224.3	-155.969	175.0
174	2413	KLX02	25.09.97	6366779.4	1549224.5	-106.175	125.0
175	2408	KLX02	25.09.97	6366774.8	1549224.6	-56.384	75.0
176	2406	KLX02	25.09.97	6366770.3	1549224.8	-6.595	25.0
177	2407	KLX02	25.09.97	6366930.8	1549225.4	-1397.163	1425.0
178	2434	KLX02	25.09.97	6366923.8	1549225.1	-1347.655	1375.0
179	2409	KLX02	25.09.97	6366916.8	1549224.8	-1298.146	1325.0
180	2433	KLX02	25.09.97	6366909.9	1549224.6	-1248.629	1275.0
181	2410	KLX02	25.09.97	6366903	1549224.3	-1199.1	1225.0
182	2432	KLX02	25.09.97	6366896.3	1549224.2	-1149.556	1175.0
183	2411	KLX02	25.09.97	6366889.8	1549224	-1099.979	1125.0
184	2431	KLX02	25.09.97	6366883.6	1549223.7	-1050.369	1075.0
185	2412	KLX02	25.09.97	6366877.5	1549223.5	-1000.744	1025.0
186	2430	KLX02	25.09.97	6366871.4	1549223.5	-951.115	975.0
187	2418	KLX02	25.09.97	6366865.4	1549223.8	-901.472	925.0
188	2429	KLX02	25.09.97	6366859.4	1549224	-851.833	875.0
189	2419	KLX02	25.09.97	6366853.4	1549224	-802.199	825.0
190	2428	KLX02	25.09.97	6366847.5	1549224	-752.547	775.0
191	2427	KLX02	25.09.97	6366841.6	1549223.9	-702.899	725.0
192	2426	KLX02	25.09.97	6366835.6	1549223.8	-653.257	675.0
193	2420	KLX02	25.09.97	6366829.8	1549223.7	-603.602	625.0
194	2425	KLX02	25.09.97	6366824	1549223.5	-553.93	575.0
195	2424	KLX02	25.09.97	6366818.3	1549223.5	-504.261	525.0
196	2423	KLX02	25.09.97	6366812.7	1549223.6	-454.577	475.0
197	3038	KLX02	06.12.99	6366925.7	1549225.2	-1361.022	1388.5
198	2523	PLX00013	02.06.98	6367010	1547440	12	1.0
199	2524	PLX00014	02.06.98	6367470	1547540	12	1.0
200	2526	PLX00015	03.06.98	6370250	1548100	3	1.0
201	2527	PLX00016	03.06.98				1.0
202	2528	PLX00017	03.06.98	6369320	1548150	9.5	1.0
203	2529	PLX00018	03.06.98	6369980	1547920	12	1.0
204	2530	PLX00019	03.06.98				1.0
205	2531	PLX00020	03.06.98	6370950	1546600	13	1.0
206	2532	PLX00021	03.06.98	6368990	1548800	5	1.0
207	2533	PLX00022	03.06.98	6369020	1548720	-33	1.0
208	2534	PLX00023	04.06.98	6369150	1548850	5	1.0
209	3031	PLX00023	14.10.99	6369150	1548850	5	1.0
210	2535	PLX00024	04.06.98	6369070	1548890	0	1.0
211	2536	PLX00025	04.06.98	6369040	1548920	0	1.0

DBINDEX	SampleID	Location	Date	Y	X	z	Depth
212	2537	PLX00026	04.06.98	6369020	1548960	0	1.0
213	2538	PLX00027	04.06.98	6369030	1549000	0	1.0
214	2539	PLX00028	04.06.98				1.0
215	2540	PLX00029	04.06.98				1.0
216	2541	PLX00030	04.06.98	6368710	1550040	0	1.0
217	2542	PLX00031	04.06.98	6368840	1549630	0	1.0
218	3016	PLX00031	12.10.99	6368840	1549630	0	1.0
219	2543	PLX00032	04.06.98	6368800	1549450	-35	1.0
220	2544	PLX00033	04.06.98	6368790	1549440	3	1.0
221	2545	PLX00034	05.06.98	6368280	1549450	3	1.0
222	2546	PLX00035	05.06.98	6368330	1549710	2	1.0
223	2547	PLX00036	05.06.98	6368470	1550020	0	1.0
224	2548	PLX00037	05.06.98	6368470	1550060	0	1.0
225	2549	PLX00038	05.06.98	6368470	1550100	0	1.0
226	2550	PLX00039	05.06.98	6368490	1550170	0	1.0
227	2551	PLX00040	05.06.98	6369600	1555200	0	1.0
228	3017	PLX00040	12.10.99	6369600	1555200	0	1.0
229	2552	PLX00041	15.06.98	6370400	1547600	5	1.0
230	2553	PLX00042	15.06.98	6370300	1547650	-35	1.0
231	2554	PLX00043	15.06.98	6368930	1549380	0	1.0
232	3010	PLX00044	12.10.99	6368462	1550042	-0.57	1.0
233	3011	PLX00045	12.10.99	6368464	1550051	-0.66	1.0
234	3012	PLX00046	12.10.99	6368469	1550066	-1.5	1.0
235	3013	PLX00047	12.10.99	6368498	1550065	-1.05	1.0
236	3014	PLX00048	12.10.99	6368511	1550057	-1.2	1.0
237	3015	PLX00049	12.10.99	6368516	1550054	-1.23	1.0
238	3018	PLX00050	13.10.99	6369097	1549074	-0.57	1.0
239	3019	PLX00051	13.10.99	6369095	1549077	-0.7	1.0
240	3020	PLX00052	13.10.99	6369095	1549078	-1.55	1.0
241	3021	PLX00053	13.10.99	6369083	1549084	-3.47	1.0
242	3022	PLX00054	13.10.99	6369087	1549044	-3.81	1.0
243	3023	PLX00055	13.10.99	6369078	1548932	-0.7	1.0
244	3024	PLX00056	13.10.99	6369078	1548937	-1.01	1.0
245	3025	PLX00057	13.10.99	6369075	1548939	-2.18	1.0
246	3026	PLX00058	13.10.99	6369076	1548952	-4.13	1.0
247	3027	PLX00059	14.10.99	6368982	1549218	-0.375	1.0
248	3028	PLX00060	14.10.99	6368985	1549219	-0.55	1.0
249	3029	PLX00061	14.10.99	6368992	1549222	-1.58	1.0
250	3030	PLX00062	14.10.99	6368977	1548961	-2.2	1.0
251	3032	PLX00063	14.10.99	6369010	1549173	-0.9	1.0
252	3033	PLX00064	14.10.99	6369013	1549176	-2.17	1.0
253	3034	PLX00065	14.10.99	6369081	1549120	-3.95	1.0

**SICADA Data**

For the rock mechanics descriptive model of Laxemar the type of data collected from SICADA are listed in Table A7-1. Apart from this some data were also collected from SKB reports and from the geological description within the Laxemar project. References to sources are given in the text in each case.

**Table A7-1. Input data collected for the rock mechanics descriptive model.**

Parameter	Borehole	Order, date	Comment
Hydraulic fracturing stress measurements	KLX02	01-79; 2001-11-21	
Fracture frequency	KLX01 and KLX02	01-79; 2001-11-21	Only KLX02 used
Crush_view	KLX01 and KLX02	01-79; 2001-11-21	Only KLX02 used
Natural joints	KLX01 and KLX02	01-79; 2001-11-21	
Rock type	KLX01 and KLX02	01-79; 2001-11-21	
RQD	KLX01 and KLX02	01-79; 2001-11-21	Only KLX02 used
Overcoring stress measurements	KZ0059B, KXZSD8HR, KXZSD8HL, KXZSD81HR, KK0045G01, KAS05, KA3579G, KA3068A, KA2870A, KA2510A, KA2198A, KA1899A, KA1625A, KA1623A, KA1192A, KA1054A, KA1045A, KA1626A	01-79; 2001-11-21	All boreholes located at ÄHRL. Not all of the data are used in the analysis.
Uniaxial compressive strength	KA0667B, KA0745B, KA0747A, KA1054A, KA1061A, KA1131B, PA1653, PA1654, PA1655, PAS00103, PAS00104, PAS00105, PAS00106, PAS00107, KXZA4, KXZA5, KXZA6, KXZC3, KXZC4, KXZC5, KXZC6, KXZC6, KA3545G, KA3557G	02-01; 2002-01-15	All boreholes located at ÄHRL
Sonic logging	KLX02	From ÄHRL (Leif Stenberg); 2001-11-#	Not yet in SICADA#

## Log-files

The logfile from the order of the uniaxial strength results is given below. For the order of the other data no log-file was provided from the SICADA administrator.

Source table: zzq\_1b0173c0005d0000, output file: /tmp/appsrv4427.outfile

Result: 73 rows found

Original search criteria

---

Date :2002-01-15 09:21:24

Tables :zzq\_1b0166c0005d0000 z,activity\_history h,zys\_act\_check a, strength\_t t

Columns :a.activity, h.start\_date, h.stop\_date, h.idcode, h.secup, h.seclow, t.seq\_no, t.diameter, t.thickness, t.p\_max, t.p\_res, t.sigma\_c, t.sigma\_1c, t.sigma\_ci, t.sigma\_cd, t.sigma\_3, t.sigma\_t, t.friction\_angle, t.comment

Criteria: h.activity\_id=z.activity\_id AND h.activity\_id=t.activity\_id AND a.activity\_type=h.activity\_type

Activity search SQL string:

```
SELECT *
FROM activity_history h,zzq_1b0165c0005d0000 a
WHERE h.activity_type=a.activity_type AND h.site in ('ÄSPÖ') AND
(VARCHAR(UPPERCASE(a.activity)) like '%UNIAXIAL STRENGTH TEST%')
```





Geology/Corelogging/petrocore

Activity id

Site Project Start date

Borehole Length Diameter m m

Bearing Inclination

° °

Completion Date

Rock Type Breccia Pegmatite Fine Grained Granite Småland Granite Åspö Diorite Hybride Rock Volcanite (mafic)

Coreloss Missing core

Alteration type Oxidized Cloritized Epidotized Tectonized Sericitized

Rock struct. Homogenous Schistose Banded Brecciated Tectonized

Nat. mineral 1 Quartz Calcite Hematite Clay Iron Hydroxide Red Feldspar Amphibole X3

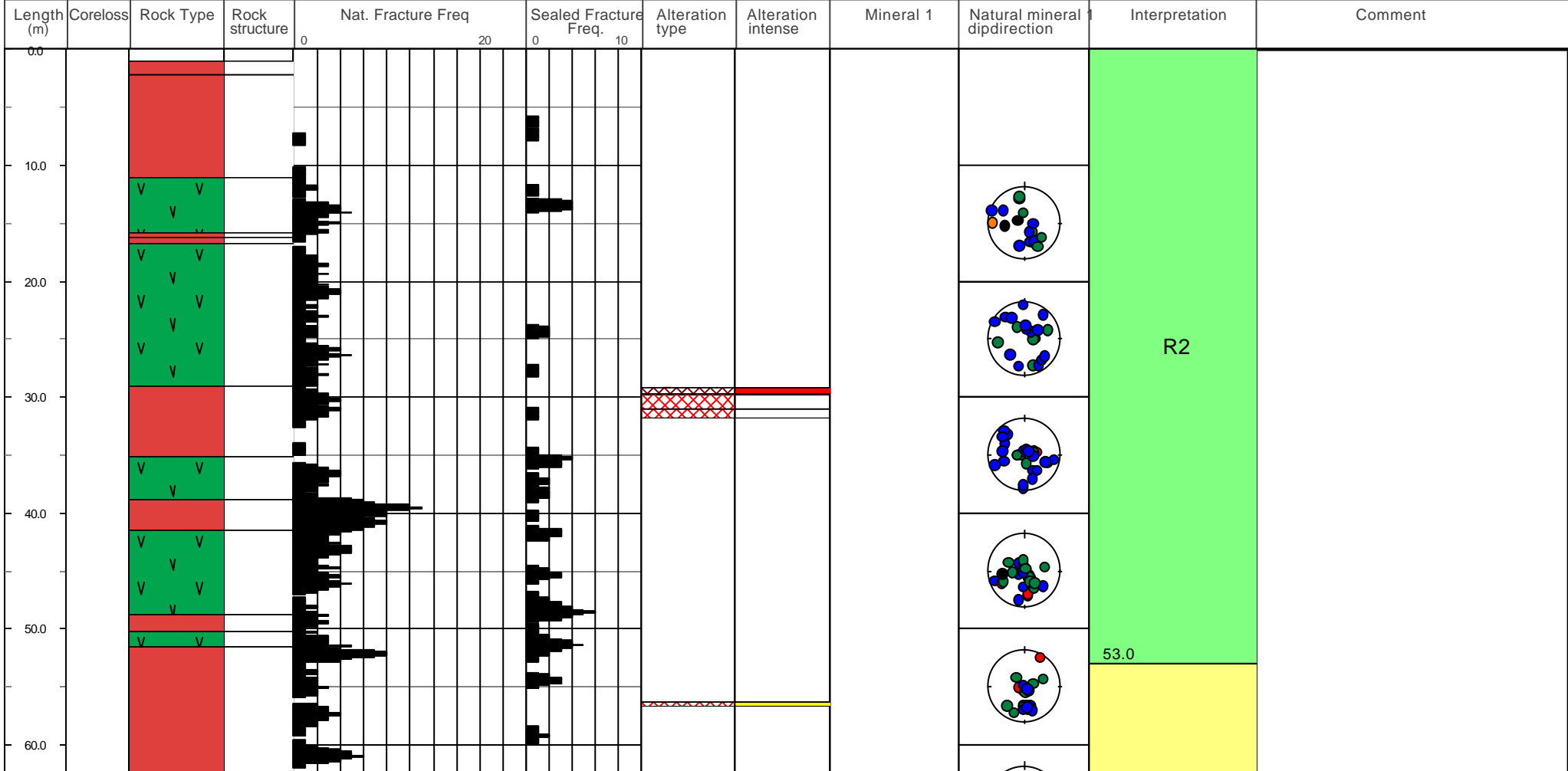
Chlorite Epidote Pyrite Biotite Fluorite Muscovite X1 X4

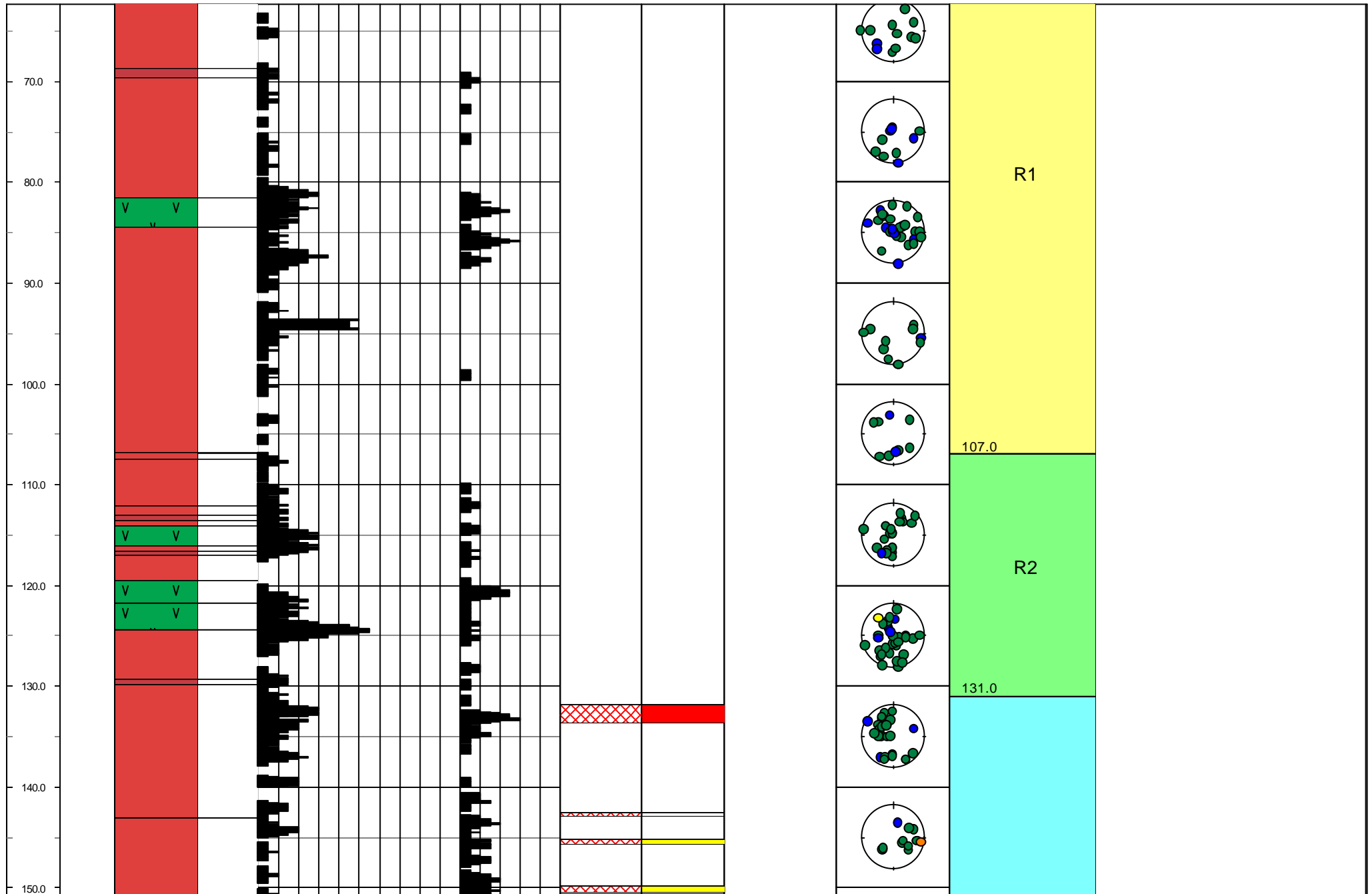
Crush mineral Chlorite Calcite Clay

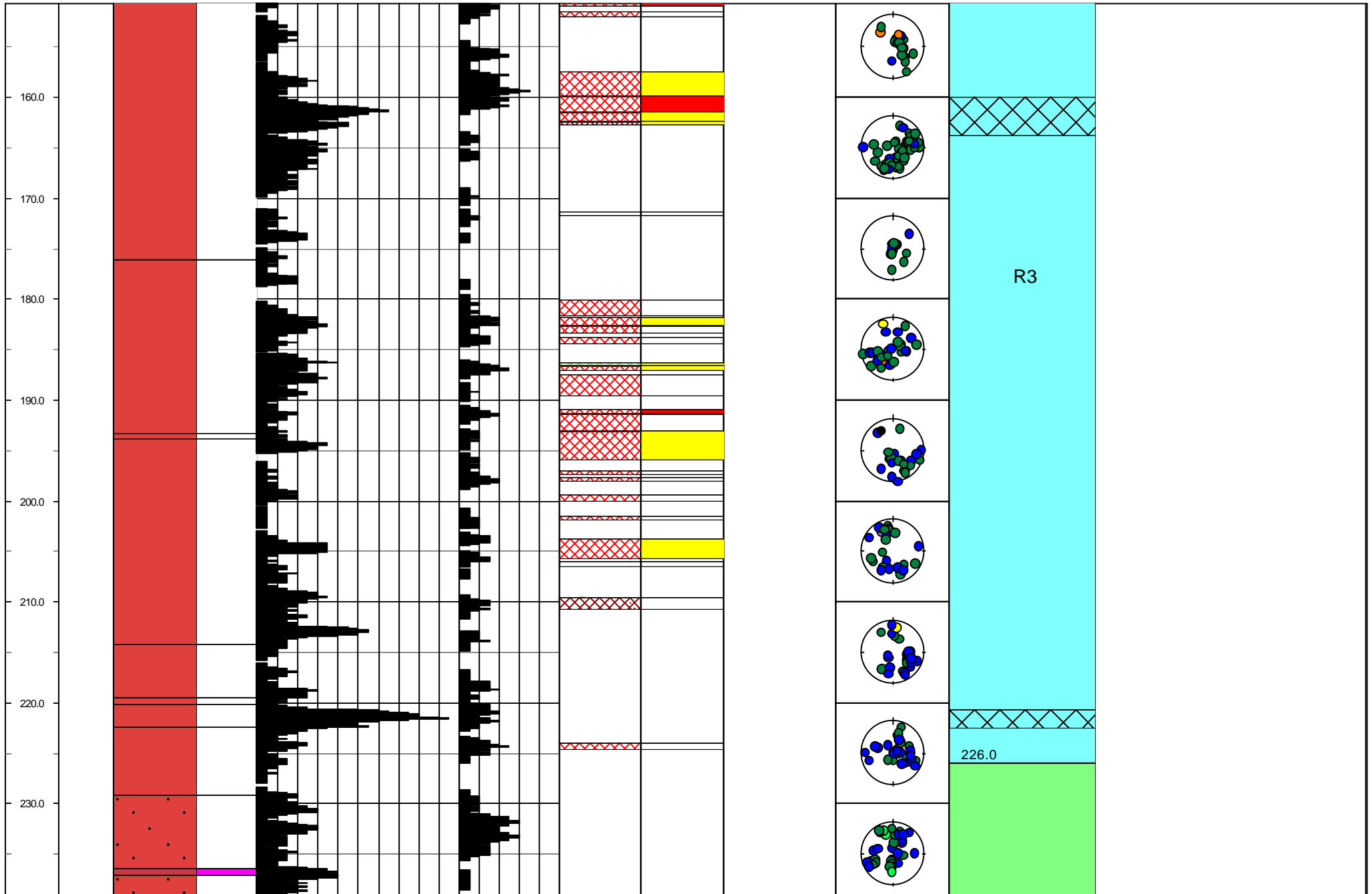
Alt. intense Medium Strong

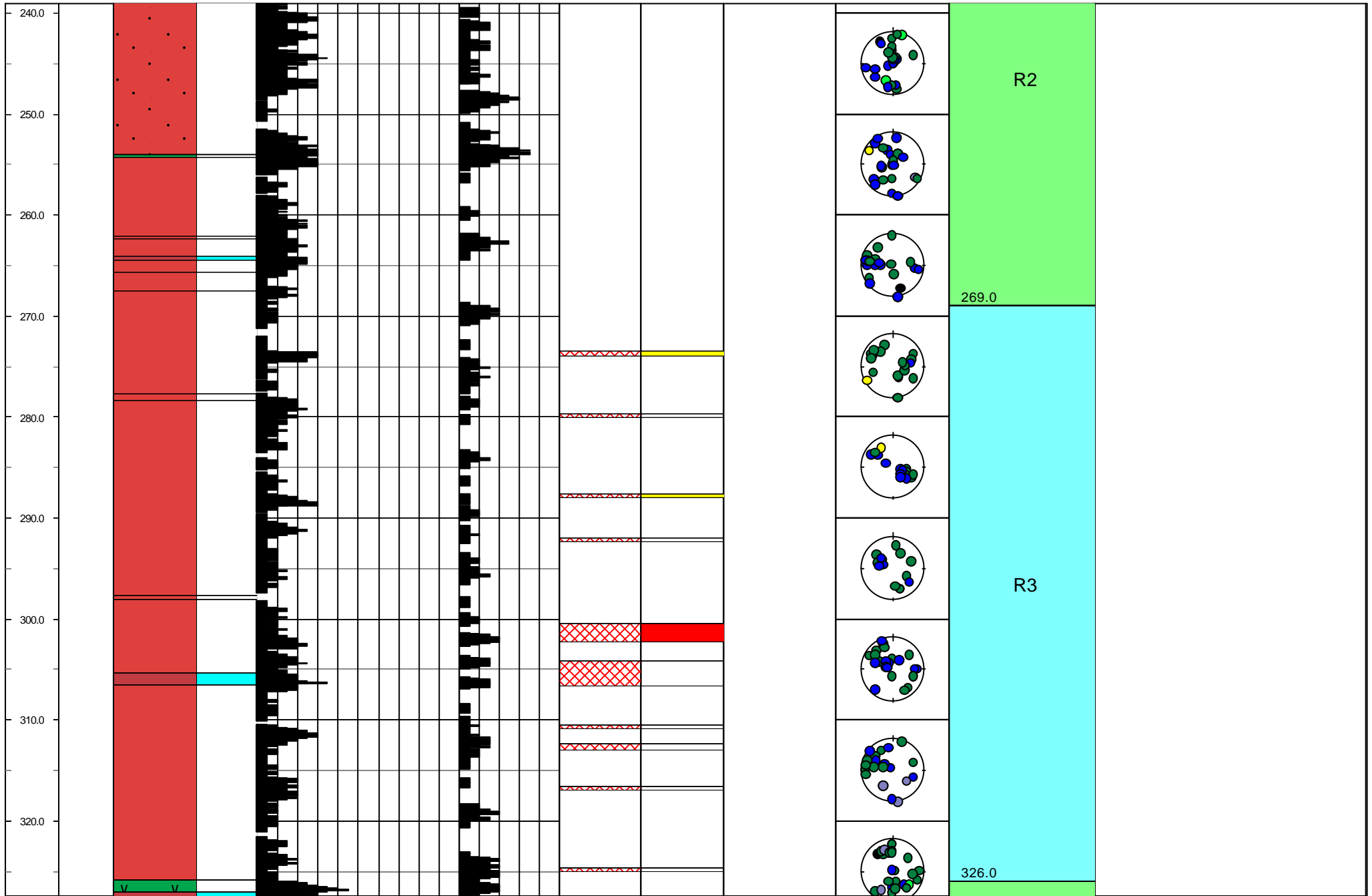
Interpretation #1 #3 #2 #5 #8 #9

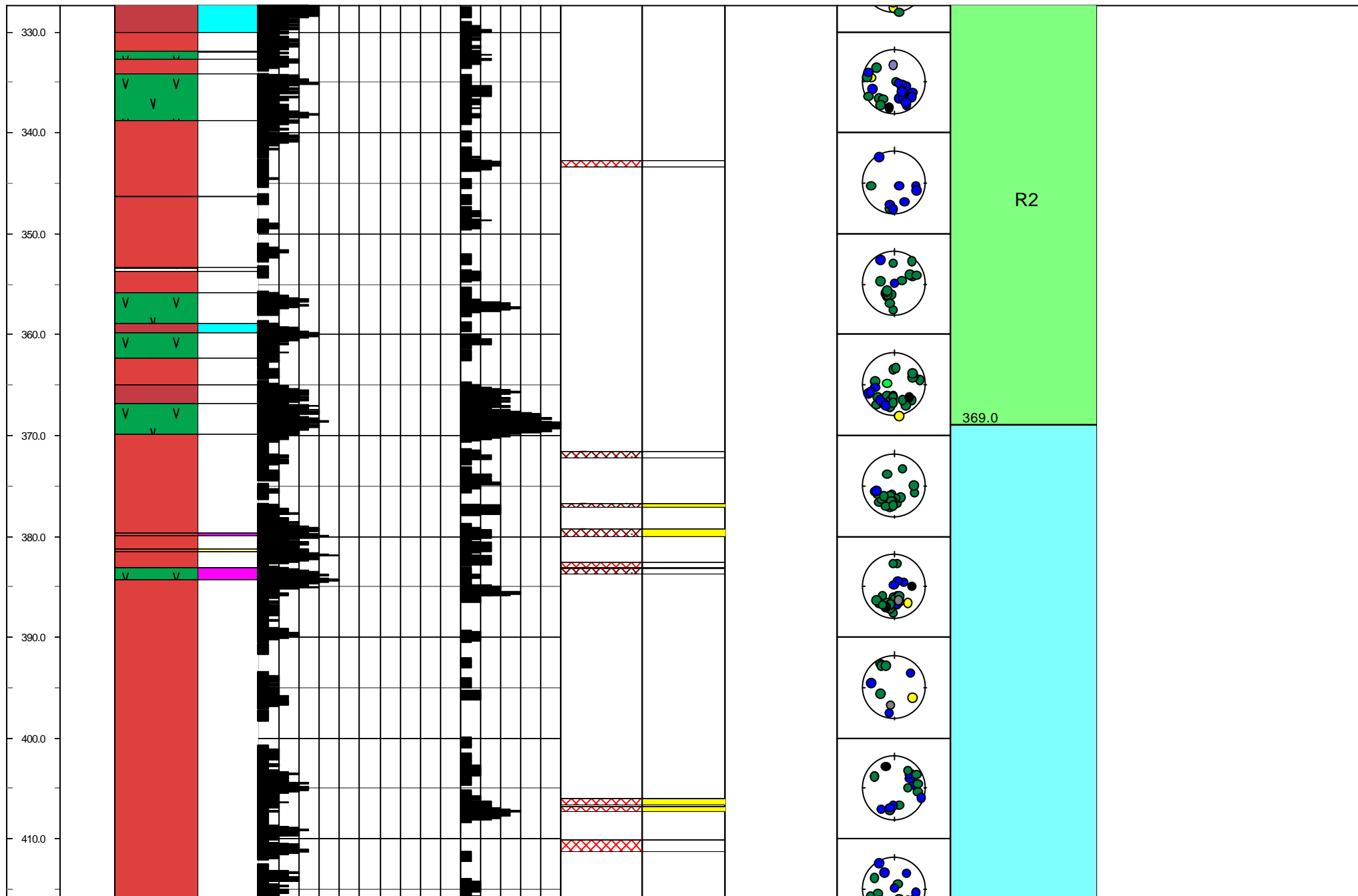
Interpreted fracture zones #1

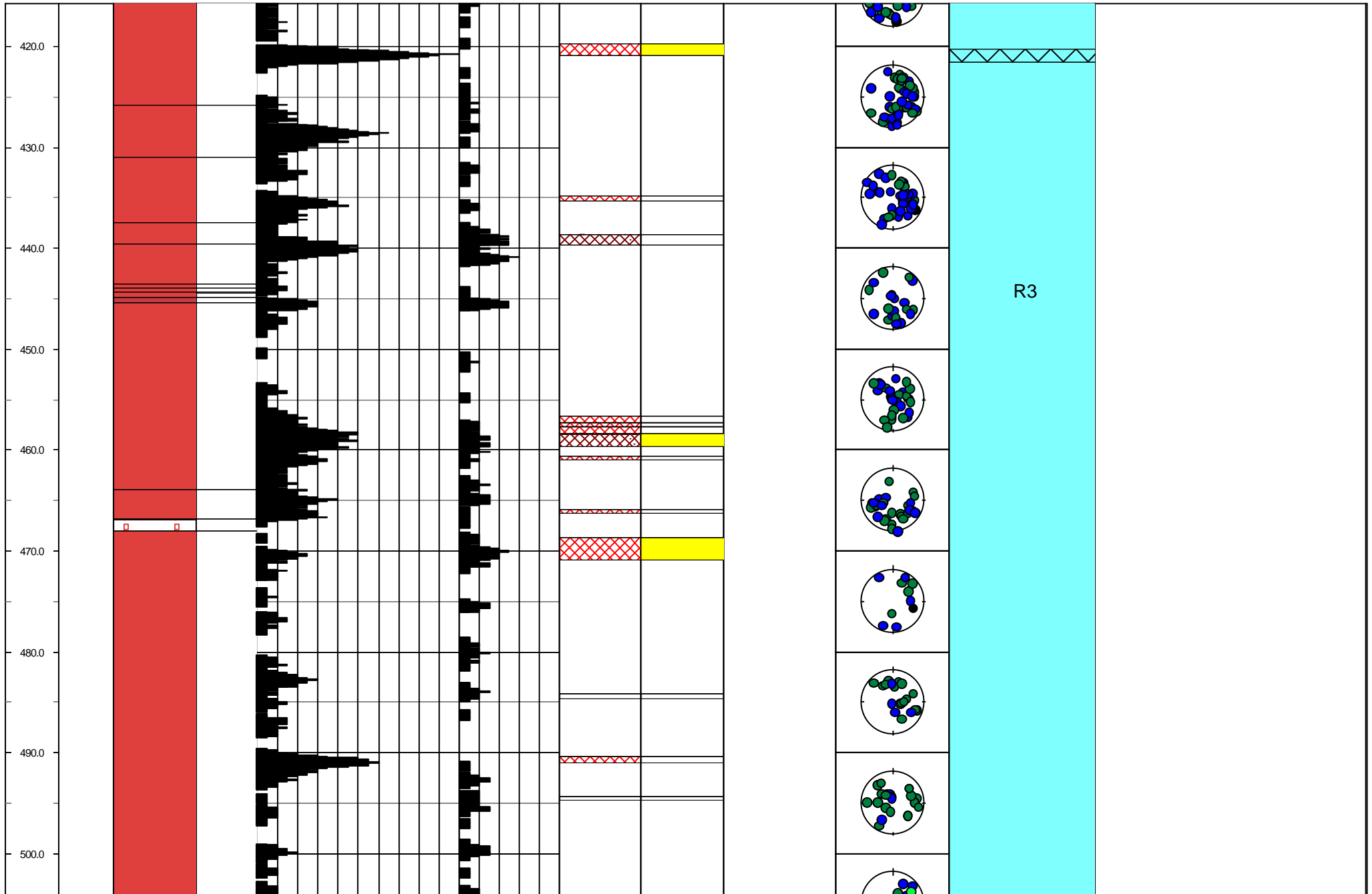


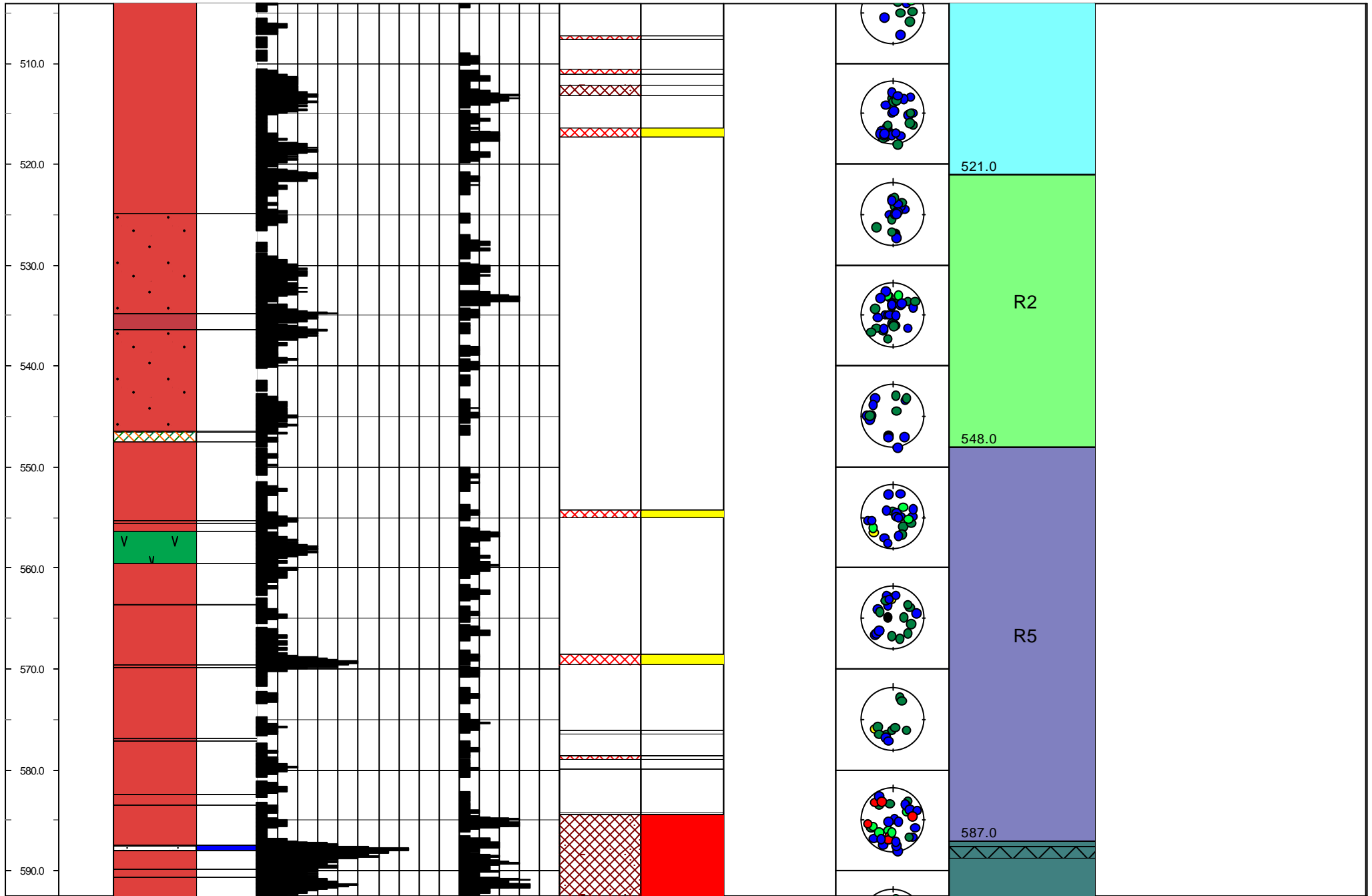






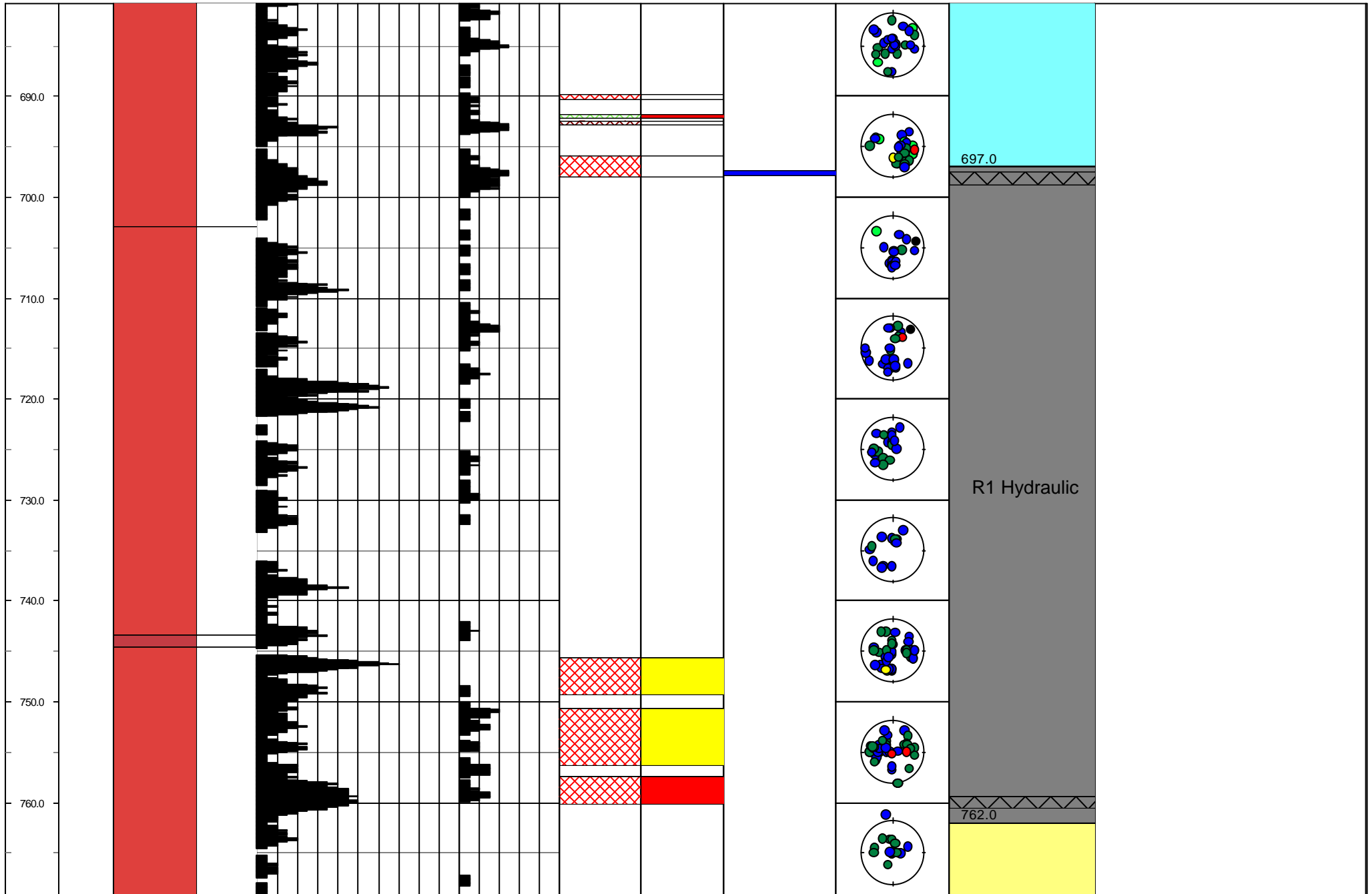


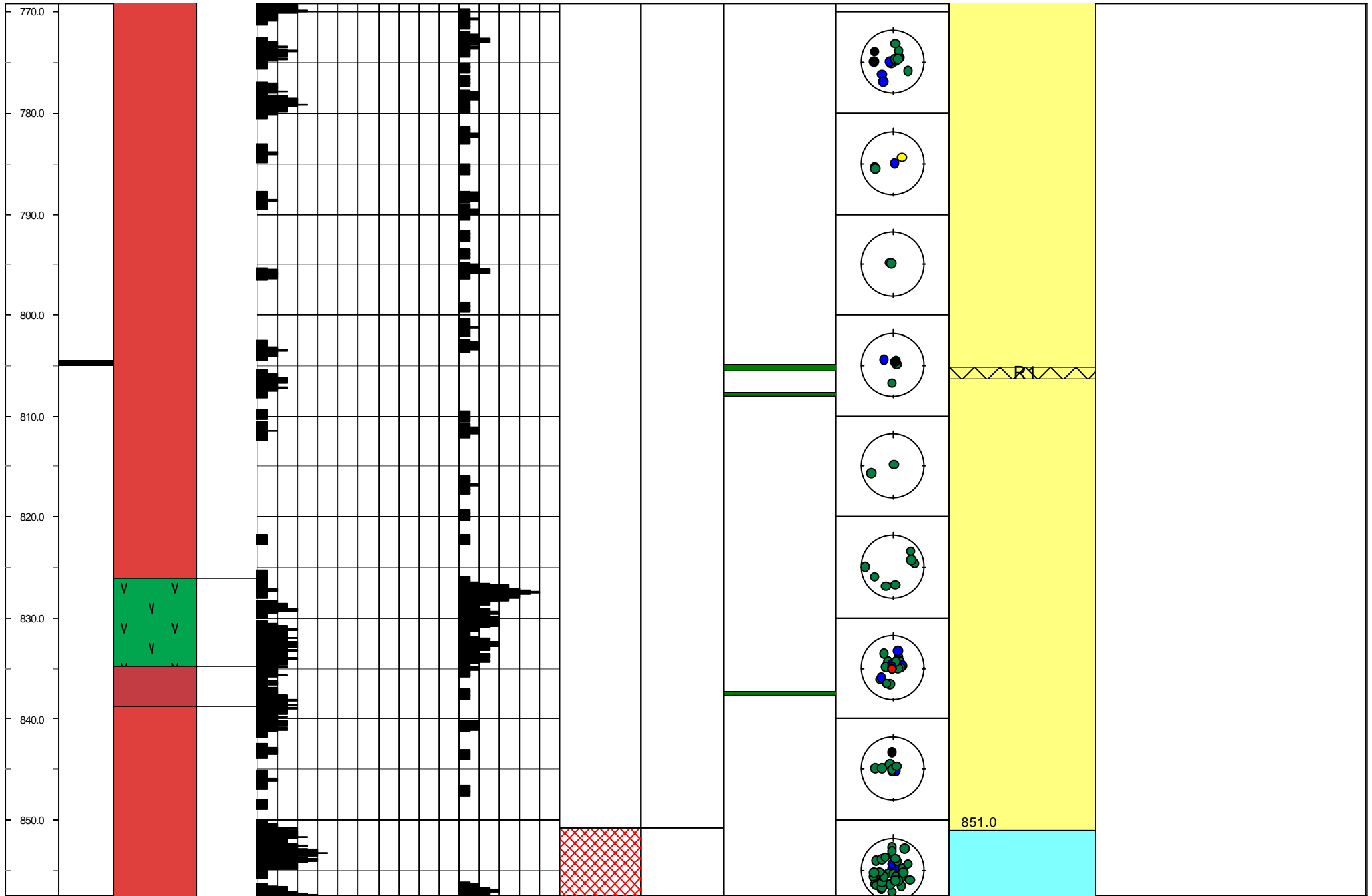




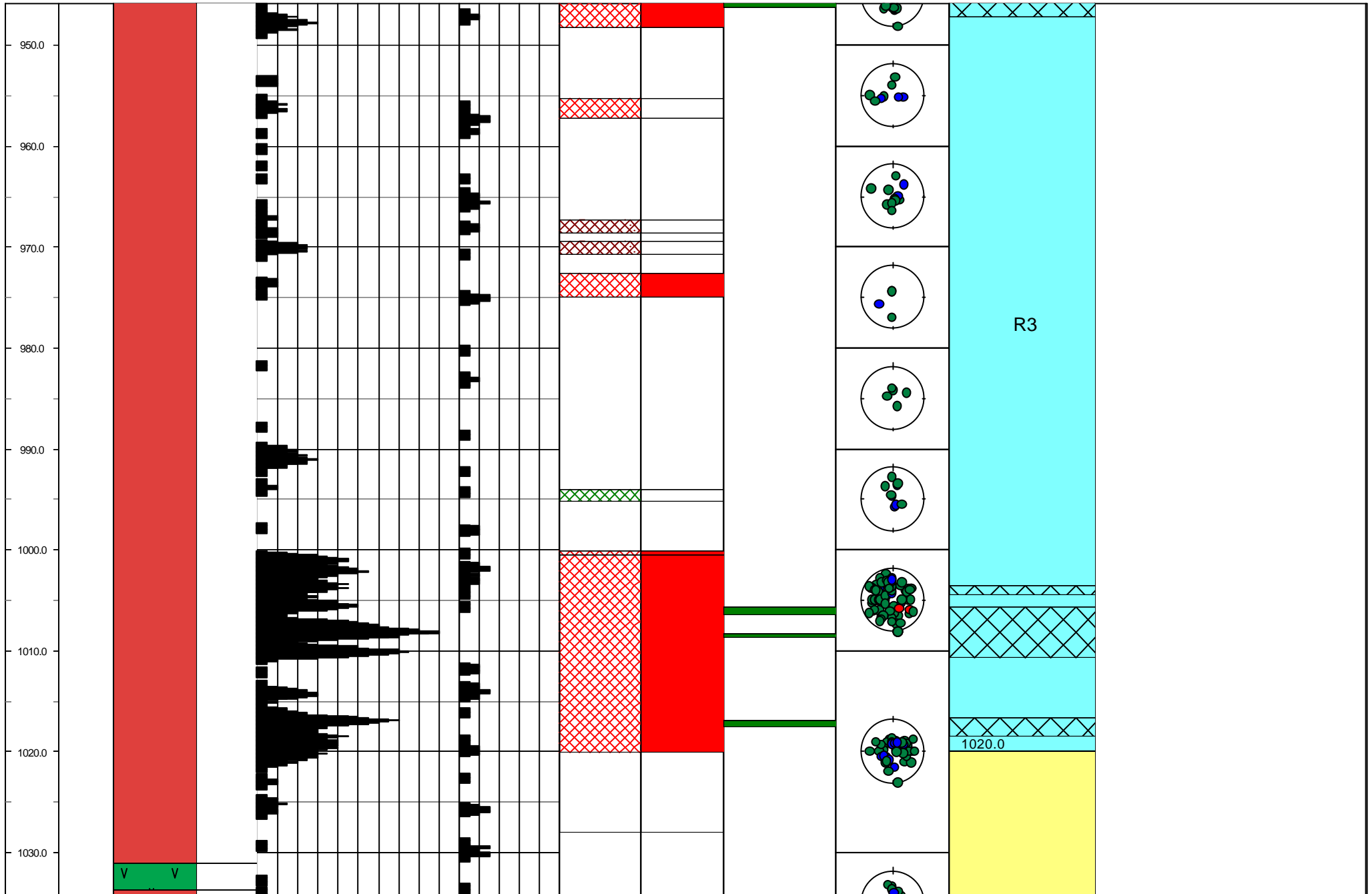


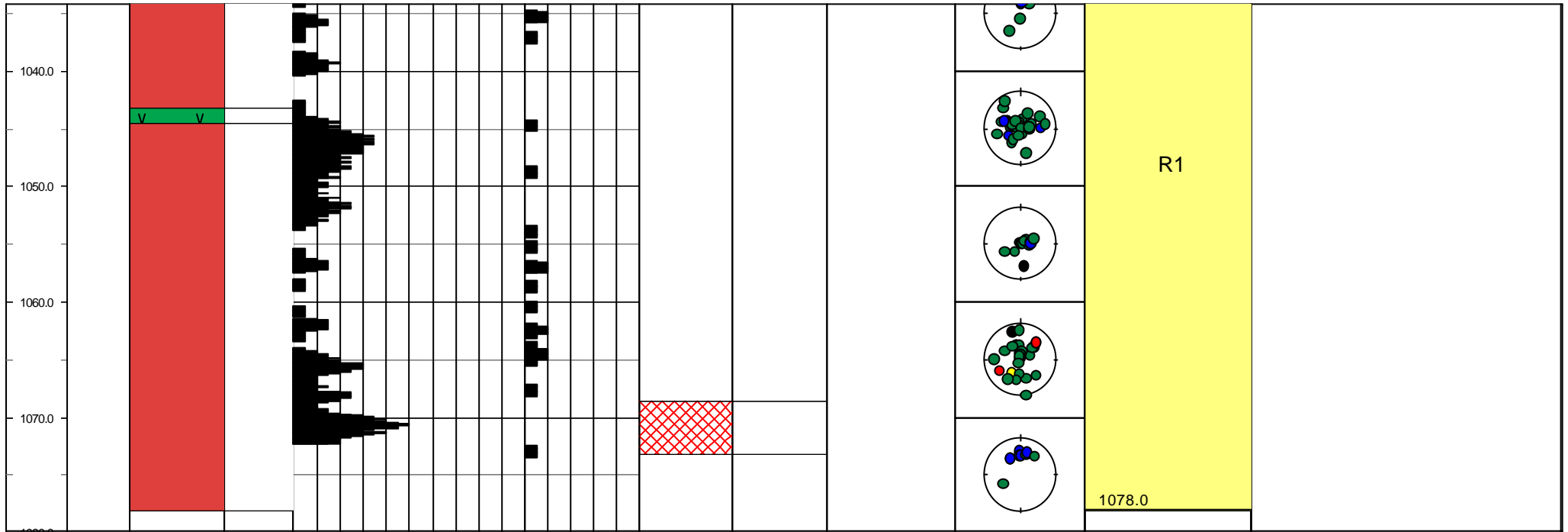






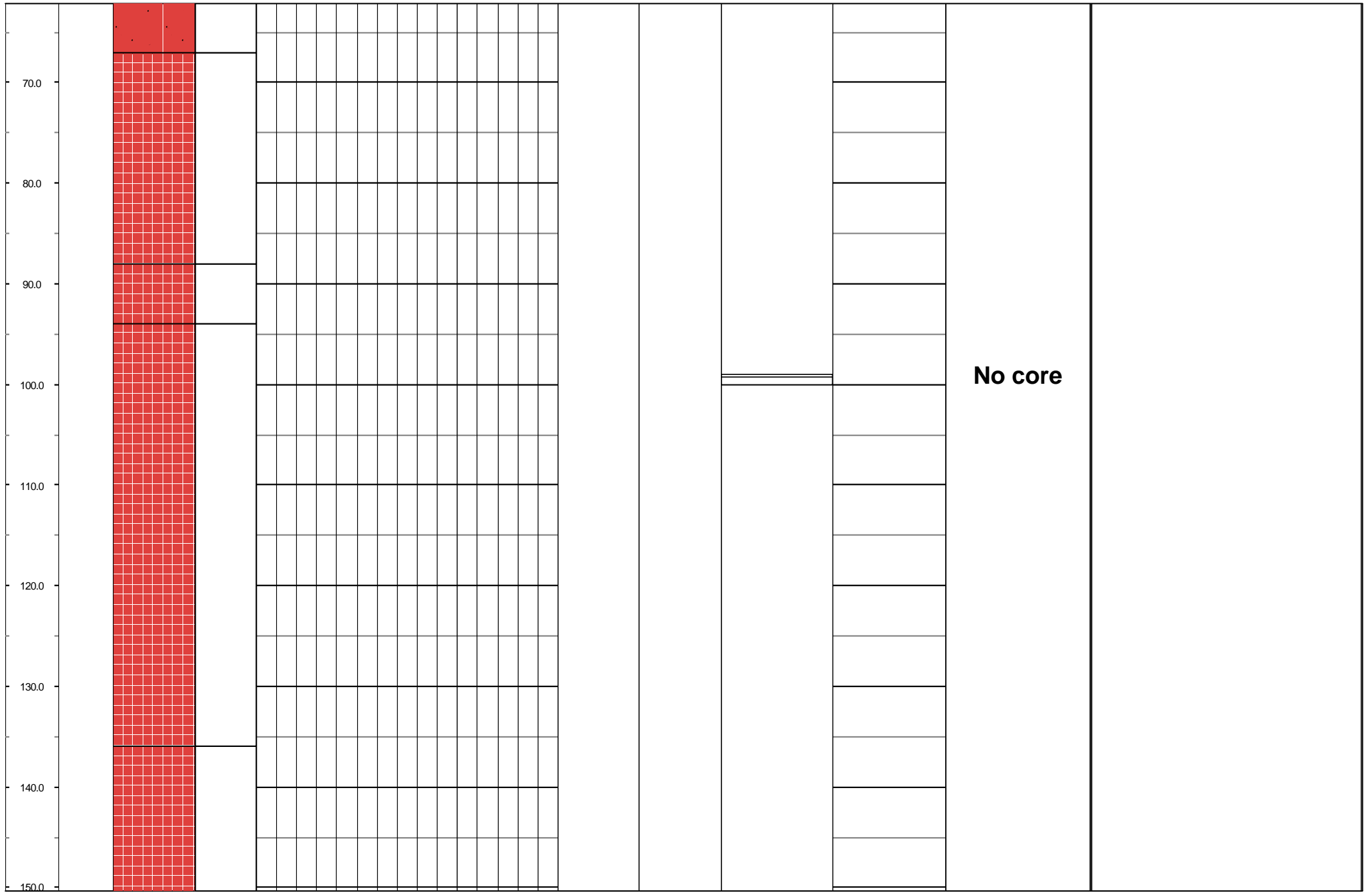






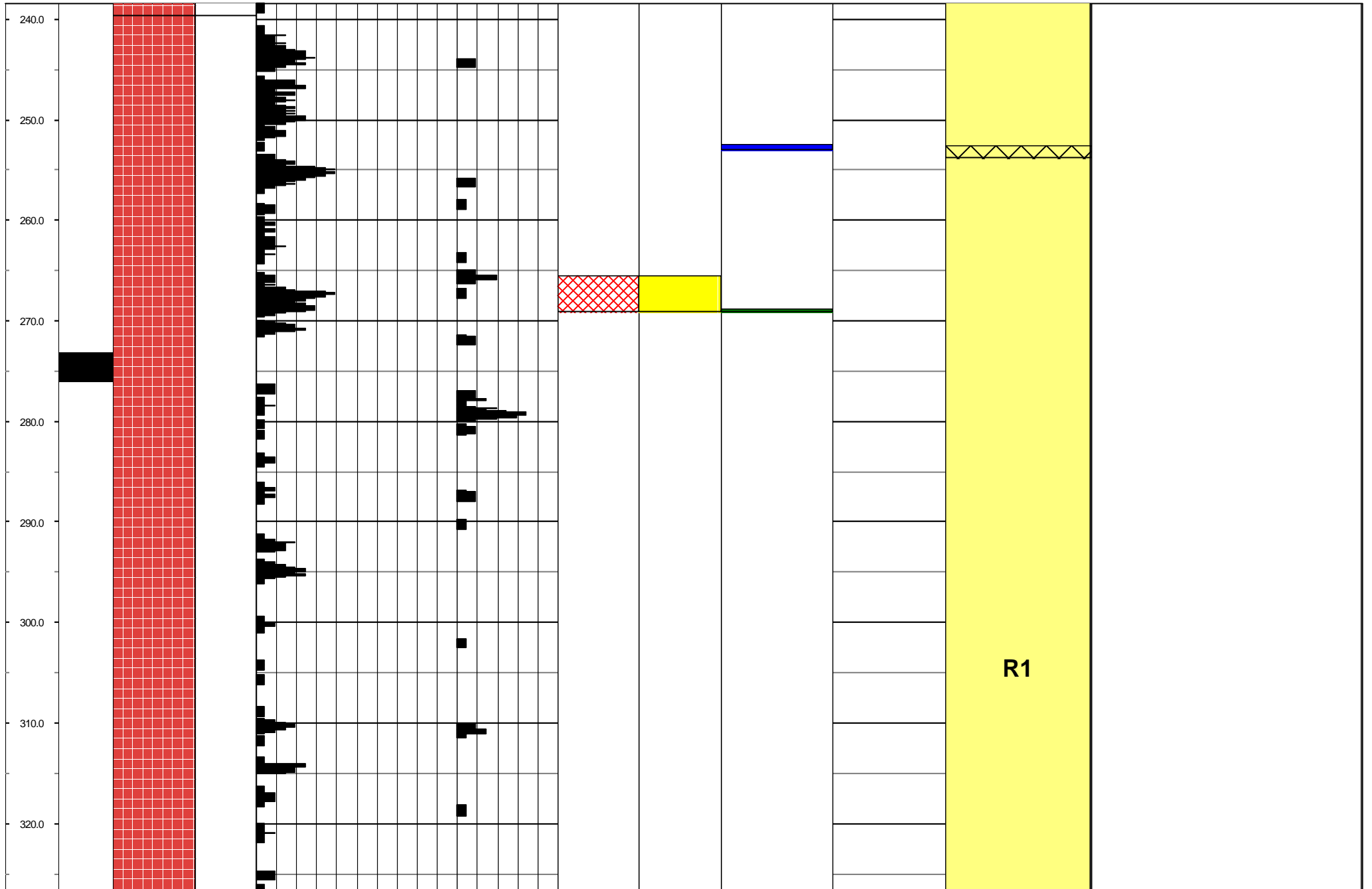
Appendix B2

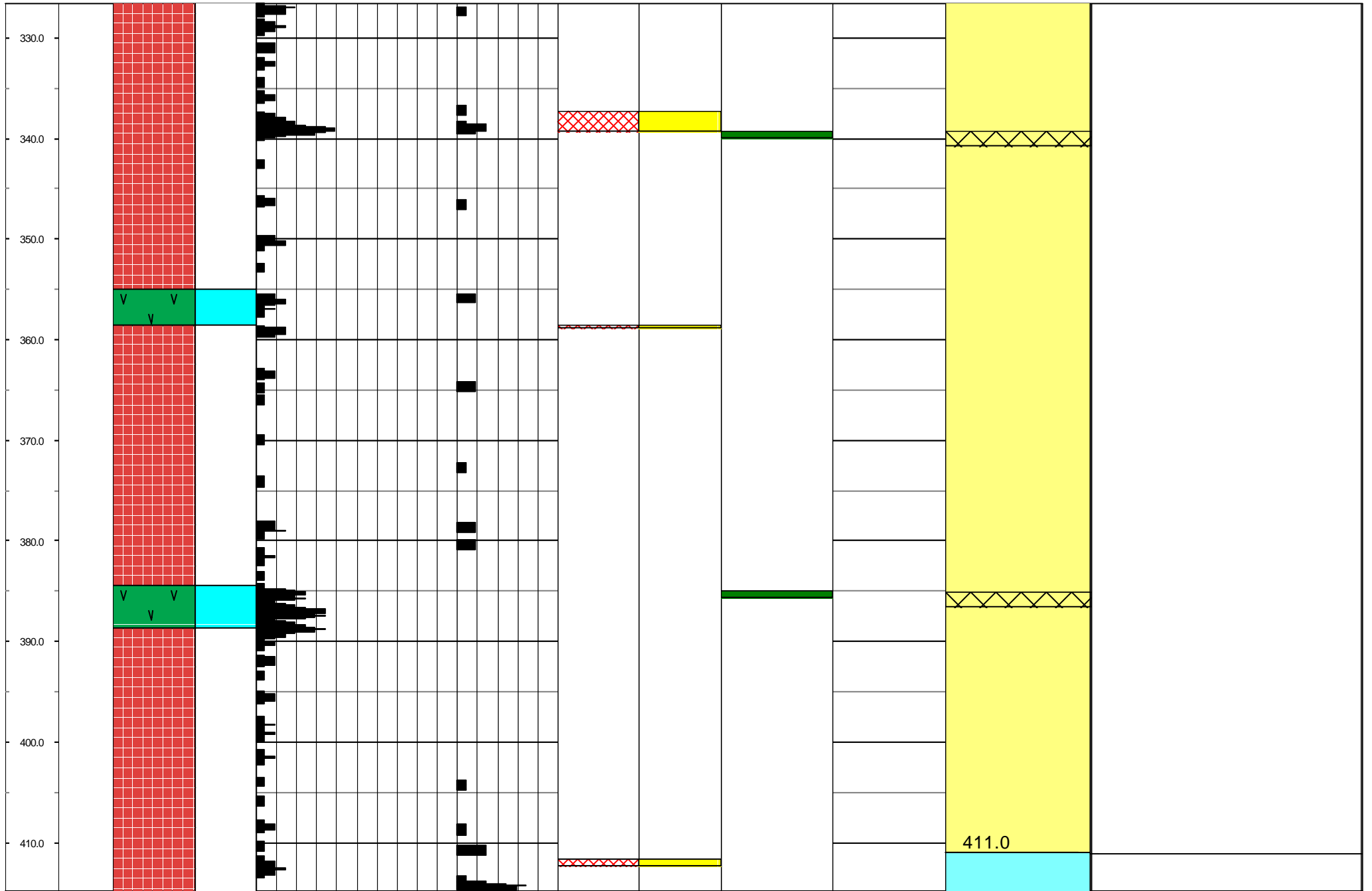
SKB		Geology\Corelogging\petroc		Site	Borehole	Bearing	Completion Date				
Activity id				Project	Length	Inclination					
				Start date	Diameter						
					m						
					m						
Rock Type		Pegmatite	Fine Grained Granite	Småland Granite	Åspö Diorite	Volcanite (mafic)					
Coreloss		Mechanical	Missing core								
Alteration type		Oxidized	Cloritized	Epidotized	Weathered	Tectonized	Alt. intense  Medium  Strong				
Rock struct.		Homogenous	Schistose								
Nat. mineral 1		Quartz	Calcite	Hematite	Chalcocopyrite	Fluorite	Amphibole	X4	Interpretation  #0  #1  #2  #3  #5  #7  #8		
Crush mineral		Chlorite	Calcite	Epidote	Hematite	Unknown	Interpreted fracture zones  #1				
Length (m)	Coreloss	Rock Type	Rock structure	Nat. Fracture Freq	Sealed Fracture Freq	Alteration type	Alteration intense	Mineral 1	Natural mineral 1 dipdirection	Interpretation	Comment
0.0				0 20	0 10						0-200 m No core (Casing)
10.0											
20.0											
30.0											
35.0											
40.0											
50.0											
60.0											

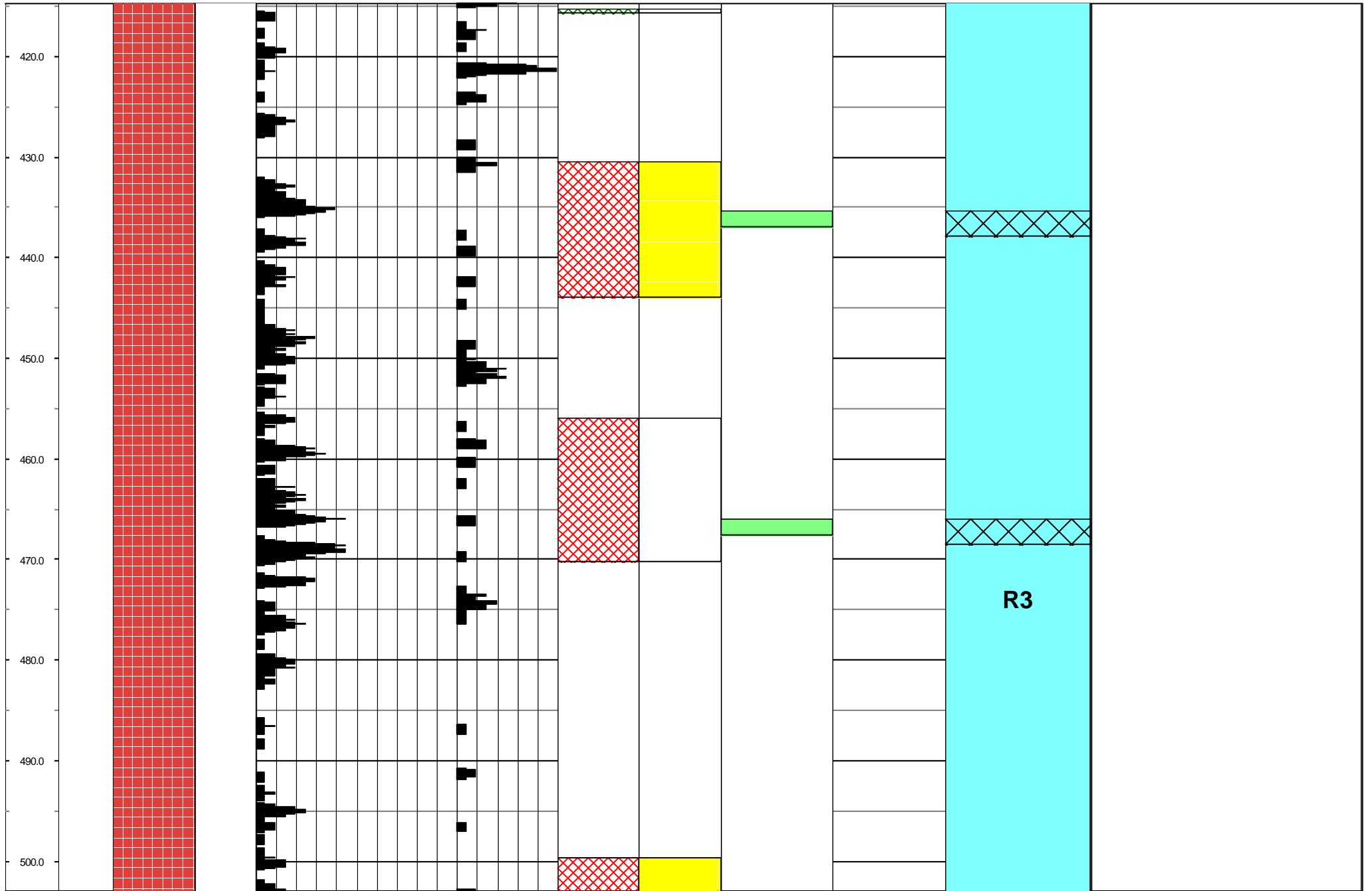


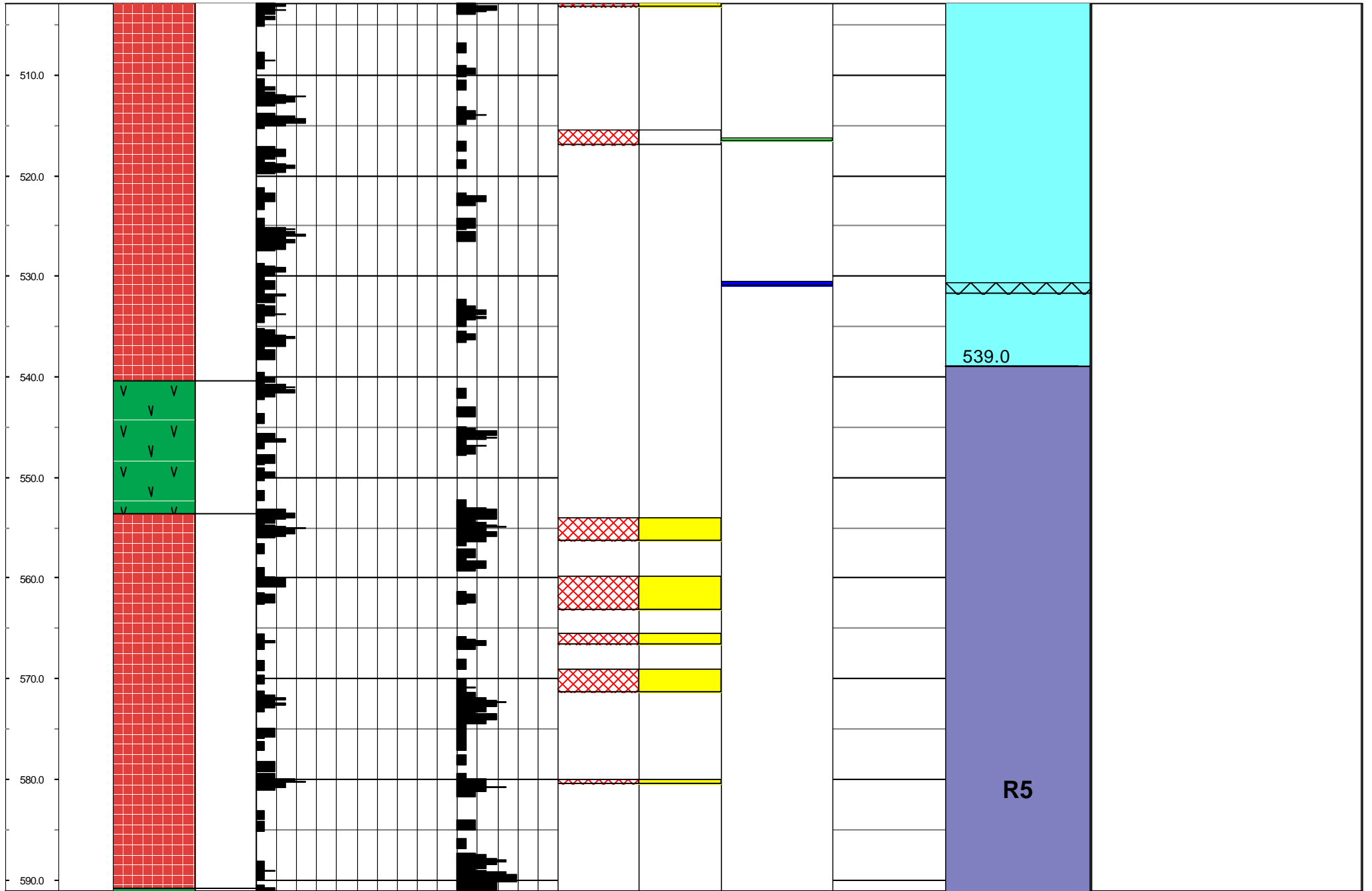


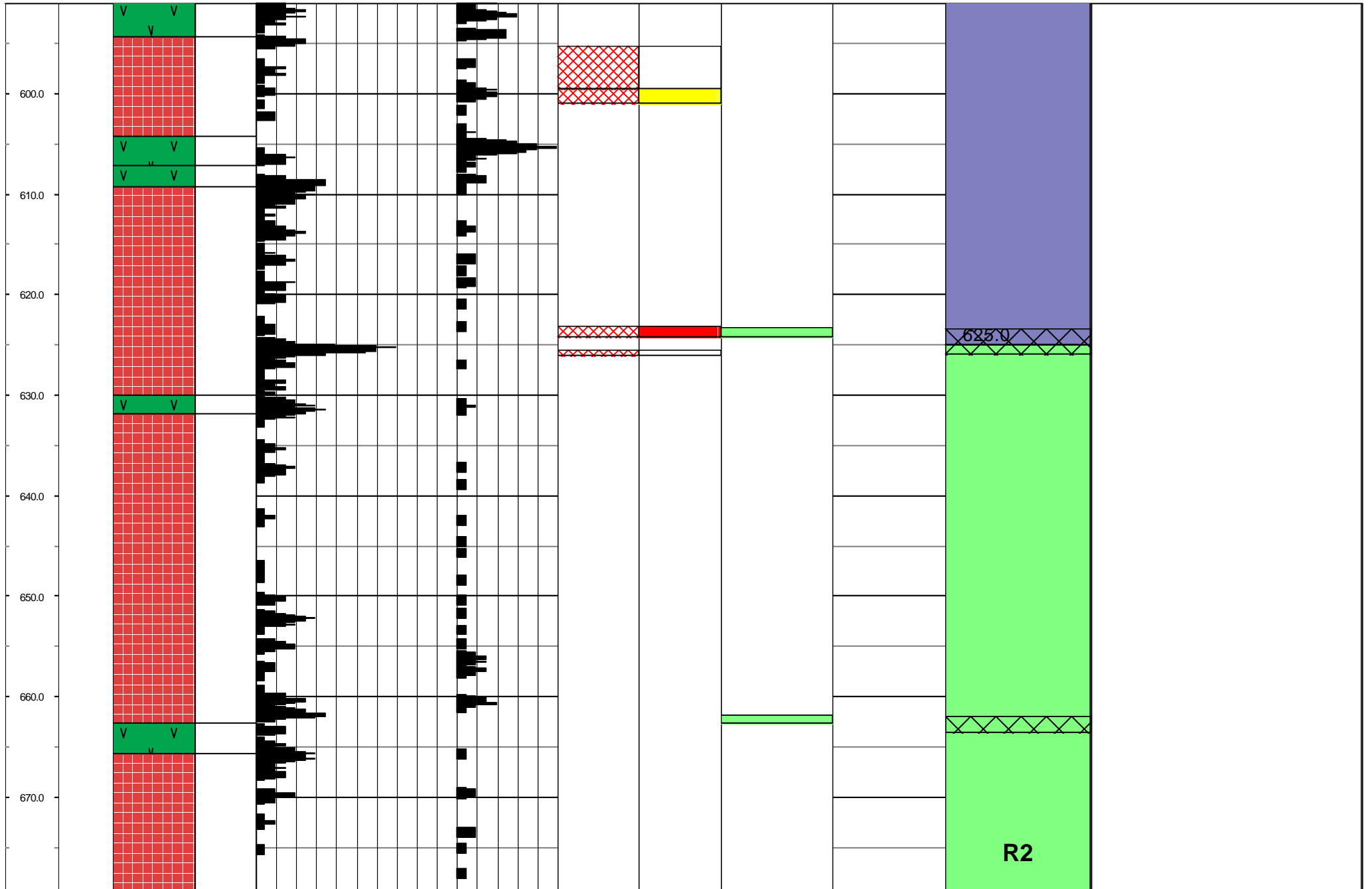


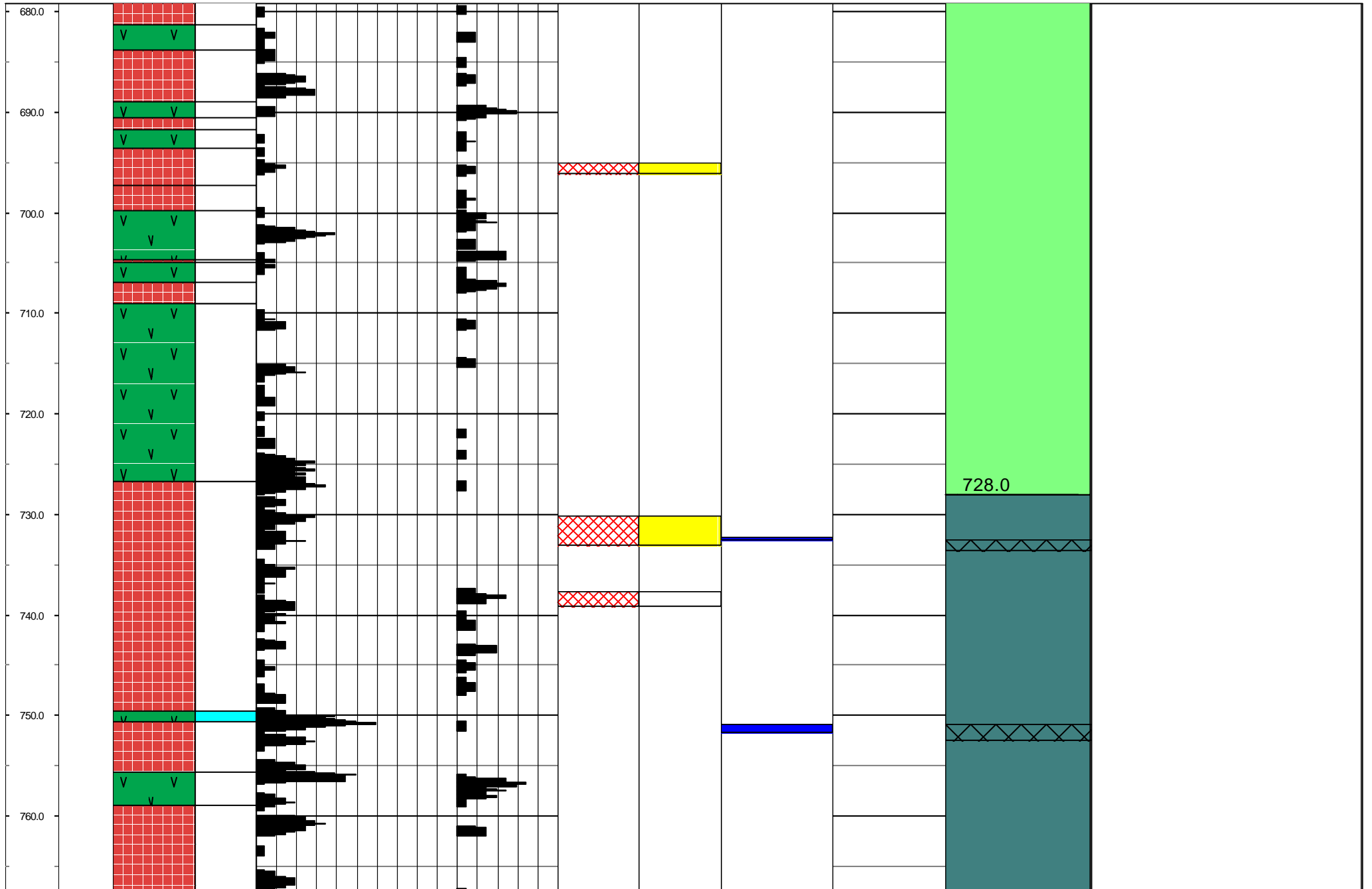


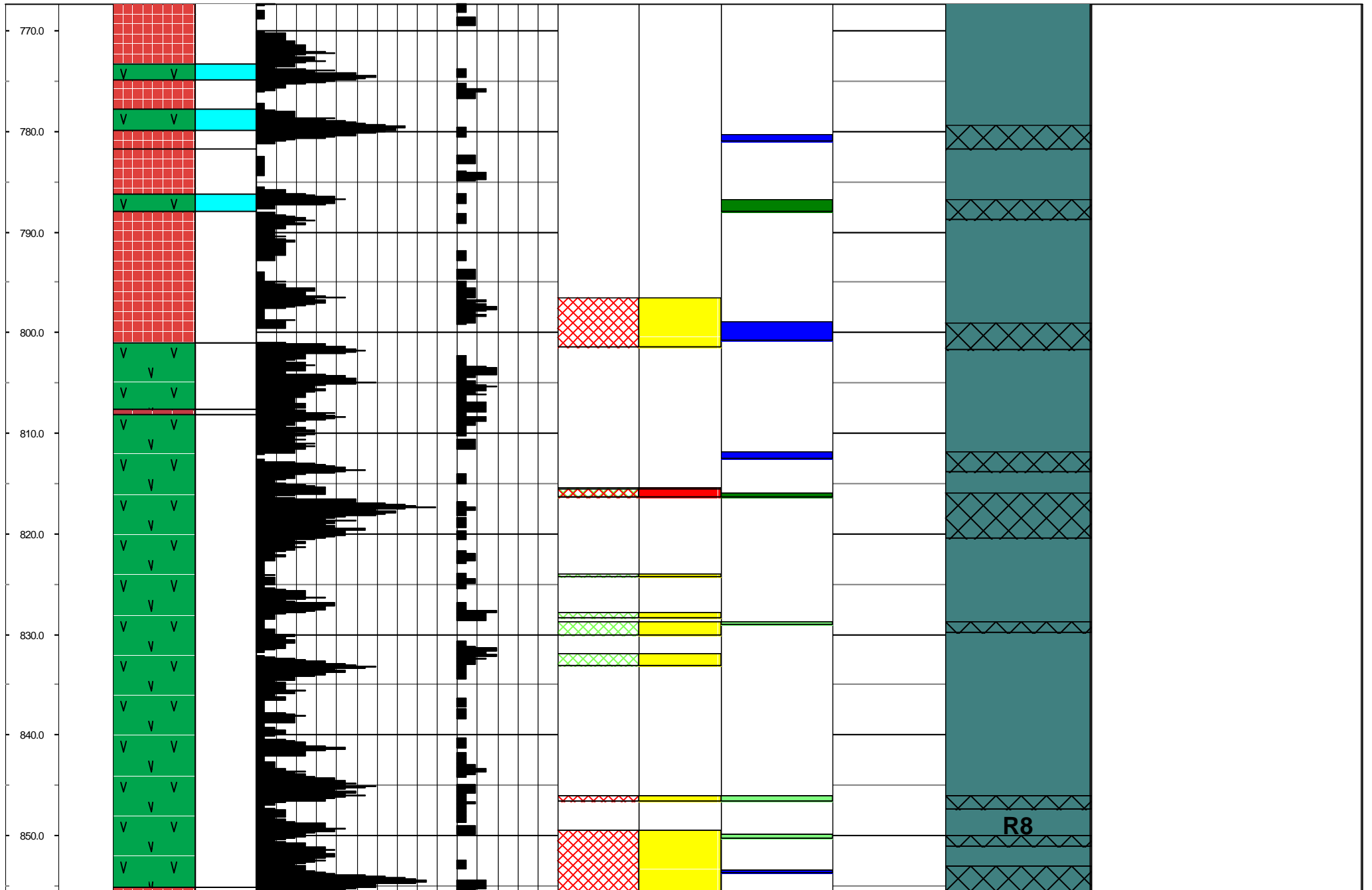


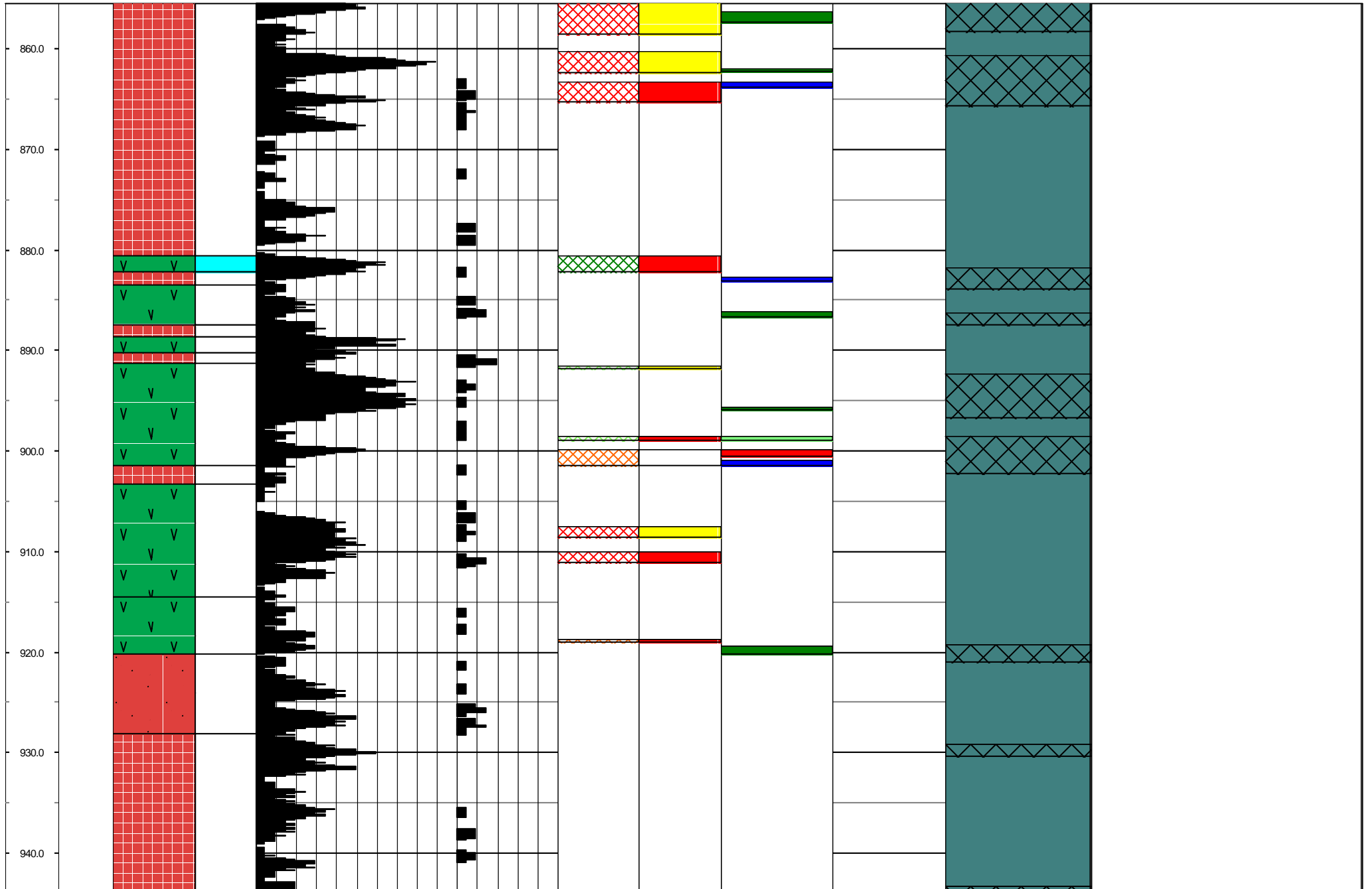




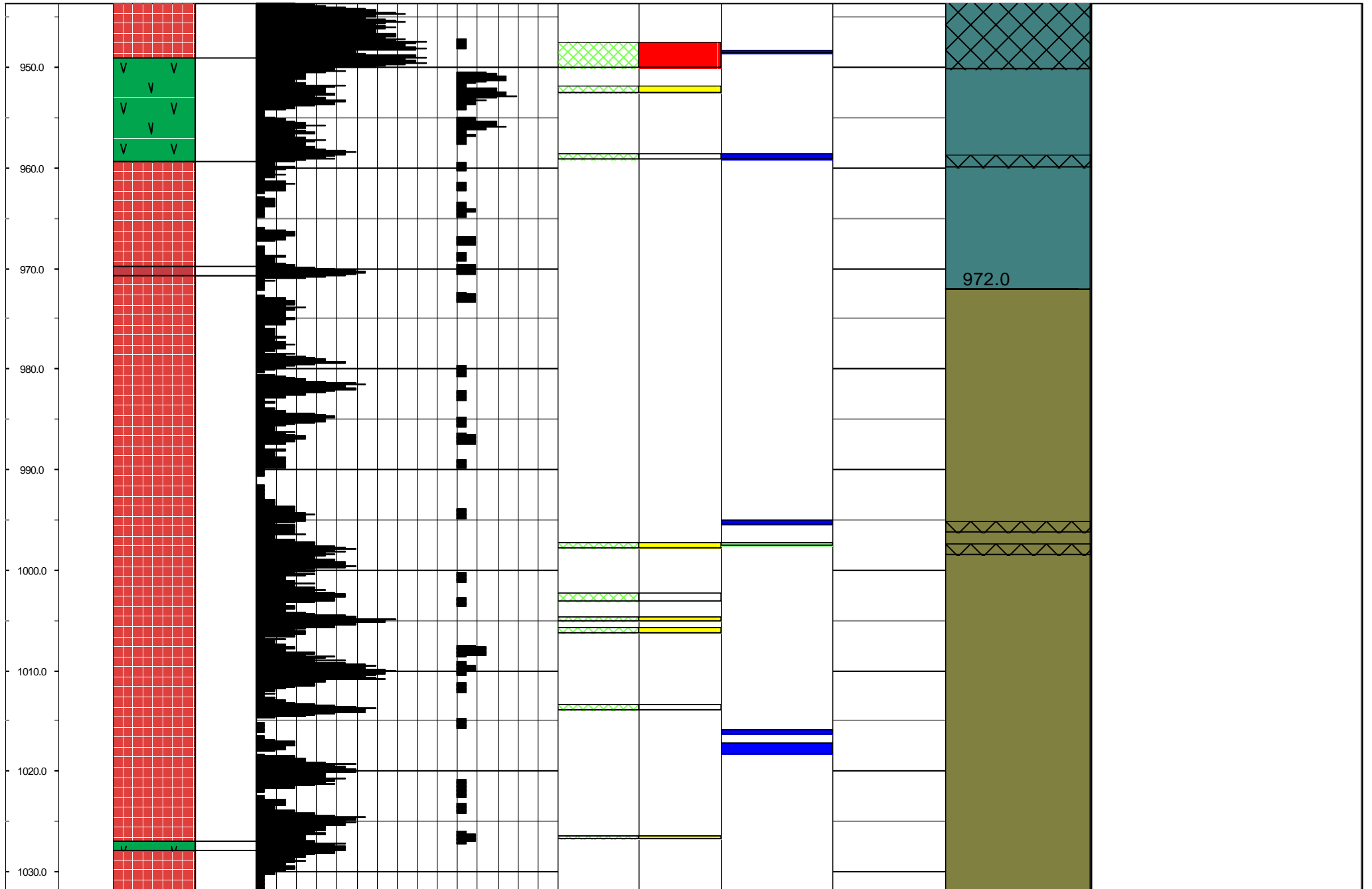


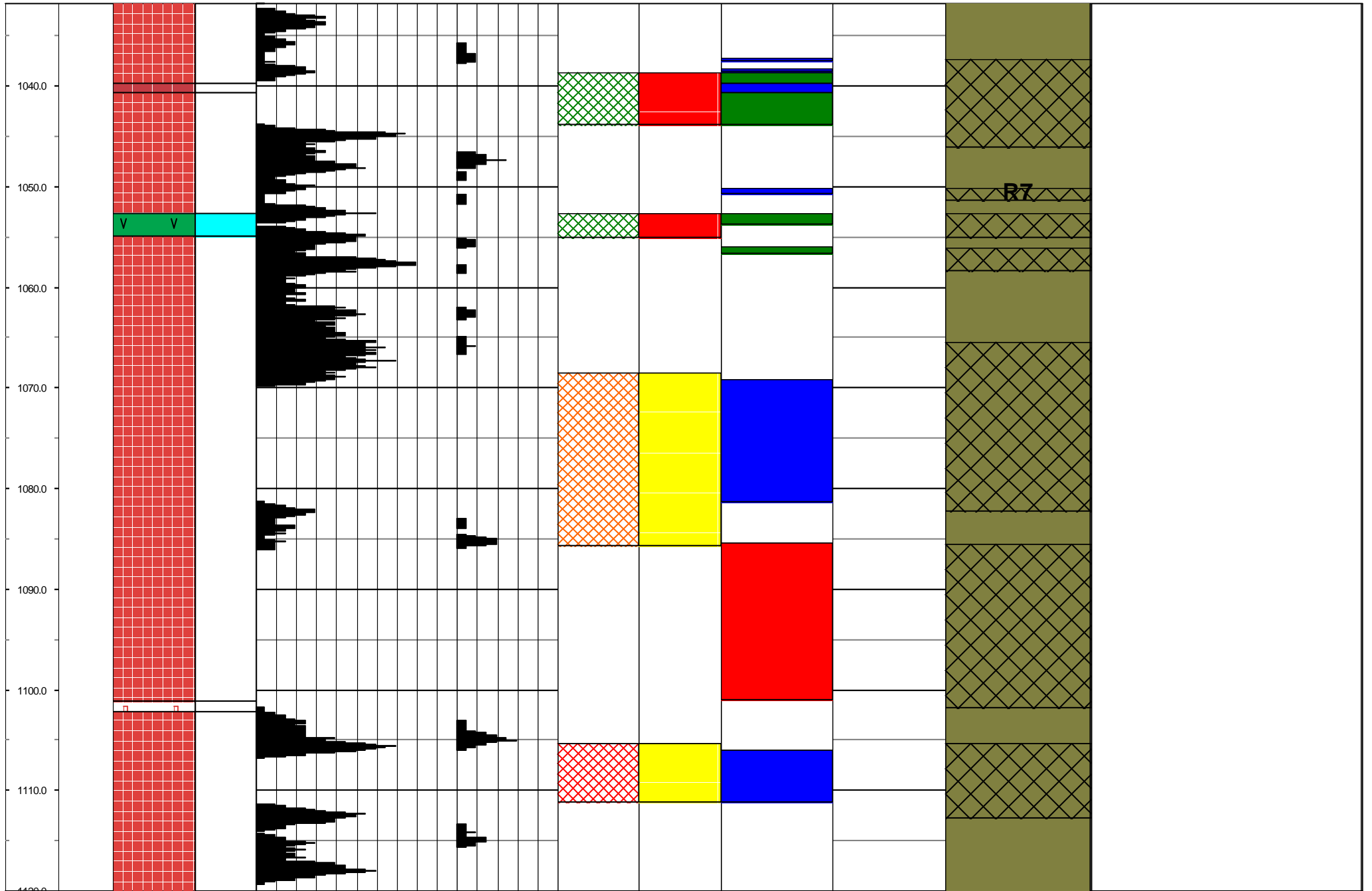


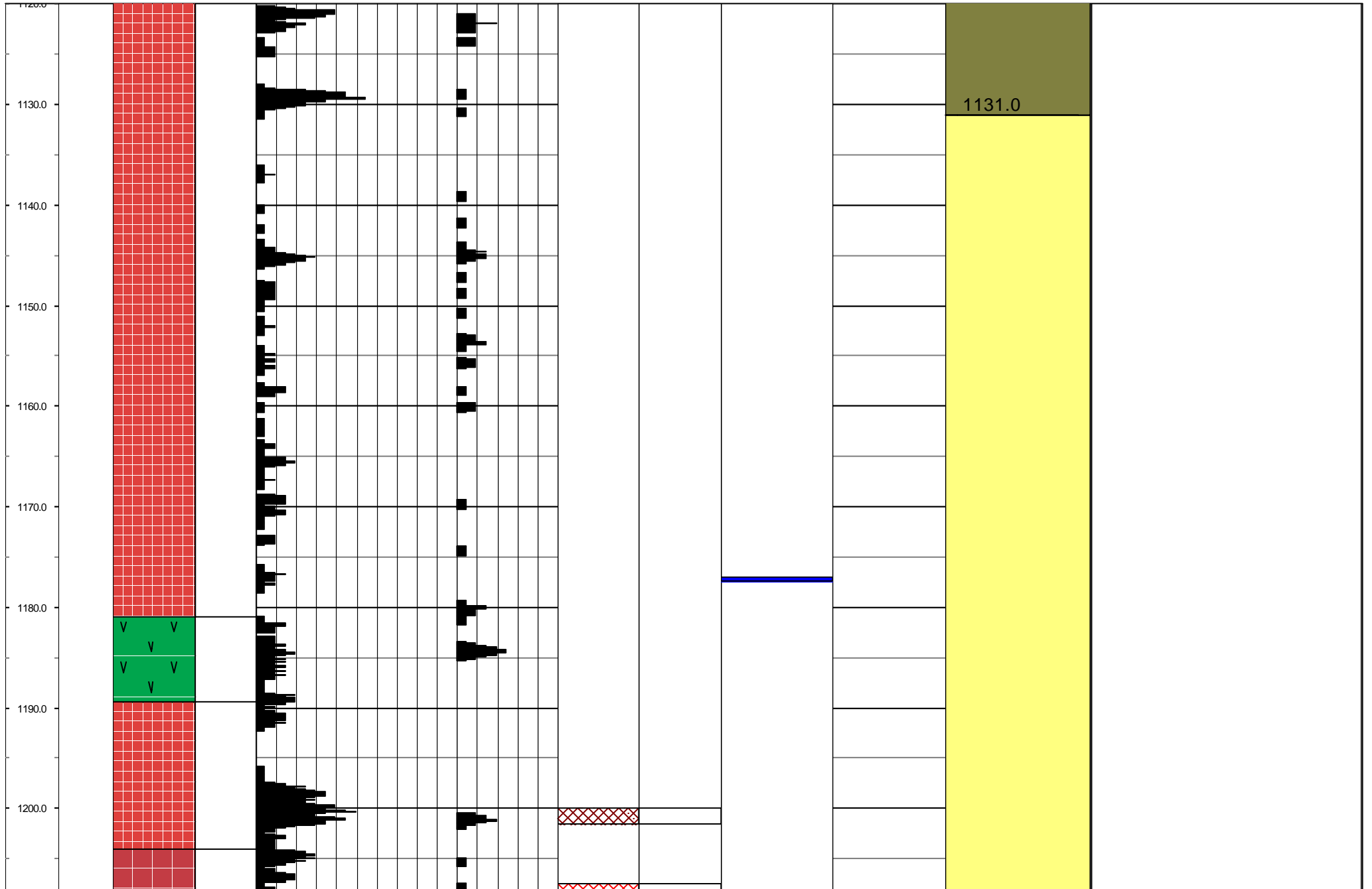


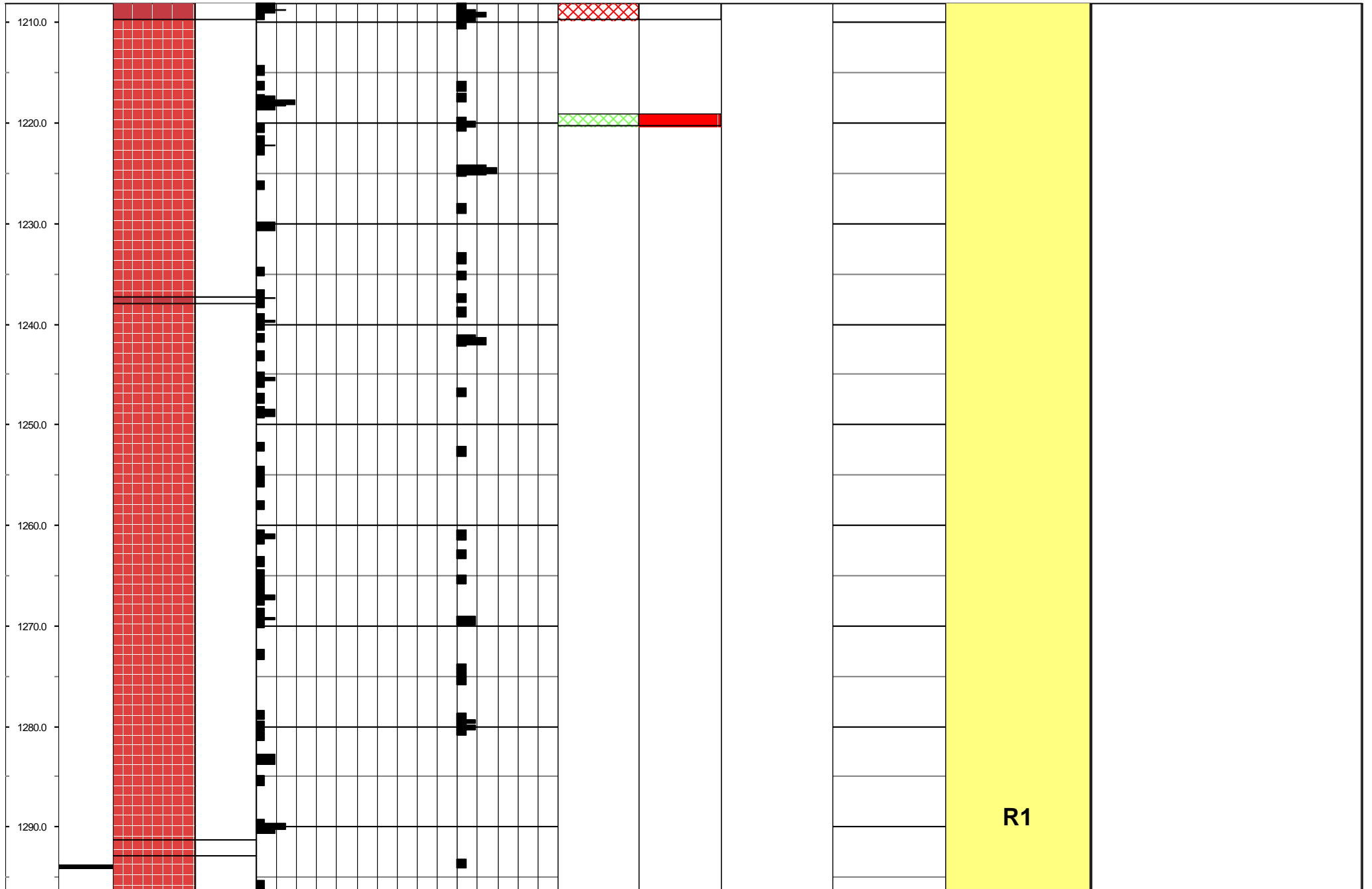


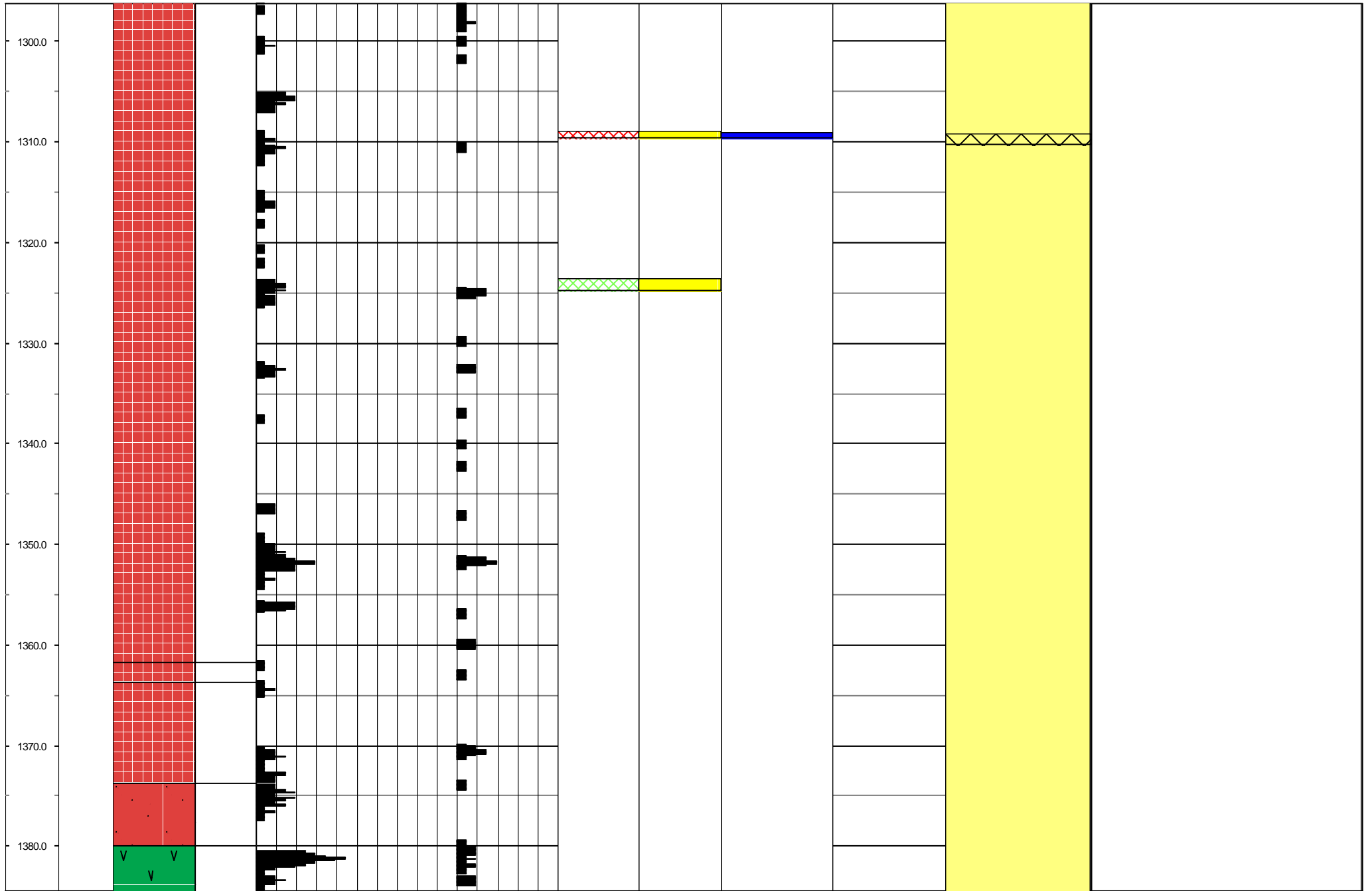


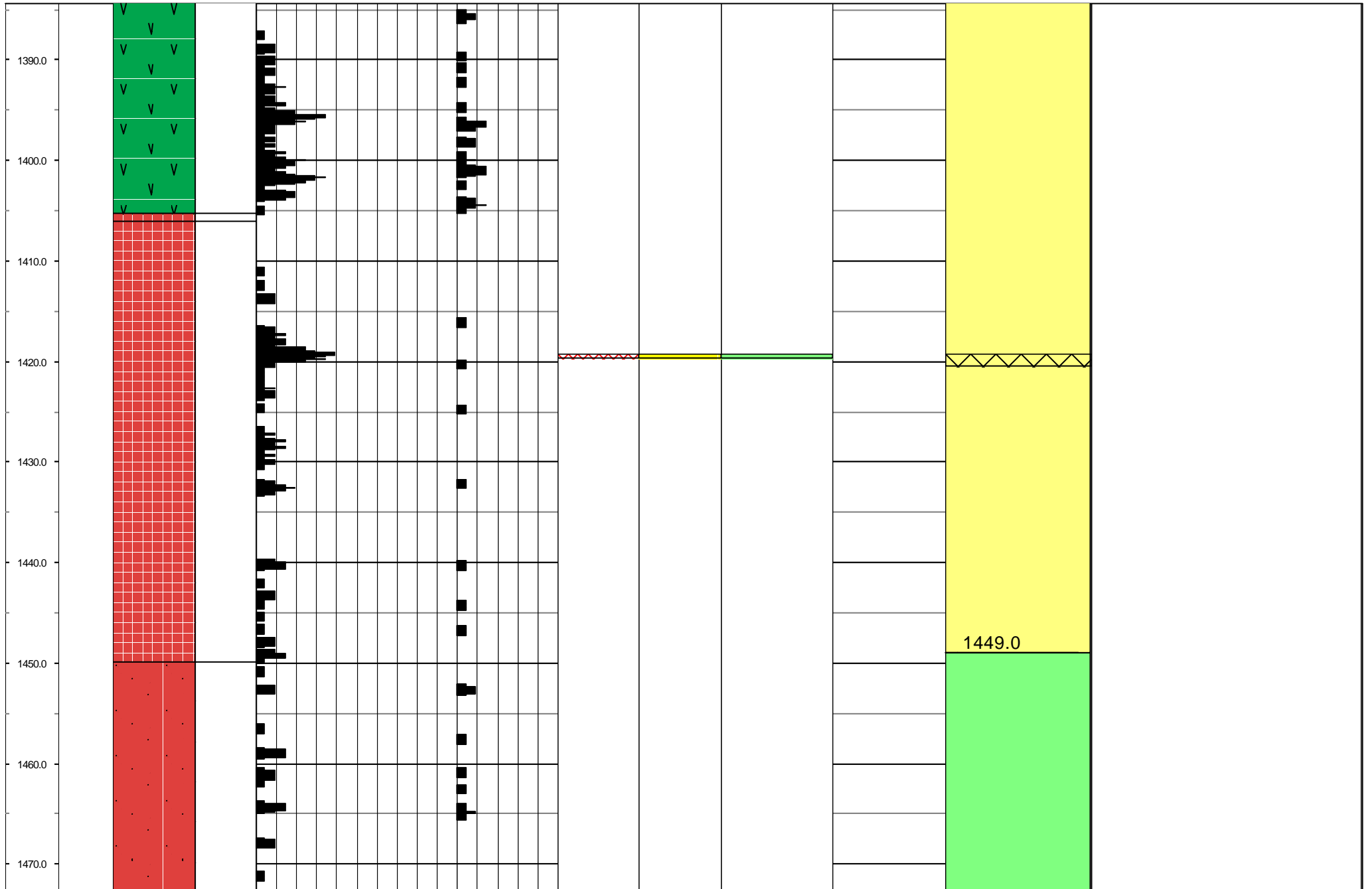


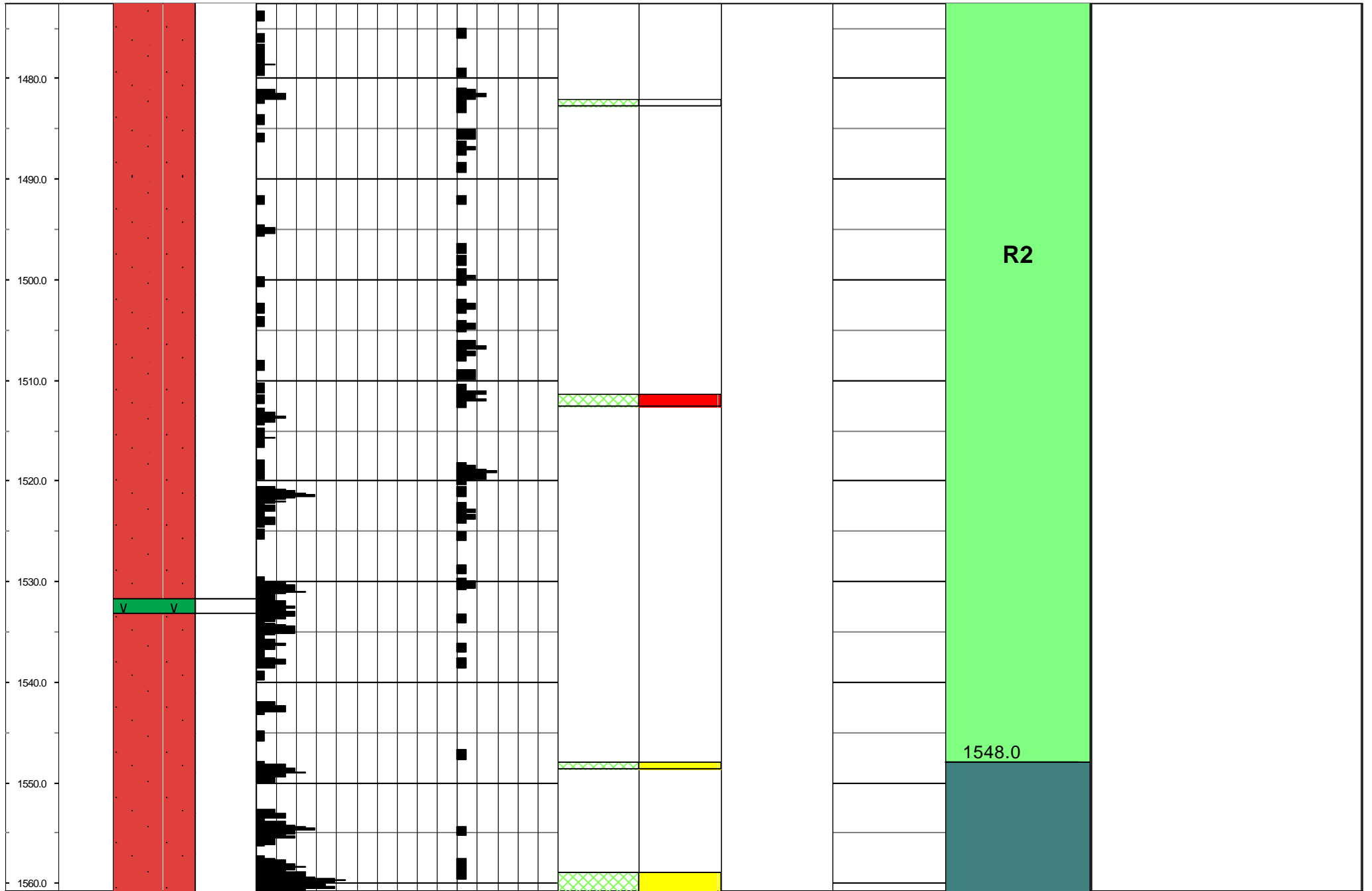


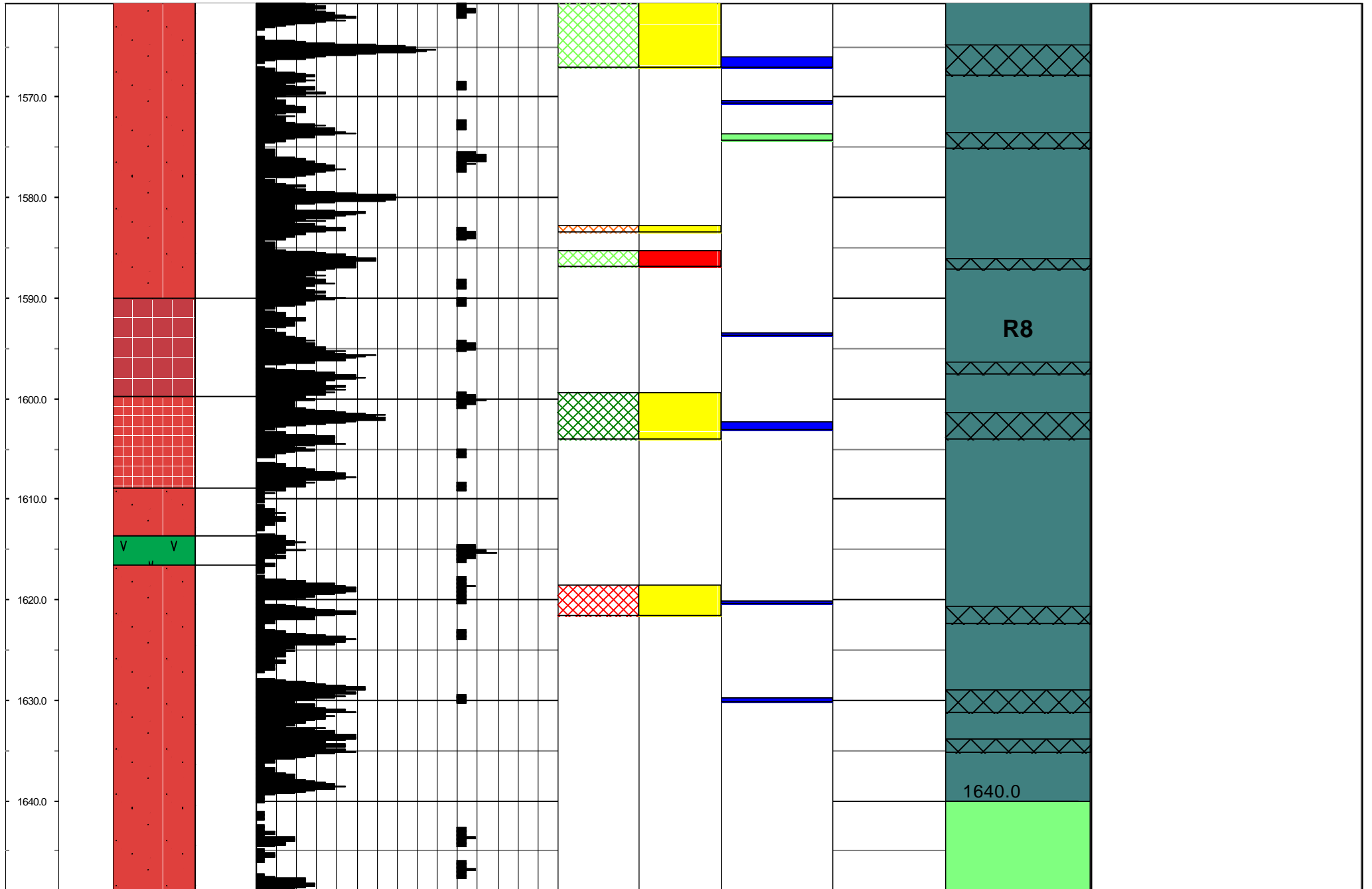




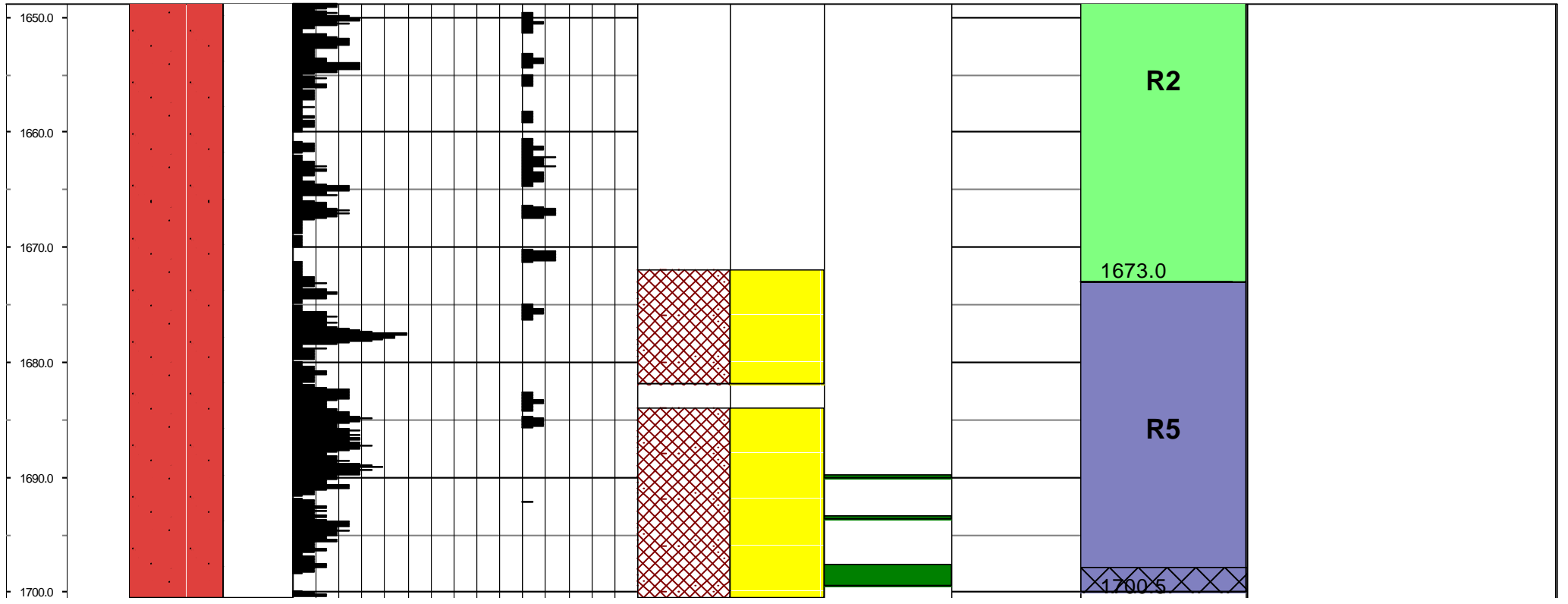






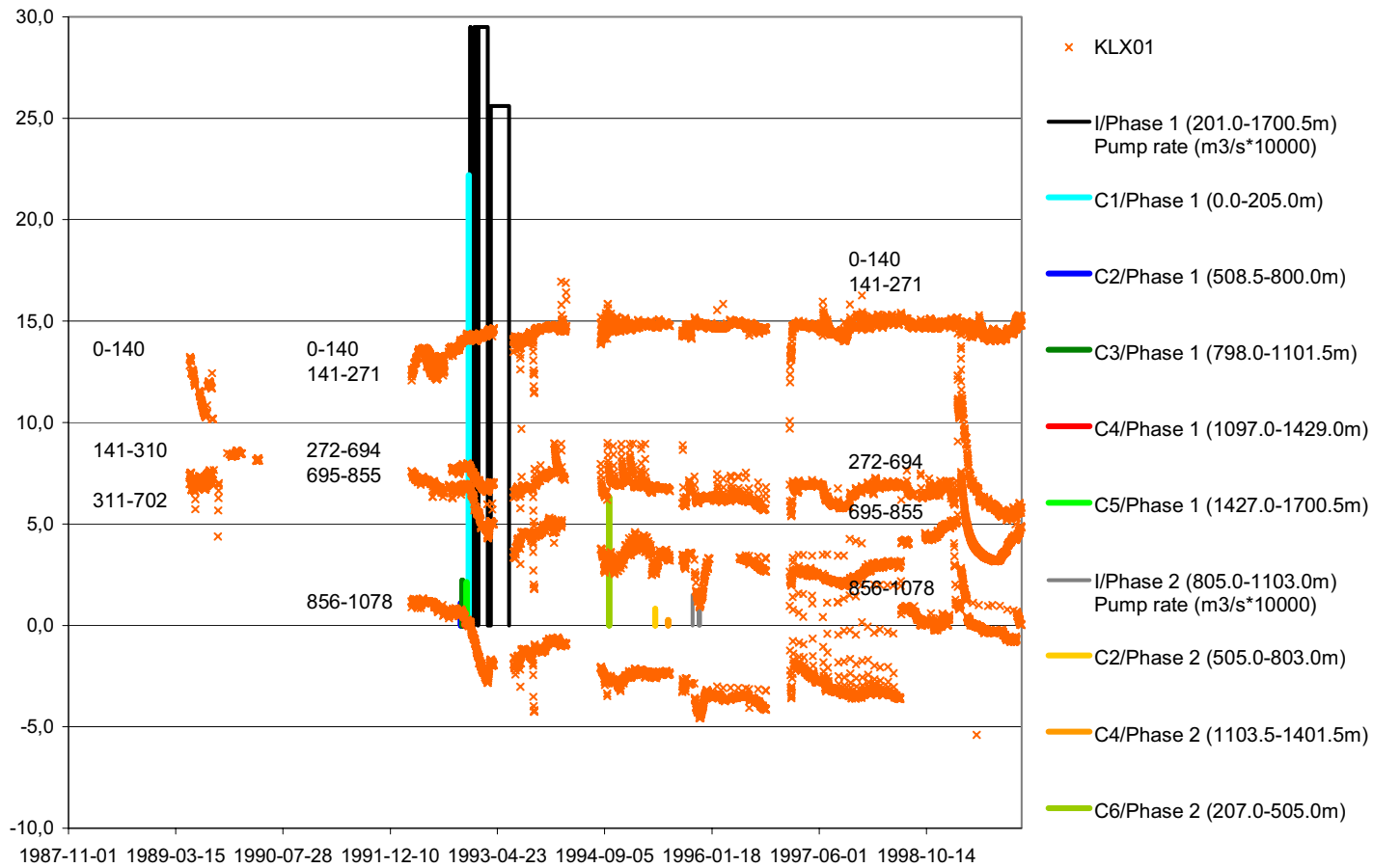




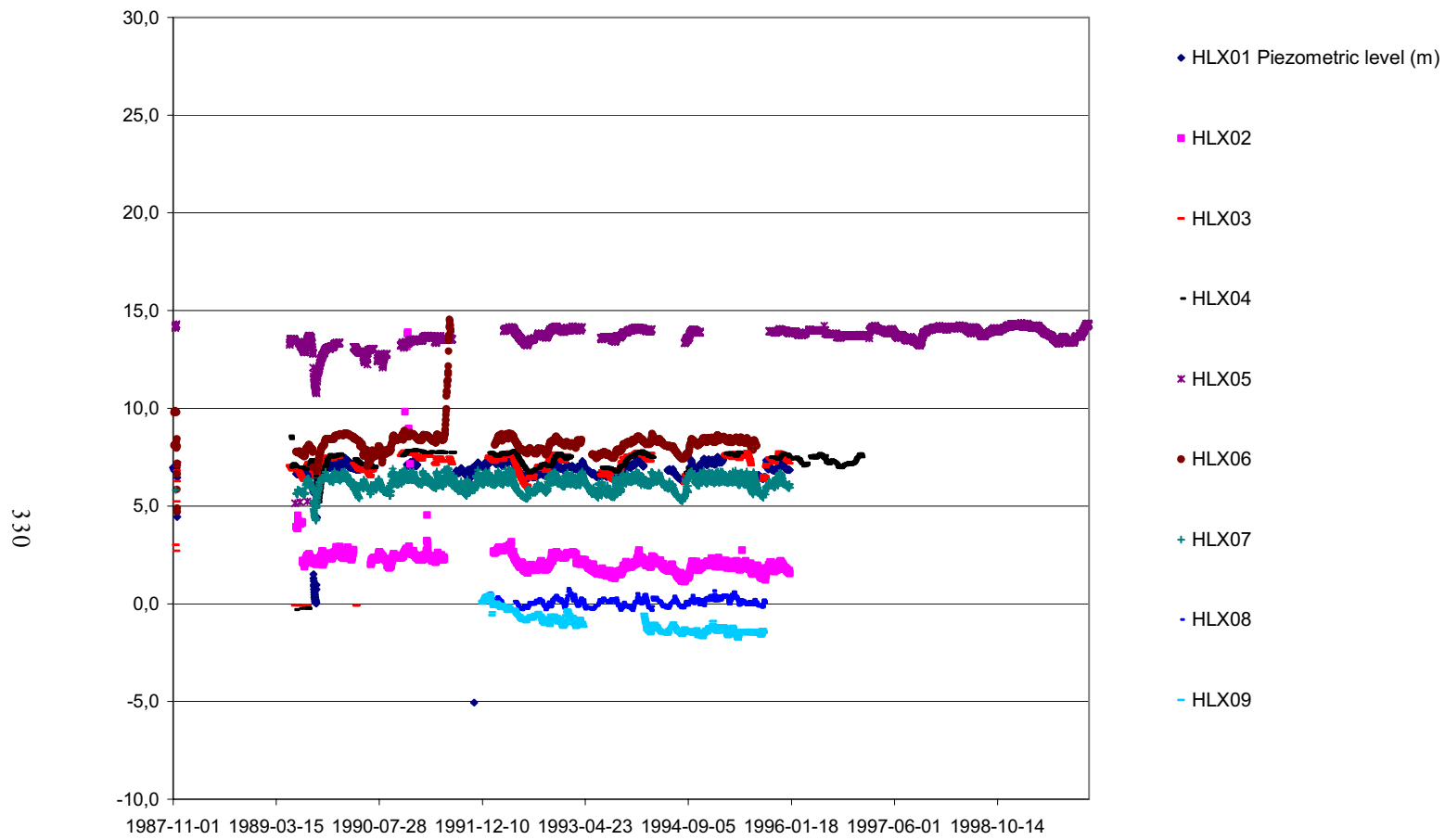


Hydrogeology – Precipitation, air temperature and piezometric levels

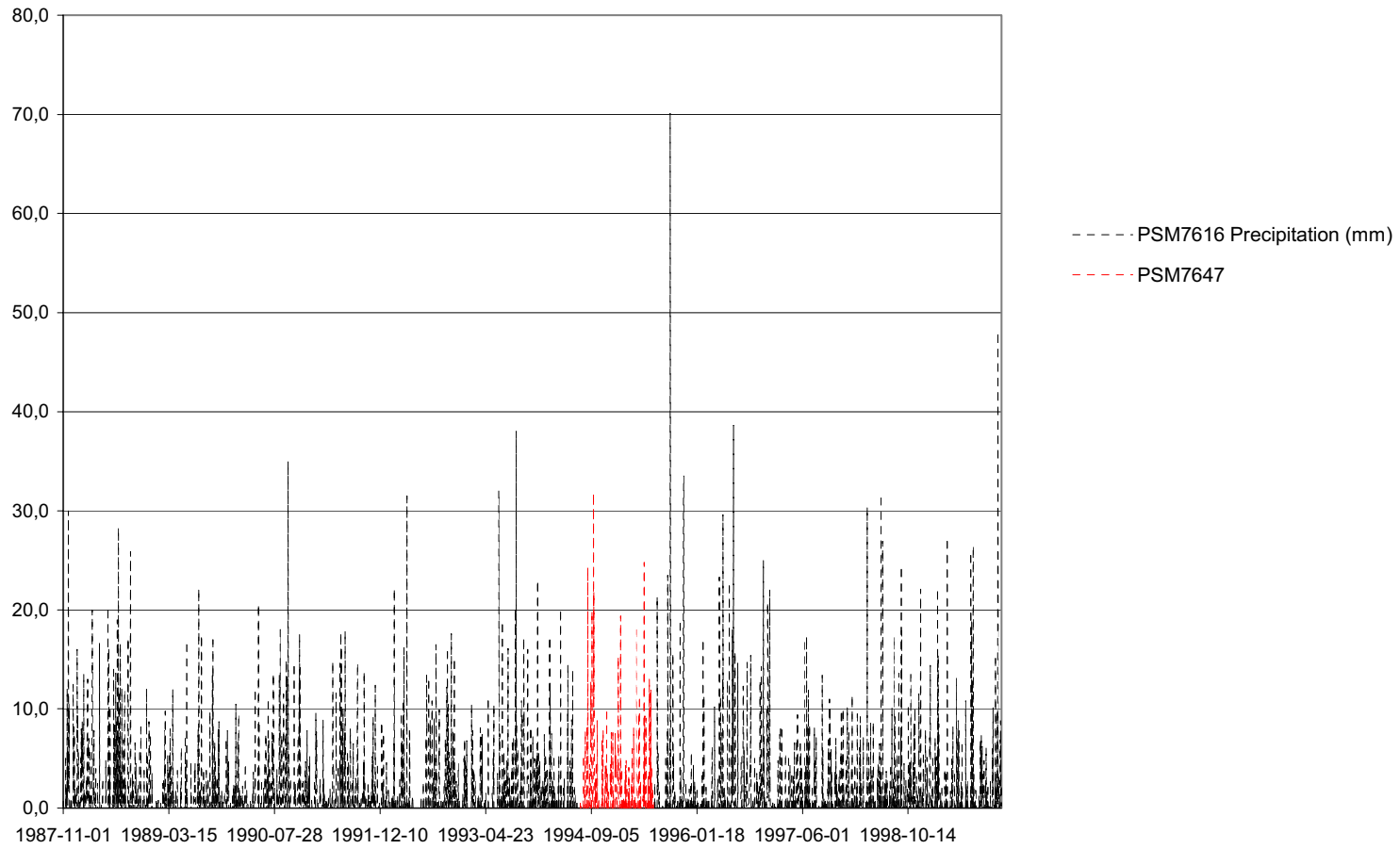
329



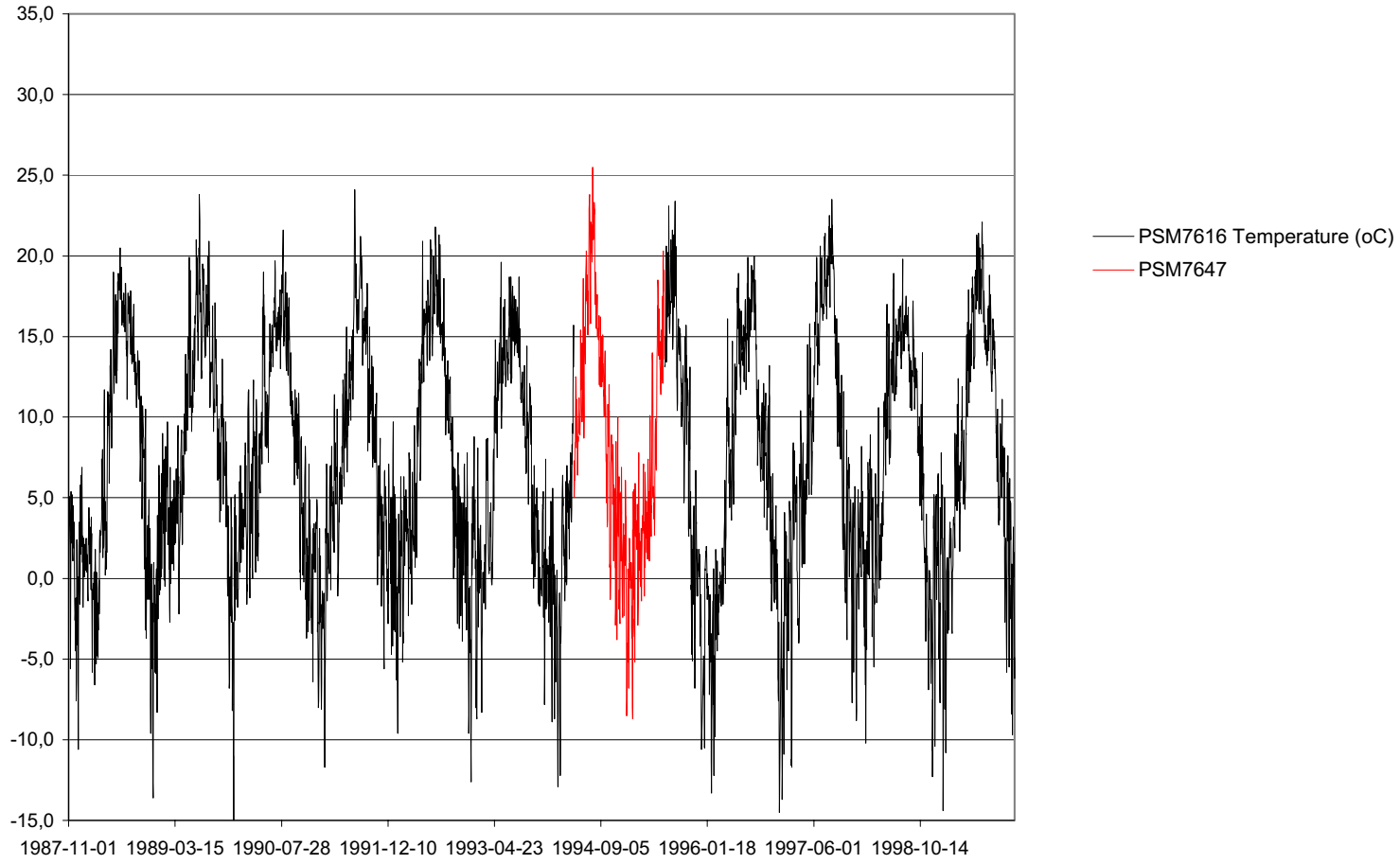
**Figure B3-1.** Piezometric levels for borehole KLX01 (numbers in the figure indicate borehole sections) and pump rates (m<sup>3</sup>/s\*10000) for hydraulic tests performed in KLX02 /Follin, 1993, 1996/. For tests C2/Phase 1 and C4/Phase 1, no transmissivities were evaluated due to the recovery periods being too short.



*Figure B3-2. Piezometric levels for boreholes HLX01-HLX09.*



*Figure B3-3. Precipitation for PSM 7616 and PSM 7647.*



*Figure B3-4. Temperature for PSM 7616 and PSM 7647.*

## Hydrogeology – Undisturbed piezometric levels

Data from TN-98-06g used for Task 5 modelling exercise within Äspö Task Force for modelling of transport of solutes.

### COMMENTS OF MEASUREMENTS OF THE PIETZOMETRIC LEVELS

- KLX01        Data for 1989 are from the period June – August 1989.
- HLX08        Data are from the period December 1991 – August 1992. Probably undisturbed conditions.
- HLX09        Data are from the period December 1991 – August 1992. Probably undisturbed conditions. The minimum values may be influenced of the tunnel construction work.

### UNDISTURBED PIEZOMETRIC LEVELS – Description of table columns

Borehole	Borehole name.
Section	The interval along the borehole between the upper and lower packer of a section.
Point of application	The point of each section where the centre of gravity of the flow or hydraulic conductivity have been estimated to be.
MASL	The vertical coordinate measured from the sea level for the point of application. MASL = metres above sea level. ( The levels are approximate as some corrections has been.)
d0	The fresh water density for the actual depth of the point of application. The density is a function of the temperature.
El. cond.90/91	Electric conductivity of water samples from the PEM-pipe.
Average Oct '89-Jan '90	An average pressue calculated for the period October 1989 – January 1990.
Min '90	The pressure values in this column is the minimum value measured during 1990.
Max '90	The pressure values in this column is the maximum value measure during 1990.
Average '90	The pressure values in this column is the measured average value during 1990.
dh '90	The pressure values in this column is the difference between Max '90 and Min '90.
Min '91	The pressure values in this column is the minimum value measured during 1991.
Max '91	The pressure values in this column is the maximum value measured during 1991.

Average '91	The pressure values in this column is the measured average value during 1991.
dh '91	The pressure values in this column are the difference between Max '91 and Min '91.
Undisturbed fresh water head	
Min	The pressure values in this column is the measured Min value recalculated to correspond the hydraulic head for a fresh water column.
Max	The pressure values in this column is the measured Max value recalculated to correspond the hydraulic head for a fresh water column.
Average	The pressure values in this column is the measured average value recalculated to correspond the hydraulic head for a fresh water column.
dh	The pressure values in this column is the difference between Max and Min.

Bore-hole	Section (m)	Point of application (m)	MASL (m)	d0 (kg/m3)	El. cond. 90/91 (mS/m)	Average		Average		Average		Undisturbed freshwater head		Average
						Oct '89 - Jan '90 (m)	Min '90 (m)	Max '90 (m)	Average '90 (m)	dh '90 (m)	Min '91 (m)	Max '91 (m)	Average '91 (m)	
LAXEMAR														
KLX01	0-140	70	-52,98	999,7	66				11,5					13,02
KLX01	141-271	180	-162,72	999,6	66			7,3						12,85
KLX01	272-694	460	-442,19	999,5	70			6,8						
KLX01	695-855	738	-719,76	999,2	61									7,21
KLX01	856-1078	933	-914,33	999,0	1860									8,96
HLX01	0-55	27	-15,00	999,7										
HLX01	56-100	78	-59,98	999,7										
HLX02	0-15	8	1,78	999,7										
HLX02	16-132	72	-54,31	999,7										
HLX03	0-10	5	5,98	999,7										
HLX03	11-100	55	-39,70	999,7										
HLX04	0-10	5	5,87	999,7										
HLX04	11-125	68	-53,16	999,7										
HLX05	0-10	5	11,20	999,7										
HLX05	11-100	55	-33,11	999,7										
HLX06	0-44	22	-3,24	999,7										
HLX06	45-100	70	-44,24	999,7										
HLX07	0-15	8	1,66	999,7										
HLX07	16-100	58	-42,90	999,7										
HLX08	0-10	5	-1,36	999,7										
HLX08	11-40	22,08	-14,19	999,7										
HLX09	0-50	25	-18,61	999,7										
HLX09	51-151	124,09	-104,87	999,7										



Hydrogeology - Hydraulic tests

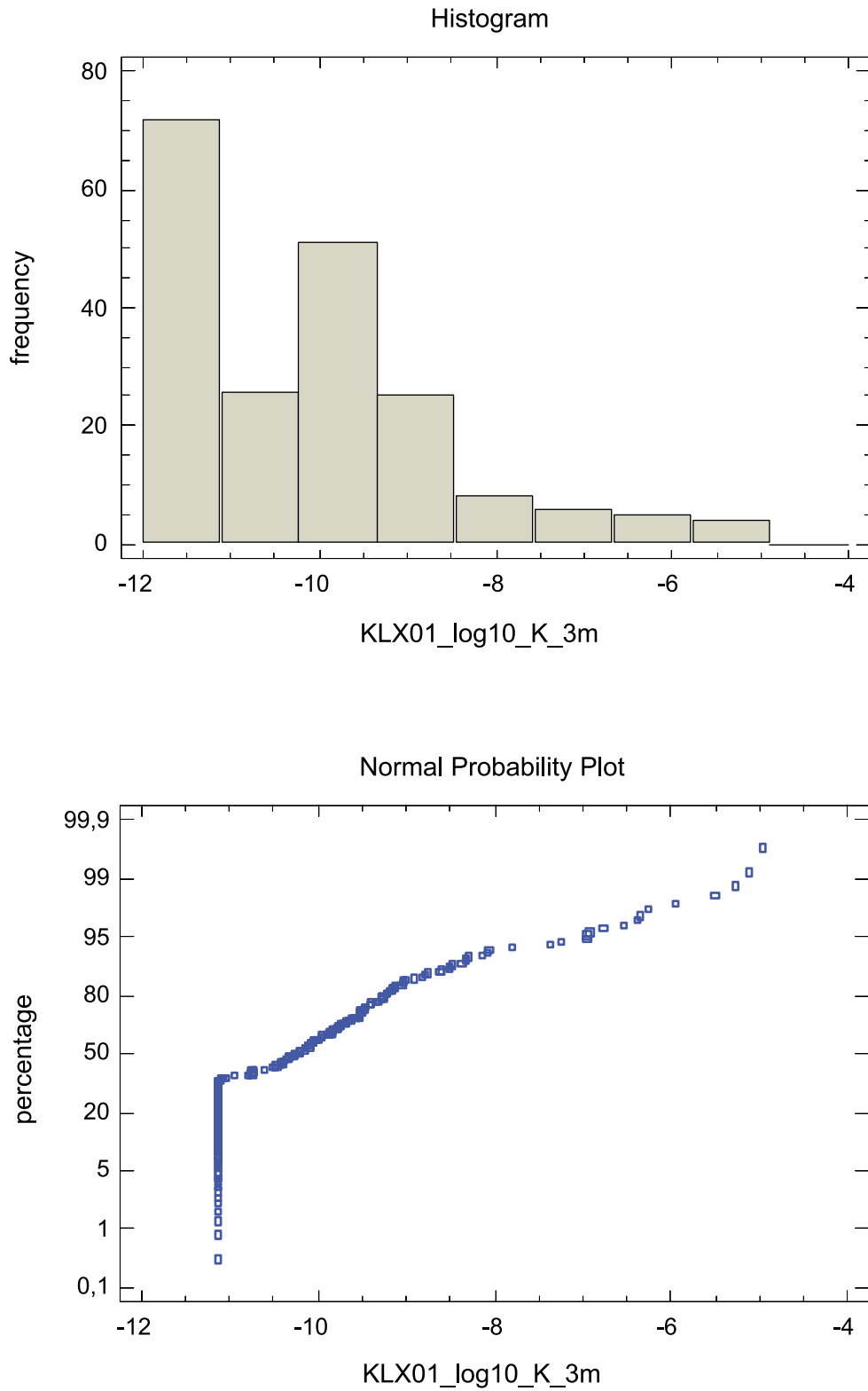
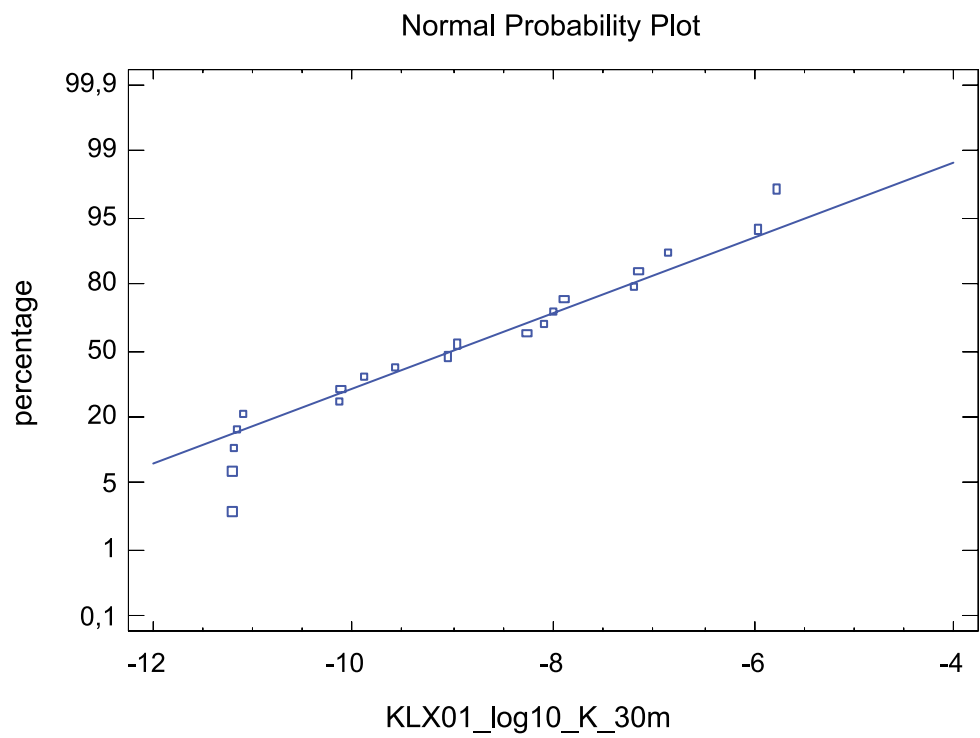
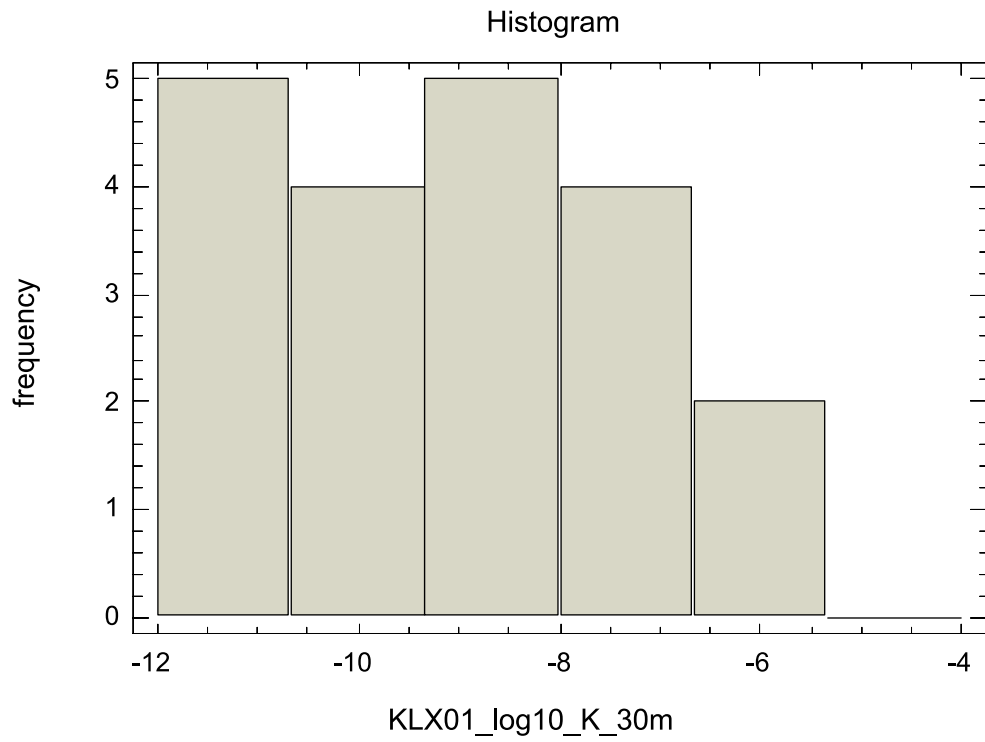
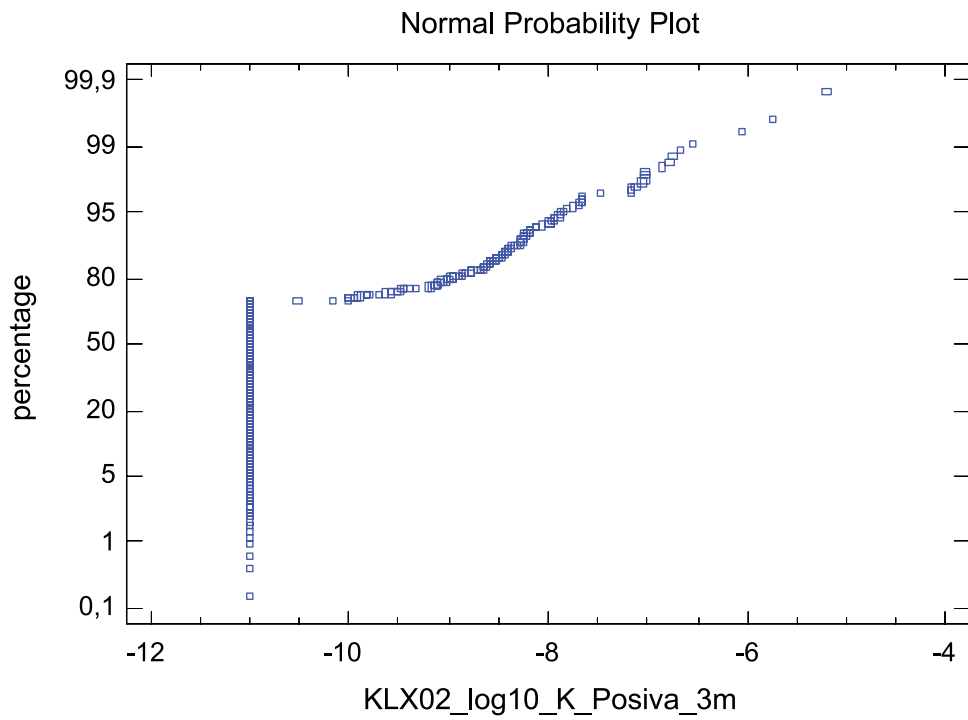
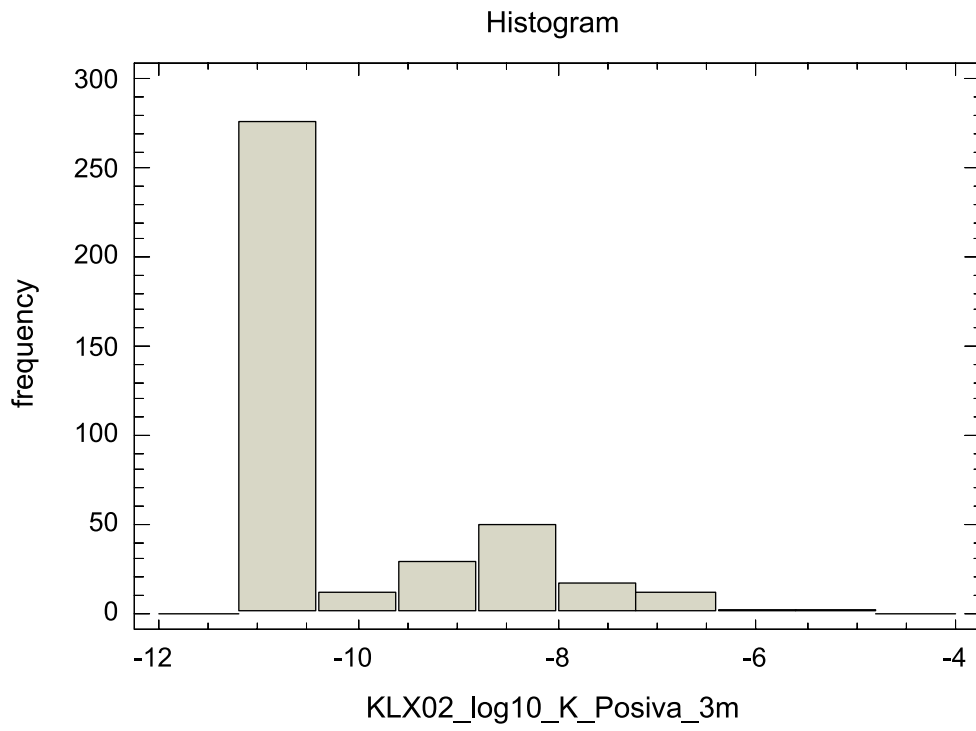


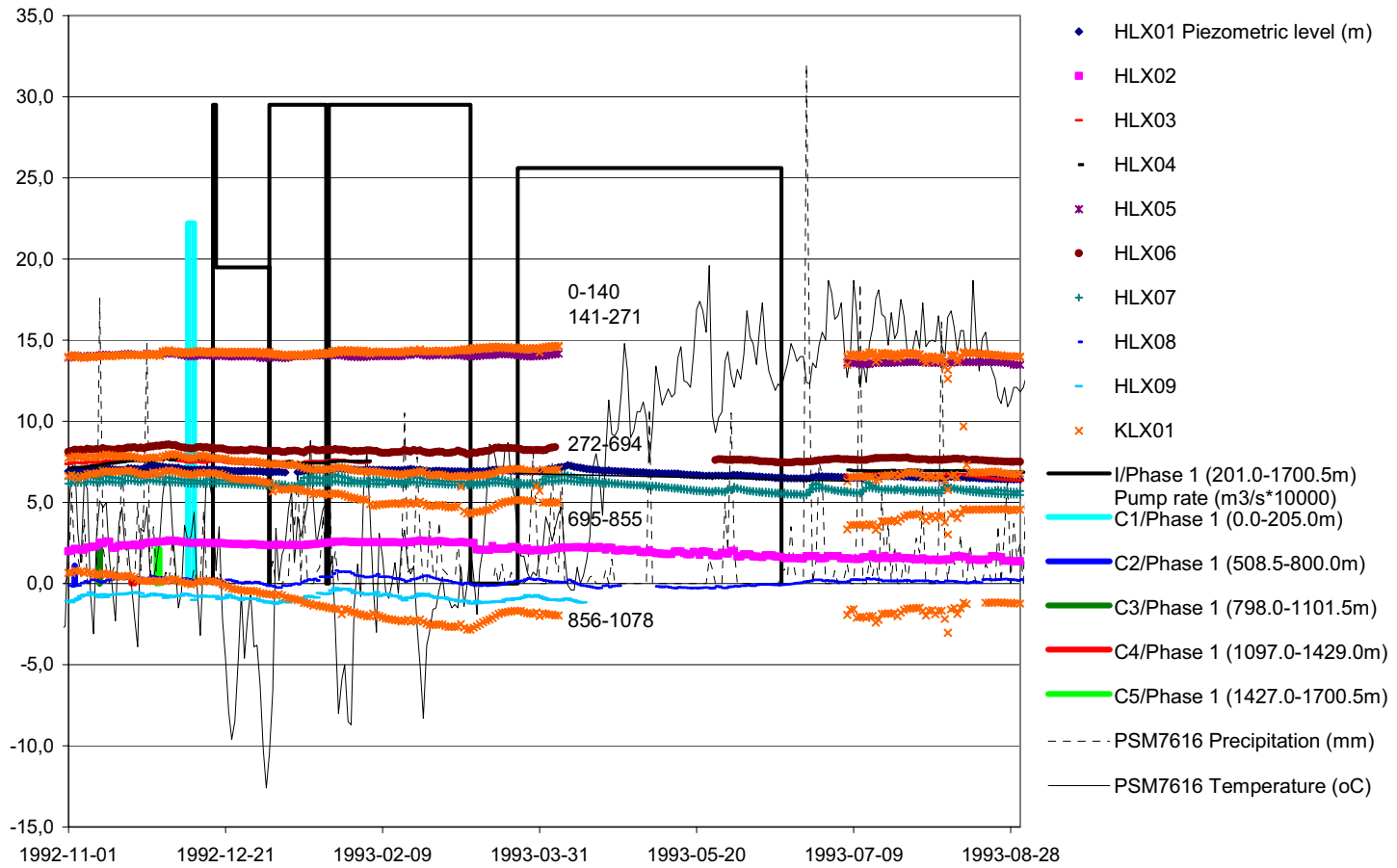
Figure B4-1. Univariate statistics for 3 m section packer tests, KLX01.



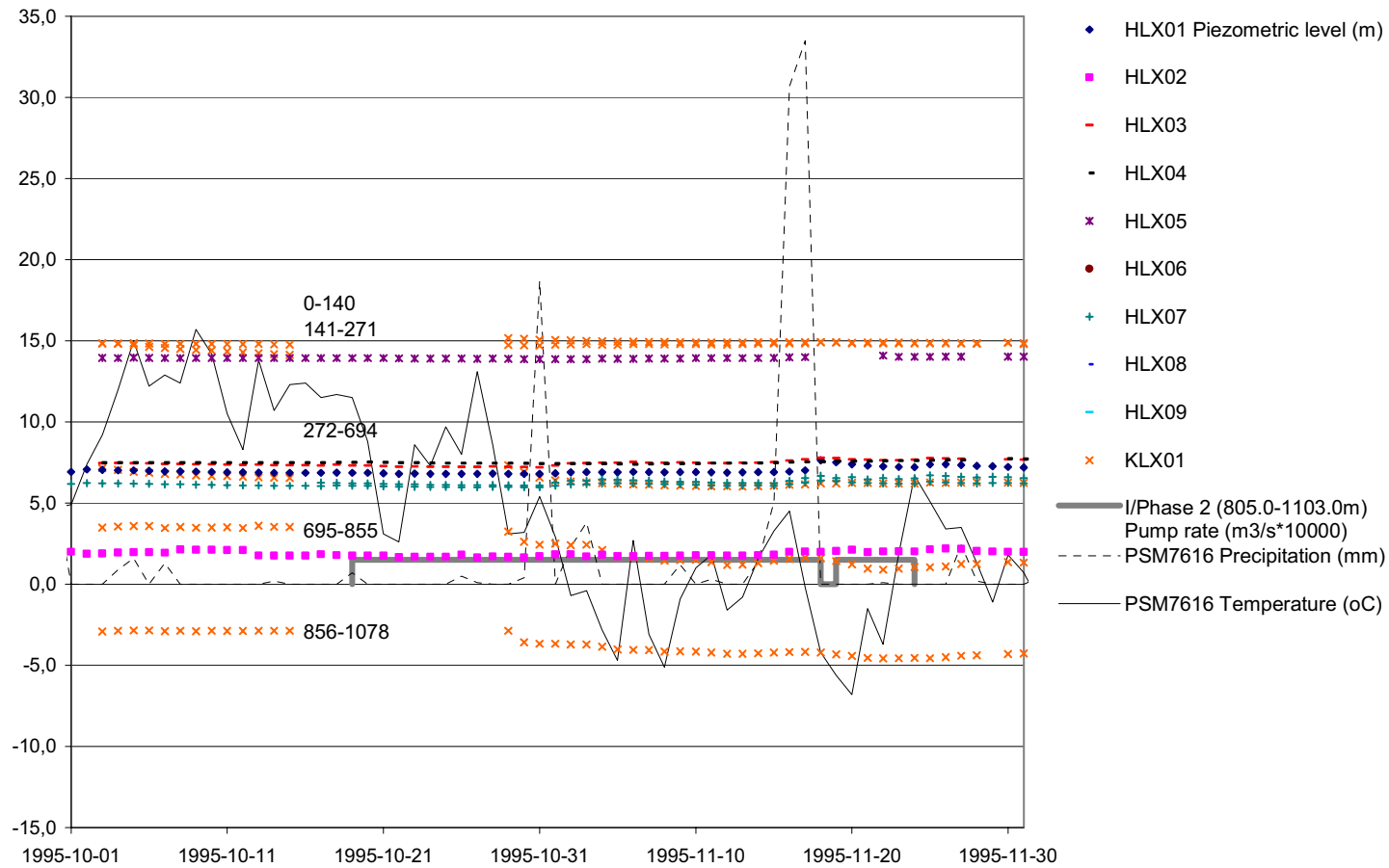
*Figure B4-2. Univariate statistics for 30 m section packer tests, KLX01.*



**Figure B4-3.** Univariate statistics for 3 m sections, Posiva Flow Log, KLX02.

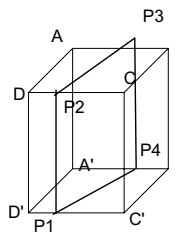


**Figure B4-4.** Piezometric levels for boreholes HLX01-HLX09 and KLX01 (numbers in figure indicate borehole sections), pump rates ( $m^3/s \cdot 10000$ ) for hydraulic tests performed in KLX02 /Follin, 1993/ and precipitation and temperature (PMS7616). For tests C2/Phase 1 and C4/Phase 1, no transmissivities were evaluated due to the recovery periods being too short.



**Figure B4-5.** Piezometric levels for boreholes HLX01-HLX09 and KLX01 (numbers in figure indicate borehole sections), pump rate ( $m^3/s*10000$ ) for a hydraulic test performed in KLX02 /Follin, 1996/ and precipitation and temperature (PMS7616).

**Laxemar geometrical**



Coordinates for modeled zones. All coordinates are given in

LR = Laxemar regional zone; LL = Laxemar local zone;

Magonly = zone indicated from magnetic data.

X=Easting Y=Northing Z=mas

1

General order in which the coordinates have been given. A represents the upper NW corner of the model block.

	X	Y	Z	A-D	Z A'-D'
A and A'	1547777,168	6E+06	50,07	50,07	-1949,93
B and B'	1550202,907	6E+06	50,07	50,07	-1949,93
C and C'	1551025,441	6E+06	50,07	50,07	-1949,93
D and D'	1548599,702	6E+06	50,07	50,07	-1949,93

New name	P1			P2			P3			P4			P5		
	X	Y	Z	X	Y	Z	X	Y	Z	X	Y	Z	X	Y	Z
ZLXEW01	1547969,0	6368029,1	-1949,9	1547969,0	6368029,1	50,1	1550414,1	6368556,1	50,1	1550414,1	6368556,1	-1949,9			
ZLXNE01	1550156,2	6365887,5	-1949,9	1549623,2	6365754,6	50,1	1550732,6	6367278,6	50,1	1550843,9	6366832,2	-1949,9			
ZLXNS01	1550739,4	6366475,6	-1949,9	1550739,4	6366475,6	50,1	1550209,2	6368511,9	50,1	1550209,2	6368511,9	-1949,9			
ZLXNS04	1550220,3	6368514,3	-1949,9	1550220,3	6368514,3	50,1	1549838,5	6369312,4	50,1	1549838,5	6369312,4	-1949,9			
ZLXNS02	1548583,7	6368161,6	-1949,9	1548583,7	6368161,6	50,1	1548583,7	6368999,5	50,1	1548583,7	6368999,5	-1949,9			
ZLXNS03	1548898,4	6368229,4	-1949,9	1548898,4	6368229,4	50,1	1549223,9	6367521,9	50,1	1549223,9	6367521,9	-1949,9			
ZLXNE02	1549987,4	6365845,4	-1949,9	1549987,4	6365845,4	50,1	1550915,0	6366547,2	50,1	1550915,0	6366547,2	-1949,9			
ZLXNE03	1548942,7	6366520,5	-1949,9	1548826,4	6366523,5	50,1	1549586,0	6367344,2	50,1	1549667,8	6367304,1	-1949,9			
ZLXNE04	1550122,1	6367081,2	-1949,9	1549556,0	6367359,0	50,1	1549928,8	6368125,1	50,1	1550555,2	6367990,1	-1923,9	1550558,3	6367977,7	-1949,9
ZLXNE05	1550452,1	6366196,9	-1949,9	1550452,1	6366196,9	50,1	1550599,4	6366479,1	50,1	1550599,4	6366479,1	-1949,9			
ZLXNE06	1550607,6	6366478,9	-1949,9	1550607,6	6366478,9	50,1	1550857,5	6366777,6	50,1	1550857,5	6366777,6	-1949,9			
ZLXNE07	1547818,6	6368632,4	-1949,9	1547818,6	6368632,4	50,1	1548076,9	6368873,2	50,1	1548076,9	6368873,2	-1949,9			
ZLXNE08	1550026,1	6368920,3	-1949,9	1550026,1	6368920,3	50,1	1550269,8	6369134,8	50,1	1550269,8	6369134,8	-1949,9			
ZLXNW01	1548122,7	6368062,2	-1949,9	1548122,7	6368062,2	50,1	1550649,1	6366822,6	50,1	1550649,1	6366822,6	-1949,9			
ZLXNW02	1550641,8	6366850,4	-1949,9	1550641,8	6366850,4	50,1	1550836,0	6366864,2	50,1	1550836,0	6366864,2	-1949,9			
ZLXEW02	1548341,4	6366535,6	-1949,9	1548341,4	6366535,6	50,1	1550934,1	6366470,8	50,1	1550934,1	6366470,8	-1949,9			
ZLXNW03	1549054,2	6369116,8	-1949,9	1549054,2	6369116,8	50,1	1550386,4	6368667,2	50,1	1550386,4	6368667,2	-1949,9			
ZLXNW04	1549171,5	6368288,3	-1949,9	1549171,5	6368288,3	50,1	1550555,2	6367990,1	50,1	1550555,2	6367990,1	-1949,9			
ZLXNW05	1548715,9	6368190,1	-1949,9	1548715,9	6368190,1	50,1	1550414,9	6367721,9	50,1	1550414,9	6367721,9	-1949,9			
ZLXNW06	1550193,1	6366489,3	-1949,9	1550193,1	6366489,3	50,1	1550667,5	6366015,0	50,1	1550667,5	6366015,0	-1949,9			
ZLXNW07	1547798,4	6368713,1	-1949,9	1547798,4	6368713,1	50,1	1548625,9	6368170,7	50,1	1548625,9	6368170,7	-1949,9			

## Laxemar geometrical base model

Coordinates (RT90-RHB70) for crossing points between modelled zones and borehole:

<b>Zone ZLXNE04</b>	X	Y	Z	Borehole length(m)
KLX01	1549914	6367530,7	-732,5	751
<b>Zone ZLXNE03</b>	X	Y	Z	
KLX02	1549224	6366881,7	-1042,5	1066
<b>Coordinates for boreholes:</b>				
KLX01	X	Y	Z	
sec up	1549923	6367485,5	16,77	
sec low	1549911	6367546,9	-1059,4	
KLX02	X	Y	Z	
sec up	1549225	6366768,1	18,31	
sec low	1549227	6366969,5	-1669,9	

## Laxemar geometrical base model

Coordinates (RT90-RHB70) for crossing points between fractured rocksegments and boreholes

<b>B8</b>	X	Y	Z	Borehole depth (m)
KLX01				
sec up	1549914,9	6367521,5	-568	
sec low	1549914,6	6367524,3	-622	

The B8 rock segment in KLX01 is one of the most fractured parts of the core in this borehole. It is characteristic because it is distinct from surrounding rock.

<b>B1 (hydraulic)</b>	X	Y	Z
KLX01			
sec up	1549914,4	6367527,3	-677
sec low	1549913,2	636731	-740

This B1 segment in KLX01 show significant hydraulic respons. If this segment corresponds to the model zone ZLXNE04, the ZLXNE04 can be estimated to have a thickness of about 15 metre. 10 metres above (SE) and 5 metres below (NW the modelled zone.

<b>B8</b>	X	Y	Z
KLX02			
sec up	1549223,1	6366842,7	-704,8
sec low	1549222,8	6366871,8	-947,1

The B8 rocksegment in KLX 02 has a high frequency of fractures compared to the higher sections. It has much less crushed zones than the lower B7 rock segment.

<b>B7</b>	X	Y	Z
KLX02			
sec up	1549222,8	6366871,8	-947,1
sec low	1549224,0	6366890,4	-1104,9

Th B7 rocksegment in KLX02 exhibit several crushed zones. If this segment corresponds to the model zone ZLXNE03, the ZLXNE03 can be estimated to have a thickness of about 20 metre.

Coordinates for boreholes:

KLX01	X	Y	Z
sec up	1549923,09	6367485,516	16,77
sec low	1549910,79	6367546,929	-1059,352

KLX02	X	Y	Z
sec up	1549224,84	6366768,086	18,31
sec low	1549227,47	6366969,52	-1669,916

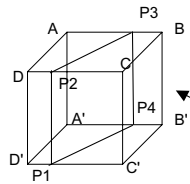
### EXPLANATION:

Segment B8 represents inhomogeneous rock segments with high frequency of zones, both with altered and fractured core (>10 fractures/m).

Segment B7 represents homogeneous rock segments with high frequency of zones, both with altered and fractured core (>10 fractures/m).



### Alternative model



Coordinates for modeled zones. All coordinates are given in RT90-

LR = Laxemar regional zone; LL = Laxemar local zone;

Magonly = zone indicated from magnetic data.

X=Eastings Y=Northing Z=masl

General order in which the coordinates have been given. A represents the upper NW corner of the model block.

	X	Y	Z	A-D	Z A'-D'
A and A'	1547777,168	6368798,416	50,07		-1949,93
B and B'	1550202,907	6369403,221	50,07		-1949,93
C and C'	1551025,441	6366104,216	50,07		-1949,93
D and D'	1548599,702	6365499,411	50,07		-1949,93

New name	P1			P2			P3			P4			P5		
	X	Y	Z	X	Y	Z	X	Y	Z	X	Y	Z	X	Y	Z
ZLXEW01	1548339,63	6366542,52	-1949,93	1 547 961,4	6368059,46	50,1	1550202,91	6369403,22	50,07	1550784,77	6367069,49	- 1 949,9			
ZLXNE01	1550156,16	6365887,48	-1949,93	1 549 623,2	6365754,60	50,1	1550732,64	6367278,56	50,07	1550843,93	6366832,23	- 1 949,9			
ZLXNS01	1550595,41	6367028,68	-1949,93	1 550 201,3	6368542,20	50,1	1550752,75	6366424,41	50,07	1550752,75	6366424,41	- 1 949,9			
ZLXNS04	1549838,50	6369312,36	-1949,93	1 549 838,5	6369312,36	50,1	1550206,44	6368543,30	50,07	1550646,80	6367622,85	- 1 220,4	1550646,80	6367622,85	-1949,93
ZLXNS02	1548583,70	6368999,51	-1949,93	1 548 583,7	6368999,51	50,1	1548583,70	6368193,58	50,07	1548583,70	6366595,13	- 1 949,9			
ZLXNS03	LL_NS3			1 548 885,1	6368258,92	50,1	1549223,90	6367521,90	50,07	1549223,90	6367521,90	- 963,0			
ZLXNE02	1549987,38	6365845,40	-1949,93	1 549 987,4	6365845,40	50,1	1550915,00	6366547,16	50,07	1550915,00	6366547,16	- 1 949,9			
ZLXNE03	1548471,93	6366011,89	-1949,93	1 548 446,7	6366113,16	50,1	1549586,02	6367344,24	50,07	1549667,85	6367304,09	- 1 949,9			
ZLXNE04	1550608,82	6366842,40	-1949,93	1 549 529,7	6367371,89	50,1	1549922,47	6368126,47	50,07	1550555,24	6367990,09	- 988,9	1550766,08	6367144,48	-1949,93
ZLXNE05	LL_NE4														
ZLXNE06	1548599,14	6365501,66	-1949,93	1 549 929,0	6365830,84	50,1	1551025,44	6366104,22	50,07	1550646,96	6367622,24	- 1 949,9			
ZLXNE07	1547818,55	6368632,43	-1949,93	1 547 818,6	6368632,43	50,1	1548076,94	6368873,16	50,07	1548076,94	6368873,16	- 1 949,9			
ZLXNE08	1550026,08	6368920,30	-1949,93	1 550 026,1	6368920,30	50,1	1550269,83	6369134,82	50,07	1550269,83	6369134,82	- 1 949,9			
ZLXNW01	1550340,93	6366973,84	-1949,93	1 548 077,4	6368084,46	50,1	1550649,07	6366822,65	50,07	1550649,07	6366822,65	- 1 949,9			
ZLXNW02	1550641,84	6366850,42	-1949,93	1 550 641,8	6366850,42	50,1	1550835,96	6366864,18	50,07	1550835,96	6366864,18	- 1 949,9			
ZLXEW02	1548142,43	6367333,42	-907,18	1 548 350,8	6366497,53	50,1	1550938,64	6366452,35	50,07	1550653,89	6367594,43	- 1 257,8			
ZLXNW03	1549054,17	6369116,81	-1949,93	1 549 054,2	6369116,81	50,1	1550386,42	6368667,20	50,07	1550386,42	6368667,20	- 1 949,9			
ZLXNW04	LL_NW4			1 549 171,5	6368288,30	50,1	1550555,24	6367990,09	50,07	1550555,24	6367990,09	- 736,2			
ZLXNW05	LL_NW5			1 548 650,8	6368208,04	50,1	1550415,40	6367721,81	50,07	1550415,40	6367721,81	- 1 034,1			
ZLXNW06	1549867,42	6366815,00	-1949,93	1 550 382,2	6366300,19	50,1	1550667,46	6366014,96	50,07	1550667,46	6366014,96	- 1 949,9			
ZLXNW07	1547798,44	6368713,11	-1949,93	1 547 798,4	6368713,11	50,1	1548589,24	6368194,77	50,07	1550424,48	6366991,84	- 1 949,9			

yellow yellow cells are copied from the geometrical base model

ISSN 1404-0344

CM Digitaltryck AB, Bromma, 2002